Wet Chemical Synthesis of Nano and Submicron Al Particles for the Preparation of Ni and Ru Aluminides

Dissertation

Zur Erlangung des Grades

des Doktors der Naturwissenschaften

der Naturwissenschaftlich-Technischen Fakultät

der Universität des Saarlandes

von

Thomas Klein

Saarbrücken

2020

Tag des Kolloquiums:	09.02.2021
Dekan:	Prof. Dr. Jörn Walter
Berichterstatter:	Prof. Dr. Guido Kickelbick
	Prof. Dr. Frank Mücklich
Vorsitz:	Prof. Dr. Gregor Jung
Akad. Mitarbeiter:	Dr. Andreas Rammo

Die vorliegende Arbeit wurde in der Zeit von Oktober 2016 bis März 2020 an der Universität des Saarlandes im Institut für anorganische Festkörperchemie im Arbeitskreis von Prof. Dr. Guido Kickelbick angefertigt.

Danksagung

Besonders danken möchte ich Herrn Prof. Dr. Guido Kickelbick, der mir die Durchführung dieser Arbeit in seinem Arbeitskreis ermöglichte, sowie für seine wissenschaftliche Unterstützung und gleichzeitige Offenheit gegenüber eigenen Ideen.

Herr Prof. Dr-Ing. Frank Mücklich danke ich für das Übernehmen der Zweitkorrektur der Arbeit.

Bei dem gesamten aktuellen und ehemaligen Arbeitskreis, Achim, Bastian, Christina, Dennis Becker, Dennis Meier, Jessica, Nadja, Nils, Mana, Max, Matthias, Patrick, Sandra und Tobias möchte ich mich für das angenehme und freundliche Arbeitsklima sowie für die Hilfe bei den kleineren und alltäglichen Laborproblemen bedanken.

Robert, Dennis Becker und Jessica danke ich für die Durchführung der XRD-Messungen sowie für die Geduld bei den zahlreichen Fragen zu der Rietveld Analyse. Susanne Harling möchte ich für die CHN Messungen danken, Michael Zimmer für die Festkörper-NMR-Messungen, Nadja für die TEM-Messungen sowie Christina und Mana für die REM Messungen. Dr. Christoph Pauly sowie Katherine Aristizabal danke ich für die Durchführung der FIB-Messungen. Susanne Limbach danke ich für die Hilfe bei organisatorischen Angelegenheiten, Sylvia sowie Stefan für die Hilfe bei den technischen Problemen der Laborgerätschaften und Jörg für die Einweisung in die TEM Messungen.

Schließlich möchte ich mich bei meinen Eltern bedanken, die mir diesen Weg ermöglicht haben und mich dabei stets unterstützt haben.

Kurzzusammenfassung

Aufgrund ihrer großen Oberfläche besitzen Nanopartikel eine im Vergleich zu Mikropartikeln stark erhöhte Reaktivität. Während diese beispielsweise bei Thermiten in Form von Nanothermiten bereits ausgenutzt wird, ist ihre Verwendung zur Herstellung von Aluminiden unüblich. Zur Herstellung von Nanopartikeln haben sich unter anderem nasschemische Methoden etabliert.

Diese Arbeit soll daher die Eignung nasschemisch hergestellter Nanopartikel zur Synthese von binären Ni and Ru Aluminiden untersuchen.

Dazu wurde zunächst die nasschemische Synthese von Al Partikeln untersucht. Es wurde eine Methode zur Synthese von Al-Partikeln mit Größen von 100 – 150 nm mittels thermischer Zersetzung von Triisobutylaluminium entwickelt. Bei der Synthese mittels katalytischer Zersetzung von Alanen wurde der Einfluss der Reaktionsparameter auf die die Größe und Morphologie der Partikel systematisch untersucht.

Um eine gute Durchmischung und einen guten Partikelkontakt zu erreichen wurde zur Synthese von binären Aluminiden eine Eintopfsynthese entwickelt. Dabei erfolgte zunächst die Synthese von Al Partikeln mittels Zersetzung von Triisobutylaluminium, bevor das zweite Metall durch Zersetzung einer geeigneten Vorstufe, wie Bis(cycloocta-1,5-dien)nickel(0) oder $Ru_3(CO)_{12}$, eingebracht wurde. Verglichen mit Systemen aus getrennt hergestellten Partikeln konnten diese Gemische durch thermische Behandlung mit höheren Umsätzen und niedrigeren Onsettemperaturen zu den jeweiligen Aluminiden umgesetzt werden.

Abstract

Due to their large surface, nanoparticles are exhibiting a highly increased reactivity compared to microparticles. While this is for example already exploited in the field of thermites in the form of nanothermites, their application for the preparation of aluminides is uncommon. Amongst others, wet chemical methods have been established for the preparation of nanoparticles.

Thus, this work studies the suitability of wet chemically prepared nanoparticles for the preparation of binary Ni and Ru aluminides.

The wet chemical synthesis of Al particles was studied. A method for the preparation of Al particles with sizes of 100 – 150 nm via a thermal decomposition of triisobutylaluminum was developed. Within the catalytic decomposition approach, the influence of the reaction parameters on the size and morphology of the resulting particles was systematically studied.

To ensure a good intermixing and a good particle contact, a one-pot synthesis protocol was developed for the preparation of binary aluminides. Within this protocol, Al particles were prepared via a decomposition of triisobutylaluminum followed by the decomposition of a suitable precursor of the additional metal, such as bis(cycloocta-1,5-diene)nickel(0) or $Ru_3(CO)_{12}$. Compared to samples prepared from separately synthesized particles, these mixtures were reacted with increased yields as well as lower onset temperatures to the respective aluminides by a thermal treatment.

Table of contents

1. Introduction ... 1

1.1 Metal nanoparticles ... 1

1.2 Reactive metal nanoparticles ... 2

1.3 Al nanoparticles ... 5

1.3.1 Synthesis of Al nanoparticles ... 5

1.3.1.1 Synthesis via physical methods ... 5

1.3.1.2 Synthesis via thermal decomposition ... 7

1.3.1.3 Synthesis via metal reduction ... 8

1.3.1.4 Synthesis via hydride reduction ... 10

1.3.1.5 Synthesis via catalytic decomposition ... 12

1.3.1.6 Additional synthesis methods ... 20

1.3.1.7 Size control ... 21

1.3.1.8 Control of morphology ... 22

1.3.2 Oxidation of Al nanoparticles ... 23

1.3.3 Applications ... 27

1.4 Aluminides ... 33

1.4.1 Ru aluminides ... 33

1.4.1.1 Ru-Al system ... 33

1.4.1.2 Properties and applications ... 34

1.4.1.3 Preparation methods ... 35

1.4.2 Ni aluminides ... 38

1.4.2.1 Ni-Al system ... 38

1.4.2.2 Properties and applications ... 40

1.4.2.3 Preparation methods ... 41

1.5 Methods ... 52

1.5.1 Calculation of Al contents from TG measurements ... 52

1.5.2 Kissinger analysis ... 54

1.5.3 Synthesis of aluminides on a hot plate ... 54

1.5.4 XRD measurements ... 55

2. Goals of this work ... 56

3. Results and discussion ... 57

3.1 Synthesis of Al particles ... 57

3.1.1 Synthesis via metal reduction ... 57

3.1.2 Synthesis via hydride reduction ... 60

3.1.3 Synthesis via catalytic decomposition 62
3.1.3.1 Comparison to the hydride reduction 62
3.1.3.2 Systematic variation of the reaction parameters 67
3.1.4 Synthesis via thermal decomposition 84
3.1.4.1 Addition to the size control 99
3.1.4.2 Application of Al seeds 100
3.1.4.3 Synthesis via hot injection 101
3.2 Synthesis of aluminides 105
3.2.1 General comments for the preparation of Ni and Ru particles 105
3.2.2 Comparison of different Al particles for the preparation of aluminides 109
3.2.3 Preparation of Ni aluminides 122
3.2.3.1 Application of micron Ni and Al powders 122
3.2.3.2 Application of wet chemically prepared Ni and Al particles 124
3.2.4 Preparation of Ru aluminides 136
3.2.4.1 Application of micron Ru and Al powders 136
3.2.4.2 Application of submicron Al and Ru nanopowder 138
3.2.4.3 Application of submicron Al and Ru nanoparticles 140
3.2.5 Synthesis of additional aluminides and aluminothermic reactions 153
4. Experimental 167
4.1 Materials 167
4.2 Methods 168
4.3 Syntheses 170
5. Summary and Outlook 178
6. References 182
7. Appendix 202
7.1 Characterization of the commercial Ni powder 202
7.2 Characterization of the commercial Co powder 202
7.3 Diffractograms of the nanocrystalline Cu_2O and V_2O_5 203
7.4 Supporting information for Chapter 3.1.3.2 204
7.5 Supporting information for Chapter 3.1.4 224

Abbreviations

acac	Acetylacetonate
BuLi	Butyllithium
Cat	Catalyst
CHN	Carbon, hydrogen, nitrogen elemental analysis
COD	Cylcooctadiene
Cp	Cyclopentadiene
Cp*	Pentamethylcyclopentadiene
CP/MAS	Cross polarization magic-angle spinning
CVD	Chemical vapor deposition
DME	Dimethylether
DLS	Dynamic light scattering
DSC	Differential scanning calorimetry
EEW	Electrical exploding wire
ESR	Electron spin resonance
Et	Ethyl group
FIB	Focused ion beam
FTIR	Fourier-transformed infrared spectroscopy
Me	Methyl group
^{n}Bu; ^{i}Bu; ^{t}Bu	n-Butyl group; Isobutyl group; tert-Butyl group
NMP	N-Methyl-2-pyrrolidone
NMR	Nuclear magnetic resonance
NP	Nanoparticles
^{n}Oct	n-Octyl group
Ph	Phenyl group
^{i}Pr	Isopropyl group
Pyr	Pyridine
PS	Polystyrene
R	Organic residue
SEM	Scanning electron microscopy
SHS	Self-sustaining high temperature synthesis

SPE-MAS	Single-excitation magic angle spinning
STA	Simultaneous thermal analysis
TEM	Transmission electron spectroscopy
Tetraglyme	Tetraethylene glycol dimethyl ether
THF	Tetrahydrofuran
TG	Thermogravimetry
TGA	Thermogravimetric analysis
TIBAl	Triisobutylaluminum
TMEDA	Tetramethylethylenediamine
TOP	Trioctylphosphine
TOPO	Trioctylphosphine oxide
UV	Ultraviolet
XRD	X-ray diffraction

1. Introduction

1.1 Metal nanoparticles

Per definition, a nanoparticle is an object with a size of 1 – 100 nm in all three dimensions whose lengths of the shortest and longest axes are not differing significantly (typically not more than a factor of 3)[1]. Accordingly, they are representing the transition region from atoms, molecules, and small clusters to bulk materials and nowadays, nanoparticles from many different materials, including metals, metal oxides, or semiconductors are readily available. Beside these synthetic nanoparticles, they can also be found in the environment, for example in living organisms such as honey bees[2] or as a result of natural processes such as volcano eruptions[3] in the form of small mineral particles.

The historical origins of the nanotechnology research have already been summarized numerous times in the literature[4–7]. The first, likely unaware, anthropogenic applications of nanoparticles can be dated back to the late antiquity, when colloidal metal nanoparticles were applied for the coloration of glasses and ceramics. Well-known examples are including the Lycurgus cup[8,9], luster ware[10] as well as colored windows of the middle ages[11], whose colors can be ascribed to colloidal Au and Ag nanoparticles (Figure 1).

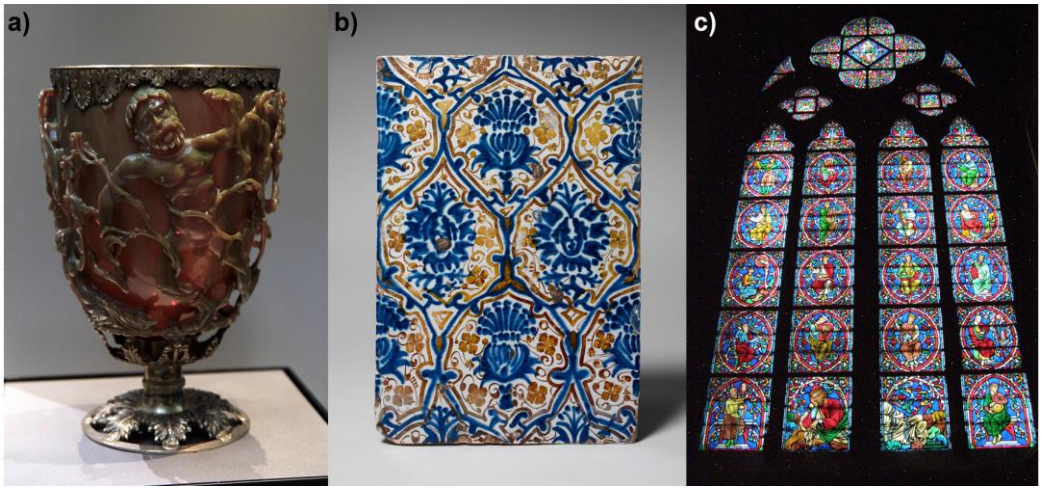

Figure 1: a) *Lycurgus Cup*[12] ***b)*** *Luster ware*[13] ***c)*** *colored window located in the Notre-Dame*[14] *(reprinted from the Wikimedia Commons public domain).*

The first systematic scientific investigations of colloidal Au solutions were carried out by Michael Faraday not earlier than around 1850, who examined the optical properties of Au colloids[15]. The heterogeneous nature of the colloidal Au solutions was confirmed for the first time by Richard Zsigmondy applying the ultramicroscope developed by Horst Siedentopf and him at around 1900[16], for

which he was awarded with the Nobel prize in chemistry in 1925 ("for his demonstration of the heterogenous nature of colloid solutions and for the methods he used, which have since become fundamental in modern colloid chemistry")[17]. However, the true potential of the nanotechnology was recognized only slowly within the following years, which was famously expressed in 1959 by Richard Feynmarn within his well-known lecture „There`s plenty of room at the bottom“[18]. Consequently, the research interest in this topic rapidly increased, particularly due to the interesting and sometimes unexpected physical as well as chemical properties of the nanoparticles, which can differ significantly from the properties of the respective bulk materials. Moreover, their properties are often found to be size dependent, which allows a precise control over these properties once the size of the particles can be controlled. The reason for these deviant and size-dependent properties can be found within the small size of the particles itself, which results in a large amount of surface atoms and thus an increased surface energy compared to the bulk materials[19] as well as the occurrence of size-dependent quantum effects[19]. Typical examples for such size-dependent properties are including melting points, reactivities, or optical properties of metal colloids. Bulk Al melts at a temperature of 660 °C[20], while Al nanoparticles with a size of 11 nm are exhibiting a melting point of 647 °C[21] and Al particles with a size of 2 nm are expected to have an even lower melting point of only 200 °C[22] as was predicted via molecular dynamic simulations. The increased reactivity of nanoparticles compared to their bulk counterparts can for example be observed during the synthesis of Ni aluminides, where Hunt et al.[23] reported an ignition temperature of 286 °C upon applying nanoparticulate reactants compared to 633 °C when micrometer sized reactants were applied. This increase in the reactivity is also well known in aluminothermic reactions, which are then often referred to as nanothermites or metastable interstitial composites, and which is exploited throughout the field of propellants and explosives[24,25]. The colors of colloidal metal nanoparticles can be ascribed to a size dependent quantum effect, the so-called localized surface plasmon resonance. Although Au and Ag nanoparticles are the most common examples for which this effect is known, it can be observed in numerous other metals such as Al, Ni, Cu or Co[26–29]. The exact position of the absorption maximum, and thus the color of the colloidal solution, is not only dependent on the element itself but also on various other parameters, such as size, morphology and dispersion medium[30] and is not necessarily located in the visible range of the spectrum.

1.2 Reactive metal nanoparticles

As described above, noble metal nanoparticles have been known for a long time and nowadays a precise control over size, geometry as well as morphology is readily possible. Details about these procedures shall however not be discussed within this manuscript and can be found in various review

articles[31,32]. In contrast, the wet chemical synthesis of reactive metal nanoparticles is still representing a challenging task. In a chemical reduction approach, their highly negative standard electrode potentials make the application of very strong reducing agents necessary, strongly restricting applicable stabilizers and solvents due to chemical incompatibilities. Moreover, the resulting bare metal nanoparticles tend to react explosively with ambient air, resulting in the often undesired formation of the respective metal oxides. Thus, a synthesis and handling of these particles under inert conditions is often mandatory. Although a passivation applying organic compounds is possible[33], such passivation is always introducing impurity atoms, which might, depending on the desired application, be problematic. Selected examples of synthesis approaches reported in the literature for the preparation of such reactive metal nanoparticles are briefly summarized in the following sections.

A common synthesis method is the chemical reduction approach, in which a metal salt is reduced to the respective metal applying a strong reducing agent. Strong reducing agents that are typically employed for the preparation of reactive metal nanoparticles are naphtalenides, which are capable of reducing many metal halogenides. For example, Mo^0, W^0, Fe^0, Ru^0, Re^0 and Zn^0 nanoparticles with sizes of 1 – 5 nm can be synthesized starting from their chlorides via Na-naphtalenide reduction in DME solutions[34]. A good dispersibility in nonpolar solvents can be realized in an optional second reaction step via oleylamine capping[34]. Similarly, Ti^0 nanoparticles with similar sizes can be obtained from Li-naphtalenide reduction of $TiCl_4$ in THF solution[35]. The synthesis of Mg^0 nanoparticles is possible via Li-naphtalenide reduction of $MgCl_2$ in THF[36] or via K-naphtalenide reduction of $MgCp_2$ in glyme[37] resulting in the formation of particles with sizes of 300 nm and 20 – 40 nm, respectively. In a similar approach, the synthesis of B^0 and Si^0 nanoparticles with sizes < 20 nm, which can be further functionalized by a capping with alcohols, is possible starting from BBr_3 or $SiCl_4$ and Na-naphtalenide[38,39].

Alkali metals can also be applied directly for the reduction of many metal chlorides, whereby it is also possible to carry out the reduction in the presence of naphthalene as an electron carrier. This method was initially reported by Rieke for the preparation of nanocrystalline, bare Mg powders, the so called Rieke-Magnesium, which was obtained from a reduction of $MgCl_2$ or $MgBr_2$ with an alkali metal in an ethereal solution[40]. However, this method can be adapted for various other metals, such as for example Zn, In, Ni, Ca, Sr, and many more[41] and can also be applied for the synthesis of reactive nanoparticles. For example, Ti^0 nanoparticles with sizes of 0.5 – 5 µm can be obtained by reducing $TiCl_4$ in hexadecane solutions applying Na/K alloy[42] as a reducing agent, while the preparation of Mn^0 nanoparticles with a size of about 2 nm is possible by reducing $MnCl_2$ with Li sand in THF solutions[43]. Similarly, the preparation of Mg^0 nanoparticles has been reported to be possible by reducing n-butylmagnesium with Li in the presence of naphthalene, wherein the size was controlled between 20 nm and 100 nm by varying the concentration of naphthalene[44]. The application of Na dissolved in

liquid ammonia has been applied in the literature for the reduction of WCl_6 resulting in the formation of W^0 nanoparticles with a size of 2 nm[45]. The biggest advantage of this method is the facile clean up due to the evaporation of the ammonia solvent upon heating to room temperature.

Moreover, the application of organometallic or hydridic reducing agents has been reported. For example, ^{n}BuLi was applied for the synthesis of Mn^0 nanoparticles with a size of 13 nm in diphenylether at a temperature of 200 °C[46], while lithium triethylborohydride (Superhydride) was employed for the preparation of Ti^0 nanoparticles with a size of 2 nm in THF solutions[47].

An alternative synthesis approach is the thermal decomposition of suitable precursors at increased temperatures. Their decomposition ideally results in the formation of only gaseous or volatile side-products, making fast and facile work-up procedures possible. For example, the synthesis of monodisperse Fe nanoparticles is possible via a thermal decomposition of $Fe(CO)_5$. Peng et al.[48] prepared Fe^0 nanoparticles with a size of 13 nm via injection of $Fe(CO)_5$ into an oleylamine solution at a temperature of 180 °C. A scale-up of this reaction was reported by Yang et al.[49] enabling the synthesis of up to 2 g Fe^0 nanoparticles per batch applying the same method as described above. Moreover, the decomposition of other iron compounds like $Fe(acac)_3$ has also been applied for the preparation of Fe^0 nanoparticles in the literature[50]. In contrast, Ni^0 nanoparticles can be prepared by decomposing $Ni(acac)_2$ in a mixture of oleylamine and oleic acid wherein the size of the resulting particles can be controlled between 23 nm and 114 nm by varying the reaction temperature in the range from 240 °C to 285 °C[51]. Despite the advantages of these methods, suitable precursors are not known for every element, are often requiring time-consuming and complex synthesis procedures or are expensive if commercially available. Accordingly, the applicability of this approach is somewhat limited for many elements.

Al nanoparticles, which are examined within this manuscript, do also fall within the category of these reactive metal nanoparticles and a detailed literature review of possible synthesis approaches, properties and applications is given within the following chapters.

1.3 Al nanoparticles

1.3.1 Synthesis of Al nanoparticles

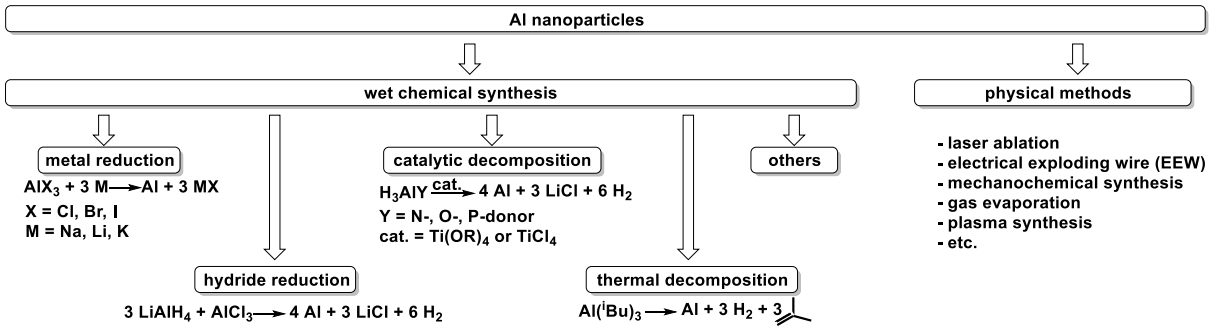

***Figure 2**: Synthesis methods of Al nanoparticles.*

An overview of literature known preparation methods of Al nanoparticles is given in Figure 2, distinguishing physical and (wet) chemical synthesis approaches. In general, the physical methods can be classified as top-down approaches, as bulk Al is employed as a metal source, which is processed in a certain way to yield Al nanoparticles. In contrast, the chemical methods are carried out in suitable solvents using molecular Al precursors, making them bottom-up synthesis approaches. The conversion of the molecular Al source to Al^0 is realized using suitable reactants in homogenous or heterogeneous reaction mixtures in terms of a chemical reduction reaction. Applying these reactions, the addition of surface-active agents is often necessary to limit the crystal growth and to prevent particle agglomeration as well as oxidation. Depending on their compatibility towards other reactants they can be added to the reaction mixture either directly at the start of the reaction or after a certain reaction time. In many syntheses, a single surface-active agent is playing multiple roles at once, such as for example oleylamine, which can be employed as a capping agent, a stabilizer, a reducing agent as well as a solvent all at once[52]. Regarding the synthesis of Al nanoparticles, typically applied compounds are carboxylic acids[53], phosphines[54], various polymers (polyepoxides[55], PVP[56], PMMA[33],…), amines[57], phosphonic acids[58] as well as silica[59].

1.3.1.1 Synthesis via physical methods

The physical methods described within this chapter are the most commonly applied approaches for the preparation of Al nanoparticles with a wide range of sizes. However, since this work focuses on wet chemical synthesis methods, and a detailed discussion of these methods, including the influence of their reaction parameters on the particle sizes and morphologies, would be well beyond the scope of this manuscript, only a brief description of the most common processes shall be given for reasons of completeness.

Laser ablation

During a synthesis via laser ablation, the surface of a bulk sample (target) is subjected to a pulsed laser beam leading to the ablation of (nano)particles from the target surface. Accordingly, the synthesis of Al nanoparticles is possible applying a bulk Al target[60–63], either in solution[61,62], or in a gas atmosphere[63] as well as in the vacuum[60] yielding stable nanoparticle dispersions or dry nanopowders respectively. Solvents used in the literature for the synthesis of Al nanoparticles are for example water[62] or ethanol[61]. The size and morphology of the resulting particles can be controlled via the applied laser parameters and a decrease of the laser pulse length was found to result in a size decrease of the prepared particles[61]. Accordingly, Stratakis et al. reported the formation of Al particles with a size of 20 nm upon applying fs pulses, while particles with a size of 60 nm were formed upon applying ps pulses[61].

Electrical exploding wire

The electrical exploding wire method is a process by which a high-density current is applied to a thin metallic wire ultimately leading to an ablation of small particles from that wire. Similar to the synthesis via laser ablation, the preparation of Al nanoparticles is possible by applying an Al wire either in a gas atmosphere, such as Ar or N_2[64–67], or in solution[68], again resulting in the formation of nanopowders or stable dispersions, respectively. Depending on the applied wire composition, atmosphere, and follow-up treatment the synthesis of various core-shell-particles is readily possible[69], while the particle sizes can be controlled by a variation of the reaction parameters including amongst others the electrical circuit parameters as well as the pressure within the exploding wire chamber[64]. Depending on these parameters, the sizes of the resulting particles are ranging from < 100 nm up to several hundred nanometers[65].

Gas evaporation

The gas evaporation synthesis is a process by which nanoparticulate Al is formed by condensation of gaseous Al inside a chamber containing a noble gas at a low pressure[70–75]. The size and morphology of the resulting particles is dependent on the atmosphere pressure, the temperature as well as the instrument geometry[73] and, by applying this method, the synthesis of particles with sizes ranging from 5 nm[70] up to several hundred nanometers[71] is possible.

High-energy ball milling

Starting from coarse grained Al powder, the synthesis of Al nanopowders is possible applying high energy ball milling techniques[76–78]. The crystallite size of the resulting powders was found to be dependent on the milling parameters such as milling speed and milling time. For example, Mhadhbi et al.[76] observed a reduction of the crystallite size from 70 nm to 20 nm upon increasing the milling time from 2 h to 8 h.

Nowadays, Al nanoparticles synthesized via physical methods are readily commercially available in various sizes[79–82]. They are commonly synthesized via the electrical exploding wire technique and are commercialized as ALEX™. However, due to their simple experimental setups, short reaction times, and facile scale-ups, wet chemical synthesis methods can be promising alternatives. Thus, a detailed literature review of the wet chemical synthesis of Al particles is given in the following chapters.

1.3.1.2 Synthesis via thermal decomposition

The wet chemical synthesis of Al nanoparticles via thermal decomposition is based on the decomposition of suitable Al precursors at increased temperatures without other reactants (Scheme 1). Although only gaseous or volatile side-products are often formed, facilitating a fast and easy work-up procedure, only a few examples can be found in the literature, which will be discussed below.

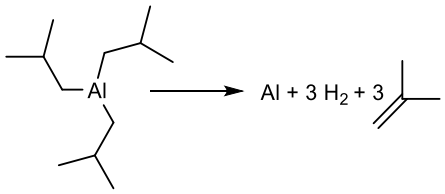

***Scheme 1**: Synthesis of Al nanoparticles via thermal decomposition of Al(^{i}Bu)$_3$.*

Clark et. al[83] applied triisobutylaluminum as an Al precursor, which was thermally decomposed in trioctylamin at a temperature of 250 °C resulting in the formation of particles with various geometries and a broad size distribution. From TEM images, the product mixture was found to contain 10 % trigonal bipyramids, 15 % octahedrons, 15 % nanorods as well as 60 % other non-defined geometries. In contrast, Zhang[84] carried out the decomposition of triisobutylaluminum in boiling diphenylether in the presence of perfluoroundecanoic acid. However, the prepared Al particles exhibited sizes of up to 1 µm and the formation of AlF_3 was problematic, particularly at increased temperatures. In the same work[84], the synthesis of Al nanoparticles with sizes of about 12 nm was accomplished by injecting ^{n}BuLi

to a mixture of $AlCl_3$ and perfluoroundecanoic acid in diphenylether at a temperature of 250 °C. Within this approach, the formation of Al is likely to proceed via a thermal decomposition of intermediately formed $AlBu_3$.

Besides these examples, several reports are known in the literature involving a thermal decomposition of intermediately formed AlH_3, which will however be discussed separately in Chapter 1.3.1.4**.**

1.3.1.3 Synthesis via metal reduction

Within the metal reduction synthesis approach, Al^{3+} is reduced to Al^0 in suitable solvents applying strong alkali metal reducing agents (Scheme 2).

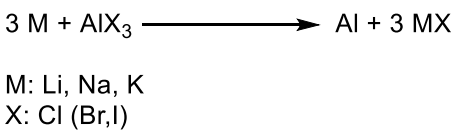

Scheme 2*: Synthesis of Al nanoparticles via metal reduction of aluminum halides.*

In general, they are based on the methods developed by Rieke for the preparation of highly reactive metal powders, which are mainly known for, but not limited to, the formation of highly reactive Mg powders, the so-called Rieke-Mg[40]. Applying these methods, the synthesis of Al is possible by reacting aluminum halides with (molten) alkali metals in THF, xylene or triethylamine solutions[85]. In general, the reaction mixture is heated until the alkali metal is molten and then stirred at room temperature for several hours with the time necessary for a complete conversion being dependent on the employed reactants and solvent. The use of naphthalene as an electron carrier is also possible and has been reported in the literature. Some examples of possible reaction systems as well as the respective reaction times are given in Table 1. A systematic study of the reaction system was carried out by Tzu-Jung[86] and the results were summarized as follows: i) Al^0 powder was obtained upon reducing $AlCl_3$ applying K in xylene, ii) the use of Na/K alloy allows a room temperature reduction in hydrocarbon solvents, iii) the use of Li results in incomplete reactions, even in the presence of naphthalene, and iv) the reduction of homogenous solutions of $AlCl_3$ in THF is possible applying K. In contrast to the observations described above, Pyo et al.[87] successfully employed Li as a reducing agent, which was reacted with $AlCl_3$ in refluxing THF for 2 h. Since the resulting powders were used for further reactions without isolation, no yields and characterizations of the resulting Al^0 powders were given within these reports.

***Table 1**: Selected reaction systems applied in the literature for the synthesis of Rieke aluminum starting from $AlCl_3$.*

Reducing agent	Solvent	Comment	Reaction time	Reference
K	xylene		6-15 h	[86]
Na/K	xylene		3 h	[86]
Li + K	xylene	incomplete reduction	7 d	[86]
K + naphthalene	xylene		3 h	[86]
Li + K + naphthalene	xylene	incomplete reduction	7 d	[86]
Na/K + naphthalene	xylene		4 h	[86]
Li + naphthalene	pyridine	incomplete reduction	3 d	[86]
Li + naphthalene	THF	incomplete reduction	3 d	[86]
K	THF		1-3 h	[85]
K	NEt_3		1-3 h	[85]
K	xylene		1-3 h	[85]
Na	xylene		1-3 h	[85]
Li	THF		reflux, 2 h	[87]

Due to the strong reducing properties of the employed alkali metals, the range of suitable Al precursors is restricted, making particularly the use of precursors containing additional reducible functional groups not possible. Accordingly, no formation of Al^0 was observed upon reacting $Al(acac)_3$ with naphtalenides, since the reduction of the acetyacetonate ligand was preferred over the Al^{3+} reduction[84]. Similarly, no Al^0 was obtained by reacting $AlCl_3$ with Na in liquid ammonia, because an ammonolysis was favored over the Al reduction in this solvent[88].

The disadvantages of this method include amongst others the heterogeneous reaction mixtures, the long reaction times as well as the formation of hard to remove alkali halogenides as side-products, particularly when THF is used as a solvent. The Al^0 synthesized applying this approach is commonly employed in the field of organic chemistry without preceding isolation, for example for the reduction of nitroarenes[87] or within the pinacol-coupling-reaction[86]. In contrast, this method is hardly applied in the literature for the synthesis of Al^0 nanoparticles, which is why no systematic studies regarding the influence of the reaction parameters on the resulting particle sizes and morphologies have been reported up to date.

1.3.1.4 Synthesis via hydride reduction

Within this approach, an Al precursor, commonly $AlCl_3$, is reacted with a strong hydridic reducing agent at increased temperatures, ultimately yielding Al^0 (Scheme 3).

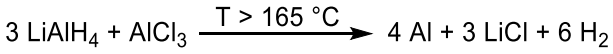

***Scheme 3**: Synthesis of Al nanoparticles via hydride reduction.*

In contrast to the synthesis via the metal reduction approach as described above, the reaction proceeds via a thermal decomposition of intermediately formed AlH_3[89], making the use of hydridic reducing agents necessary. Throughout the literature, $LiAlH_4$ is applied almost exclusively as a reducing agent. On one hand it is representing an additional Al source and its application is thus resulting in increased yields. On the other hand, less impurity atoms will be introduced into the resulting particles compared to the application of, for example, borohydrides.

These syntheses are based on the work of Haber and Buhro, who prepared nanocrystalline Al by reacting $LiAlH_4$ and $AlCl_3$ in refluxing mesitylene[89]. However, since no additional stabilizers were present in the reaction mixture, the Al^0 was obtained as a nanocrystalline, but strongly agglomerated powder, with particle sizes of > 200 nm. The resulting particles exhibited a purity of only 87 % Al and contained 3.0 % C, 4.0 % O and 3.3 % Cl as impurities. In the following years, many other procedures based on this method have been published in the literature, in which a control over particle sizes and agglomeration was achieved by a variation of the reaction conditions and the addition of stabilizers (Table 2).

For example, Cui et al.[54,90] employed the same reaction system as described by Haber and Buhro, $LiAlH_4$ and $AlCl_3$ in refluxing mesitylene, but achieved a control over the particle sizes and agglomeration by the addition of PPh_3. In their studies, particles with a size of about 50 nm formed upon applying a PPh_3:$AlCl_3$ ratio of 20:1, while a ratio of 5:1 resulted in the formation of particles with a size of about 110 nm.

***Table 2**: Selected reaction conditions applied in the literature for the synthesis of Al nanoparticles via hydride reduction. Unless stated otherwise $LiAlH_4$ was applied as a reducing agent.*

Al-Precursor	Solvent	Reaction time [h]	Temperature [°C]	Stabilizer	Particle size [nm]	Reference
$AlCl_3$	mesitylene	16	164	---	90 - >200	[89]
$AlCl_3$	mesitylene	1	164	PPh_3	50 - 130	[54,90]
$AlCl_3$	mesitylene	24	165	PVP	50 - 160	[91]
				PMMA	<300	
$AlCl_3$	mesitylene	2	164	oleic acid	85	[92]
$AlCl_3$	THF	4	25[(1)]	---	10 - 20	[93]
$Al(acac)_3$	mesitylene	72	164	---	50 - 250	[94]
$Al(O^iPr)_3$	toluene	0.25	30[(1)]	oleic acid	5 - 10	[95]
$Al(NO_3)_3$[(2)]	H_2O/ EtOH	2-3	reflux	---	7 - 56	[96]
$SiCl_4$	toluene	2	25[(1)]	PVP	2 - 15	[56]

[(1)]sonochemical reaction [(2)]benzildiethylenetriamine as reducing agent

Oleic acid, a common nanoparticle stabilizer, can also be employed within this reaction system, which was reported by Lee et al.[92]. However, in contrast to PPh_3, it was added only after a reaction time of 2 h, due to its chemical incompatibility particularly towards $LiAlH_4$, ultimately yielding particles with a size of about 85 nm and an oxide layer thickness of 8 nm. The resulting particles contained a high organic content, observed as a mass loss of up to 20 % in TG measurements. Moreover, the use of polymeric stabilizers, such as PVP or PMMA, was reported[91], resulting in the formation of particles with sizes of 50 – 150 nm and < 300 nm, respectively. However, like the particles prepared in the presence of oleic acid, high organic contents of 32 % and 64 % were determined in these particles via TG measurements.

The reaction temperatures can be significantly lowered upon applying sonochemical synthesis approaches as was reported by Mahendiran et al.[93]. In their studies, Al nanoparticles with a size of 10 – 20 nm were sonochemically prepared by reacting $AlCl_3$ and $LiAlH_4$ in THF at room temperature without any other stabilizer being present.

Besides $AlCl_3$, only a few examples are known in the literature applying alternative Al precursors. Ghanta et al.[94] employed $Al(acac)_3$, which was reduced with $LiAlH_4$ in refluxing mesitylene yielding particles with a broad particle size distribution ranging from 50 nm to 250 nm. In addition, compared to $AlCl_3$, a longer reaction time of 72 h was necessary, and the particles contained a carbonaceous residue, whose exact chemical nature could not be identified. Another precursor applied in the

literature is $Al(NO_3)_3$, which was reduced to Al^0 using benzildiethylenetriamine in a refluxing water/ethanol mixture resulting in the formation of particles with a size of about 7 nm[96]. Furthermore, particles with sizes of 5 – 10 nm were sonochemically synthesized by reducing $Al(O^iPr)_3$ applying $LiAlH_4$ in the presence of oleic acid at room temperature in toluene solution[95].

A different approach, with $LiAlH_4$ being the only Al source, was reported by Gottapu et al.[56]. Within their approach $SiCl_4$ was reacted with $LiAlH_4$ in the presence of PVP, resulting in the formation of Al^0 and the gaseous side-products H_2 and $H_x(SiCl)_{4-x}$ as well as insoluble LiCl, which had to be separated in an additional clean-up step. The reaction was carried out at room temperature using an ultrasonic assisted approach and the size of the resulting particles was 2 – 15 nm.

In general, the disadvantages of this hydride reduction approach include long reaction times, high reaction temperatures, heterogeneous reaction mixtures and additional clean-up steps to completely remove the formed LiCl.

1.3.1.5 Synthesis via catalytic decomposition

The synthesis of Al^0 via catalytic decomposition is based on the catalytic decomposition of AlH_3 in solution (Scheme 4).

$$H_3AlY \xrightarrow{\text{cat.}} Al + {}^3/_2\, H_2 + Y$$

Y = N-, O-, P- donor

cat. = $Ti(OR)_4$ or $TiCl_4$

***Scheme 4**: Synthesis of Al nanoparticles via catalytic decomposition.*

To keep the generally polymeric and insoluble AlH_3 in solution, it is typically employed in the form of suitable AlH_3 adducts, which are known to form stable and homogeneous solutions in various solvents. In contrast to the method described above, in which intermediately formed H_3Al is thermally decomposed, the decomposition is carried out in the presence of a catalyst. Thus, no increased reaction temperatures are necessary, although they might of course be useful regarding a decrease of the reaction times. Within this approach, amine alanes such as dimethylethylamine alane or triethylamine alane, are the most widely applied Al precursors, while Ti compounds, particularly $Ti(O^iPr)_4$, are employed almost exclusively as decomposition catalysts. It has to be noted that these alanes could of course be thermally decomposed to Al^0 at temperatures > 165 °C[89], however, such an approach has no significance in the literature. The advantages of this synthesis method include its short reaction times of a few minutes as well as its easy work-up procedures, since only gaseous or volatile side-products are often formed. Accordingly, the catalytic decomposition is the most widely used

method in the literature for the preparation of Al^0 nanoparticles via wet chemical synthesis processes. A summary over selected reaction conditions applied in the literature is given in Table 3.

***Table 3**: Selected reaction conditions applied in the literature for the synthesis of Al nanoparticles via catalytic decomposition of alanes.*

Precursor	Catalyst	Solvent	Temperature	Stabilizer	Size [nm]	Reference
H_3AlNMe_2Et	$Ti(O^iPr)_4$	mesitylene	>100 °C	-	40 - 180	[89]
H_3AlNMe_2Et	$Ti(O^iPr)_4$	THF/1,4-dioxane	40+70 °C	oleic acid	70 - 220	[53]
H_3AlNMe_2Et	$Ti(O^iPr)_4$	toluene	25 °C(1)	oleic acid	n/a	[97]
H_3AlNMe_2Et	$Ti(O^iPr)_4$	dodecane	70 °C(1)	oleic acid	5	[98]
H_3AlNMe_2Et	$Ti(O^iPr)_4$	dodecane	70 °C(1)	oleic acid	5/30(2)	[99]
H_3AlNMe_3 $H_3AlNMePyr$	$Ti(O^iPr)_4$	diethylether	25 °C	$C_8F_{19}COOH$ $C_{10}F_{21}COOH$ $C_{13}F_{27}COOH$	50 - 100(2)	[100]
$H_3AlNMePyr$	$TiCl_4$	diethylether	25 °C	$C_{13}F_{27}COOH$	20 - 200	[101]
H_3AlNMe_2Et $H_3AlN[(C_4H_8)(CH_3)]$	$Ti(O^iPr)_4$	touene/ diethylether	25 °C +110 °C	$C_{13}F_{27}COOH$ $C_{13}F_{27}CH_2OH$ $C_{13}H_{27}COOH$ HDIPA	various(2)	[102]
H_3AlNMe_2Et	$Ti(O^iPr)_4$	toluene	25 °C	1,2-epoxyisobutane 1,2-epoxyhexane 1,2-epoxydodecane	20 - 30	[55]
H_3AlNMe_2Et	$Ti(O^iPr)_4$	toluene	70 °C(1)	1,2-epoxyisobutane 1,2-epoxyhexane 1,2-epoxydodecane	20 - 30	[103]
H_3AlNMe_2Et	$Ti(O^iPr)_4$	toluene/ diethylether	85 °C	1,2-epoxyhexane	30	[104]
H_3AlNMe_2Et	$Ti(O^iPr)_4$	toluene	85 °C	1,2-epoxy-9-decene/ tetradecadiene	20 - 25	[105]
H_3AlNMe_2Et	$Ti(O^iPr)_4$	toluene	85 °C	PMMA	35	[33]
H_3AlNMe_3	$Ti(O^iPr)_4$	toluene	110 °C	TMEDA	100 – 500(2)	[57]
H_3AlNMe_3	$Ti(O^iPr)_4$	toluene	110 °C	TMEDA	100 - 500(2)	[106]
H_3AlNEt_3	$Ti(O^iPr)_4$	heptane	25 °C	Pd, Ag, Ni, Au	150	[107]
$H_3Al(OEt)_2$	$Ti(O^iPr)_4$	diethylether	25 °C	PMAA	50	[108]
H_3AlNMe_2Et	$Ti(O^iPr)_4$; $TiCl_4$; $VO(O^iPr)_3$	1,4-dioxane; THF; NMP; TMEDA	40 °C	---	62 - 157(2)	[109]

(1)sonochemical reaction (2)depending on the applied reaction parameters

Like the hydride reduction approach, this synthesis approach is also based on the work of Haber and Buhro[89]. In their studies, H_3AlNMe_2Et was decomposed in mesitylene solutions applying $Ti(O^iPr)_4$ as a catalyst at temperatures > 100 °C. Since no additional stabilizer was present in the reaction mixture, large particles with sizes > 100 nm were formed. However, compared to the synthesis starting from $AlCl_3$ and $LiAlH_4$, a much higher purity of 99 % Al^0 was observed, with 0.23 % C, 0.25 % O, 0.14 % Cl as well as 0.32 % Ti being present as impurities. In the following years, this method has been applied numerous times for the synthesis of Al nanoparticles and the size as well as the agglomeration of the particles was controlled by the addition of stabilizers and a variation of the reaction conditions.

Stabilizer

Common stabilizers applied for this purpose are carboxylic acids. For example, reaction systems containing H_3AlNMe_2Et, $Ti(O^iPr)_4$ and oleic acid were used by Bunker[97], Lewis[98] and Fernando[99], who carried out the decompositions in non-polar solvents, typically toluene or dodecane. Moreover, they applied an ultrasonic assisted synthesis approach leading to the formation of very small particles with sizes down to 5 nm, with the exact size being controlled in the range from 5 to 30 nm by the amount of oleic acid added to the reaction system[99]. Similarly, Jouet et al.[100,101] and Meziani et al.[102] applied various perfluorated carboxylic acids and alcohols for the passivation of the Al particles, which were synthesized starting from H_3AlNMe_3, $H_3AlNMePyr$ and $H_3Al[(C_4H_8)(CH_3)]$. Meziani et al.[102] found, upon decomposing $H_3Al[(C_4H_8)(CH_3)]$, the perfluorated alcohol $C_{13}F_{27}CH_2OH$ to be a poor stabilizer resulting in the formation of particles with sizes > 200 nm, while particles with sizes < 200 nm were observed upon applying $C_{13}F_{27}COOH$, $C_{13}H_{27}COOH$ or 5-(hexadecyloxy)isophthalic acid (HDIPA)[102]. Moreover, HDIPA was also found to lead to slower decomposition reactions as well as the formation of highly air stable Al particles. Jouet[100] reported $C_8F_{19}COOH$ not to be a suitable stabilizer since the Al particles settled out during the synthesis, which was in contrast not observed upon applying $C_{10}F_{21}COOH$ or $C_{13}F_{27}COOH$.

An alternative class of stabilizers often applied for the preparation of Al nanoparticles are alkylepoxides, which form, after initiation by the bare Al particle surface, a continuous shell of polyepoxide on the particle surface[55,103–105] (Figure 3). By a variation of the alkyl chain length or using copolymerizable epoxides, the stability of the formed Al particles can be controlled, which is particularly important for a possible application in the field of energetic materials. Accordingly, the application of 1,2-epoxyisobutane results in the formation of pyrophoric particles, while more stable, non-pyrophoric particles are formed upon applying 1,2-epoxyhexane[55]. Ultimately, particles stable in ambient air for several months and also being nearly unreactive towards water can be obtained by the

use of copolymerizable 1,2-epoxydodecane and tetradecadiene[105] as stabilizers. As can be seen above, the stability of the Al nanoparticles is increasing with an increasing chain length of the employed epoxide. However, an increasing chain length is also associated with higher organic contents or decreased contents of Al^0 respectively, leading, depending on the Al: polymer ratio, to organic contents of up to 40 – 50 %[103].

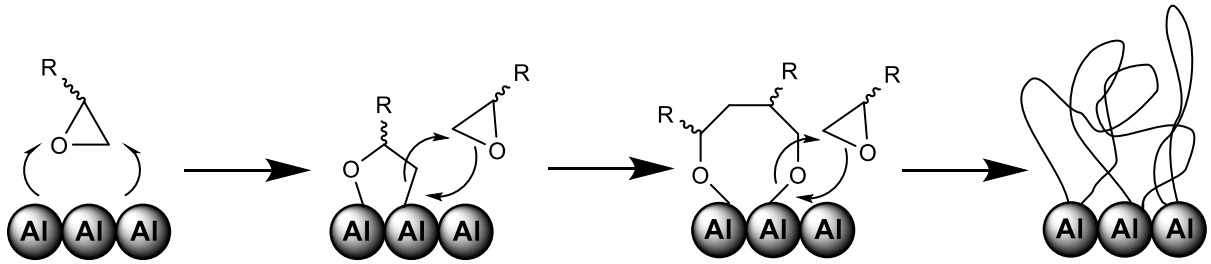

***Figure 3**: Polymerization of alkyl epoxides on Al^0 surfaces; Adapted with permission from Hammerstroem, D. W.; Burgers, M. A.; Chung, S. W.; Guliants, E. A.; Bunker, C. E.; Wentz, K. M.; Hayes, S. E.; Buckner, S. W.; Jelliss, P. A. Aluminum Nanoparticles Capped by Polymerization of Alkyl-Substituted Epoxides: Ratio-Dependent Stability and Particle Size.* Inorg. Chem. ***2011**,* 50*, 5054–5059. Copyright (2011) American Chemical Society*[103].

Another polymeric stabilizer applied within the literature is PMMA[33]. It can be easily removed by an UV-induced decomposition, enabling a controlled release of the Al^0 cores. In further studies polydopamine was employed[110], leading to particles stable in an aqueous environment for at least 15 days. Moreover, Atmane et al.[108] covalently attached functionalized diazonium salts, functioning as photo initiators for the polymerization of methycrylic acid, to the Al^0 particle surfaces, ultimately leading to the formation of PMMA-Al-core-shell-particles (Figure 4).

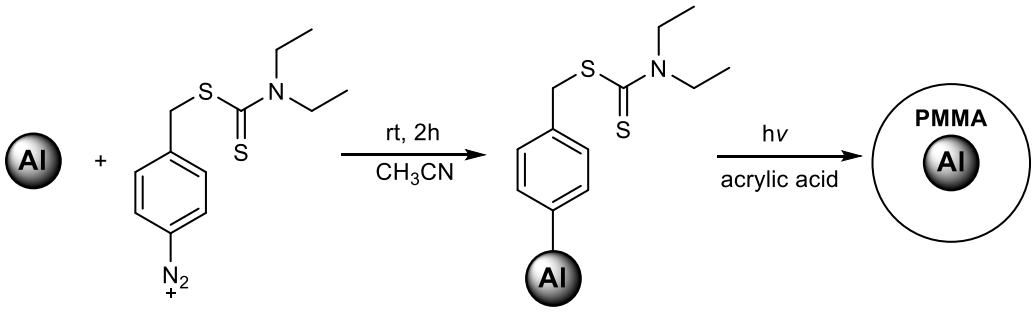

***Figure 4**: Synthesis of PMMA@Al core shell nanoparticles; Adapted with permission from Atmane, Y. A.; Sicard, L.; Lamouri, A.; Pinson, J.; Sicard, M.; Masson, C.; Nowak, S.; Decorse, P.; Piquemal, J. Y.; Galtayries, A.; Mangeney, C. Functionalization of Aluminum Nanoparticles Using a Combination of Aryl Diazonium Salt Chemistry and Iniferter Method.* J. Phys. Chem. C ***2013**,* 117*, 26000–26006.. Copyright (2003) American Chemical Society*[108].

Tertiary amines are representing another class of suitable stabilizers[57,106]. As they are chemically compatible to the typically applied alane precursors, they can be added to the reaction mixture at the start of the reaction. In contrast, the stabilizers described above are typically added only after a reaction time of a few minutes. Johnson et al.[57] decomposed $(H_3Al(NMe_3)_2$ in toluene solutions

applying $Ti(O^iPr)_4$ as a catalyst in the presence of TMEDA at a temperature of 110 °C. The particles sizes were controlled in the range from 100 nm up to 500 nm, by varying the reaction parameters.

Foley et al.[107] prepared transition metal coated Al nanoparticles (Pd, Ag, Au and Ni). The coating was carried out by simply stirring the Al particles in dimethoxyethane solutions containing the dissolved metal acetylacetonates in terms of an electroless deposition reaction. The synthesis of the bare Al particles, was carried out as reported above, by decomposing H_3AlNEt_3 with $Ti(O^iPr)_4$ in heptane without any additional stabilizer being present.

A variety of different stabilizers was employed by Smith[111], who prepared Al nanoparticles via a sonochemical assisted decomposition of H_3AlNMe_2Et in dodecane solutions in the presence of several stabilizers, including oleic acid, 2-hexadecanone, 1-octanol, Span 80, dodecyl aldehyde, 1,2-epoxydodecane, arachidyl dodecanoate, octadecylamine, chloro(dimethyl)octadecylsilane, Ni-stearate as well as hexadecanethiole. Except for hexadecanethiole, Al particles were found to form in every sample with sizes ranging from 20 to 100 nm. Upon applying chloro(dimethyl)octadecylsilane particles with a cubic morphology were obtained, while spherical particles were observed for the other stabilizers. Moreover, upon triplicating the concentrations of oleic acid and octadecylamine the particle sizes were found to decrease from 30 nm to 5 nm and from 20 nm to 10 nm respectively. In contrast, no variation of the particles size was observed upon triplicating the concentrations of 1-octanol and chloro(dimethyl)octadecylsilane.

Additionally, it has to be noted that coordinating solvents, such as TMEDA, can play multiple roles of solvent and stabilizer at the same time. Accordingly, the addition of a stabilizer is not absolutely necessary in these solvents[109], as will be discussed further below.

Precursor

H_3AlNMe_2Et is the most widely applied Al precursor and only a few studies have been conducted applying alternate precursors such as H_3AlNMe_3, H_3AlNEt_3 or H_3AlPyr (Table 3). For example, Jouet et al. reported a slower decomposition to occur when $H_3AlNMePyr$ is applied compared to H_3AlNMe_3, also leading to the formation of more stable dispersions due to the stronger stabilizing properties of pyridine[100]. Similarly, Meziani et al.[102] reported a faster decomposition to occur upon employing H_3AlNMe_2Et compared to $H_3Al[(C_4H_8)(CH_3)]$. Moreover, in the same work, an influence of the precursor on the particle morphology was reported, leading to the formation of particulate structures with a size of about 40 nm upon decomposing H_3AlNMe_2Et in the presence of $C_{13}F_{27}COOH$ as a stabilizer at room temperature, while the use of $H_3Al[(C_4H_8)(CH_3)]$ resulted in the formation of more complex, network-like structures[102].

Atmane et al.[108] applied $H_3Al(OEt)_2$ as a precursor, which was prepared *in situ* by reacting $LiAlH_4$ and $AlCl_3$ in diethylether. The decomposition was achieved by adding $Ti(O^iPr)_4$, resulting in the formation of Al^0 particles with a size of 50 nm without any stabilizer being present. However, the small sizes of these particles are not necessarily due to the applied precursor, as the reaction was conducted in a coordinating solvent, which is also influencing the sizes of the formed particles as will be discussed below.

The concentration of the applied precursor is capable of influencing the size and morphology of the resulting Al particles, as was reported by Lu et al.[112] for the decomposition of 1-methylpyrrolidone alane in THF solutions in the presence of cumyl dithiobenzoate terminated polystyrene. In their studies particles with a size of 224 nm were obtained upon applying a precursor concentration of 50 mM, while particles with a size of 184 nm and a broader size distribution were observed applying a concentration of 15 mM. Moreover, aggregated and coalescenced particles were obtained upon applying an increased concentration of 80 mM.

Solvents

In general, the decomposition can be carried out in non-polar, hydrocarbon solvents or in polar, coordinating solvents, such as ethers or amines. Particularly the coordinating solvents are representing an additional possibility to control the sizes of the resulting Al particles, since they are capable of acting as capping agents. For example, McClain et al.[53] decomposed H_3AlNMe_2Et applying $Ti(O^iPr)_4$ as a catalyst at temperatures of 40 °C and 70 °C in the presence of oleic acid as a stabilizer. They used mixtures of THF and 1,4-dioxane as solvents and the size of the particles was controlled from 55 nm to 220 nm by varying the solvent ratio. Similarly, Clark et al.[109] reported a reduction of the particle size upon applying bidentate instead of monodentate solvents during the decomposition of H_3AlNMe_2Et and reported the formation of particles with sizes of 157 nm in THF, 62 nm in 1,4-dioxane, 101 nm in TMEDA, and 134 nm in NMP. Similar observations were made by Higa et al., who reported the formation of particles with sizes < 100 nm upon decomposing H_3AlNMe_3 in TMEDA solutions at a temperature of 110 °C, while significantly larger particles with sizes ranging from 100 nm up to 500 nm were formed upon conducting the reaction in toluene solutions in the presence of only a small amount of TMEDA[57,106]. However, upon exchanging TMEDA for toluene the decomposition rate was found to be several orders of magnitude higher[57], which was attributed to a stabilization of the alane precursor by TMEDA. Analogous observations were reported by Meziani et al.[102], who observed the formation of particles with a size of 50 – 100 nm upon decomposing $H_3Al[(C_4H_8)(CH_3)]$ in the presence of $C_{13}F_{27}COOH$

in refluxing toluene/ethyl ether mixtures, while particles with a size of < 50 nm were formed upon employing DMA as a solvent at a temperature of 90 °C.

Temperature

The decomposition was carried out in a wide temperature range from room temperature up to 110 °C (Table 3). However, the influence of the decomposition temperature on the size and morphology of the resulting particles has not been widely studied.

According to Higa et al.[106], the influence of the reaction temperature on the size of the particles resulting from the decomposition of H_3AlNMe_3 in the presence of TMEDA can be neglected. In contrast, Lu et al.[112] reported a decrease of the particle size from 320 nm to 224 nm upon increasing the temperature from 40 °C to 50 °C during the decomposition of 1-methylpyrrolidone alane in THF solutions in the presence of cumyl dithiobenzoate terminated polystyrene. Meziani et al.[102] reported a change of the morphology of the resulting products from network-like to particulate with sizes of 50 – 100 nm upon decomposing $H_3Al[(C_4H_8)(CH_3)]$ in the presence of $C_{13}F_{27}COOH$ at room-temperature and 110 °C, respectively.

In addition to the size and morphology, the reaction temperature has a large influence on the time necessary to achieve a complete decomposition. For example, the reaction time decreased from 12 h to 20 min upon increasing the reaction temperature from room-temperature to 110 °C in the system applied by Meziani et al.[102]. Similar observations were made by McClain et al.[53], who reported a decrease of the decomposition time from 2 h to 30 min upon decomposing H_3AlNMe_2Et in THF/1,4-dioxane mixtures in the presence of oleic acid at temperatures of 40 °C and 70 °C respectively, while the reaction took even 12 h to complete at room temperature.

Catalyst

Although $Ti(O^iPr)_4$ has been applied almost exclusively as a decomposition catalyst, the concentration and chemical nature of the catalyst have been reported to play an important role during the decompositions. The concentration of the decomposition catalyst was reported by Johnson et al.[57] to play an important role regarding the Al particle sizes resulting from the decomposition of H_3AlNMe_3 in the presence of TMEDA in toluene solutions. They reported a reduction of the particle size from 500 nm to 100 nm to occur upon increasing the catalyst $Ti(O^iPr)_4$ concentration from 0.02 % to 2.2 %, while the use of $TiCl_4$ instead of $Ti(O^iPr)_4$ led to the formation of larger particles with broader size distributions[57]. Similar results were obtained by Lu et al.[112] upon decomposing 1-methylpyrrolidone

alane in THF solutions in the presence of cumyl dithiobenzoate terminated polystyrene, who observed a decrease of the particle sizes from 250 nm down to 134 nm upon increasing the $Ti(O^iPr)_4$ concentration from 0.2 mM to 0.4 mM. This behavior can be explained by the formation of a larger amount of Al seeds during the early stages of the reaction, thus decreasing the particles sizes. Clark et al.[109] decomposed H_3AlNMe_2Et at a temperature of 40 °C applying various catalysts and found the decomposition to be complete after 30 min for $TiCl_4$, 2 h for $Ti(O^iPr)_4$ and 24 h for $VO(O^iPr)_3$. No differences in the size of the resulting particles was observed, which was at about 60 nm in all samples. Moreover, the chemical nature of the catalyst might influence the morphology of the resulting particles as will be in Chapter 1.3.1.8.

Reaction time

The Al nanoparticle size can be controlled by decreasing the reaction time in terms of a premature quenching of the reaction mixture. This has been employed by Clark et al.[113] for the synthesis of particles with sizes ranging from 53 nm to 160 nm, with the reaction mixture being quenched after a time of 30 min and 2 h, respectively. Moreover, as summarized above, the reaction time is strongly dependent on the reaction temperature and increasing reaction temperatures are leading to decreased reaction times.

As was summarized in the previous sections, a large variety of reaction conditions has been employed in the literature for the synthesis of Al nanoparticles via the catalytic decomposition approach and Al particles with various sizes have already been synthesized (Table 3). However, the reaction systems are often not comparable, for example due to varying reactant concentrations or varying experimental equipment. Moreover, the influence of the reaction parameters on the size and morphology of the formed Al particles has been hardly systematically studied.

Reaction mechanism

Ti compounds have been applied almost exclusively as decomposition catalysts in the literature (Table 3). The catalytic effect of Ti on the decomposition reaction of various alanes has been known for a long time and is already being exploited for the optimization of hydrogen storage systems based on solid alanes such as $LiAlH_4$ or Na_3AlH_6[114]. However, the underlying decomposition mechanism has not yet been fully understood and various models, such as a destabilization of the Al-H bond, an altering of the Fermi energy levels or an increase of the mobility of mobile species, have been postulated in the

literature[115]. A more detailed discussion would be beyond the scope of this work and can for example be found in a review article published by Frankcombe[115].

Similarly, the catalytic effect of Ti on the decomposition of AlH_3 and its adducts in solution as well as its superior activity compared to other transition metals is well-known in the literature[116–118]. Similar as described above, the decomposition mechanism has not been understood until very recently, when it was studied by Clark et al.[109] applying NMR and ESR techniques. According to their results, $Ti(O^iPr)_3$, which is formed from the initial $Ti(O^iPr)_4$-AlH_3-complex via reductive H_2 elimination, is representing the catalytically active species and Al^0 is formed via repeated alane coordinations followed by reductive H_2 eliminations. The mechanism as postulated by Clark et al. is shown in Figure 5.

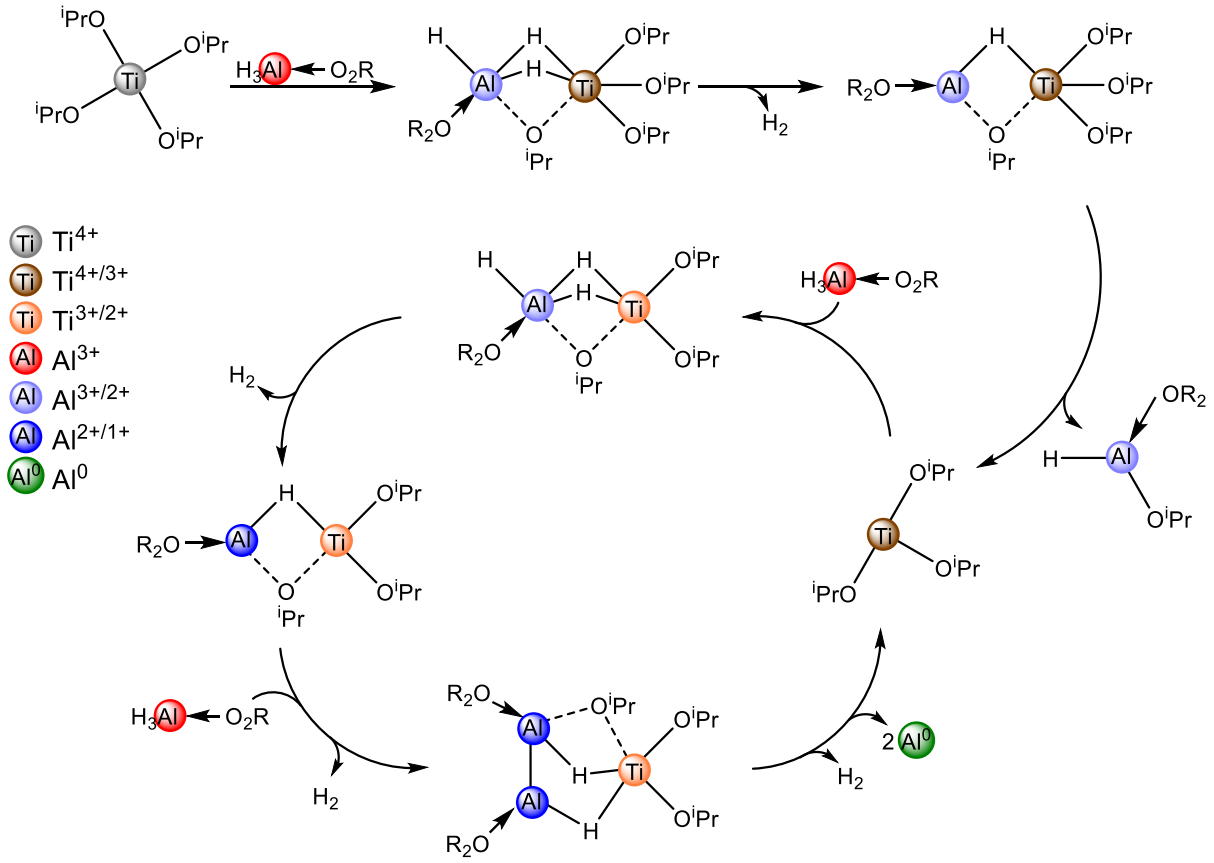

***Figure 5**: Mechanism of the $Ti(O^iPr)_4$ catalyzed decomposition of alane adducts; Adapted with permission from Clark, B. D.; DeSantis, C. J.; Wu, G.; Renard, D.; McClain, M. J.; Bursi, L.; Tsai, A.-L.; Nordlander, P.; Halas, N. J. Ligand-Dependent Colloidal Stability Controls the Growth of Aluminum Nanocrystals.* J. Am. Chem. Soc. ***2019**,* 141*, 1716–1724 Copyright (2019) American Chemical Society*[109].*

1.3.1.6 Additional synthesis methods

Besides the methods described above, a few additional methods have been reported in the literature, not fitting in any of these categories. For example, Tiwari et al.[119] synthesized Al nanoparticles with a size of 20 nm via photochemical reduction of $AlCl_3$ applying $LiNbO_3$ as a photocatalyst in aqueous

solutions. Moreover, Cokoja[120] prepared spherical Al particles with a size of 20 nm via hydrogenolysis of $[(AlCp^*)_4]$ in mesitylene solutions at a temperature of 150 °C applying a hydrogen pressure of 3 bar.

1.3.1.7 Size control

As reported in Chapter 1.1, the properties of metal nanoparticles are dependent on their size. Accordingly, the synthesis of particles with tailored properties is possible once their size can be controlled. For metal nanoparticles, the size of the particles resulting from a certain synthesis is dependent on the ratio of the nucleation rate and the growth rate at the start of the reaction[121–123]. Assuming an identical growth rate, a fast nucleation will result in the formation of small particles, while a slow nucleation will lead to the formation of large particles (Figure 6). Accordingly, the size of these nanoparticles can be controlled by altering the ratio of both rate constants, which can be typically realized by changing various reaction parameters, such as the reaction temperature, the nature and concentration of the stabilizer, the solvent, the reactant concentrations, etc.[121–123].

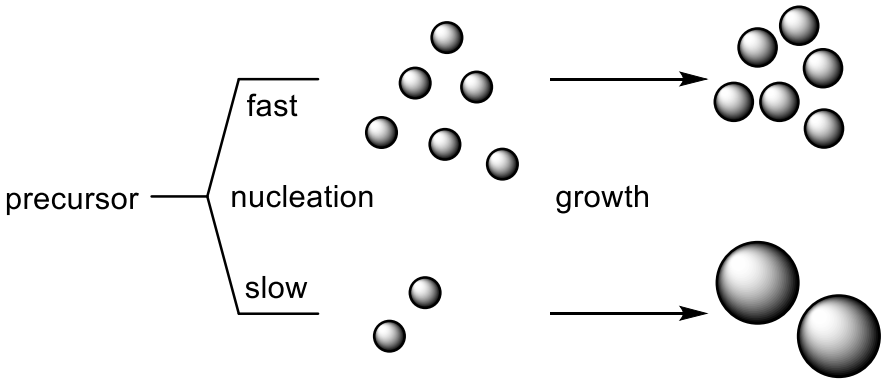

***Figure 6**: Synthesis of metal nanoparticles with various sizes (without considering Ostwald ripening). Adapted with permission from Shevchenko, E. V.; Talapin, D. V.; Schnablegger, H.; Kornowski, A.; Festin, Ö.; Svedlindh, P.; Haase, M.; Weller, H. Study of Nucleation and Growth in the Organometallic Synthesis of Magnetic Alloy Nanocrystals: The Role of Nucleation Rate in Size Control of $CoPt_3$ Nanocrystals.* J. Am. Chem. Soc. ***2003**, 125, 9090–9101. Copyright (2003) American Chemical Society* [121].

For the catalytic reduction method, the effect of the reaction parameters on the size of the resulting particles has already been described in Chapter 1.3.1.5. The size of the resulting particles can be reduced by i) increasing the amount of stabilizer, ii) the chemical nature of the stabilizer, iii) applying coordinating solvents, and iv) increasing the catalyst concentration. In contrast, the observed influence of the reaction temperature on the particle sizes is not consistent throughout the literature[57,106,112]. Similarly, the effect of the applied precursor on the sizes of the resulting particles has not yet been studied in the literature.

1.3.1.8 Control of morphology

The morphology of a given nanoparticle is determined by the growth rates of individual lattice planes. By adding surfactants which are coordinating selectively to particular planes, the growth of this plane can be slowed down or can be completely inhibited, thus influencing the morphology of the resulting particle (Figure 7).

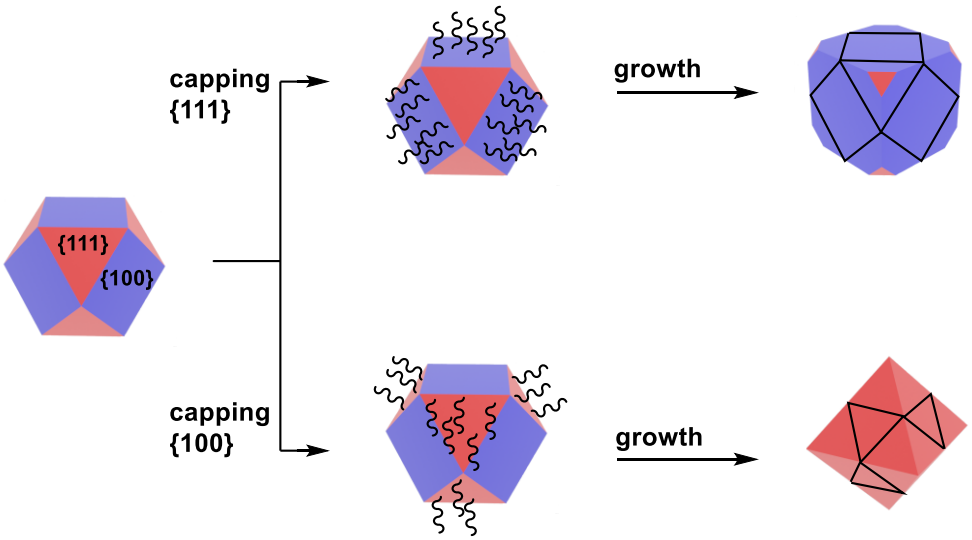

***Figure 7**: Synthesis of nanoparticles with controlled morphologies by applying surfactants*[124].

For the catalytic decomposition approach, the morphology of the resulting Al particles has been hardly studied in more detail and the particles are commonly obtained as quasi spherical or irregularly formed particles or as a mixture of various morphologies. For example, for the synthesis of Al nanoparticles via catalytic decomposition of H_3AlNMe_2Et applying $Ti(O^iPr)_4$ in THF/1,4-dioxane solutions in the presence of oleic acid, mixtures of various morphologies have been reported independently of the solvent composition[53]. A typical composition was determined to consist of 30 % truncated trigonal bipyramids, 30 % octahedrons, 10 % icosahedrons and 30 % irregular formed particles.

Only a few reports are known in the literature, studying the wet chemical synthesis of Al nanoparticles with a controlled morphology. Lu et al.[112] achieved a control over the particle morphology by decomposing 1-methylpyrrolidine alane in THF in the presence of cumyldithiobenzoate terminated polystyrene. This bulky polymer preferably coordinates to the {100} surfaces and via a variation of its concentration, the growth rate along the <100> and <111> directions could be controlled. Thus, upon increasing its concentration from 0.30 mM to 0.70 mM a change in the morphology of the resulting particles according to the following series was observed: cubes/ trigonal bipyramids → cuboctahedrons/ anticuboctahedrons → truncated octahedrons/ truncated triangular platelets → octahedrons/ triangular platelets (Figure 8). Even lower concentrations of the stabilizer were found to not sufficiently stabilize the resulting particles.

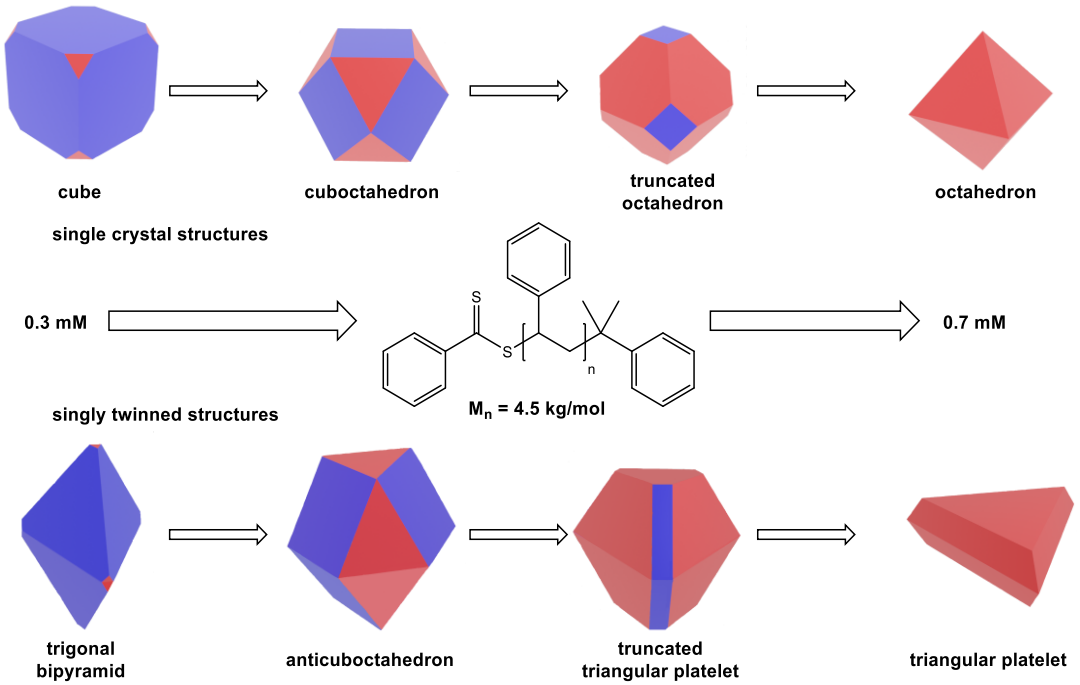

***Figure 8**: Synthesis of Al nanoparticles with a controlled morphology applying cumyldithiobenzoate terminated polystyrene as a surfactant*[112].

The synthesis of Al nanocubes has been reported recently by decomposing H_3Al in THF solutions at a temperature of 65 – 70 °C applying Tebbes reagent ($Cp_2TiClCH_2AlMe_2$) as a decomposition catalyst[113]. Cubes with sizes ranging from 53 nm to 160 nm were obtained by prematurely quenching the reaction mixtures at different times. The reaction mechanism has not yet been fully understood, it is however assumed, that the formation of a C-Al bond between Al and a Cp-ligand, formed via H_2 elimination as a result of a Cp-H-bond activation is playing an essential role[113]. The product mixture consisted of 65 % cubes, 20 % bipyramids, 5 % pentagonal rods and 10 % other geometries.

The synthesis of Al nanorods has been reported to be possible by decomposing TIBAl in trioctylamine at a temperature of 250 °C[83]. The resulting nanorods exhibited a hexagonal cross-section, a growth along the <110> direction as well as a diameter of 272 nm and a length of 992 nm. The product mixture consisted of 15 % rods, 5 % trigonal bipyramids, 20 % octahedrons and 60 % other geometries.

1.3.2 Oxidation of Al nanoparticles

Bare Al nanoparticles are a pyrophoric solid and are passivated by the formation of a thin oxide layer almost immediately upon air contact. This oxide layer formation can not only be observed following air contact, but also in the presence of organically bound oxygen, such as in oleic acid[99] or epoxides[103]. The oxide layer thickness can for example be experimentally determined via HRTEM analysis and is varying from 0.2 nm to 6.9 nm depending on the applied synthesis method and conditions. Selected

oxide layer thicknesses reported in the literature are summarized in Table 4. As described in Chapter 1.3.1.5, the Al oxidation can be slowed down or inhibited with the help of various stabilizers.

***Table 4**: Oxide layer thicknesses of Al nanoparticles reported in the literature.*

Oxide layer thickness [nm]	Particle size [nm]	Synthesis method	Stabilizer	Reference
2 - 4	50	cat. decomposition	---	[108]
2 - 4	110	cat. decomposition	---	[125]
2 - 4	160	cat. decomposition	---	[113]
3	100	cat. decomposition	---	[126]
2 - 4	70 - 220	cat. decomposition	oleic acid	[53]
0.2 - 1.7	140 - 290	EEW (Ar + 10 % H_2)	---	[69]
1.5 - 2.1	120 - 160	EEW (Ar)	---	[69]
4.9 - 6 .9	210 - 330	EEW (Ar + 10 % N_2)	---	[69]
4	30	gas condensation	---	[127]
6	25	gas condensation	---	[128]
3	nanorods; d: 275 nm	thermal decomposition	trioctylamine	[83]

Due to the oxide layer growth being controlled by the diffusion of Al and O species, which is dependent on the particle size, apart from a time dependence, a dependence of the oxide layer thickness from the particle size can be expected[129]. Accordingly, thinner oxide layers can be expected to form on larger particles and, assuming that the smallest particles (< 10 nm) are fully oxidized, following oxide thickness-particle diameter correlation can be calculated (Figure 9):

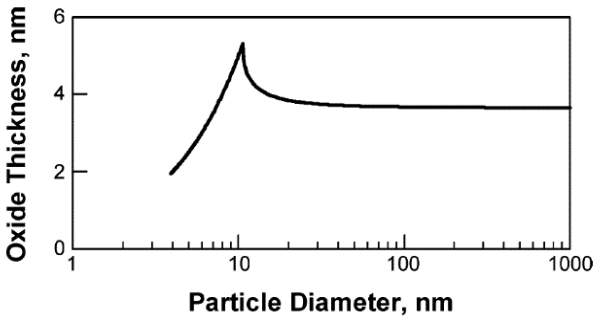

***Figure 9**: Calculated oxide layer thickness of Al particles as a function of the particle diameter. Reprinted with permission from Trunov, M. A.; Umbrajkar, S. M.; Schoenitz, M.; Mang, J. T.; Dreizin, E. L. Oxidation and Melting of Aluminum Nanopowders.* J. Phys. Chem. B ***2006**,* 110*, 13094–13099. Copyright (2006) American Chemical Society*[129].

Because of this oxidation, the active Al^0 content is generally decreasing with decreasing particle sizes. Accordingly, nanoparticles are exhibiting high oxide contents, while they can be neglected for bulk Al or micrometer-sized Al particles. Consequently, the application of oxide passivated Al nanoparticles, for example for the preparation of intermetallic compounds, will result in the introduction of impurity phases within the final product, with the content of this phase being dependent from the size of the applied nanoparticles. Of course, the formation of these phases might also have an influence on the physical and chemical properties of the resulting products. Since Al_2O_3 is capable of acting as a heat sink, the application of oxide passivated Al nanoparticles can moreover alter the thermodynamic properties of certain reactions, such as for example SHS reactions[23]. This will be summarized in more detail in Chapter 1.4.2.3.

Upon exposing Al nanoparticles to increased temperatures in oxygen containing atmospheres, further oxidation will occur, leading to characteristic TGA traces exhibiting multiple stepwise mass increases. These traces can be divided into 4 different stages[130,131] and a typical example is shown in Figure 10.

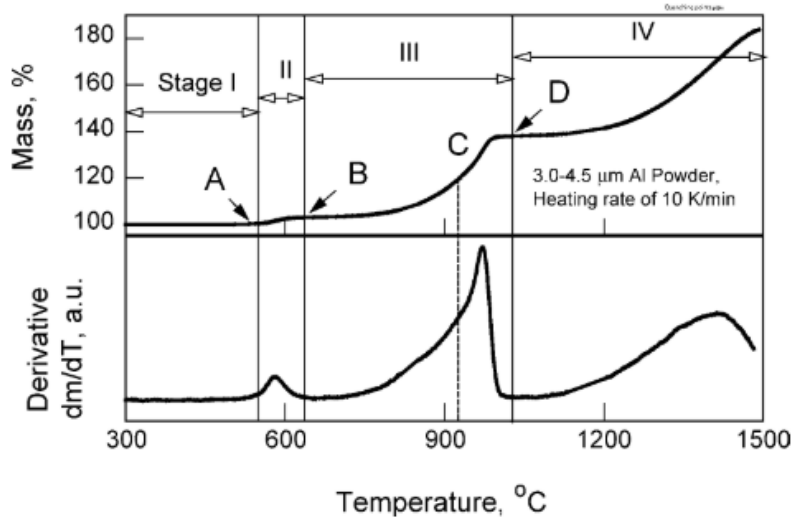

***Figure 10**: TGA trace of Al particles in an oxidizing atmosphere as well as its segmentation into 4 stages based on the underlying processes. Reprinted from Combustion and Flame, 140, Trunov M.A.; Schoenitz M.; Zhu X.; Dreizin E.L., Effect of polymorphic phase transformations in Al_2O_3 film on oxidation kinetics of aluminum powders, 310-318, Copyright (2005), with permission from Elsevier*[131].

In the first stage, a slow mass increase can be observed, with the Al^{3+} diffusion through the existing amorphous oxide layer being the rate determining step[131,132]. Upon reaching a critical thickness (about 2 – 4 nm[131,133]), the amorphous alumina will transform to denser γ-Al_2O_3 (Table 5), resulting in an exposition of fresh, bare Al^0 to the atmosphere. This freshly exposed Al^0 will oxidize very fast until a complete covering of the surface is evident again, ultimately resulting in the step wise mass increase followed by the formation of a plateu visible in stage 2[130,131]. Within stage 3 the oxidation rate is initally increasing upon increasing the temperature until again reaching a plateau. At this temperatures, the

O^{2-} diffusion is representing the rate determing step[131,132]. As the diffusion rate is increasing with increasing temperatures, a steepening mass increase can be observed in the beginning of stage 3. At the end of stage 3, γ-Al_2O_3 transforms to even denser α-Al_2O_3 resulting in a decrease of the diffusion rates and the formation of a plateu[130,131]. Upon further increasing the temperatures in stage 4, the diffusion rates are increasing again, thus leading to the observed increasing oxidation rates. The TGA trace shown in Figure 10 can be typically observed for micro-meter sized particles, while for nanoparticles particulary the sections 3 and 4 are not necessarily present, due to their complete oxidation before reaching these stages (Figure 18b).

***Table 5**: Densities of selected alumina polymorphs.*

Al_2O_3-polymorph	**Density [g/cm^3]**	**Reference**
amorphous	2.66 - 3.30	134,135
γ	3.2	136
δ	3.2	136
θ	3.56	136
α	3.99	20

However, the TG measurements are strongly dependent on the experimental setup, which was demonstrated by Labourer et al.[137], particularly resulting in a missing comparability of TG analyses published throughout the literature. For example, as reported within their work[137], Chen et al.[138] observed a shift of the oxidation onset temperature from 493 °C to 564 °C upon increasing the heating rate from 5 K/min to 90 K/min. Similarly, an increase of the sample mass was reported to lead to lower onset temperatures as well as peak temperatures[137], while an increase of the atmosphere oxygen content led to a decrease of the onset temperatures[137].

1.3.3 Applications

Due to their highly exothermic reactions with many materials, such as for example O_2, H_2O, metals, or metal oxides, many of the applications of Al nanoparticles can be found within the field of (nano)energetic materials. Besides, they are employed in optical as well as medical applications.

Optical and medical applications

The plasmon resonance of Al nanostructures can be tuned over a wide wavelength range and is dependent on various parameters such as their size, their oxide content as well as their substrate[139]. For example, Knight et al.[139] prepared Al nanodisks, whose scattering intensities were tuned from 250 nm to 650 nm by varying their size from 70 nm to 180 nm. Due to these plasmonic properties, combined with the low costs and high abundance, Al nanoparticles are a promising possibility to increase the efficiency of solar cells currently being discussed in the literature[54,140–142]. In addition, Al nanorods have been employed for the preparation of pixels and might be applied within color displays[143,144]. Moreover, these optical properties can be exploited for medical applications, such as the detection of biomolecules[145]. This detection is based on the enhancement of the fluorescence of a fluorophore in the presence of a metal substrate (the so-called metal-enhanced fluorescence (MEF)) and Al nanoparticles have been shown to be a suitable metal substrate[145].

Propellants and Explosives

Due to their violent reaction with water, Al nanoparticles can be applied for the production of hydrogen[146] or as a solid rocket propellant (so-called ALICE)[147,148] (Scheme 5):

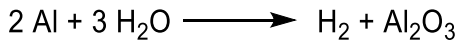

***Scheme 5**: Reaction of Al with water.*

The propellant was prepared by dispersing Al nanoparticles with a size of about 80 nm and an Al^0 content of about 75 % in water and then freezing the resulting mixture at a temperature of – 30 °C. It can be ignited applying small amounts of conventional explosives and its advantages include its environmental friendliness, its cheap and readily available raw materials as well as its proper functionality under water[147,148].

Similarly, Al nano or mesoparticles can be added as an additional component to conventional propellants such as for example ammonium perchlorate[149–151]. In these mixtures, Al particles inhibit an

undesired decomposition of the conventional propellant at low temperatures, while the decomposition at high temperatures is catalyzed[149], ultimately resulting in increased rates of combustion[150]. Al nanoparticles were also found to improve the ignition characteristics of conventional diesel fuel, leading to increased ignition probabilities on a hot plate[152].

The addition of Al nanoparticles to conventional explosives such as cyclotrimethylenetrinitramine (RDX)[153,154], trinitrotoluene[155,156], or 2,4,6,8,10,12-hexanitro-2,4,6,8,10,12-hexaazaisowurtzitane (CL20)[157] has also been studied in the literature. Similar as reported above for conventional propellants, the Al nanoparticles catalyze the decomposition of these explosives[153] and their ignition sensitivity might be increased[157]. Moreover, the application of Al nanoparticles within other energetic materials, such as nitrocellulose or Teflon[158], has been reported to lead to complete and fast reactions due to short diffusion path lengths.

Aluminothermic reactions

Another possible application lies within the field of aluminothermic reactions, in which Al is reacted with a suitable metal oxide (Scheme 6):

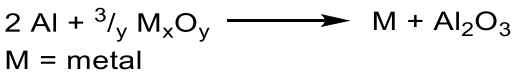

***Scheme 6**: General aluminothermic reaction.*

These reactions are generally characterized by highly negative heats of reaction. By far the most well-known example is the thermite reaction, the reaction of Al and Fe_2O_3, which is amongst others applied for the welding of rails[159]. However, Al is known to react with many other metal oxides in a similar matter (Table 6). The reaction products are often formed in their liquid state since the reaction temperature often exceeds their melting point. Accordingly, a separation of the formed metal from the lighter alumina side product (the so-called slag), which floats on the liquid metal, is readily possible.

***Table 6**: Selected examples of aluminothermic reactions including their enthalpies of reaction and adiabatic temperatures as well as the melting points of the metal reaction products.*

Aluminothermic reaction	T_{ad} (°C)[160]	T_{mp} (°C)[160]	- ΔH (J/g)[161]
$Al + {}^3/_4\ MnO_2 \rightarrow {}^3/_4\ Mn + {}^1/_2\ Al_2O_3$	3905	1244	4859
$Al + {}^1/_2\ MoO_3 \rightarrow {}^1/_2\ Mo + {}^1/_2\ Al_2O_3$	4008	2617	4702
$Al + {}^3/_{10}\ V_2O_5 \rightarrow {}^3/_5\ V + {}^1/_2\ Al_2O_3$	3512	1902	4569
$Al + {}^3/_8\ Co_3O_4 \rightarrow {}^9/_8\ Co + {}^1/_2\ Al_2O_3$	3908	1222	4234
$Al + {}^1/_2\ Fe_2O_3 \rightarrow Fe + {}^1/_2\ Al_2O_3$	3349	1536	3955
$Al + {}^3/_2\ NiO \rightarrow {}^3/_2\ Ni + {}^1/_2\ Al_2O_3$	3251	1453	3440
$Al + {}^3/_4\ PbO_2 \rightarrow {}^3/_4\ Pb + {}^1/_2\ Al_2O_3$	> 3727	327	3062
$Al + {}^1/_2\ WO_3 \rightarrow {}^1/_2\ W + {}^1/_2\ Al_2O_3$	4007	3407	2914
$Al + {}^1/_2\ Cr_2O_3 \rightarrow Cr + {}^1/_2\ Al_2O_3$	2108	1857	2602
$Al + {}^3/_4\ TiO_2 \rightarrow {}^3/_4\ Ti + {}^1/_2\ Al_2O_3$	1526	1670	1527

T_{ad}: adiabatic temperature; T_{mp}: melting point of the metal reaction product

In contrast to conventional thermites, nanothermites or metastable interstitial composites are prepared from nanoscaled oxidizers and reducing agents. These nanothermites are exhibiting significantly increased reactivities as well as ignition sensitivities[162]. For example Weir et al.[163] studied the ignition of Al-MoO_3 thermites via electrical discharge and found the nanothermites to be significantly more sensitive to ignition than their micrometer sized counterparts (Table 7). The reactivity of the Al-MoO_3 system was examined by Sun et al.[164] and they found the maximum reaction rate of a conventional thermite to be 0.6 W/g_{Al}, while it increased to 2-5.5 W/g_{al} upon employing nanoscaled Al.

***Table 7**: Electrical discharge ignition characteristics of Al-MoO_3 thermites. The MoO_3 particle size was 44 nm in all samples[163].*

Al size (nm)	Ignition voltage (V)	Minimum ignition energy (mJ)
20000	> 10.000	---(1)
4000	> 10.000	---(1)
2000	2000	4.0
100	1000	1.0
50	500	0.3

(1) no ignition was observed

Aluminides

Al nanoparticles can be applied for the synthesis of various intermetallic compounds. Strictly speaking, the term “aluminide” refers to compounds consisting of Al and at least one additional, more electropositive element. However, due to historical reasons and the quantification of the electronegativity being nontrivial, within this work, every intermetallic Al containing compound will be referred to as aluminide. Al is known to form such intermetallic compounds with many metals and Figure 11 summarizes the elements, from which at least one binary aluminide is known according to the FactSage Phase Diagram Database[165]. Their synthesis is commonly possible starting from the elements and is, similar to the aluminothermic reactions, often characterized by a highly negative heat of reaction (Table 8).

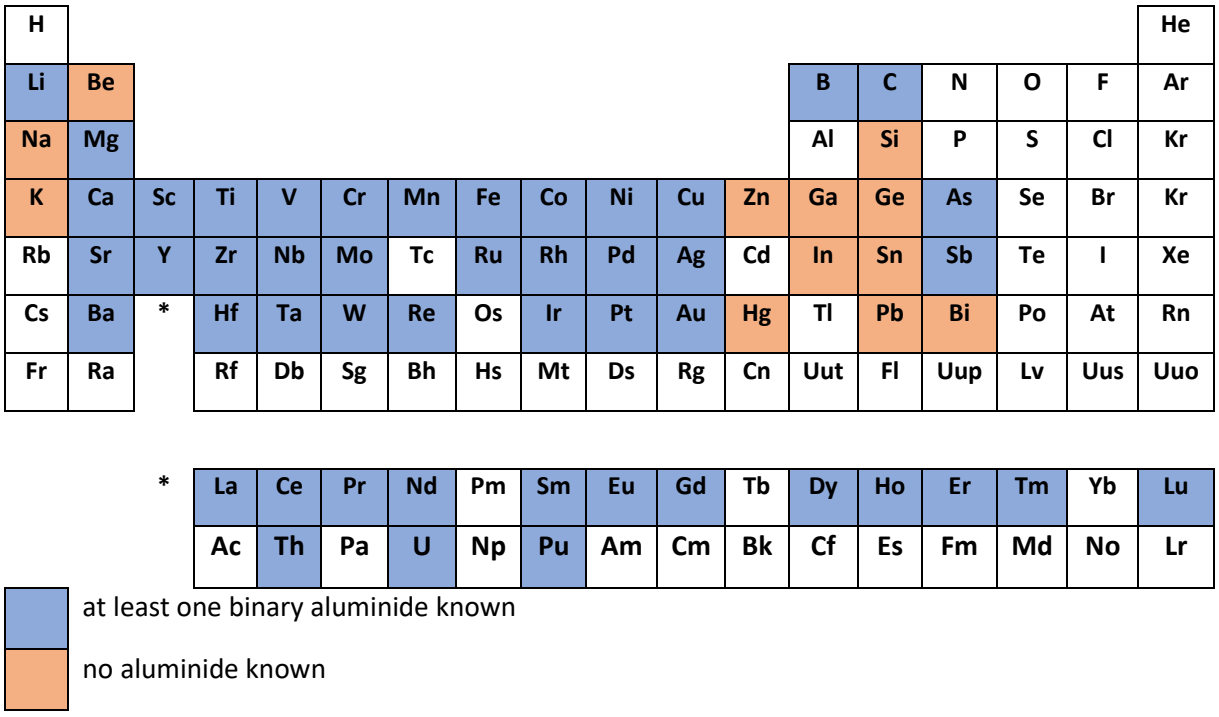

***Figure 11**: Overview of known binary aluminides[165].*

***Table 8**: Selected examples of binary aluminides including their enthalpies of formation, the adiabatic temperatures of their formation and the states of the formed products (all values are from reference[161] unless stated otherwise).*

Aluminide	T_{ad} [°C]	State of product	$-\Delta H_f \left[\frac{kJ}{mol\ atoms}\right]$
AlPt	3106	s	100
AlPd	2380	l	92
Al_2B	1465	l	73
AlRu	1977[166]	s	62[167]
AlNi	> 1251	s-l	59
AlB_2	> 979	l-g	50
AlCo	> 1639	s-l	38
AlFe	1162	s	37
AlTi	1324	s	37
AlMn	530	s	21
AlCu	662	s	20
$AlAg_2$			1-5[168]

T_{ad}: adiabatic temperature; s: solid; l: liquid; g: gaseous

As stated above, their synthesis is possible starting from the elements via various techniques such as melt metallurgy, reactive infiltration[169] or reactions in solid samples[170,171]. These reactions in the solid samples can be divided into sintering approaches and combustion syntheses depending on the reaction parameters applied within these methods (Figure 12)[172,173]. While the inherent self-heating of the sample due to the strongly exothermic reaction is exploited within the combustion syntheses, it should be avoided during a synthesis via a reactive sintering approach[173]. Depending on the reaction initiation, the combustion syntheses can be further divided into SHS reactions and thermal explosion methods. In a SHS reaction, the reaction mixture is initiated via a local energy input and the reaction front subsequently propagates self-sustainingly throughout the entire sample. Besides applying a local heat source, an initiation is possible applying laser pulses[174], microwave radiation[175], electric energy (such as a spark[166]) or mechanical energy[176]. In contrast, in a thermal explosion, the reaction mixture is initiated by heating the whole sample at once and no local spot of initiation can be defined.

Within the sintering approaches, the reaction is also commonly initiated by heating the whole sample at once, but, as stated above, the self-heating of the sample is avoided[173]. Depending on the exact experimental set-up, these methods can be further divided into reactive sintering, reactive annealing, reactive hot isostatic pressing, and reactive hot pressing[172]. In a reactive sintering approach, the reaction is initiated by heating the whole sample at once and a porous sample is employed. Upon

employing a non-porous sample, the approach is referred to as reactive annealing. If the sample is compacted during the reaction applying a hydrostatic pressure, the approach is known as reactive hot isostatic pressing, while an uniaxial pressure is applied within the reactive hot pressing approach (Figure 12).

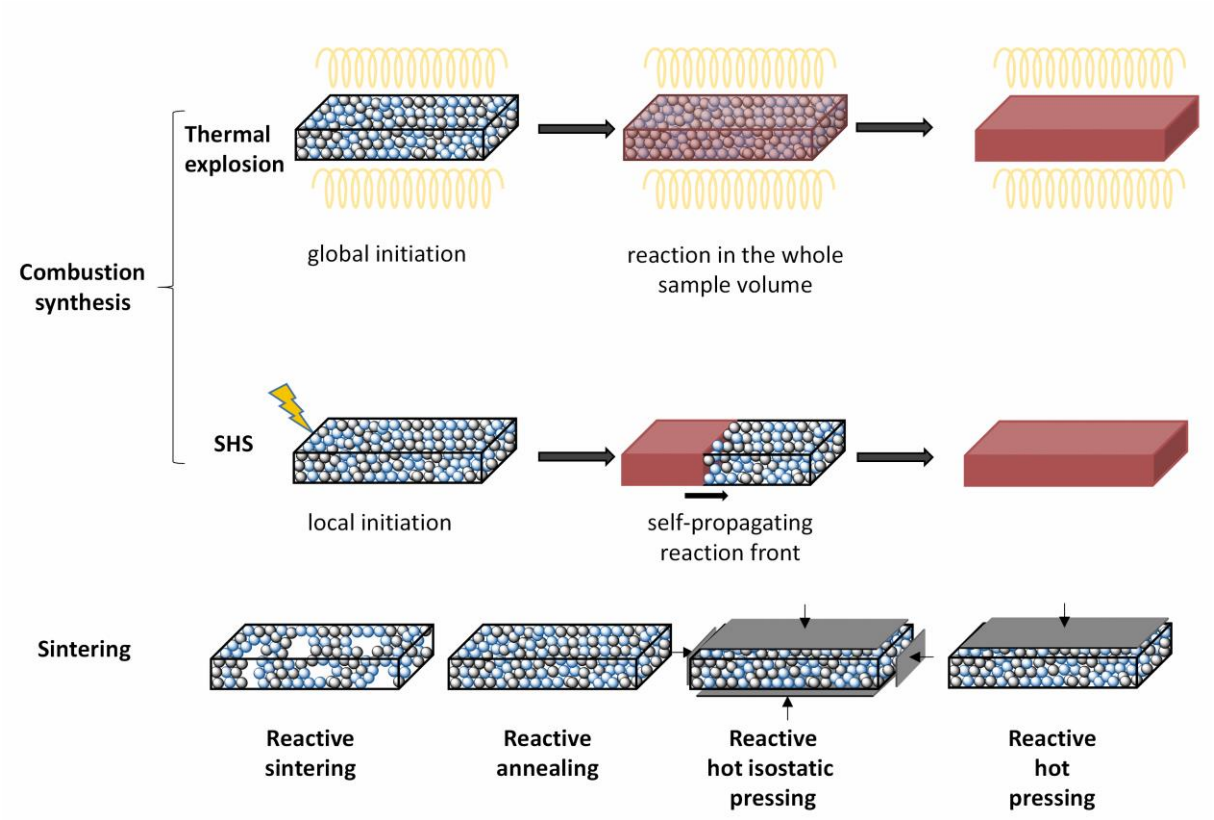

***Figure 12**: Synthesis of aluminides via combustion and sintering approaches*[172,173].

Within all these approaches, the educts can be employed in the form of powder mixtures, multilayers, for example prepared applying CVD techniques, as well as other morphologies such as core-shell particles[177]. Particularly the preparation of multilayers is characterized by a high experimental effort, however also resulting in an excellent interfacial contact between the elements and a minimum formation of passivation layers. Powder mixtures can be employed in the form of loose powders as well as compacted pellets. The mixing of these elemental powders can be carried out applying various techniques ranging from simple physical mixing in an agate mortar, an ultrasonic bath or a turbulate mixer to a treatment in a planetary ball mill. While an efficient mixing is expected to occur upon applying a planetary ball mill, it might also result in an activation of the powders[178] or in the undesired, premature formation of intermetallic phases[179].

Moreover, the synthesis has been reported to be possible via wet chemical or mechanochemical approaches[179–181]. A more detailed discussion of the preparation methods reported in the literature

for NiAl and RuAl, which were primarily studied within this work, will be given in the following chapters.

1.4 Aluminides

This work mainly focused on preparation of Ru and Ni aluminides starting from wet chemically prepared nano and submicron particles. Thus, the Ru-Al and Ni-Al systems as well as their properties, applications and preparation methods will be described in more detail within the following chapters.

1.4.1 Ru aluminides

1.4.1.1 Ru-Al system

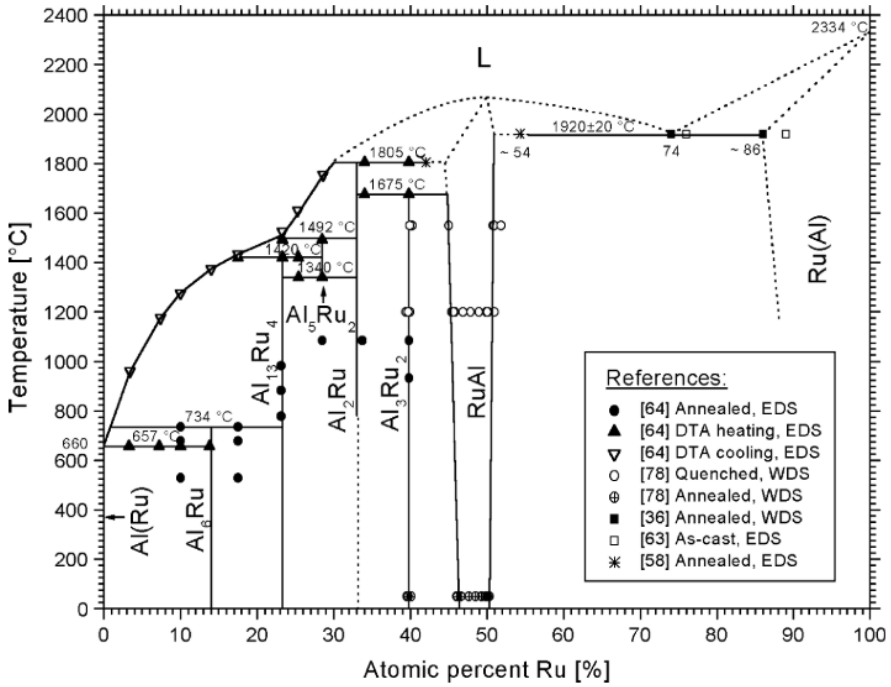

***Figure 13**: Binary Ru-Al equilibrium phase diagram. The legend within the figure stems from the original source. Reprinted from Intermetallics, 13, Mücklich F.; Ilić, N., RuAl and its alloys. Part I. Structure, physical properties, microstructure and processing, 5-21, Copyright (2005), with permission from Elsevier[182].*

Figure 13 shows the binary Ru-Al phase diagram. As can be seen, 6 intermetallic compounds are known to be existent, including the room temperature stable phases Al_6Ru, $Al_{13}Ru_4$, Al_2Ru, Al_3Ru_2 and AlRu[183–186], as well as the high temperature phase Al_5Ru_2[186]. From these compounds, Al_6Ru is exhibiting the lowest melting point and melts incongruently at a temperature of 734 °C[186]. In contrast, Al_6Ru, $Al_{13}Ru_4$, Al_5Ru_2, and Al_2Ru all have significantly higher melting points and are melting incongruently at

temperatures of 734 °C, 1420 °C, 1492 °C and 1805 °C[186]. Al_5Ru_2 is known to be existent only in the small temperature range from 1340 °C up to its melting point of 1492 °C and below 1340 °C it decomposes to Al_2Ru and RuAl[186]. RuAl is the only congruently melting compound and is exhibiting the highest melting point of these compounds at a temperature of about 2050 °C[187].

The compounds Al_6Ru, $Al_{13}Ru_4$, Al_5Ru_2, Al_2Ru und Al_3Ru_2 are line phases and thus all exhibiting very small stability ranges. In contrast, RuAl is exhibiting a broader stability range, particularly on the Al rich side, ranging from 53.4 – 49.9 at% Al at room temperature and from 54.2 – 50.0 at% Al at 1200 °C[188]. While the solubility of Ru in Al can be neglected, a solid solution of Al in Ru can contain up to 14 at% Al[189].

Due to their differing crystal structures, which are summarized in Table 9, the identification of these compounds within a reaction mixture is possible applying X-ray diffraction techniques. For example, RuAl crystallizes in the space group $Pm\bar{3}m$, thus exhibiting a B2 structure, with the lattice parameter being dependent on the exact composition and being linearly decreasing from 0.29932 nm at 54.2 at% Al to 0.29892 nm at 49.9 at% Al[188].

***Table 9**: Crystallographic data and enthalpies of formation of Ru aluminides.*

Aluminide	Space group	a(nm)	b(nm)	c(nm)	β (°)	$-\Delta H_f$[(1)] $\left[\frac{kJ}{mol\ atoms}\right]$	$-\Delta H_f$[(1)] $\left[\frac{J}{g}\right]$
Al	$Fm\bar{3}m$	4.05[190]					
Al_6Ru	*Cmcm*	7.49[191]	6.55	8.96		31	819
$Al_{13}Ru_4$	*C2/m*	15.82[192]	8.19	12.74	107.77	50	1135
Al_5Ru_2	*Cmcm*	0.78[186]	0.66	0.42		45	928
Al_2Ru	*Fddd*	8.01[193]	4.72	8.78		66	1283
Al_3Ru_2	*I4/mmm*	3.08[193]	3.08	14.33		64	1173
AlRu	$Pm\bar{3}m$	3.03[183]				62	975
Ru	$P6_3/mmc$	2.72[194]					

(1)theoretical values from[167]

1.4.1.2 Properties and applications

Due to its broad stability range compared with its high-temperature properties, RuAl is by far the most promising Ru aluminide regarding possible applications, which is why the following discussion will be limited to RuAl. In the following chapter, a few of its properties will be summarized, while a detailed overview on its properties and applications can be found in various review articles[182,195].

RuAl is exhibiting a high resistance towards oxidation, particularly at increased temperatures. Single-phase RuAl was altered only up to a depth of 5 µm upon heat-treating a sample at a temperature of 1000 °C for 300 h[196] and a layer of α-Al_2O_3 was observed to form on the sample surface, with the subjacent layer being Ru rich due to Al depletion. In contrast, near stoichiometric RuAl was found to be more prone towards oxidation and an oxide layer with a thickness of 25 µm was observed to form after a heat treatment at a temperature of 1000 °C for 200 h[197]. This observation was explained by the oxidation of excess Ru, leading to the formation of volatile RuO_3 or RuO_4 species, which lead to the formation of a more porous α-Al_2O_3 layer upon evaporation. This porous α-Al_2O_3 layer cannot protect the sample from oxidation as efficient as a non-porous layer, thus leading to the observed increased oxidation sensitivity.

Moreover, RuAl is exhibiting an excellent corrosion resistance in acid as well as alkaline conditions. In conc. HNO_3, aqua regia, 80 % H_2SO_4, 48 % HF and 50 % NaOH, the rates of corrosions were < 0.1 mm/a even at temperatures > 100 °C. Similar rates of corrosion were observed in aqueous solutions of $FeCl_3$ and NaCl. Only a solution of NaOCl (15 %) was found to result in a severe corrosion leading to corrosion rates > 3000 mm/a[198].

Its most important mechanical properties are including its ductility under compression[199,200], with Ru rich RuAl exhibiting a higher ductility compared to Al rich RuAl, as well as its high hardness[199] even at increased temperatures of up to 1100 °C[201].

Additionally, its physical, chemical and mechanical properties can be specifically altered by alloying with ternary elements such as for example C[198], Co[202,203], Fe[202,203], Ti[202,203] or Mo[204]. This might be particularly important regarding the synthesis of aluminides starting from wet-chemically synthesized particles, which might contain C, H, N, P and O containing impurities originating from the applied reagents, solvents, or stabilizers. For example small amounts of C have been reported to reduce the hardness of RuAl[198], while alloying with B increases its ductility and strength[199].

Although possible applications of RuAl are limited by its high costs, it is nonetheless a promising material for high temperature applications also requiring materials with high strengths, such as engines[205,206], cutting tools[207], exhaust manifolds[208] as well as bond coats and thermal barriers[209,210] or metallizations[211].

1.4.1.3 Preparation methods

The synthesis of RuAl is commonly starting from the elements, for example applying melt metallurgy techniques such as vacuum arc melting[197]. In this process, both elements are melted in vacuo, mixed and the product is formed after a homogenization at temperatures > 1000 °C. However, typically no

single-phase products are obtained applying this technique, since intergranular Ru rich phases were found to form[197].

Moreover, the preparation is possible applying mechanochemical synthesis approaches, in which Ru and Al powders are reacted within a planetary ball mill[179,212]. The crystallite size of the resulting single phase RuAl can be controlled by adjusting the milling time, with smaller crystallites being formed at increased milling times[179]. However, increased milling times might also lead to an increased amount of impurity phases being introduced in the resulting products due to abrasion from the grinding bowl[179].

Many other synthesis methods are relying on the high heat of formation of RuAl (Table 9) and the self-sustaining character of the reaction. Since an initiation of the self-sustaining reaction is possible in the solid-state, the necessary reaction temperatures are often being low compared to the high temperatures particularly applied during the melt processes. For example, the synthesis of single phase RuAl is possible starting from Ru/Al multilayers, which can be synthesized via magnetron sputtering[166,213]. For these multilayers, their bilayer thickness is representing an important reaction parameter, which amongst others is controlling the multilayer ignition temperature. A sample with a bilayer thickness of 22 nm was found to ignite at a temperature of 408 °C, while a sample with a bilayer thickness of 222 nm ignited at 608 °C[213]. Another parameter that is influenced by the bilayer thickness is the reaction front velocity, which is increasing with increasing bilayer thickness[166]. In these multilayers, the RuAl formation was shown via high speed time resolved X-ray experiments to proceed in a single step reaction via crystallization from the melt[166,214]. Upon igniting on a hot plate, the SHS reaction is initiated by the formation of at least one intermetallic phase, which was evidenced by the observation of Al_6Ru right before the ignition of the samples[213]. The Al_6Ru formation followed an Ru grain boundary diffusion in Al, which was found to play a crucial role within this ignition process and which was exhibiting an activation energy of 75 kJ/mol[213]. Upon applying slow heating rates, a dependence of the bilayer thickness of the multilayers on the phase formation sequence was reported. In the case of a bilayer thickness < 22 nm and a heating rate of 20 K/min, the formation of RuAl was reported to occur in a two-step process[214]. In the first step, at temperatures < 425 °C, Al diffusion into Ru is taking place, resulting in the formation of a Ru(Al) solid solution. In the second step, RuAl is formed in a diffusion-controlled process without the formation of any intermediate products[214]. In contrast, upon heating a multilayer with a bilayer thickness of 88 nm and a heating rate of 20 K/min, the formation of a Ru(Al) solid solution was reported to occur at temperatures < 350 °C[215]. This solid solution then decomposes yielding Al_6Ru, which then reacts with Ru forming RuAl at around 500 °C.

The synthesis is also possible applying powder metallurgy techniques. As stated above, loose powders as well as compacted pellets can be applied, which can be heated with or without the application of an external pressure[170,196,216,217]. Applying these methods, the preparation is typically carried out well

below the melting point of Ru and RuAl using several temperature steps, with the last step commonly being a homogenization at temperatures of 1400 – 1600 °C.

Upon reacting loose Al and Ru powders, no reaction was observed in DTA measurements upon reaching the Al melting point[170], which can be attributed to a poor particle contact. Naturally, this contact will significantly improve as soon as liquid Al is present, ultimately leading to an initiation of the reaction. Accordingly, the onset temperature was 755 °C and a decrease of the Al particle size was reported to lead to increased onset temperatures within these loose powder mixtures[170].

Reactive sintering

In contrast to the loose powders, the onset of the reaction in compacted Ru-Al pellets was found to occur well below the melting point of Al[170], indicating an initiation via solid-state reactions. Wolff et al.[170] reported no clear trend to be visible in the reaction onset temperature upon increasing the heating rate, while Mohamed et al.[216] reported increasing onset temperatures with increasing heating rates. The application of low heating rates < 30 K/min was reported to lead to the formation of multi-phase products containing large amounts of unreacted Ru, while a complete conversion to RuAl was observed upon applying high heating rates > 70 K/min[170]. Similar observations were made by Mohamed et al.[216], who reported the formation of multiphase products, containing RuAl as well as $RuAl_2$, upon applying a heating rate of 5 K/min, while single-phase RuAl was formed upon heating with 15 K/min. In these systems, the formation of pores was problematic, leading to the formation of porous products[170,217]. As reported by Gobran et al.[217], the Ru:Al particle size ratio is an important parameter within this system, with a small ratio being advantageous towards complete reactions as well as low onset temperatures. Moreover, the onset temperatures was found to increase with increasing Ru:Al size ratio and was determined to be about 625 °C for a ratio of 0.24 and about 635 °C for a ratio of 0.67.

Reactive hot pressing

By the application of an external pressure, the amounts of pores within the prepared samples can be reduced, leading to the formation of RuAl with 95 % of its theoretical density, which is considerably higher compared to the products obtained without any additional external pressure (up to 81 % of its theoretical density)[170,217]. However, the resulting products are typically containing multiple phases including Ru, RuAl, $RuAl_2$ and Ru_2Al_3[170,217], making a homogenization at increased temperatures (1400 – 1600 °C) necessary to obtain single phase products. Within the literature, heat transfer effects

to the pressure die, leading to an inhibited Ru diffusion due to the decreased temperatures, have been discussed to be responsible for the formation of these multiphase products[217]. Accordingly, due to shorter diffusion paths, the use of smaller Ru particles results in reactions that are more complete[217].

A synthesis applying a wet chemical approach has not been reported yet in the literature up to date.

1.4.2 Ni aluminides

1.4.2.1 Ni-Al system

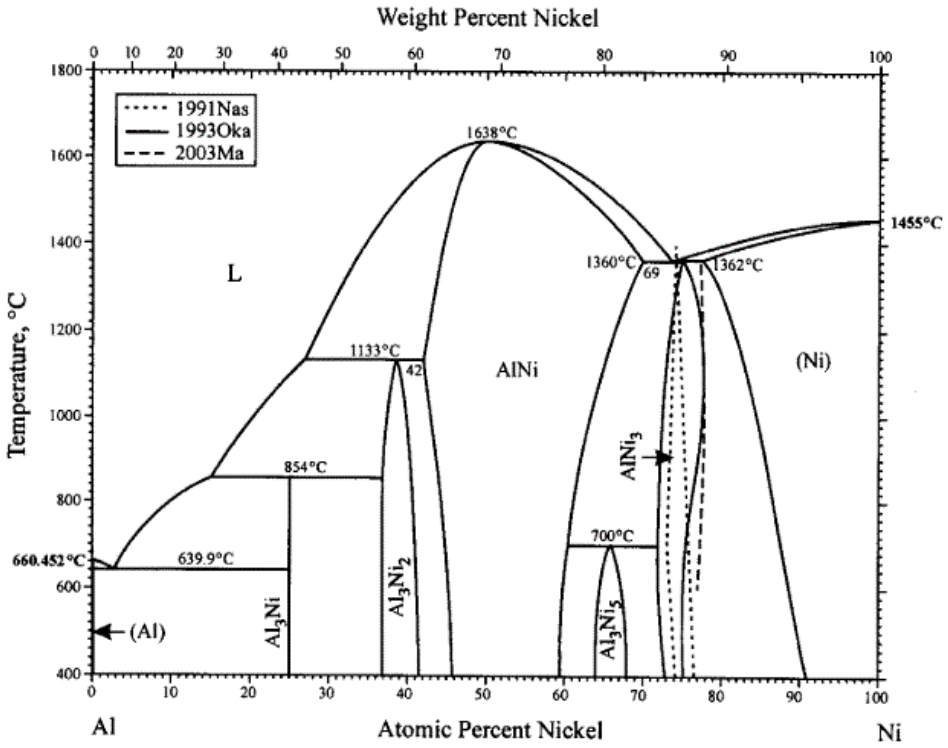

***Figure 14**: Binary Ni-Al equilibrium phase diagram. The legend within the figure stems from the original source. Reprinted by permission from Springer Nature Customer Service Centre GmbH: Springer Nature, Journal of Phase Equilibria and Diffusion, Al-Ni (aluminum-nickel), Okamoto H., 25, 394 (2004), Copyright (2004) [(https://www.springer.com/journal/11669)](https://www.springer.com/journal/11669)[218].*

Figure 14 shows the binary equilibrium Ni-Al phase diagram. Ni-Al intermetallic compounds have been known for a long time, and Wöhler already reported in 1860[219] about an intermetallic compound of the proposed composition Al_6Ni, while Brunck reported about a compound of the composition Al_3Ni in 1901[220]. The first Ni-Al phase diagram was published in 1908 by Gwyer[221] containing the phases $NiAl_3$, NiAl as well as a compound of the proposed composition $NiAl_2$. A few years later, the compound $NiAl_2$ was found to actually be Ni_2Al_3 and an additional phase of the composition Ni_3Al was detected via X-ray diffraction[222,223]. With the discovery of Ni_5Al_3 in 1978 by Enami and Nenno[224] all of the Ni-Al

intermetallic compounds known up to date have been detected. As can be seen, five stable Ni-Al intermetallic phases, $NiAl_3$, Al_3Ni_2, NiAl, Ni_5Al_2 and Ni_3Al, are existing, which are moreover all stable at room temperature.

The compounds $NiAl_3$, Ni_2Al_3, Ni_5Al_3 and Ni_3Al are melting incongruently at temperatures of 854 °C[222], 1133 °C[222], 700 °C[218], and 1362 °C[225], respectively. Particularly the question whether Ni_3Al is formed from a peritectic reaction of the melt and NiAl or from a peritectic reaction of the melt and Ni remained unclear for a long time[218,222,225,226]. NiAl is the only phase melting congruently at a temperature which was long assumed to be 1638 °C[222] before being corrected to 1681 °C by Bitterlich et al. in 2002[227].

While $NiAl_3$ is the only line phase within the Ni-Al system, Al_3Ni_2, NiAl, Ni_5Al_2 as well as Ni_3Al are all exhibiting a more or less broad stability range. Ni_2Al_3 is stable from 37.7 at% Ni to 42.2 at% Ni at a temperature of 500 °C[228], while Ni_3Al and Ni_5Al_3 are stable from about. 72 – 77 at% Ni and 64 – 68 at% Ni respectively[226]. In contrast, NiAl has a broad stability range, ranging from 45.2 at% Ni to 60.0 at% Ni at a temperature of 500 °C[228], with the phase border on the Ni rich side shifting to 69.5 at% Ni at a temperature of 1395 °C[228]. Similar to the Ru-Al system, the solubility of Ni in Al can be neglected[229], while solid solutions of Al in Ni can contain up to about 22 at% Ni at a temperature of 1362 °C[225,226].

The Ni-Al phases (Table 10) can be distinguished applying X-ray diffraction techniques. Since Ni is considerably smaller than Al, a decrease of the lattice parameter could be expected to occur upon increasing the Ni content within NiAl. However, this decrease can only be observed for NiAl with > 50 % Ni and, contrary to this expectation, a decrease in the lattice parameter can be observed upon decreasing the Ni content within Al rich NiAl. As a result, a lattice parameter maximum can be observed at a stoichiometry of $Ni_{50}Al_{50}$ (Figure 15a), which is explained in the literature by the formation of vacancies within Al rich NiAl[228]. Thus, a determination of the exact composition of NiAl is not possible only considering the lattice parameter and only a derivation from the ideal composition can be determined. For Ni_2Al_3, the ratio of the lattice parameters a/c can be used to determine the exact phase composition (Figure 15b**)**.

***Table 10**: Crystallographic data and enthalpies of formation of Ni aluminides.*

Aluminide	Space group	a(nm)	b(nm)	c(nm)	γ (°)	$-\Delta H_f \left[\frac{kJ}{mol\ atoms}\right]$	$-\Delta H_f \left[\frac{J}{g}\right]$
Al	$Fm\bar{3}m$	4.05[190]					
Al_3Ni	*Pnma*	6.60[230]	7.35	4.80		37[231]	1180
Al_3Ni_2	$P\bar{3}m1$	4.03[230]	4.03	4.89	120	63[232]	1624
AlNi	$Pm\bar{3}m$	2.88[233]				66[232]	1553
Al_3Ni_5	*Cmmm*	7.44[224]	6.68	3.72		54[234] (1)	1164
$AlNi_3$	$Pm\bar{3}m$	3.57[235]				39[232]	776
Ni	$Fm\bar{3}m$	3.52[233]					

(1) theoretical value

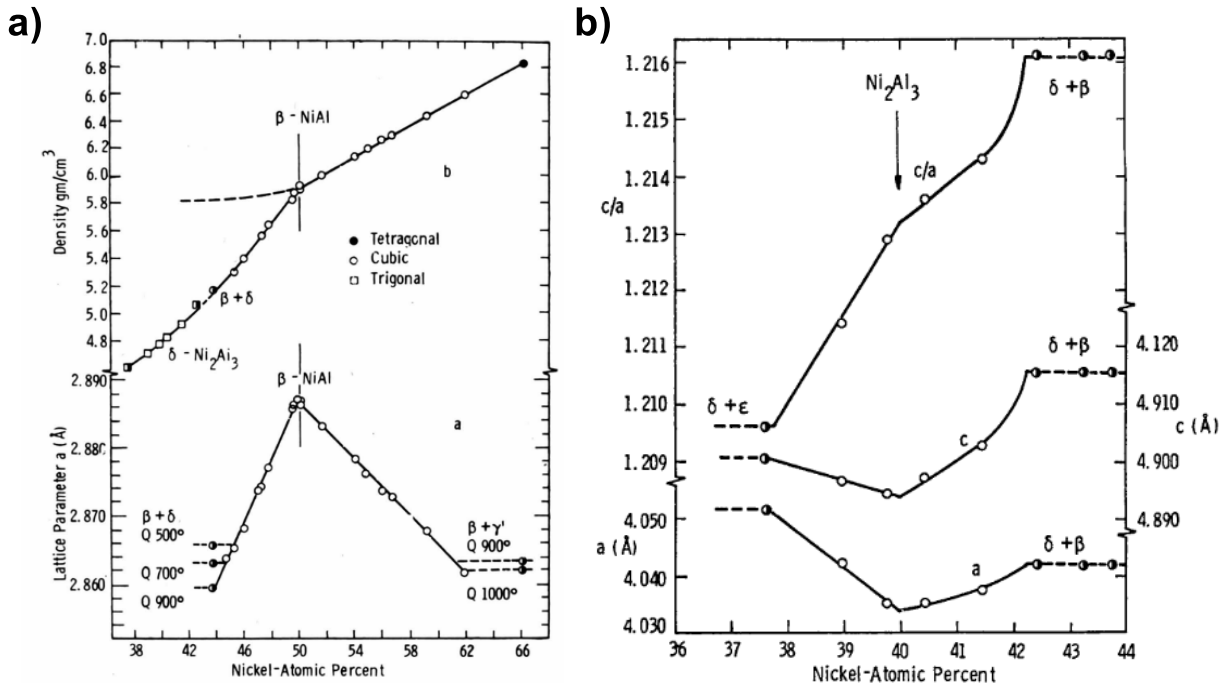

***Figure 15**: Dependency of the **a)** NiAl and **b)** Ni_2Al_3 lattice parameters from their composition. Reproduced with permission of the International Union of Crystallography (https://journals.iucr.org/). Taylor, A.; Doyle, N. J. Further Studies on the Nickel–Aluminium System. I. β-NiAl and δ-Ni_2Al_3 Phase Fields.* J. Appl. Crystallogr. ***1972**,* 5*, 201–209*[228]*.*

1.4.2.2 Properties and applications

Due to its broad stability range as well as its chemical, physical, and mechanical properties, NiAl is one of the most applied Ni aluminides for technical applications. Thus, the following sections shall focus on the properties and preparation methods of NiAl.

Similar to RuAl, NiAl is exhibiting a very high oxidation resistance, particular at increased temperatures > 1000 °C, which can be further improved by alloying with ternary elements, such as for example 0.1 at% Zr[236,237]. Doychak et al. observed the formation of an oxide layer with a thickness of about 1 µm upon treating a NiAl sample for 25 h at a temperature of 1100 °C[238]. During the oxidation, the meta stable phases $NiAl_2O_4$, δ-Al_2O_3 and θ-Al_2O_3 are initially formed, which then transform to α-Al_2O_3, ultimately passivating the underlying material[239].

The corrosion resistance of NiAl in acidic environments as well as the influence of various alloying elements was studied by Albiter et al.[240]. Within these studies, NiAl was observed to have an excellent corrosion resistance and the corrosion rate in 0.5 M H_2SO_4 was 1 mm/a and was hardly affected by the addition of 2 – 6 % Mo, 2 – 6 % Ga or 6 % Fe. In contrast, the corrosion rate in 0.5 M HNO_3 was lowered from 10 mm/a to < 1 mm/a by the addition of 2 % Ga. Similar as reported above for RuAl, many of its physical and chemical properties can be controlled by the addition of ternary elements such as B[241], Be[241], C[241], Ga[240], Mo[240]. For example, the yield strength can be increased by 1700 MPa/at% via C addition[241].

Moreover, many of the chemical and mechanical properties of NiAl were found to be dependent on many parameters, including for example the exact sample stoichiometry or the applied preparation method. A discussion of these influences would be beyond the scope of this work. They are, however, summarized in the literature in the form of various review articles[242–244]. Within these reviews a more detailed discussion of the properties discussed above, as well as the influence of various ternary alloying elements is also given.

Due to its high thermal stability as well as its excellent corrosion and oxidation resistance, even at increased temperatures, NiAl is widely employed as a coating material[245–249] in high temperature applications such as turbines, engines[245], or tools[250]. An application as a structural material also seems to be possible[251–255], including the field of astronautics[256]. Moreover, its mechanical and chemical properties might be useful within the field of electronics, for example for the construction of electric circuits[257,258]. Raney-Nickel, which is a common catalyst applied within the field of organic chemistry for the reduction of multiple bonds[259,260], is also consisting of a mixture of various Ni aluminides[261] and is activated by Al leaching with NaOH.

1.4.2.3 Preparation methods

Over the years, various methods have been applied throughout the literature for the preparation of NiAl. For instance, a wet chemical synthesis of NiAl and Ni_3Al was reported by Haber et al.[180]. They reacted $NiCl_2$ with $LiAlH_4$ in refluxing mesitylene and nanocrystalline aluminide powders were obtained

after vacuum sintering the resulting products at a temperature of 650 – 750 °C. Upon conducting the reaction in ethereal solutions, an oxygen abstraction from the solvent was observed, resulting in the formation of aluminum oxides. Moreover, the synthesis is possible by reacting $Ni(COD)_2$ and $AlEt_3$ under 5 bar hydrogen pressure at room temperature followed by sintering in an Ar atmosphere at a temperature of 300 °C[181]. The crystallite size of the resulting powders was about 4 nm. A similar approach is starting from $Ni(COD)_2$ and $Al(Cp^*)_4$, which can be converted to NiAl nanoparticles at 150 °C under 3 bar hydrogen pressure without any additional sintering being necessary[120]. The crystallite size of the resulting powder was determined to be about 2 nm

However, similar to RuAl, the synthesis of NiAl is commonly starting from elemental and commercially available Ni and Al powders. For example, NiAl can be prepared via mechanochemical approaches applying high energy ball milling[262,263], in which the crystallite sizes of the resulting powders can be controlled via a variation of the milling time[263]. Moreover, ball milling is a facile method for the preparation of Ni aluminides containing ternary additions and, for instance, Mo containing Ni aluminides were prepared by milling Ni and Al powder in the presence of Mo powder[264].

A synthesis applying the reactive infiltration method, in which a heated, porous solid Ni mold is infiltrated by liquid Al applying a high pressure has also been reported in the literature[169]. However, following the infiltration step, a homogenization step at temperatures of 1000 – 1200 °C is necessary to ultimately obtain Ni aluminides[169].

Besides the self-explaining syntheses via melt metallurgy approaches such as arc-melting, various sintering and combustion synthesis methods are the most common approaches for the preparation of NiAl reported in the literature. Within these approaches, powder mixtures as well as multilayer systems can be employed. However, no general reaction mechanism for these reactions can be postulated, since it was found to be dependent on the applied reaction conditions and parameters and various mechanisms have been proposed throughout the literature. Some examples of possible reaction mechanisms are summarized within the following sections, including single step reactions as well as reactions proceeding via the formation of several intermediate products such as $NiAl_3$ and Ni_2Al_3.

Multilayer

The Ni/Al-multilayers applied for the synthesis of Ni aluminides are typically prepared via magnetron sputtering techniques[265,266]. Similar as described for the Ru-Al systems, a decreasing bilayer thickness of these multilayers results in a decrease of the hot plate ignition temperatures. A Ni/Al multilayer with a 30 nm bilayer thickness was reported to ignite at a temperature of 232 °C, while a multilayer

with a bilayer thickness of 139 nm exhibited an ignition temperature of 297 °C[265].

Applying fast heating rates, i.e. during a locally initiated SHS reaction, the reaction was shown to proceed via a single-step mechanism according to the following reaction scheme[267–269]:

$$Ni(s) + Al(s) \longrightarrow Ni(s) + Al(m) \longrightarrow Ni(s) + AlNi_x(m) \longrightarrow NiAl(s)$$

***Scheme 7**: Formation of NiAl from Ni/Al multilayers applying fast heating rates[267].*

After reaching the Al melting point, solid Ni dissolves in the Al melt until reaching its saturation concentration resulting in a NiAl crystallization from this melt without the formation of any intermediate products. The formation of additional intermetallic phases, which was sometimes observed within this kind of samples, can thus likely be attributed to heat loss effects, leading to a rapid cooling of non-homogenously mixed solutions.

Zhu et. al[270] employed Ni/Al multilayers for the synthesis of NiAl via a thermal explosion reaction applying a heating rate of 40 K/min. They also found NiAl to form by crystallization from a melt, however, the formation of the intermediate phases $NiAl_3$ and Ni_2Al_3 was observed during the sample heat up and Ni dissolution at the interfacial area. Upon further heating, the intermediate products decomposed in a peritectic reaction ultimately forming a melt, from which NiAl ultimately crystallized. Applying slow heating rates, the formation of several, partially meta stable intermediate products was also observed applying XRD techniques[269,271,272] (Scheme 8). In contrast to the synthesis via the SHS technique, the reactions are typically initiated in the solid-state at temperatures of about 200 – 300 °C well below the melting point of the Ni-Al-eutectic. Accordingly, they are initiated without the presence of any liquid phase[271,272]. Besides, the phase sequence was found to be dependent on the bilayer thickness and upon applying small bilayer periods < 12.5 nm Al_3Ni was observed to be the first phase being formed, while at bilayer periods > 12.5 nm metastable Al_9Ni_2 was being formed first[272].

$$Ni + Al \longrightarrow Ni + Al + Ni_2Al_9 \longrightarrow Ni + Al_3Ni \longrightarrow Al_3Ni_2 \longrightarrow AlNi$$

***Scheme 8**: Formation of NiAl from Ni/Al multilayers applying slow heating rates (42 K/min)[269].*

Nowadays, such Ni/Al multilayer are readily commercially available, marketed by the Indium Corporation® as Nanofoil®[273].

Powder

The synthesis of Ni aluminides is possible employing Ni and Al powder mixtures, which can be reacted in the form of loose powders as well as compacted samples with and without the application of an external pressure.

SHS reaction

Employing compacted pellets, early studies applying time-resolved XRD studies, proposed the formation of several intermediate products, which could however, not be fully identified[274]. Tingaud et al.[275] as well as Biswas et al.[276] later identified Ni_2Al_3 and $NiAl_3$ as intermediate products and following reaction mechanism was proposed: i) melting of Al, ii) dissolution of Ni in the Al melt and formation of Ni_2Al_3 and $NiAl_3$ at the interfacial area, iii) further growth of these phases via diffusion processes, iv) melting of Ni_2Al_3 and $NiAl_3$ v) crystallization of NiAl from the melt[275]. However, recent studies could not confirm these results and proposed a single step reaction mechanism, similar as reported for the multilayer systems. For example, Curfs et al.[277] studied locally initiated SHS reactions within compacted powder pellet samples via in-situ XRD techniques and observed a single-step reaction mechanism with NiAl crystallizing from the melt. Similarly, as described above, the formation of several additional compounds such as Ni_3Al, Ni_2Al_3 and Ni_5Al_3 was observed, which were however shown to form only during the slow cooling of the sample. The formation of any additional phases during the cooling was also proposed by Fan et al.[278], who also observed the formation of Ni_3Al and Ni_2Al_3 as side-products, and ascribed them to an incomplete intermixing due the large sized reactant powders resulting in long diffusion paths.

Combustion synthesis and reactive sintering

The formation of NiAl starting from Ni and Al powders with sizes ranging from 5 – 40 µm via thermal explosion reactions was studied by Mukasyan et al.[171]. Applying a heating rate of 50 K/min, NiAl was found to crystallize from a melt without the formation of any intermediate products during the course of the reactions in time-resolved XRD studies. The lowest onset temperature was equal to the eutectic temperature of the Ni-Al system of 640 °C. Although, depending on the experimental conditions, solid-solid reactions were reported to occur below the eutectic temperature of 640 °C in these systems[279,280], as was stated by Thiers[281], a sharp increase in the heat release and thus in the reaction rate can be often observed as soon as a liquid phase is formed, which results in an improved interfacial contact between Ni and Al. In general, such pre-combustion or pre-ignition reactions can preferably be

observed applying slow heating rates. For example, Plazanet et al.[282] employed compacted Ni-Al powder mixtures, which were heated at heating rates ranging from 1 – 30 K/min. Within these studies, a single exothermic signal was observed upon applying heating rates > 5 K/min, with the exact onset temperatures being dependent on the heating rate as well as the green density of the pellet. Upon increasing the heating rate from 5 K/min to 30 K/min (70 % green density) the onset temperature decreased from 570 °C to 535 °C, while an increase of the green density from 62 % to 95 % (20 K/min) resulting in a decrease of the onset temperature from 560 °C to 510 °C. When slow heating rates < 5 K/min were applied, two exothermic signals were observed during STA scans. During the first exothermic reaction, $NiAl_3$ and Ni_2Al_3 are formed at the interfacial area via solid-state reactions, while the formation of NiAl was observed in a second exothermic reaction starting at the eutectic temperature of 640 °C.

Another very important parameter within this reaction system is the interelemental Ni-Al contact. An improved interfacial contact between Al and Ni, can be realized by treating the Ni and Al powders in a ball mill before the reaction, which results in the formation of “fresh” surfaces due to a breakup of the surface oxide layers. Accordingly, Muskayan et al.[171] observed a decrease of the onset temperature by 300 °C upon such a ball mill treatment and ascribed them to facilitated solid-state reactions. Similar observations were reported by White et al.[178], who also reported a 3 fold lower activation energy for the reaction upon employing ball mill treated powder mixtures (84 kcal/mol and 28 kcal/mol). Accordingly, the application of such mechanically activated powder mixtures is often preferred over their non-activated counterparts throughout the literature.

The synthesis of NiAl starting from ball-milled Ni and Al powder mixtures was studied by Mukasyan et al.[171] via time-resolved XRD techniques applying a heating rate of 50 K/min. In contrast, to the non-ball milled mixtures, no formation of a liquid phase was detected. Accordingly, the onset temperatures were well below the eutectic temperature of 640 °C. Instead, solid Ni, Al and NiAl were coexisting for a short period, before NiAl was the only phase being observed. During the course of the reaction, no other intermediate intermetallic phases were detected within these studies. However, particularly upon applying slower heating rates, the formation of various intermediate products is possible and has been observed numerous times. For example, Miura et al[283] studied the effect of the heating rates and sample green densities in such ball-milled Ni-Al powder mixtures, applying compaction pressures of 100 – 300 MPa as well as heating rates ranging from 1-10 K/min. Within their studies, an increase of the heating rate from 1 to 10 K/min resulted in an increase of the onset temperatures from about 470 °C to about 500 °C, while the onset temperature increased from about 500 °C to about 520 °C upon decreasing the compaction pressure from 300 to 100 MPa. Moreover, in contrast to the reports above,

the intermediate products $NiAl_3$ und Ni_2Al_3 were detected under the synthesis parameters applied within these studies.

The formation of such intermediate phases has been reported numerous times throughout the literature and many reaction sequences have been proposed. For example, Dong et al.[284] applied ball milled Ni-Al powder mixtures compacted at a pressure of 200 MPa, which were heated at rates < 5 K/min, and proposed Ni_2Al_3 to be the first phase being formed at a temperature of 540 °C. Particularly, no formation of $NiAl_3$ was proposed, while at lower temperatures of 540 – 640 °C the 5 phases Ni, Ni_3Al, NiAl, Ni_2Al_3 and Al were coexisting. In contrast, Biswas et al.[276], who also employed compacted and ball milled Ni and Al powder mixtures as well as heating rates ranging from 5 to 60 K/min proposed the following reaction mechanism: i) formation of $NiAl_3$, ii) formation of a melt with a eutectic composition, iii) formation of Ni_2Al_3 at the Ni particle surface, iv) diffusion of Ni and Al through this layer, and v) formation of NiAl by crystallization from the melt.

Reactive hot pressing

In order to obtain more dense reaction products, the synthesis is often carried out applying an external pressure during the reaction. However, similar to the Ru-Al system, the formation of multiphase products due to incomplete reactions was often observed. Again, these observations were attributed to heat loss effects due to heat transfer effects from the sample to the pressure dye[285–287], preventing the combustion reactions to run to completeness.

For example, Zhu et al.[287] employed ball-milled, compacted Ni-Al particle mixtures, which were heated applying heating rates of 10 K/min and 50 K/min under a pressure of 50 MPa. Upon heating an isolated sample with a heating rate of 50 K/ min the formation of single-phase NiAl was observed, while upon employing a non-isolated sample a multiphase product was obtained, which was ascribed to heat loss effects as described above. For this heating rate, only a single exothermic signal was observed during a STA scan. However, upon applying a heating rate of 10 K/min a multistep, diffusion-controlled reaction was observed and following reaction mechanism was proposed:

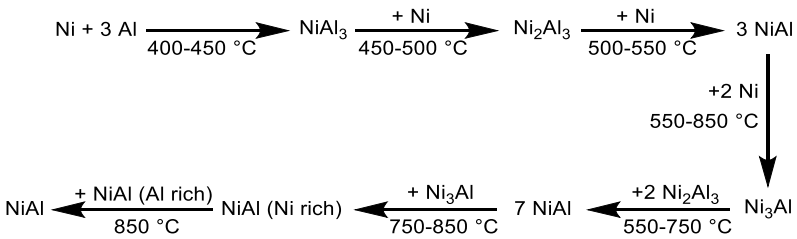

***Scheme 9**: Formation of NiAl from ball-milled and compacted Ni-Al powder mixtures applying a heating rate of 10 K/min and an external pressure of 50 MPa [287].*

Similar multi-step reactions where described by Bhaumik et al. and by Farber et al.. Bhaumik et al.[288] employed ball milled Ni and Al powders, which were reacted applying a heating rate of 40 K/min and a pressure of 3 GPa. A multi-step reaction mechanism was proposed, including the formation of $NiAl_3$ and Ni_2Al_3 as intermediate products, which ultimately resulted in the formation of multiphase reaction products, which was again ascribed to heat loss effects. Similarly, Farber et al.[285] prepared NiAl starting from ball milled Ni and Al powders, which were compacted at a pressure of 3 GPa, and reacted applying heating rates ranging from 1 - 50 K/min under a pressure of 50 MPa. They proposed the formation of $NiAl_3$ at the interfacial area, which then reacts with excess Ni to form Ni_2Al_3 and NiAl upon further heating.

As can be seen, no general reaction mechanism for the formation of NiAl can be established, since it was found to be dependent on various reaction parameters including sample pre-treatment, heating rate as well as applied pressure. However, particularly upon applying an external pressure as well as slow heating rates, the formation of various intermediate products such as $NiAl_3$ and Ni_2Al_3 has been reported many times.

Influence of impurity phases

If the reaction is conducted in the presence of impurity phases or atoms, these impurities might have an influence on the reaction. Considering reactive, non-inert compounds, an undesired reaction with at least one of the reactants might occur, leading to the formation of additional impurity phases that will be included within the final product. For example, within this work, the formation of iron aluminum carbides was often observed upon reacting iron and aluminum in the presence of organic and thus carbon containing compounds. If the impurity phase shows no reactivity towards the reactants and does not decompose and evaporate during the heat-up, it will however still be included within the final product. Although the presence of such additional compounds is undesired in many cases, it might be exploited to alter the physical, mechanical as well as chemical properties of the resulting products. Typical examples are including alloying with an ternary element (Chapter 1.4.2.2) or the addition of stainless steel fibers[289]. If organic compounds are present, the porosity of the reaction mixture can be expected to increase upon decomposition or evaporation of these molecules. Accordingly, products with increased porosities can be expected to form.

Moreover, inert impurities might influence the thermodynamic and thus the mechanistic characteristics of these reactions. Since the presence of an additional, inert phase can be understood as a dilution of the reaction system, the heat of the reaction effectively decreases[290] also decreasing the maximum reaction temperatures as well as the reaction front propagation velocities of the self-

sustaining reactions[291]. Naiborodenko et al.[292] proposed an influence of the maximum reaction temperature on the reaction mechanism of the NiAl formation and distinguished 3 different cases upon reacting compacted Ni and Al particle mixtures applying a SHS reaction:

i) The melting point of NiAl is higher than the maximum reaction temperature, which is higher than the melting points of Ni, Al, and any intermediate product (Ni_2Al_3 and $NiAl_3$). This case was reported to be occur for a dilution < 15 % and NiAl was proposed to crystallize from a saturated melt. The dilution was realized by the addition of NiAl to the reaction mixture.

ii) The melting points of NiAl and Ni are higher than the maximum reaction temperature, which is higher than the melting points of Al and any intermediate product. In this case, solid Ni was proposed to dissolve in the melt and NiAl then forms via crystallization from a saturated melt.

iii) The maximum reaction temperature is lower than the melting points of NiAl, Ni and at least one intermediate product. In this case Ni_2Al_3 forms on the Ni surface and Ni and Ni_2Al_3 then dissolve in the melt, from which NiAl ultimately crystallizes. This case was reported to occur for a dilution > 25 % and resulted in the formation of multiphase products containing NiAl, Ni_2Al_3, Ni.

Ultimately, such a dilution might lead to a loss of the self-sustaining properties of such a reaction system[290]. The dilution, which is necessary for such a loss of the self-sustaining properties can be calculated theoretically and the results can be plotted in the form of so-called SHS diagrams (Figure 16). For example, Zhu et al.[293] studied the ignition of Ni (4.5 µm) and Al (15 µm) powders in the presence of 3 – 15 % Al_2O_3 (1 µm) via inductive heating and observed a failure of the mixture to ignite in samples containing more than 12 % Al_2O_3. In addition, an increase of the Al_2O_3 content was associated with a decrease of the combustion velocity and a decrease of the sample heating rate. The hardness of the prepared NiAl was reported to increase with increasing Al_2O_3 content before reaching a maximum at about 10 % Al_2O_3 due to increased porosities and the formation of brittle Ni_2Al_3. Similarly, incomplete reactions during the synthesis of Ni_3Al starting from Ni and Al powders have also been reported by Lebrat et al.[294] to occur in samples containing about 10 % Al_2O_3.

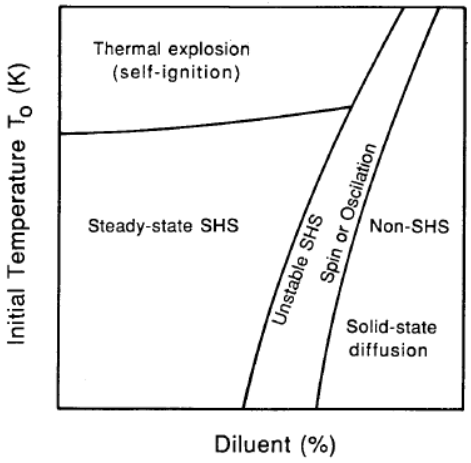

***Figure 16**: SHS diagram. Reprinted by permission from Springer Nature Customer Service Centre GmbH: Springer Nature, Metallurgical transaction A Physical metallurgy and materials science, Reaction synthesis processes: mechanisms and characteristics, Munir Z. A., 23, 7-13 (1992), Copyright (1992) (http://link.springer.com/journal/11661)*[290].

Influence of particle sizes

The influence of the Al particle sizes within the combustion synthesis of NiAl was examined by Li et al.[295]. They employed Ni powders with sizes ranging from 3 to 27 µm and Al powders with sizes from 5 to 150 µm, which were compacted and ignited using a propane torch. Upon applying Ni particles with a size of 8 µm and Al particles with varying sizes, only the sample containing Al particles with a size of 5 µm could be ignited, while no ignition was observed in samples containing Al with a size > 5 µm. This behavior was attributed to a longer time necessary to melt the larger Al particles, thus leading to higher heat losses and ultimately preventing an ignition. In contrast, a further decrease of the particle size down to the submicron range had no influence on the reaction as well as the formed products. Similar results, with the observation of an upper limit regarding the Al particle size, were reported for the synthesis of Ni_3Al via reactive sintering[296,297]. Upon applying large Al particles, no continuous phase, which is capable of completely enclosing the Ni particles, could form, thus resulting in porous products as well as incomplete reactions.

Similarly, the influence of the Ni particles size has been studied several times within the literature. Li et al.[295] reported a decrease of the combustion temperature as well as the reaction front velocity to occur upon increasing the Ni particle size from 3 to 27 µm upon igniting their reaction mixtures applying a propane torch. Within their studies, these observations were attributed to kinetic factors as well as a change in the thermal conductivities. Similar observations were reported by Biswas et al[298]. They prepared NiAl via thermal explosion reactions applying Al powder with a size of 42 µm and Ni powder with a size ranging from 11 to 130 µm. The samples were homogenized in a ball mill,

compacted applying a pressure of 75 – 150 MPa and heated at heating rates of 5 – 60 K/min. The results of these studies are summarized in Table 11.

***Table 11**: Combustion and reaction characteristics of ball milled and compacted NI-Al powder mixtures applying Ni powders with various sizes and various heating rates. The Al particle size was 42 µm in all samples. Reprinted from Acta Materialia, 50,Biswas A.; Roy S. K.; Gurumurthy K. R.; Prabhu N.; Banerjee S., A study of self-propagating high-temperature synthesis of NiAl in thermal explosion mode, 757-773, Copyright (2002), with permission from Elsevier[298].*

<table>
<tr><td></td><td colspan="5">Effect on combustion and the product phase microstructure</td></tr>
<tr><td rowspan="3">Particle diameter of nickel (µm)</td><td>129.57</td><td>No combustion</td><td>Multiple phase porous product, poor conversion, large amount of unreacted nickel and Al_3Ni, Low T_{ig}, T_c<m.pt. of NiAl</td><td>Multiple phase porous product with Ni(Al)-Ni_3Al eutectic, better conversion, less amount of unreacted nickel, no Al_3Ni, High T_{ig}, T_c<m.pt. of NiAl</td><td>Single phase dense NiAl; Cast microstructure, coarse dendrites; High T_{ig}, T_c>m.pt. of NiAl</td></tr>
<tr><td>110.83</td><td>No combustion</td><td>Multiple phase porous product, poor conversion, large amount of unreacted nickel and Al_3Ni, Low T_{ig}, T_c<m.pt. of NiAl</td><td>Multiple phase porous product with Ni(Al)-Ni_3Al eutectic, better conversion, less amount of unreacted nickel, no Al_3Ni, High T_{ig}, T_c<m.pt. of NiAl</td><td>Single phase dense NiAl; Cast microstructure, coarse dendrites; High T_{ig}, T_c>m.pt. of NiAl</td></tr>
<tr><td>10.94</td><td colspan="2">Single phase NiAl; Cast microstructure, fine dendrites; Low T_{ig}, high T_c, T_c>m.pt. of NiAl</td><td colspan="2">Single phase NiAl; Cast microstructure, fine dendrites; High T_{ig}, high T_c, T_c>m.pt. of NiAl</td></tr>
<tr><td></td><td colspan="2">5-10</td><td>15-25</td><td>30-35</td><td>>35</td></tr>
<tr><td></td><td colspan="5">Rate of Heating (°C/min)</td></tr>
</table>

T_{ig}: ignition temperature; m.pt.: melting point; T_c: maximum reaction temperature

Hence, the use of smaller Ni particles resulted in more complete reactions, lower ignition temperatures as well as higher maximum reaction temperatures. Moreover, at a given composition, increasing heating rates resulted in increased reaction temperatures as well as increased maximum reaction temperatures. Within their work, the increase in the combustion temperature upon decreasing the Ni particle size was explained by an increase of the Ni-Al interfacial area. The increase in the onset temperature with increasing heating rates was explained by the formation of smaller amounts of Al_3Ni via solid-state reactions prior to the combustion, which is leading to shorter residence times at the eutectic melting point and thus higher onset temperatures. The increased amount of Al_3Ni formed prior to the combustion at low heating rates was also discussed to lead to lower combustion temperatures, which are not allowing enough time for a complete homogenization and are thus leading to the formation of multiphase products.

A decrease of the minimum heating rate necessary for a successful SHS reaction upon decreasing the particle sizes was also reported by Dumez et al.[299], who also plotted the results in form of a SHS diagram

(Figure 17). Within Figure 17a, the arrows indicate the shift of the phase boundaries when the grain sizes are decreased and I is referring to a diffusion-controlled reaction, II to an unstable SHS reaction and III to a stable SHS reaction.

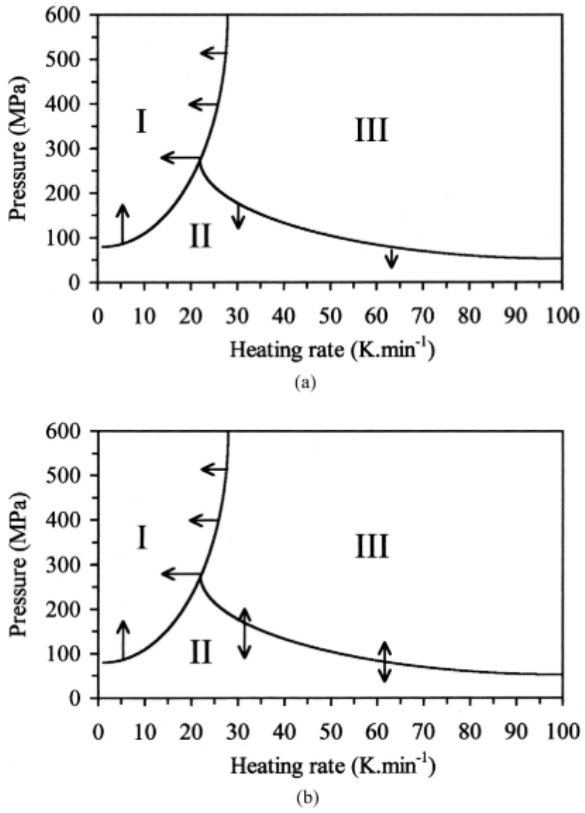

***Figure 17**: Effect of a a) particle size and b) porosity decrease on the mode of a combustion synthesis. Reprinted from Journal of Alloys and Compounds, 268, Dumez M.C.; Marin-Ayral R. M.; Tédenac J. C., The role of experimental parameters in combustion synthesis of NiAl under high gas pressure, 141-151, Copyright (1998), with permission from Elsevier*[299].

Besides the particle sizes, the reaction mechanism as well as the composition of the resulting product is determined by many other parameters including for example porosity[299], sample preparation[178] or the applied pressure[299], which shall however not be discussed in more detail within this manuscript.

Although a reduction of the particle sizes has been found to be advantageous towards the synthesis of NiAl via thermal combustion approaches, only a few studies are known in the literature applying nanoparticulate reactants. One reason for this is, that upon applying oxide passivated Al nanoparticles, the particle size reduction is linked to an increase of the Al_2O_3 content of the sample. Nonetheless, the synthesis starting from Ni particles with a size of 1 µm and Al particles with sizes ranging from 25 nm to 20 µm was conducted by Hunt et al[23]. Within these studies, compacted Ni-Al powder mixtures were ignited by a 50 W CO_2 laser and the influence of the Al particle size was studied. The time upon an ignition was observed reduced from 4 s to 0.2 s upon reducing the particle size from 20 µm to 25 nm, which was explained by the Al melting point depression of these nanoparticles. Due to the reduced

heating periods, the ignition temperature also decreased from 631 °C to 377 °C. Moreover, the ignition temperature was found to be dependent on many other parameters such as the green density and the heating rate[300]. Moreover, the use of nanoparticles led to a reduction of the burn rate from 62 to 8 mm/s[23], which was attributed to increased Al_2O_3 contents acting as a heat sink[23,301]. In addition, Hunt et al.[302] found the activation energy of the reaction system to decrease upon decreasing the Al and Ni particle sizes and reported the activation energy in samples prepared from micrometer sized powders (107 - 163 kJ/mol) to be significantly higher than those prepared from nanoparticulate reactants (17 - 104 kJ/mol), which was ascribed to a different reaction mechanism with the initiation occurring via solid-state reactions rather than solid-liquid reactions.

1.5 Methods

1.5.1 Calculation of Al contents from TG measurements

The Al^0 content of Al nanoparticles can be calculated from TGA measurements in an oxidizing atmosphere according to equation 1. This calculation is based on the total mass increase from the mass minimum to the mass maximum due to the Al oxidation (Chapter 1.3.2), which is measured in the TG analysis. A complete oxidation of the Al is assumed, which can be confirmed by an X-ray analysis of the residue remaining after a TG measurement. Moreover, potential impurity phases can be detected in the XRD measurements, which might then be considered in these calculations, if necessary.

$$w(Al^0) = \frac{\Delta m \cdot 2\, M_{Al}}{3\, M_O} \quad (1)$$

$w(Al^0)$: Mass content of Al^0
Δm: Total mass increase observed in the TGA trace
M_{Al}, M_O: Molar masses Al (26.98 g/mol) and O (15.99 g/mol)

Due to the assumption of a complete oxidation of the particles, an ignition of the Al particles has to be avoided during the measurements, since it might lead to the formation of aluminum nitrides and oxynitrides apart from aluminum oxide[303]. An ignition of the particles does particularly occur applying high sample masses, high heating rates or high oxygen contents[137]. It can often be easily recognized in the TGA traces by the formation of rectangular angles as well as a slight temperature increase (Figure 18a).

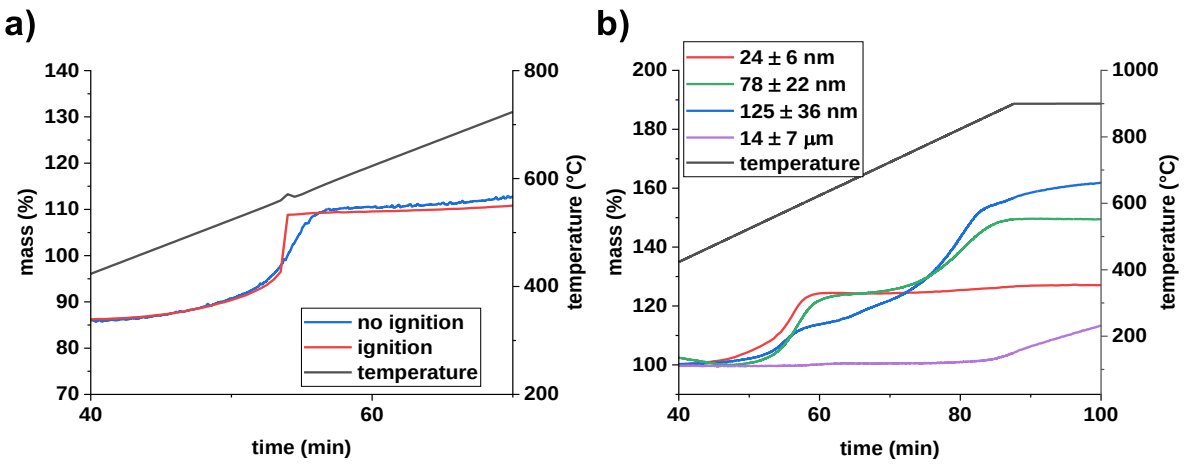

***Figure 18**: **a)** TGA traces of Al nanoparticles with and without ignition (N_2: O_2 32:8; 10 K/min) and **b)** TGA traces of Al particles with various sizes (N_2: O_2 32:8; 10 K/min).*

If the calculations are based on the as measured TG traces, the calculated Al^0 content refers to the Al^0 content in the as prepared samples including organic passivation layers as well as residual solvents. By normalizing the TGA traces to their mass minimum, the calculated Al^0 contents are an indication of the Al^0/Al_{total} ratio, assuming no mass loss overlapping the mass gain is occurring after reaching the minimum and that only Al^0 as well as Al_2O_3 are being present at the mass minimum. An estimation of the mass loss occurring after reaching the mass minimum can be given by comparing the TG mass losses and the organic contents determined from CHN analyses.

Moreover, since the observed TG trace is dependent on the Al particle sizes as well as morphologies (Figure 18b), several models for the calculation of the particle sizes from the TG traces have been proposed within the literature utilizing a simulation of the TGA traces. However, they require the knowledge of the exact particle size distribution[304] or are assuming monodisperse and spherical particles[130] and where thus not suitable for the particles studied within this work and shall thus not be discussed in more detail.

1.5.2 Kissinger analysis

According to Kissinger[305], the kinetics of the most solid-state reactions can be described by the following equation:

$$\frac{dx}{dt} = A(1-x)^n \, e^{-\frac{E_A}{RT}} \quad (2)$$

dx/dt: Reaction rate
A: Constant
x: Turnover
n: Empirical order of reaction
T: Temperature
E_A: Activation energy
R: Ideal gas constant 8.3145 J/(mol K)

Applying a given heating rate β, the reaction rate will increase with increasing temperature until reaching its maximum value due to an increased turnover. The maximum rate of reaction will be observed at a temperature T_m, which can be determined by calculating the maximum of equation (2):

$$\frac{E\beta}{RT_m^2} = An(1-x)_m^{n-1} \, e^{-\frac{E_A}{RTm}} \quad (3)$$

T_m: Temperature at which the highest reaction rate occurs
β: Heating rate

Starting from equations 2 and 3, Kissinger derived following correlation, independently of the reaction order:

$$\frac{d(ln\frac{\beta}{T_m^2})}{d(\frac{1}{T_m})} = -\frac{E_A}{R} \quad (4)$$

According to equation 4, the activation energy of a solid-state reaction can be determined from the slope of a plot of $1/T_m$ against $\ln(\beta/T_m^2)$.

1.5.3 Synthesis of aluminides on a hot plate

The experimental set-up consisted of an isolated stainless-steel plate, in which three 650 W heating cartridges were embedded (Figure 19). The temperature of the steel block could be controlled from 25 °C to 650 °C via a PID temperature controller, whose temperature sensor was embedded about 0.5 mm beneath the surface of the steel plate. To determine the ignition temperature of an Al-metal powder mixture, the plate was heated to a set temperature, equilibrated until a constant temperature was reached and a small amount of the compacted sample (1 – 3 mg) was dropped onto the plate using a tweezer. An ignition and thus a reaction of the powder mixture was recognized with the naked eye by the formation of sparks (Figure 19). If no reaction was observed, the temperature of the plate

was raised, and the procedure was repeated. The ignition temperature was then determined as the median of the lowest temperature at which an ignition was observed and the highest temperature at which no ignition was observed. These reactions were carried out in an atmosphere of ambient air. In these measurements a constant temperature distribution in the reaction spot (Ø 2 cm) was assumed and the temperature of the temperature controller was assumed to be the surface temperature. By applying this technique high heating rates can be realized, which is important in these systems. In the case of metallic reactive systems, the application of slow heating rates is not appropriate because of sub-critical diffusion processes dissipating heat and delaying or suppressing the ignition.

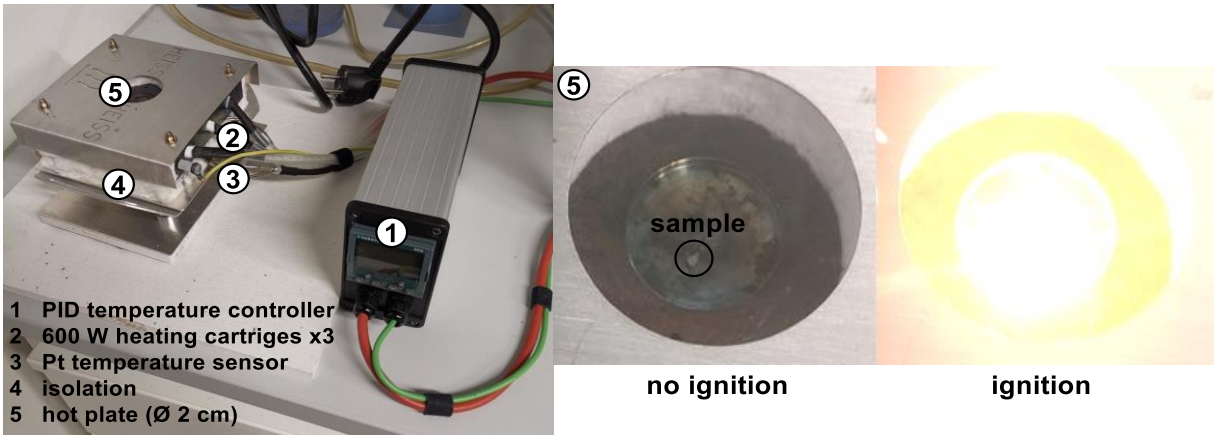

***Figure 19**: Experimental set-up of the hot-plate applied within this work and examples of a negative and a positive ignition event.*

1.5.4 XRD measurements

Due to the small sample amounts available as well as the high number of samples, the XRD measurements were conducted on glass sample holders. Due to the application of these glass sample holders, a very broad signal was observed in all samples at 2θ angles < 40 °, which is why the measurements were typically fitted and plotted starting from a 2θ angle of 30 ° or 35 °. A measurement of an empty sample holder is shown in Figure 20.

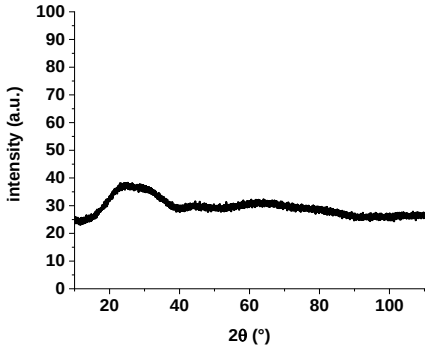

***Figure 20**: XRD measurement of an empty glass sample holder.*

2. Goals of this work

The goal of this work was the synthesis of aluminides starting from wet chemically prepared nanoparticulate reactants (Figure 21). For this purpose, the work was divided into two parts:

- The goal of the first part of the work was the wet chemical synthesis of metal nanoparticles, which were then reacted in the second part to yield the respective aluminides. Since the synthesis of many metal nanoparticles such as Ag, Au, Ni, Ru and many more has already been studied in detail in the literature and the synthesis of particles with various sizes as well as morphologies is possible, this work mainly focused on the preparation of Al nanoparticles. Due to their high reactivity, reports on the wet chemical synthesis of Al nanoparticles are limited and a study of the influence of the reaction parameters on the size and morphology of the resulting Al nanoparticles is often lacking. Nonetheless, different synthesis approaches have been reported throughout the literature. Accordingly, the goal of this part of the work was the synthesis of Al nanoparticles suitable for the preparation of various aluminides. The Al particles prepared via different synthesis approaches should be compared, and the influence of various reaction parameters on the size and morphology of the resulting particles should be examined in order to allow a preparation of the particles with a controlled size and morphology. Moreover, the reaction conditions should be optimized towards short reaction times in homogeneous solutions, which might allow the preparation of Al nanoparticles via a large scale, continuous synthesis approach in the future.

- The goal of the second part of the work was the synthesis of various aluminides starting from the wet chemically prepared metal nanoparticles, focusing on the synthesis of Ni and Ru aluminides. The suitability of the Al particles prepared applying different synthesis methods should be evaluated and the influence of various reaction parameters such as particles sizes, reaction conditions, contents of oxide and organics on the aluminide formation should be examined.

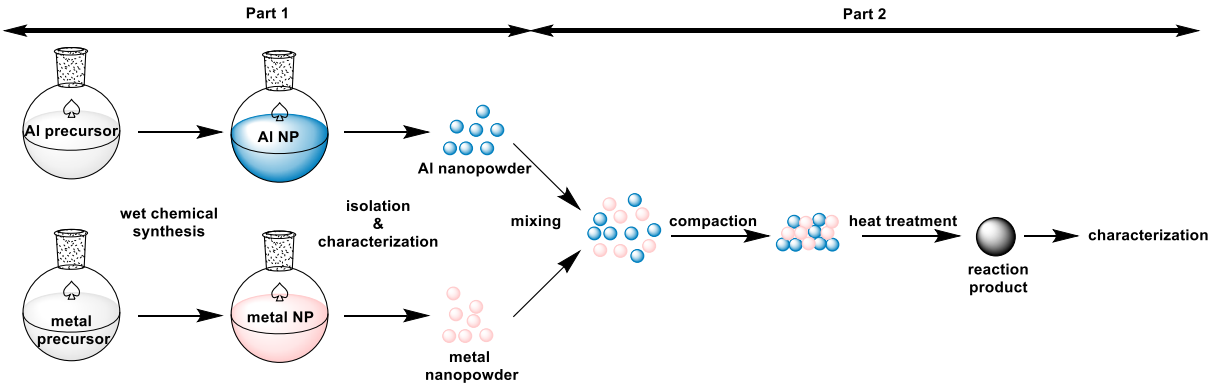

***Figure 21**: Procedure for the synthesis of aluminides applied within this work.*

3. Results and discussion

3.1 Synthesis of Al particles

Within this work, Al particles were synthesized applying various wet chemical methods introduced in Chapter 1.3.1. In the following chapters a characterization of these particles is given and their suitability for the preparation of Ni and Ru aluminides is evaluated.

3.1.1 Synthesis via metal reduction

Although the reduction of $AlCl_3$ with alkali metals is known to yield finely dispersed Al^0 (see Chapter 1.3.1.3), the resulting powder is commonly not isolated and characterized but is applied *in situ* for further reactions. Thus, within this work, the method adapted from Pyo et al.[87], in which $AlCl_3$ is reduced by Li in refluxing THF solutions, was applied for the preparation of Al^0 powder, which was then isolated, characterized and employed for the preparation of aluminides (Scheme 10). After the synthesis the powder was slowly air passivated and the characterizations were carried out applying this air passivated powder.

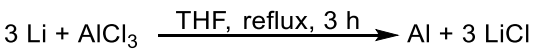

***Scheme 10**: Synthesis of Al starting from $AlCl_3$ and Li.*

The formation of Al^0 was confirmed by XRD measurements (Figure 22a), in which the reflections of fcc-Al are clearly visible. The Al^0 crystallite size was determined to be 12(5) nm via Rietveld refinements. Although no other phases were detected, this does not exclude the presence of a passivating oxide layer, which is known to consist of amorphous Al_2O_3 at room temperature. Accordingly, the formation of Al^0 as well as Al_2O_3 was observed applying ^{27}Al-SPE/MAS NMR techniques (Figure 22b), in which the signal at 1642 ppm can be assigned to Al^0, while the signal at 5 ppm can be assigned to the amorphous surface Al_2O_3 mentioned above. The Al^0 was found to form large agglomerated and sintered structures, detected by DLS measurements as well as TEM images (Figure 22c and d). In the DLS measurements (Figure 22c), a hydrodynamic radius of 118 ± 5 nm as well as larger agglomerates with radii of up to 1000 nm were observed, while the TEM images revealed severely agglomerated and sintered structures. Due to this sintering, no reasonable particle size distribution could be determined from these TEM images.

The small crystallite sizes observed in the Rietveld refinements are also evident in the TG measurements (Figure 23a), in which only a small, single mass increase step of 15.4 % was observed

starting at a temperature of about 400 °C. The presence of only a single mass increase step can be understood as a consequence of the small Al crystallites, as was discussed in Chapter 1.3.2. After normalization to the mass minimum, the Al^0 content was calculated from the mass increase and found to be as low as 17.3 %. This small value is in agreement with the small crystallite sizes determined in the XRD analysis, which can be expected to have a large amount of surface Al_2O_3 in the form of an amorphous oxide layer due to their small size. The mass loss of 15.3 % observed up to a temperature of 400 °C can be ascribed to the presence of residual solvents and organics.

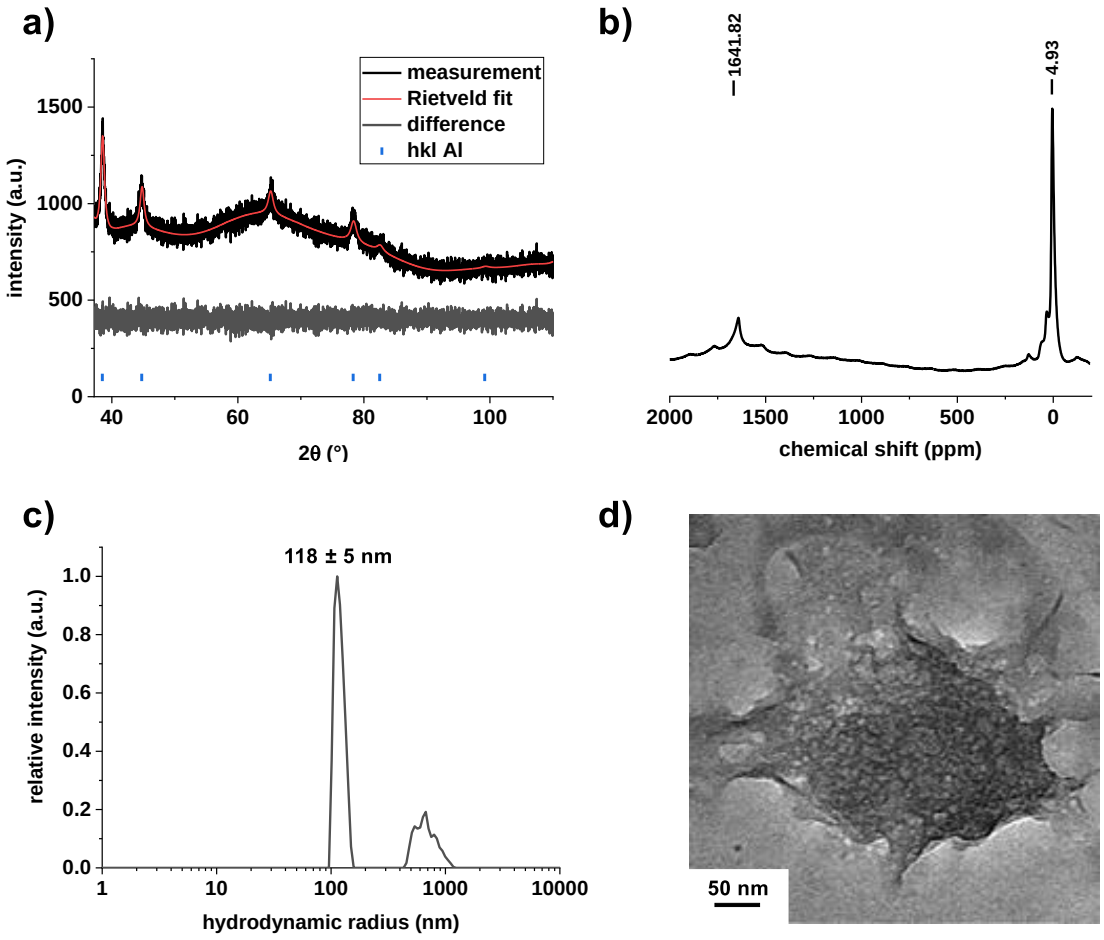

***Figure 22**: **a)** XRD measurement and Rietveld refinement, **b)** ^{27}Al-SPE/MAS NMR (104 MHz), **c)** DLS measurement in MeOH, and **d)** TEM image of Al^0 nanopowder prepared via reduction of $AlCl_3$ with Li.*

A capping of the resulting Al^0 powder was easily possible by adding oleic acid in a second, optional synthesis step prior to the particle isolation. The oleic acid coordination on the surface was confirmed by FTIR measurements, in which the signals belonging to the symmetric and asymmetric stretching modes of the carboxylate group (1560 cm^{-1} and 1452 cm^{-1}) were observed as well as in the TG measurements, in which an increased mass loss of 28.5 % was evident (Figure 23a and b). The high intensity signal in the FT-IR spectra at wavelengths < 1000 cm^{-1} can be assigned to the presence of

surface oxides. The TEM image (Figure 23c) again confirmed the formation of severely agglomerated and sintered particles. Accordingly, although the oleic acid was found to coordinate to the particle surface, it could not prevent the particle sintering. This can be explained the fact, that the oleic acid was added only in a second synthesis step, after the reduction was already complete. Accordingly, it was added to an already agglomerated and sintered particle mixture, as was shown above. However, due to the chemical incompatibility of Li, $AlCl_3$, and oleic acid, an addition at the start of the reaction was not suitable.

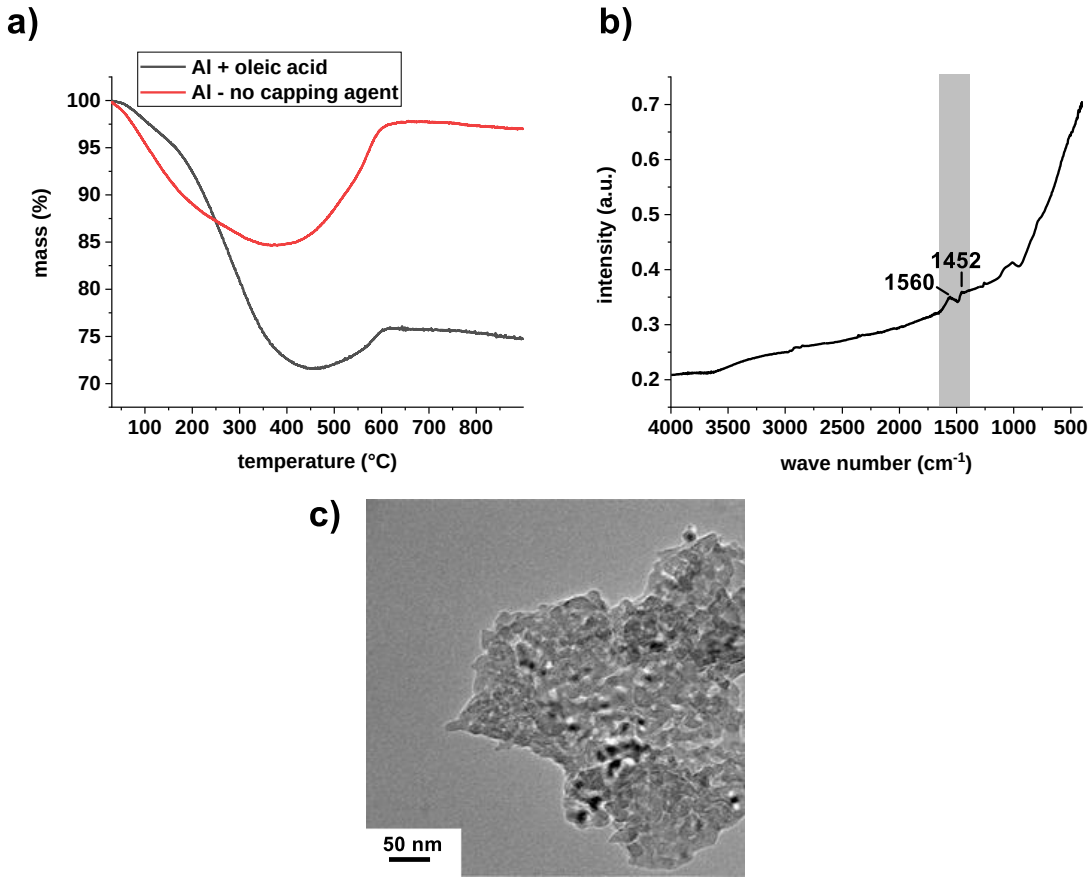

***Figure 23**: **a)** TG measurements (10 K/min: N_2:O_2 32:8) of bare and oleic acid capped Al nanopowder, **b)** ATR-FTIR spectrum, and **c)** TEM image of oleic acid capped Al nanopowder prepared via reduction of $AlCl_3$ with Li. The signal marked with a grey box in part b) can be assigned to the symmetric and asymmetric carboxylate stretching modes.*

In an attempt to prevent the particle agglomeration and sintering, the reaction was carried out in the presence of TOP as well as in coordinating and stabilizing tetraglyme and trioctylamine solutions. However, in all cases, a much slower reaction was observed and after 4 h only minor amounts of Al were isolated, which can likely be attributed to the altered electrochemical and sterical properties of formed Al^{3+} complexes.

Due to the drawbacks of this synthesis approach, particularly the heterogeneous reaction mixtures, the long reaction times of several hours, as well as the poor results observed upon applying these

particles for the formation of aluminides (see Chapter 3.2.2), no additional attempts regarding a reaction optimization, particle size variation or minimization of the particle agglomeration/ sintering were made. Of course, several methods are known to conduct the reduction in homogenous reactions mixtures, such as the application of Li naphtalenide or Li in liquid NH_3. However, they have been reported in the literature to lead to incomplete reductions[86,88] and were thus also not further examined within the present work.

3.1.2 Synthesis via hydride reduction

Within this synthesis approach, $AlCl_3$ is reduced by $LiAlH_4$ in refluxing mesitylene (Scheme 11). The reaction proceeds via an intermediate formation of AlH_3[89], which is then thermally decomposed at 165 °C to yield Al^0. The synthesis was carried out according the methods reported by Cui et al.[90] in the presence of PPh_3 as a stabilizer. This approach was chosen, since PPh_3 does not contain oxygen and does not, in contrast to the commonly applied carboxylic acid, lead to the formation of an oxide layer due to the presence of organically bound oxygen[99]. After the synthesis the powder was slowly air passivated and the characterizations were carried out applying this air passivated powder.

$$3\ LiAlH_4 + AlCl_3 \xrightarrow[\text{mesitylene}]{\substack{PPh_3 \\ 165\ °C,\ 2\ h}} 4\ Al + 3\ LiCl + 6\ H_2$$

***Scheme 11**: Synthesis of PPh_3 capped Al particles starting from $LiAlH_4$ and $AlCl_3$.*

Again, the formation of Al^0 was clearly confirmed by XRD measurements and ^{27}Al-SPE/MAS NMR techniques (Figure 24a and c). The reflections of fcc-Al are again clearly visible with no other crystalline phases being present. The signal at 1639 ppm in the solid-state NMR can be ascribed to Al^0, while the low intensity signal at around 0 ppm is due to the presence of amorphous surface Al_2O_3. In agreement with the literature[90], the size the resulting Al nanoparticles could be controlled by changing the Al : PPh_3 ratio, as was evidenced by DLS as well as XRD measurements (Figure 24b). Rietveld refinements revealed that the crystallite size was reduced from 118(2) nm when 2.3 eq of PPh_3 were used down to 65(1) nm when 5.8 eq of PPh_3 were applied, with the same trend being visible in the DLS measurements as well. The DLS measurements were carried out in methanol, since PPh_3 was largely removed upon washing (Chapter 3.1.3.1) resulting in a very poor dispersibility in nonpolar solvents. The hydrodynamic radius decreased from 50 ± 8 nm and 51 ± 14 nm when 2.3 eq and 3.5 eq of PPh_3 were used down to 25 ± 3 nm and 39 ± 8 nm when 4.7 eq and 5.8 eq of PPh_3 were applied. The differences between the values observed in XRD and DLS measurements can be explained by the different measurement methods used in these studies. The DLS measurement determines the number

weighted mean hydrodynamic radii of the particles dispersed in a solvent. This value is not necessarily equal to the actual particle size, since for example agglomerates will also be detected, while large sedimented particles will not be detected. In contrast, XRD analysis provides volume weighted mean values of the crystalline components only. The use of even higher amounts of PPh_3 was not possible since the solubility limit of PPh_3 in mesitylene was reached. Similarly, the use of less than 2.3 eq PPh_3 was problematic since an Al film formation on the surface of the reaction vessel started to occur. However, these results are in good agreement with the results reported by Cui et al.[90] who observed a size reduction from ~ 110 nm down to ~ 50 nm upon increasing the amount of PPh_3 from 1.25 eq up to 5 eq. A representative TEM image, in which strongly sintered and agglomerated particles were observed, as well as a TG measurement of these particles will be discussed in the following chapter.

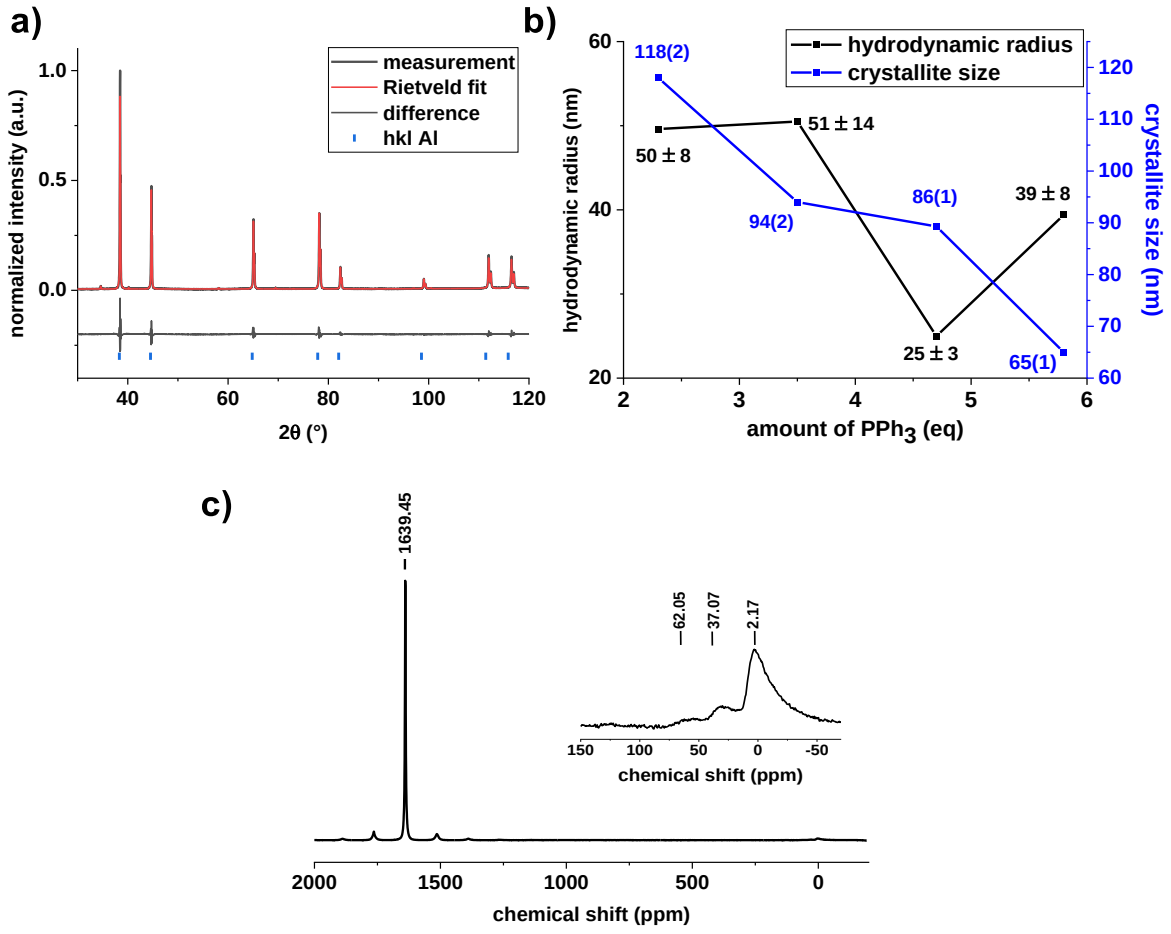

***Figure 24**: **a)** XRD measurement and Rietveld refinement of Al nanoparticles synthesized via a hydride reduction approach, **b)** hydrodynamic radii in methanol and crystallite sizes of Al nanoparticles synthesized via a hydride reduction approach in the presence of varying amounts of PPh_3, and **c)** ^{27}Al-SPE/MAS NMR (104 MHz) of Al nanoparticles synthesized via a hydride reduction approach.*

The use of other phosphines or phosphine oxides as stabilizers was also possible, as was evidenced by successful syntheses conducted in the presence of P(^{n}Bu$_3$), TOP, TOPO and PPh_3O (Figure 25). As

expected, a lower amount of 1.1 eq of the stronger coordinating TOP was sufficient to stabilize the resulting Al nanoparticles, which exhibited a crystallite size of 95(6) nm and hydrodynamic radius of 47 ± 9 nm. The formation of particles with large hydrodynamic radii of 95 ± 27 nm was observed upon applying P(^{n}Bu$_3$) as a stabilizer, even when the synthesis was carried out directly in a P(^{n}Bu$_3$) solution (30 eq). In general, trialkyl phosphines are exhibiting increased Lewis basicities compared to PPh$_3$ and are thus also commonly applied as nanoparticle stabilizers. A typical example is trioctylphosphine, which was also applied within this work for the preparation of Al particles (Chapter 3.1.3.2). Accordingly, the poor stabilizing properties observed for P(^{n}Bu$_3$) are likely due to sterical reasons, particularly due to its small size.

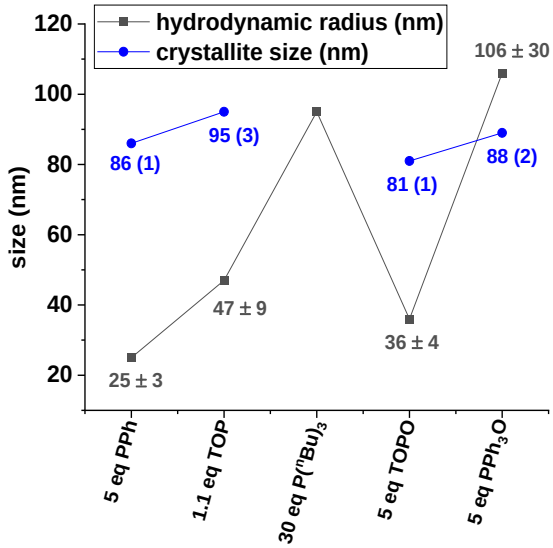

***Figure 25**: Crystallite sizes determined from Rietveld refinements and hydrodynamic radii in methanol of Al particles prepared via $LiAlH_4$ reduction of $AlCl_3$ in the presence of different phosphine stabilizers.*

3.1.3 Synthesis via catalytic decomposition

3.1.3.1 Comparison to the hydride reduction

Since the hydride reduction and the catalytic decomposition are both proceeding via a decomposition of H_3Al compounds, both approaches were compared regarding the size and morphology of the resulting particles. Therefore, Al particles were prepared via both methods under similar experimental conditions, particularly using the same stabilizer and reactant concentrations. Accordingly, the catalytic decomposition was carried out by decomposing H_3AlNEt_3 applying Ti(^{i}OPr)$_4$ as a decomposition catalyst in toluene solutions and in the presence of a PPh$_3$ stabilizer (Scheme 12). After

the synthesis the powder was slowly air passivated and the characterizations were done applying this air passivated powder.

$$H_3AlNEt_3 \xrightarrow[\text{toluene}]{\substack{PPh_3 \\ \text{cat. } Ti(O^iPr)_4 \\ 90\ ^\circ C,\ 15\ min}} Al + NEt_3 + {}^3/_2H_2$$

***Scheme 12**: Synthesis of PPh_3 capped Al particles via catalytic decomposition of H_3AlNEt_3.*

Again, the formation of fcc-Al was confirmed by XRD measurements as well as ^{27}Al-SPE/MAS NMR techniques (Figure 26a and b) and, similar as reported above, no other crystalline phases were detected in the diffraction patterns. The amorphous alumina from the surface passivation layer was again observed in the ^{27}Al SPE/MAS NMR spectrum by the signal at around 0 ppm. However, in contrast to the observations made for the hydride reduction approach, only a small and inconsistent dependence of the crystallite size from the concentration of PPh_3 was observed (Figure 26c). The largest crystallite size of 66(2) nm was observed for the particles synthesized in the presence of 4.7 eq of PPh_3 and the smallest crystallites with sizes of 51(1) nm were observed for the particles synthesized in the presence of 3.5 eq of PPh_3. Similarly, only a minor influence was observed in the DLS measurements, where the largest particles with a hydrodynamic radius of 105 ± 6 nm were observed when 2.3 eq of PPh_3 were used. The large radii observed for the particles synthesized in the presence of 4.7 eq PPh_3 are due to the presence of some large agglomerates and a broad particle size distribution. The distribution maximum was however at a similar size compared to the sample synthesized in the presence of 3.5 eq of PPh_3 with a size of 72 ± 2 nm. The less pronounced and inconsistent influence of the amount of PPh_3 in these decompositions can likely be explained by the release of 1 eq of NEt_3 from the triethylamine alane used as a precursor during the reaction, which can also act as capping agent itself. Moreover, it is exhibiting a higher basicity and a smaller size compared to PPh_3 and is thus negatively affecting the stabilizing effect of PPh_3 due to competitive interactions.

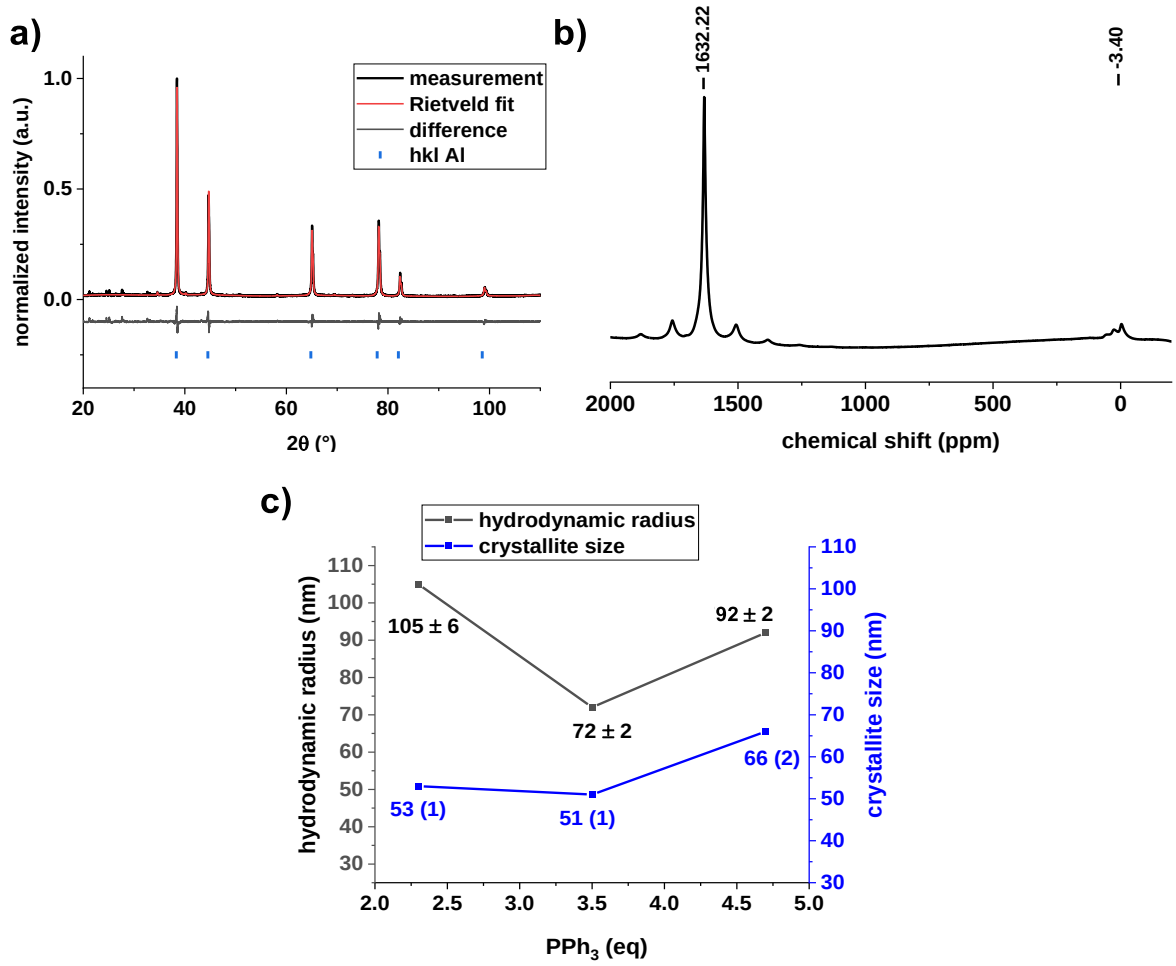

***Figure 26**: **a)** XRD measurement and Rietveld refinement of Al nanoparticles synthesized via a chemical reduction approach, **b)** ^{27}Al-SPE/MAS NMR (104 MHz) of Al nanoparticles synthesized via a chemical reduction approach, and **c)** hydrodynamic radii as well as crystallite sizes of Al nanoparticles synthesized via a chemical reduction approach in the presence of varying amounts of PPh_3.*

Comparing the DLS measurements of the particles formed in the presence of 4.7 eq PPh_3 (Figure 27a), smaller particles as well as narrower particle size distribution were observed when the hydride reduction approach was applied compared to the catalytic decomposition approach. However, as can be seen in the TEM images (Figure 27b and c), the particles synthesized via a hydride reduction approach are severely agglomerated and aggregated, with the single particles being hardly visible. For the particles synthesized via the catalytical decomposition approach, an agglomeration of the particles is also visible, the single particles are however clearly visible. For these particles, the size determined from the TEM measurements was 78 ± 26 nm (Figure 27d) and is in good agreement with the crystallite size of 66(2) nm, however smaller than the hydrodynamic radius of 92 ± 15 nm, which can be attributed to agglomeration effects. A reason for the stronger agglomeration in case of the hydride reduction might be the slower reaction from a heterogenous reaction mixture. Due to their severe aggregation, no particle size distribution could be obtained for these particles from the TEM images.

Accordingly, the much smaller hydrodynamic radii observed for these particles in the DLS measurements is likely due to the deposition of these large agglomerates during the equilibration step, only leaving a small amount of non-agglomerated particles in solution.

TGA measurements (Figure 27e) were carried out in an atmosphere of synthetic air (N_2:O_2 32:8; 40 ml/min) in order to obtain a controlled oxidation of the Al nanoparticles. The oxidation of the particles is evident at temperatures > 500 °C in both samples, where the typical twostep oxidation pattern can be observed. The steep mass increase at a temperature of 900 °C is due to an isothermal segment of 15 min at this temperature, which was applied to allow a complete oxidation of the particles. The lower total mass gain observed for the particles synthesized via the catalytical decomposition approach is indicating a lower total Al^0 content and Al^0 contents of 56 % and 77 % were calculated for the particles prepared via the catalytic decomposition and the hydride reduction respectively. The lower Al^0 contents can be explained by the lower degree of agglomeration and sintering observed above, assuming a similar oxide shell thickness in both cases.

Moreover, an increased mass loss of 21.7 % up to a temperature of 400 ° C was observed for the particles prepared via the catalytic decomposition approach, compared to 9.4 % for the particles synthesized via the hydride reduction approach. This higher organic content is likely also caused by the larger surface area due to the lower degree of agglomeration and sintering as well as by the presence of coordinating NEt_3. This was further evidenced by CHN analyses: 10.56 % CHN content (7.47 % C, 2.40 % H, 0.69 % N) for the particles synthesized via catalytic decomposition compared to 2.34 % CHN content (0.89 % C, 1.33 % H and 0.12 % N) for the particles synthesized via hydride reduction. For the CHN analyses, the particles were dried in vacuo at 80 °C for 7 days and the presence of nitrogen was still observed in the particles synthesized via the catalytic decomposition approach. This supports the hypothesis that the NEt_3 released upon the decomposition of the alane precursor acts as an additional capping agent. Moreover, the presence of phosphorous was confirmed by applying solid-state NMR techniques for the particles prepared via the catalytic decomposition approach, while no residual phosphorus was observed for the particles prepared via the hydride reduction approach. This further confirms the lower organic contents of the particles prepared via the hydride reduction approach. For the particles prepared via the catalytic decomposition approach signals in the range from 20 – 50 ppm were observed within the ^{31}P NMR spectra (Figure 27f), which lies in a typical range reported for PPh_3 capped metal nanoparticles[306,307], confirming the PPh_3 capping of the formed Al particles (cf. free PPh_3 – 8 ppm[306]).

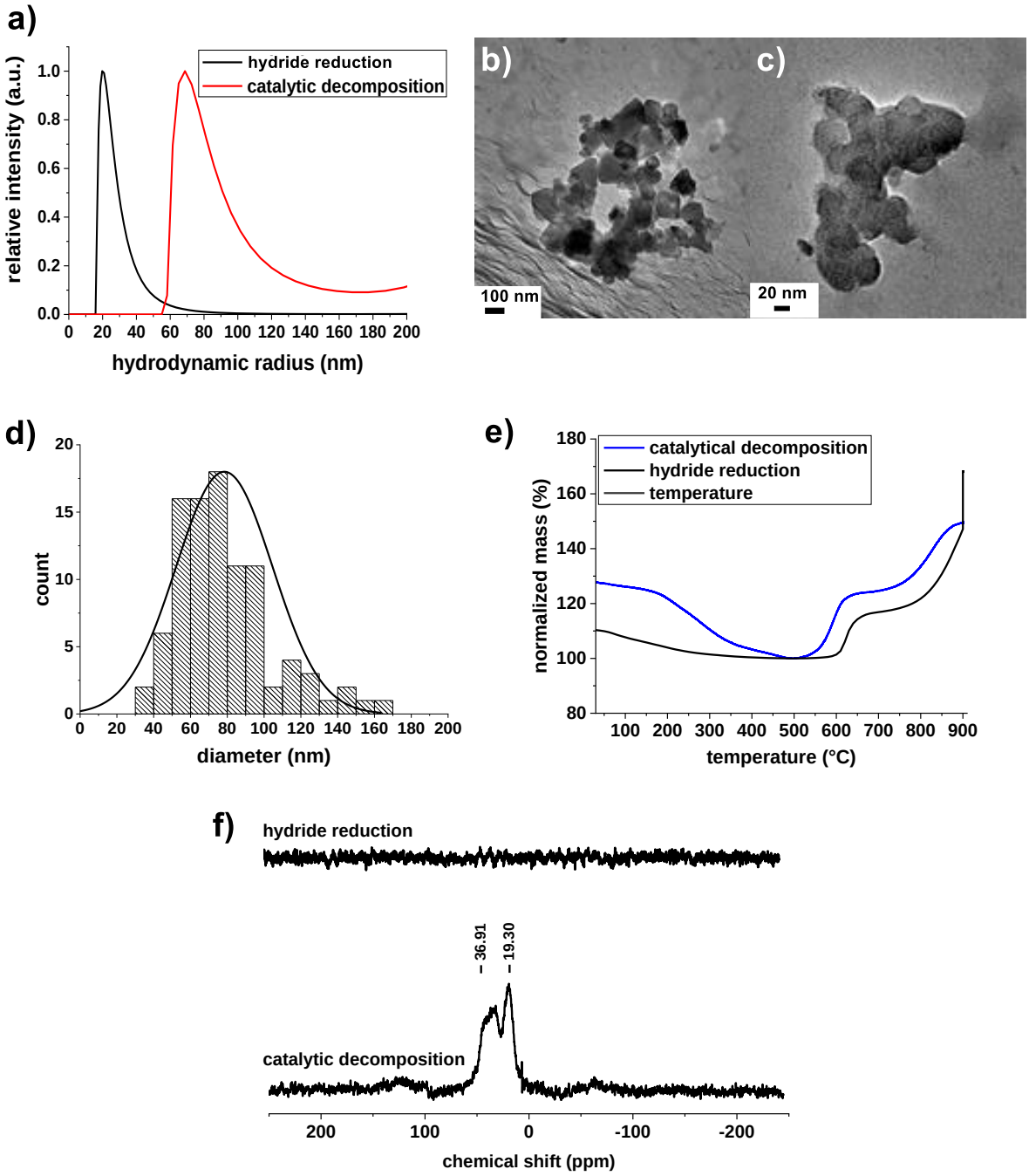

***Figure 27**: **a)** DLS measurements of Al particles synthesized via hydride reduction and catalytic decomposition in the presence of 4.7 eq of PPh_3 in methanol, **b)** TEM image of Al particles synthesized via catalytic decomposition in the presence of 4.7 eq of PPh_3, **c)** TEM images of Al particles synthesized via hydride reduction in the presence of 2.3 eq of PPh_3, **d)** particles size distribution for the particles prepared via catalytic decomposition in the presence of 4.7 eq of PPh_3 obtained from the TEM image by counting 95 particles, **e)** TGA measurements of Al nanoparticles synthesized via hydride reduction and catalytic decomposition approaches in the presence of 4.7 eq PPh_3 (10 K/min; N_2:O_2 32:8), and **f)** ^{31}P CP/ MAS solid-state NMR (162 MHz) of the Al particles prepared via hydride reduction and catalytic decomposition approaches in the presence of 4.7 eq of PPh_3.*

Although the hydride reduction and the catalytic decomposition both are proceeding via a H_3Al decomposition, the hydride reduction approach has several disadvantages, including for example the heterogenous reaction mixtures, the long reaction times as well as the high reaction temperatures of

165 °C. Moreover, the particles were more severely sintered and thus, no more efforts were made to further study or optimize this synthesis approach. The catalytic decomposition was found to be a more promising approach for the preparation of non-agglomerated Al particles from homogenous solutions. Accordingly, this synthesis approach was studied in more detail and the reaction parameters were systematically varied as will be described in the following chapter.

3.1.3.2 Systematic variation of the reaction parameters

As summarized in Chapter 1.3.1.5, the catalytic decomposition was applied many times for the preparation of Al nanoparticles throughout the literature. Although numerous reaction conditions have been applied and particles with sizes from 5 up to several hundred nanometers were prepared, a systematic study of the influence of the reaction parameters on the size and morphology of the resulting particles was hardly carried out. In many of these studies similar reactants, particularly H_3AlNMe_2Et as a precursor and $Ti(O^iPr)_4$ as a catalyst, were applied and the reaction systems were mainly differing in the applied stabilizer. Moreover, the studies can often not be compared directly, due to varying reactant concentrations, slightly different synthesis protocols or different experimental set-ups.

Thus, to study the influence of the reaction parameters on the size and morphology of the resulting Al particles, a systematic variation of the reaction parameters in the catalytic decomposition system was carried out. Various precursors, including a phosphine alane, a carbene alane, a H_3Al-THF adduct, and amine alanes containing various amines were applied. The decompositions were carried out in varying polar and non-polar solvents, such as THF, diethylene ether, hexane, cyclohexane, and toluene. Moreover, the reaction temperature was varied from 25 °C to 100 °C and several transition metal catalysts, also containing different alkoxy ligands were studied. Also, different amine and phosphine stabilizers, such as PPh_3, TOP and $N(Oct)_3$ were applied.

The resulting Al particles were characterized applying XRD, DLS, and TEM techniques and the reaction conditions were optimized towards homogenous reaction mixtures, short reaction times as well as particle sizes < 50 nm. Regarding these requirements, the best results were obtained applying H_3AlNEt_3 or $H_3Al(THF)$ as a precursor, $Ti(O^iPr)_4$ as a catalyst, $N(Oct)_3$ or PPh_3 as stabilizers, and toluene as a solvent.

The results have been published as a paper in *Dalton Transactions* from The Royal Society of Chemistry.

Klein, T.; Kickelbick, G. Aluminum Nanoparticle Preparation via Catalytic Decomposition of Alane Adducts – Influence of Reaction Parameters on Nanoparticle Size, Morphology and Reactivity. *Dalt. Trans.* **2020**, *49*, 9820–9834 – Reproduced by permission of The Royal Society of Chemistry.[308] (https://doi.org/10.1039/D0DT01820A)

Author contributions:

T. Klein had the original idea, carried out all the synthetic work, characterized the particles, and interpreted the results. He carried out the DLS and TEM measurements and conducted the Rietveld refinements. He prepared the initial draft of the manuscript.

G. Kickelbick gave scientific input, supervised the work, and discussed the results. He proof-read and edited the final manuscript.

Dalton Transactions

ROYAL SOCIETY OF CHEMISTRY

PAPER

Cite this: *Dalton Trans.*, 2020, **49**, 9820

Aluminum nanoparticle preparation *via* catalytic decomposition of alane adducts – influence of reaction parameters on nanoparticle size, morphology and reactivity†

Thomas Klein and Guido Kickelbick *

Al nanoparticles represent one of the most challenging classes of metal nanoparticles in synthesis and handling due to their high chemical reactivity and their affinity to oxidation. A promising wet chemical preparation route is the catalytic decomposition of alane adducts. In the current systematic study, we investigated the influence of various reaction parameters, such as precursors, catalysts, solvents, reaction temperatures, capping agents, and concentrations of the reactants on the size and morphology of the resulting Al nanoparticles. One major goal was the optimization of the reaction parameters towards short reaction times. Our studies revealed that Ti alkoxides, such as $Ti(O^iPr)_4$, are much more efficient decomposition catalysts compared to other related metal catalysts. Optimized conditions for full conversion times smaller than 15 min are temperatures between 90–100 °C and non-polar solvents such as toluene. Amine alanes containing short alkyl chains, for example H_3AlNMe_2Et or H_3AlNEt_3, were the most suitable precursors, leading to the formation of the smallest nanoparticles. The use of weakly coordinating capping agents like amines and phosphines should be preferred over the commonly employed carboxylic acids because they do not accelerate the formation of an amorphous oxide shell upon binding to the particle surface. In conclusion, the best reaction parameters for a fast synthesis of Al nanoparticles *via* a catalytic decomposition approach are the combination of sterically less hindered amine alanes applying a Ti catalyst in toluene solutions in the presence of amine or phosphine stabilizers at elevated temperatures.

Received 20th May 2020,
Accepted 22nd June 2020

DOI: 10.1039/d0dt01820a

rsc.li/dalton

Introduction

Al nanoparticles are exhibiting a very high reactivity and can thus be employed in various applications, such as nanothermites,[1] explosives,[2] environmentally friendly propellants,[3] as well as self-propagating reaction syntheses.[4] Most commonly Al nanoparticles are synthesized *via* physical methods including gas evaporation methods,[5] plasma synthesis,[6] laser ablation[7,8] and exploding wire techniques.[9,10] The most frequently applied wet chemical synthesis approach is the catalytic decomposition approach, introduced by Haber and Buhro.[11] Within this approach, alane adducts (typically amine alanes) are decomposed applying $Ti(O^iPr)_4$ as a catalyst. In the original report,[11] H_3AlNMe_2Et was decomposed in mesitylene using $Ti(O^iPr)_4$ as a catalyst resulting in the formation of relatively large Al grain sizes >100 nm, since no stabilizer was present in the reaction mixture. The clean-up of the resulting nanoparticles is very convenient, since typically only gaseous and/or volatile side products are formed. The decomposition mechanism was clarified very recently by Clark *et al.*[12] applying EPR and NMR techniques. Their studies revealed $Ti(O^iPr)_3$ to be the catalytically active species, which is produced from the initially formed AlH_3–$Ti(O^iPr)_4$ complex by reductive elimination of H_2 and abstraction of one isopropoxy ligand by Al. Subsequently, $Ti(O^iPr)_3$ catalyzes the decomposition of 2 AlH_3 to 2 Al^0 *via* a 4 step decomposition mechanism containing several reductive elimination steps of H_2.

Typical capping agents used in this approach are carboxylic acids,[13–19] epoxides,[20–24] and the coating with transition metals.[25] The size of the resulting Al particles can be controlled by changing the amount of the stabilizer[16] or changing the solvent composition.[13,19] Bulkier amine alanes, such as $H_3AlNMePyr$ and $H_3AlN[(C_4H_8)(CH_3)]$, have been reported to

Saarland University, Inorganic Solid State Chemistry, Campus C4.1, 66123 Saarbrücken, Germany. E-mail: guido.kickelbick@uni-saarland.de

†Electronic supplementary information (ESI) available: Crystallite sizes, hydrodynamic radii and reaction conditions for Al particles prepared from additional transition metal catalysts; DLS measurements of the particles prepared in various solvents; TEM images of the particles prepared from various precursors; XRD and DLS measurements of the particles prepared in the presence of various amounts of PPh_3; CHN analyses of the particles prepared in the presence of various stabilizers; DLS measurements of the particles prepared applying various catalyst concentrations; syntheses and characterizations (NMR and IR measurements) of the alane precursors. See DOI: 10.1039/d0dt01820a

decompose more slowly compared to H_3AlNMe_3 and H_3AlNMe_2Et.[17,19] Similarly, the decompositions have been reported to be faster and more efficient upon increasing the reaction temperature.[19]

Although, the catalytic decomposition of amine alanes is the most frequently applied method for the wet chemical preparation for Al nanoparticles, to the best of our knowledge, a systematic variation of the reaction conditions has not been carried out until yet. For example, $Ti(O^iPr)_4$ has been applied almost exclusively as a decomposition catalyst, while H_3AlNMe_2Et or H_3AlNMe_3 are typically applied as alane precursors and only a few studies are known applying alternative precursors. Although a broader variety of solvents and stabilizers has been reported, these studies can often not be directly compared to each other, due to various reasons such as varying synthetic protocols, changing experimental setups, or altering reactant concentrations. Accordingly, a judgement of the influence of the reaction conditions in the catalytic decomposition of molecular precursors for the formation of Al particles is difficult. This was our motivation to systematically study the influence of reaction parameters, such as precursors, catalysts, catalyst ratio, solvents, reaction temperatures, capping agent composition, and concentration on the decomposition reaction. Particularly, besides the commonly applied amine alanes, other classes of alanes, such as phosphine or carbene alanes are known, which have not been applied within this reaction system yet and which might represent an additional option to control the particle size and morphology. A similar possibility represents the application of Ti catalysts with varying alkoxy ligands, which also has not been reported before. Moreover, our goal was also the optimization of the reaction parameters towards short reaction times, homogeneous reaction mixtures, and a one-pot procedure, regarding a possible future continuous wet-chemical synthesis of these Al particles.

Experimental

Materials

Tributylamine (NBu_3, >98%) was purchased from TCI Japan (Tokyo, Japan) and trioctylamine ($N(Oct)_3$ < 92.5%) as well as $Ti(O^tBu)_4$ (>98%) were obtained from Merck (Darmstadt, Germany). Triphenylphosphine (PPh_3, 99%) and $Ti(O^nBu)_4$ (97%) were purchased from Sigma-Aldrich (St. Louis, USA). Trioctylphosphine (TOP, 97%), $Ti(O^iPr)_4$ (97%), titanium(IV) 2-ethylhexoide (97%), and tributylphosphine ($P(Bu)_3$, 93%) were supplied by abcr (Karlsruhe, Germany). Triphenylamine (98%) and 1,2-epoxyhexane (96%) were obtained from Alfa Aesar (Ward Hill, USA). Tricyclohexylphosphine (>97%) was delivered from Carbosynth (Berkshire, United Kingdom). Toluene, THF, hexane, acetonitrile, and diethyl ether were purified in a MBraun solvent purification system. All chemicals were used as received unless stated otherwise. The reactions were carried out under an Ar atmosphere using either a glove box or Schlenk line techniques.

Synthesis

The synthesis of the different alane precursors was carried out according to known procedures and is reported in the literature. H_3AlNEt_3,[26] H_3AlNMe_2Et,[26] H_3AlNBu_3,[26] $H_3AlNOct_3$ [26] and H_3AlNMe_3 [27] were chosen as amine based alanes, while $[H_2Al(PMDTA)]^+[AlH]^-$ [28] and $H_3Al{\cdot}DABCO$ were chosen as amine based ionic and polymeric alanes, respectively. $H_3Al{\cdot}DABCO$[29] was obtained as a mixture of polymeric $H_3Al{\cdot}DABCO$ and H_3AlNEt_3. $H_3Al{\cdot}THF$,[30] $H_3Al{\cdot}PCy_3$ [31] and $H_3Al{\cdot}IMes$[32,33] were synthesized representing O, P and C based alanes. *N*,*N*,*N*′,*N*′-Tetraoctylethylendiamine (TOEDA)[34] was also synthesized following literature procedures. Precautions must be taken, as explosions may occur if the syntheses are not carried out properly. Moreover, the prepared amine alanes themselves are revealing explosion hazards.

Al nanoparticles *via* catalytic decomposition. In an atmosphere of Ar, 2.5 ml (16 mmol) of H_3AlNEt_3 and 21 g (81 mmol) of PPh_3 were dissolved in 100 ml of toluene. To this solution 16 µl of $Ti(O^iPr)_4$ in 20 ml of toluene were added. The resulting mixture heated to 90 °C and stirred at this temperature for 15 min. The formed grey solid was collected by centrifugation (10 000 rpm; 10 min), washed three times with 20 ml of toluene and dried *in vacuo* at room temperature. During the work-up steps, the Al particles dispersions were carefully exposed to the ambient air, to allow a passivation of the particles by the formation of a passivating oxide layer. After drying at reduced pressure, the air passivated particles were found to be not spontaneously combustible in all samples. For reproducibility reasons, every decomposition was carried out within the same reaction flask as well as heating equipment.

Characterization

Transmission electron microscope (TEM) measurements were carried on a JEOL JEM-2010. TEM samples were prepared by drop coating nanoparticle dispersions in methanol on the carbon coated copper grids (Plano S160-3). The particle size distributions were obtained from the TEM or SEM images by measuring 100 particles using the software ImageJ.[35]

Powder X-ray diffraction (PXRD) patterns were measured on a Bruker D8-A25-Advance diffractometer in a Bragg–Brentano geometry using Cu K_α radiation. A 2θ-range from 7 to 120° was recorded using a step size of 0.013° and a total measurement time of 1 h. The samples were prepared by drop coating the dispersed and homogenized nanoparticles in hexane onto glass sample holders. Sample compositions and crystallite sizes were determined from Rietveld refinements using TOPAS 5.1.[36] The background was fitted applying a Chebychev polynom (15^{th} degree) and a fundamental parameter approach[37] was used to calculate the instrumental line broadening. Crystal structures obtained from the crystallographic open database (COD)[38] were used to carry out the Rietveld refinements. For pure Al the entry COD ID 2300250 and for γ-Al_2O_3 the entry COD ID 2107301 were used in the refinements.

The elemental analyses were conducted on an Elementar Vario Micro cube. Thermogravimetric analyses (TGA) were carried out on a Netzsch TG F1 Iris using a heating rate of 10 K min^{-1} in an atmosphere of synthetic air (N_2/O_2 32 : 8, 40 ml min^{-1}). The samples were heated up to 900 °C in open alumina crucibles and hold at this temperature for 15 min.

Dynamic light scattering (DLS) measurements were carried out at 25 °C using an ALV Compact Goniometer. A scattering angle of 90° was used and the samples were prepared by dispersing the particles in methanol. The dispersions were ultrasonicated for 10 min, filtered through 0.45 μm PTFE filters and equilibrated for 5 minutes before the measurements.

The onset temperatures given within this manuscript are referring to the temperatures at which a first gas evolution and a formation of a grey dispersion was visible by the naked eye upon heating the reaction mixture to a temperature of 100 °C.

Results and discussion

Within our studies Al nanoparticles were produced *via* catalytic decomposition of alane precursors (Scheme 1). The advantages of this approach are the facile synthetic parameters including: (i) homogenous solutions, (ii) short reaction times, (iii) moderate reaction conditions, and (iv) straightforward workup due to the formation of volatile side-products. Accordingly, we systematically varied and optimized the reaction parameters aiming at small particle sizes as well as short reaction times. Since increased reaction temperatures were found to be advantageous regarding short reaction times, the decompositions were generally carried out at temperatures between 90 °C and 100 °C within this work.

Influence of the decomposition catalyst

$Ti(O^iPr)_4$ has been applied almost exclusively as a catalyst for the synthesis of Al nanoparticles starting from alane precursors. Ti compounds are known to catalyse the decomposition of alanes in the solid state[39] as well as in solution.[40,41] However, the reason for the superior activity of Ti-based catalysts in these decompositions has not yet been fully understood.[39] The decomposition mechanism of amine alanes in coordinating solvents was suggested recently identifying $Ti^{3+}(O^iPr)_3$ to be the catalytically active species.[12] As reported in the literature,[12,41,42] Ti is known to show a superior catalytic activity compared to other transition metals. Accordingly, we focused in our study on the application of various Ti alkoxides. Besides $Ti(O^iPr)_4$ only very few other Ti compounds have been applied as a catalyst. For example, $TiCl_4$ was reported to result in a faster decomposition but similar particle size compared to $Ti(O^iPr)_4$.[12] To study the influence of the alkoxy ligand we applied various Ti alkoxides, which particularly differed in the bulkiness of the ligands. Additionally Sn compounds have been applied, which are often considered as alternatives to Ti Lewis acid catalysts.

During these studies, H_3AlNEt_3 was used as a precursor together with 5 eq. of PPh_3 as stabilizer and toluene as the solvent. H_3AlNEt and PPh_3 as well as the reactant concentrations have been selected based on the observations described further below. Fig. 1 summarizes the reaction conditions as well as the hydrodynamic radii and the crystallite sizes of the resulting particles. Without applying a catalyst, no decomposition of H_3AlNEt_3 could be observed after heating to reflux for 2 h, which agrees with its reported decomposition temperature of about 165 °C.[11] A decomposition reaction started at considerably lower temperatures upon adding Ti^{4+} compounds to the reaction mixture. Applying $Ti(O^iPr)_4$ and $Ti(O^nBu)_4$ a visible gas evolution started to occur at around 50 °C that stopped after about 5 min. In contrast, the bulky Ti compounds $Ti(O^tBu)_4$ and $Ti(OC_8H_{17})_4$ showed a lower reactivity and no gas evolution was evident until reaching a temperature of 60 °C. The hydrodynamic radii as well as the crystallite sizes of the resulting particles increased with increasing bulkiness of the Ti catalyst (Fig. 2d) and particles with a hydrodynamic radius of 44 ± 1 nm were observed for $Ti(O^nBu)_4$, while a radius of 105 ± 4 nm was determined applying $Ti(OC_8H_{17})_4$. The same trend can be observed if the crystallite sizes were compared, which increased from 68(4) nm and 62(3) nm when $Ti(O^iPr)_4$ and $Ti(O^nBu)_4$ were used up to 85(5) nm applying $Ti(OC_8H_{17})_4$.

Scheme 1 Synthesis of Al nanoparticles *via* a catalytic decomposition approach.

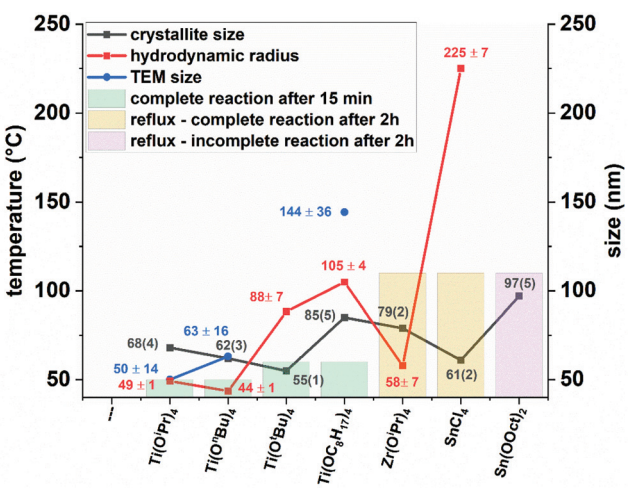

Fig. 1 Crystallite sizes and reaction conditions observed for decomposition of H_3AlNEt_3 applying different transition metal catalysts. The concentrations used were as follows: 35 mM H_3AlNEt_3, Al : PPh_3 5 : 1 and cat. : Al 2 ppm. The crystallite sizes were determined from Rietveld refinements of the dried powders. The bars are representing the observed onset temperatures of the decompositions.

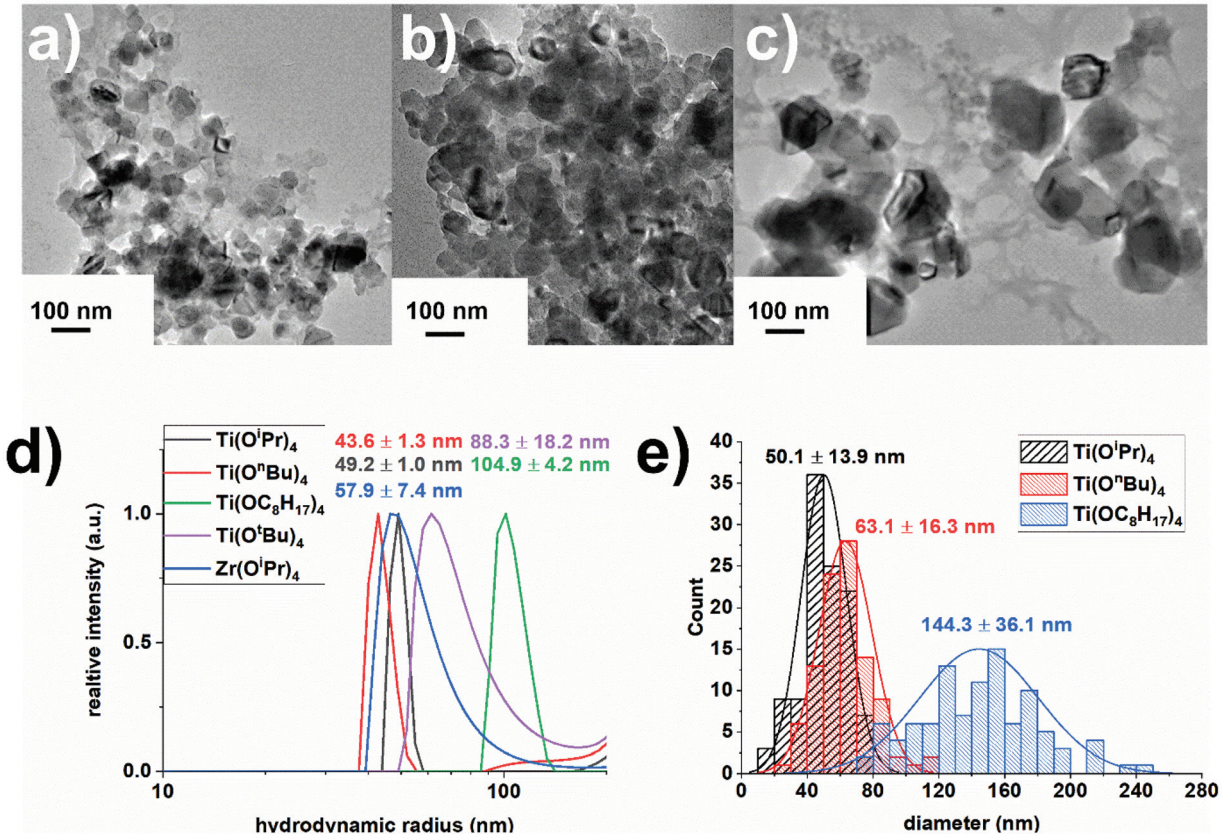

Fig. 2 TEM image of Al particles obtained by applying (a) Ti(O^{i}Pr)$_4$, (b) Ti(O^{n}Bu)$_4$, and (c) Ti(OC$_8$H$_{17}$)$_4$ as a catalyst; (d) DLS measurements of Al nanoparticles synthesized applying different decomposition catalysts in methanol; (e) particle size distributions of the particles shown in (a)–(c).

We assume that with increasing bulkiness of the Ti catalyst the decomposition reactions become slower due to steric reasons. Thus, less nuclei are formed during the initial stages of the decomposition and therefore larger particles are observed.

In all samples the crystallite sizes are smaller than the hydrodynamic radii (note, that in Fig. 1 the hydrodynamic radii are given, while the crystallite size is referring to a diameter). The sizes determined from the DLS measurements are number weighted mean values of the hydrodynamic radii of the particles in solution. The values determined from the Rietveld refinements are volume weighted mean values of the crystalline contents only, whereas the TEM sizes are the number weighted mean values of the particles including the crystalline and amorphous contents. Accordingly, the large values determined for the hydrodynamic radii in some samples within Fig. 1 can likely be ascribed to the formation of agglomerates.

The size increase upon applying bulkier alkoxides at the metal centre, as well as the broadening of the particle size distribution is further confirmed from TEM images (50.1 ± 13.9 nm for Ti(O^{i}Pr)$_4$), 63.1 ± 16.3 for Ti(O^{n}Bu)$_4$ and 144.3 ± 36.1 for Ti(OC$_8$H$_{17}$)$_4$ (Fig. 2)). These sizes are in good agreement to the crystallite sizes determined from Rietveld refinements indicating the Al particles being single crystallites.

Other metal compounds showed a very poor catalytic effect within these decompositions, resulting in long reaction times as well as incomplete reactions (Fig. S1†).[12,41,42] Sn compounds, which are often considered as alternatives to Ti Lewis acid catalysts, also showed very poor catalytic properties (Fig. 1).

In summary, if short reaction times, small particle sizes and mild reaction conditions are required, preferably Ti catalysts with small ligands are clearly preferred. Hence, all other studies were carried out using Ti(O^{i}Pr)$_4$ as a decomposition catalyst.

Influence of the type of solvent

Within the literature, the decomposition of amine alanes is mostly carried out in nonpolar solvents, particularly toluene, as well as polar, coordinating solvents such as THF and diethyl ether. To compare the performance of these solvents we have thus carried out the decomposition in toluene, THF, and diethyl ether solutions under comparable conditions. Besides, tetraglyme was selected as a highly coordinating example, to further study the influence of the coordinating properties of the solvent on the particle formation. Moreover, cyclohexane and hexane were chosen as nonaromatic analogues to toluene, which are particularly differing in their boiling points.

The presence of large amounts of stabilizer, such as 5 eq. TOP or $N(Oct)_3$, might influence the decomposition of the alane precursor. Thus, these reactions were carried out in the presence of a small amount of 1,2-epoxyhexane (Al : epoxyhexane 4 : 1), which has been shown in the literature to be an effective capping agent.[23] Fig. 3 summarizes the reaction conditions as well as the crystallite sizes found for the Al nanoparticles obtained in various solvents.

The decomposition in polar, coordinating solvents was examined using diethyl ether, tetraglyme and THF as examples. In general, these solvents were found to be not suitable for the preparation of Al particles under the conditions applied within our work. Although, the use of THF was reported in previous publications to result in faster reaction rates compared to 1,4-dioxanes,[12] which was attributed to an increased stability of the intermediately formed Ti–H–Al clusters upon applying the bidentate 1,4-dioxane.[12] The structure of these intermediately formed species as well as the influence of coordinating molecules on these species has already been extensively studied and confirmed in the literature[12] and shall thus not be discussed in more detail within this study. Based on the enhanced stabilization of the intermediately formed Ti–H–Al clusters, the application of these coordinating solvents resulted in slow and thus incomplete reactions and low yields. The use of the highly coordinating tetraglyme thus resulted in a very high onset temperature of 180 °C and very small crystallite sizes, which can be attributed to an incomplete reaction. Although a lower onset temperature of 65 °C could be observed applying THF, the reactions were still found to be incomplete and very low yields of Al nanoparticles with larger diameters were isolated. In diethyl ether, no formation of Al particles could be observed at reflux temperature upon heating for 3 h.

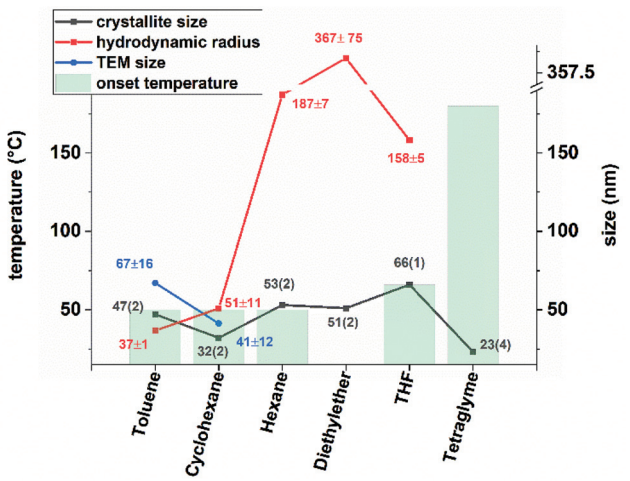

Fig. 3 Crystallite sizes, hydrodynamic radii, TEM sizes and reaction conditions observed for decomposition of H_3AlNEt_3 in different solvents. The concentrations used were as follows: 35 mM H_3AlNEt_3, Al : epoxyhexane 4 : 1 and cat. : Al 2 ppm. The crystallite sizes were determined from Rietveld refinements of the dried powders. The bars are representing the observed onset temperatures of the decompositions.

However, when diethyl ether was removed *in vacuo*, the concentration of the catalyst increased, finally leading to a decomposition of the alanes, resulting in the formation of Al powder with large crystallite sizes. This result is in good agreement with reports in the literature, where the reaction mixtures in diethyl ether were typically stirred overnight. Tertiary amines or phosphines like $N(Oct)_3$ or TOP were also found to lead to slow decomposition rates and low yields upon examining various stabilizers (see below) and were thus not further studied at this point. Moreover, the much larger hydrodynamic radii compared to the crystallite size observed for THF and diethyl ether is indicating a high degree of agglomeration. Again, the large hydrodynamic radii observed in some samples in Fig. 3 can be ascribed to the formation of agglomerates, which were in some samples also visible with the naked eye.

In a next step, non-coordinating, nonpolar solvents have been applied since they are not capable of stabilizing the intermediately formed Ti–H–Al clusters by coordination and can thus be expected to lead to increased decomposition rates. Hexane, cyclohexane, and toluene have been chosen as examples. Applying these solvents increased reaction rates and thus more complete reactions as well as lower onset temperatures were observed compared to the coordinating solvents reported above. The most promising results were observed applying cyclohexane and toluene. In both cases, the onset temperature of the decomposition was 50 °C and no more gas evolution was evident after heating for about 5 minutes. The crystallite sizes were determined to be 32(2) nm in the case of cyclohexane and 47(2) nm when toluene was used as a solvent. However, due to its lower boiling point, slower decomposition reactions and thus longer reaction times and larger Al crystallites were observed when hexane was used as a solvent. We assume, that the slower decomposition might lead to the formation of less nuclei during the initial stages of the decomposition and therefore lead to the formation of the observed larger particles.

DLS measurements (Fig. S2†) confirmed these results and for the particles synthesized in hexane large hydrodynamic radii as well as the formation of large agglomerates were clearly visible. Similar hydrodynamic radii were observed for the particles synthesized in toluene and cyclohexane, for which hydrodynamic radii of 37 ± 1 nm and 51 ± 11 nm could be determined. However, much broader particles size distributions were observed when cyclohexane was used as a solvent, which can likely be attributed to the more pronounced agglomeration of the particles visible in the TEM images, compared to the sample prepared in toluene.

Since the most promising results were obtained when cyclohexane and toluene were used as solvents the resulting particles were further characterized applying TEM. Nanoparticles obtained in cyclohexane formed large spherical agglomerates (Fig. 4) and the particle size was determined to be 41.2 ± 11.6 nm, which is in good agreement with the crystallite size determined from the Rietveld refinements. The particle diameter of the particles obtained from toluene was 67.12 ± 15.6 nm, which is also in good agreement with the value

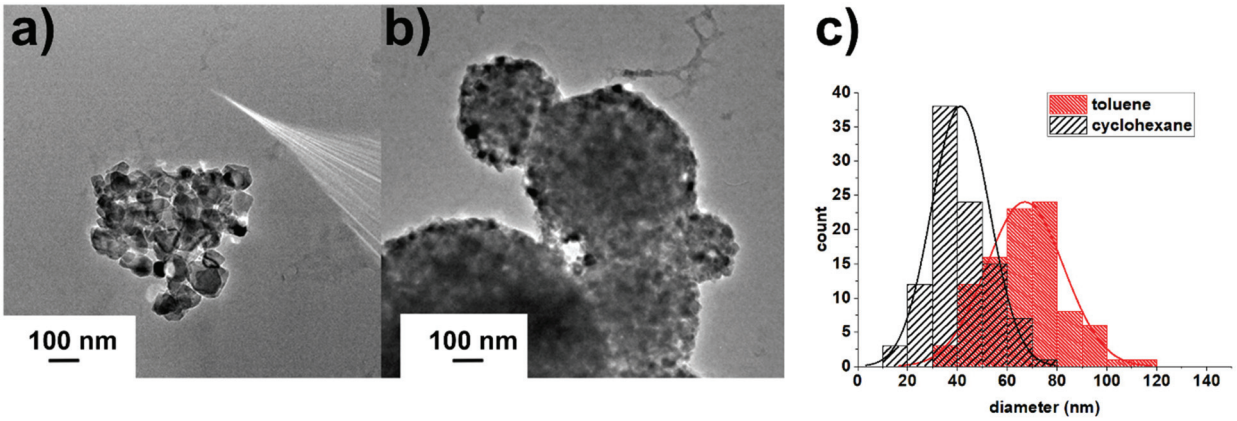

Fig. 4 TEM images of Al nanoparticles synthesized from H_3AlNEt_3 in different solvents. The concentrations used were as follows: 35 mM H_3AlNEt_3, Al : epoxyhexane 4 : 1 and cat. : Al 2 ppm. (a) Toluene, (b) cyclohexane, (c) particle size distributions of the Al particles shown in (a) and (b).

obtained from the Rietveld refinements. Although an agglomeration is also visible, it is clearly much less pronounced compared to the particles synthesized in cyclohexane.

As indicated by the results summarized above, the use of non-polar, non-coordinating solvents should be clearly preferred if short reaction times are the goal. This does particularly not exclude the general applicability of polar solvents as was also demonstrated several times throughout the literature.[12,17] The shortest reaction times together with the highest yields could be observed for the reactions carried out in toluene and cyclohexane. Due to a much lower degree of agglomeration further studies were carried out in toluene solutions.

Influence of the type of precursor

The most common Al precursors for the synthesis of Al nanoparticles are amine alanes, particularly the commercially available H_3AlNMe_2Et. Many more alane adducts, containing varying amines as well as other ligands such as phosphines or carbenes alanes are known. However, these compounds have, to the best of our knowledge, not been applied for the preparation of Al nanoparticles. Studies from the literature indicate, that the applied Al precursor might have a significant influence on the size and morphology of the formed Al particles.[17,19] We thus applied various molecular AlH_3 adducts to examine their general suitability for the synthesis of Al nanoparticles and to study the effect of the alane ligand on the decomposition as well as on size and morphology of the resulting Al particles.

H_3AlNMe_3, H_3AlNMe_2Et, H_3AlNEt_3, H_3AlNBu_3, and $H_3AlNOct_3$ were chosen as model systems for the amine alane precursors containing amines with different alkyl chain lengths. $H_3Al{\cdot}DABCO$ was selected as a precursor exhibiting a polymeric structure,[43] while $[H_2Al(PMDTA)]^+[AlH]^-$ was chosen as an ionic precursor. $H_3Al{\cdot}THF$ and PCy_3 were chosen as model systems of oxygen- and phosphorous-based donor molecules. As a representing carbon-based precursor, we used $H_3Al{\cdot}IMes$. In the case of the phosphine and carbene alanes the presence of bulky ligands is mandatory due to stability reasons.

The different Al containing precursors were employed in the synthesis of Al nanoparticles in toluene using $Ti(O^iPr)_4$ as a decomposition catalyst and 0.25 eq. $N(Oct)_3$ as a stabilizer. As was evidenced by PXRD measurements of the resulting powders, all precursors could be decomposed to fcc Al^0. Fig. 5 summarizes the onset temperatures of the decompositions as well as the crystallite sizes and hydrodynamic radii of the resulting particles.

A decrease of the decomposition rate of AlH_3 derivates can be correlated to an increase of the strength of the donor–acceptor interactions within the AlH_3 derivates.[41] Accordingly, the phosphine alane, bearing the weakest donor–acceptor interactions, decomposes at the lowest temperature of 45 °C, while decomposition of the carbene alane was found to be much slower, due to its strong donor–acceptor interactions. When $H_3Al{\cdot}IMes$ was used as a precursor, no abrupt gas evolution could be observed. Instead, a slow formation of a grey dispersion was occurring upon heating to reflux for 15 min, thus resulting in increased reaction times of 30 min. The decomposition of the amine alanes as well as of the THF adduct occurred at similar temperatures starting at 50 °C and in all cases, the gas evolution ceased after a few minutes indicating the decomposition being complete within 5 min. $[H_2Al(PMDTA)]^+[AlH]^-$ as well as the polymeric precursor $H_3Al{\cdot}DABCO$ both decomposed to Al^0 with crystallite sizes of 74(3) nm and 46(4) nm under the conditions described above. However, both compounds exhibited a poor solubility resulting in inhomogeneous reaction mixtures containing large agglomerates and were thus not further examined.

The particle sizes of the resulting Al nanoparticles increased with increasing size of the substituents at the amine. H_3AlNMe_2Et and H_3AlNEt_3 resulted in crystallite sizes of 22(1) nm and 34(3) nm, respectively, while sizes of 66(2) nm and 60(2) nm were determined when H_3AlNBu_3 and $H_3AlNOct_3$ were employed as precursors. The TEM images reveal highly agglomerated particles (Fig. S3†) with mean par-

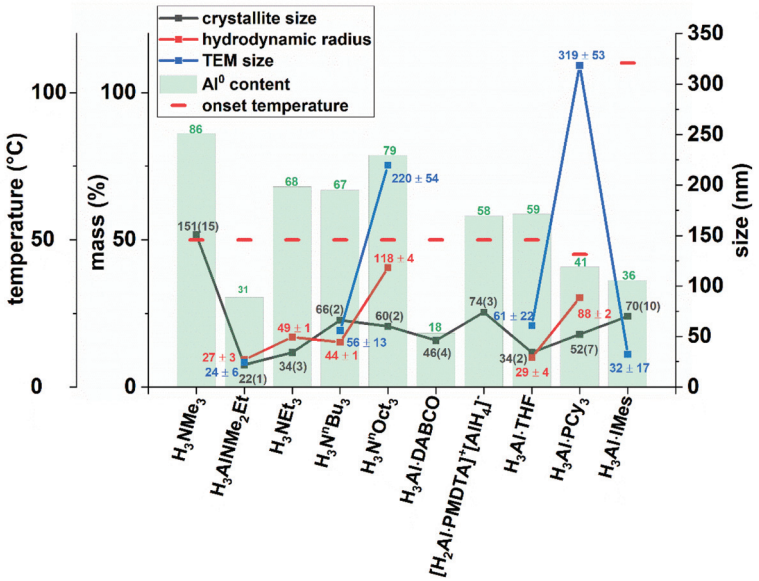

Fig. 5 Crystallite sizes, TEM sizes, hydrodynamic radii and reaction conditions as well as Al^0 contents observed for the synthesis of Al nanoparticles using various Al containing precursors in toluene. The concentrations used were as follows: 35 mM H_3AlNEt_3, Al : $N(Oct)_3$ 4 : 1 and cat. : Al 2 ppm. The crystallite sizes were determined from Rietveld refinements of the dried powders. The Al^0 contents have been calculated from the TG mass gains without normalizing to the mass minimum. The bars are representing the observed onset temperatures of the decompositions.

ticles sizes of 24.4 ± 6.3 nm for H_3AlNMe_2Et, 55.9 ± 12.6 nm for H_3AlNBu_3, and 219.6 ± 54.2 nm for $H_3AlNOct_3$. This size increase might be explained by the stability of intermediately formed Ti–H–Al species, which can be expected to exhibit a lower stability upon applying bulky amines like $NOct_3$ due to steric reasons. These observations would thus be in agreement with literature,[12] where less stable intermediate species were found to form in THF solutions compared to dioxane solutions resulting in the formation of larger particles in THF.

In the case of H_3AlNMe_3 very large crystallites (151(15) nm) as well as an increased deposition on the walls of the reaction vessel could be observed. Since the stabilizing influence of the amine coordinated to the alane and its effect on particle formation has already been discussed in the literature,[17] the large crystallites observed when H_3AlNMe_3 was used can likely be ascribed to its poor stabilizing abilities and its volatility compared to the other bulkier ligands. Thus, due to the increased reaction temperatures, H_3AlNMe_3 is assumed to quickly evaporate from the reaction mixture and is thus not capable of stabilizing the growing Al particles, resulting in the formation of the observed large crystallite sizes.

Applying $H_3Al{\cdot}PCy_3$, $H_3Al{\cdot}THF$ $H_3Al{\cdot}IMes$ as precursors resulted in the formation of particles with crystallite sizes of 52(7) nm, 34(2) nm, and 70(10) nm and TEM sizes of 318.5 ± 53.3 nm, 60.7 ± 22.3 nm, and 32.1 ± 17.0 nm, respectively. The nanoparticles resulting from the decomposition of $H_3Al{\cdot}IMes$ formed agglomerates with diameters larger than 1 μm. Within these agglomerates single particles with sizes of about 32 ± 17 nm are visible. Non-particular structures could be observed when $H_3Al{\cdot}PCy_3$ was used a precursor (see Fig. S3b and S3f†). These structures consisted of large, porous and network like structures with sizes of up to a few micrometres. PCy_3 can be expected a poor nanoparticle stabilizing agent, thus resulting in the formation of these large, poorly defined nanostructures. The formation of similar complex product mixtures was also reported by Meziani[19] using the precursor $H_3AlN[(C_4H_8)(CH_3)]$. The formation of these non-particular nanostructures could be also observed applying the bulkier amines $N(Oct)_3$ and $N(Bu)_3$. Due to these structures, the TEM size of the particles prepared from $H_3Al{\cdot}PCy_3$ is much larger than the crystallite size determined from Rietveld refinements and the TEM sizes for $H_3AlNOct_3$ and $H_3Al{\cdot}PCy_3$ can thus not be compared to the crystallite sizes determined from the Rietveld refinements as well as to the DLS measurements.

Fig. 6 shows the DLS measurements of the Al particles synthesized starting from various precursors in methanol. Upon increasing the amine chain length, an increase in the hydrodynamic radii could be observed, confirming the results from the XRD, TEM and TG analyses. In the reactions starting from the carbene alane no particles were found in solution, likely due to a complete precipitation caused by the large agglomerates visible in the TEM images.

TGA experiments can be used to examine the oxidation of the Al nanoparticles under controlled experimental conditions. To obtain a controlled oxidation without ignition, the experiments were carried out applying a heating rate of 10 K min^{-1} in an atmosphere of synthetic air (N_2 : O_2 32 : 8). The TGA curves for the nanoparticles synthesized from different precursors reveal in all cases a mass loss upon heating, which is complete at temperatures of 400–450 °C (Fig. 6a). This mass loss results from the decomposition of the stabilizer as well as the evaporation of residual solvent and moisture. Starting at

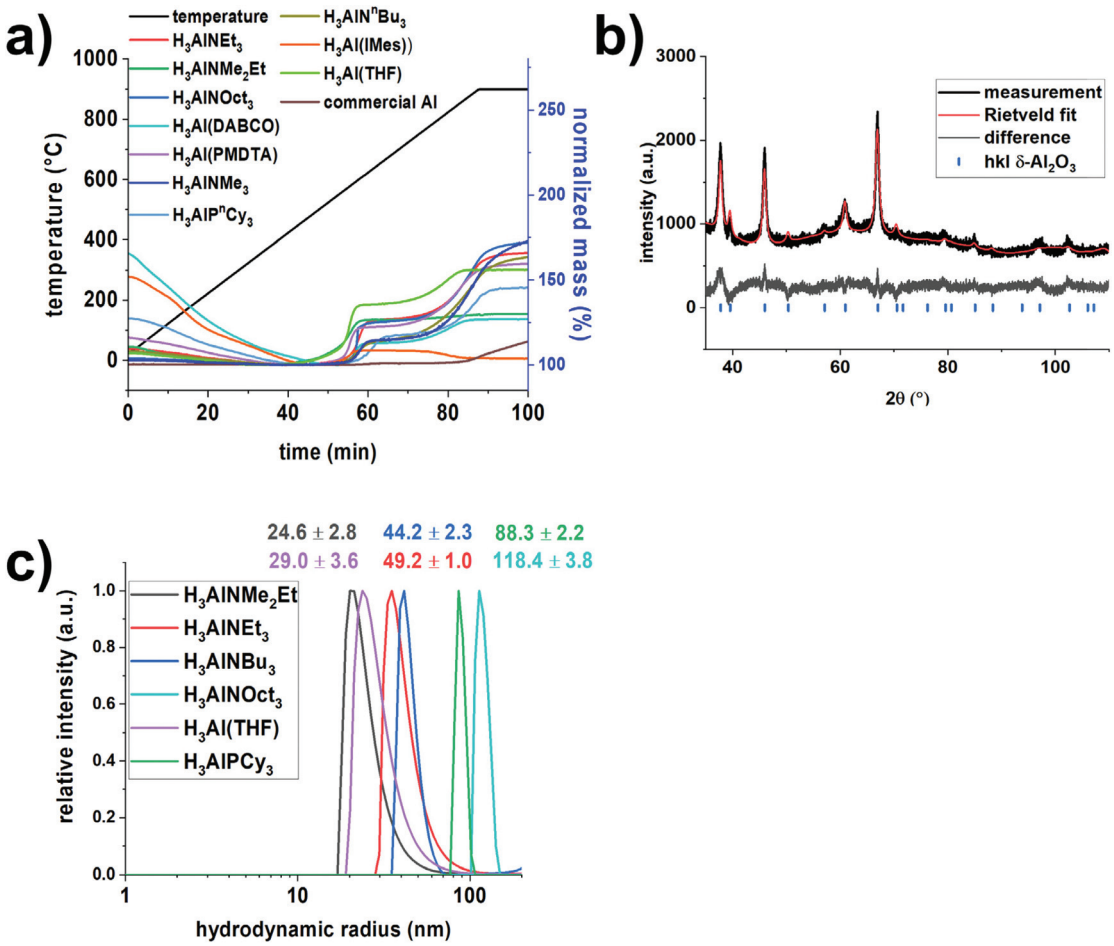

Fig. 6 (a) TGA measurements of Al nanoparticles synthesized using various precursors (10 K min^{-1}; $N_2 : O_2$ 8 : 32), (b) XRD measurement and Rietveld refinement of Al nanoparticles after the TG measurement in an atmosphere of $N_2 : O_2$ 8 : 32, (c) DLS measurements of Al nanoparticles synthesized using various precursors; agglomerates with sizes >200 nm are not shown.

around 500 °C a mass increase due to the Al oxidation in a well-known two step pattern can be observed.[44]

Neglecting any oxidation of the particles before reaching the mass minimum, the content of the organics can be estimated from the TGA measurements. Fig. 7 summarizes the mass losses observed in the TG measurements as well as the CHN analyses of the synthesized Al particles. The organic contents are ranging from 39.6% when H_3Al·DABCO is used as a precursor down to 3.8% when $H_3AlN^nOct_3$ is the precursor. The very high organic content in case of polymeric precursors is due to the very poor solubility in toluene as described above, resulting in a high residual content of DABCO in the final particles. Moreover, very high organic contents of 34.2% could be observed when the carbene alane was used as a precursor, with mass losses occurring up to temperatures of 800 °C, which likely can be ascribed to small amounts of LiCl being present in the sample and explaining the discrepancy between TG and CHN analyses. When the amine alanes were applied in the syntheses, organic contents <10% could be determined in all samples and a good agreement between the values of the organic contents determined *via* TG and CHN analyses could be observed. No nitrogen could be detected in these particles indicating a complete removal of the formed amine and the trioctylamine stabilizer during the work-up.

The total Al content of the synthesized powders can be estimated based on the mass gains during the TG measurements in an atmosphere of synthetic air ($N_2 : O_2$ 32 : 8) (eqn (1)), assuming a complete oxidation of the Al powders. The complete oxidation of the Al nanopowders after conducting the TGA analyses was confirmed by PXRD measurements, in which a formation of δ-Al_2O_3 was detected (Fig. 6b). The calculated Al^0 contents are summarized in Fig. 5.

$$w(\mathrm{Al}) = \frac{m_{\mathrm{gain}} \cdot 2 \cdot M_{\mathrm{Al}}}{M_{\mathrm{O}} \cdot 3} \quad (1)$$

w_{Al}: content of Al^0 in mass percent, m_{gain}: mass increase in percent from the mass minimum to the maximum in the TG traces, M_{Al}, M_O: molar mass of Al and O respectively.

For the particles synthesized from H_3AlNMe_2Et, for which the smallest crystallite sizes were observed, very low Al^0 contents were calculated, due to the expected larger content of surface Al_2O_3. For the particles synthesized from the additional amine

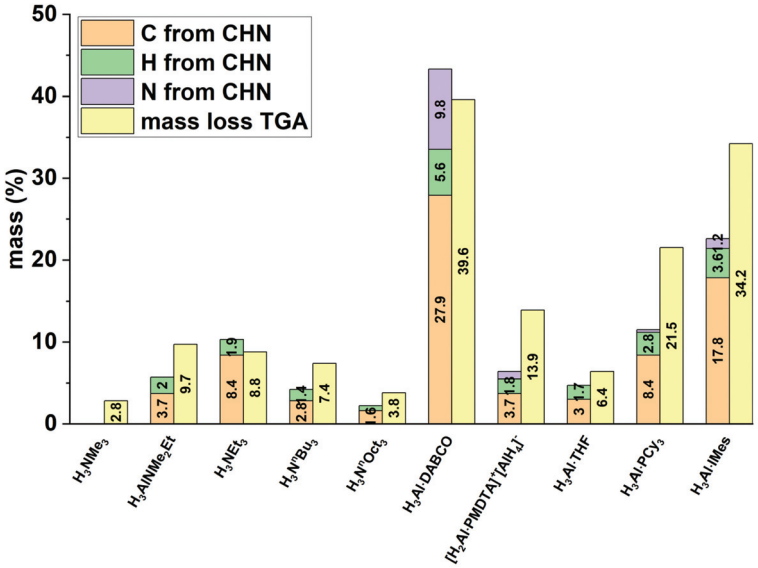

Fig. 7 CHN analyses and TG mass losses of Al nanoparticles synthesized using various precursors as well as Al contents calculated from the TG measurements.

precursors, the THF as well as the PCy_3 precursor, the calculated Al^0 contents were in the range between 50 to 80%. For the particles synthesized starting from $H_3Al{\cdot}IMes$ and $H_3Al{\cdot}DABCO$ very low Al^0 contents of 10% and 30% respectively could be calculated due to their high organic contents. The mass loss at temperatures >600 °C within the $H_3Al{\cdot}IMes$ sample can likely be attributed to a sublimation of small amounts of residual LiCl present in the sample. However, due to several reasons, no dependency of the Al^0 content and the crystallite size could be observed: (i) overlapping of mass losses and mass gains, (ii) possible additional mass losses at higher temperatures >500 °C, (iii) varying initial Al_2O_3 contents due to inconsistent particle shapes and morphologies (*cf.* presence of non-particular structures), (iv) agglomeration and sintering of the particles (v) varying organic contents.

The polymeric $H_3Al{\cdot}DABCO$ as well as the ionic $[H_2Al{\cdot}PMDTA]^+$ $[AlH_4]^-$ were both found not to be suitable precursors for the preparation of Al particles. The AlH_3–carbene adduct exhibited the slowest decomposition and yielded severely sintered and agglomerated particles. For the amine alanes the best results regarding particle sizes and morphologies could be observed when adducts contain small amines were applied. An exception is H_3AlNMe_3, which yielded very large crystallites, likely due to its poor stabilizing properties. When amines with higher carbon content were used, the formation of larger particles as well as the formation of non-particular structures could be observed. Similar observations were made when $H_3Al{\cdot}PCy_3$ was used as a precursor.

Influence of the stabilizer

The most common capping agents used for the synthesis of Al nanoparticles are based on carboxylic acids, which are known to lead to an oxidation of the surface of the particles.[16] They are commonly added to the reaction mixture a certain time after the addition of the decomposition catalyst. Contrary, we were optimizing the reaction parameters towards short reaction times and one-pot procedures and thus only examined stabilizers, which did not affect the precursor alanes and therefore could already be added to the reaction mixture before the decomposition process. Accordingly, we focused on the application of amines and phosphines, which have been reported to be suitable stabilizers for Al[45,46] and which could be added to the reaction mixture directly at the start of the reaction. Moreover, it is not possible to introduce any additional oxygen *via* these stabilizers.

Based on the results of Cui *et al.*,[45] who successfully prepared Al nanoparticles *via* reduction of $AlCl_3$ with $LiALH_4$ in the presence of PPh_3, 5 eq. of PPh_3 were chosen as a reference system. Besides, TOP has been chosen as an alternative phosphine stabilizer since it is a commonly applied and well-known nanoparticle stabilizer. To compare the performance of phosphine and amine stabilizers, the decompositions have moreover been carried out in the presence of $N(Oct)_3$ in a next step. In addition, several structurally related amines and phosphines have been tested.

Based on the results described above, the reactions were carried out in toluene using H_3AlNEt_3 as a precursor and $Ti(OiPr)_4$ as a decomposition catalyst (Fig. 8).

Without any stabilizer, the formation of large agglomerates as well as an Al film formation on the surface of the reaction vessel could be observed. The resulting powder consisted of large Al crystallites with sizes of 103(12) nm and the formation of large agglomerates was visible in DLS measurements. By applying a precursor containing a bulkier amine, *e.g.* $H_3AlNOct_3$, the formation of an Al film on the surface of the reaction vessel could be avoided. However, the formation of

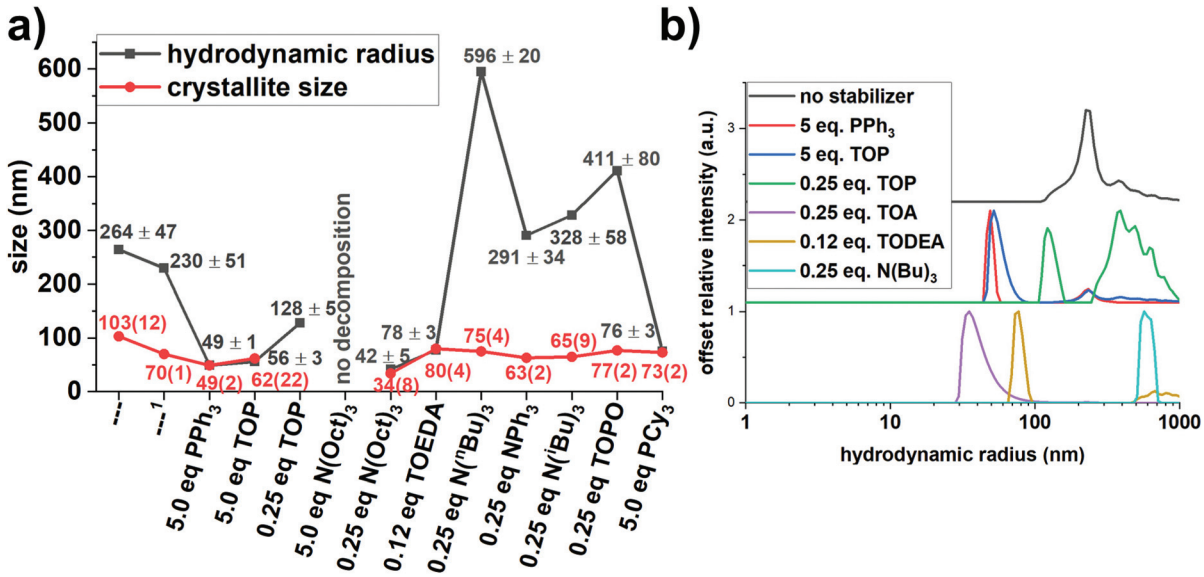

Fig. 8 (a) Crystallite sizes and hydrodynamic radii in MeOH observed for Al nanoparticles prepared applying different stabilizers in toluene. The concentrations used were as follows: 35 mM H_3AlNEt_3 (unless stated otherwise), and cat. : Al 2 ppm. The crystallite sizes were determined from Rietveld refinements of the dried powders. [1] $H_3AlNOct_3$ as precursor, (b) DLS measurements of the samples summarized in (a).

agglomerates was still evident, making the use of additional stabilizers inevitable. The crystallite size of the resulting powder was found to be 70(1) nm and thus as expected smaller than in the powder synthesized using H_3AlNEt_3 as precursor.

Based on the reports of Cui *et al.*,[45] who employed PPh_3 as a stabilizer during the synthesis of Al nanoparticles starting from $LiAlH_4$ and $AlCl_3$, the decomposition was carried out in the presence of 5 eq. of PPh_3 resulting in the formation of particles with crystallite sizes of 49(2) nm and hydrodynamic radii of 49 ± 1 nm. In the TEM images, a mixture of particular and non-particular structures could be observed, similar as described above (Fig. 9a).

Upon replacing PPh_3 with 5 eq. of more basic stabilizers such as TOP or $N(Oct)_3$, significantly slower decompositions and thus decreased yields of Al nanoparticles could be observed. While, for PPh_3 165 mg of Al particles could be isolated, only 10 mg of nanoparticles were obtained for TOP and no formation of a solid was visible in $N(Oct)_3$ after 15 min. These results are consistent with our previous observations when the decompositions were carried out in coordinating solvents. For TOP, the crystallite sizes and hydrodynamic radii were comparable to the results for PPh_3, however almost no particular structures could be observed in the TEM images (Fig. 9b). A decomposition in the presence of TOP and $N(Oct)_3$ could be achieved in the presence of 0.25 eq. of the stabilizers. An amount of 0.25 eq. was chosen based on the observation reported above, that an excess of these stabilizers leads to slow and incomplete decompositions. For the more basic $N(Oct)_3$, particles with crystallite sizes of 34(8) and a hydrodynamic radius of 42 ± 5 nm could be observed, while the particles formed in the presence of TOP were found to be severely agglomerated (see Fig. 8b). Applying the smaller amines N^nBu_3, N^iBu_3 and NPh_3 as well as TOPO the formation of large agglomerates was observed in all cases (Fig. 8a) due to their poor stabilizing properties. As a result, large hydrodynamic radii compared to the crystallite sized could be determined, as can be seen in Fig. 8.

CHN analyses of the Al particles synthesized in the presence of various stabilizers proved that the total content of

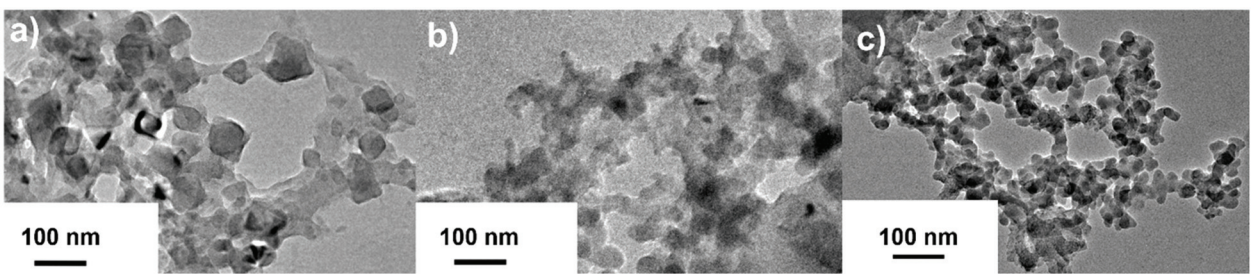

Fig. 9 TEM images of Al nanoparticles synthesized in the presence of (a) 5 eq. PPh_3, (b) 5 eq. TOP, and (c) 0.25 eq. $N(Oct)_3$.

organics was well below <10% in all cases (Table S1†), indicating a removal of the stabilizers during the reaction work-up. This result is in contrast to the typically employed oleic acid, which is capable of strongly coordinating to the particle surface thus potentially resulting in very high organic contents up to 80%.[17] These low contents of organics might however be favourable for certain applications like the formation of intermetallic compounds from these particles.

We can conclude that the choice of an appropriate stabilizer is crucial for a successful, fast synthesis of Al nanoparticles. On one hand, the formation of large agglomerates is easily possible if a too weak stabilizer is applied and on the other hand, yields might significantly decrease if a too high amount of stabilizer is added to the reaction mixture. We thus typically carried out our syntheses in the presence of 5 eq. PPh_3 or 0.25 eq. of $N(Oct)_3$.

Influence of concentrations

To examine the influence of the concentrations of the different reactants, the decomposition was carried out applying different concentrations of the stabilizer, catalyst and precursor. Based on the results described above, the reactions were carried out in toluene while $Ti(OiPr)_4$ was used as a catalyst and H_3AlNEt_3 was applied as a precursor (Table 1).

When PPh_3 was used as a stabilizer only a very small and somewhat inconsistent influence on the particle sizes could be observed (Fig. S4†), which is in contrast to results reported in the literature[45] for the synthesis of Al nanoparticles *via* a chemical reduction approach. The used amine alane precursors are containing 1 eq. of amines, which are present in every decomposition and which are obviously capable of influencing the particle sizes resulting in said inconsistent influence of the PPh_3 concentration. However, the presence of an additional stabilizer is still mandatory, as was discussed above.

Upon decreasing the concentration of the alane precursor from 140 mM down to 35 mM, a decrease in the crystallite size from 66(1) to 49(2) nm could be observed. In the TEM images, a decrease in the particle size from 78.4 ± 26.3 nm down to 50.1 ± 13.9 nm could be observed as well as much more narrower particle size distribution (Fig. 10).

Increasing the concentration of the decomposition catalyst leads to the formation of smaller nanoparticles with significantly narrower particle size distributions. As could be determined from the TEM images, the particle size reduced from

Table 1 Reaction conditions, crystallite sizes and hydrodynamic radii in methanol observed for Al nanoparticles synthesized in toluene applying different concentrations of the reactants. The crystallite sizes were determined from Rietveld refinements of the dried powders

Capping agent	Concentration H_3AlNEt_3 [mM]	$Ti(OiPr)_4$: Al [ppm]	Hydrodynamic radius [nm]	Crystallite size [nm]
2.3 eq. PPh_3	140	2	105 ± 6	53(1)
3.5 eq. PPh_3	140	2	72 ± 2	51(1)
4.7 eq. PPh_3	140	2	92 ± 15	66(1)
5.0 eq. PPh_3	35	2	49 ± 1	49(2)
5.0 eq. PPh_3	35	34	30 ± 1	24(1)

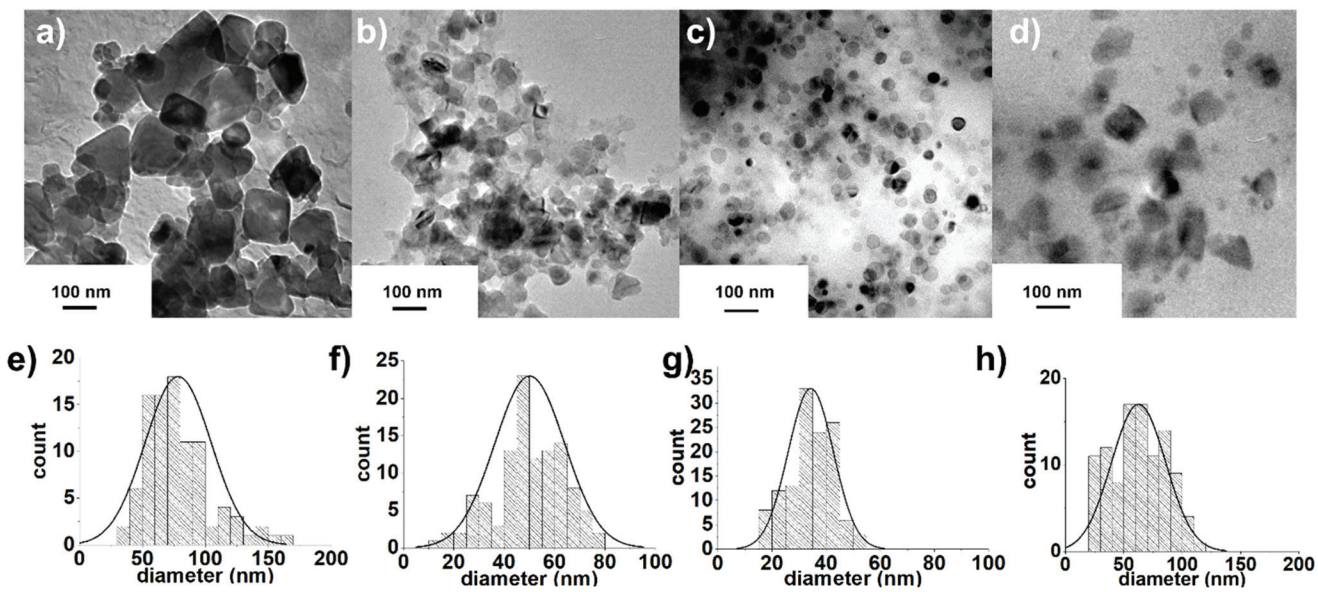

Fig. 10 TEM images and particles size distributions of Al nanoparticles synthesized in the presence of 5 eq. PPh_3 applying different concentrations of the precursor and catalyst (a) + (e) 140 mM H_3AlNEt_3 and 2 ppm $Ti(O^iPr)_4$, (b) + (f) 35 mM H_3AlNEt_3 and 2 ppm $Ti(O^iPr)_4$, (c) + (g) 35 mM H_3AlNEt_3 and 34 ppm $Ti(O^iPr)_4$, and (d) + (h) 35 mM $H_3Al{\cdot}THF$ and 24 ppm $Ti(O^iPr)_4$.

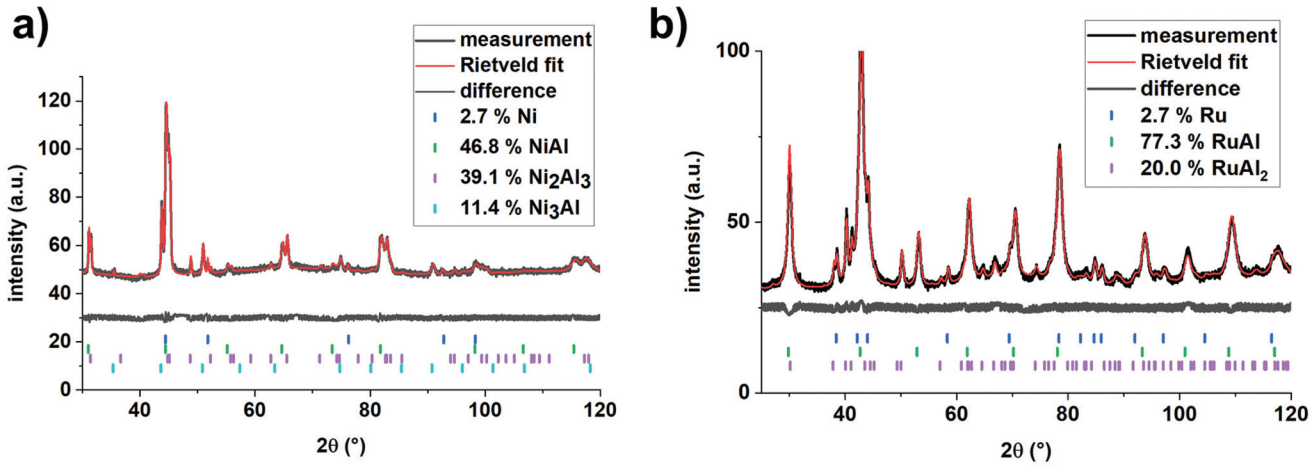

Fig. 11 XRD measurements and Rietveld refinements of reacted mixtures prepared from Al particles with (a) Ni particles and with (b) Ru particles as precursors. The reactions have been carried out by heating to 800 °C under an Ar atmosphere applying a heating rate of 60 K min^{-1}. The Al particles were prepared from a decomposition of 140 mM H_3AlNEt_3 applying 2 ppm $Ti(O^iPr)_4$ as a catalyst in toluene solutions in the presence of 5 eq. PPh_3.

50.1 ± 13.9 nm down to 34.3 ± 8.3 nm (Fig. 10). Moreover, the formation of non-particular structures could be completely avoided by increasing the catalyst concentration, due to the much faster and thus kinetically controlled decompositions. Furthermore, the agglomeration of the particles was found to be much less upon increasing its concentration. The crystallite size decreased from 49(2) nm to 24(1) nm, which is in good agreement with the results observed by TEM analysis. The decrease of the particle sizes could also be observed in the DLS measurements, where a decrease of the hydrodynamic radius from 49 ± 1 nm to 29 ± 1 nm as well as a decrease in the amount of agglomerates could be observed (Fig. S5†).

A possible application of the prepared Al nanoparticles is the formation of Al intermetallic compounds, the so-called aluminides. They are commonly prepared starting form micron powders, but the results reported in the literature indicate, that the application of nanoparticular reactants has several advantages such as lowered ignition temperatures and decreased activation energies.[47,48] Since the wet chemical approaches have several advantages such as short reaction times, simple experimental set-ups and facile scale-ups, the suitability of the Al particles for the preparation of Ni and Ru aluminides was tested.

For this purpose, the Al particles prepared from a decomposition of 140 mM H_3AlNEt_3 applying 2 ppm $Ti(O^iPr)_4$ as a catalyst in toluene solutions in the presence of 5 eq. PPh_3 as a stabilizer have been exemplary selected. These particles have been thoroughly mixed in a 1 : 1 molar ratio with Ni or Ru particles in an agate mortar. About 15 mg of the resulting mixture was compacted in a hydraulic press (350 MPa; ∅ 6 mm) and the prepared pellet was then heated to 800 °C under an atmosphere of Ar applying a heating rate of 60 K min^{-1}. The Ni and Ru particles have been prepared following literature procedures[49,50] and a characterization of these particles can be found elsewhere.[51] In Fig. 11 the formation of several Ni and Ru containing intermetallic phases can be clearly detected in the PXRD patterns. Thus, the Al particles synthesized *via* the catalytic decomposition approach are suitable precursors for the preparation of aluminides.[52,53] Further studies on the formation of these intermetallic compounds would however be well beyond the scope of this manuscript and will be examined in more detail in a future work.

Conclusions

The synthesis of Al nanoparticles was carried out applying a wet chemical catalytic decomposition approach while systematically varying the reaction parameters and optimizing them towards short reaction times, regarding a possible future continuous synthesis of these Al nanoparticles.

Ti catalysts are necessary in the decomposition reaction since the use of other Lewis acid catalysts results in increased reaction times. Best results were obtained using $Ti(O^iPr)_4$ and $Ti(O^nBu)_4$, while more bulky Ti catalysts like $Ti(O^tBu)_4$ were found to be slightly less efficient.

Temperatures of at least 90 °C lead to short reaction times and complete decomposition typically within less than 5 minutes. The shortest reaction times, lowest reaction temperatures, and the smallest particle sizes with the most defined morphologies were obtained in toluene solutions. When polar, coordinating solvents were applied, the yield of the resulting Al nanoparticles was found to significantly decrease resulting in incomplete decompositions after a reaction time of 15 min.

The use of amine alanes with short alkyl chains or the alane THF adduct resulted in the best results smallest particle sizes as well as nearly spherical morphologies. When longer alkyl chain containing amines and a phosphine alane were used an increased formation of complex, non-particular structures could be observed. The decomposition of a carbene alane resulted in the formation of strongly agglomerated particles. Alanes with a polymeric or an ionic structure can also

be decomposed under the selected conditions, but these precursors show a very poor solubility in toluene.

A stabilizer is necessary in all cases to prevent the formation of large agglomerates and the formation of an Al film on the surface of the reaction vessel. Applying amine- or phosphine-based stabilizers resulted in the formation of particles with low organic contents (<10%) making the use of these particles for the formation of intermetallic compounds possible. However, applying a too high amount of stabilizer might result in significantly decreased yields.

Upon reducing the precursor concentration, a decrease in the particles size as well as a narrower particle size distribution could be observed. Increasing the concentration of the decomposition catalyst was also found to result in smaller particles with narrower particles size distribution. Moreover, the formation of complex non-particular structures could be prevented and significantly less agglomeration was observed.

Abbreviations

TOP	Trioctylphosphine
$N(Oct)_3$	Trioctylamine
TOEDA	*N*,*N*,*N*′,*N*′-Tetraoctylethylendiamine
IMes	1,3-Bis-(2,4,6-trimethylphenyl)imidazolylidene
PMDTA	*N*,*N*,*N*′,*N*″,*N*″-Pentamethyldiethylenetriamine

Conflicts of interest

There are no conflicts to declare.

Acknowledgements

We thank Susanne Harling for performing the elemental analyses. We further thank Dr Robert Haberkorn and Dennis Becker for providing the XRD measurements and their notes regarding the Rietveld refinements. We also thank Nadja Klippel for recording some of the TEM images.

References

1 J. A. Puszynski, C. J. Bulian and J. J. Swiatkiewicz, Processing and Ignition Characteristics of Aluminum-Bismuth Trioxide Nanothermite System, *J. Propul. Power*, 2007, **23**(4), 698–706.

2 J. Wang, W. P. Bassett and D. D. Dlott, Shock Initiation of Nano-Al/Teflon: High Dynamic Range Pyrometry Measurements, *J. Appl. Phys.*, 2017, **121**(8), 085902.

3 G. A. Risha, T. L. Connell Jr., R. A. Yetter, D. S. Sundaram and V. Yang, Combustion of Frozen Nanoaluminum and Water Mixtures, *J. Propul. Power*, 2014, **30**(1), 133–142.

4 K. Woll, A. Bergamaschi, K. Avchachov, F. Djurabekova, S. Gier, C. Pauly, P. Leibenguth, C. Wagner, K. Nordlund and F. Mücklich, Ru/Al Multilayers Integrate Maximum Energy Density and Ductility for Reactive Materials, *Sci. Rep.*, 2016, **6**(November 2015), 19535.

5 S. Yatsuya, S. Kasukabe and R. Uyeda, Formation of Ultrafine Metal Particles by Gas Evaporation Technique. I. Aluminium in Helium, *Jpn. J. Appl. Phys.*, 1973, **12**(11), 1675–1684.

6 A. Pivkina, D. Ivanov, Y. Frolov, S. Mudretsova and J. Schoonman, Structure, Thermal Properties, and Combustion Behavior of Plasma Synthesized Nano-Aluminum Powders, *AIP Conf. Proc.*, 2006, **849**, 164–173.

7 E. Stratakis, M. Barberoglou, C. Fotakis, G. Viau, C. Garcia and G. A. Shafeev, Generation of Al Nanoparticles via Ablation of Bulk Al in Liquids with Short Laser Pulses, *Opt. Express*, 2009, **17**(15), 12650–12659.

8 C. A. Crouse, E. Shin, P. T. Murray and J. E. Spowart, Solution Assisted Laser Ablation Synthesis of Discrete Aluminum Nanoparticles, *Mater. Lett.*, 2010, **64**(3), 271–274.

9 A. A. Gromov, U. Förter-Barth and U. Teipel, Aluminum Nanopowders Produced by Electrical Explosion of Wires and Passivated by Non-Inert Coatings: Characterisation and Reactivity with Air and Water, *Powder Technol.*, 2006, **164**(2), 111–115.

10 M. I. Lerner, E. A. Glazkova, A. S. Lozhkomoev, N. V. Svarovskaya, O. V. Bakina, A. V. Pervikov and S. G. Psakhie, Synthesis of Al Nanoparticles and Al/AlN Composite Nanoparticles by Electrical Explosion of Aluminum Wires in Argon and Nitrogen, *Powder Technol.*, 2016, **295**, 307–314.

11 J. A. Haber and W. E. Buhro, Kinetic Instability of Nanocrystalline Aluminum Prepared by Chemical Synthesis; Facile Room-Temperature Grain Growth, *J. Am. Chem. Soc.*, 1998, **120**(42), 10847–10855.

12 B. D. Clark, C. J. DeSantis, G. Wu, D. Renard, M. J. McClain, L. Bursi, A.-L. Tsai, P. Nordlander and N. J. Halas, Ligand-Dependent Colloidal Stability Controls the Growth of Aluminum Nanocrystals, *J. Am. Chem. Soc.*, 2019, **141**(Iii), 1716–1724.

13 M. J. McClain, A. E. Schlather, E. Ringe, N. S. King, L. Liu, A. Manjavacas, M. W. Knight, I. Kumar, K. H. Whitmire, H. O. Everitt, P. Nordlander and N. J. Halas, Aluminum Nanocrystals, *Nano Lett.*, 2015, **15**(4), 2751–2755.

14 C. E. Bunker, M. J. Smith, K. A. Shiral Fernando, B. A. Harruff, W. K. Lewis, J. R. Gord, E. A. Guliants and D. K. Phelps, Spontaneous Hydrogen Generation from Organic-Capped Al Nanoparticles and Water, *ACS Appl. Mater. Interfaces*, 2010, **2**(1), 11–14.

15 W. K. Lewis, A. T. Rosenberger, J. R. Gord, C. A. Crouse, B. A. Harruff, K. A. S. Fernando, M. J. Smith, D. K. Phelps, J. E. Spowart, E. A. Guliants and C. E. Bunker, Multispectroscopic (FTIR, XPS, and TOFMS-TPD) Investigation of the Core-Shell Bonding in Sonochemically Prepared Aluminum Nanoparticles Capped with Oleic Acid, *J. Phys. Chem. C*, 2010, **114**(14), 6377–6380.

16 K. A. S. Fernando, M. J. Smith, B. A. Harruff, W. K. Lewis, E. A. Guliants and C. E. Bunker, Sonochemically Assisted

Thermal Decomposition of Alane N,N- Dimethylethylamine with Titanium(IV) Isopropoxide in the Presence of Oleic Acid to Yield Air-Stable and Size-Selective Aluminum Core - Shell Nanoparticles, *J. Phys. Chem. C*, 2009, **113**(2), 500–503.

17 R. J. Jouet, A. D. Warren, D. M. Rosenberg, V. J. Bellitto, K. Park and M. R. Zachariah, Surface Passivation of Bare Aluminum Nanoparticles Using Perfluoroalkyl Carboxylic Acids, *Chem. Mater.*, 2005, **17**(11), 2987–2996.

18 R. J. Jouet, R. H. Granholm, H. W. Sandusky and A. D. Warren, Preparation and Shock Reactivity Analysis of Novel Perfluoroalkyl-Coated Aluminum Nanocomposites, *Mater. Sci. Technol.*, 2006, **22**(4), 422–429.

19 M. J. Meziani, C. E. Bunker, F. Lu, H. Li, W. Wang, E. A. Guliants, R. A. Quinn and Y. P. Sun, Formation and Properties of Stabilized Aluminum Nanoparticles, *ACS Appl. Mater. Interfaces*, 2009, **1**(3), 703–709.

20 S. W. Chung, E. A. Guliants, C. E. Bunker, D. W. Hammerstroem, Y. Deng, M. A. Burgers, P. A. Jelliss and S. W. Buckner, Capping and Passivation of Aluminum Nanoparticles Using Alkyl-Substituted Epoxides, *Langmuir*, 2009, **25**(16), 8883–8887.

21 D. W. Hammerstroem, M. A. Burgers, S. W. Chung, E. A. Guliants, C. E. Bunker, K. M. Wentz, S. E. Hayes, S. W. Buckner and P. A. Jelliss, Aluminum Nanoparticles Capped by Polymerization of Alkyl-Substituted Epoxides: Ratio-Dependent Stability and Particle Size, *Inorg. Chem.*, 2011, **50**(11), 5054–5059.

22 B. J. Thomas, C. E. Bunker, E. A. Guliants, S. E. Hayes, A. Kheyfets, K. M. Wentz, S. W. Buckner and P. A. Jelliss, Synthesis of Aluminum Nanoparticles Capped with Copolymerizable Epoxides, *J. Nanopart. Res.*, 2013, **15**(6), 1729.

23 P. A. Jelliss, S. W. Buckner, S. W. Chung, A. Patel, E. A. Guliants and C. E. Bunker, The Use of 1,2-Epoxyhexane as a Passivating Agent for Core-Shell Aluminum Nanoparticles with Very High Active Aluminum Content, *Solid State Sci.*, 2013, **23**, 8–12.

24 W. Zeng, S. W. Buckner and P. A. Jelliss, Poly(Methyl Methacrylate) as an Environmentally Responsive Capping Material for Aluminum Nanoparticles, *ACS Omega*, 2017, **2**(5), 2034–2040.

25 T. J. Foley, C. E. Johnson and K. T. Higa, Inhibition of Oxide Formation on Aluminum Nanoparticles by Transition Metal Coating, *Chem. Mater.*, 2005, **17**, 4086–4091.

26 P. J. Reuvers and C. J. Smit, Preparation and Properties of Alane Dimethylethylamine, a Liquid Precursor for MOCVD, *Chem. Mater.*, 1994, **6**(21), 190–195.

27 J. K. Ruff and M. F. Hawthorne, The Amine Complexes of Aluminum Hydride. I, *J. Am. Chem. Soc.*, 1960, **82**(9), 2141–2144.

28 J. L. Atwood, K. D. Robinson, C. Jonesb and C. L. Raston, Cationic Aluminium Hydrides: $[H_2AlL]$ + $[AlH_4]$-, L = N,N, N′,N",N"-Pentamethyldiethylenetriamine and 1,4,8,11-Tetramethyl-1,4,8,11-Tetraazacyclotetradecane, *J. Chem. Soc., Chem. Commun.*, 1991, **3**, 1697–1699.

29 H. C. Brown and B. Singaram, Molecular Addition Compounds. 7. Synthesis of Addition Compounds of Boron Trifluoride, Borane, and Alane with N, N, N, 'N′-Tetramethylethylenediamine and Triethylenediamine by Precipitation from Ether Solvents, *Inorg. Chem.*, 1980, **19**(2), 455–457.

30 A. E. Finholt, A. C. Bond and H. I. Schlesinger, Lithium Aluminum Hydride, Aluminum Hydride and Lithium Gallium Hydride, and Some of Their Applications in Organic and Inorganic Chemistry, *J. Am. Chem. Soc.*, 1947, **69**(5), 1199–1203.

31 F. R. Bennett, F. M. Elms, M. G. Gardiner, G. A. Koutsantonis, C. L. Raston and N. K. Roberts, Stable Tertiary Phosphine Adducts of Alane, *Organometallics*, 1992, **11**(4), 1457–1459.

32 X. Bantreil and S. P. Nolan, Synthesis of N-Heterocyclic Carbene Ligands and Derived Ruthenium Olefin Metathesis Catalysts, *Nat. Protoc.*, 2011, **6**(1), 69–77.

33 L. Hintermann, Expedient Syntheses of the N-Heterocyclic Carbene Precursor Imidazolium Salts IPr·HCl, IMes·HCl and IXy·HCl, *Beilstein J. Org. Chem.*, 2007, **3**, DOI: 10.1186/1860-5397-3-22.

34 J. G. H. du Preez, D. P. Shillington and B. J. A. M. van Brecht, Polynitrogen Reagents in Metal Separation. Part 1. Ditertiary and Diquaternary Ammonium Extractants for Cobalt(II) and Copper(II) in HCL Medium, *Solvent Extr. Ion Exch.*, 1984, **2**(6), 839–858.

35 C. A. Schneider, W. S. Rasband and K. W. Eliceiri, NIH Image to ImageJ: 25 Years of Image Analysis, *Nat. Methods*, 2012, **9**(7), 671–675.

36 Bruker AXS Karlsruhe, *Topas 5.1. General Profile and Structure Analysis Software for Powder Diffraction Data*, Karlsruhe, 2014.

37 R. W. Cheary, A. A. Coelho and J. P. Cline, Fundamental Parameters Line Profile Fitting in Laboratory Diffractometers, *J. Res. Natl. Inst. Stand. Technol.*, 2004, **109**, 1–25.

38 A. Merkys, A. Vaitkus, J. Butkus, M. Okulič-Kazarinas, V. Kairys and S. Gražulis, COD::CIF::Parser: An Error-Correcting CIF Parser for the Perl Language, *J. Appl. Crystallogr.*, 2016, **49**, 292–301.

39 T. J. Frankcombe, Proposed Mechanisms for the Catalytic Activity of Ti in $NaAlH_4$, *Chem. Rev.*, 2012, **112**(4), 2164–2178.

40 S. Zhang, A. Taniguchi, Q. Xu, N. Takeichi, H. T. Takeshita, N. Kuriyama and T. Kiyobayashi, Understanding the Effect of Titanium Species on the Decomposition of Alanates in Homogeneous Solution, *J. Alloys Compd.*, 2006, **413**(1–2), 218–221.

41 V. V. Gavrilenko, L. A. Chekulaeva and L. I. Zakharkin, Decomposition of Solvates of Aluminum Hydride and Its Derivatives in Ethereal Solutions under the Influence of Titanium Compounds, *Russ. Chem. Bull.*, 1977, **26**(6), 1131–1134.

42 D. L. Anton, Hydrogen Desorption Kinetics in Transition Metal Modified NaAlH4, *J. Alloys Compd.*, 2003, **356–357**, 400–404.

43 K. Wade and A. J. Banister, *The Chemistry of Aluminium, Gallium, Indium and Thallium: Comprehensive Inorganic Chemistry*, Pergamon Press, 1st edn, 1973.
44 M. A. Trunov, M. Schoenitz, X. Zhu and E. L. Dreizin, Effect of Polymorphic Phase Transformations in Al_2O_3 Film on Oxidation Kinetics of Aluminum Powders, *Combust. Flame*, 2005, **140**(4), 310–318.
45 Y. Cui, D. Huang, Y. Li, W. Huang, Z. Liang, Z. Xu and S. Zhao, Aluminium Nanoparticles Synthesized by a Novel Wet Chemical Method and Used to Enhance the Performance of Polymer Solar Cells by the Plasmonic Effect, *J. Mater. Chem. C*, 2015, **3**(16), 4099–4103.
46 C. E. Johnson and K. T. Higa, Preparation of Nanometer Sized Aluminum Powders, *MRS Proc.*, 1996, **457**, 131–135.
47 E. M. Hunt and M. L. Pantoya, Ignition Dynamics and Activation Energies of Metallic Thermites: From Nano- to Micron-Scale Particulate Composites, *J. Appl. Phys.*, 2005, **98**(3), 034909.
48 E. M. Hunt, K. B. Plantier and M. L. Pantoya, Nano-Scale Reactants in the Self-Propagating High-Temperature Synthesis of Nickel Aluminide, *Acta Mater.*, 2004, **52**(11), 3183–3191.
49 S. Carenco, C. Boissière, L. Nicole, C. Sanchez, P. Le Floch and N. Mézailles, Controlled Design of Size-Tunable Monodisperse Nickel Nanoparticles, *Chem. Mater.*, 2010, **22**(4), 1340–1349.
50 N. G. Garcia-Pena, R. Redon, A. Herrera-Gomez, A. L. Fernandez-Osorio, M. Bravo-Sanchez and G. Gomez-Sosa, Solventless Synthesis of Ruthenium Nanoparticles, *Appl. Surf. Sci.*, 2015, **340**, 25–34.
51 T. Klein and G. Kickelbick, Synthesis of Submicron Aluminum Particles via Thermal Decomposition of Alkyl Aluminum Precursors in the Presence of Metal Seeds and Their Application in the Formation of Ruthenium Aluminides, *Nanotechnology*, 2020, **31**, 265605.
52 T. Klein, C. Pauly, F. Mücklich and G. Kickelbick, Al and Ni nanoparticles as precursors for Ni aluminides, *Intermetallics*, 2020, **124**, 106839.
53 T. Klein, C. Pauly, F. Mücklich and G. Kickelbick, Al and Ru nanoparticles as precursors for Ru–Al intermetallics, *Intermetallics*, in press.

In conclusion, from these studies it can be learned that the synthesis of Al nanoparticles is possible applying a large variety of reaction conditions via the catalytic decomposition approach. By varying the parameters, such as the nature and concentration of the precursor, of the catalyst, and of the stabilizer as well as the reaction temperature and the solvent, the size of the resulting nanoparticles can be tuned from 20 nm up to >100 nm. Similarly, the morphology of the particles can be varied from spherical particles to non-particulate, network-like morphologies.

Although the optimized reaction conditions determined for the preparation of Al particles with sizes < 50 nm within short reaction times from homogeneous solutions were found to be similar to the reaction conditions commonly applied in the literature, the paper fills the knowledge gap regarding the systematic variation of the reaction parameters.

Moreover, this synthesis approach has various advantages compared to the syntheses via hydride or metal reductions, including the very short reaction times of a few minutes, the mild reaction conditions as well as the possibility to add the stabilizer directly at the start of the reaction and not only after a certain reaction time. Although a reaction time of 15 min was generally applied within this manuscript, a visible gas evolution ceased in less than 5 min. Accordingly, the synthesis might be possible applying even shorter reaction times, particularly if a hot-injection method would be introduced. Thus, the synthesis of Al particles with various sizes in a large-scale might be possible applying this approach in a future work.

3.1.4 Synthesis via thermal decomposition

As was discussed in Chapter 1.3.1.2, the thermal decomposition is an attractive synthesis approach for the preparation of nanoparticles, and has already been applied for the synthesis of many, also reactive, metal nanoparticles. However, for the preparation of Al particles, this method has been hardly applied and only a few reports are known in the literature. Thus, due to the numerous advantages of this method, such as the formation of gaseous or volatile side-products and short reaction times, further studies regarding the applicability of a thermal decomposition approach for the synthesis of Al particles were conducted within this work and a new synthesis protocol was introduced.

Within this method, triisobutylaluminum was thermally decomposed in refluxing diphenylether in the presence of metallic nanoparticulate seeds (Ni, Ru or Ag). The metallic nanoparticles were likely acting as nucleation seeds and their addition was necessary to prevent an Al film formation on the surface of the reaction vessel. The resulting particles were characterized applying XRD, DLS, TG, FTIR as well as TEM techniques. This approach resulted in the formation of submicron Al particles with sizes of about 150 nm and a content of the seed metal of < 5 %, as was determined from Rietveld refinements. In

addition, since no addition of an organic stabilizer was necessary, the total organic content was determined to be well below < 10 %. However, if desired, a functionalization of the resulting particles with oleic acid was readily possible in a second, optional reaction step, resulting in the formation of oleic acid capped Al particles. Moreover, by the addition of PPh_3 during the decomposition reaction, the size of the resulting particles could be decreased to about 80 nm as was evidenced by TEM images.

The suitability of these particles for the preparation of Ru alumindes was shown by reacting them with Ru nanopowder, which was mechanochemically synthesized from $RuCl_3$ and $NaBH_4$. Al and Ru powders were thoroughly mixed in an agate mortar, compacted in a hydraulic press, and then reacted by heating the resulting pellet in an atmosphere of Ar up to 800 °C applying a heating rate of 60 K/min. The reaction products were characterized applying XRD, STA and FIB techniques. Although the XRD measurements revealed RuAl to be the only crystalline phase being present, the FIB measurements clearly showed the presence of a second, amorphous and oxide rich phase due the application of oxide passivated submicron Al particles.

The results of these studies were published as a paper in *Nanotechnology* from IOP Publishing:

Klein, T.; Kickelbick, G. Synthesis of Submicron Aluminum Particles via Thermal Decomposition of Alkyl Aluminum Precursors in the Presence of Metal Seeds and Their Application in the Formation of Ruthenium Aluminides. *Nanotechnology* **2020**, *31*, 265605 (https://doi.org/10.1088/1361-6528/ab7ef5)[309].

Author contributions:

T. Klein had the original idea, carried out all the synthetic work, characterized the particles, and interpreted the results. He carried out the DLS, FTIR, TG, STA and TEM measurements and prepared the initial draft of the manuscript.

G. Kickelbick gave scientific input, supervised the work, and discussed the results. He proof-read and edited the final manuscript.

Nanotechnology

Synthesis of submicron aluminum particles via thermal decomposition of alkyl aluminum precursors in the presence of metal seeds and their application in the formation of ruthenium aluminides

To cite this article before publication: Thomas Klein *et al* 2020 *Nanotechnology* in press https://doi.org/10.1088/1361-6528/ab7ef5

IOP Publishing Journal Title
Journal **XX** (XXXX) XXXXXX https://doi.org/XXXX/XXXX

Synthesis of submicron aluminum particles via thermal decomposition of alkyl aluminum precursors in the presence of metal seeds and their application in the formation of ruthenium aluminides.

Thomas Klein, Guido Kickelbick[1]

Inorganic Solid State Chemistry, Saarland University, Campus C4.1, 66123 Saarbrücken, Germany

E-mail: guido.kickelbick@uni-saarland.de

Received xxxxxx
Accepted for publication xxxxxx
Published xxxxxx

Abstract

Submicron Al particles can be used in energy materials, as reducing agents, or for the formation of aluminides. Their low highly positive standard potential and their reactivity towards oxygen makes their synthesis a challenging task. Here we present a thermal decomposition approach starting from triisobutylaluminium (TIBAL) as a precursor. This compound can be decomposed in refluxing diphenylether as a high-boiling solvent and in the presence of metallic nanoparticles of Ni, Ru or Ag acting as seeds. The resulting particles revealed sizes of around 100 nm. Passivation of the resulting submicron Al particles is possible in an optional second step after the synthesis by adding oleic acid resulting in the formation of oleic acid capped Al particles. The suitability of these submicron particles for the synthesis of aluminides was studied by reacting the synthesized particles with Ru powders, resulting in the formation of the respective aluminide.

Keywords: nanoparticles, thermal decomposition, intermetallics

1. Introduction

Submicron Al particles exhibit a high reactivity and energy density and are thus widely used in energetic materials. Examples include environmentally friendly propellants (ALICE)[1], explosives[2], nanothermites[3], and self-propagating reaction systems.[4] Commonly, Al submicron and nanoparticles are synthesized using physical synthesis methods, like pulsed laser ablation[5][6] (20-60 nm), electrical exploding wire[7][8] (70 – 500 nm), gas evaporation[9](50 - >500 nm), or plasma synthesis[10] (around 50 nm). In contrast, wet chemical synthesis methods are rarely used even though simple synthesis procedures are known and no special equipment is needed for this preparation method.

The wet chemical synthesis of Al submicron and nanoparticles is typically carried out via chemical reduction or catalytic decomposition approaches, both first described by Haber and Buhro in 1998.[11] In the chemical reduction approach, an Al salt is reduced to metallic Al^0 using strong reducing agents. In this approach, the most common Al-precursor used is $AlCl_3$[11][12]. Additionally coordination compounds, such as $Al(acac)_3$, have also been reported as precursors in the literature.[13] Typically $LiAlH_4$ is used as a

reducing agent[11][12][13], since it is capable of playing dual roles of a strong reducing agent and an additional Al source thus resulting in increased yields. The use of other reducing agents, e.g. Na/K[14] or K-naphthalenide[15], is however also possible. The sizes of these particles are ranging from 20 to 400 nm.[12] The largest drawback of these methods is the formation of side-products (typically LiCl when $AlCl_3$ and $LiAlH_4$ are used), making the clean-up and purification of the resulting Al particles rather difficult.

The second synthetic approach is the catalytic decomposition of alanes. Within this approach amine alanes such as H_3AlNMe_2Et[11][16][17][18], H_3AlNMe_3[19], H_3AlNEt_3[20], $H_3AlN(C_4H_8)(CH_3)$[17] or $H_3AlNMePyr$[21] are decomposed using $Ti(OiPr)_4$[11][16][17][19] or $TiCl_4$[21] as a catalyst. The ether adducts of AlH_3 are known to decompose under similar conditions[22], their use in the wet chemical synthesis of Al nanoparticles is however much more uncommon compared to their amine counterparts. The decomposition reactions are performed at moderate temperatures ranging from 25 °C up to 70 °C or under ultrasonication[23][24] resulting in volatile and easy to remove side-products (H_2 and the corresponding amine). The particle sizes of the resulting Al particles are ranging from around 5 up to 200 nm and possible applications of such particles can be found in the field of energetic materials.[21] However, reaction times are long and the formed amine is capable of coordinating to the particle surface competing with other added stabilizers.

Moreover, a few reports are known in the literature which are discussing the synthesis of Al nanoparticles using alternative reaction pathways, e.g. a reductive elimination starting from H_2AlCp^* or $HAlCP^*_2$[25] as well as a photochemical reduction approach using $NbLiO_3$ as a photocatalyst.[26]

Due to their very high reactivity an amorphous Al_2O_3 passivating layer with a thickness of 0.2 - 6.9 nm[27] is formed at the particle surface immediately upon air contact. With increasing oxide layer thickness and decreasing particle size the Al^0-content of the particles is decreasing. Uncontrolled oxidation can be avoided applying various passivating agents such as oleic acid[18][23][28], perfluorated carboxylic acids[19][21][29], phosphines[12], amines[30], or thin transition metal coatings.[20] Also, polymers like PVP[31], PMMA[16], and polyepoxides[32][33] can be used to protect the surface.

Although, the Al particles synthesized via the methods described above are often referred to be pure Al, one has to keep in mind that a large amount of organic stabilizer is still coordinated to the surfaces of the resulting particles. Evaporation or decomposition of these capping molecules during heating can produce gaseous species, which might introduce porosity into the samples. This can lead to changes of the green density of the pellets, which has been reported to have an influence on the self-propagating reaction. For example, Dong et. al[34] observed increasing onset temperatures with decreasing green densities during the formation of NiAl. Moreover, the stabilizer has to be considered as a source of additional impurities such as carbon and/ or oxygen in the final product, which is why we were particularly interested in an alternative, stabilizer free synthesis approach.

Generally, metal nanoparticles can also be produced by thermal decomposition of suitable precursors in the presence of a stabilizer. This method represents a facile synthesis for the preparation of many metal nanoparticles, such as Ni[35][36], Fe[37], or Ru[38]. The main advantages of this approach are short reaction times and the formation of mainly gaseous side-products resulting in high purity products. This makes them an attractive synthesis route, especially for non-noble metal nanoparticles.

However, to our knowledge, little is known in literature about the synthesis of Al particles via a thermal decomposition pathway. The only reports using a thermal decomposition approach for the synthesis of submicron Al structures were published very recently, wherein Al-nanorods were synthesized by thermal decomposition of triisobutylaluminum in trioctylamine[39] or wherein relatively large nanoparticles were synthesized in diphenylether in the presence of perfluoroundecanoic acid as a capping agent.[40]

In our study, we investigated a thermal decomposition route to the synthesis of metallic, submicron Al particles. Within this approach, triisobutylaluminum was used as an Al source and metallic nanoparticles of Ag, Ni and Ru were applied as nanoparticular seeds. Although no additional capping agent is required, the particles can be passivated by simply adding oleic acid to the reaction mixture resulting in the formation of passivated Al core-shell particles. Using the resulting Al particles, the formation of Ru intermetallics was possible in good yields by heating compacted and thoroughly mixed Ru-Al powder mixtures to 800 °C under an atmosphere of flowing Ar.

2. Experimental

2.1 Materials

Triisobutylaluminium (solution; 1 M in Hexane) and trioctylphosphine (90 %) were purchased from Sigma-Aldrich (St. Louis, USA). Diphenylether (99 %), oleic acid (90 %) and nickel(II)acetylacetonate (95 %) were obtained from Alfa-Aesar (Kandel, Germany). Triphenylphosphine (99 %), $RuCl_3 \cdot xH_2O$ (39-42 % Ru; 99.9 % Ru), Al powder (99.7 %; 325 mesh) and Ru powder (99.8 %; 60 µm) were purchased from ABCR (Karlsruhe, Germany). Sodium borohydride (> 98 %) was purchased from applichem (Darmstadt, Germany). All chemicals were used as received without further purification unless stated otherwise. Diphenylether and oleic acid were dried at 100 °C in vacuo for 2 h, stored over molecular sieves (3 Å) and filtered through 0.45 µm syringe filters prior to use. Triphenylphosphine was dried in vacuo at 80 °C. All reactions were carried out under an argon atmosphere applying Schlenk techniques.

2.2 Syntheses

Ag Nanoparticles

Ag nanoparticles were synthesized following the method of Park et. al.[41] 1.7 g (10 mmol) $AgNO_3$ were added to a mixture of 0.5 ml oleylamine and 4.5 ml of oleic acid. The mixture was degassed at 70 °C for 1 h and then heated to 180 °C using an Al heating mantle. A temperature of 180 °C was maintained for 2 min. The black solid formed was dispersed in 5 ml of toluene and the particles were precipitated by adding 40 ml ethanol. The Ag nanoparticles were centrifuged (8000 rpm, 10 min) and washed by three additional cycles of redispersing in 5 ml toluene, precipitating with 40 ml of ethanol and centrifuging (8000 rpm, 10 min). The obtained black solid was dried in vacuo at 80 °C. XRD, TG and TEM measurements of the resulting Ag nanoparticles are shown in the supporting information (Figure S10).

Ru Nanopowder

Ru nanopowder were synthesized using a mechanochemical synthesis route.[42] Briefly, 1 g $RuCl_3 \cdot xH_2O$ (39-42 % Ru) (5 mmol) and 2 g (53 mmol) of $NaBH_4$ were milled for 30 min in an agate mortar. 40 ml of ethanol were added and the mixture was centrifuged (8000 rpm, 10 min). The resulting black powder was washed one more time with 40 ml of ethanol and afterwards two times with 40 ml of water (8000 rpm, 10 min). The product was dried in vacuo at 80 °C. Precautions must be taken since the dried Ru nanopowder tend to react explosively when exposed to air. XRD, TG and TEM measurements of the resulting Ru nanopowder are shown in the supporting information (Figure S12).

Ni Nanoparticles

Ni nanoparticles were synthesized following the method of Carenco et. al.[35] 2 g of $Ni(acac)_2$ (8 mmol) were dissolved in 21 g of oleylamine and 2.3 g (6 mmol) of TOP and were degassed at 100 °C for 1 h. The temperature was raised to 220 °C and the mixture was maintained at 220 °C for 2 h resulting in the formation of a black solid. After cooling to room temperature 40 ml of acetone were added and the mixture was centrifuged (8000 rpm; 10 min). The particles were washed by three cycles of redispersing in 5 ml of hexane, adding 40 ml of acetone and centrifuging (8000 rpm; 10 min). The obtained black solid was dried in vacuo at 80 °C. XRD, TG and TEM measurements of the resulting Ni nanoparticles are shown in the supporting information (Figure S11).

Submicron Al particles

60 ml of diphenylether were degassed at 100 °C for 30 min. After cooling to 40 °C 2 ml of Triisobutylaluminium (1 M in hexane) (2 mmol) and a small amount of seed nanoparticles of Ag, Ru or Ni was added (M: Al 1: 80). When Ru or Ni were used, 50 mg (0.2 mmol) of PPh_3 were added to increase their dispersibility. The hexane was removed in vacuo and the mixture was homogenized using an ultrasonication bath for 15 min. The mixture was refluxed for 15 min resulting in the formation of a black/ grey solid. After cooling to room temperature 0.3 ml (1 mmol) of oleic acid were added and the mixture was stirred for an additional 30 min. The grey solid was centrifuged (8000 rpm; 10 min), washed three times with 15 ml of diethylether (8000 rpm; 10 min) and dried in vacuo at room temperature.

Synthesis of Aluminides

The samples for the preparation of aluminides were prepared by thoroughly mixing both components in an ultrasonication bath using hexane as a dispergent. In case compacted pellets were used for the synthesis, the resulting powder mixtures were compacted in a hydraulic press (Ø 6 mm; 1 t; 15 min; 190 MPa). The pellets or the loose powders were heated in a tube furnace to 800 °C using a heating rate of 200 °C/ h under a flowing Ar atmosphere (100 ml/min) in open alumina crucibles. A temperature of 800 °C was maintained for 2 h before cooling to room temperature using a cooling rate of 200 °C/h. High heating rates of 1 °C/ s were realized by heating the compacted pellets or loose powders up to 800 °C in a TGA/ DSC thermal analyzer under an atmosphere of flowing Ar (40 ml/min) in open alumina crucibles. After reaching 800 °C the samples were immediately cooled down to room temperature with a cooling rate of 20 °C/ min without any additional isothermal segment. After cooling down to room temperature, the samples were homogenized and their composition was determined from Rietveld refinements.

2.3 Methods

Dynamic light scattering (DLS) measurements were carried out at room temperature using an ALV Compact Goniometer at a scattering angle of 90 °. The samples were prepared by dispersing the particles in hexane applying an ultrasonication bath for 20 min. Before the measurement, the samples were equilibrated for 5 minutes. Infrared spectra of the dried powders were recorded using a Bruker Vertex 70 ATR-FTIR spectrometer. The elemental analyses were performed on an Elementar Vario Micro cube. Thermogravimetric analyses (TGA) were conducted on a Netzsch TG F1 Iris under a constant flow of N_2/O_2 32:8 (40 ml/min) using a heating rate of 10 K/ min. The samples were heated up to 900 °C and hold at this temperature for 15 min. The measurements were carried out in open alumina crucibles. Powder X-ray diffraction (PXRD) measurements were carried out on a Bruker D8-A25-Advance diffractometer in a Bragg-Brentano geometry using Cu Kα-radiation. Diffraction patterns were recorded from 7 to 120° (2θ) with a step size of 0,013° and a total measurement time of 1 h. The specimens were prepared by drop coating the dispersed and homogenized samples directly onto glass sample holders. Sample composition and crystallographic structure were determined via Rietveld refinements using TOPAS 5.1.[43] A Chebychev polynom (15^{th} degree) was used for background fitting and instrumental line broadening was taken into account by a fundamental parameter approach.[44] The crystal data was compared with published

crystal structures from the crystallographic open database (COD)[45] and the inorganic crystal structure database (ICSD). Entries with the following ID's were used for the Rietveld refinements: Al: 2300250 (COD), Ni: 2100640 (COD), Ru 1539052 (COD), Ag_2Al 1509011(COD), γ-Al_2O_3 2107301(COD), RuAl 1527371(COD), $RuAl_2$ 58156(ICSD), Ru_4Al_{13} 58158(ICSD). Simultaneous thermal analyses (STA) were measured on a Mettler-Toledo STAre system under a constant flow of Ar (40 ml/min). The samples were heated up to 800 °C using a heating rate of 1 °C/s. Immediately after reaching 800 °C the samples were cooled down to room temperature using a cooling rate of 20 °C/ min. For the STA measurements, open alumina crucibles were used. Solid-state ^{27}Al SPE-MAS NMR measurements were carried out on a Bruker AV400WB spectrometer in ZrO_2 rotors using solid α-Al_2O_3 as an external standard. Transmission electron microscope (TEM) images were recorded on a JEOL JEM-2010. TEM samples were prepared by drop coating a particle dispersion in hexane directly on the carbon coated copper grids (Plano S160-3). Scanning electron microscope (SEM) measurements were done on a JEOL JSM-7000F microscope. The powders were measured directly without any additional pretreatment. Focused ion beam (FIB) measurements were done on a Helios NanoLab660 from FEI using a gallium ion beam. The samples were coated with conductive carbon prior to the measurements.

3. Results and Discussion

Metallic submicron Al particles have been successfully prepared by thermally decomposing triisobutylaluminum (TIBAl) in the presence of Ag, Ni or Ru nanoparticles (for characterization of the Ag, Ni and Ru nanoparticles see supporting information figures S10, S11 and S12). By using these metallic seeds, the synthesis of aluminides starting from the resulting Al particles is possible without introducing any additional impurities. TIBAl is a well-known precursor for the synthesis of Al films via chemical vapor deposition (CVD) processes and was chosen as a precursor for the synthesis of these submicron particles because of its relatively low decomposition temperature (~250 °C) compared to other organoaluminum compounds. The decomposition is known to be a two-step process, with the first β-hydride elimination occurring at about 120 °C. In a second step at temperatures >200 °C, the resulting diisobutylaluminumhydride (DIBAlH) then completely decomposes yielding elemental Al, hydrogen and isobutylene (Scheme 1)[46].

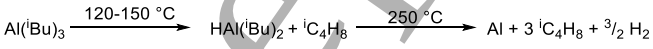

Scheme 1. General decomposition pathway of TIBAl.

Only gaseous side products, namely hydrogen and isobutylene, are formed during this reaction, which allows a very simple work-up and the synthesis of high purity products. It also has to be noted that the reason why diphenylether was chosen as a solvent was its high boiling point and its inertness towards TIBAL. The use of other high boiling solvents is also possible as was evidenced by successful syntheses conducted in tetraglyme, paraffin oil as well as hexadecane. However, when non-polar, non-coordinating solvents like paraffin oil and hexadecane were used an increased Al film formation at the walls of the reaction vessel could be observed compared to the syntheses carried out in polar, weakly coordinating solvents. No decomposition at all could be observed when 1-hexadecene or benzylether were used as a solvent. This might be explained by the formation of thermally more stable Al-adducts, which might form after a deprotonation of these solvents by triisobutylaluminum. These species are not capable of undergoing beta-hydride-eliminations resulting in higher decomposition temperatures.

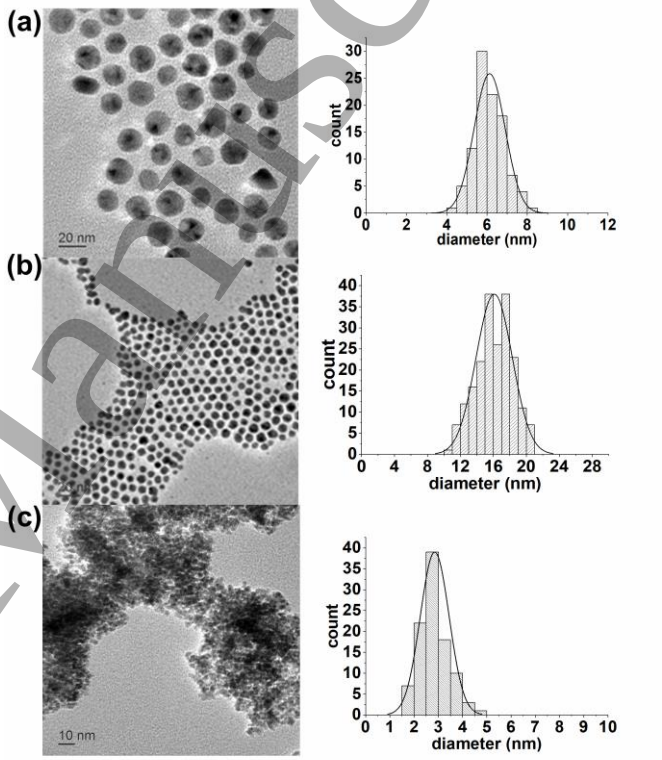

Figure 1. TEM images and particles size distributions (obtained from measuring 100 particles) of the metal nanoparticles used as seeds for the synthesis of submicron Al particles via a thermal decomposition approach a) Ni b) Ag c) Ru.

When the decomposition was carried out without any additional metallic nanoparticles present in the reaction mixture, no formation of Al particles could be observed. Instead, the formation of a metallic Al film on the heated surface of the reaction vessel was taking place. The addition of typical nanoparticle stabilizers (stabilizer: Al 1:10) prior to the decomposition and the use of stabilizing solvents (tetraglyme) could also not prevent this film formation. The examined stabilizers were oleylamine, trioctylphosphineoxide (TOPO) and PPh_3. When oleic acid was used, as a stabilizer the film formation was not evident, however the resulting

hydrophobic oleic acid capped particles were strongly agglomerated due to the polarity of the diphenylether.

The coating of the reaction vessel could however be prevented by the addition of metallic nanoparticles (Figure 1) prior to the TIBAl decomposition. We believe that the Al is still formed at the surfaces, but due to the extremely large surface area of the metallic seed nanoparticles, the formation of submicron and nanostructures is favored over the film formation (Figure S1). The decomposition and the formation of submicron Al particles could be observed using different metallic nanoparticles (Ag, Ru and Ni) acting as seeds but is likely not restricted to these few examples as was indicated by a successful synthesis in the presence of SiO_2 nanoparticular seeds. One criticism can be that due to the presence of the seed metal in the final sample, the resulting particles might technically not be considered to be "pure" Al. However, the seed metal content in the samples was found to be lower than 4 wt.% (Table 1). Moreover, if a further chemical reaction of the particles, like the formation of aluminides, is targeted an additional metal has to be used nonetheless. Since the formation of the Al particles was found to be successful in the presence of various metal seeds, one can simply apply seeds of the targeted metal aluminide thus ultimately introducing no impurities.

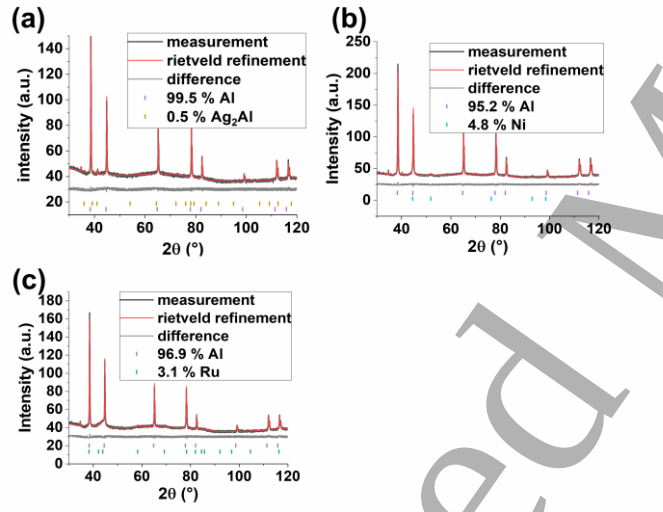

Figure 2. PXRD-measurements and Rietveld-refinements of a) Al from Ni seeds b) Al from Ru seeds c) Al from Ag seeds, synthesized via thermal decomposition of TIBAl in Ph2O using different metal nanoparticles as seeds.

After the synthesis, the Al particles were passivated by adding oleic acid. Since synthesis and passivation were carried out in two separate steps, synthesis of „unpassivated", submicron Al particles is possible by skipping the passivation step.

The presence of the seed metal in the resulting particles could be observed in PXRD measurements, however no formation of a core-shell morphology was visible neither in TEM (Figure S2) nor in FIB measurements (Figure 7b). Instead, agglomerates of small particles present besides the large Al particles were visible in the TEM image, indicating the formation metal-Al particle mixtures rather than the formation of core-shell morphologies. EDX analysis of a single particle (Figure S3) revealed the formation of pure Al particles, further confirming that no formation of core-shell morphologies or a dissolution of the seed metal in the Al is occurring.

The formation of fcc-Al could be confirmed by PXRD measurements. No signals referring to aluminum oxide could be identified (Figure 2). This does however not exclude the existence of a passivating oxide layer, which is consisting of amorphous alumina at room temperature and can thus not be detected in PXRD measurements. The composition of the samples, as well as the crystallite size, were both determined via Rietveld refinements and are summarized in Table 1. Despite the much higher molecular weight of the seed metals, the Al contents of the submicron particles are very high (>96 wt. %) and only small amounts of the seed metals can be found. The crystallite sizes of Al are 88 nm for Al from Ni seeds, 171 nm for Al from Ru seeds and 102 nm for Al from Ag seeds. The different crystallite sizes observed when different metallic seeds are used are likely caused by different degrees of agglomeration of these seeds in diphenylether. Accordingly, the Ru nanoparticle seeds, which were synthesized using a mechanochemical approach with no stabilizer added, formed large agglomerates resulting in a decreased surface area and are thus leading to larger Al particles. For all samples, these values show good agreement with the particle sizes determined via TEM measurements (see below). The determined lattice parameters of 4.049 – 4.050 Å show good agreement with values reported in the literature (4.03 - 4.05[47,48]). The presence of Ag_2Al after the synthesis indicates that the formation of Al is indeed occurring at the surface of the seed metal nanoparticles. As expected, when Ni or Ru were used as seeds no intermetallics could be detected, since the onset of the formation reactions require much higher temperatures. In addition, as can be seen by examining the Rietveld refinement particularly in the 2θ range including the (111) and (002) reflections, no peak shifting out of their ideal positions can be observed and only a very small broadening of the (002) reflection compared to the (111) reflection is evident. Both is indicating towards a very small amount of stacking faults being present in the synthesized metal particles, as can be expected based on the high reaction temperature of 260 °C as well as on the high stacking fault energy of aluminum.[49]

Table 1. Sample compositions and crystallite sizes of submicron Al particles synthesized via thermal decomposition of TIBAL in Ph_2O using different metal nanoparticle seeds. Values were determined via Rietveld-refinements of the respective PXRD-measurements.

sample	Al [wt. %]	M [wt. %]	crystallite size [nm]	lattice parameter Al [Å]
Al(Ni)	96.46	3.54 (Ni)	Al: 87(3) Ni: 6(1)	4.049

Al(Ru)	96.94	3.06 (Ru)	Al: 171(17) Ru: 3(1)	4.050
Al(Ag)	99.54	0.52 (Ag_2Al)	Al: 102(3) Ru: 45(1)	4.050

The TEM image of oleic acid capped submicron Al particles synthesized using Ni seeds reveals particles with a mean diameter of 125±36 nm (Figure 3a). The particles show a broad particle size distribution and a quasi-spherical shape. They are agglomerated, while the single particles are clearly visible. No sintering was detected. The sizes determined via TEM measurements are about 37 nm larger than the sizes determined via Rietveld analysis. It is well known from literature [7],[23] that the use of oleic acid as a capping agent will lead to the formation of an oxidic passivation layer, due to the presence of organic provided oxygen even under inert conditions. Due to the formation of this amorphous oxide layer and the organic passivation layer, the particle sizes determined via TEM measurements are expected to be larger than those determined via Rietveld analyses. The Al particles synthesized using Ag seeds show triangular or hexagonal shapes (Figure 3c) with a mean radius of 122±21 nm. As can be seen in the inset they also show a rather broad size distribution while no sintering of the particles is visible. The size of the Al particles from Ag seeds was determined as the height of the triangular or hexagonal particles and is thus larger than the value determined via Rietveld analysis. As described above, the Ru seed particles showed agglomeration and thus exhibited a poor dispersability. The surface provided by the Ru nanoparticles can be expected to be smaller compared to that provided by the Ni seeds. The particles obtained from Ag seeds exhibited a triangular or hexagonal morphology induced by the morphology of the Ag seeds. Hence, the various seed particles have a specific influence on the resulting Al particle growth mechanisms.

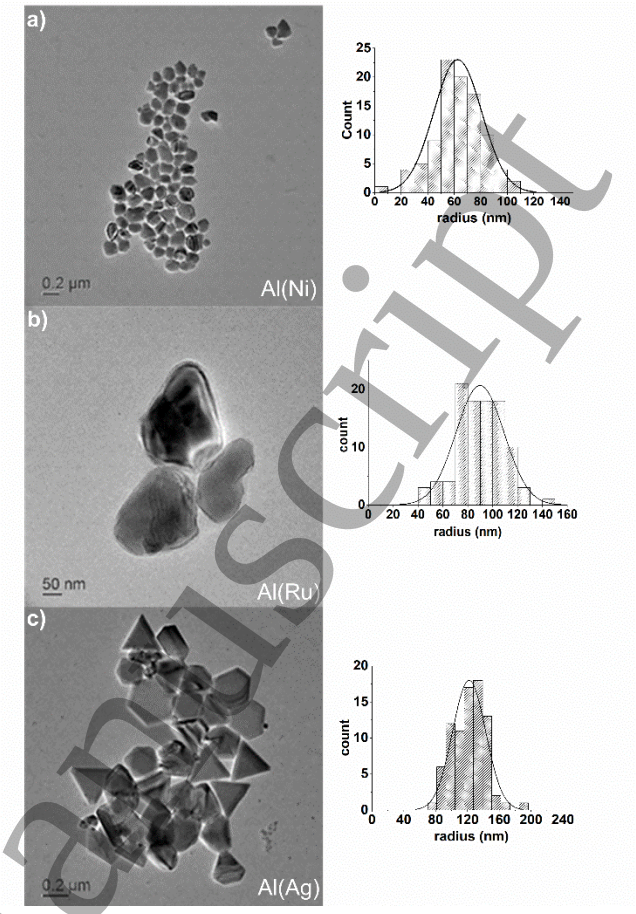

Figure 3. TEM images and particles size distributions (obtained from measuring 100 particles) of the metal nanoparticles used as seeds for the synthesis of submicron Al particles via a thermal decomposition approach a) Ni b) Ag c) Ru.

Ag seeds seem to support the formation of triangular or hexagonal shaped platelets (Figure S4). This is most likely based on the development of stacking faults within the originally formed very small Al seeds, which is a known phenomenon and has been observed upon deposition of Al on Ag surfaces.[50][51][52] It is also known that in case of fcc metals the nanoparticle grow from nuclei containing stacking faults will lead to the formation of triangular or hexagonal shaped platelets[53][54].

The TEM image of the Al particles from Ru seeds (Figure 3b) shows quasi-spherical particles with a broad size distribution, while no sintering of the particles is visible. Due to their very poor dispersibility, very few particles were found on the copper grid and no particle size distribution could be determined for the Al particles from Ru seeds. Instead, the mean radius was determined from SEM measurements and is 90±19 nm. As can be seen a broad size distribution could be observed, with no visible sintering of the Al particles.

EDX analysis (Figure S3) revealed the presence of Al and oxygen, which indicates the presence of an oxygen containing passivating layer. However, the exact nature of the passivating layer is unclear since it is not possible to distinguish between the carbon contained within the sample and the carbon copper

grid. No signals belonging to Ag could be detected, confirming the very low silver content determined via Rietveld analysis as well as the formation of Al and seed metal particle mixtures rather than core-shell morphologies. The Cu signals are originating from the carbon coated copper grids used for the measurement, while the Si signal stems from the Si-Li detector.

The hydrodynamic radii determined via DLS-measurements were 85(3) nm for the Al particles from Ni seeds, 86(3) nm for the Al particle from Ru seeds and 111(8) nm for the Al particles from Ag seeds (Figure S5). For the Al particles from Ni seeds, the hydrodynamic radius prior to the addition of oleic acid was 70(2) nm. The formation of larger agglomerates in these samples is clearly visible. The larger hydrodynamic radii compared to the particle sizes observed in XRD and TEM measurements are indicating the formation of agglomerates, which also could be seen in the TEM measurements.

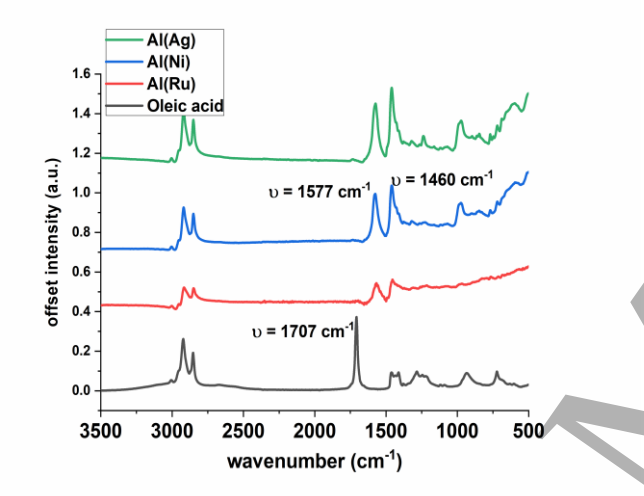

Figure 4. ATR-FTIR spectra of neat oleic acid and of oleic acid capped submicron Al particles synthesized via thermal decomposition of TIBAL in Ph_2O using different metal nanoparticles as seeds.

The presence of an organic passivation layer was confirmed by FTIR-analysis of the dried submicron particles. Figure 4 shows the FTIR-spectra of neat oleic acid and of oleic acid capped Al particles. The most prominent signals in the FTIR-spectrum of the neat oleic acid are the carbonyl stretching at ~1700 cm^{-1} and the C-H stretching modes in the region of 2700-3000 cm^{-1}. In the spectra of the oleic acid capped Al particles the C-H modes at 2700-3000 cm^{-1} remained largely unchanged, indicating that the alkyl chain is still intact. However, the carbonyl stretching at ~1700 cm^{-1} is no longer visible and two new peaks at ~1460 cm^{-1} and 1580 cm^{-1} have appeared which belong to the symmetric and the asymmetric carboxylate stretching modes, respectively. Deacon et. al.[55] assigned frequency differences of these two peaks of ~200 cm^{-1} to a bridging bonding geometry, differences of <80 cm^{-1} to a bidentate bonding geometry and differences of ~300 cm^{-1} to a monodentate bonding geometry. The observed frequency difference of ~120 cm^{-1} is thus pointing towards a bidentate or maybe a bridging bonding geometry. A bridging bonding geometry was also reported by Jouet et al.[19]. However, it has to be noted, that other binding geometries are also being discussed in the literature[16][27], which would however result in the presence of an OH signal at wavenumbers > 3000 cm^{-1}, clearly not observable in our measurements.

3.1 Thermal analysis of the formed Al particles

Oxidation of the submicron Al particles was examined under controlled experimental parameters using TG measurements making it possible to calculate the Al contents of the particles from the resulting mass changes. TG measurements were conducted in an atmosphere of N_2:O_2 32:8 using a heating rate of 10 °C/min in order to obtain a controlled oxidation of the Al particles without ignition.

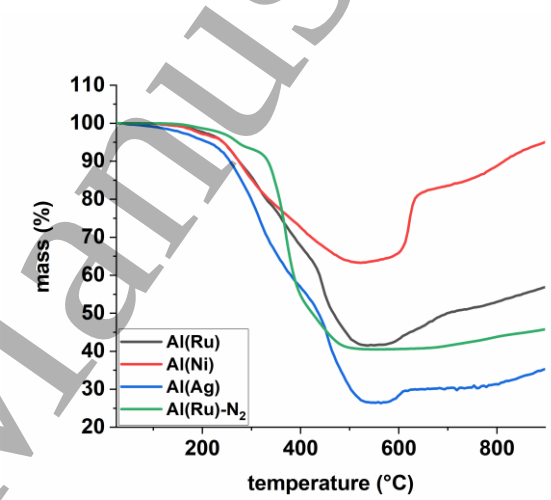

Figure 5. TG analyses of oleic acid capped submicron Al particles synthesized via thermal decomposition of TIBAL in Ph_2O using different metal nanoparticles as seeds (10 K/ min; 40 ml/ min synthetic air unless stated otherwise). Samples were hold at 900 °C for an additional 15 min to ensure complete oxidation (not shown). Synthesis were carried out using a metal: Al ratio of 1:80 and an oleic acid: Al ratio of 1:2.

In the TGA curves of submicron Al particles synthesized using different metal nanoparticular seeds almost no mass loss can be observed up to ~150 °C (Figure 5). Around 150 °C the mass loss starts in all samples and is finished at around 500 °C. At temperatures > 500 °C the mass is increasing in a well-known two step pattern due to oxidation of Al.[56]

In the temperature range between 500 and 600 °C, a slow mass increase is observed due to the diffusion of oxygen through the oxide layer. At around 600 °C, the amorphous alumina transforms into denser γ-alumina leading to an exposure of the Al^0 core to the atmosphere resulting in a sharp mass increase, followed by the formation of a plateau. With increasing temperatures, oxygen diffusion is increasing again

leading to faster mass gains until the Al is completely

From these TGA curves, the total organics content can be estimated from the mass loss if any oxidation of the Al particles occurring before the mass minimum is neglected. The Al content can be estimated from the observed mass increases (Scheme 2), assuming that only alumina was present at the end of reaction. XRD measurements of the particles after the TGA analyses indeed showed almost exclusively the presence of δ-Al_2O_3 (Figure S6). The values determined from the mass increases (Eq. 1) can be understood as minimum Al^0 contents since only Al oxidized after the mass minimum is taken into account and any oxidation occurring at lower temperatures is neglected. The determined organic and Al contents are summarized in Table 2.

$$w(Al)=\frac{m_{gain}\cdot 2\cdot M_{Al}}{M_O\cdot 3} \quad \text{(Eq. 1)}$$

Scheme 2. General equation for the calculations of the Al contents from the TGA measurements using the mass gain (Eq. 1).

The mass losses are ranging from 36.73 % for the Al particles from Ni seeds and 58.47 % for the Al particles from Ru seeds up to 73.84 % for the Al particles from Ag seeds. It has to be noted that the organic contents determined via TGA measurements are representing minimum values, since on one hand the end of the mass loss step cannot be clearly identified due to the starting mass increase and on the other hand Al oxidation is to be expected not only to occur at temperatures >600 °C. For comparison, elemental analyses of the particles are summarized in Table 3. The organic contents determined via CHN analyses (taken as sum of carbon and hydrogen content) ranged from 39.8 % for the Al particles from Ni seeds and 60.5 % for the Al particles from Ru seeds up to 71.8 % for the Al particle from Ag seeds. When the oxygen content expected for oleic acid is calculated based on the measured carbon content good agreement between the organic contents determined via both methods can be observed. Moreover, the determined ratios of carbon and hydrogen are showing good agreement with the values expected for oleic acid and oleate respectively.

A minimum Al^0 content was calculated from the mass gains, only considering Al oxidized at temperatures > 600 °C. As it is rather difficult to determine the exact onset of the mass gain, it was defined at the temperature of the mass minimum. The minimum Al-contents calculated were 37.7 % for Al from Ni seeds, 19.1 % for Al from Ru seeds and 11.4 % for Al from Ag seeds.

Moreover, we ascribe the significantly different organic contents to the very different dispersibilities of the various metal nanoparticle seeds of Ni, Ru and Ag. The Ni nanoparticles showed a poor dispersibility in diphenylether and agglomerated very quickly due to their magnetism resulting in their deposition on the stirring bar. Similarly, the Ru nanoparticles were synthesized using a mechanochemical approach without applying any stabilizer resulting the formation of large agglomerates. The Ag nanoparticles showed a good dispersibility and the resulting yellow/ orange dispersions were stable until the end of the reaction. The good dispersibility of the Ag seeds is based on the presence of oleic acid and oleylamine on their surface. The organic content determined from TG measurements was found to be about 25 %. Due to these differences the submicron Al particles, synthesized using Ag nanoparticle seeds showed the largest surface and thus the highest contents of organics.

The Al_2O_3 content of the Al particles can be estimated as the balance of the Al and organic contents determined from the TG measurements as well as the seed metal content determined from the Rietveld refinements. In this estimation any oxidation of the seed metals as well as any mass loss occurring after reaching the mass minimum is neglected. The calculated Al_2O_3 contents are ranging from 20.74 % for Al(Ni) to 14.25 % for Al(Ag) and are thus, as to be expected, increasing as the particle size decrease.

Table 2. TGA of oleic acid capped submicron Al particles synthesized via thermal decomposition of TIBAL in Ph2O using different metal nanoparticles as seeds. Synthesis were carried out using a metal: Al ratio of 1:80 and an oleic acid: Al ratio of 1:2.

Sample	Mass loss [%]	Residual mass [%]	Al-content[a] [%]	Al_2O_3-content [%]
Al(Ni)	36.73	96.81	37.73	20.74
Al(Ru)	58.03	58.47	19.05	19.86
Al(Ag)	73.84	36.28	11.39	14.25

[a] calculated from mass gain.

Table 3. CHN analyses of oleic acid capped submicron Al particles synthesized via thermal decomposition of TIBAL in Ph_2O using different metal nanoparticles as seeds. Synthesis were carried out using a metal: Al ratio of 1:80 and an oleic acid: Al ratio of 1:2.

Sample	C [%]	H [%]	N [%]	O[a] [%]	∑ [%]	C/H
Al(Ni)	30.37	4.92	---	4.49	39.78	6.17
Al(Ru)	46.67	6.97	---	6.90	60.54	6.69
Al(Ag)	55.53	8.05	---	8.22	71.80	6.89
oleic acid	76.60	12.06	---			6.35
oleate	76.87	11.74	---			6.55

[a] expected value for oleic acid calculated from the measured C content.

3.2 Variation of particle size

As a model system for systematic studies of size control, we applied the particles prepared with Ag nanoparticular seeds. While keeping all other parameters constant the Ag:Al ratio was changed in the synthetic procedures. A higher Ag:Al ratio should, in theory, lead to a size decrease of the resulting Al

particles, since, assuming the concentration of Al stays constant, an increased Ag concentration would lead to an increased surface area, allowing more simultaneous nucleation and would thus result in smaller Al particles. However, almost no change in the crystallite size of the particles could be observed when the Ag:Al ratio was altered. As was evidenced by DLS measurements the Ag nanoparticles formed agglomerates even after being ultrasonicated in diphenylether for 20 min (Figure S8a), which is resulting in a decreased surface area. To overcome this problem a weakly coordinating ligand, PPh_3, was added to the reaction mixture in order to improve the dispersibility of the Ag nanoparticles. The addition of this molecule resulted in the formation of fewer agglomerates which can be observed in DLS as well as UV/VIS-measurements, where red shifted and less broad LSPR peaks are detected (Figure S8b). By adding PPh_3 and increasing the amount of Ag in the thermal decomposition reaction, the crystallite size of the Al particles could be reduced to 61 nm which was confirmed by Rietveld analysis as well as TEM measurements (Table 4). The particle size obtained from TEM images (Figure 6a and 6b) was 80.5±15.7 nm. A narrower particle size distribution was reached and the shape was quasi-spherical contrary to the trigonal and hexagonal shapes obtained in the syntheses without any additional stabilizer (Figure 3c). Thus, since the morphology of the Al particles is also changed upon adding PPh_3 to the synthesis, it is not only increasing the dispersibility of the seed nanoparticles but is also affecting the particle growth.

Table 4. Sample compositions and crystallite sizes of submicron Al particles synthesized via thermal decomposition of TIBAL Ph_2O using different Ag:Al ratios in the presence of PPh_3. Values were determined via Rietveld-refinements of the respective XRD-measurements.

Sample	Ag:Al	PPh_3:Ag [%]	Al [wt. %]	M [wt. %]	Crystallite size [nm]
Al(Ag)	2:100	50:1	99.15	0.85 (Ag_2Al)	Al: 61(3)
Al(Ag)	1:100	50:1	99.70	0.30 (Ag_2Al)	Al: 85(2)
Al(Ag)	1:80	---	99.54	0.52 (Ag_2Al)	Al: 102(3)

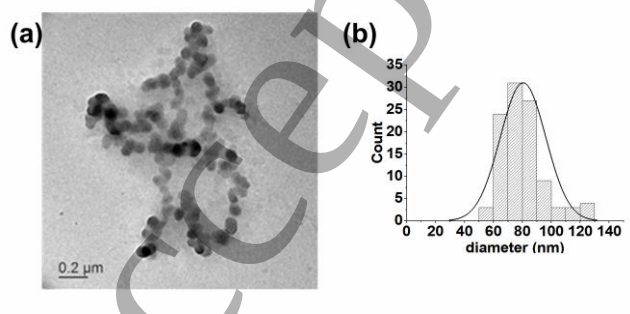

Figure 6. a) TEM images of submicron Al particles synthesized using Ag seeds in the presence of PPh_3 b) particle size distribution obtained from TEM images by measuring 104 particles.

3.3 Particle preparation without capping agent

Since the oleic acid was added in an additional step after the synthesis, it is easily possible to synthesize submicron Al particles with very low organic contents by simply omit using a capping agent after the decomposition reaction. Instead, the resulting powders were centrifuged and dried in vacuo yielding surfactant free submicron Al powders. It has to be noted that these particles were passivated upon air contact through the formation of a thin oxide layer. Especially the low organic contents of the resulting particles are making them interesting precursors for the formation of aluminides, since no major introduction of carbon and/ or oxygen impurities is possible in the final product, contrary to when for example oleic acid capped particles are used (Figure S7).

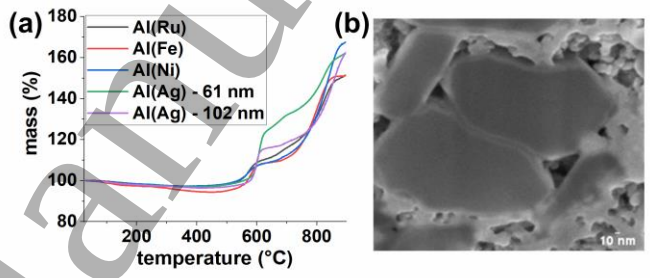

Figure 7. a) TGA analyses of uncapped submicron Al particles synthesized via thermal decomposition of TIBAL in Ph_2O using different metal nanoparticles as seeds (10 K/ min; synthetic air). Samples were hold at 900 °C for an additional 15 min to ensure complete oxidation (not shown). Syntheses were carried out using a metal:Al ratio of 1:80 b) FIB measurement of synthesized submicron Al particles from Ru seeds in a Ru environment.

The content of organics was determined using CHN- and TG- analysis. As can be seen in Figure 7a and Table 5 the organic content of the samples was well below 5 % in all cases and is probably due to moisture and residual solvent. Again, the typical two-step oxidation pattern is clearly visible for all the samples. The Al particles from Ag seeds with a crystallite size of 61 nm shown in the TG measurement below were synthesized in the presence of PPh_3 in order to reduce their particle size. Despite the use of PPh_3 in the synthesis only a small amount of organics could be detected in TGA as well as CHN analyses, indicating the weakly coordinating nature of the surfactant which is basically completely washed away during the work-up procedure. Because of their still very low organics contents these particles are good candidates for the use in the synthesis of different intermetallic compounds.

The Al_2O_3 contents estimated from the TG measurements are ranging from 11.96 % for Al(Ni) to 18.26 % for Al(Ag). These values are lower than the values determined for the oleic acid capped particles, since i) no additional oxygen was introduced

by addition of the oleic acid and ii) no or just minimal overlap of mass loss and gain during the TG measurements.

The smaller size of the Al particles from Ag seeds is also indicated by a higher mass increase in the first oxidation step (Figure 7a), where only Al close to the surface is oxidized. Accordingly, the larger Al particles from Ag seeds with sizes of 100 nm showed a smaller mass increase in this first oxidation step. Due to the oxidation of Al to Al_2O_3 the observed residual masses are greater than 100 %. For pure Al a residual mass of 189 % can be expected. The observed lower values are due to the oxide layers present on the particle surfaces at the start of the measurements, causing the samples not to be pure Al. As can be expected based on the low organic content no signals could be detected in the FTIR measurements (Figure S9b). The increase in absorption at wavelengths below 1000 cm^{-1} can be attributed to Al_2O_3 at the particle surfaces.

Figure S9a shows the ^{27}Al-SPE-MAS-NMR of surfactant free Al particles from Ru seeds. The signal at 1632 ppm can be assigned to Al^0, while the low intensity signal at around 0 ppm can be assigned to Al_2O_3 present at the particle surface. Since electron microscopic measurements only revealed the particle surfaces, we further examined the cross-sections of the synthesized Al particles using FIB techniques. FIB measurements revealed the core-shell structure of the uncapped submicron Al particles (Figure 7b): A continuous shell, which we ascribe to the presence of amorphous alumina, surrounds the Al particles. The thickness of this shell is in the range of 5 – 7 nm, which is in the same range of typical values for the thickness of the oxide shell reported in the literature.[57]

Table 5. TGA and CHN analyses of uncapped submicron Al particles synthesized via thermal decomposition of TIBAL in Ph_2O using different metal nanoparticles as seeds. Syntheses were carried out using a metal:Al ratio of 1:80 in open alumina crucibles. No nitrogen was detected in the CHN analyses.

sample	Mass loss [%]	Residual mass [%]	Al-content[a] [%]	Al_2O_3-content [%]	∑(C+H) [%]
Al(Ni)	2.8	169.8	81.7	11.96	1.03
Al(Ru)	3.2	158.2[b]	81.7	12.04	1.88
Al(Ag) 61 nm	3.1	166.3	78.1	18.26	0.92
Al(Ag) 102 nm	3.6	166.8	79.2	16.66	

[a] calculated from mass gain [b] calculated using the limit value of an asymptotic fit to the measurement data.

3.4 Formation of Aluminides

Aluminides are intermetallic compounds of Al with at least one (more electropositive) additional element, which are attractive materials for the use in high temperature applications, due to their high-temperature strength[58], as well as chemical[59], and oxidation resistance[60]. Aluminides can be synthesized via highly exothermic self-propagating high-temperature syntheses starting from the elemental powders. Very short reaction times and high purity products are characteristic for these types of reactions. The use of the synthesized Al particles for the formation of metal aluminides was examined by reacting the "uncapped" submicron particles with Ru powders. To exclude the influence of impurities, the formation of Ru-aluminides was carried out using Al particles synthesized with Ru seeds. In order to investigate the influence of the Al particle size on the formation of the respective aluminides, the observed results were compared to the results obtained when larger commercial Al powders with a particles size of around 14 µm were used (for the characterization of the Al powder see supporting information figure S14).

Six different intermetallic compounds are known in the Ru-Al system[61]: $RuAl_6$, Ru_4Al_{13}, Ru_2Al_5, $RuAl_2$, Ru_2Al_3 and RuAl. Due to RuAl exhibiting a good chemical and oxidation resistance as well as a good high-temperature strength and being the only phase not representing a stoichiometric compound, it is the most important phase for possible technical applications.

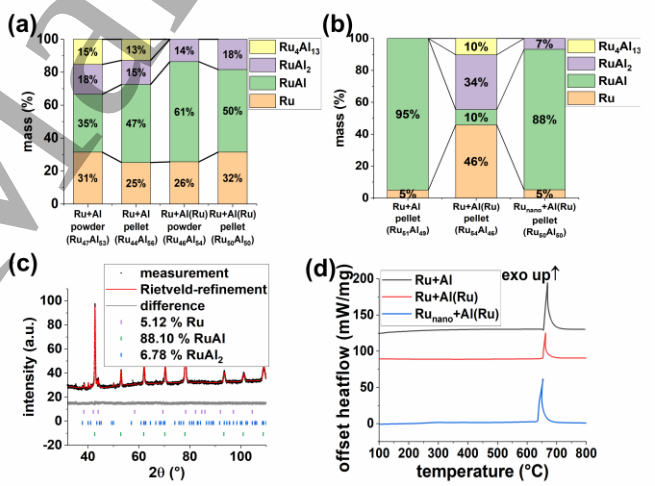

Figure 8. Sample compositions of Al and Ru powder mixtures in a 1:1 stoichiometry after heating up to 800 °C under an atmosphere of Ar determined via Rietveld refinements at a heating rate of a) 3.3 K/min and b) 60 K/min. Ru and Al are referring to the commercial Ru and Al; Al(Ru) is referring to the synthesized Al powders. Compositions noted in brackets describe the total sample composition estimated from Rietveld refinements assuming the formation of ideally stoichiometric phases c) PXRD measurement and Rietveld-refinement of the Al(Ru) and Ru_{nano} sample shown in b) d) STA measurements of compacted Ru – Al powder mixtures using a heating rate of 60 K/min under an atmosphere of flowing Ar.

The synthesis of the target compound RuAl was investigated using the synthesized Al particles as well as commercial Al powder. The Al particles and Ru were mixed

in a stoichiometric ratio of 1:1 assuming an Al^0 content of the synthesized Al particles of 70 % as determined from TGA measurements, while the presence of an oxide shell was neglected for the commercial Al powder. The exothermic reaction in a loose powder sample of micrometer sized Ru and Al was reported to occur at 755 °C [59]. Thus, the samples were heated up to a maximum temperature of 800 °C in order to be capable to detect every exothermic or endothermic reactions during the STA scans that might possibly occur during the heat up. The yield of RuAl was similar, but low in every sample upon heating up to 800 °C using a slow heating rate of 200 °C/h (Figure 8a). When commercial Al powder was used only 35 % of RuAl was formed in the case of loose powder while 47 % of RuAl was formed using the pellets. Applying the synthesized Al particles, the yields were a bit higher, 61 %/ of RuAl for the loose powders and 50 % of RuAl for the pellets. The same is true for the amount of unreacted Ru, which was present in contents ranging from 25 % up to 32 %. However, no formation of the Al rich phase Ru_4Al_{13} could be observed in the samples in which the synthesized particles were used, while it was present up to 15 % when the commercial Al-powder was used. Similar observations were made by Mohamed et al.[62] who observed the formation of $RuAl_2$ containing multiphase products in compacted Ru-Al powder mixtures (Ru: 6 µm; Al: 20 µm) applying slow heating rates of 0.08 K/min. According to the literature[62] in case of commercial Ru and Al powders RuAl was formed almost exclusively when a high heating rate of 60 K/min was used. However, for the Al(Ru) and Ru particle mixtures only multiphase products could be observed (Figure 8a and 8b) using both slow and fast heating rates, particularly showing a very high amount of 45 % of unreacted Ru. When the large commercial Ru powder (60 µm) was substituted with smaller, nanocrystalline Ru powder (crystallite size 2-3 nm) more complete reactions and higher contents of RuAl (up to 88 %) could be determined after heating up to 800 °C (Figure 8b and 8c**)**. Thus, as reported earlier by Wolff[59] the Al/ Ru particle size ratio as well as the Ru particle size are playing important roles in the synthesis of RuAl starting from these submicron particles.

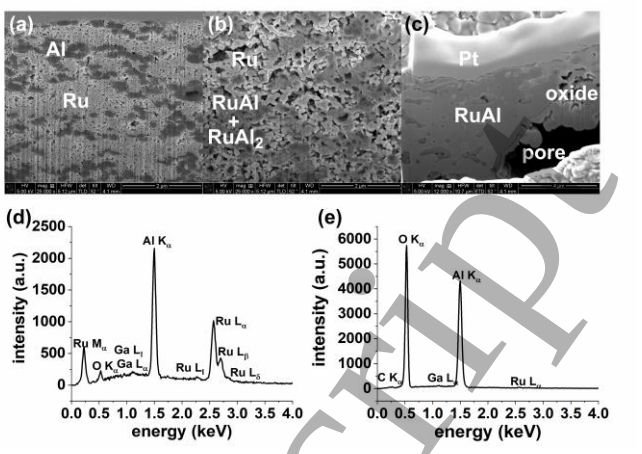

Figure 9. a) FIB images of as prepared compacted Ru_{nano} and Al(Ru) particle mixtures b) FIB images of compacted Ru_{nano} and Al(Ru) particle mixtures after heating up to 800 °C using a heating rate of 60 K/min understoichiometric in Al c) FIB images of compacted Ru_{nano} and Al(Ru) particle mixtures after heating up to 800 °C using a heating rate of 60 K/min with Ru:Al ratio of 1:1 d) EDX measurements of the compacted and reacted Ru-Al powder mixtures of the RuAl phase and e) the oxide rich phase.

STA scans of the commercial Al – Ru powder mixtures reveal a temperature onset of the exothermic reaction 656 °C, right after the beginning of the eutectic melting of the Al-Ru mixture at 649 °C (Figure 8d). The Al(Ru)-Ru_{nano} powder mixtures shows a temperature onset at 634 °C well before the melting of the eutectic composition. Again, the onset temperatures are higher than the values reported in the literature for multilayer systems (408-608 °C)[63] due to the presence of an amorphous passivating layer. Good agreement to values reported in the literature for powder mixtures can however be found[64] (625-640 °C). Also, the reported strong dependence of the onset temperature from the Ru particles size[64],[59] can be clearly observed.

In the unreacted Ru_{nano} and Al(Ru) compacted powder pellets (Figure 9a) a statistical distribution of Al and Ru was observed, while no formation of any intermetallic phases was visible. Moreover, only a very few pores could be detected, resulting in a large contact area between Al and Ru. In a Ru rich sample, after the heat treatment at 800 °C the porosity of the sample was enhanced, caused by the increased density of the reaction product (ρ_{RuAl}: 7.76-8.01 g/cm^3 [61]; ρ_{Al}: 2.70 g/cm^3 [65]; ρ_{Ru}: 12.1 g/cm^3 [65]; $\rho_{Ru\text{-}Al}$: 7.4 g/cm^3). The Al particles (dark particles in the left image) are no longer visible confirming a complete conversion of the Al, which was no longer detectable using XRD measurements. As can be clearly seen in Figure 9b multiple phases were formed, also indicated by the sample composition determined via XRD measurements: $Ru_{70}Al_{30}$ (58.3 % Ru, 32.3 % RuAl and 9.46 % $RuAl_2$). Figure 9c shows a reacted, stoichiometric Ru-Al pellet. The formation of two different phases as well as of pores, again due to the increased density of the reaction product is clearly visible. PXRD measurements indicated the formation of nearly single-phase RuAl, which can be assigned to the darker colored phase via EDX measurements (Figure

9d). EDX analysis also revealed the second amorphous phase, to be oxygen rich, which is thus likely to originate from the oxide layer on the particle surface (Figure 9e).

4. Conclusions

Submicron Al particles have been successfully synthesized using a thermal decomposition approach. Triisobutylaluminum was decomposed in refluxing diphenylether in the presence of metallic nanoparticles of Ni, Ru or Ag acting as seeds yielding metallic submicron Al particles with sizes of about 100-150 nm. The presence of the metallic nanoparticle seeds was necessary to prevent the formation of an Al film on the surface of the reaction flask. No additional stabilizer was necessary for the formation of these particles, making the synthesis of Al particles with organic contents < 5 % easily possible. The resulting particles were passivated by an amorphous oxide layer with a thickness of roughly 5 nm upon air contact resulting in Al^0 contents of about 70-80 %. However, if desired, passivation of these particles was easily possible in an additional, second step after the synthesis by adding oleic acid resulting in the formation of oleic acid@Al core-shell particles. The size of the particles can be controlled by adding weakly coordinating triphenylphosphine during the thermal decomposition, resulting in the formation of Al particles with sizes of about 70 nm. Due to the weakly coordinating nature of PPh_3 low contents of organics (< 5 %) could still be observed in the resulting Al particles after simple washing with toluene.

The low organic contents are making the obtained particles to promising precursors for the synthesis of various aluminides, we tested their suitability for the formation of Ru aluminides. Using Al particles from Ru seeds, “single-phase” RuAl could be obtained by heating compacted powder mixture pellets up to 800 °C under an atmosphere of flowing Ar. However, the use of high heating rates of 60 K/min and small Ru crystallites (2-3 nm) was essential, when slower heating rates (200 °C/ h) and/ or large Ru particles (60 µm) were used the formation of multiphase products was taking place. The onset of the reaction was observed at 628 °C well before the eutectic of the Ru-Al system. The presence of the passivating oxide layer on the Al particle surface further lead to the formation of a second oxide rich phase.

Acknowledgements

We thank Dr. Michael Zimmer for conducting the ^{27}Al-SPE-MAS measurements and Susanne Harling for doing the elemental analyses. We further thank Dr. Robert Haberkorn and Dennis Becker for performing the XRD measurements as well as their advices regarding the Rietveld refinements and Nadja Klippel and Christina Odenwald for the TEM and SEM measurements. We also thank Dr. Christoph Pauly for the FIB characterizations.

References

[1] Risha G A, Connell Jr. T L, Yetter R A, Sundaram D S and Yang V 2014 Combustion of frozen nanoaluminum and water mixtures *J. Propul. Power* **30** 133–42

[2] Wang J, Bassett W P and Dlott D D 2017 Shock initiation of nano-Al/Teflon: High dynamic range pyrometry measurements *J. Appl. Phys.* **121** 085902

[3] Puszynski J A, Bulian C J and Swiatkiewicz J J 2007 Processing and Ignition Characteristics of Aluminum-Bismuth Trioxide Nanothermite System *J. Propuls. Power* **23** 698–706

[4] Woll K, Bergamaschi A, Avchachov K, Djurabekova F, Gier S, Pauly C, Leibenguth P, Wagner C, Nordlund K and Mücklich F 2016 Ru/Al Multilayers Integrate Maximum Energy Density and Ductility for Reactive Materials *Sci. Rep.* **6** 19535

[5] Stratakis E, Barberoglou M, Fotakis C, Viau G, Garcia C and Shafeev G A 2009 Generation of Al nanoparticles via ablation of bulk Al in liquids with short laser pulses *Opt. Express* **17** 12650–9

[6] Crouse C A, Shin E, Murray P T and Spowart J E 2010 Solution assisted laser ablation synthesis of discrete aluminum nanoparticles *Mater. Lett.* **64** 271–4

[7] Gromov A A, Förter-Barth U and Teipel U 2006 Aluminum nanopowders produced by electrical explosion of wires and passivated by non-inert coatings: Characterisation and reactivity with air and water *Powder Technol.* **164** 111–5

[8] Lerner M I, Glazkova E A, Lozhkomoev A S, Svarovskaya N V., Bakina O V., Pervikov A V. and Psakhie S G 2016 Synthesis of Al nanoparticles and Al/AlN composite nanoparticles by electrical explosion of aluminum wires in argon and nitrogen *Powder Technol.* **295** 307–14

[9] Yatsuya S, Kasukabe S and Uyeda R 1973 Formation of Ultrafine Metal Particles by Gas Evaporation Technique. I. Aluminium in Helium *Jpn. J. Appl. Phys.* **12** 1675–84

[10] Pivkina A, Ivanov D, Frolov Y, Mudretsova S and Schoonman J 2006 Structure, thermal properties, and combustion behavior of plasma synthesized nano-aluminum powders *AIP Conf. Proc.* **849** 164–73

[11] Haber J A and Buhro W E 1998 Kinetic instability of nanocrystalline aluminum prepared by chemical synthesis; facile room-temperature grain growth *J. Am. Chem. Soc.* **120** 10847–55

[12] Cui Y, Huang D, Li Y, Huang W, Liang Z, Xu Z and Zhao S 2015 Aluminium nanoparticles synthesized by a novel wet chemical method and used to enhance the performance of polymer solar cells by the plasmonic effect *J. Mater. Chem. C* **3** 4099–103

[13] Ghanta S R and Muralidharan K 2010 Solution phase

chemical synthesis of nano aluminium particles stabilized in poly(vinylpyrrolidone) and poly(methylmethacrylate) matrices. *Nanoscale* **2** 976–80

[14] Purdy A P, Miller J B, Stroud R M and Pettigrew K A 2011 Aluminum Nanoparticle Synthesis by Reduction of Halides with Na/K *MRS Proc.* **1056** 1056-HH03-18

[15] Garza-Rodríguez L A, Kharisov B I and Kharissova O V 2009 Synthesis and Reactivity in Inorganic , Metal-Organic , and Nano-Metal Chemistry Overview on the Synthesis of Activated Micro- and Nanostructurized Rieke Metals : History and Present State Overview on the Synthesis of Activated Micro- and Nanostructurized *Synth. React. Inorg. Met. Chem.* **3174** 37–41

[16] Zeng W, Buckner S W and Jelliss P A 2017 Poly(methyl methacrylate) as an Environmentally Responsive Capping Material for Aluminum Nanoparticles *ACS Omega* **2** 2034–40

[17] Meziani M J, Bunker C E, Lu F, Li H, Wang W, Guliants E A, Quinn R A and Sun Y P 2009 Formation and properties of stabilized aluminum nanoparticles *ACS Appl. Mater. Interfaces* **1** 703–9

[18] McClain M J, Schlather A E, Ringe E, King N S, Liu L, Manjavacas A, Knight M W, Kumar I, Whitmire K H, Everitt H O, Nordlander P and Halas N J 2015 Aluminum Nanocrystals *Nano Lett.* **15** 2751–5

[19] Jouet R J, Warren A D, Rosenberg D M, Bellitto V J, Park K and Zachariah M R 2005 Surface passivation of bare aluminum nanoparticles using perfluoroalkyl carboxylic acids *Chem. Mater.* **17** 2987–96

[20] Foley T J, Johnson C E and Higa K T 2005 Inhibition of Oxide Formation on Aluminum Nanoparticles by Transition Metal Coating Inhibition of Oxide Formation on Aluminum Nanoparticles by Transition Metal Coating *Chem. Mater.* **17** 4086–91

[21] Jouet R J, Granholm R H, Sandusky H W and Warren A D 2006 Preparation and shock reactivity analysis of novel perfluoroalkyl-coated aluminum nanocomposites *AIP Conf. Proc.* **845 II** 1527–30

[22] Fei F, Zhuang J, Wu W, Song M, Zhang D, Li S, Su W and Cui Z 2015 A printed aluminum cathode with low sintering temperature for organic light-emitting diodes *RSC Adv.* **5** 608–11

[23] Fernando K A S, Smith M J, Harruff B A, Lewis W K, Guliants E A and Bunker C E 2009 Sonochemically assisted thermal decomposition of alane N,N-dimethylethylamine with titanium (IV) isopropoxide in the presence of oleic acid to yield air-stable and size-selective aluminum core - shell nanoparticles *J. Phys. Chem. C* **113** 500–3

[24] Bunker C E, Smith M J, Shiral Fernando K A, Harruff B A, Lewis W K, Gord J R, Guliants E A and Phelps D K 2010 Spontaneous hydrogen generation from organic-capped al nanoparticles and water *ACS Appl. Mater. Interfaces* **2** 11–4

[25] Ganesamoorthy C, Loerke S, Gemel C, Jerabek P, Winter M, Frenking G and Fischer R a 2013 Reductive elimination: a pathway to low-valent aluminium species *Chem. Commun.* **49** 2858–60

[26] Tiwari D and Dunn S 2012 Photochemical reduction of Al3+ to Al0 over a ferroelectric photocatalyst — LiNbO3 *Mater. Lett.* **79** 18–20

[27] Kwon Y S, Gromov A A and Strokova J I 2007 Passivation of the surface of aluminum nanopowders by protective coatings of the different chemical origin *Appl. Surf. Sci.* **253** 5558–64

[28] Lewis W K, Rosenberger A T, Gord J R, Crouse C A, Harruff B A, Fernando K A S, Smith M J, Phelps D K, Spowart J E, Guliants E A and Bunker C E 2010 Multispectroscopic (FTIR, XPS, and TOFMS-TPD) investigation of the core-shell bonding in sonochemically prepared aluminum nanoparticles capped with oleic acid *J. Phys. Chem. C* **114** 6377–80

[29] Lee H M and Yun J-Y 2011 Preparation of Aluminum-Oleic Acid Nano-Composite for Application to Electrode for Si Solar Cells *Mater. Trans.* **52** 1222–7

[30] Arora N and Jagirdar B R 2012 Monodispersity and stability: case of ultrafine aluminium nanoparticles (<5 nm) synthesized by the solvated metal atom dispersion approach *J. Mater. Chem.* **22** 9058–63

[31] Gottapu S, Padhi S K, Krishna M G and Muralidharan K 2015 Poly(vinylpyrrolidone) stabilized aluminum nanoparticles obtained by the reaction of SiCl4 with LiAlH4 *New J. Chem.* **39** 5203–7

[32] Chung S W, Guliants E A, Bunker C E, Hammerstroem D W, Deng Y, Burgers M A, Jelliss P A and Buckner S W 2009 Capping and Passivation of Aluminum Nanoparticles Using Alkyl-Substituted Epoxides *Langmuir* **25** 8883–7

[33] Hammerstroem D W, Burgers M A, Chung S W, Guliants E A, Bunker C E, Wentz K M, Hayes S E, Buckner S W and Jelliss P A 2011 Aluminum nanoparticles capped by polymerization of alkyl-substituted epoxides: Ratio-dependent stability and particle size *Inorg. Chem.* **50** 5054–9

[34] Dong S, Hou P, Yang H and Zou G 2002 Synthesis of intermetallic NiAl by SHS reaction using coarse-grained nickel and ultrafine-grained aluminum produced by wire electrical explosion *Intermetallics* **10** 217–23

[35] Carenco S, Boissière C, Nicole L, Sanchez C, Le Floch P and Mézailles N 2010 Controlled design of Size-tunable monodisperse nickel nanoparticles *Chem. Mater.* **22** 1340–9

[36] Ramírez-Meneses E, Betancourt I, Morales F, Montiel-Palma V, Villanueva-Alvarado C C and Hernández-Rojas M E 2011 Superparamagnetic nickel nanoparticles obtained by an organometallic approach *J. Nanoparticle Res.* **13** 365–74

[37] Peng S, Wang C, Xie J and Sun S 2006 Synthesis and

stabilization of monodisperse Fe nanoparticles *J. Am. Chem. Soc.* **128** 10676–7

[38] Pelzer K, Vidoni O, Philippot K, Chaudret B and Collière V 2003 Organometallic synthesis of size-controlled polycrystalline ruthenium nanoparticles in the presence of alcohols *Adv. Funct. Mater.* **13** 118–26

[39] Clark B D, Jacobson C R, Lou M, Yang J, Zhou L, Gottheim S, DeSantis C J, Nordlander P and Halas N J 2018 Aluminum Nanorods *Nano Lett.* **18** 1234–40

[40] Zhang L 2013 *On the chemical synthesis of manganese-based high magnetocrystalline anisotropy energy density magnetic nanoparticles* (University of Alabama)

[41] Park J, Kwon S G, Jun S W, Kim B H and Hyeon T 2012 Large-scale synthesis of ultra-small-sized silver nanoparticles *ChemPhysChem* **13** 2540–3

[42] Garcia-Pena N G, Redon R, Herrera-Gomez A, Fernandez-Osorio A L, Bravo-Sanchez M and Gomez-Sosa G 2015 Solventless synthesis of ruthenium nanoparticles *Appl. Surf. Sci.* **340** 25–34

[43] Bruker AXS, Karlsruhe G 2014 Topas 5.1. General Profile and Structure Analysis Software for Powder Diffraction Data.

[44] Cheary R W, Coelho A A and Cline J P 2004 Impact of nanomaterial arrangement on the reliability and the electron mobility in AlGaN/GaN HEMTs *J. Res. Natl. Inst. Stand. Technol.* **109** 1–25

[45] Merkys A, Vaitkus A, Butkus J, Okulič-Kazarinas M, Kairys V and Gražulis S 2016 COD::CIF::Parser: An error-correcting CIF parser for the Perl language *J. Appl. Crystallogr.* **49** 292–301

[46] Ziegler K, Nagel K and Pfohl W 1960 Metallorganische Verbindungen. XXXVIII Pyrolyse von Aluminiumtrialylen *Justus Liebigs Ann. Chem.* **345** 210–21

[47] Mulder F M, Assfour B, Huot J, Dingemans T J and Wagemaker M 2010 Hydrogen in the Metal - Organic Framework Cr MIL-53 *J. Phys. Chem. C* **5** 10648–55

[48] Woodward P M and Karen P 2003 Mixed valence in YBaFe2O5 *Inorg. Chem.* **42** 1121–9

[49] Liu L H, Chen J H, Fan T W, Liu Z R, Zhang Y and Yuan D W 2015 The possibilities to lower the stacking fault energies of aluminum materials investigated by first-principles energy calculations *Comput. Mater. Sci.* **108** 136–46

[50] Fournée V, Cai T, Thiel P A and Ledieu J 2003 Influence of strain in Ag on Al(111) and Al on Ag(100) thin film growth *Phys. Rev. B - Condens. Matter Mater. Phys.* **67** 155401

[51] Bufford D, Liu Y, Zhu Y, Bi Z, Jia Q X, Wang H and Zhang X 2013 Formation mechanisms of high-density growth twins in aluminum with high stacking-fault energy *Mater. Res. Lett.* **1** 51–60

[52] Bufford D, Bi Z, Jia Q X, Wang H and Zhang X 2012 Nanotwins and stacking faults in high-strength epitaxial Ag/Al multilayer films *Appl. Phys. Lett.* **101** 223112

[53] Xia Y, Xiong Y, Lim B and Skrabalak S E 2009 Shape-controlled synthesis of metal nanocrystals: Simple chemistry meets complex physics? *Angew. Chemie - Int. Ed.* **48** 60–103

[54] Xiong Y, Siekkinen A R, Wang J, Yin Y, Kim M J and Xia Y 2007 Synthesis of silver nanoplates at high yields by slowing down the polyol reduction of silver nitrate with polyacrylamide *J. Mater. Chem.* **17** 2600–2

[55] Deacon G B and Phillips R J 1980 Relationships Between the Carbon-Oxygen Stretching Frequencies of Carboxylato Complexes and the Type of Carboxylate Coordination *Rev. Chem.* **33** 227–50

[56] Trunov M A, Schoenitz M, Zhu X and Dreizin E L 2005 Effect of polymorphic phase transformations in Al2O3 film on oxidation kinetics of aluminum powders *Combust. Flame* **140** 310–8

[57] Trunov M A, Schoenitz M and Dreizin E L 2006 Effect of polymorphic phase transformations in alumina layer on ignition of aluminium particles *Combust. Theory Model.* **10** 603–23

[58] Fleischer R L, Briant C L, Field R D and Engines E A 1991 Tough, Ductile High-Temperature Intermetallic Compounds: Results of a Four-Year Survey. *Mat. Res. Soc. Symp. Proc.* **213** 463–74

[59] Wolff I M 1996 Synthesis of RuAl by reactive powder processing *Metall. Mater. Trans. A Phys. Metall. Mater. Sci.* **27** 3688–99

[60] Soldera F, Ilić N, Brännström S, Barrientos I, Gobran H and Mücklich F 2003 Formation of Al2O3scales on single-phase RuAl produced by reactive sintering *Oxid. Met.* **59** 529–42

[61] Mücklich F and Ilić N 2005 RuAl and its alloys. Part I. Structure, physical properties, microstructure and processing *Intermetallics* **13** 5–21

[62] Mohamed K E, Stover D and Buchkremer H P 1997 Some reactive processing aspects of high-temperature aluminides Nb3Al and RuAl *J. Mater. Eng. Perform.* **6** 771–9

[63] Pauly C, Woll K, Bax B and Mücklich F 2015 The role of transitional phase formation during ignition of reactive multilayers *Appl. Phys. Lett.* **107** 113104

[64] Gobran H A, Ilić N and Mücklich F 2004 Effects of particle size and pressure on the reactive sintering of RuAl intermetallic compound *Intermetallics* **12** 555–62

[65] Rumble J R, Lide D R and Bruno T J 2017 *Handbook of Chemistry and Physics* (CRC Press)

These studies revealed that the thermal decomposition of organoaluminium compounds is a valuable method for the preparation of nano and submicron Al particles. The advantages of this synthesis approach include its simple experimental set-up, the very short reaction times of about 15 min as well as the possibility to conduct the reaction without the presence of an additional stabilizer. The biggest disadvantage is the high reaction temperatures of 270 °C.

The resulting particles were suitable for the preparation of Ru aluminides and in Chapter 3.2 it will be shown that the particles resulting from the described approach are more suitable for the preparation of Ni and Ru aluminides than the particles resulting from the metal reduction, hydride reduction, and catalytic decomposition approaches. This was attributed to the low organic content of the particles as well as their submicron size. Particularly their size of 100 – 150 nm seems to represent a good compromise between small size and thus increased reactivity and an oxide content low enough to allow a preparation of the aluminides in a reasonable yield of > 90 %.

In the following chapters a few additional aspects of the developed synthesis approach will be briefly summarized, which have not been included in the published manuscript.

3.1.4.1 Addition to the size control

As stated in the manuscript above, the size of the submicron Al particles could be reduced by adding PPh_3 to the reaction mixture. However, the size and morphology of the resulting Al was quiet sensitive regarding the amount of PPh_3 added to the reaction mixture. Upon applying a lower amount of PPh_3 the formed Al particles were not sufficiently stabilized, resulting in the formation of very large, as well as highly agglomerated particles (Figure 28a). In contrast, upon applying larger amounts of PPh_3, the formation of more complex, largely non-particulate structures was observed (Figure 28b). Since without the addition of PPh_3 particles with a size of about 150 nm were observed, these observations indicate that the PPh_3 is strongly influencing the formation of the Al particles via the thermal decomposition of triisobutylaluminum. However, due to time limitations this influence could not be studied in more detail within in this work. Nonetheless, it would be an interesting topic of a possible future work, possibly allowing the formation of Al particles with a wider range size and possibly additional morphologies.

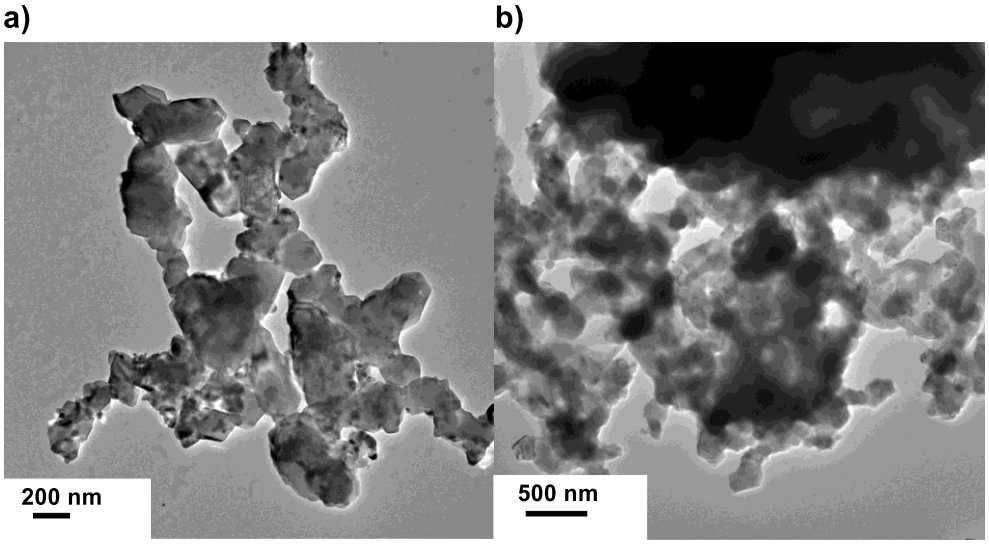

***Figure 28**: TEM images of Al particles prepared by decomposing triisobutylaluminum in refluxing diphenylether using reactant ratios of **a)** Ag:Al 2:100 and PPh_3: Ag 20:1 and **b)** Ag:Al 1:100 and PPh_3: Ag 100:1.*

3.1.4.2 Application of Al seeds

The synthesis of Al nanoparticles was successfully carried out in the presence of many metallic as well as oxidic seeds such as Ni, Ag, Ru, Fe, SiO_2 and Fe_2O_3. Thus, the suitability of the resulting particles themselves as nucleation seeds was examined in a next step, since this would allow the preparation of Al particles with strongly reduced contents of impurity phases. To test their suitability, Al particles prepared in the presence of Ru seeds and containing about 3 wt% Ru, as determined by Rietveld refinements, were employed as seeds in the thermal decomposition approach. The synthesis and the clean-up of the resulting particles was carried out identically as reported above.

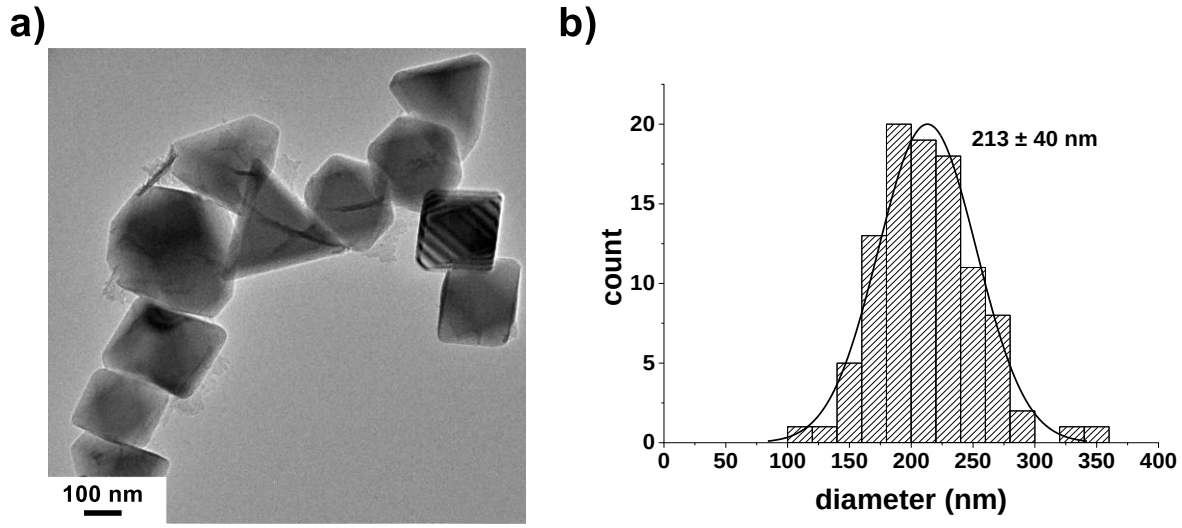

***Figure 29**: **a)** TEM image and **b)** particle size distribution of submicron Al particles prepared via thermal decomposition of triisobutylaluminum in refluxing diphenylether applying submicron Al seeds.*

The synthesis was successfully carried out in the presence of Al nucleation seeds. The size of the particles was 213 ± 40 nm (Figure 29) which is slightly larger than the sizes of the particles prepared in the presence of Ni, Ru and Ag nanoparticulate seeds, which typically exhibited sizes of about 150 nm. However, a much lower Ru content, below the XRD detection limit, was observed in the Al particles upon applying the Al(Ru) seeds, as was indicated by the absence of any Ru reflections (Figure 30). Of course, the Ru content could be further decreased by repeatedly applying the Al particles resulting from this synthesis as nucleation seeds for another Al synthesis batch.

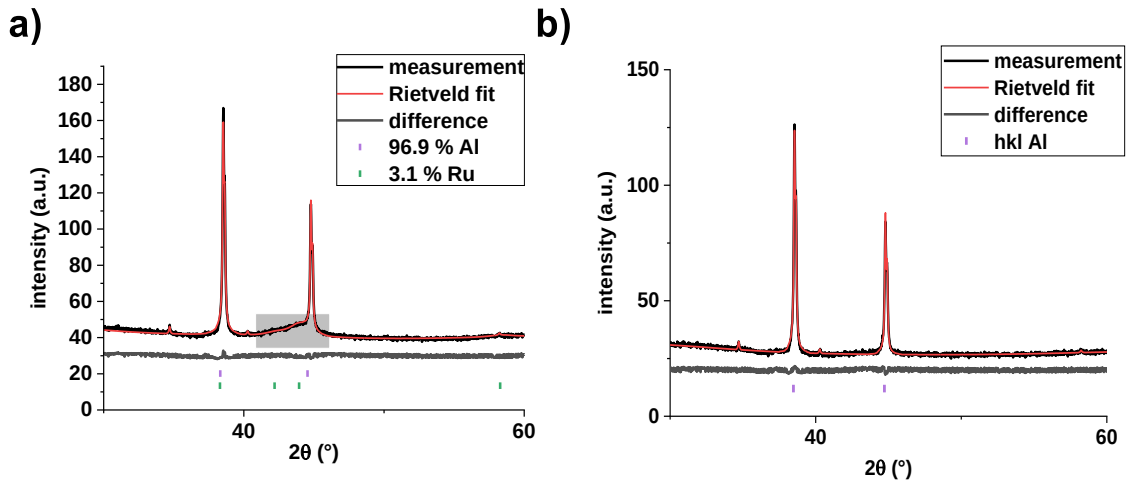

***Figure 30**: XRD measurement and Rietveld refinement of Al nanoparticles synthesized in the presence of **a)** Ru seeds and **b)** Al seeds. The broad signals marked in grey are the Ru (0 2 0) and (0 1 1) reflections. The particles shown in a) were applied as seeds for the preparation of the particles shown in b).*

3.1.4.3 Synthesis via hot injection

The synthesis approach reported above was conducted as a conventional heat-up approach, in which a reaction mixture is heated slowly from room temperature to the reaction temperature. Another approach, which is also commonly applied for the preparation of metal nanoparticles, is the hot-injection method, in which the metal precursor is rapidly injected into a preheated reaction mixture. Consequently, rapid nucleation occurs, resulting in the formation of smaller particles, which also often exhibit narrower particle size distributions. To apply this method for the preparation of Al particles, a diphenylether solution containing dispersed Ag seeds, was heated to reflux and triisobutylaluminum dissolved in diphenylether was then injected into this preheated solution.

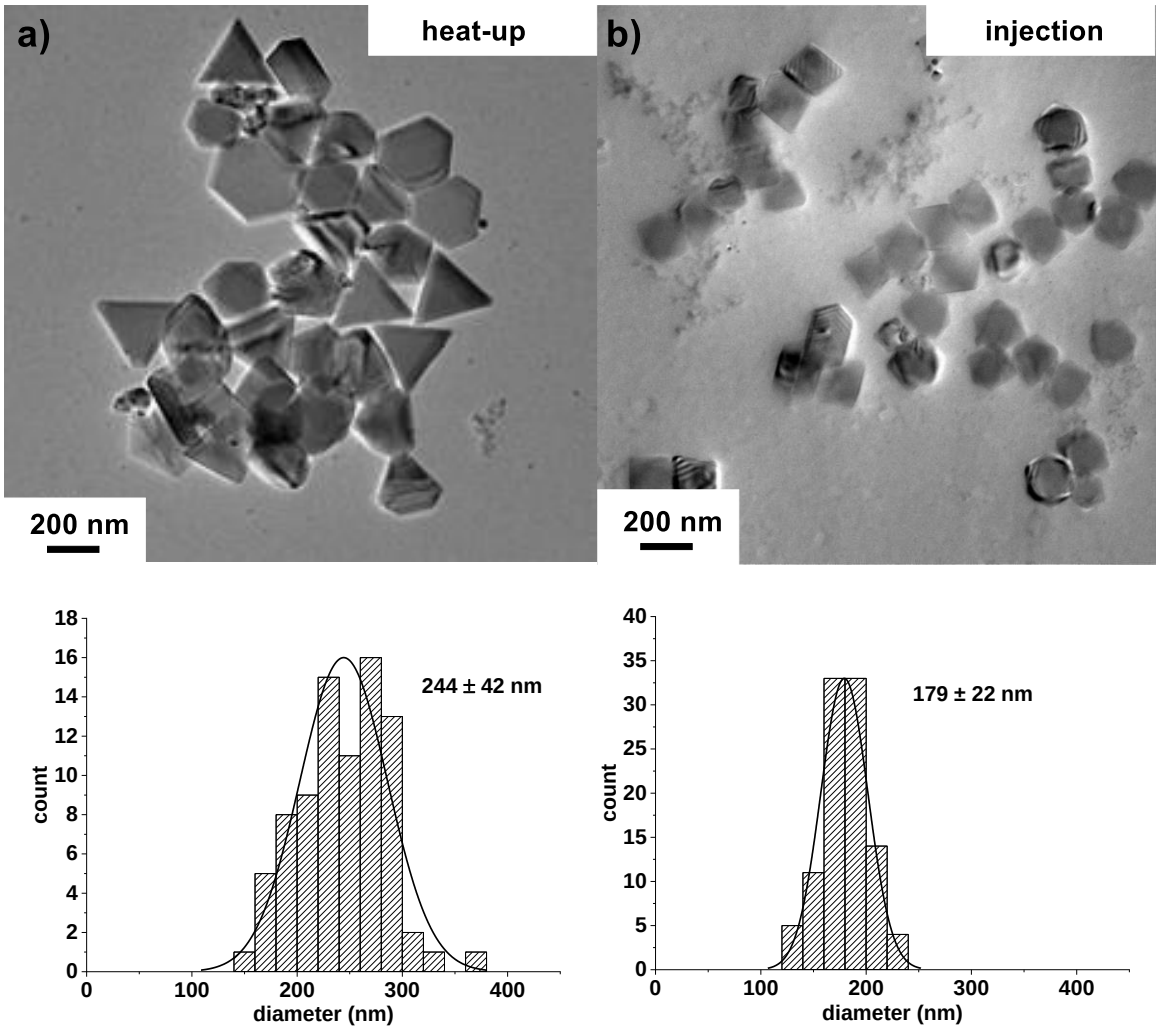

***Figure 31**: TEM images and particle size distributions of Al particles prepared via thermal decomposition of triisobutylaluminum in refluxing diphenylether in the presence of Ag seeds applying a **a)** heat-up approach and **b)** hot-injection approach. The concentration of the reactants was identical in both samples.*

Applying this hot-injection approach, the synthesis of Al particles was also possible. A reduction of the particle size from 244 ± 42 nm to 179 ± 22 nm was observed, as well as a narrower particle size distribution with relative standard deviation of 12 % compared to 17 % when a heat-up approach was applied (Figure 31). Moreover, a change in the morphology to more irregular formed particles was observed, due to the more rapid decompositions.

The reduction of the particle size was also detected in normalized TG measurements (Figure 32a), where a larger mass increase in the first oxidation step was observed, while the total mass increase was lower compared to the particles prepared via a heat-up approach. Although, the change in the morphology must be considered, both aspects are another indication of the smaller particle sizes observed in the TEM images as discussed in Chapter 1.3.2. The organic content of the particles was still

well below < 10 %. The steep mass increase at a temperature of 900 °C is due to a 15 min isothermal segment at this temperature, which was applied to allow a complete oxidation of the samples.

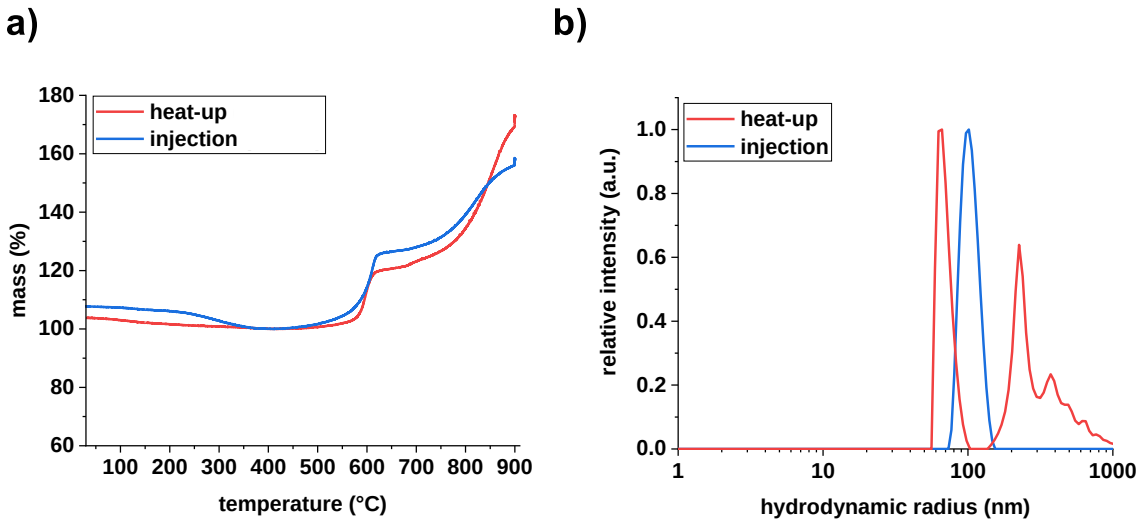

***Figure 32**: **a)** TG measurements in an atmosphere of synthetic air (N_2:O_2 32:8; 10 K/min) and **b)** DLS measurements in MeOH of Al particles synthesized via a heat-up and a hot-injection approach.*

Moreover, a much smaller degree of agglomeration was observed upon applying the hot-injection method, which is obvious from the TEM images (Figure 31) as well as DLS measurements (Figure 32b). Within the DLS measurements, the formation of large agglomerates with sizes ranging from 200 – 1000 nm was observed upon applying a heat-up approach, which were absent when the particles were prepared via a hot-injection approach. In addition, upon dispersing these particles in hexane, the lower degree of agglomeration could be observed with the naked eye. Upon dispersing the particles prepared via the heat-up approach in hexane, the resulting dispersions completely settled after about 2 h, while dispersions prepared from the particles synthesized via the hot-injection approach were stable for at least 22 d and only a few particles settled at the bottom of the vial (Figure 33).

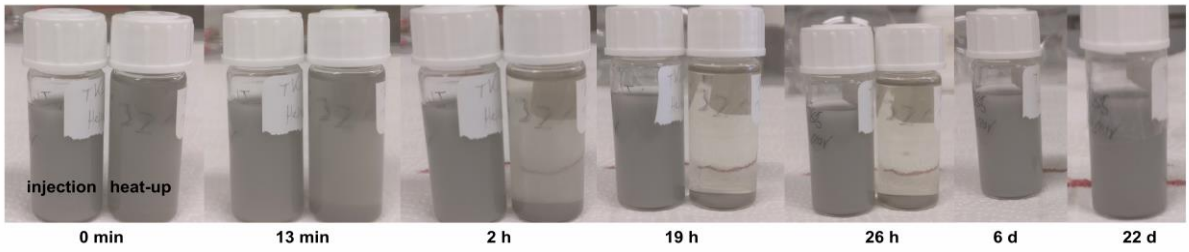

***Figure 33**: Photographs of Al particle dispersions in hexane, prepared from Al particles synthesized via a heat-up and a hot-injection approaches after various times.*

The most important characteristics of the different synthesis approaches and of the resulting particles are briefly summarized in Table 12. The most promising results were observed applying the catalytic

decomposition and the thermal decomposition approaches, due the homogeneous reaction mixtures, the short reaction times and the formation of non-agglomerated particles. The drawback of the thermal decomposition approach is the increased reaction temperature of 260 °C. In contrast, heterogeneous reaction mixtures, long reaction times, and the formation of severely agglomerated particles were observed upon applying the metal reduction and the hydride reduction approaches. In a next step, the particles resulting from these methods were tested regarding their suitability for the preparation of Ni and Ru aluminides, which will be discussed in the following chapters.

***Table 12**: Selected characteristics of the wet chemical synthesis approaches for the preparation of Al particles applied within this work.*

	Metal reduction	**Hydride reduction**	**Catalytic decomposition**	**Thermal decomposition**
Al precursor	$AlCl_3$	$AlCl_3$ + $LiAlH_4$	H_3AlNEt_3	$Al(^iBu)_3$
Solvent	THF	mesitylene	toluene	diphenylether
Reaction mixture	heterogeneous	heterogeneous	homogeneous	homogeneous
Reaction time	3 h	1 h	15 min	15 min
Reaction temperature	70 °C	165 °C	90 °C	260 °C
Resulting particles	agglomerated/ sintered	agglomerated/ sintered	non-agglomerated	non-agglomerated
Crystallite size	12 nm	65 - 120 nm	50 – 100 nm	100 – 200 nm

3.2 Synthesis of aluminides

3.2.1 General comments for the preparation of Ni and Ru particles

Within this work, the synthesis of the Ni and Ru nanoparticles was carried out following published literature procedures. Although the wet chemical synthesis of these particles generally is more common compared to the preparation of the Al particles, the following sections aim to demonstrate that not all the resulting metal nanoparticles are suitable for the preparation of aluminides. Accordingly, the synthesis method for these nanoparticles needs to be carefully selected to allow a successful aluminide synthesis.

Ni nanoparticles

The applied Ni particles play a crucial role in the formation of Ni aluminides since impurities are easily introduced via these particles into the final product. Within this work, the Ni nanoparticles were commonly prepared via a thermal decomposition of $Ni(acac)_2$ in oleylamine in the presence of TOP or PPh_3 at a temperature of 220 °C according to published literature procedures[310] (for a characterization of the Ni nanoparticles see Chapter 7.5). However, this method easily resulted in the introduction of Ni phosphides in the final product (Figure 34a). This was particularly problematic when the Ni particles were prepared in the presence of PPh_3 as a stabilizer. In contrast, the Ni phosphide formation was not evident upon replacing PPh_3 by TOP, unless higher reaction temperatures > 220 °C were applied during the synthesis. These nickel phosphides result from the reaction of Ni^0 with phosphines, which has already been applied in the literature for the preparation of Ni_2P nanoparticles[311]. As result, the Ni particles prepared in the presence of phosphines are easily obtained as mixture of Ni^0 and various Ni phosphides (Figure 34b), particularly if a too high reaction temperature is chosen. In Figure 34b the reflection of Ni can be clearly recognized after sintering at 500 °C in an atmosphere of Ar. However, other phases, including Ni_3P as well as at least one additional phase, which could not be further identified, are clearly visible. Generally, if large amounts of phosphides were present, it was easily recognized by the fact that the Ni nanoparticles were no longer attracted to a neodymium magnet. Alternatively, numerous other methods are known in the literature not relying on phosphine stabilizers, such as for example polyol synthesis approaches[312].

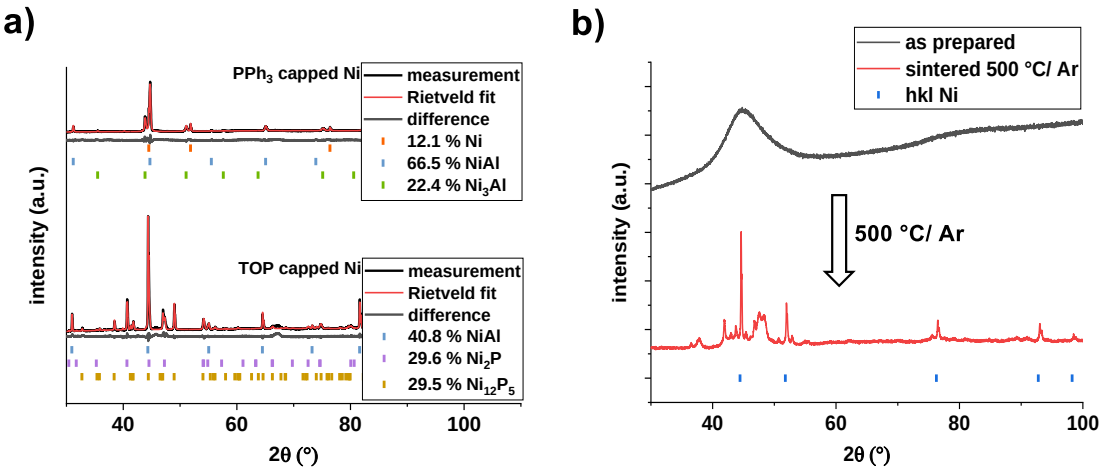

***Figure 34**: **a)** XRD measurements and Rietveld refinements of the reaction products obtained from a mixture of Al nanoparticles and Ni nanoparticles prepared in the presence of PPh_3 and TOP upon heating to 1100 °C in an atmosphere of Ar and **b)** XRD measurements of Ni nanoparticles prepared in the presence of PPh_3 before and after sintering at 500 °C in an Ar atmosphere.*

Ru nanoparticles

Within this work, various methods for the wet chemical preparation of Ru nanoparticles were applied[313–318]. However, the particles obtained from these methods typically exhibited a very large organic content or could not be isolated from the reaction mixture due to their excellent dispersibility. For example, Ru nanoparticles prepared by the reduction of $RuCl_3$ or $Ru(acac)_3$ in oleylamine solutions[313,314] exhibited hydrodynamic radii of 40 ± 4 nm and 2 ± 1 nm as well as organic contents of 62.5 % and 91.1 % respectively (Figure 35). Particularly, these high organic contents are problematic regarding the preparation of Ru alumindes, since the resulting particles were exhibiting an almost liquid consistency, making the preparation of pellets impossible. Several methods were tested to reduce the organic contents, including chemical treatments as well as plasma etching procedures. However, none of them considerably lowered the organic contents (Figure 36) and the particles still exhibited a liquid consistency. When the samples were thermally treated at a temperature of 800 °C in an atmosphere of nitrogen a carbon content of >30 % was still observed in the samples by CHN analysis. Upon thermally treating the samples at a temperature of 800 °C in an atmosphere of ambient air, a complete removal of the organics was observed. However, such a treatment might lead to particle oxidation as well as sintering and was thus not further applied within this work. Since the application of nanoparticles with high organic contents resulted in incomplete reactions when applied for the preparation of aluminides (Chapter 3.2.2), and the removal of the organics was non-trivial in some samples, syntheses leading to the formation of metal nanoparticles with low contents of organics were preferred throughout this work.

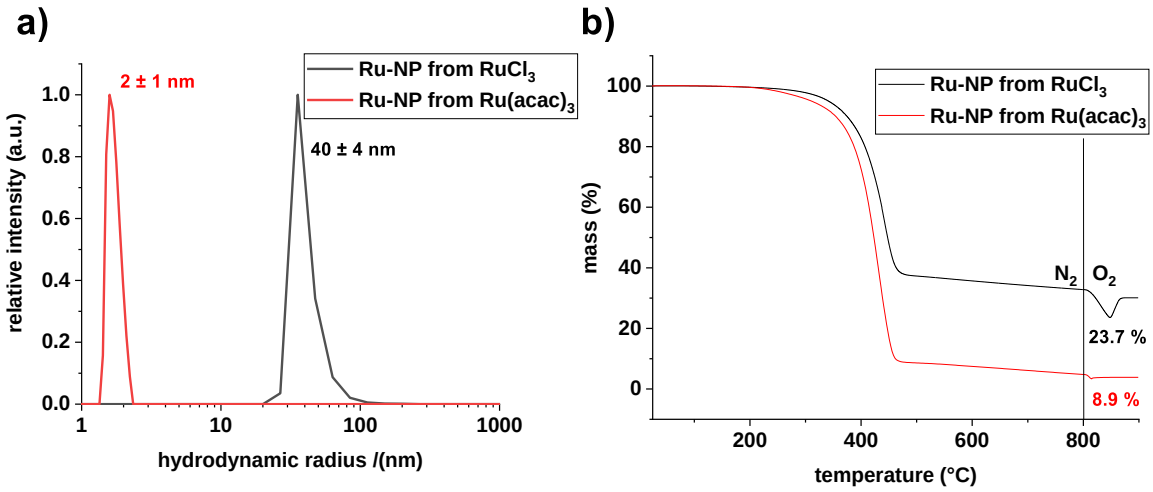

***Figure 35**: **a)** DLS measurements in hexane and **b)** TG measurements (10 K/min; N_2 up to 800 °C and N_2:O_2 32:8 from 800 - 900 °C) of Ru nanoparticles prepared from $RuCl_3$ and $Ru(acac)_3$ in oleylamine solutions.*

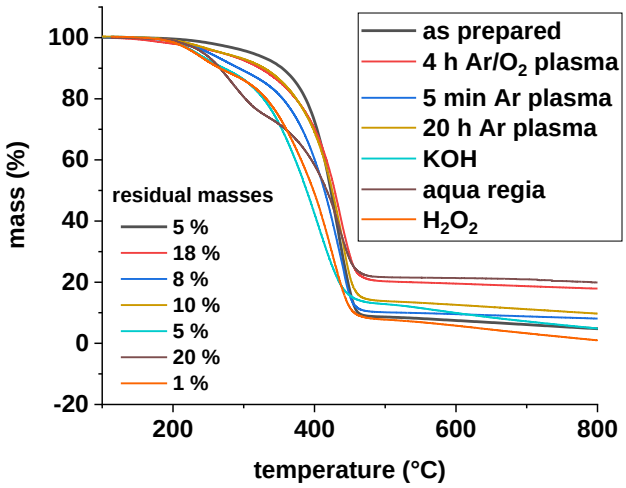

***Figure 36**: TG measurements of Ru nanoparticles prepared from $Ru(acac)_3$ in oleylamine solutions treated via various methods to reduce the content of organics (800 °C; 10 K/min; N_2).*

Accordingly, mechanochemical approaches were applied for the preparation Ru nanoparticles[319] (for a characterization of the resulting particles see Chapter 7.4 as well as a thermal decomposition of $Ru_3(CO)_{12}$ in oleylamine solutions. This thermal decomposition results in the formation of Ru particles with a hydrodynamic radius of 13 ± 4 nm, a TEM size of 6.4 ± 0.8 nm and an organic content of 18.9 % (Figure 37). These Ru nanoparticles were suitable for the preparation of Ru aluminides. Upon mixing with Al particles prepared from a thermal decomposition of TIBAl, compacting and heating the resulting pellet to 800 °C in an atmosphere of Ar, the formation of Ru aluminides was clearly observed (Figure 38).

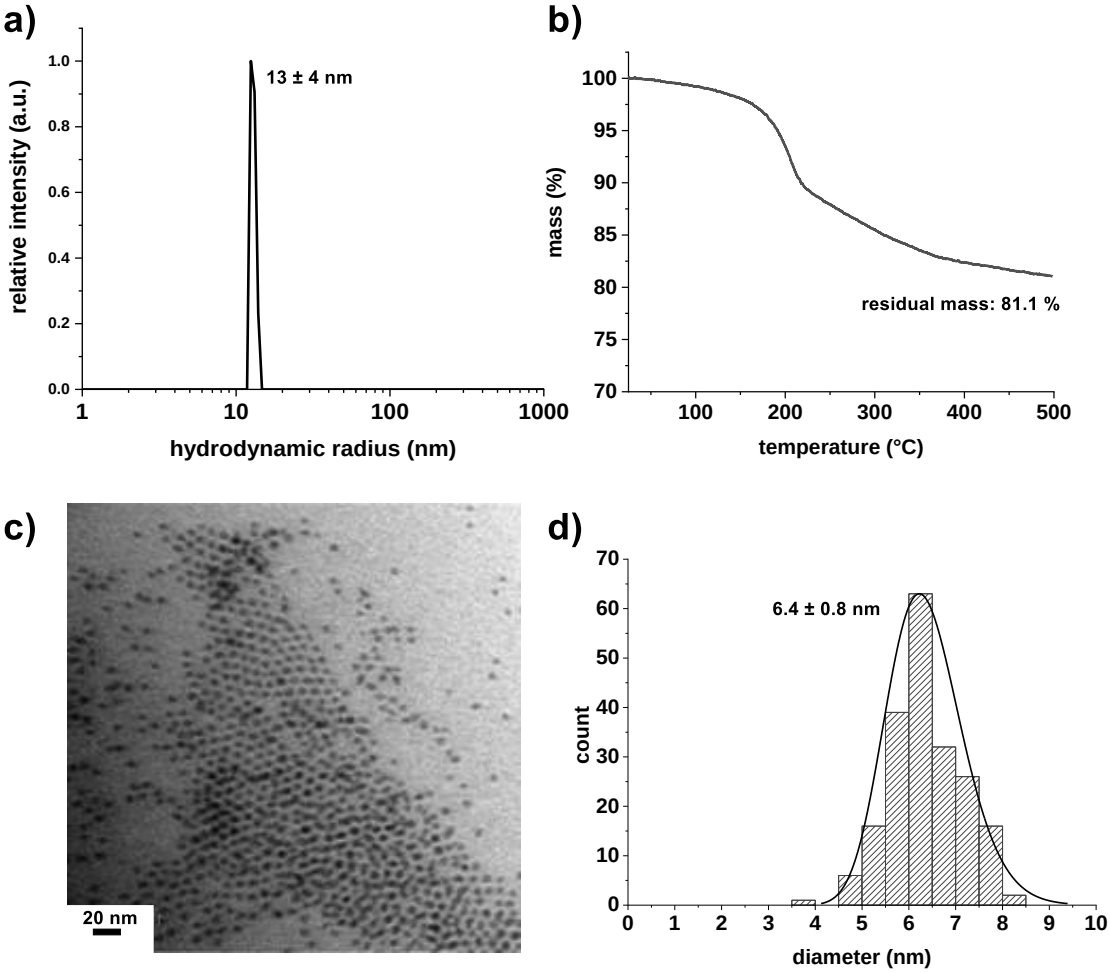

***Figure 37**: **a)** DLS measurements in hexane, **b)** TG measurements (10 K/min; N_2), **c)** TEM image, and **d)** particle size distribution obtained from the TEM image by measuring 200 particles of Ru nanoparticles prepared from $Ru_3(CO)_{12}$ in oleylamine solutions.*

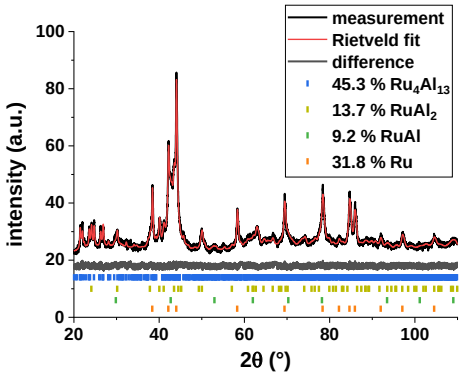

***Figure 38**: Reaction product obtained from a mixture of Al particles prepared via a thermal decomposition approach and Ru nanoparticles prepared via decomposition of $Ru_3(CO)_{12}$ in oleylamine by heating to 800 °C (60 K/min) in an Ar atmosphere.*

3.2.2 Comparison of different Al particles for the preparation of aluminides

Al particles prepared via different synthesis methods (metal reduction, catalytic reduction, and thermal decomposition) were compared regarding their suitability for the preparation of Ni and Ru aluminides starting from wet chemically synthesized reactants. The Al particles obtained from the metal reduction approach were prepared by reducing $AlCl_3$ with Li in refluxing THF solutions, exhibited a crystallite size of 12(5) nm and were severely agglomerated. For the catalytic reduction approach, Al particles resulting from the decomposition of H_3AlNEt_3 in toluene solutions applying $Ti(O^iPr)_4$ as a decomposition catalyst in the presence of PPh_3 as a stabilizer were chosen as an example. They exhibited a crystallite size of 34(4) nm, a TEM size of 50 ± 14 nm and an Al^0 content of 68 %. The particles prepared via the thermal decomposition approach were prepared by decomposing triisobutylaluminum in refluxing diphenylether in the presence of Ni and Ru seeds. They exhibited sizes of 125 ± 36 nm and 180 ± 38 nm (determined from TEM or SEM) and Al^0 contents of about 82 % and 69 %. A detailed characterization of these wet chemically prepared Al particles can be found in the previous chapters. Moreover, commercial Al with a particle size of 14 ± 7 nm, as determined from SEM images, was applied. The Al^0 content of these particles was determined via titration[103,320,321] and found to be > 99 %. A characterization of this commercial Al can be found in Chapter 3.1.4. These Al particles were reacted with Ni and Ru particles to compare their suitability for the preparations of Ni and Ru aluminides. The employed Ni nanoparticles were prepared by decomposing $Ni(acac)_2$ in oleylamine/ TOP mixtures and exhibited a size of 8 ± 1 nm. In contrast, the Ru nanopowder was prepared via a mechanochemical synthesis approach by reacting $RuCl_3$ and $NaBH_4$ in an agate mortar. A characterization of the Ni and Ru particles is given in Chapter 7.5. Moreover, micrometer sized commercial Ni and Ru powders with sizes of 7 ± 2 µm and 57 ± 12 µm were applied. A characterization of these commercial particles can be found in Chapters 7.1 and 7.5. The most relevant properties of the employed particles are summarized in Table 13.

***Table 13**: TEM sizes, crystallite sizes, Al^0 contents, and organic contents of the different metal particles applied for the preparation of aluminides.*

	Synthesis method	TEM size [nm]	Crystallite size [nm]	Al^0 content [%](1)	Organic content [%](2)
Al	Metal reduction	agglomerates	12(5)	17.3	15.2
	Catalytic decomposition	spherical 50 ± 14	34(3)	68.0	8.8
	Thermal decomposition (Ni)	spherical 125 ± 36	87(3)	81.7	2.8
	Thermal decomposition (Ru)	spherical 180 ± 38	171(17)	69.0	3.2
	commercial	14 ± 7 µm (3)	318(16)	99(4)	< 1
Ni	Nanoparticles	spherical 8 ± 1	10(1)	---	< 1
	commercial	7 ± 2 µm(3)	258(8)	---	---
Ru	Nanopowder	agglomerates 3 ± 1	2(1)	---	---
	commercial	57 ± 12 µm(3)	172(6)	---	---

(1)determiend from TGA mass gains (2)determined from the mass loss in TG analysis (3)determined from SEM measurements (4)titrational method

Ni aluminides

The Al particles prepared via different synthesis approaches are differing in various parameters, including their size, morphology as well as contents of Al^0 and organics (Table 13). Particularly, decreasing Al^0 contents were determined from the TGA measurements with decreasing size of the particles. Moreover, rather high organic contents were observed for the particles prepared from the metal reduction and hydride reduction approaches due to residual solvents and stabilizers, while low organic contents < 5 % were determined for the particles prepared via thermal decomposition as well as for the commercial powders.

To test the suitability for the preparation of Ni aluminides, the Al particles were thoroughly mixed in a 1:1 stoichiometry with Ni particles prepared from a decomposition of $Ni(acac)_2$[310]. For mixing, the Ni and Al particles were treated in an agate mortar for 10 min. The resulting mixtures were then compacted to a pellet in a hydraulic press (350 MPa, Ø 0.6 mm; 1 t; 10 min) and heated to a temperature of 800 °C applying a heating rate of 60 K/min in an Ar atmosphere. After cooling to room temperature, the reacted pellets were homogenized and their compositions were determined from Rietveld refinements (Figure 39). Since high batch-to-batch variations were observed, the best results for each pellet composition is shown in Figure 39.

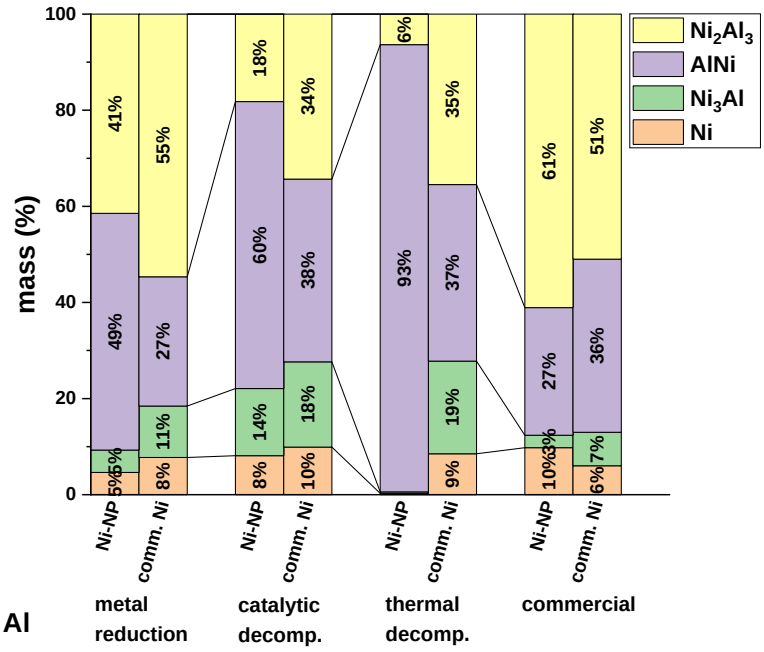

***Figure 39**: Compositions of various reacted Al-Ni pellets prepared from wet chemically synthesized Al particles and Ni nanoparticles (800 °C; Ar; 60 K/min) determined from Rietveld refinements (only intermetallic phases being present in the sample are shown for comparability reasons; other phases, particularly Al_2O_3, are not shown).*

The formation of multiphase reaction products containing Al_3Ni_2, NiAl, Ni_3Al as well as unreacted Ni was observed in all samples, independently from the synthesis method applied for the preparation of the Al particles as well as for the samples containing commercial, micrometer sized Ni and Al powders (Figure 39). However, particularly upon applying Al particles prepared from the metal reduction approach, γ-Al_2O_3 was the main reaction product (Figure 40a), which can be attributed to the high content of surface oxide due to their small crystallite sizes of 12 nm. In contrast, for the products obtained from the larger Al particles synthesized via the thermal and catalytic decomposition approaches, Al_2O_3 contents < 20 % were typically observed. Since an Al_2O_3 content > 50 % in the final sample was considered too high, no further studies applying the Al particles obtained from the metal reduction approach were conducted within this work.

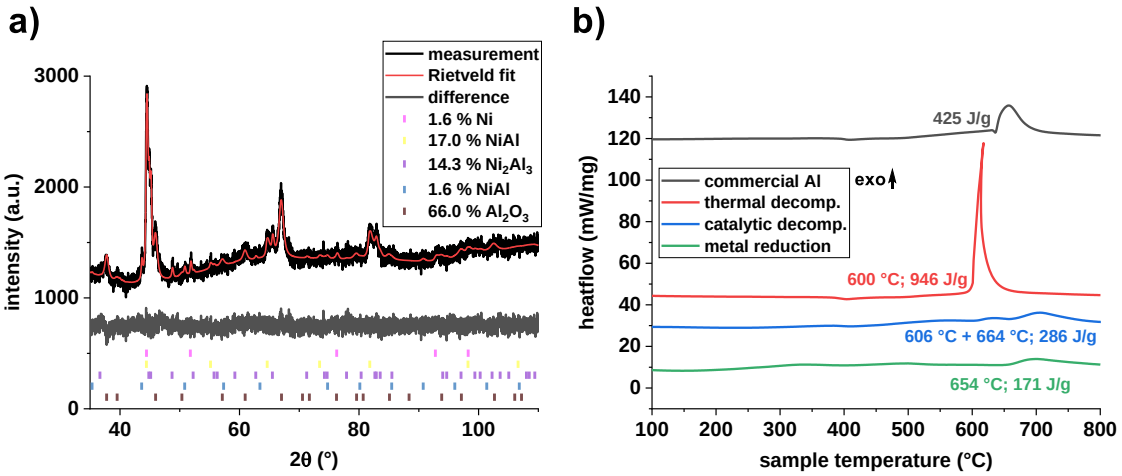

***Figure 40**: **a)** XRD measurement and Rietveld refinement of a reacted Al-Ni pellet prepared from Ni nanoparticles and Al particles synthesized via the metal reduction approach (800 °C; Ar; 60 K/min) and **b)** STA traces of various Al-Ni pellets prepared from wet chemically synthesized Al and Ni nanoparticles (800 °C; Ar; 60 K/min).*

Upon applying commercial, micrometer sized Ni particles incomplete reactions, resulting in the formation of only a small amount of NiAl of up to 38 % and Ni-rich as well as Al-rich phases were observed in all samples, independently from the Al particle size. The incomplete reactions can likely be attributed to large diffusion pathways. Due to these large diffusion pathways, the time at increased reaction temperatures was not sufficient to allow a complete intermixing, thus resulting in the observed multiphase sample compositions.

However, upon applying Ni nanoparticles, the formation of similar multiphase product mixtures was generally observed. The yield of NiAl was typically only slightly higher than in the samples prepared from the micrometer sized Ni powders, which can be ascribed to the shortened diffusion pathways as well as larger interfacial areas. As will be discussed in Chapter 3.2.3 the formation of these multiphase reaction products despite the shorter diffusion pathways, can likely be ascribed to incomplete reactions due to heat losses as well as a poor intermixing. Upon reaching the onset temperature of the highly exothermic reaction, the temperature within the sample can be expected to raise and also exceed the external oven temperature. However, due to the application of small sample amounts of about 5 mg, only a small temperature increase, as well as a fast adoption of the external oven temperature can also be expected to occur. Accordingly, the time at these increased temperatures is too short to allow a complete mixing and thus a complete conversion to NiAl. Such a formation of multiphase products in the Ni-Al system, which has been ascribed to incomplete reaction due to heat losses, has also been reported in the literature before[287] and could be prevented by isolating the reacting sample. Accordingly, upon applying a larger pellet with a mass of 1 g, the formation of NiAl in a quantitative yield was observed, further confirming the aspects discussed above. It has to be noted, that another temperature program with a heating rate of 3.3 K/min and an isothermal segment of 2 h

at 800 °C was applied for the reaction of this 1 g pellet. However, upon reducing the sample amount to about 15 mg the formation of a multiphase product was again observed applying this temperature program.

The content of the target phase NiAl was found to increase from 49 % to 60 % to 93 % upon replacing the Al particles prepared via the metal reduction approach for the particles prepared via the catalytic decomposition approach and the particles prepared via the thermal decomposition approach respectively. Within this series the particle size of the Al particles increases, and the above observation is thus in contrast to the expectation based on increasing interfacial areas and decreasing diffusion pathways with decreasing Al particle sizes. However, with a decreasing Al particle size, the Al_2O_3 content is increasing, which is acting as a diluent, effectively lowering the mass normalized heat of reaction. Accordingly, lower reaction temperatures are reached within the sample, ultimately leading to more incomplete reactions as discussed above. A more detailed study of the influence of the Al_2O_3 content within this type of reaction will be given further below.

Figure 40b shows the STA traces obtained in an Ar atmosphere applying a heating rate of 60 K/min for the reaction of the different Al particles with Ni nanoparticles. As can be clearly seen, a strongly exothermic reaction was observed for the Al particles prepared via thermal decomposition which correlates to the high yield of 93 % NiAl. The tilt of the STA trace of this strongly exothermic reaction visible in Figure 40b (red trace) is due to the plot of the heatflow as a function of the sample temperature. Upon the onset of the reaction, the exothermic nature of the reaction leads to an internal sample heat up with a heating rate larger than the set heating rate of the thermal analyzer. Accordingly, the sample temperature rises faster than intended for a short period of time before again being controlled by the thermal analyzer. Ultimately, this behavior results in said tilt of the STA traces visible in Figure 40b and the further STA traces shown within this manuscript. For the other Al particles, significantly lower heatflows were observed due to i) melting of Al (for the commercial Al), ii) dilution of the reaction system by Al_2O_3 (for the smaller Al particles), and iii) incomplete reactions (particular due to residual Ni; the heats of formation of NiAl and Ni_2Al_3 are of the same order of magnitude). Moreover, with increasing oxide content of the Al particles, the onset of the reaction shifted from 600 °C to 654 °C, which can be attributed to the poorer interfacial contact between Ni and Al.

Ru aluminides

Similar as described above, the suitability of the different Al particles for the preparation of Ru aluminides was studied by reacting them with Ru nanopowder as well as with commercial Ru powder. The Al and Ru particles were ultrasonicated for 15 min in hexane dispersions and were then treated in

an agate mortar for an additional 10 min. The resulting mixtures were then compacted to a pellet in a hydraulic press (350 MPa, Ø 0.6 mm; 1 t; 10 min) and heated to a temperature of 800 °C applying a heating rate of 60 K/min in an Ar atmosphere. After cooling to room temperature, the reacted pellets were homogenized and their compositions were determined from Rietveld refinements (Figure 41). Due to the very poor results observed above, the Al particles prepared via the metal reduction approach were not further examined in this reaction system.

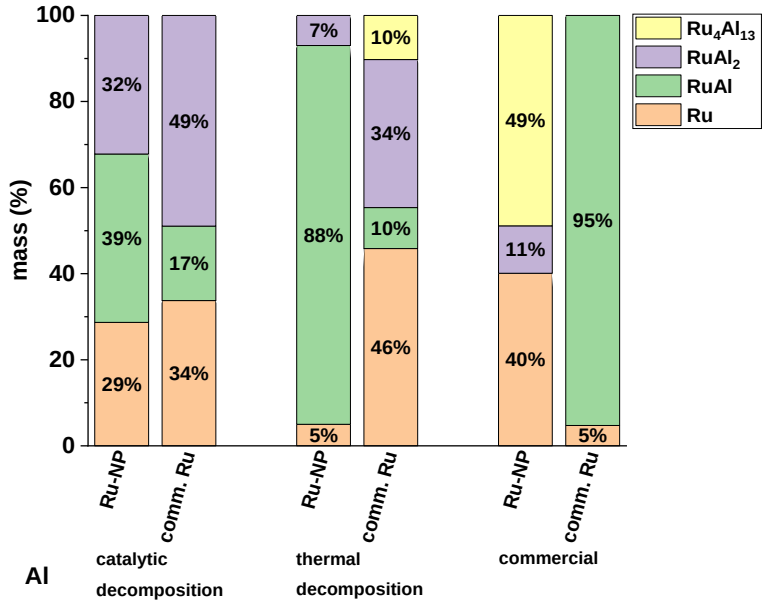

***Figure 41**: Compositions of various reacted Al-Ru pellets prepared from chemically synthesized Al and Ru particles (800 °C; Ar; 60 K/min) determined from Rietveld (only intermetallic phases being present in the sample are shown for comparability reasons; other phases, particularly Al_2O_3, are not shown).*

Upon reacting nano and submicron Al particles with micrometer sized Ru or upon reacting Ru nanopowder with micrometer sized Al, the formation of multiphase products consisting of RuAl, Al rich phases and unreacted Ru was observed (Figure 41). Again, these incomplete reactions can be attributed to long diffusion pathways, similar as reported above for the Ni-Al mixtures. The most promising results were obtained for the Al particles prepared via the thermal decomposition approach, while the application of the particles prepared via the catalytic decomposition approach again resulted in incomplete reactions. This behavior might again be attributed to the varying Al_2O_3 content, although one has to keep in mind that low Ru : Al particle size ratios have been reported in the literature to be necessary to achieve complete conversions[217]. Accordingly, the increased yield might also be attributed to the smaller Ru:Al particle size ratio upon applying the Al particles prepared via the thermal decomposition approach.

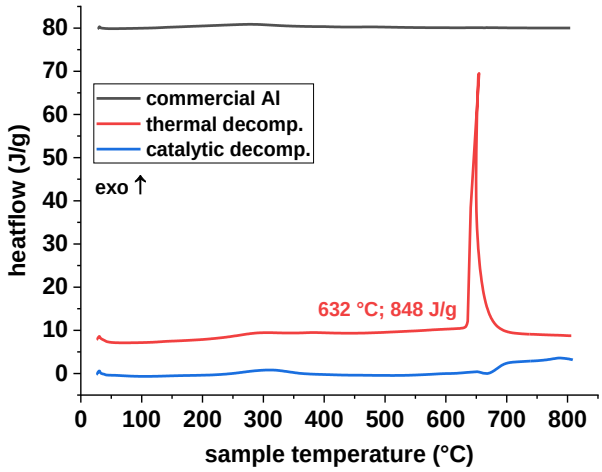

***Figure 42**: STA traces of various Al-Ru pellets prepared from wet chemically synthesized Al particles and Ru nanopowder (800 °C; Ar; 60 K/min).*

Figure 42 shows the STA traces obtained in an Ar atmosphere applying a heating rate of 60 K/min for the reaction of the different Al particles with Ru nanopowder. Again, as was already discussed for the Ni-Al system, the observations of the Rietveld refinements are confirmed, and a strongly exothermic reaction was observed only for the sample prepared applying the Al synthesized via the thermal decomposition approach. In contrast, for the Al synthesized via the catalytic decomposition approach and for the commercial Al, incomplete reactions and thus weak exothermic signals were observed.

In summary, the most promising results regarding the preparation of Ni and Ru aluminides were observed upon applying the Al particles prepared via the thermal decomposition approach. To further study the reasons for these observations, the influence of the organic and oxide contents was studied in more detail, as will be discussed below.

Influence of organic contents

Further studies were carried out to understand the different behavior during the aluminide formation of the Al particles prepared via different synthesis approaches. Particularly upon applying wet chemically synthesized Al and metal particles, which were separately prepared and then mixed in a second step, several parameters, such as organic and oxidic impurity phases, can be expected to affect the aluminide formation. To examine the influence of the organic content, the system prepared from the Al particles synthesized via a thermal decomposition of TIBAl and mechanochemically prepared Ru was chosen, since RuAl was obtained in high yields within this reaction system. Polystyrene (PS) was chosen as an organic compound since it does not contain any functional groups possibly interacting

with the particle surface and since it is known to decompose yielding volatile or gaseous compounds[322]. Accordingly, the Al particles were dispersed in a polystyrene containing toluene solution from which the toluene was subsequently removed in vacuo. The resulting Al-polystyrene composites were then mixed with nanocrystalline Ru powder, compacted and then heated to 800 °C in an Ar atmosphere applying a heating rate of 60 K/min. Figure 43a shows the compositions of the sample prepared in the presence of 0 %, 34 %, and 46 % polystyrene as well as the STA measurements of the respective reactions. As can be seen, the presence of polystyrene within this particle mixture resulted in much more incomplete reactions, indicated by the presence of large amounts of Ru_4Al_{13} as well as unreacted Ru, which were observed in both samples containing polystyrene.

In the STA traces (Figure 43b), the endothermic signal observed at temperatures from 400 – 500 °C can be assigned to the thermal decomposition of the polystyrene. In the sample containing no polystyrene the reaction was observed to start at a temperature of 633 °C, while in the samples containing polystyrene a melting of the Al was clearly observed prior to the reaction, as is indicated by the endothermic signal starting at a temperature of 652 °C. After the melting, the reaction is accordingly initiated in a solid-liquid reaction, as is indicated by the exothermic signal, which can be observed directly following the melting. The significantly lower heat flow in these samples can be explained by the incomplete reactions as well as the lowered energy density of the reacting pellet due to the organic content. The later onset of the reaction in the polystyrene containing samples can be explained by the poorer interelemental contact in these samples, which can be explained by the formation of pores due to the decomposition of the polystyrene. Once the Al starts to melt, the interelemental contact can be expected to improve, ultimately enabling the reaction via a solid-liquid reaction. Accordingly, the more incomplete reactions can likely be attributed to the lower temperatures reached within the samples, due to the increased content of pores and organics. Thus, from these studies it can be learned that the application of nanoparticles with low organic contents should clearly be preferred.

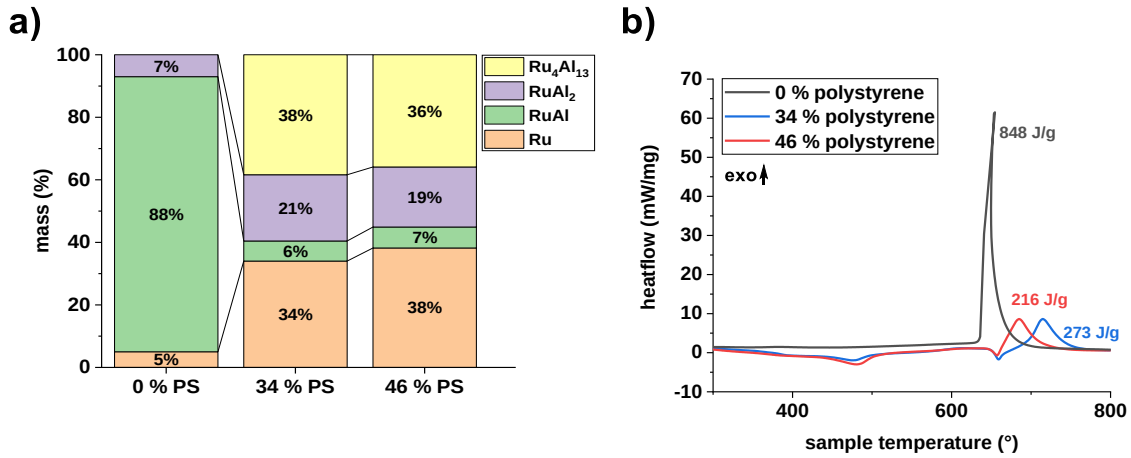

***Figure 43**: **a)** Sample compositions of reacted Al-Ru pellets containing varying amounts of polystyrene (800 °C; Ar; 60 K/min) determined from Rietveld refinements. The Al particles were prepared applying a thermal decomposition of triisobutylaluminum and the Ru nanopowder was prepared by a mechanochemical reaction of $RuCl_3$ and $NaBH_4$ **b)** STA traces of the samples shown in a).*

Influence of oxide content

To further study the influence of the oxide content on the formation of the aluminides, the system consisting of the Al particles synthesized via a thermal decomposition of TIBAl and mechanochemically prepared Ru powder was once more chosen. The main oxygen source within this system is the amorphous oxide layer of the applied Al particles, although a minor amount of oxygen might also be introduced via an oxidation of the Ru nanopowder. To study the influence of an increase of the oxygen content, it was introduced via various strategies: i) addition of commercial Al_2O_3 nanoparticles, ii) oxidation of the Al particles by heating in an atmosphere of synthetic air, or iii) oxidation of the Al particles in conc. HNO_3. However, all of these methods are just a model of the real reaction system, since either the oxide layer thickness or the structure of the Al_2O_3 is changed, while in reality, the oxide content is increased by a reduction of the Al particle size with the oxide layer thickness and structure remaining unchanged (Figure 44). For example, upon heating the Al particles in an atmosphere of synthetic air, an increase of the oxide layer thickness as well as a change of the Al_2O_3 modification will occur, while an oxidation in HNO_3 was reported to lead to a grow of the amorphous oxide layer without a change in the modification[323]. Nonetheless, these studies might give an idea how the Ru aluminide formation is influenced by the presence of additional oxidic phases.

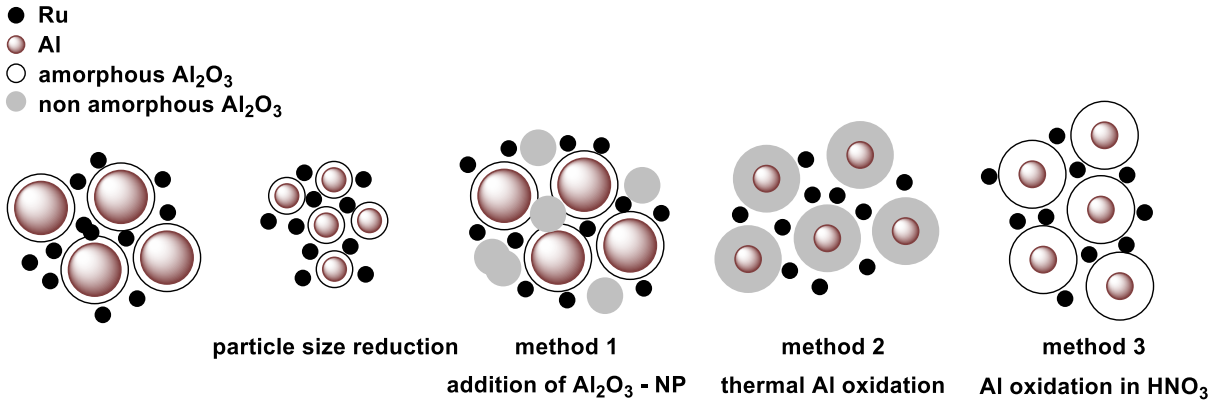

***Figure 44**: Possible methods to increase the oxide content within a metal particle mixture.*

In the first approach, additional Al_2O_3 was introduced into the reaction system by the addition of commercial Al_2O_3 nanoparticles. Within this approach, the oxide content is increased, a contact between Al and Ru is however still given. The presence of this direct Al-Ru contact can be concluded from the STA traces (Figure 45a), where no shift of the onset temperature to increased temperatures can be observed. However, significantly more incomplete reactions were observed in the samples containing additional Al_2O_3 nanoparticles, which is indicated by large amounts of unreacted Ru still being present in the reacted samples (Figure 45b). Due to these incomplete reactions, as well as due to the dilution of the reaction systems by Al_2O_3, strongly decreased heatflows were observed in the STA measurements. Again, the dilution leads to decreased energy densities and thus lower maximum reaction temperatures, which are in turn leading to the observed incomplete reactions.

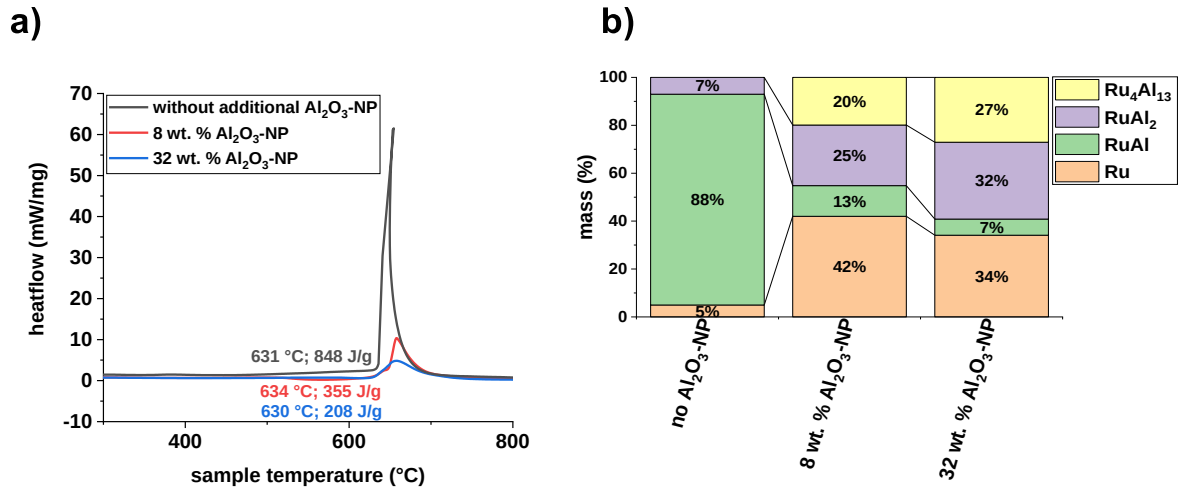

***Figure 45**: **a)** STA traces of Al-Ru pellets prepared from submicron Al, Ru nanopowder and commercial Al_2O_3 nanoparticles (800 °C; Ar; 60 K/min). The Al particles were prepared applying a thermal decomposition of triisobutylaluminum and the Ru nanopowder was prepared by a mechanochemical reaction of $RuCl_3$ and $NaBH_4$; **b)** Sample compositions of the samples after the reactions shown in a) determined from Rietveld refinements.*

In the second approach, the applied Al particles were oxidized by heating them to various temperatures in an atmosphere of synthetic air at a heating rate of 10 K/min in a TG thermal analyzer. The Al^0 contents of the oxidized particles after the heat treatment were calculated from the mass gains and are given within Figure 46a. The application of Al powder which was oxidized at increased temperatures led to significantly decreased yields of the target compound RuAl, as well as significantly increased amounts of residual Ru (Figure 46a). This behavior can be explained by a change of the alumina polymorph during the heat up for the oxidation of the Al particles. In an Al particle passivated by an amorphous oxide layer, this amorphous alumina transforms into denser γ-Al_2O_3 upon reaching a temperature of about 550 °C[130,131]. Thus, in a compacted metal Al particle mixture, which is reacted in an inert atmosphere, bare Al is exposed to the environment upon reaching this transformation temperature, enabling a facile metal - Al reaction via solid-state reactions. In contrast, in the Al particles applied within this method, this transformation already took place during the oxidation of the Al particles. Thus, upon heating the metal Al particle mixtures, no bare Al is exposed to the environment, inhibiting the desired intermetallic reaction. This poorer particle contact was also observed in the STA measurements (Figure 46b), in which the onset temperature shifted from 631 °C for the as prepared Al particles to 653 °C for the Al particles oxidized at a temperature of 620 °C. Due to the more incomplete reactions and the dilution of the reaction system, significantly lower heatflows were observed upon applying the oxidized Al particles. Analogous as described above, increased oxide contents are representing a dilution of the reaction system, leading to decreased maximum temperatures within the reacting sample and thus more incomplete reactions. These observation are in agreement with reports in the literature, in which incomplete reactions have been linked to heat loss effects occurring during the reaction[287].

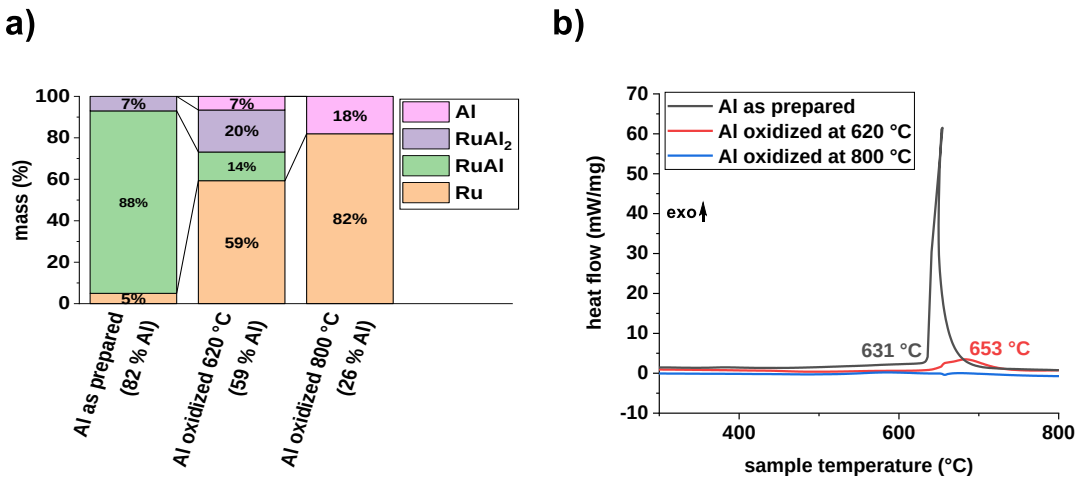

***Figure 46**: **a)** Sample compositions of reacted Al-Ru pellets prepared from Al particles oxidized at different temperatures in an atmosphere of synthetic air and Ru nanopowder (800 °C; Ar; 60 K/min) determined from Rietveld refinements. The value in the brackets is the Al^0 content of the applied Al particles. The Al particles were prepared applying a thermal decomposition of triisobutylaluminum and the Ru nanopowder was prepared by a mechanochemical reaction of $RuCl_3$ and $NaBH_4$; **b)** STA traces of the samples shown in a).*

In the third approach, the Al particles were oxidized by a treatment in 69 % HNO_3 for several minutes at room temperature, followed by rinsing with distilled water and drying. This method has been reported in the literature to lead to the formation of an amorphous oxide layer, with the layer thickness being dependent on the treatment time[323]. Accordingly, in a XRD measurement of the oxidized Al particles no crystalline Al_2O_3 was observed. The Al^0 content of the oxidized Al particles calculated from TG measurements was 49 % after 10 min and 10 % after 20 min. By applying this oxidation method, the additional Al_2O_3 is introduced in the form of amorphous alumina, as it is the case upon a particle size reduction. However, the oxide layer thicknesses increased compared to untreated, but smaller Al particles. Upon mixing these oxidized Al particles with Ru nanopowder and heating the resulting, compacted pellets to 800 °C in an Ar atmosphere, the formation of incomplete reactions was again observed and the product mixtures consisted of unreacted Al, a small amount of RuAl as well as Al rich $RuAl_2$ and Ru_4Al_{13} (Figure 47a). A good particle contact seems however to be given, which is indicated by the low onset temperature of 592 °C (Figure 47b). The amorphous Al_2O_3 is capable of undergoing the phase transformation to denser γ – Al_2O_3, as discussed above, enabling this good interelemental contact. The even lower onset temperature compared to the untreated particles might be attributed to a changed morphology of the formed oxide layer, which was reported to be much more porous[323] or to the smaller size of the Al^0 cores. In general, these observations agree with the results observed for the previous two methods and are also pointing towards the dilution effect being the reason for the observed incomplete reactions. Again, the observed lower heatflows are a result of the incomplete reactions, as was already discussed above. In a FIB cross section image (Figure 47c), the formation of porous products was observed. This increased porosity might also be attributed to the low heats of reactions, which are leading to low maximum reaction temperatures within the reacting samples, which are not sufficient to lead to the formation of a liquid phase.

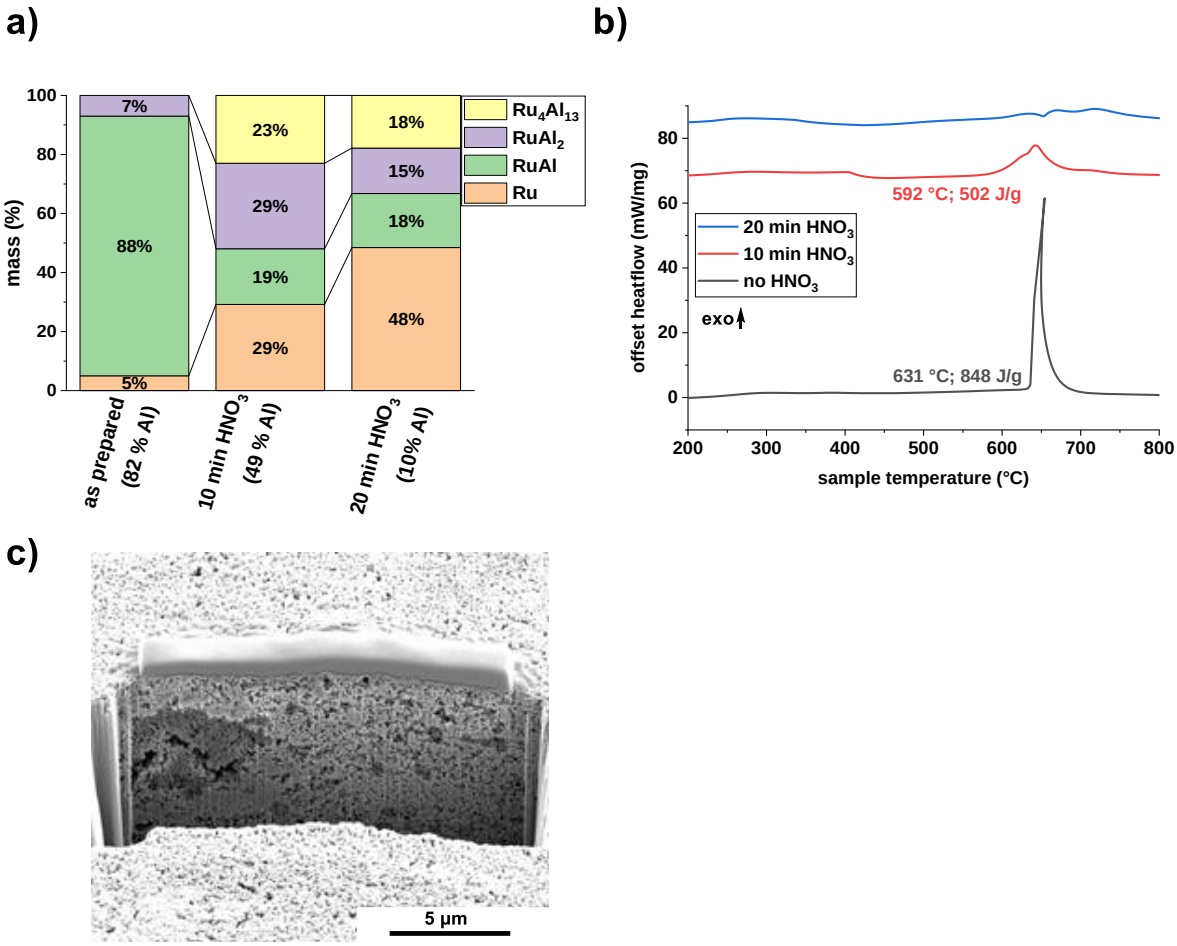

***Figure 47**: **a)** Sample compositions of reacted Al-Ru pellets prepared from Al particles oxidized in 69 % HNO_3 and Ru nanopowder (800 °C; Ar; 60 K/min) determined from Rietveld refinements. The value in the brackets is the Al^0 content of the applied Al particles. The Al particles were prepared applying a thermal decomposition of triisobutylaluminum and the Ru nanopowder was prepared by a mechanochemical reaction of $RuCl_3$ and $NaBH_4$; **b)** STA traces of the samples shown in a); **c)** FIB cross section image the reaction product prepared from the Al particles oxidized in 69 % HNO_3 for 10 min.*

From the studies conducted within this chapter, it can be concluded that under the reaction conditions applied within this work, the best results regarding the preparation of aluminides were observed upon applying the Al particles prepared via a thermal decomposition of triisobutylaluminum. Their superior suitability compared to the Al particles prepared via the catalytic decomposition and metal reduction approaches can be explained by their submicron size and thus lower contents of Al_2O_3 as well as by their very low organic contents < 5 %. Both aspects were shown to be important parameters for the synthesis of aluminides in high yields. Upon increasing the oxide content or the content of organics, incomplete reactions as well as the formations of multiphase products was observed. This observation is likely based on a dilution of the reaction system by the organics or oxides, which is resulting in a decreased energy density leading to lower maximum reaction temperatures. Accordingly, further

studies regarding the preparation of Ni and Ru aluminides summarized within the following chapters were conducted applying particles prepared via the thermal decomposition synthesis method.

3.2.3 Preparation of Ni aluminides

3.2.3.1 Application of micron Ni and Al powders

Firstly, the formation of NiAl starting from commercial, micrometer sized Ni and Al powders was studied to compare their performance with the performance of wet chemically prepared Ni and Al particles. The size of the particles was determined from SEM images and was 7 ± 2 µm for Ni and 14 ± 7 µm for Al. A characterization of these particles is given in Chapters 7.1 and 7.5. The Ni and Al powders were dispersed in a 1:1 molar ratio in hexane, thoroughly mixed in an agate mortar and then compacted in a hydraulic press (350 MPa, Ø 0.6 mm; 1 t; 10 min) to a pellet with a mass of about 15 mg. The resulting pellets were reacted by heating to a temperature of 800 °C applying a controlled heating rate in a TGA/DSC thermal analyzer in an Ar atmosphere. After the reaction the pellets were homogenized and their composition was determined from Rietveld refinements.

Upon applying these small pellets prepared from micrometer sized Ni and Al particles, incomplete reactions resulting in the formation of multiphase reaction products were observed, independently of the applied heating rate (Figure 48a). After the reaction, the samples typically consisted of residual Ni, Ni_3Al, Ni_2Al_3 as well as NiAl, which was attributed to long diffusion pathways as well as high heat losses preventing the reaction to run to completeness. Accordingly, the sample is not being held at an increased temperature long enough to allow a complete diffusion and intermixing, as was already discussed in Chapter 3.2.2. This was further experimentally shown in a publication, which can be found in Chapter 3.2.3.2, wherein these incomplete reactions were only observed in small pellets (< 15 mg), while large pellets (1 g) resulted in the formation of single phase NiAl**.** The incomplete reaction as well as the formation of multiphase products could also be clearly observed in a cross-section SEM image (Figure 49).

The reactions are initiated in the compacted pellets via solid-state reactions well below the Al-Ni eutectic with the onset temperature increasing from 557 °C to 624 °C upon increasing the heating rate from 5 K/min to 60 K/min (Figure 48b). The observed heats of reaction are slightly lower than the values expected based on the determined compositions (the literature values of the heats of formation of the single Ni aluminides are given in Table 10). For example, for a heating rate of 60 K/min a value of 1240 J/g was observed, while the calculated value is 1430 J/g. Since no diluent is present, the lower

values can likely be explained by melting processes occurring during the reactions. In a loose Ni-Al powder mixture, the onset of the reaction is only occurring after the formation of a liquid phase, resulting in an improved interelemental contact. Accordingly, a small endothermic signal can be observed in the STA trace prior to the exothermic reaction signal.

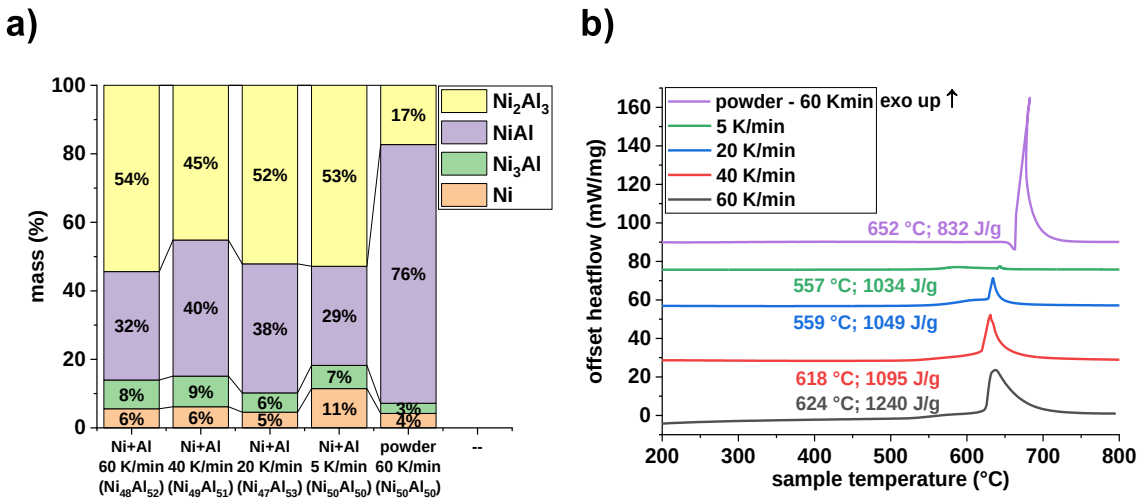

***Figure 48**: **a)** Compositions of reacted Ni-Al pellets and a loose powder mixture prepared from commercial Ni and Al powders (800 °C; Ar; 60 K/min) determined from Rietveld refinements. The compositions given in brackets describe the total sample compositions estimated from Rietveld refinements assuming the formation of ideally stoichiometric phases; **b)** STA traces of the reactions leading to the formation of the products shown in a) (800 °C; Ar; 60 K/min).*

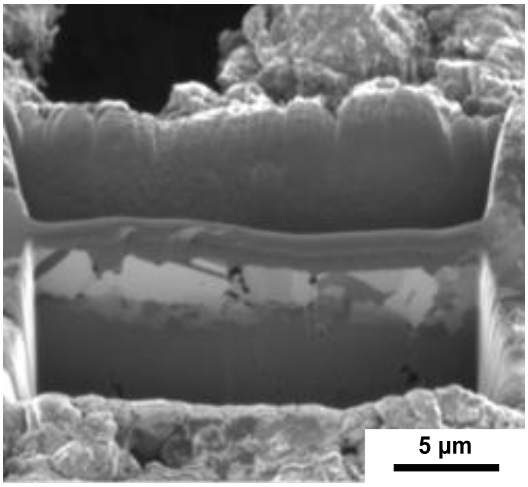

***Figure 49**: Cross-section SEM image of a reacted Ni-Al pellet prepared from commercial Ni and Al powders (800 °C; Ar; 60 K/min).*

As can be seen from the previous section, the formation of multiphase products was problematic upon applying micrometer sized reactants, which was attributed to long diffusion pathways. Accordingly, in

the next chapter, the micrometer sized powders were replaced by wet chemically prepared nanoparticulate reactants, in order to improve the intermixing and prepare NiAl with increased yields.

3.2.3.2 Application of wet chemically prepared Ni and Al particles

Due to the reasons discussed in Chapter 3.2.2., the preparation of NiAl starting from wet chemically prepared Ni and Al particles was studied applying the Al particles prepared via a thermal decomposition of triisobutylaluminum. Ni nanoparticles with a size of 8 ± 1 nm were prepared by decomposing $Ni(acac)_2$ or $Ni(COD)_2$. The Ni and Al powders were mixed in an agate mortar, compacted in a hydraulic press, and then heated to 800 °C in an atmosphere of Ar applying a heating rate of 60 K/min. Upon applying small sample sizes of a few mg prepared from separately synthesized powders, the formation of multiphase reaction products containing Al, $NiAl_3$, Ni_2Al_3, NiAl, Ni_3Al as well as unreacted Ni was observed. These incomplete reactions were shown to be a result of heat loss effects resulting in the sample not to be at an increased temperature for a sufficient time to allow a complete reaction. The observed compositions were similar to the compositions observed upon applying the micrometer sized Ni and Al powders (Chapter 3.2.3.1). Since the diffusion pathways potentially might be decreased due to the strongly reduced particle sizes, this is strongly indicating that poor and irreproducible intermixing is also playing a significant role. This is further evidenced by the observation of extremely large batch to batch variations as can be seen by the formation of 93 % NiAl within Chapter 3.2.2 compared to a maximum of only 21 % NiAl observed in these studies. However, an application of a ball mill for mixing purposes, which would allow a more controlled mixing, was not possible due to the small sample amounts.

To prepare samples containing NiAl as the only crystalline phase in a controlled way, a novel two-step synthesis protocol for the preparation of Ni-Al precursor powders was developed. In a first step, submicron Al was prepared by thermally decomposing triisobutylaluminum in refluxing diphenylether in the presence of nanoparticulate Ni seeds. In a second step, $Ni(COD)_2$ was added to this mixture and thermally decomposed. The resulting particle mixtures were characterized applying TEM, XRD and FIB techniques. Upon heating these Ni-Al powder mixtures to a temperature of 800 °C in an atmosphere of Ar applying a heating rate of 60 K/min the formation of NiAl as the only crystalline phase was observed without any mixing being necessary prior to the thermal treatment. In addition, amorphous and oxide-rich phases were detected, which were attributed to the presence of oxidic passivation layers. The formation of NiAl as the only crystalline phase was attributed to the excellent intermixing and particle contact that was realized by applying this synthesis protocol. The excellent interelemental contact was evidenced by an onset temperature well below the melting point of the Ni-Al eutectic even when the powders were applied as a loose powder.

The results have been published as a paper in *Intermetallics* from Elsevier.

Klein, T.; Pauly, C.; Mücklich, F.; Kickelbick, G. Al and Ni Nanoparticles as Precursors for Ni Aluminides. *Intermetallics* **2020**, *124*, 106839.[324] Reprinted with permission from Elsevier. (https://doi.org/10.1016/j.intermet.2020.106839)

Author contributions:

T. Klein had the original idea, carried out all the synthetic work and evaluated the results. He carried out the Rietveld refinements, the STA, DLS, TG, and TEM measurements and prepared the initial draft of the manuscript.

C. Pauly carried out and evaluated the FIB measurements, gave scientific input, prepared the initial draft of the manuscript, and proof-read the final manuscript.

F. Mücklich proof-read and edited the final manuscript.

G. Kickelbick gave scientific input, supervised the work, and discussed the results. He also proof-read and edited the final manuscript.

Intermetallics 124 (2020) 106839

Contents lists available at ScienceDirect

Intermetallics

journal homepage: http://www.elsevier.com/locate/intermet

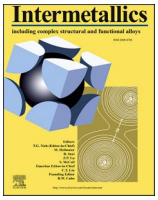

Al and Ni nanoparticles as precursors for Ni aluminides

Thomas Klein [a], Christoph Pauly [b], Frank Mücklich [b], Guido Kickelbick [a,*]

[a] Saarland University, Inorganic Solid-State Chemistry, Campus C4$_1$, 66123, Saarbrücken, Germany
[b] Saarland University, Functional Materials, Department of Materials Science, 66123, Saarbrücken, Germany

ARTICLE INFO

Keywords:
A. aluminides
A. intermetallics
A. nanocrystalline metals
C. heat treatment
C. nanocrystals
C. reaction synthesis

ABSTRACT

Aluminides, intermetallic compounds of Al with at least one additional element, are promising materials particularly for high-temperature applications due to their physical and chemical properties. They are typically prepared starting from the elements using compacted, micrometer sized powders or multilayer systems, while the application of nanoparticles as precursors is much more uncommon although the high interface area can have advantages in the reactivity of the materials. We prepared Ni aluminides starting from submicron Al particles and Ni nanoparticles applying a self-propagating reaction. Upon applying separately prepared particles multiphase products containing Ni, Ni_3Al, NiAl, Ni_2Al_3 as well as $NiAl_3$ were observed depending on the sample size and heating rates. The preparation of single phase NiAl was possible applying particle mixtures synthesized by a two-step protocol. In a first step, submicron Al particles were synthesized via thermal decomposition of triisobutylaluminum. On the surface of the formed Al particles nanocrystalline Ni was deposited in a second step via thermal decomposition of bis(cycloocta-1,5-dien)nickel(0) resulting in the formation of well-mixed Ni–Al particle blends. Heating of powder compacts or loose powders under an atmosphere of Ar resulted in the formation of single phase NiAl at low as well as at high heating rates with no other intermetallic phases being present.

1. Introduction

Aluminides are promising materials for high-temperature applications because of their oxidation resistance as well as chemical resistance combined with their high-temperature strength [1–5]. They are commonly synthesized starting from the elements via various methods, such as melt metallurgy or reactive methods [6]. Applying highly exothermic self-propagating reactions has the advantage of short reaction times and the synthesis of high purity products. Examples for metal aluminides are binary Ni, Fe, Ti and Ru aluminides, as well as ternary, quaternary or even materials with a larger amount of elements [7–11].

In the Ni–Al system [12] five different intermetallic phases are known, namely $NiAl_3$, Ni_2Al_3, NiAl, Ni_5Al_3 and Ni_3Al. While the thermal stability of $NiAl_3$ and Ni_5Al_3 is limited and the stability ranges of Ni_2Al_3 and Ni_3Al are small, NiAl exhibits a wide stability range at room temperature of around 10 at% Al as well as a high thermal stability. Its properties like a very high melting point (1638 °C), as well as corrosion and oxidation resistance make it to the most important nickel aluminide for technical applications, such as coatings or as a material for reactive bonding [13,14]. Besides NiAl, Ni_3Al is also an interesting material for industrial applications because of its high-temperature properties [15].

The synthesis of single-phase NiAl can be carried out starting from Ni and Al powders applying reactive sintering [16,17], self-propagating high-temperature reactions [18,19], or mechanochemical approaches [20]. Moreover, the synthesis applying wet-chemical approaches [21] or multilayer systems [22–24] has been reported in the literature.

In sputter-deposited multilayer systems, a dependence of the ignition temperature from the bilayer thickness was reported [22]. A multilayer with a bilayer thickness of 30 nm exhibited an ignition temperature of 232 °C, while an ignition temperature of 297 °C was observed in a system with a bilayer thickness of 139 nm [22]. In such systems it was proven that NiAl forms from the melt in a single reaction step [25–27] without any other intermetallic intermediate products. In contrast, when slow heating rates <1 K min^{-1} were applied, the formation of several intermediate products such as Ni_2Al_9, Al_3Ni and Al_3Ni_2 could be observed [27,28].

Starting from compacted micrometer sized Al and Ni particles, a synthesis of NiAl is also possible, whereby higher ignition temperatures are typically observed. For example, Hunt et al. [29] reported an ignition temperature of 633 °C in a compacted mixture of 20 μm Al and 1 μm Ni particles.

In contrast to these micrometer sized powders, which are commonly

* Corresponding author.
E-mail address: guido.kickelbick@uni-saarland.de (G. Kickelbick).

https://doi.org/10.1016/j.intermet.2020.106839
Received 7 March 2020; Received in revised form 9 April 2020; Accepted 12 May 2020

applied in such syntheses, only a few studies about the synthesis of Ni aluminides applying nanoparticular reactants [29–31] have been reported. In the studies conducted by Hunt et al. [29], commercial, oxide-passivated Al and Ni nanoparticles were used. The Al particles had sizes of 25 nm up to 1 μm, while Ni particles with a size of 1 μm were applied. Upon decreasing the Al particle size, a decrease in the ignition time and temperature from 633 °C to 286 °C could be observed, while the burn-rates were found to be decreasing. The lower burn-rates were explained by the increasing amount of Al_2O_3 present in the samples with the smaller Al particles, which is acting as a heat sink and thus lowering the burn rate.

Dong et al. [30] studied the formation of NiAl applying Ni powder with a size of 44 μm and Al powder with a size of 40 nm. They also reported a low onset temperature of the reaction of 470 °C. Moreover, they reported a shift of the onset temperatures to lower temperatures upon increasing the heating rate or the green densities.

Hence, the application of nanometer sized reactants is leading to various advantages especially regarding the reaction onset temperatures. The particles applied in these studies are typically of a commercial origin and/or have been synthesized applying physical approaches. For example, the particles employed by Dong et al. were obtained via wire electrical explosion [30]. However, to our knowledge, only little is known about the synthesis of Ni aluminides starting from wet chemically synthesized Ni and Al nanoparticles. Wet chemical processes have the advantages of possible short reaction times, easy experimental set-ups, as well as the possibilities of facile scale-ups and continuous syntheses approaches. Additional compounds like surfactants or residual solvents might however introduce impurities as well as porosities in the final intermetallic compounds. These open questions were the motivation of our studies about the suitability of wet chemically synthesized powders for the synthesis of aluminides.

2. Materials and methods

2.1. Materials

Triisobutylaluminum (1 M in hexanes), trioctylphosphine (TOP; 90%), 1,5-cyclooctadiene (COD; 99%), and oleylamine (C_{18} content 80–90%) were obtained from Sigma-Aldrich (St. Louis, USA). Diphenylether (99%) and nickel(II)acetylacetonate (95%) were delivered by Alfa-Aesar (Kandel, Germany). Diphenylether and oleylamine were dried in vacuo at 100 °C for 2 h, stored over molecular sieves (3Å) for several days and filtered through 0.45 μm syringe filters prior to use. Absolute THF was obtained from a MBraun solvent purification system and MeOH (99.8%; extra dry) was provided by Acros Organics (Geel, Belgium). All other chemicals were used as received without any further purification. Unless stated otherwise, all reactions were carried out under an Ar atmosphere applying standard Schlenk techniques. Bis (cycloocta-1,5-dien)nickel(0) was synthesized following a literature procedure [32].

3. Methods

Elemental analyses were carried out with an Elementar Vario Micro cube.

Powder X-ray diffractograms (PXRD) were measured in a Bragg-Brentano geometry using Cu K_α-radiation on a Bruker D8-A25-Advance diffractometer. The diffraction patterns were recorded using a step size of 0,013° from 7 to 120° (2θ) and a total measurement time of 1 h. The specimens were prepared from the homogenized and dispersed samples by drop coating them directly onto the sample holders. Rietveld refinements using TOPAS 5.1 [33] were applied to determine the sample compositions as well as the crystallographic structures. Instrumental line broadening was taken into account by a fundamental parameter approach [34] and the background was fitted using a Chebychev polynom (15th degree). The Rietveld refinements were carried out applying published crystal structures from the crystallographic open database (COD) [35], the inorganic crystal structure database (ICSD) or the materials project [36]. Entries with the following ID's were used for the refinements: Al 2300250 (COD), Ni 2100640 (COD), NiAl 9008802 (COD), Ni_3Al 20000627 (COD), $NiAl_3$ 58040 (ICSD), Ni_2Al_3 mp-1057 (materials project), Ni_3P 9011823 (COD), Ag_2Al 1509011 (COD), γ-Al_2O_3 2107301 (COD).

TEM images were recorded on a JEOL JEM-2010 applying an accelerating voltage of 200 kV. TEM samples were prepared by drop casting the nanoparticle dispersion directly onto the carbon coated copper grids followed by air drying.

Focused ion beam (FIB) measurements were carried out on a Helios NanoLab600 from FEI using a gallium ion beam. The powder compacts were contacted with conductive carbon prior to the measurements. The particle size distributions were obtained from the TEM or SEM images by measuring 100 particles using the software ImageJ [37].

Thermogravimetric analyses (TGA) were carried out in open alumina crucibles on a Netzsch TG F1 Iris under a constant flow of N_2/O_2 32:8 (40 ml min^{-1}) or N_2 (40 ml min^{-1}) using a heating rate of 10 K min^{-1}. Simultaneous thermal analyses (STA) were conducted in open alumina crucibles on a Mettler-Toledo STAre system under a constant flow of Ar (40 ml min^{-1}). A heating rate of 60 K min^{-1} was used and the maximum temperature in the measurements was 800 °C. For all samples, a second scan was performed and, after confirming the absence of any signals (particularly Al melting), used as a background curve.

Ignition temperatures of the compacted pellets were determined by dropping small amounts (1–2 mg) of the pellets onto a heated hot plate. The lowest temperature at which an ignition could be observed with the naked eye was defined as the ignition temperature. The experiments were carried out under an atmosphere of ambient air.

3.1. Syntheses

3.1.1. Al–Ni powder mixtures

60 ml of diphenylether were degassed at 100 °C for 30 min. After cooling to 40 °C 2 ml of triisobutylaluminium (1 M in hexane) (2 mmol) and 3.0 mg (0.05 mmol) of Ag nanoparticles were added. Afterwards hexane was removed in vacuo and the mixture was homogenized using an ultrasonication bath for 15 min. Subsequently the mixture was refluxed for 15 min resulting in the formation of a grey solid. After cooling to room temperature, $Ni(COD)_2$ was added and the mixture was heated to 120 °C for additional 2 h. The black solid was centrifuged (8000 rpm; 10 min), washed three times with 15 ml of diethylether (8000 rpm; 10 min) and dried in vacuo at room temperature.

3.2. Synthesis of aluminides

The samples were prepared by thoroughly mixing both components in an agate mortar using hexane as a dispergent. Compacted pellets were obtained using a hydraulic press (Ø 6 mm; 1 t; 15 min; 350 MPa). The reactions were carried out using a controlled heating rate in a tube furnace or in a TGA/DSC thermal analyzer under a flowing Ar atmosphere (40 ml min^{-1}) in open alumina crucibles. After cooling to room temperature, the pellets were homogenized and their composition was determined from Rietveld refinements.

3.3. Ni nanoparticles

Ni nanoparticles were prepared according to the method published by Carenco et al. [38]. Briefly, 2 g of $Ni(acac)_2$ (8 mmol) were dissolved in 21 g of oleylamine and 2.3 g (6 mmol) of TOP and the mixture was degassed at 100 °C for 1 h. The solution was heated to 220 °C for 2 h and after cooling to room temperature, 40 ml of acetone were added. The particles were collected by centrifugation (8000 rpm; 10 min) and washed by three cycles of redispersing in 5 ml of hexane, precipitating with 40 ml of acetone and centrifugation (8000 rpm; 10 min). The

particles were dried in vacuo at 80 °C.

3.4. Submicron Al particles

Submicron Al particles were prepared according to published literature methods [39]. Briefly, 60 ml of diphenylether were degassed at 100 °C for 30 min. After cooling to room temperature, 3.0 mg of Ni nanoparticles (0.05 mmol) and 2 ml of triisobutylaluminium (1 M in hexane) (2 mmol) were added. Hexane was removed in vacuo, followed by homogenization of the reaction mixture in an ultrasonication bath for 15 min. The mixture was refluxed for 15 min resulting in the formation of a black/grey solid. The solid was separated by centrifugation (8000 rpm; 10 min), washed three times with 15 ml of diethylether (8000 rpm; 10 min) and dried in vacuo at room temperature. Within this manuscript, the particles obtained via this method are referred to as Al(Ni).

3.4.1. Bis(cycloocta-1,5-dien)nickel(0) (Ni(COD)$_2$)

$Ni(COD)_2$ was prepared following a published literature procedure [32]. Briefly, 10.8 g (45 mmol) of $NiCl_2(H_2O)_6$ were added to 125 ml pyridine. The resulting mixture was refluxed for 3 h and the formed blue solid ($NiCl_2(pyridine)_4$) was separated by filtration and dried in vacuo at room temperature. 8.92 g (20 mmol) of ($NiCl_2(pyridine)_4$ were degassed at room temperature for 15 min and the flask was refilled with Ar. This procedure was repeated two more times. 7.4 ml (60 mmol) 1,5-Cyclooctadiene and 12 ml THF were added and the mixture was stirred at room temperature for 15 min. 0.92 g (40 mmol) Na was added in small pieces and the mixture was stirred for 3 h at room temperature under the exclusion of light. 24 ml methanol were added and the formed yellow solid was allowed to settle. The methanol was decanted and the solid was washed 3 more times with 12 ml of methanol. The product was dried in vacuo and stored at – 10 °C.

^{1}H NMR (400 MHz; C_6D_6) δ: 4.31 (br s; CH), 2.07 (br s; CH_2) ppm.
^{13}C NMR (101 MHz; C_6D_6) δ: 89.7 (CH), 30.9 (CH_2) ppm.

4. Results and discussion

4.1. Ni aluminides

The preparation of NiAl applying combustion syntheses like self-sustaining, high-temperature reactions or thermal explosions is well known in the literature [19,40,41] and the formation of single-phase NiAl has been reported to be possible by applying these syntheses [40,41]. However, one has to keep in mind that in these reports often multi-gram pellets were used. Also, it has been reported that high heat losses may prevent the reaction from becoming self-sustaining [17,40] resulting in the formation of multiphase products due to incomplete reactions. Since high heat losses are expected to occur particularly in samples with high surface-to-volume ratios and/or small sample sizes and for wet chemically synthesized nanoparticles such large quantities are typically not available, we examined the product formation in samples with various geometries applying commercial Ni and Al powders in a first step.

For these studies, pellets prepared from commercial Ni and Al powder with particles sizes of 7 ± 2 μm and 14 ± 7 μm were reacted by heat treatment up to 800 °C applying a heating rate of 3.3 K min^{-1} under a flowing Ar atmosphere and holding this temperature for additional 2 h. A dependence of the final sample composition from the amount and shape of the pellet could be clearly observed (Fig. 1a). While the formation of single phase NiAl could be observed for pellets generated from 1 g of a 1:1 Ni–Al powder mixture as well as for 250 mg of loose powder in a 1:1 ratio, the use of smaller amounts of sample resulted in an increasing amount of additional phases. Similar observations were made when pellets with a mass of 250 mg were prepared in various sizes. The pellets were prepared with diameters of 6 mm, 10 mm as well as 16 mm applying a pressure of 290 MPa. In these samples, increasing amounts of additional phases (Ni_2Al_3, Ni_3Al and unreacted Ni) were observed to form with increasing surface-to-volume ratio of the sample (Fig. 1a). Accordingly, the yield of NiAl decreased from 67% in the pellet with a diameter of 6 mm–46% in the pellet with a diameter of 16 mm. These results are in good agreement with previous reports [17,40], since

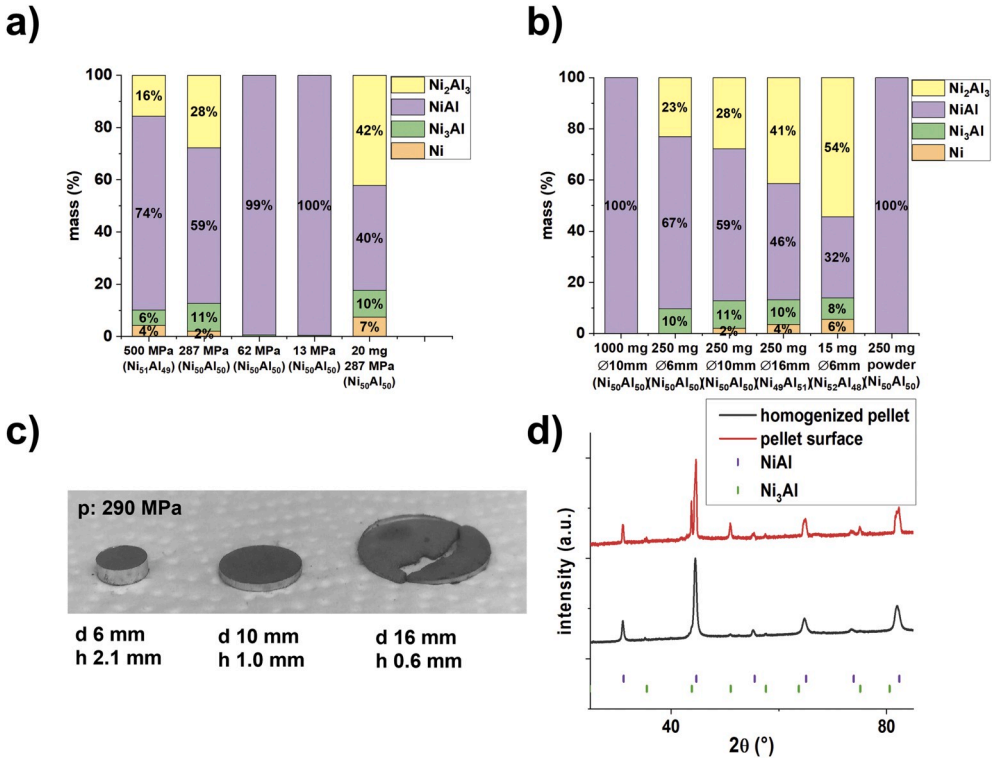

Fig. 1. a) Sample compositions of homogenized Ni–Al powder mixtures obtained from different pellets determined from Rietveld refinements after heating to 800 °C using a heating rate of 3.3 K min^{-1} in a flowing Ar atmosphere and holding at 800 °C for 2 h. The compositions given in brackets describe the total sample compositions estimated from Rietveld refinements assuming the formation of ideally stoichiometric phases. **b)** Sample compositions of homogenized Ni–Al powder mixtures obtained from different pellets (1 cm diameter and 250 mg sample; various pressures) determined from Rietveld refinements after heating to 800 °C using a heating rate of 3.3 K min^{-1} in a flowing Ar atmosphere and holding at 800 °C for 2 h. **c)** Picture of the different pellets used during these studies **d)** XRD measurements of a homogenized pellet and of its surface.

higher heat losses are expected to occur upon increasing the surface-to-volume ratio of the pellets. Due to these heat losses, the time at increased temperatures >800 °C is reduced leading to poorer intermixing and thus incomplete reactions. This could be also observed in the 1 g pellet, which yielded single phase NiAl after being homogenized, but in which the formation of Ni_3Al could be detected on the pellet surface (Fig. 1d). Heat losses at the pellet surface are most likely the reasons for this observation. Analogous observations were made in various pellets (diameter 1 cm and 250 mg sample) prepared applying different pressures (Fig. 1b): The highest yields of NiAl were detected when low pressures were applied during the preparation of the pellets. In pellets prepared by application of low pressures, a less dense sample can be expected to be formed. The effect of the green density during the formation of NiAl via SHS reaction has already been discussed in the literature [30] and a decreasing porosity was reported to result in enhanced thermal conductivities as well as in a facilitated diffusion due to increased interfacial areas. Accordingly, dense samples can be expected to exhibit higher heat losses during the reactions, again resulting in reduced times at increased temperatures >800 °C leading to poorer intermixing and thus incomplete reactions. Accordingly, the yield of NiAl was found to decrease from 99% to 59% upon increasing the pressure from 62 MPa to 287 MPa, before it increases again to 74% upon further increasing the pressure to 500 MPa. As discussed above, the decrease in the yield can be attributed to an increase in the thermal conductivity, while the increase in the yield upon further increasing the pressure can be attributed to the increased interfacial areas.

The onset temperature of the reaction in an Ar atmosphere was 623 °C for the compacted pellets (Fig. 2a), which is slightly below the melting point of the Ni–Al eutectic at 640 °C. No melting peak could be observed indicating a very fast consumption of Al. For the loose powders, a reaction via solid-state diffusion is inhibited due to the poor contact between Ni and Al. Thus, no exothermic reaction can be observed until reaching the melting point of Al, leading to a violent solid-liquid reaction. (Fig. 2a). On a hot plate no ignition could be observed until reaching the maximum temperature of the plate (>600 °C). One also has to keep in mind that particularly using small sample amounts in which high heat losses are occurring the reaction might at least not completely proceed via a self-sustaining route. As reported in the literature the formation of NiAl is believed to be a diffusion-controlled solid-state reaction rather than becoming self-sustaining when slow heating rates are applied [28,42], as it is the case in these studies. As a result, the formation of intermediate products according to the Ni–Al phase diagram can typically be observed applying these slow heating rates.

Accordingly, the amount of NiAl slightly increased from 39% to 45% upon increasing the reaction time at 800 °C from 2 h to 12 h due to a more complete diffusion (Fig. 2b). Similarly, more complete reactions with a yield of 72% NiAl could be observed when the Al particle size was reduced from 14 μm to about 150 nm due to better intermixing as well as shorter diffusion paths (Fig. 2b). Note that the final sample composition is slightly understoichiometric in Al due to the smaller particle size of the Al(Ni) particles, leading to an increased content of the surface oxide resulting in a lower total Al^0 content (around 80% as determined via TGA measurements compared to >99% for the commercial Al). When the heating rate was increased from 3.3 K min^{-1} to 60 K min^{-1}, the formation of multiphase products could be observed in all samples, with the sample compositions being independent from the particle sizes (Fig. 2b). Similar compositions with only a minor proportion of NiAl were detected in all samples. Since reaction times were very short (no isothermal segment was used after reaching 800 °C), the formed multiphase products are once again the result of incomplete reactions caused by high heat losses. Similar as was discussed for the micrometer sized reactants, due to these heat losses, the time at increased temperatures >800 °C, caused by the high heat of reaction, is reduced leading to poorer intermixing and thus incomplete reactions.

As described above, all attempts of the preparation of single phase NiAl applying separately synthesized and mixed Ni and Al nanoparticles failed in our reaction system and multiphase products were obtained. These observations can likely be ascribed to a poor intermixing as well as long diffusion paths.

Thus, in order to obtain higher yields of NiAl, a one-pot synthesis protocol was developed which directly yields Ni/Al particle mixtures suitable for the synthesis of Ni aluminides. In a first step, submicron Al particles were synthesized via a thermal decomposition of Al^iBu_3 in phenylether [39]. In a second step, after cooling to room temperature, Ni $(COD)_2$ was added and the reaction mixture was heated up again to 120 °C for additional 2 h. Since no isolation of the formed Al particles was necessary, less agglomeration occurs resulting in improved mixing of the particles with better contact between Ni and Al. XRD measurements of the resulting materials revealed that Ni and Al were formed with no detectable formation of any Ni–Al intermetallics. The crystallite sizes determined via Rietveld refinements are 98(5) nm for Al and 2(1) nm for Ni with a total sample composition of $Ni_{54}Al_{46}Ag_{0.04}$. The Ag_2Al was formed during the synthesis of the Al particles in which Ag nanoparticles were used as nucleation seeds. The resulting Ni–Al powder mixtures were compacted and heated up to 800 °C under an Ar atmosphere, resulting in the formation of NiAl as the only intermetallic phase (Fig. 3). One has however to keep in mind, that the compositions were

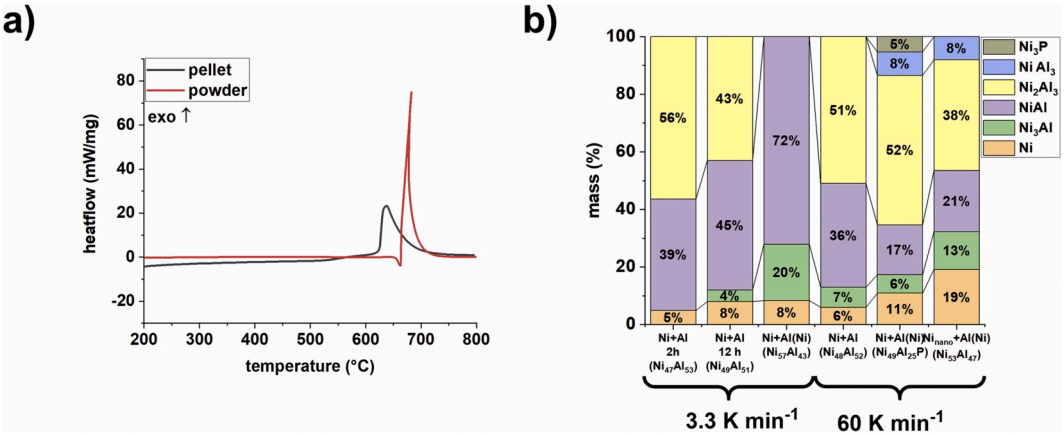

Fig. 2. a) STA measurements of loose and compacted Ni–Al powder mixtures under a flowing Ar atmosphere applying a heating rate of 60 K min^{-1}. **b)** Sample compositions determined from Rietveld refinements of various compacted Ni–Al powder mixtures. The compositions given in brackets describe the total sample compositions estimated from Rietveld refinements assuming the formation of ideally stoichiometric phases and the applied heating rates are given below the brackets.

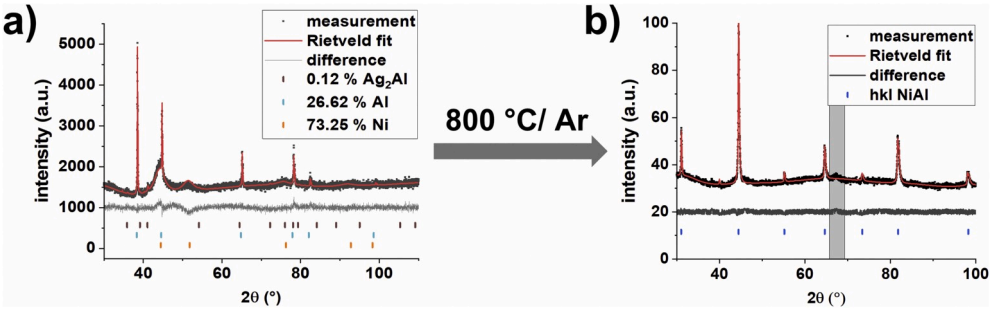

Fig. 3. a) XRD measurement and Rietveld refinement (GoF 1.21) of an as synthesized Ni–Al powder mixture. **b)** XRD measurement and Rietveld refinement (GoF 1.21) of a compacted Ni–Al powder mixture after heating up to 800 °C using a heating rate of 60 K min^{-1} a flowing Ar atmosphere. The reflection highlighted in grey can be attributed to γ-Al_2O_3.

determined using XRD measurements and amorphous phases (particularly oxidic phases) are neglected in the calculation of the yields.

TEM and FIB cross-section images of the unreacted and reacted powder pellets reveal that Ni and Al are present well mixed in the unreacted sample (Fig. 4a and b) and no formation of any intermetallic phase is visible. The homogeneity of the reacted sample is shown in the low-magnification cross-section image (Fig. 5a). It is obvious from the TEM images that the small Ni crystallites with a size of 2(1) nm as observed in the XRD measurements are forming larger agglomerates with a mean size of 68 ± 17 nm. However, the much smaller crystallites are still clearly visible in the TEM image. In addition, as expected, the mixtures were rather consisting of a mixture of Ni and Al particles than core-shell structures. Nevertheless, a deposition of the Ni agglomerates on the Al surfaces can be observed, resulting in a very good contact as well as intermixing between Ni and Al. The formation of an oxide shell on the Al particle surfaces could also be observed in this sample. In the reacted sample (Fig. 4c) the single particles of Ni and Al are no longer visible indicating a complete reaction of both particles. Instead, the formation of the new NiAl phase can be observed as was evidenced by PXRD measurements (see above), while no formation of any other intermetallic phases was detected. However, a second phase could be clearly observed. Because the resolution of the available EDS technique was too low to determine the phase composition directly, an EDS line scan (Fig. 4d) was carried out along the line shown in Fig. 4e applying an accelerating voltage of 5.0 kV. Upon crossing the second, darker appearing phase, the intensities of the oxygen K_α and the carbon K_α are increasing, confirming the second phase to be oxide rich. Thus, this phase mainly consists of Al_2O_3, which is known to exist as amorphous Al_2O_3 at room temperature and which transforms to γ-Al_2O_3 upon heating to temperatures >500 °C [43]. The γ-Al_2O_3 was visible in the

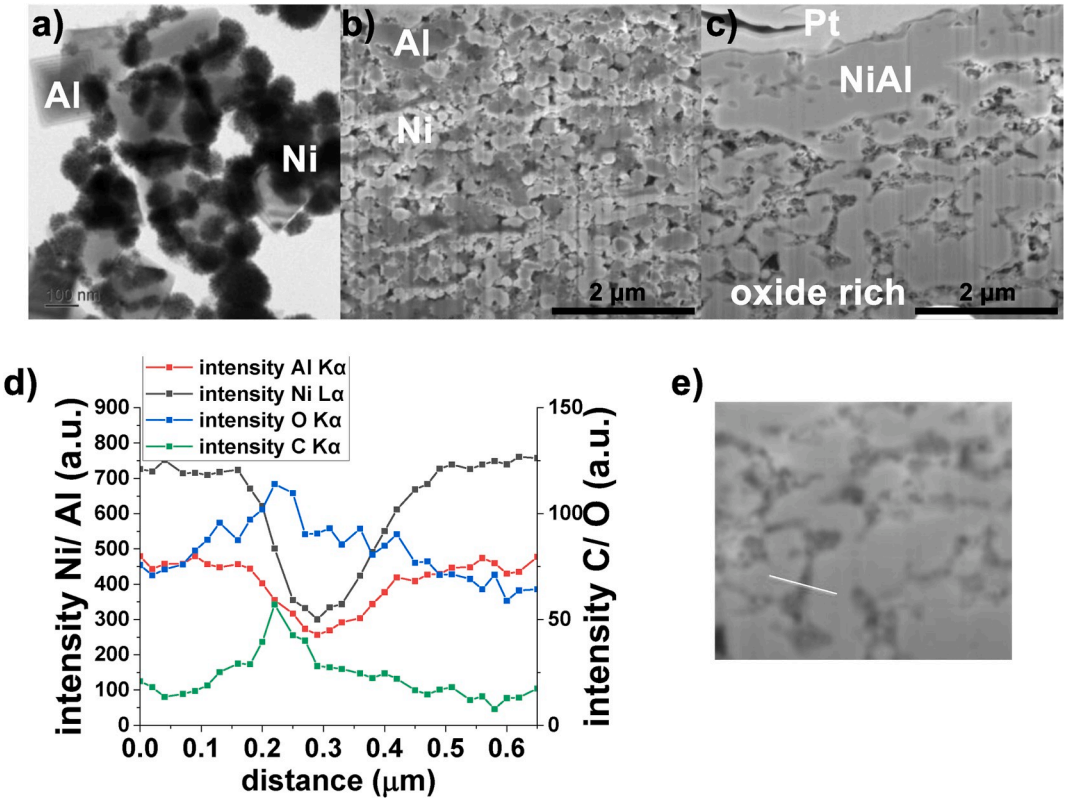

Fig. 4. a) TEM image of as prepared compacted Ni–Al powder pellets synthesized using a one-pot procedure (Ni:Al 1:1). **b)** FIB cross-section image of as prepared compacted Ni–Al powder pellets synthesized using a one-pot procedure (Ni:Al 1:1). **c)** FIB cross-section image of compacted Ni–Al powder pellets synthesized using a one-pot procedure (Ni:Al 1:1) after heating up to 800 °C using a heating rate of 60 K min^{-1} under a flowing Ar atmosphere. **d)** EDS measurements of the reacted sample along the line shown in **e**). The length of the line shown in **e)** is 0.65 µm. Angle of observation in b), c) and e) is 52°.

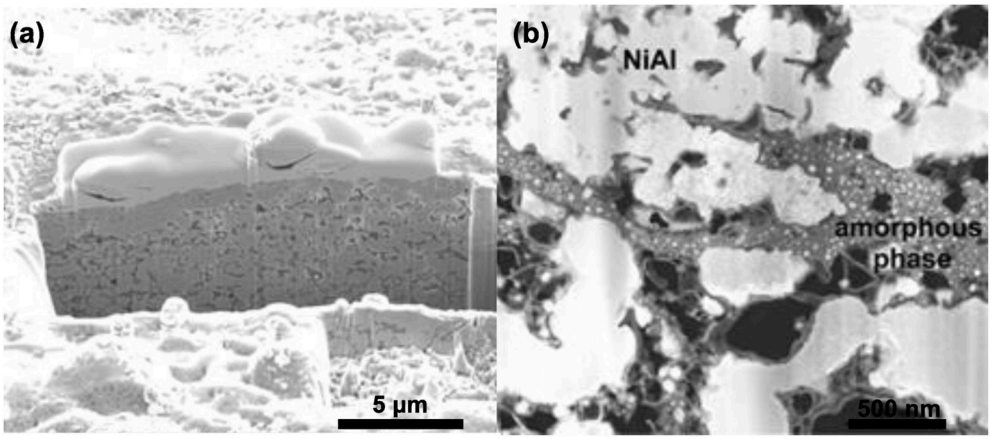

Fig. 5. a) Low magnification cross-section image of a reacted sample. **b)** Dark field STEM image of the reacted Ni–Al powder mixture after heating to 800 °C under a flowing Ar atmosphere using a heating rate 60 K min^{-1}.

XRD measurements of the reacted samples (Fig. 3b), wherein the very broad reflections can be attributed to its very poor crystallinity or amorphicity. Besides, carbonaceous residues due to the decomposition of residual organics could be clearly observed as can be seen in Fig. 4d. Moreover, the decomposition of these organic residues likely is the reason for formation of the porous structure visible in Fig. 4c. The total carbon content in a reacted sample was 2.2% as determined via CHN analysis. No residual hydrogen and nitrogen could be detected in the sample. Accordingly, the presence of the oxygen can be attributed to the amorphous oxide layers at the Al particle surface, while the presence of carbon is likely due to the decomposition of small residual amounts of COD and solvent. Moreover, it has to be noted that the presence of oxygen and carbon within the NiAl phase can be assigned to the poor resolution of the EDS technique.

A STEM-DF image (Fig. 5b) further confirmed that NiAl is the only intermetallic phase present. Moreover, small inclusions of the amorphous phase in the NiAl phase can be detected in these images as well as small particle-like inclusions of the NiAl in the amorphous phase.

Similar compositions were observed using slow heating rates of 3.3 K min^{-1} and 5 K min^{-1} as well as fast heating rates of 60 K min^{-1} and the yields were significantly higher than those observed above for the micrometer sized particles (Fig. 6a). Applying slow heating rates of 3.3 K min^{-1}, the formation of >93% of NiAl is indicating a nearly complete reaction between the elemental powders. For fast heating rates of 60 K min^{-1} single phase NiAl could be observed. In both cases, the higher yields are likely to be caused by the one pot synthesis procedure, resulting in the formation of very small Ni crystallites leading to a good mixing and contact between Ni and Al as well as very short diffusion pathways. These short diffusion pathways seem to be advantageous regarding a complete conversions, since for particle mixtures as well as for multilayer systems the reaction is initiated by an asymmetric solid-state diffusion of Ni into Al [44,45].

STA measurements (Fig. 6b) showed a dependency of the reaction onset from the heating rate. The visible tilt of the STA signals is due to the strong exothermic reactions leading to heating rates >60 K min^{-1} for a short period of time. While for high heating rates of 60 K min^{-1} and 40

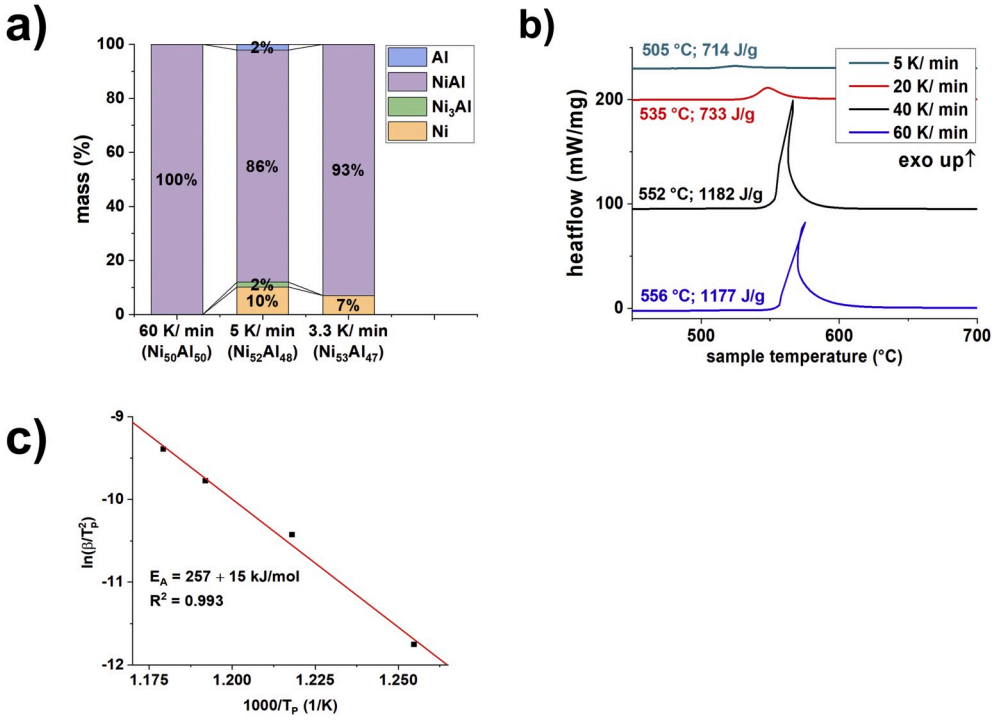

Fig. 6. a) Sample compositions determined from Rietveld refinements of reacted Ni–Al powder mixtures after heating up to 800 °C under an Ar atmosphere (note: the sample heated with 3.3 K min^{-1} was held for an additional 2 h at 800 °C). **b)** STA measurements of compacted Ni–Al powder mixtures in a flowing Ar atmosphere applying various heating rates up to 800 °C. The compositions given in brackets describe the total sample compositions estimated from Rietveld refinements assuming the formation of ideally stoichiometric phases. **c)** Kissinger plot obtained from the data shown in b).

K min^{-1} an onset between 552 °C and 556 °C could be observed, it was lowered to 505 °C when a heating rate of 5 K min^{-1} was used. Such a decrease of the onset temperature with decreasing heating rates has been known for a long time in the literature and was theoretically described by Kissinger [46,47]. According to his work, the peak temperature occurs when the reaction rate reaches its maximum value, which is in turn dependent on the applied heating rate. In all measurements it was well below the melting temperature of the lowest melting Ni–Al eutectic (640 °C) indicating an initiation in the solid state. A signal broadening as well as a decrease in the relative intensity was observed in these samples upon decreasing the heating rate, further indicating the diffusion-controlled reaction pathway at these low heating rates as described above. The reaction enthalpy of 1182 J g^{-1} is significantly lower than the value reported in the literature (1377 J g^{-1} [48]) and can be ascribed to the presence of the amorphous, oxidic phases. A comparison of both values indicates towards a weight proportion of 14.2% of the amorphous phase. This value is in good agreement with a value of 8.5% determined from Rietveld analyses applying a CaF_2 internal standard.

The onset temperature of the reaction is known to be dependent on the particles sizes, which has been reported for (compacted) particle mixtures [49] as well as multilayers [22]. In both systems, the onset temperature has been reported to shift to lower temperature with decreasing Ni and/or Al particle sizes, which is consistent with the observations described above. The exact onset temperature is dependent from various other parameters such as green density or heating rates [42], which makes a comparison of the determined temperatures with values reported in the literature rather difficult. However, for NiAl the observed value of 551 °C is in good agreement with values typically reported [40,42,49]. Contrary to the powder mixture consisting of commercial powders, a peak in the temperature-time curves can be clearly observed, indicating the onset of the strongly exothermic reaction. According to Kissinger [46], the activation energy of a solid-state reaction can be determined from STA measurements conducted at different heating rates. In a plot of $\ln(\beta/T_p^2)$ as a function of $1000/T_p$, the slope is equal to E_A/R, where β is the heating rate in K min^{-1}, T_p are the peak temperatures in K, E_A is the activation energy in Jmol^{-1} and R is the gas constant (8.3145 J mol^{-1} K^{-1}). The activation energy determined via this method was found to be 257 ± 15 kJ mol^{-1} and is therefore situated within a broad range of activation energies reported for NiAl in the literature [22] ranging from 17 kJ mol^{-1} [50] up to 350 kJ mol^{-1} [51]. A value of 76–79 kJ mol^{-1} was reported as the activation energy for Ni grain boundary diffusion in multilayers ignited on a hot plate and the large value observed in these experiments is thus pointing towards volume diffusion being the dominating process. The value determined for Ni volume diffusion in bulk Al was reported to be 146 kJ mol^{-1} [52], the determined value of 257 kJ mol^{-1} does however agree well with the activation energy determined for Ni bulk diffusion in NiAl (230–290 kJ mol^{-1}) [53].

A comparison of the STA traces obtained from the compacted powders as well as loose powders revealed similar onset temperatures (Fig. 7a), which can be likely ascribed to the good mixing and contact between the Ni and Al particles obtained through the one pot synthesis approach. In addition, in both samples the formation of NiAl could be observed in good yields >96% (Fig. 7b). In contrast to the results described in Fig. 2a, the reaction is initiated via solid-state diffusion in both samples. Due to a better interconnectivity in the compacted pellet, a more violent reaction can be observed compared to the loose powder.

To test the suitability of this method for the synthesis of NiAl intermetallics with different stoichiometries (Ni_3Al, NiAl and $NiAl_3$), powder mixtures showing different Ni:Al ratios were synthesized with the same synthesis protocol as described above. The resulting powders were compacted and heated up to 800 °C under an Ar atmosphere, resulting in yields ranging from 61% for Ni_3Al and 65% for $NiAl_3$ up to 100% for NiAl (Fig. 8a). Although these yields were in all cases higher than the yields observed above for the microparticle mixtures, it has to be noted that the adjustment of the total sample composition in the reaction mixture is challenging due to surface oxidation effects upon air contact. This is particularly true for the compounds possessing small stability ranges (Ni_3Al, $NiAl_3$) resulting in the formation of the observed multiphase products. In contrast, NiAl, which is exhibiting a larger stability range of about 10 at. % at room temperature [12], is much easier to synthesize applying this one-pot procedure since small variations of the total sample composition are tolerated. The formation of Al_4C_3 in the $NiAl_3$ samples is caused by the presence of small residual amounts of COD in the powder. Again, the compositions determined applying low heating rates of 3.3 K min^{-1} were found to be very similar to these reported below. However, one has also to keep in mind that these samples were kept for an additional 2 h at a temperature of 800 °C.

We were able to show that the onset temperatures are shifting to higher temperatures with increasing Ni mass weight. However, in all cases the onset temperature was well below the melting point of the eutectic composition (640 °C): 531 °C for Al_3Ni, 551 °C for NiAl and 582 °C for Ni_3Al (Fig. 8c). This dependence of the onset temperature from the sample composition is consistent with reports in the literature applying micrometer sized powders [54]. Even though only one exothermic signal can be observed, further investigations would be necessary to identify possibly occurring intermediate products or to clarify if the reaction is actually proceeding via a one-step reaction pathway. For comparison, in the samples containing the large, commercial Ni and Al powders (7±2 μm and 14±7 μm) the onset temperatures of the reactions were similar in all samples at around 625 °C (Fig. 8b), which is slightly below the melting point of the Ni–Al eutectic (640 °C). Except for the sample with an Al_3Ni composition, no melting peak could be observed

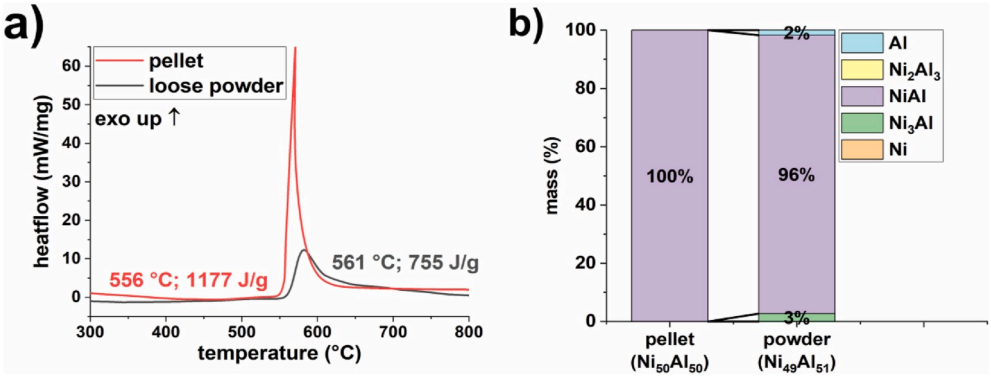

Fig. 7. a) STA measurements of compacted and loose Ni–Al powder mixtures in a flowing Ar atmosphere applying a rate of 60 K min^{-1} up to 800 °C. **b)** Sample compositions determined from Rietveld refinements of reacted compacted and loose Ni–Al powder mixtures after heating up to 800 °C in an Ar atmosphere. The compositions given in brackets describe the total sample compositions estimated from Rietveld refinements assuming the formation of ideally stoichiometric phases.

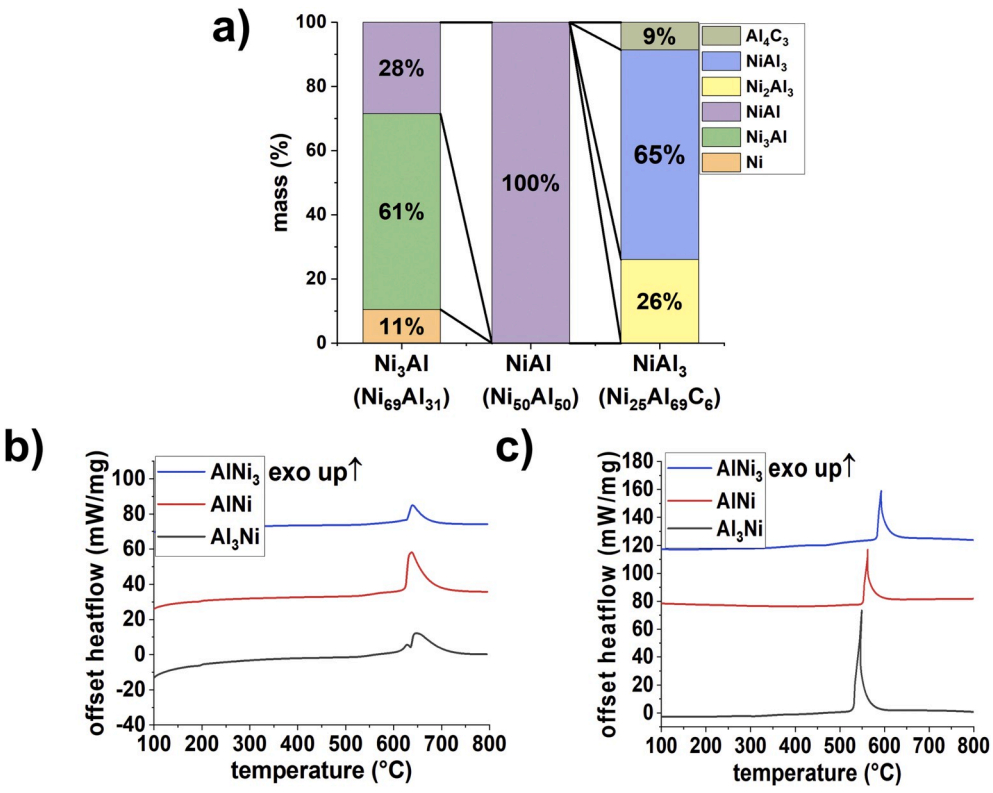

Fig. 8. a) Sample compositions of Ni–Al powder mixtures determined from Rietveld refinements after heating up to 800 °C using a heating rate of 60 K min^{-1} in a flowing Ar atmosphere. The compositions given in brackets describe the total sample compositions estimated from Rietveld refinements assuming the formation of ideally stoichiometric phases. **b)** STA measurements of compacted Ni–Al powder mixtures (commercial Ni + Al) in a flowing Ar atmosphere using a heating rate of 60 K min^{-1}. **c)** STA measurements of compacted Ni–Al powder mixtures (nanoparticular Ni + Al) in a flowing Ar atmosphere using a heating rate of 60 K min^{-1}.

indicating a very fast consumption of Al.

The ignition temperatures determined under an atmosphere of ambient air on a hot plate were found to be similar to the values determined from the STA measurements and showed the same dependency from to Ni content: $NiAl_3$: 558 °C; NiAl: 560 °C and Ni_3Al: 569 °C. The reaction on the hot plate was violent and easily visible with the naked eye, indicating a selfsustaining reaction. The formation of NiAl could again be confirmed by PXRD measurements (Fig. 9a). The pellets made of micrometer sized commercial powders showed no ignition on the hot plate up to its maximum temperature of about 600 °C. In a sample dropped onto the hot plate just below the ignition temperature and which was then immediately removed again, a small amount of NiAl as well as the formation of NiO could be detected (Fig. 9b). The observed onset temperatures are significantly higher than the values reported for Ni–Al multilayers (200–300 °C [22]), due to various reasons like for example the presence of the amorphous oxide passivation layers, different crystallite sizes, interface areas, and degrees of interfacial intermixing. The activation energy for the ignition of these multilayer on the hot plate was determined with 76–79 kJ mol^{-1} [22] and was attributed to Ni grain boundary diffusion. As discussed above, this value is significantly lower than the value of 257 kJ mol^{-1} observed in this work, which can likely be ascribed to volume diffusion processes.

5. Conclusions

Starting from elemental Ni and Al, heat transfer effects were found to be problematic regarding the synthesis of Ni aluminides particularly in specimens with a low amount of Ni and Al or a high surface-to-volume ratio. This could be observed in both, samples prepared from microscopic as well as nanoparticular reactants. Samples with NiAl being the only intermetallic phase formed, even when small sample amounts were used, could be prepared from Ni–Al powders obtained from a two-step synthesis protocol. In the first step, submicron Al particles were obtained by thermal decomposition of triisobutylaluminum in refluxing

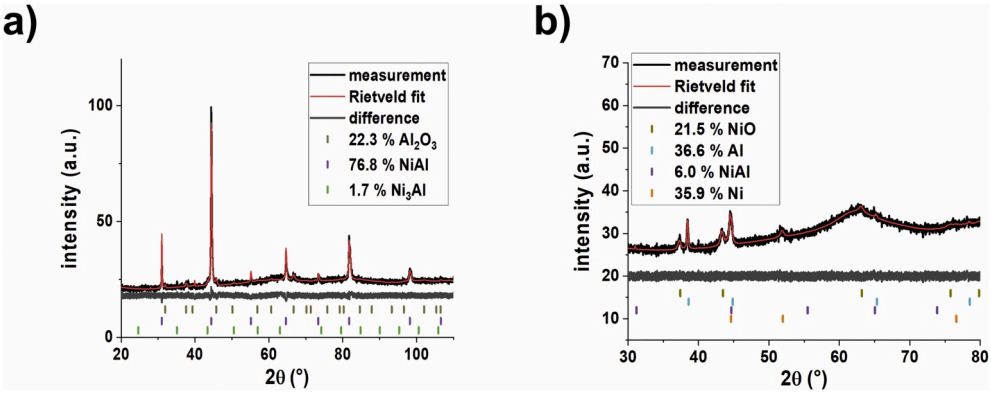

Fig. 9. XRD measurement and Rietveld refinement of **a)** a Ni–Al powder mixture ignited under an atmosphere of ambient air (GoF 1.31) **b)** a Ni–Al powder mixture dropped onto the hot plate just below the ignition temperature (GoF 1.04).

diphenylether. In the second step metallic Ni was deposited via thermal decomposition of bis(cycloocta-1,5-dien)nickel(0) at a temperature of 120 °C. The resulting powders consisted of submicron Al particles and nanocrystalline Ni, resulting in a good intermixing and good contact between both reactants. By heating these powder mixtures up to a temperature of 800 °C under an Ar atmosphere, the formation of NiAl as the only crystalline phase could be observed at low heating rates of 5 K min^{-1} as well as at high heating rates of 60 K min^{-1}. In the formed aluminide a second, amorphous and carbon and oxygen rich phase could be detected, resulting from the passivating oxide layers as well a residual organic content.

Declaration of competing interest

There are no conflicts to declare.

CRediT authorship contribution statement

Thomas Klein: Conceptualization, Methodology, Investigation, Validation, Writing - original draft. **Christoph Pauly:** Investigation, Writing - original draft. **Frank Mücklich:** Resources, Writing - review & editing. **Guido Kickelbick:** Conceptualization, Resources, Writing - review & editing.

Acknowledgments

We thank Susanne Harling for carrying out the elemental analyses and Dr. Robert Haberkorn and Dennis Becker for performing the XRD measurements as well as their advices regarding the Rietveld refinements.

References

[1] F. Soldera, N. Ilić, S. Brännström, et al., Formation of Al_2O_3 scales on single-phase RuAl produced by reactive sintering, Oxid. Met. 59 (2003) 529–542.
[2] I.M. Wolff, Synthesis of RuAl by reactive powder processing, Metall. Mater. Trans. A 27 (1996) 3688–3699.
[3] R.L. Fleischer, C.L. Briant, R.D. Field, E.A. Engines, Tough, ductile high-temperature intermetallic compounds: results of a four-year survey, Mater. Res. Soc. Symp. Proc. 213 (1991) 463–474.
[4] H. Clemens, S. Mayer, Design, processing, microstructure, properties, and applications of advanced intermetallic TiAl alloys, Adv. Eng. Mater. 15 (2013) 191–215.
[5] H. Clemens, S. Mayer, Advanced intermetallic TiAl alloys, Mater. Sci. Forum 879 (2017) 113–118.
[6] K. Morsi, Review: reaction synthesis processing of Ni-Al intermetallic materials, Mater. Sci. Eng. A 299 (2001) 1–15.
[7] S. Niemann, W. Jeitschko, Ternary Aluminides AT_2Al_{20} (A = Rare Earth Elements and Uranium; T = Ti, Nb, Ta, Mo, and W) with $CeCr_2Al_{20}$-Type Structure, J. Solid State Chem. 114 (1995) 337–341.
[8] V.M.T. Thiede, T. Ebel, W. Jeitschko, Ternary aluminides LnT_2Al_{10} (Ln = Y, La–Nd, Sm, Gd–Lu and T = Fe, Ru, Os) with $YbFe_2Al_{10}$ type structure and magnetic properties of the iron-containing series, J. Mater. Chem. 8 (1998) 125–130.
[9] R.E. Watson, M. Weinert, Transition-metal aluminide formation Ti, V, Fe, and Ni aluminides, Phys. Rev. B 58 (1998) 5981–5988.
[10] R.E. Watson, M. Weinert, M. Alatalo, Transition-metal aluminide formation: The 4d aluminides, Phys. Rev. B 65 (2001), 014103.
[11] N. Zhou, S. Jiang, T. Huang, et al., Single-phase high-entropy intermetallic compounds (HEICs): bridging high-entropy alloys and ceramics, Sci. Bull. 64 (2019) 856–864.
[12] H. Okamoto, Al-Ni (Aluminum-Nickel), J. Phase Equil. 14 (1993) 257–259.
[13] Y. Zhang, J.A. Haynes, G. Wright, et al., Effects of Pt incorporation on the isothermal oxidation behavior of chemical vapor deposition aluminide coatings, Metall. Mater. Trans. A 32 (2001) 1727–1741.
[14] B. Boettge, J. Braeuer, M. Wiemer, et al., Fabrication and characterization of reactive nanoscale multilayer systems for low-temperature bonding in microsystem technology, J. Micromech. Microeng. 20 (2010) 64018.
[15] P. Jozwik, W. Polkowski, Z. Bojar, Applications of Ni_3Al based intermetallic alloys—current stage and potential perceptivities, Materials 8 (2015) 2537–2568.
[16] H.X. Zhu, R. Abbaschian, Reactive processing of nickel-aluminide intermetallic compounds, J. Mater. Sci. 38 (2003) 3861–3870.
[17] C. Nishimura, C.T. Liu, Reactive sintering of Ni_3Al under compression, Acta Metall. Mater. 41 (1993) 113–120.
[18] D. Tingaud, L. Stuppfler, S. Paris, et al., Time-resolved X-ray diffraction study of SHS-produced NiAl and NiAl-ZrO_2 composites, Int. J. Self-Propag. High-Temp. Synth. 16 (2007) 12–17.
[19] C. Curfs, X. Turrillas, G.B.M. Vaughan, et al., Al-Ni intermetallics obtained by SHS; A time-resolved X-ray diffraction study, Intermetallics 15 (2007) 1163–1171.
[20] V.K. Portnoi, A.M. Blinov, I.A. Tomilin, T. Kulik, Mechanochemical synthesis of Mo-doped nickel aluminides, Inorg. Mater. 38 (2002) 900–904.
[21] J.A. Haber, N.V. Gunda, J.J. Balbach, et al., Chemical syntheses of nanocrystalline nickel aluminides, Chem. Mater. 12 (2000) 973–982.
[22] G.M. Fritz, S.J. Spey, M.D. Grapes, T.P. Weihs, Thresholds for igniting exothermic reactions in Al/Ni multilayers using pulses of electrical, mechanical, and thermal energy, J. Appl. Phys. 113 (2013) 14901.
[23] X. Qiu, R. Liu, S. Guo, et al., Combustion synthesis reactions in cold-rolled Ni/Al and Ti/Al multilayers, Metall. Mater. Trans. A 40 (2009) 1541–1546.
[24] R. Knepper, M.R. Snyder, G. Fritz, et al., Effect of varying bilayer spacing distribution on reaction heat and velocity in reactive Al/Ni multilayers, J. Appl. Phys. 105 (2009) 83504.
[25] A.S. Rogachev, S.G. Vadchenko, F. Baras, et al., Structure evolution and reaction mechanism in the Ni/Al reactive multilayer nanofoils, Acta Mater. 66 (2014) 86–96.
[26] A.S. Rogachev, S.G. Vadchenko, F. Baras, et al., Combustion in reactive multilayer Ni/Al nanofoils: Experiments and molecular dynamic simulation, Combust. Flame 166 (2016) 158–169.
[27] J.C. Trenkle, L.J. Koerner, M.W. Tate, et al., Time-resolved x-ray microdiffraction studies of phase transformations during rapidly propagating reactions in Al/Ni and Zr/Ni multilayer foils, J. Appl. Phys. 107 (2010) 113511.
[28] P. Zhu, J.C.M. Li, C.T. Liu, Reaction mechanism of combustion synthesis of NiAl, Mater. Sci. Eng. A 329–331 (2002) 57–68.
[29] E.M. Hunt, K.B. Plantier, M.L. Pantoya, Nano-scale reactants in the self-propagating high-temperature synthesis of nickel aluminide, Acta Mater. 52 (2004) 3183–3191.
[30] S. Dong, P. Hou, H. Yang, G. Zou, Synthesis of intermetallic NiAl by SHS reaction using coarse-grained nickel and ultrafine-grained aluminum produced by wire electrical explosion, Intermetallics 10 (2002) 217–223.
[31] E.M. Hunt, J.J. Granier, K.B. Plantier, M.L. Pantoya, Nickel aluminide superalloys created by SHS of nano-particle reactants, MRS Proc. 800 (2003) AA4.6.
[32] R.L. Jezorek, N. Zhang, P. Leowanawat, et al., Air-stable nickel precatalysts for fast and quantitative cross-coupling of aryl sulfamates with aryl neopentylglycolboronates at room temperature, Org. Lett. 16 (2014) 6326–6329.
[33] Bruker AXS. Karlsruhe, Topas 5.1. General Profile and Structure Analysis Software for Powder Diffraction Data, 2014.
[34] R.W. Cheary, A.A. Coelho, J.P. Cline, Fundamental parameters line profile fitting in laboratory diffractometers, J. Res. Natl. Inst. Stand. Technol. 109 (2004) 1–25.
[35] A. Merkys, A. Vaitkus, J. Butkus, et al., COD::CIF::Parser: an error-correcting CIF parser for the Perl language, J. Appl. Crystallogr. 49 (2016) 292–301.
[36] A. Jain, S.P. Ong, G. Hautier, et al., Commentary: the materials project: a materials genome approach to accelerating materials innovation, Apl. Mater. 1 (2013), 011002.
[37] C.A. Schneider, W.S. Rasband, K.W. Eliceiri, ImageJ, Nat. Methods 9 (2012) 671–675.
[38] S. Carenco, C. Boissière, L. Nicole, et al., Controlled design of Size-tunable monodisperse nickel nanoparticles, Chem. Mater. 22 (2010) 1340–1349.
[39] T. Klein, G. Kickelbick, Synthesis of submicron aluminum particles via thermal decomposition of alkyl aluminum precursors in the presence of metal seeds and their application in the formation of ruthenium aluminides, Nanotechnology 31 (2020) 265605.
[40] H.X. Zhu, R. Abbaschian, Reactive processing of nickel-aluminide intermetallic compounds, J. Mater. Sci. 38 (2003) 3861–3870.
[41] Q. Fan, H. Chai, Z. Jin, Dissolution-precipitation mechanism of self-propagating high-temperature synthesis of mononickel aluminide, Intermetallics 9 (2001) 609–619.
[42] L. Plazanet, F. Nardou, Reaction process during relative sintering of NiAl, J. Mater. Sci. 33 (1998) 2129–2136.
[43] M.A. Trunov, M. Schoenitz, X. Zhu, E.L. Dreizin, Effect of polymorphic phase transformations in Al_2O_3 film on oxidation kinetics of aluminum powders, Combust. Flame 140 (2005) 310–318.
[44] K.J. Blobaum, D. Van Heerden, A.J. Gavens, T.P. Weihs, Al/Ni formation reactions: characterization of the metastable Al_9Ni_2 phase and analysis of its formation, Acta Mater. 51 (2003) 3871–3884.
[45] J.M. Pauls, C.E. Shuck, A. Genç, et al., In-situ transmission electron microscopy determination of solid-state diffusion in the aluminum-nickel system, J. Solid State Chem. 276 (2019) 114–121.
[46] H.E. Kissinger, Reaction kinetics in differential thermal analysis, Anal. Chem. 29 (1957) 1702–1706.
[47] H.E. Kissinger, Variation of peak temperature with heating rate in differential thermal analysis, J. Res. Natl. Bur. Stand. 57 (1956) 217–221.
[48] T.P. Weihs, D.I. Glocker, S.I. Shah, Handbook of Thin Film Process Technology, IOP Publishing Ltd., Bristol, 1997.
[49] H. Sina, S. Iyengar, S. Melin, Ignition temperatures for Cu-Al and Ni-Al reactions in elemental powder mixtures using Differential Scanning Calorimetry, in: Advances in Powder Metallurgy & Particulate Materials - 2012 : Proceedings of the 2012 International Conference on Powder Metallurgy & Particulate Materials : PowderMet 2012, June 10-13, Nashville, vol. 9, 2012, 9–40–09–51.
[50] E.M. Hunt, M.L. Pantoya, Ignition dynamics and activation energies of metallic thermites: from nano- to micron-scale particulate composites, J. Appl. Phys. 98 (2005) 34909.
[51] J.D.E. White, R.V. Reeves, S.F. Son, A.S. Mukasyan, Thermal explosion in Ni-Al system: influence of mechanical activation, J. Phys. Chem. A 113 (2009) 13541–13547.

[52] G. Erdélyi, D.L. Beke, F.J. Kedves, I. Gödény, Determination of diffusion coefficients of Zn, Co and Ni in aluminium by a resistometric method, Philos. Mag. B 38 (1978) 445–462.

[53] S. Frank, S.V. Divinski, U. Södervall, C. Herzig, Ni tracer diffusion in the B2-compound NiAl :Influence of temperature and composition, Acta Mater. 49 (2001) 1399–1411.

[54] K.A. Philpot, Z.A. Munir, J.B. Holt, An investigation of the synthesis of nickel aluminides through gasless combustion, J. Mater. Sci. 22 (1987) 159–169.

From these studies it can be concluded that the preparation of NiAl is possible applying wet chemically prepared Ni and Al particles. Particularly upon applying small sample amounts, the intermixing of the particles as well as the interelemental contact were found to be important parameters to obtain nearly quantitative yields. This was particularly true for the samples prepared from separately synthesized Ni and Al particles, in which the formation of multiphase products was observed. Accordingly, the powders obtained from the developed one-pot synthesis approach are representing ideal precursors for the formation of Ni aluminides. Due to the excellent intermixing and interelemental contact, no time-consuming mixing was necessary prior to the aluminide formation and an initiation via solid-state reactions was observed even upon applying loose powders. In contrast to the samples prepared from separately synthesized particles, the formation of products containing NiAl as the only crystalline phase was readily possible.

3.2.4 Preparation of Ru aluminides

3.2.4.1 Application of micron Ru and Al powders

Firstly, the formation of Ru aluminides was studied applying commercial, micrometer sized Ru and Al powders. The sizes of these powders were determined to be 57 ± 12 µm for Ru and 14 ± 7 µm for Al by SEM measurements and a characterization of these powders is given in Chapter 7.4. The Ru and Al powders were dispersed in a 1:1 molar ratio in hexane, treated for 10 min in an ultrasonication bath, thoroughly mixed in an agate mortar, and then compacted in a hydraulic press (350 MPa; Ø 0.6 mm; 1 t; 10 min). The prepared pellets with a mass of up to 15 mg were reacted by heating to a temperature of 800 °C applying a controlled heating rate in a TGA/DSC thermal analyzer in an Ar atmosphere. The reacted pellets were then homogenized, and their composition was determined from Rietveld refinements.

Generally, the formation of RuAl was possible applying these small pellets (< 15 mg) prepared from micrometer sized powders. However, the application of high heating rates was necessary, while at heating rates < 60 K/min the formation of multiphase products containing RuAl, as well as Al rich phases such as $RuAl_2$ and residual unreacted Ru was observed (Figure 50a). Due to the more and more incomplete reactions, the heat flow determined from the STA traces also decreased with decreasing heating rates from 814 J/g at 60 K/ min to 394 J/g for 5 K/min. This result is in good agreement with reports in the literature were heating rates > 15 K/min[216] or 30 K/min[170] have been reported to be necessary for a complete conversion to RuAl, while lower heating rates led to the formation of multiphase products (also see Chapter 1.4.1**)**. The reaction initiated via solid-state reactions well below the melting point of the Al-Ru eutectic (657 °C) upon applying slow heating rates of 20 K/min and

5 K/min, which is also in agreement with reports in the literature[170] (Figure 50b). Similar to the literature reports[216] an increase of the onset temperature with increasing heating rates was observed. Thus, upon applying a heating rate of 60 K/min, for which the highest onset temperature can be expected to occur, the reaction ultimately initiated via a liquid-solid reaction, which is evidenced by a small endothermic signal in the STA traces prior to the occurrence of the highly exothermic signal (marked with a red circle in Figure 50b). On a hot plate, these powder mixtures could not be ignited in an atmosphere of ambient air up to its maximum temperature of 650 °C.

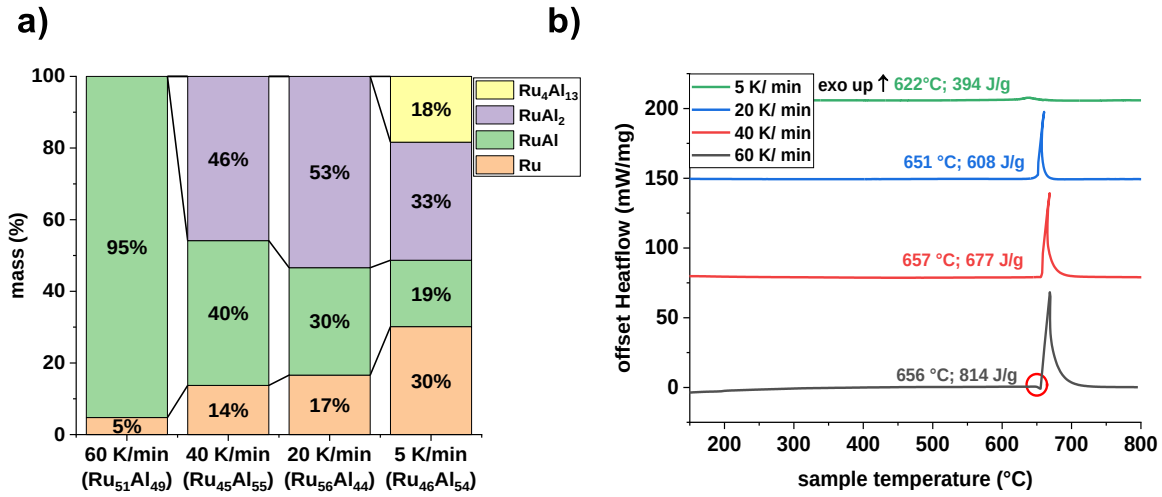

***Figure 50**: **a)** Compositions of reacted Ru-Al pellets prepared from commercial Ru and Al powders applying various heating rates in an Ar atmosphere determined from Rietveld refinements. The compositions given in brackets describe the total sample compositions estimated from Rietveld refinements assuming the formation of ideally stoichiometric phases; **b)** STA traces of the reactions leading to the formation of the products shown in a) (800 °C; Ar).*

Moreover, the influence of the applied pressure during the preparation of the pellets was studied. However, only a minor influence of the applied pressure during the pellet preparation was observed and a constant onset temperature ranging from 650 °C to 654 °C as well as nearly quantitative yields of RuAl were determined in all samples (Figure 51). A heating rate of 60 K/min was applied in all samples. Only for the sample prepared applying a pressure of 690 MPa a more incomplete reaction was observed, which is likely based on an increased heat conductivity due to a good compaction of the pellet. In contrast, loose powders are not suitable for the preparation of Ru aluminides. The reaction initiated only after a formation of a liquid phase due to a poor interelemental contact within these loose powders, which of course improved after melting (Figure 51a). For the same reason, incomplete reactions and multiphase reaction products were observed within this sample.

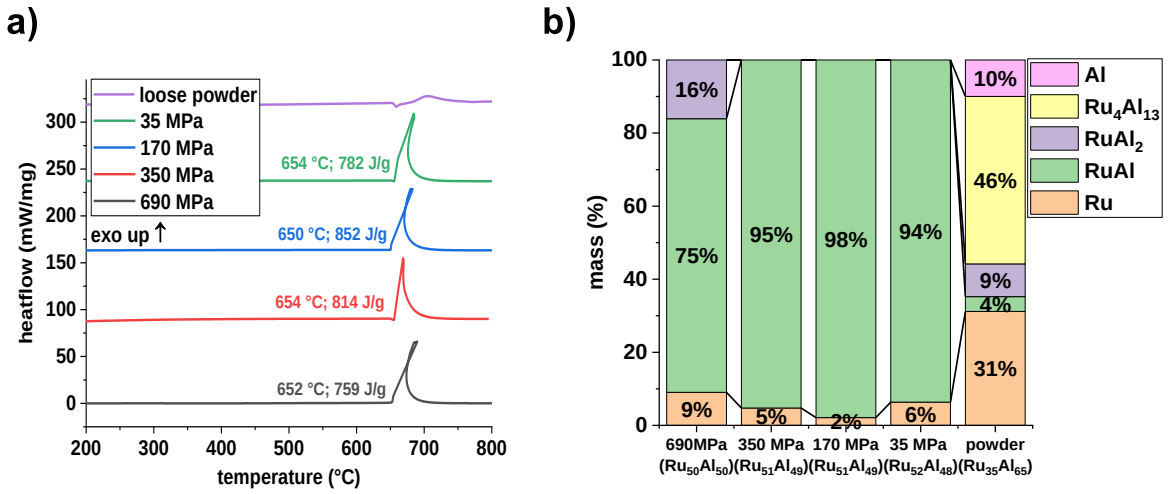

***Figure 51**: **a)** STA traces of Ru-Al pellets prepared from commercial Ru and Al powders under varying compaction pressures (800 °C; Ar; 60 K/min); **b)** Compositions of the samples after the measurements shown in a) determined from Rietveld refinements. The compositions given in brackets describe the total sample compositions estimated from Rietveld refinements assuming the formation of ideally stoichiometric phases.*

3.2.4.2 Application of submicron Al and Ru nanopowder

In a next step, the preparation of Ru aluminides starting from wet chemically prepared particles was studied. Due to the reasons discussed in Chapter 3.2.2, submicron Al particles with a size of about 150 nm, prepared via thermal decomposition of triisobutylaluminum, were applied. As was shown in the literature[217], the Ru:Al particle size ratio is representing an important parameter within this reaction system and, in order to achieve a high yield of RuAl, a small Ru:Al size ratio should clearly be preferred. The more complete conversions to RuAl upon applying small Ru particles were ascribed to shortened diffusion path lengths, resulting in more complete mixing process[217]. Thus, a mechanochemical approach[319] has been applied for the preparation of Ru nanopowder, in which Ru is prepared from $RuCl_3$ and $NaBH_4$. The crystallite size of the resulting Ru nanopowder was 2(1) nm and a characterization of the powder can be found in Chapter 7.4. The pellet preparation and thermal treatment was carried out as reported above for the commercial powders applying a compaction pressure of 350 MPa.

The preparation of RuAl in good yields of about 90 % was possible applying these chemically prepared submicron Al and nano Ru powders. A detailed discussion of the result is included in the publication in Chapter 3.1.4. Thus, only a few additional aspects shall be discussed within this chapter.

Similar as reported above for the commercial Al and Ru powders, the application of heating rates > 60 K/min was necessary to obtain RuAl in high yields and incomplete reactions were observed upon applying heating rates < 60 K/min or upon applying loose Ru and Al powders. These incomplete reactions were evidenced by the presence of large amounts of unreacted Ru as well as $RuAl_2$ (Figure

52a). The reactions were found to initiate via solid-state reactions as was evidenced by the absence of any endothermic signals in the STA traces (Figure 52b). Slightly lower onset temperatures compared to the commercial samples were observed, which can be explained by the higher reactivity of the applied nanopowders. Due to the incomplete reactions as well as the presence of oxidic passivation layers, the determined heatflows of up to 848 J/g were lower than the literature reported value for the formation of RuAl of 975 J/g[167].

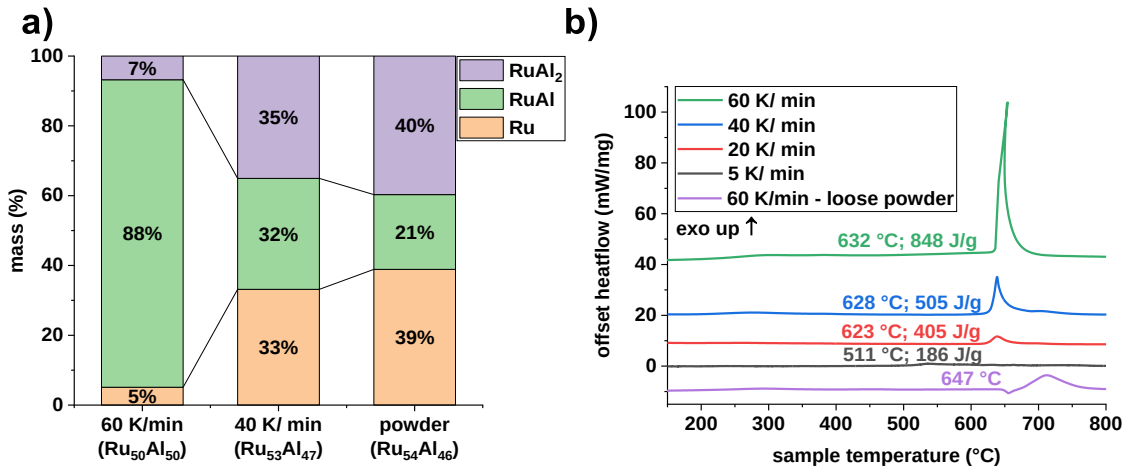

***Figure 52**: **a)** Compositions of reacted Ru-Al pellets and loose powder prepared from submicron Al and nano Ru powders applying various heating rates in an Ar atmosphere determined from Rietveld refinements (800 °C; Ar). The compositions given in brackets describe the total sample compositions estimated from Rietveld refinements assuming the formation of ideally stoichiometric phases; **b)** STA traces of the reactions leading to the formation of the products shown in a) (800 °C; Ar).*

As qualitatively shown in Chapter 3.1.4, amorphous Al_2O_3 was present within the prepared samples, even if the reaction was carried out in an Ar atmosphere due to the presence of oxidic passivation layers. To quantify its content within the sample different approaches were applied: i) comparison of the measured heat of reaction and the literature value (975 J/g[167]), ii) Rietveld refinement of the reacted sample in the presence of a CaF_2 internal standard, and iii) oxidation in a TG thermal analyzer in an atmosphere of synthetic air, followed by a determination of the composition of the oxidized samples by Rietveld refinements and calculation of the initial oxide content from the mass gain and the determined composition. The determined crystalline contents resulting from the different methods are summarized in Table 14.

***Table 14**: Oxide content in RuAl samples prepared from submicron Al and Ru nanopowders determined from various methods.*

Method	Crystalline content [wt%]
i) heatflow comparison	87
ii) CaF_2 internal standard	67
iii) oxidation in a TG analyzer	76

The values determined from the methods ii) and iii) are showing a good agreement and a mean value of 72 wt% of the crystalline phase was determined, indicating the content of the amorphous phase to be 28 wt% (Table 14). In contrast, a much larger content of 87 wt% was determined from the heatflow comparison. This larger value can likely be attributed to additional heat released from an aluminothermic reaction occurring between RuO_x and Al. The presence of these surface Ru oxides can be strongly assumed due to the fact of an explosive reaction of the Ru nanoparticles with ambient air, although no direct proof for the formation of this surface Ru oxides was obtained.

3.2.4.3 Application of submicron Al and Ru nanoparticles

To evaluate the applicability of wet-chemically synthesized Ru nanoparticles, Ru nanoparticles were prepared via a decomposition of $Ru_3(CO)_{12}$ in oleylamine solutions. The size of the resulting particles was 6 ± 1 nm and a characterization of these particles is given in Chapter 3.2.1. Again, submicron Al particles with a size of 150 nm were applied, which were prepared via a thermal decomposition approach.

Since for the Ni-Al system good results were obtained applying a two-step synthesis protocol as reported in Chapter 3.2.3.2, a similar approach was applied for the preparation of Ru-Al particle mixtures. In a first step, submicron Al was prepared by thermally decomposing triisobutylaluminum in refluxing diphenylether in the presence of nanoparticulate Ru seeds. In a second step, $Ru_3(CO)_{12}$ in oleylamine was added to this mixture and thermally decomposed. The resulting Al-Ru particle mixtures were characterized applying TEM, XRD, TG and FIB techniques.

For the preparation of Ru aluminides, these Al-Ru mixtures were compacted in a hydraulic press and heated to a temperature of 800 °C in an atmosphere of Ar as well as on a hot plate in an atmosphere of ambient air. The characterization of the reacted samples was carried out applying XRD and FIB techniques as well as Rietveld refinements.

Upon heating the samples in an Ar atmosphere, the formation of multiphase products mainly consisting of Ru, RuAl, Ru_2Al_3, $RuAl_2$ and amorphous oxide rich phases was observed. The phase fractions were found to be dependent on the sample composition, the heating rate, and the sample amount, while the onset of the reaction was observed to be about 600 °C in all samples.

Upon heating the samples in an atmosphere of ambient air on a hot-plate very low onset temperatures of about 300 °C were observed, which were attributed to additional heat released from the oxidation of Ru and organics.

These results have been published as a paper in *Intermetallics* from Elsevier.

Klein, T.; Pauly, C.; Mücklich, F.; Kickelbick, G. Al and Ru Nanoparticles as Precursors for Al-Ru Intermetallics. *Intermetallics* **2020**, *124*, 106851[325]. Reprinted with permission from Elsevier. (https://doi.org/10.1016/j.intermet.2020.106851)

Author contributions:

T. Klein had the original idea, carried out all of the synthetic work and evaluated the results. He also carried out the Rietveld refinements, the STA, DSC, DLS, TG, and TEM measurements and prepared the initial draft of the manuscript.

C. Pauly carried out and evaluated the FIB measurements, gave scientific input, prepared the initial draft of the manuscript and proof read the final manuscript.

F. Mücklich proof-read and edited the final manuscript.

G. Kickelbick gave scientific input, supervised the work and discussed the results. He also proof-read and edited the final manuscript.

Intermetallics 124 (2020) 106851

Contents lists available at ScienceDirect

Intermetallics

journal homepage: http://www.elsevier.com/locate/intermet

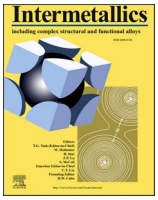

Al and Ru nanoparticles as precursors for Ru–Al intermetallics

Thomas Klein [a], Christoph Pauly [b], Frank Mücklich [b], Guido Kickelbick [a,*]

[a] Saarland University, Inorganic Solid State Chemistry, Campus C41, 66123, Saarbrücken, Germany
[b] Saarland University, Functional Materials, Department of Materials Science, 66123, Saarbrücken, Germany

ARTICLE INFO

Keywords:
A. aluminides
A. intermetallics
A. nanocrystalline metals
C. heat treatment
C. nanocrystals
C. reaction synthesis

ABSTRACT

Intermetallic compounds of Al and Ru are exhibiting promising physical and chemical properties, such high-temperature strength and oxidation resistance. Compacted micron-sized Ru and Al powders or multilayer systems are usually the starting points for their synthesis. Nanoparticles are rarely applied in the preparation of such intermetallic compounds. Here we present the preparation of Ru aluminides starting from Al and Ru nanoparticles. Al particles showing diameters as small as 125 nm were synthesized via thermal decomposition of triisobutylaluminum in refluxing phenylether, while the Ru nanoparticles were prepared by thermal decomposition of $Ru_3(CO)_{12}$ at 300 °C in the presence of oleylamine. Both synthetic steps can be carried out subsequently in a one pot reaction and the resulting powders consisted of well-dispersed and intermixed Ru and Al particles. Upon thermal treatment of the mixed particles in an Ar atmosphere we observed the formation of multiphase products mainly consisting of Ru, RuAl, Ru_2Al_3 and $RuAl_2$. The phase fractions were found to be dependent on the sample mass used for the reaction and the Al:Ru ratio. Ignition temperatures of the self-propagating reaction could be decreased to 300 °C in an ambient atmosphere. Accordingly, the preparation of Ru–Al intermetallic compounds starting from wet chemically synthesized Al and Ru nanoparticles was found to be readily possible, particularly under an atmosphere of ambient air.

1. Introduction

Intermetallic Al compounds, historically called aluminides, are promising materials for high temperature applications due to their physical and chemical properties, such as high-temperature strength as well as their oxidation and chemical resistance [1–5]. The most common examples are binary Ni, Fe and Ti aluminides [4–7], such as NiAl, FeAl and TiAl, ternary and other compounds have also been reported in the literature [8–10]. In contrast, RuAl, which is exhibiting a CsCl structure, and which is known since at least 1960 [11], is a more rarely employed example [12–14]. Previous studies showed that RuAl has also a potential in high temperature applications, such as metallization [15], or exhausts [16] or bond coatings for thermal barrier coatings [17].

Among the six different Ru–Al intermetallic compounds known [18] ($RuAl_6$ ($MnAl_6$ type [19]), Ru_4Al_{13} (Fe_4Al_{13} type [20]), Ru_2Al_5 (Fe_2Al_5 type [21], $RuAl_2$ ($MoSi_2$ type [22] and $TiSi_2$ type [23]), Ru_2Al_3 (Os_2Al_3 type [24] and Ni_2Al_3 type [22]) and RuAl), RuAl is the most promising compound regarding high temperature applications, due to its very high melting point as well as its excellent corrosion and oxidation resistance. A detailed overview over its physical, chemical and mechanical properties as well as its possible applications is given in various reviews [18,25]. The preparation of RuAl is typically carried out starting from elemental Al and Ru using casting [26], mechanical alloying [27,28], reactive sintering, reactive hot isostatic pressing [1,2,29,30], or multilayer [31,32] techniques.

Particularly reactive synthesis approaches, such as self-propagating reactions, are facilitating a fast and simple preparation of these compounds because of short reaction times and simple experimental setups. However, when this reaction type is applied using loose, micrometer sized Al and Ru powders, no reaction could be observed upon reaching the melting point of Al [2]. Contrary, when consolidated Ru–Al powder mixtures were used, the reaction initiated via solid-state reactions. Moreover, the use of high heating rates was found to be advantageous towards the preparation of single-phase products [2,29]. The Ru:Al particle size ratio is an important parameter in these reactions [30]. Decreasing the Ru:Al particle size ratio leads to a reduction of the ignition temperature and smaller particle size ratios are also supporting the formation of single-phased products indicating that the Ru diffusion is the limiting step during this reaction.

When the reaction is carried out in a hot isostatic press, more dense

* Corresponding author.
E-mail address: guido.kickelbick@uni-saarland.de (G. Kickelbick).

https://doi.org/10.1016/j.intermet.2020.106851
Received 20 March 2020; Received in revised form 26 April 2020; Accepted 27 May 2020
Available online 12 July 2020

structures can be prepared [2]. However, due to increased heat losses the formation of multiphase products is preferred making an additional homogenization step at increased temperatures necessary [2,30]. For Ru–Al multilayer systems the ignition temperature under an atmosphere of ambient air is dependent on the bilayer thickness and it decreased from 608 °C for 222 nm bilayer thickness down to 408 °C for 22 nm bilayer thickness [31].

To the best of our knowledge, no studies on the synthesis of Ru aluminides applying nanoparticular reactants have been described yet. Since the application of Ru and Al nanoparticles would allow very small particle size ratios as well as a good intermixing of both compounds, we herein examined the formation of Ru aluminides starting from synthesized, nanoparticular Ru and Al reactants. Wet-chemical synthesis methods comprise several advantages compared to other methods of particle preparation, such as short reaction times, simple experimental set-ups as well as the possibilities of facile scale-ups or continuous synthesis approaches. Therefore, we employed these techniques for the preparation of Al and Ru particles. However, the application of wet chemical approaches also often leads to the presence of additional compounds like stabilizers and residual solvents in the reacting particle mixtures, which might, for example, lead to the formation of impurities, e.g. carbides, nitrides or oxides, or additional porosities in the final reaction product. We investigated these yet unaddressed questions in our studies.

2. Experimental

2.1. Materials

Triruthenium dodecacarbonyl (99%), $RuCl_3{\cdot}xH_2O$ (39-42% Ru; 99.9 %-Ru) and Ru powder (99.8%; 60 μm) were purchased from abcr (Karlsruhe, Germany). Triisobutylaluminum (1 M in hexanes) and oleylamine (C_{18} content 80-90%) were obtained from Sigma-Aldrich (St. Louis, USA). Sodium borohydride was delivered by applichem (Darmstadt, Germany) and phenylether (99%) by Alfa-Aesar (Kandel, Germany). Oleylamine and diphenlether were dried in vacuo at 100 °C for 2 h, stored over molecular sieves (3Å) for several days and filtered through 0.45 μm syringe filters prior to use. All other chemicals were used as received without any further purification. Unless stated otherwise, all reactions were carried out under an Ar atmosphere applying standard Schlenk techniques.

2.2. Methods

Powder X-ray diffractograms (PXRD) were measured on a Bruker D8-A25-Advance diffractometer in a Bragg-Brentano geometry using Cu K_α-radiation. A step size of 0.013° from 7 to 120° (2θ) and a total measurement time of 1 h was used to record the diffraction patterns. The specimen were prepared from the dispersed samples in hexane by drop coating them directly onto the sample holders. Sample compositions as well as the lattice parameters were determined from Rietveld refinements using TOPAS 5.1 [33]. A fundamental parameter approach [34] was used to consider the instrumental line broadening while a Chebychev polynom (15th degree) was used for background fitting. The Rietveld refinements were carried out using the published crystal structures from the Crystallographic Open Database (COD) [35] or the Inorganic Crystal Structure Database (ICSD). Entries with the following ID's were used for the refinements: Al 2300250 (COD), Ru 1539052 (COD), γ-Al_2O_3 2107301(COD), RuAl 1527371 (COD), $RuAl_2$ 58156 (ICSD), Ru_4Al_{13} 58158 (ICSD), Ru_2Al_3 609226 (ICSD), RuO_2 2101931 (COD).

A Bruker Vertex 70 ATR-FTIR spectrometer equipped with a DIAMOND ATR-QL measurement cell from Bruker was used to record the ATR-FTIR spectra in a range from 4000 to 400 cm^{-1} and a resolution of 4 cm^{-1} using an average of 16 scans for both, background and sample.

TEM images were recorded on a JEOL JEM-2010 applying an accelerating voltage of 200 kV. TEM specimens were prepared by drop casting nanoparticle dispersions in hexane directly onto the carbon coated copper grids followed by air drying.

Focused ion beam (FIB) measurements were carried out using a gallium ion beam on a Helios NanoLab600 from FEI. Conductive carbon was used to contact the powder compacts prior to the measurements. From the TEM or SEM images the average particle sizes and particle size distributions were obtained by measuring 100 particles using the software ImageJ [36].

Thermogravimetric analyses (TGA) were conducted on a Netzsch TG F1 Iris under a constant flow of N_2/O_2 32:8 (40 ml/min) or N_2 (40 ml/min) in open alumina crucibles using a heating rate of 10 °C min^{-1}. FTIR analysis of the evolved gases was carried out by coupling the microbalance to the Bruker Vertex 70 via a transfer line heated to 200 °C.

Simultaneous thermal analyses (STA) were carried out on a Mettler-Toledo STAre system under a constant flow of Ar (40 ml min^{-1}) in open alumina crucibles. A heating rate of 60 °C min^{-1} was used and the maximum temperature was set to 800 °C. After confirming the absence of any signals (particularly Al melting), a second scan was used as a background scan for every sample.

DSC measurements were performed on a Netzsch DSC 204 F1 Phoenix in pierced aluminum crucibles under an atmosphere of N_2/O_2 32:8 (100 ml min^{-1}) or N_2 (100 ml min^{-1}) using a heating rate of 10 °C min^{-1}.

Ignition temperatures of the pellets were determined on a hot plate using small amounts (1-2 mg) of the pellets. The lowest temperature at which an ignition could be observed with the naked eye was defined as the ignition temperature. The experiments were carried out under an atmosphere of ambient air.

2.3. Syntheses

2.3.1. Nanocrystalline Ru powder

Nanocrystalline Ru powder was synthesized following a literature-known method [37]. Under an atmosphere of ambient air 1 g $RuCl_3{\cdot}xH_2O$ (39-42% Ru) (5 mmol) and 2 g (53 mmol) of $NaBH_4$ were treated for 30 min in an agate mortar. 40 ml of ethanol were slowly added and the solid was isolated by centrifugation (8000 rpm; 10 min). The mixture was washed with 40 ml of ethanol and then two additional times with water (8000 rpm; 10 min). The residue was dried at 80 °C in vacuum yielding 250 mg (78%) of black Ru nanopowder. The resulting agglomerated particles were applied as seeds for the preparation of the Al particles, due to their low organic content. This nanocrystalline Ru powder, was severely agglomerated, in contrast to the Ru nanoparticles reported below.

2.3.2. Ru nanoparticles

150 mg of $Ru_3(CO)_{12}$ (0.23 mmol) were dissolved in 20 ml of oleylamine and heated to 200 °C for 2 h. After cooling to room temperature, 20 ml of methanol were added and the solid was collected by centrifugation (13,000 rpm; 10 min). The particles were isolated by three cycles of dispersing in 5 ml of toluene, precipitating with 30 ml of methanol and centrifugation (13,000 rpm; 10 min). The resulting brown-black solid was dried in vacuum at room temperature yielding 54 mg (62%) of Ru nanoparticles.

2.3.3. Al nanoparticles

Submicron Al particles were synthesized according to a previously published procedure [38]. Within this approach, triisobutylaluminum was decomposed in refluxing phenyl ether in the presence of nanoparticular Ru seeds, resulting in the formation of submicron Al particles with sizes of about 150 nm.

2.3.4. Al–Ru powder mixtures

60 ml of phenylether were degassed at 100 °C for 30 min. After cooling to 40 °C, 2 ml of triisobutylaluminium (1 M in hexane) (2 mmol)

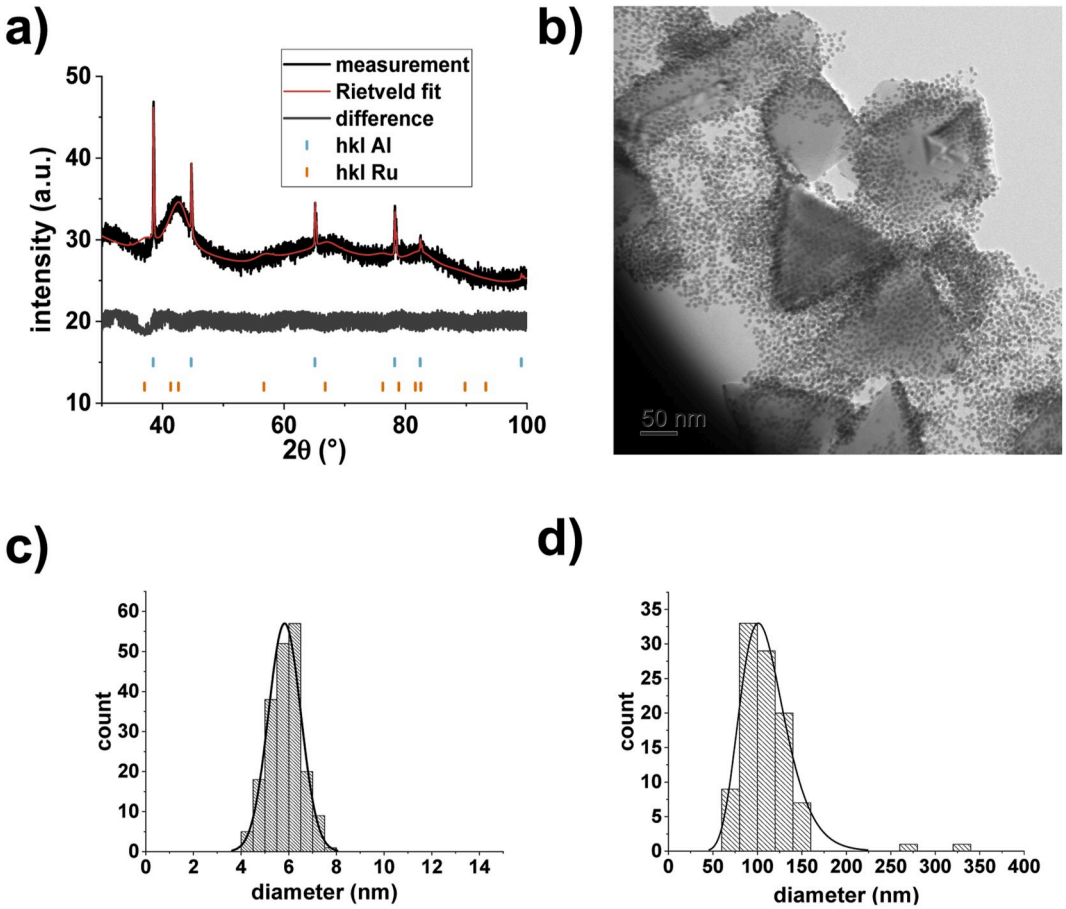

Fig. 1. a) PXRD measurement and Rietveld refinement of as synthesized Al–Ru particle mixtures, b) TEM images of the as synthesized Al–Ru particle mixture, c) particle size distribution of the Ru particles in the synthesized Al–Ru particle mixture obtained from measuring 200 particles, d) particle size distribution of the Al particles in the synthesized Al–Ru particle mixture obtained from measuring 100 particles.

and 3.0 mg (0.03 mmol) of nanocrystalline Ru powder were added. The hexane was removed in vacuo and the mixture was homogenized using an ultrasonication bath for 15 min. The mixture was refluxed for 15 min resulting in the formation of a grey solid. After cooling to room temperature, varying amounts of $Ru_3(CO)_{12}$ dissolved in 20 ml of oleylamine were added. The orange-grey mixture was heated to 200 °C for an additional 2 h. The mixture was centrifuged (13,000 rpm; 10 min), washed by three cycles of dispersing in 5 ml of toluene, precipitating with 30 ml of methanol and centrifuging (13,000 rpm; 10 min) and dried in vacuo at room temperature.

2.3.5. *Synthesis of aluminides*

Compacted pellets of the Al–Ru powder mixtures were obtained using a hydraulic press (Ø 6 mm; 1 t; 15 min; 350 MPa). The reactions were carried out using a controlled heating rate in a TGA/DSC thermal analyzer under a flowing Ar atmosphere (40 ml min^{-1}) in open alumina crucibles. After cooling to room temperature, the pellets were homogenized and their composition was determined via Rietveld refinements.

3. Results and discussion

Ru aluminides are possible materials for high temperature applications due to their excellent thermal properties. Although there are a couple of reports in the literature about the synthesis of Ru aluminides starting from micrometer sized elemental powders, little is known about the synthesis of these aluminides starting from nanoparticular, wet chemically synthesized reactants. Thus, within this manuscript the preparation of Ru aluminides starting from wet chemically prepared Al and Ru particles was studied.

3.1. *Precursor synthesis*

For the Ni–Al system good results could be obtained via a two-step synthesis protocol [39]. In a first step, submicron Al particles were prepared via thermal decomposition of triisobutylaluminum in refluxing diphenyl ether and in a second step metallic Ni was deposited via thermal decomposition of $Ni(COD)_2$. From the resulting Ni–Al powder mixtures, NiAl could be obtained as the only intermetallic phase upon heating to 800 °C under an Ar atmosphere. Thus, a similar approach was developed for the Ru–Al system in the current study. Due to the straightforward thermal decomposition of $Ru_3(CO)_{12}$ we have chosen this compound as a Ru source. However, when $Ru_3(CO)_{12}$ was added to the reaction mixture in diphenylether after the synthesis of the submicron Al nanoparticles as it was carried out with $Ni(COD)_2$, no formation of metallic Ru could be observed in XRD measurements even after heating to reflux for several hours. Instead, the isolated solid still showed an orange coloration indicating an incomplete decomposition of the $Ru_3(CO)_{12}$. Thus, $Ru_3(CO)_{12}$ was added to the reaction mixture in an oleylamine solution, in which a decomposition could be observed upon heating to 200 °C for an additional 2 h. The Al:Ru ration of the powders can be controlled via the $Ru_3(CO)_{12}/Al^iBu_3$ ratio during the decomposition. A characterization of the as prepared loose Al–Ru particle mixtures is given in section 3.1.1.

For the synthesis of Ru aluminides, compacted pellets prepared from these dried Al–Ru particle mixtures were employed, which were prepared in a hydraulic press applying a pressure of 350 MPa. The

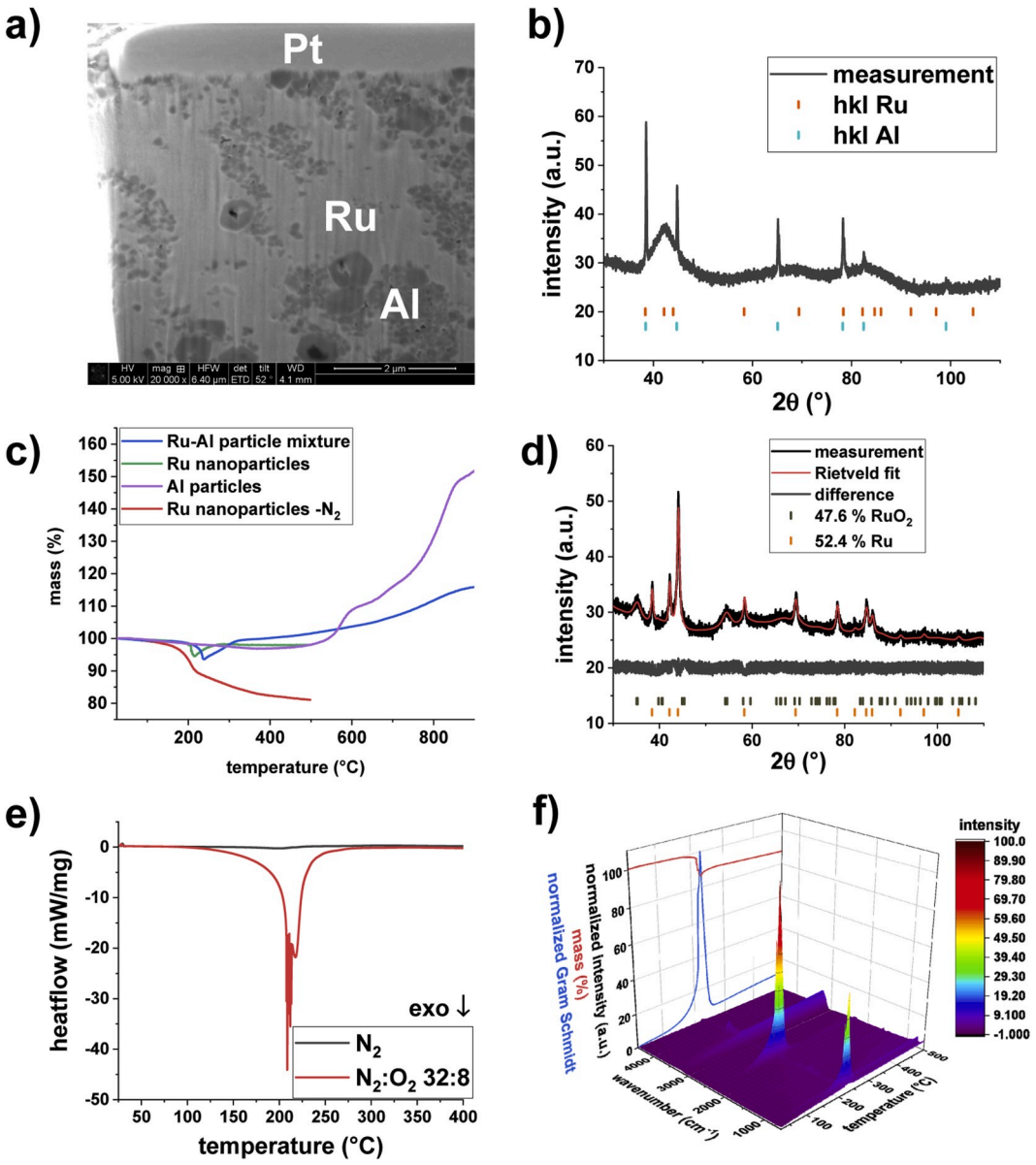

Fig. 2. a) FIB cross-section image, b) XRD measurement of the unreacted Al–Ru pellet, **c)** TG measurements of Ru and Al particles as well as Ru–Al particle mixtures using a heating rate of 10 °C min^{-1} in an atmosphere of synthetic air (N_2:O_2 32: 8), d) XRD measurement and Rietveld refinement of the Ru nanoparticles after the DSC measurement in N_2:O_2 shown in d), e) DSC measurements of Ru nanoparticles under N_2 and N_2:O_2 atmospheres using a heating rate of 10 °C min^{-1}, **f)** FTIR analysis of the evolved decomposition gases during the TG measurement of Ru nanoparticles under an atmosphere of synthetic air (10 °C min^{-1}; N_2:O_2 8:32).

aluminides were then prepared by heating small amounts (3-15 mg) of these pellets under an atmosphere of Ar in a STA/DSC thermal analyzer using various heating rates ranging from 5 °C min^{-1} up to 60 °C min^{-1} as well as on a hot plate under an atmosphere of ambient air. To determine the composition of the reacted samples, they were homogenized in an agate mortar and analyzed by PXRD applying Rietveld refinements. A characterization of the unreacted Al–Ru pellets is given in section 3.1.2.

3.1.1. *Characterization of the as prepared loose Al–Ru precursors*

The formation of metallic Al and Ru could be confirmed by PXRD measurements (Fig. 1a). Crystallite sizes were 110(7) nm for Al and 2(1) nm for Ru as determined from Rietveld refinements. Broad reflections in the powder pattern also indicate the very small crystallite sizes of Ru, while Al is obviously exhibiting a much better crystallinity based on the larger crystallite size. Upon sintering at 600 °C for 2 h under an atmosphere of Ar metallic Ru could however be clearly identified in a sample synthesized without the presence of Al. TEM images (Fig. 1b) further revealed the presence of Ru nanoparticles with a diameter of 5.8 ± 0.7 nm (Fig. 1c), while the size of the Al particles was 111 ± 35 nm (Fig. 1d). Although a core-shell structure would be advantageous for the reaction because the whole surface of the Al particles would be covered and thus protected against oxidation, we only observed the presence of small Ru particles next to the larger Al particles.

The resulting Ru:Al particle size ratio is about 0.05 (Fig. 1). This size ratio has been reported to play an important role in the preparation of Ru aluminides starting from micrometer sized Al and Ru powders [30]. According to these results small Ru particles compared to the Al particles are necessary to achieve a large interfacial contact area as well as a complete diffusion of Ru and thus a good intermixing in the reacting sample. Accordingly, the prepared Ru–Al powder mixtures seemed to be good candidates for the preparation of Ru aluminides and no further attempts have been made to further decrease the Al particle size.

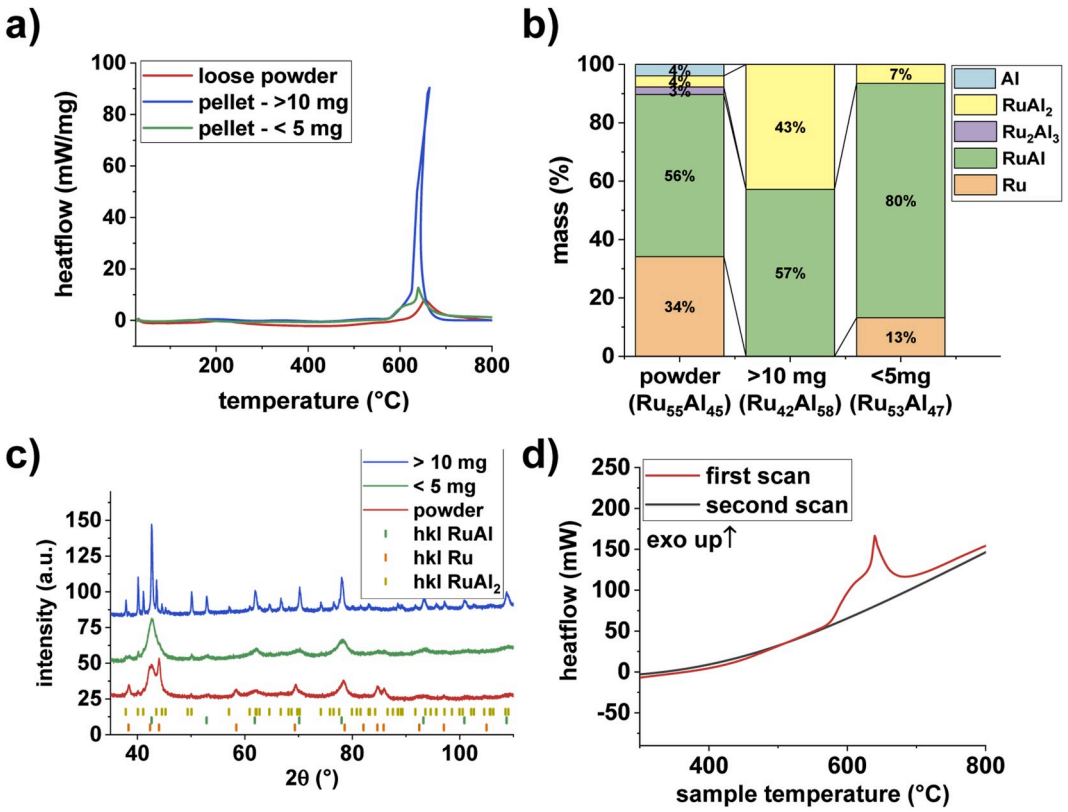

Fig. 3. a) STA measurements of Al–Ru particle mixtures under a flowing Ar atmosphere using a heating rate of 60 °C min^{-1}, **b)** sample composition of the resulting products after the STA measurements up to a temperature of 800 °C determined from Rietveld refinements. The compositions given in parentheses describe the total sample compositions estimated from Rietveld refinements assuming the formation of ideally stoichiometric phases. The error of the composition data was found to be <1%, **c)** PXRD measurements of the products obtained from large and small sample amounts after the STA measurements up to a temperature of 800 °C, **d)** second STA scan of the pellet with a mass <5 mg under the same conditions as described in a).

3.1.2. Characterization of the compacted Al–Ru pellets

In a FIB cross-section image (Fig. 2a) of the unreacted, compacted powder mixture, the Al and Ru rich domains are clearly visible. While for Al, single, distinct particles with a size of 111 ± 35 nm can be observed (Fig. 1d), the Ru particles appear as a continuous phase, due to their very small sizes which are below the SEM resolution limit. Moreover, a good contact between the Al and Ru particles as well as only a few pores can be detected, which both is advantageous for the formation of the aluminides. No formation of any intermetallic phase in the compacted samples could be observed, which was also confirmed by a XRD measurement of the unreacted pellet (Fig. 2b).

TG measurements (Fig. 2c) of the compacted Ru–Al pellets in an atmosphere of synthetic air (N_2:O_2 32:8) revealed a mass loss starting at a temperature of 225 °C directly followed by a sharp mass increase. Upon further increasing the temperature a slow mass gain can be observed until a constant plateau is reached. This trace clearly is a combination of the TG traces observed for the pure Ru and Al particles. In the TG measurements of the Ru nanoparticles under an atmosphere of synthetic air up to a temperature of 500 °C, a mass loss starting at around 200 °C directly followed by a sharp mass gain can be observed. The mass loss is a result of the decomposition of the stabilizing oleylamine, residual carbonyl ligands and a loss of residual diphenylether, which could be further confirmed by gas-phase IR spectroscopy of the evolved gases during these measurements, where the formation of CO_2, CO as well as NH_3 could be observed. The sharp mass increase could only be observed when the measurements were carried out in an atmosphere of synthetic air, while it was absent in a N_2 atmosphere, indicating an oxidation reaction. XRD measurements of Ru nanoparticles after thermal treatment to a temperature of 350 °C under an atmosphere of synthetic air further revealed the formation of RuO_2 (Fig. 2d). The TG measurements of the Al particles show a two-step mass increase due to oxidation reactions starting at a temperature of about 500 °C.

DSC measurements (Fig. 2e) of the Ru nanoparticles further revealed this oxidation to be a highly exothermic reaction. The noise visible in the DSC trace is due to a sample movement inside the pierced crucible and could not be avoided, making an integration of the signal not reliable (~4400 J g^{-1}). Nevertheless, the determined value of >4000 J g^{-1} appears to be extremely large compared to the enthalpy of formation of RuO_2 reported in the literature (~2350 J g^{-1} at 150 °C [40]), particularly since the yield of RuO_2 was only about ~50% as determined from Rietveld refinements (Fig. 2d) and a small mass loss is further expected to occur due to the loss of organic residues. These results indicate that further exothermic processes are likely to be occurring simultaneously to the Ru oxidation, such as the oxidation of carbon-containing residues. An exothermic removal of carbonaceous residues has been reported in the literature to occur in a similar temperature range [41]. An exothermic removal of carbonaceous residues has been reported in the literature to occur in a similar temperature range This was proven by FTIR analysis of the evolved gases during the exothermic event (Fig. 2f), in which the formation of CO_2 is clearly visible.

3.2. Aluminide formation

Starting from these pellets, Ru aluminides have been prepared by heating them to increased temperatures under atmospheres of Ar or ambient air. The results observed for the reactions carried out in atmospheres of Ar and ambient air will be discussed separately in the following sections.

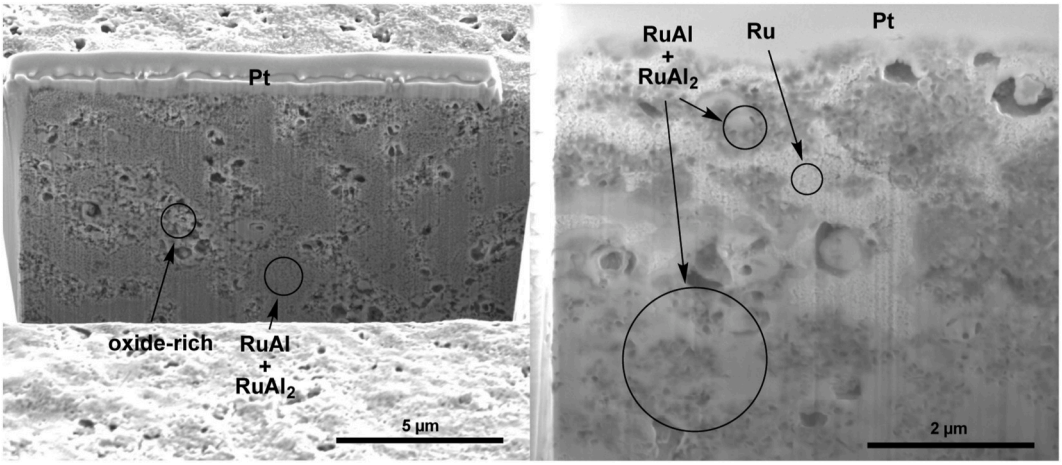

Fig. 4. FIB cross-section images of the reaction product in the compacted pellets after heating up to 800 °C under an atmosphere of Ar using a heating rate of 60 °C min^{-1} applying **a)** larger sample amounts and **b)** smaller sample amounts.

3.2.1. Aluminide formation under Ar atmosphere

These reactions has been carried out in in a STA/DSC thermal analyzer by heating small amounts (3-15 mg) of the pellet or a small amount of loose powder under an Ar atmosphere using a controlled heating rate ranging from 5 °C min^{-1} up to 60 °C min^{-1}.

3.2.1.1. Comparison of the loose as prepared Al–Ru mixture and the compacted pellets. For these studies the samples have been heated to a temperature of 800 °C applying a heating rate of 60 °C min^{-1}. The powders have been prepared applying a $^1/_3$ $Ru_3(CO)_{12}/Al^iBu_3$ ratio of 0.65.

When the Al–Ru particle mixtures where heated as a loose powder under an atmosphere of Ar, the onset of reaction was observed to be well below the melting point of Al at 627 °C. After the reaction, a large amount of Ru was still found to be present as well as a small amount of elemental Al, thus indicating an incomplete reaction (Fig. 3a, b and c). This result is in contrast to the observations reported in the literature [2], in which a reaction in loose powders was reported to occur only right after the melting of the Al. We assign the earlier onset in this system to the applied one-pot synthesis procedure resulting in rather good contact between Al and Ru even without applying pressure. The incomplete reactions are consistent with reports in literature [2], in which the formation of RuAl starting from micrometer sized Ru and Al particles via reactive powder processing was studied and which were ascribed to a lacking contiguity in these powders. Thus, all other studies were carried out applying the compacted pellets prepared as described above.

In the compacted samples, the onset of the reaction could be observed at a much lower temperature between 575 °C and 585 °C due to an improved contact between the Ru and Al particles, also resulting in a higher conversion of the Ru particles (Fig. 3a and 3b). In Fig. 3a, the heatflow is plotted against the sample temperature. Upon the onset of a strongly exothermic reaction, the heat released during this reaction leads to an internal heating of the sample. The heating rate of the sample due to this internal heating can easily exceed the programmed heating rate of the thermal analyzer. As a result, the sample temperature increases unexpectedly fast for a very short period of time ultimately leading to the visible tilt of the STA trace shown in Fig. 3a. The onset well below the melting point of the Al–Ru eutectic indicates a start of the reaction via self-propagating processes, which is consistent with reports in literature [30].

3.2.1.2. Influence of the sample amount. For these studies the samples have been heated to a temperature of 800 °C applying a heating rate of 60 °C min^{-1}. The powders have been prepared applying a $^1/_3$ $Ru_3(CO)_{12}/Al^iBu_3$ ratio of 0.65. An influence of the total sample mass could be clearly observed: When the reaction was carried out in a small pellet (<5 mg), incomplete reactions as well as nanocrystalline to amorphous products were formed. These incomplete reactions are evidenced by the presence of large amounts of unreacted Ru as was determined from Rietveld refinements (Fig. 3b and c) and were further confirmed by the absence of any signals in a second STA scan under the same reaction conditions (Fig. 3d). However, when larger pellets (>10 mg; same thickness) were used, enhanced crystalline products and more complete conversions of Ru could be observed (Fig. 3c). Upon applying a small sample mass, the released heat of reaction dissipates and no self-heating of the sample occurs. As a result, incomplete reactions and low intensity STA signals can be observed. In contrast, upon applying larger sample amounts, a self-heating of the sample occurs (as is evidenced by the tilt of the STA signal) and more complete and violent reactions can be observed. Such heat transfer effects have been reported before in the literature to play an important role in the Al–Ru system [30], and the better crystallinity and higher Ru conversions can thus be explained by the higher temperatures achieved within the larger sample. The varying total sample compositions in Fig. 3b determined from the Rietveld analyses can be explained by amorphous sample contents, which was detected via a CaF_2 internal standard in the nanocrystalline samples and which could not be observed in samples exhibiting a good crystallinity. Also it has to be noted, that similar to previous reports [30], a homogenization of the formed multiphasic products is possible by sintering in vacuum at increased temperatures.

The described observations were supported by the FIB cross-section images (Fig. 4a and b), in which the formation of a two-phase intermetallic region could be observed. Also an increased porosity compared to the unreacted pellets was detected, which is most likely based on the release of decomposition gases from the organic residues and the higher density of the formed RuAl compared to an applied Ru:Al reactant mixture in a 1:1 molar ratio ρ_{RuAl}: 7.76–8.01 g cm^{-3} [18]; ρ_{Al}: 2.70 g cm^{-3} [42]; ρ_{Ru}: 12.1 g cm^{-3} [42]. In contrast, when small sample amounts were used the formation of two different intermetallic phases as well as a large amount of unreacted Ru (brightest phase) is clearly visible. Within the intermetallic phases residual unreacted Al particles can still be observed, which also confirms an incomplete reaction due to high heat losses occurring within this sample. The formation of amorphous oxide-rich phases is due the presence of passivation layers on the Al as well as Ru particles. The phases present in the sample have been determined applying Rietveld refinements and have been assigned to phases visible in the SEM images in agreement with prior work [38].

These results are in agreement with reports in the literature for the Ni–Al system, in which high heat losses have been reported to prevent

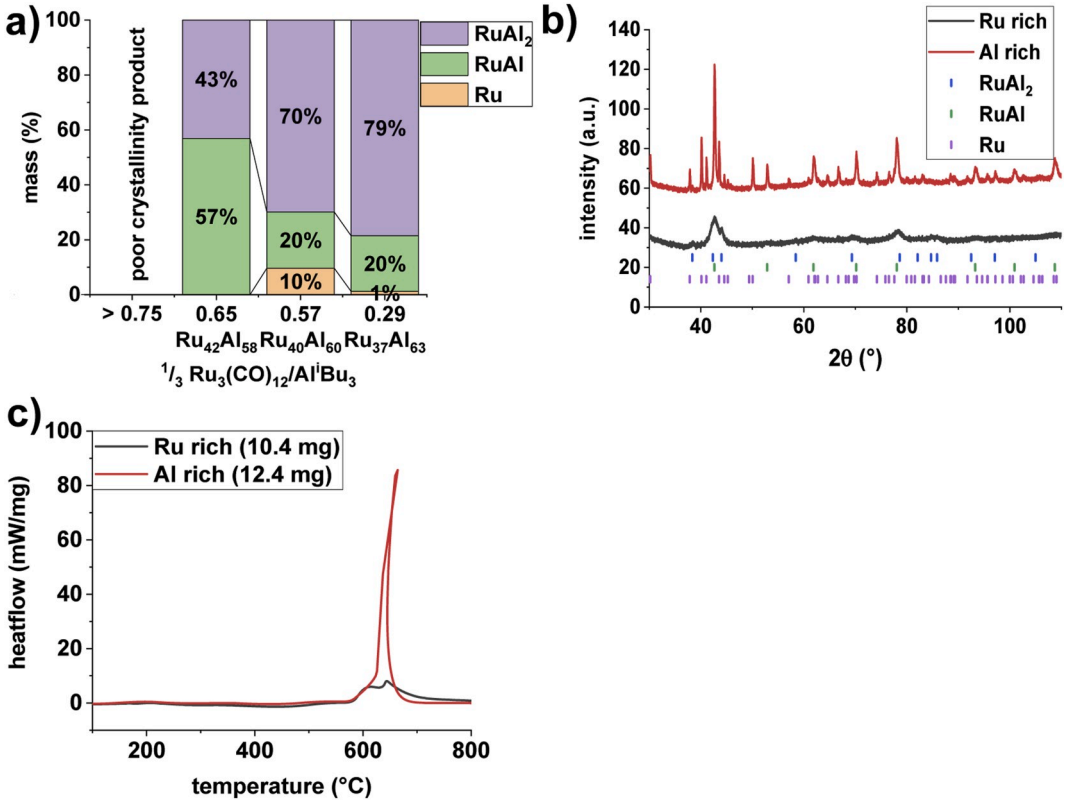

Figure 5. a) sample compositions of various samples synthesized applying varying $Ru_3(CO)_{12}/Al^iBu_3$ ratios after heating to 800 °C using a heating rate of 60 °C min^{-1} under an atmosphere of Ar determined from Rietveld analysis, **b)** XRD measurements of the Ru and Al rich samples after the STA measurements shown in c), **c)** STA measurements of a Ru and Al rich sample under an atmosphere of Ar applying a heating rate of 60 °C min^{-1}.

the reaction from becoming self-sustaining [43,44] thus leading to the occurrence of incomplete reaction as well as multiphase products. Similarly, the application of samples with a large surface to volume ratio or the application of only a small amount of a sample have been reported to result in much more incomplete reaction compared to samples with a smaller surface to volume ratio, in which the formation of single phase NiAl could be observed [39].

3.2.1.3. Influence of the sample composition. For these studies the samples with a mass of about 10 mg have been heated to a temperature of 800 °C applying a heating rate of 60 °C min^{-1}. The total Al:Ru ratio can be controlled by varying the molar ratio of $Ru_3(CO)_{12}$ and Al^iBu_3 during the decomposition, which can be clearly seen in Fig. 5a. Accordingly, upon increasing the $^1/_3$ $Ru_3(CO)_{12}/Al^iBu_3$ ratio, the formation of more Ru rich phases could be detected in the sample heated to a temperature of 800 °C. Thus, it is possible to control the final sample composition by changing the amount of $Ru_3(CO)_{12}$ during the decomposition. Moreover, Al rich samples exhibited a significantly increased reactivity and violent exothermic reaction could be observed in the STA traces resulting in the formation of highly crystalline products (Fig. 5b and 5c**).** In contrast, weak exothermic signals as well as the formation of amorphous products could be observed in Ru rich samples. This behavior can be explained by the fact that no Ru rich aluminides (>50 at. % Ru) are known to exist. Accordingly, excess Ru acts as a diluent decreasing the heat flow observed in the STA measurements. In contrast, several intermetallic compounds also exhibiting highly negative heats of formation (e.g. Al_2Ru −66 kJ mol^{-1} $atoms^{-1}$ [45]) can be found on the Al rich side of the Al–Ru phase diagram. In conclusion, more intense signals can be observed in the Al rich samples. Secondly, for multilayer systems the reaction was shown to initiate with the formation of $RuAl_6$. Accordingly,

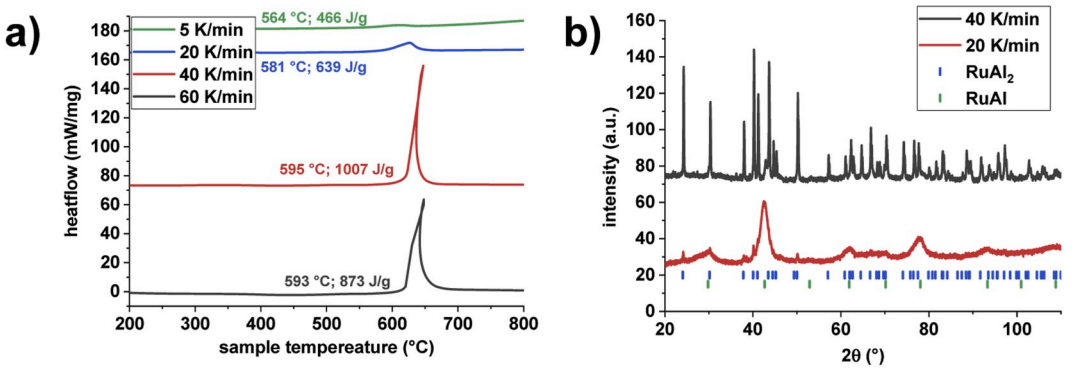

Fig. 6. a) STA measurements of an Al rich sample using various heating rates under an atmosphere of Ar **b)** XRD measurements of samples heated up to 800 °C under an atmosphere of Ar applying heating rates of 40 °C min^{-1} and 20 °C min^{-1}.

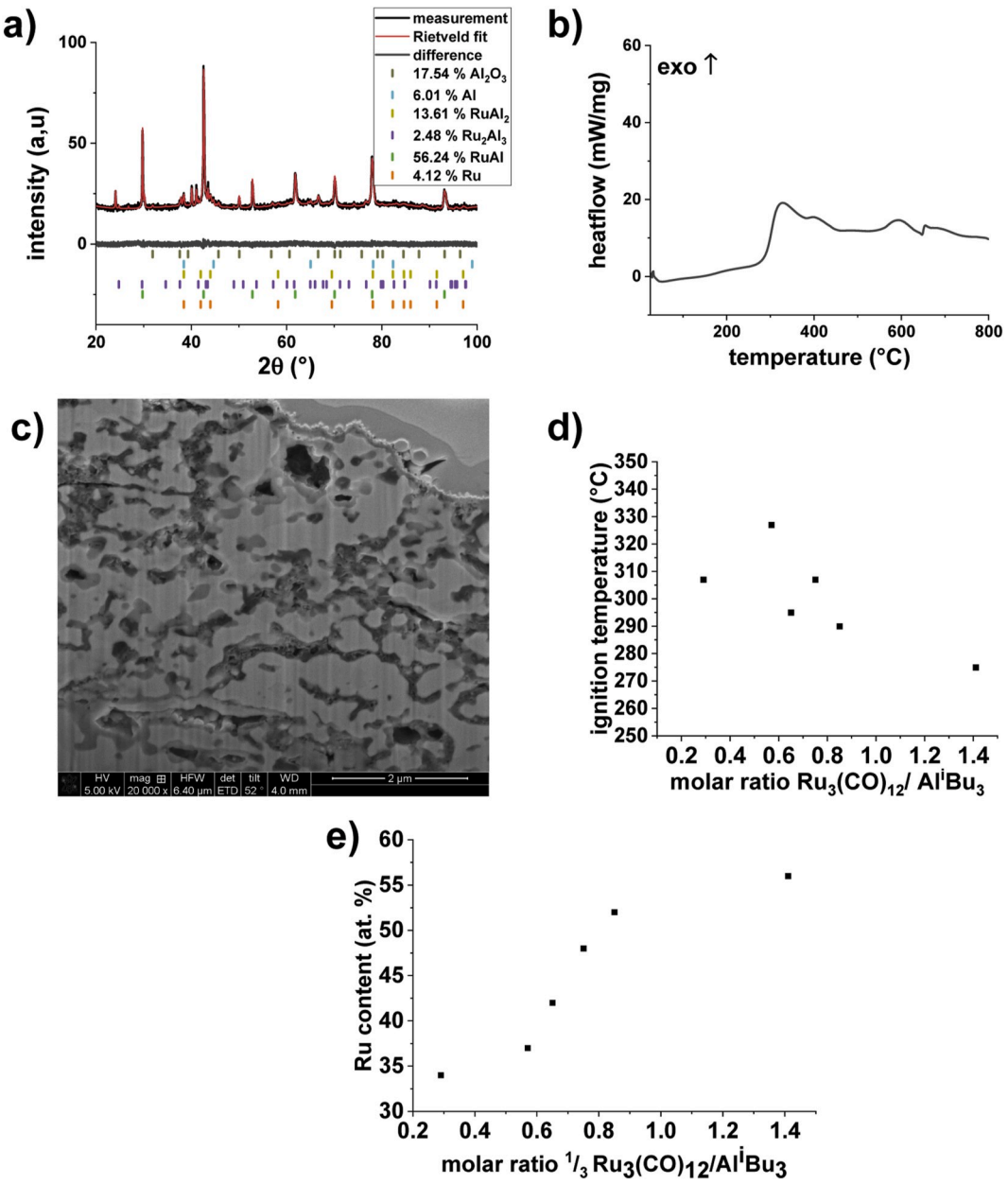

Fig. 7. a) XRD measurement and Rietveld refinement of a Ru–Al particle mixture ignited at 320 °C under an atmosphere of ambient air; **b)** STA measurement of a compacted Ru–Al particle mixture under an atmosphere of synthetic air (N_2:O_2 32:8; 60 °C min^{-1}); **c)** FIB measurement of a Ru–Al particle mixture ignited under an atmosphere of ambient air at a temperature of 320 °C; **d)** determined ignition temperature under an atmosphere of ambient air for different ratios of Ru/Al^iBu_3 during the syntheses; **e)** determined ignition temperature under an atmosphere of ambient air for different ratios of Ru/Al (Ru content = Ru content in the metallic phases without considering Al_2O_3; was determined from the reacted samples via Rietveld refinements); **e)** Ru content in the intermetallic phases in dependence of the $Ru_3(CO)_{12}/Al^iBu_3$ ratio during the synthesis determined via Rietveld refinements of the reacted samples.

a more intense reaction can be observed in the Al rich samples. This is further supported by an increase of the Ru–Al interface area upon increasing the content of the larger sized Al. An increase in the interfacial area between Al and Ru has been reported in the literature to lead to lower onset temperatures [30]. Due to this increased reactivity a molar ratio of $^1/_3$ $Ru_3(CO)_{12}/Al^iBu_3$ of 0.65 has been applied to study the aluminide formation under an Ar atmosphere.

3.2.1.4. Influence of the heating rate. Starting from micrometer sized Al and Ru powders, the formation of RuAl has been reported to be strongly dependent on the applied heating rate. At low heating rates, the formation of multiphasic products as well as incomplete reactions were reported [2,29]. In order to realize complete reactions resulting in the formation of single phase RuAl, the application of increased heating rates is necessary, with a value of 15 °C min^{-1} reported by Mohamed et al. [29], while Gobran et al. reported a value of >70 °C min^{-1} to be necessary [2].

These studies have been conducted applying a sample amount of 10 mg and a $^1/_3$ $Ru_3(CO)_{12}/Al^iBu_3$ ratio of 0.65 and heating rates ranging from 5 °C min^{-1} up to 60 °C min^{-1}.

When high heating rates of 40 °C min^{-1} and 60 °C min^{-1} were applied, highly exothermic reactions could be observed in the STA measurements and products with a high crystallinity were formed. Low heating rates of 20 °C min^{-1} and 5 °C min^{-1} led to the formation of products with poor crystallinity and weakly exothermic reactions (Fig. 6a and 6b). This behavior can likely be explained by increased heat

losses occurring when low heating rates are applied, leading to controlled reactions in the solid state [29]. Thus, for these wet chemically prepared Al and Ru nanoparticles the application of increased heating rates >40 °C min^{-1} is advantageous, similar as reported in the literature for the micrometer sized powders.

3.2.2. Aluminide formation in an atmosphere of ambient air

Ignition temperatures of self-sustaining systems can be determined using hot-plate experiments, in which a small sample amount is dropped directly on a preheated plate hold at a defined temperature. In contrast to regular ignition tests, this method allows the realization of fast heating rates as well as low heat losses. For Ru/Al multilayers the ignition temperatures determined from this method are decreasing from 608 °C to 408 °C upon decreasing the bilayer thickness of the respective multilayer from 222 nm to 22 nm [31]. To our knowledge, for powder mixtures, no such measurements have been published in the literature yet. When a mixture of large Ru and Al particles (Ru 57 ± 12 μm; Al 14 ± 7 μm) was dropped onto a hot plate under an atmosphere of ambient air no ignition could be observed up to the maximum possible temperature of 617 °C, indicating that no (self-sustaining) reaction took place. When the synthesized Al–Ru particle mixtures were dropped onto the hot plate, the ignition temperatures were found to be dependent on the sample composition and was ranging from 290 °C for a Ru:Al molar ratio of 1.4 to 330 °C for a Ru:Al molar ratio of 0.6. These values are amazingly low compared to sputtered multilayer systems. The minimum ignition temperature of these multilayer systems under an atmosphere of ambient air was determined to be 408 °C for a multilayer with a bilayer thickness of 22 nm and increased to 608 °C for multilayers with a bilayer thickness of 222 nm [31]. In contrast, in this work much larger particles with sizes of 111 nm (Al) and 6 nm (Ru) have been applied. While ignition occurred immediately when a hot plate temperature of 600 °C was used, a delay of several seconds was observed when a temperature of around 300 °C was applied. Within this delay, at first the formation of gaseous species was visible, likely due to the decomposition of the organic residues. After this decomposition process the color of the sample changes from metallic grey to slightly whitish, just before ignition occurs. When the sample was removed from the hot plate after changing its color to whitish, the ignition could not be prevented, indicating the self-propagating behavior of the reaction. However, no differences in the sample compositions as well as the crystallinities could be observed in the XRD analyses of two small pellet pieces cut out of the same pellet ignited at 320 °C and 600 °C, indicating that the temperature reached within the sample is larger than 600 °C in both cases. XRD analysis of the ignited particle mixture under an atmosphere of ambient air at a temperature of 320 °C revealed the formation of a multiphase product, with RuAl being the main constituent (Fig. 7a). Again, the incomplete reactions are likely due to high heat losses occurring especially since the ambient temperature is much lower (~25 °C). The very low ignition temperatures compared to the microscopic particle mixtures and the multilayer systems can likely be ascribed to the exothermic oxidation of the Ru nanoparticles as described in section 3.1.2. Although the support of this oxidation reaction is not necessarily needed, as was shown by the synthesis carried out in Ar atmosphere reported above, its support results in these significantly lowered ignition temperatures. The ignition of self-sustaining reactions via secondary, exothermic reactions is well known in the literature [46]. However, it is not regularly applied, since this secondary reaction mixture will be maintaining in the reaction product as an impurity phase. No RuO_2 can be observed in the reacted pellets since it is expected to react with Al to form Al_2O_3 as well as additional Ru. Although the oxidation of carbon residues also contributes to this exothermic reaction (see above), similar onset temperatures were also observed when carbon free ruthenium nanopowder prepared by the reaction between $RuCl_3$ and $NaBH_4$ in an aqueous solution. These very low onset temperatures could also be confirmed by STA measurements under an atmosphere of synthetic air (N_2:O_2 32:8), in which an onset temperature of 289 °C was determined (Fig. 7b). In the STA

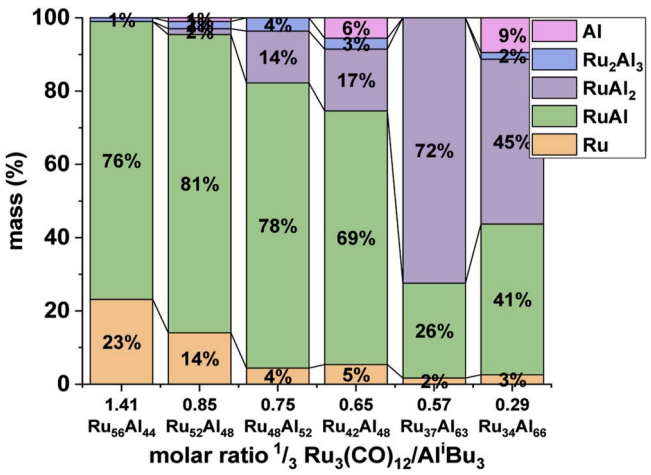

Fig. 8. Sample compositions (not considering Al_2O_3) of pellets prepared from Al–Ru mixtures synthesized applying varying $Ru_3(CO)_{12}/Al^iBu_3$ ratios after ignition in an atmosphere of ambient air at a temperature of 320 °C determined from Rietveld refinements. The error of the composition data was found to be <1%.

measurements under an atmosphere of Ar, this oxidation is not possible and thus much higher onset temperatures were observed as was shown above. A FIB cross-section image of a sample ignited at a temperature of 320 °C under an atmosphere of ambient air (Fig. 7c) further confirmed the observations made above. As can be seen, no unreacted Al and Ru particles are visible and the formation of at least three different intermetallic phases could be observed. As described above an increased porosity as well as an additional phase can be clearly seen likely due the decomposition of organic residues. The decrease of ignition temperatures in ambient air can have two different explanation. The first is that the oxidation of a fraction of the nanoscale Ru particles itself releases sufficient energy to heat the sample internally and trigger the reaction between aluminium and the remaining ruthenium. RuO_2 is then consumed by a reaction with aluminum to form intermetallic phases and aluminum oxide. The second possible explanation is that the oxidation of ruthenium to RuO_2 transforms the reaction from a pure metal/metal reaction at least partly into a metal/oxide reaction, i.e. a thermite reaction of RuO_2 with aluminum. The resulting formation of aluminum oxide releases a large amount of energy which would lead internal heating of the sample, facilitating further reactions. These thermite reactions are, in general, well-studied in the field of energetic materials although no research on the Al/RuO_2 system can be found in literature [47–51]. While they are easily possible in micro-scaled powders, thermite reactions show a tremendous increase of reaction velocity when particle sizes reach the nanoscale as is the case here. For such systems, the nano-thermites, the term “metastable intermolecular composites” (MIC) has been coined. Ignition temperatures in MICs are often found to be greatly reduced when compared to their micro-scaled counterpart which raised the question whether oxide decomposition and gas-phase transfer of oxygen are necessary or if solid-state diffusion of oxygen plays a role [52,53]. However, to elucidate the question whether a thermite reaction is involved in the reactions presented here would require dedicated experiments involving pure RuO_2 nanopowders and gas release measurements. While it is interesting and should be pursued in further studies, we consider it to be beyond the scope of this work.

When the amount of Ru during the decomposition reaction was increased the ignition temperatures of the resulting powder mixtures tend to decrease (Fig. 7d). However, it should be mentioned that the realization of exact stoichiometry in these syntheses is difficult to control. As a result, the amount of $Ru_3(CO)_{12}$ necessary to obtain samples with the desired stoichiometry has to be determined experimentally (Fig. 7e). Within this figure, the Ru content was calculated neglecting

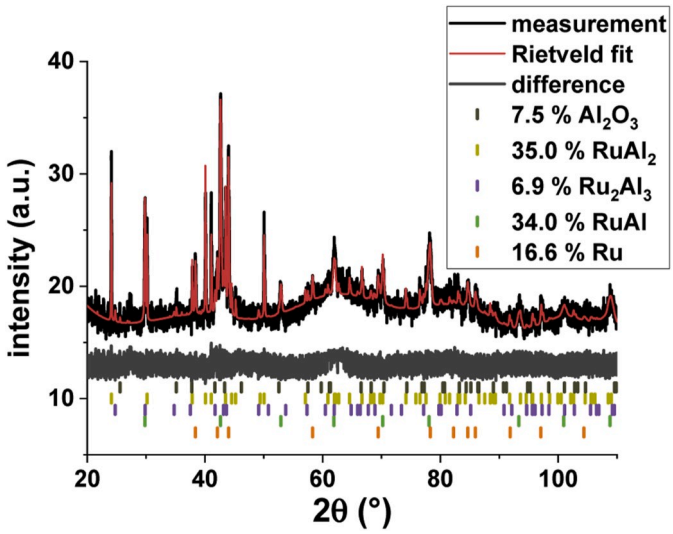

Fig. 9. XRD measurement and Rietveld refinement of a 1:1 mixture of submicron Al particles and $Ru_3(CO)_{12}$ after ignition under an atmosphere of ambient air at 170 °C.

the amorphous Al_2O_3 content for comparability reasons.

Nonetheless, the final sample composition could be modified by changing the $Ru_3(CO)_{12}/Al^iBu_3$ ratio during the precursor synthesis (Fig. 8). As expected, the total Ru content increased upon increasing the amount of $Ru_3(CO)_{12}$ during the synthesis. Hence, the Ru rich samples tended to contain a larger amount of unreacted Ru while the Al rich samples contained larger amounts of the Al rich phase $RuAl_2$ as well as unreacted Al.

Moreover, about 5 wt % of carbon could be detected in the pellets by CHN analyses after ignition in an atmosphere of ambient air, resulting from the decomposition of residual organic contents and residual carbonyl ligands.

3.2.3. *Formation of aluminides from $Ru_3(CO)_{12}$ and Al particles*

Ruthenium aluminides with no residual carbon content (according to CHN analysis in which no CHN content could be detected) could be prepared by directly igniting a mixture of Al particles and $Ru_3(CO)_{12}$. In this sample an ignition temperature of 170 °C could be observed, which is just above the thermal decomposition temperature of $Ru_3(CO)_{12}$ at about 150 °C. A long delay could be observed upon dropping the sample onto the hot plate: After about 6 s a black smoke and a dark red flame started to emanate from the sample which is due to a decomposition of the $Ru_3(CO)_{12}$ in the gas phase. After the first reaction was complete, an ignition of the sample was clearly visible after about 8 s. However, as evidenced by XRD measurements the formation of multiphase products could be observed, again due to incomplete reaction caused by heat transfer effects (Fig. 9). In addition, a large amount of gases formed during the reaction due to the evolving CO, which might be problematic for the formation of nonporous products.

3.2.4. *Formation of aluminides from separately prepared Ru and Al particles*

A synthesis of the respective intermetallic compounds was also found to be possible starting from pellets prepared from separately synthesized and dried Ru and Al particles, applying similar methods. The Al particles have been prepared by decomposing triisobutylaluminum, while the Ru particles were prepared by decomposing $Ru_3(CO)_{12}$. In a sample containing 41% Ru, the ignition under an atmosphere of ambient air was shifted to slightly higher temperatures (>380 °C), likely due to a poorer contact and intermixing between the two particles. However, no self-propagating reaction could be observed under an Ar atmosphere upon heating up to 800 °C applying a heating rate of 60 °C min^{-1}. In this case, an exothermic reaction could be observed over a broad temperature range with the melting of the Al still being clearly visible (Fig. 10b). Accordingly, the final product consisted of a large amount of unreacted Ru as well as Al-rich phases and only minor proportions of RuAl, further indicating the incomplete reactions (Fig. 10a). Thus, the synthesis of the particles in one pot should be preferred over the separate preparation of the particles, even though the stoichiometry is harder to control.

4. Conclusions

Ru aluminides can be prepared starting from submicron Al particles and Ru nanoparticles synthesized by wet chemical reactions. Particle mixtures as precursors for the aluminides are obtained applying a two-step protocol, in which submicron Al particles are prepared via a thermal decomposition of triisobutylaluminum in a first step and Ru nanoparticles by thermal decomposition of $Ru_3(CO)_{12}$ in oleylamine in the same mixture in a second step. Ru aluminides formed by heat treatments under atmospheres of Ar as well as ambient air by self-propagating reactions. The final sample compositions were found to be dependent on the sample amount as well as the Ru to triisobutylaluminum ratio. While an ignition temperature of about 600 °C is observed under an Ar atmosphere, an ignition temperature as low as 300 °C is observed under an atmosphere of ambient air on a hot plate. This very low ignition temperature is the result of a highly exothermic oxidation of the Ru and

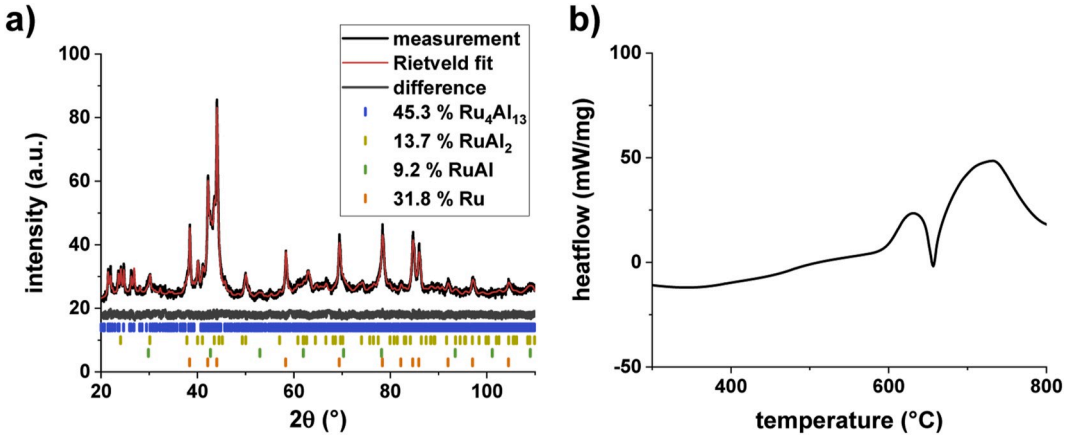

Fig. 10. a) XRD measurement and Rietveld refinement of a pellet prepared from separately synthesized and subsequently mixed Ru and Al powders after heating to 800 °C using a heating rate of 60 °C min^{-1} under an atmosphere of Ar **b)** STA measurement of a pellet prepared from separately synthesized and subsequently mixed Ru and Al powders after heating to 800 °C using a heating rate of 60 °C min^{-1} under an atmosphere of flowing Ar.

organics, which is providing additional heat to start the self-sustaining intermetallic phase formation. The resulting aluminides were containing carbon resulting from organic residues as well as oxide phases from the passivating layers as well as the oxidation reaction. Carbon free Ru-Aluminides could be formed starting from submicron Al particles and $Ru_3(CO)_{12}$ under an atmosphere of ambient air at temperatures as low as 150 °C.

Declaration of competing interest

The authors declare that they have no known competing financial interests or personal relationships that could have appeared to influence the work reported in this paper.

CRediT authorship contribution statement

Thomas Klein: Conceptualization, Methodology, Investigation, Validation, Writing - original draft. **Christoph Pauly:** Investigation, Writing - original draft. **Frank Mücklich:** Resources, Writing - review & editing. **Guido Kickelbick:** Conceptualization, Resources, Writing - review & editing.

Acknowledgments

We thank Susanne Harling for doing the elemental analyses as well as Dr. Robert Haberkorn and Dennis Becker for performing the XRD measurements and their advices regarding the Rietveld refinements. We thank Katherine Aristizabal for conducting the FIB characterizations.

References

[1] F. Soldera, N. Ilić, S. Brännström, et al., Formation of Al_2O_3 scales on single-phase RuAl produced by reactive sintering, Oxid Met 59 (2003) 529–542.
[2] I.M. Wolff, Synthesis of RuAl by reactive powder processing, Metall Mater Trans A 27 (1996) 3688–3699.
[3] R.L. Fleischer, C.L. Briant, R.D. Field, E.A. Engines, Tough, ductile high-temperature intermetallic compounds: results of a four-year survey, MRS Symp. Proc. 213 (1991) 463–474.
[4] H. Clemens, S. Mayer, Design, processing, microstructure, properties, and applications of advanced intermetallic TiAl alloys, Adv. Eng. Mater. 15 (2013) 191–215.
[5] H. Clemens, S. Mayer, Advanced intermetallic TiAl alloys, Mater. Sci. Forum 879 (2017) 113–118.
[6] S.C. Deevi, V.K. Sikka, Nickel and iron aluminides: an overview on properties, processing, and applications, Intermetallics 4 (1996) 357–375.
[7] F. Scheppe, P.R. Sahm, W. Hermann, et al., Nickel aluminides: a step toward industrial application, Mater. Sci. Eng., A 329–331 (2002) 596–601.
[8] S. Niemann, W. Jeitschko, Ternary-Aluminides-AT_2Al_{20} (A = Rare Earth Elements and Uranium; T = Ti, Nb, Ta, Mo, and W) with $CeCr_2Al_{20}$-Type Structure, J. Solid State Chem. 114 (1995) 337–341.
[9] V.M.T. Thiede, T. Ebel, W. Jeitschko, Ternary aluminides LnT_2Al_{10} (Ln = Y, La–Nd, Sm, Gd–Lu and T = Fe, Ru, Os) with $YbFe_2Al_{10}$ type structure and magneticproperties of the iron-containing series, J. Mater. Chem. 8 (1998) 125–130.
[10] N. Zhou, S. Jiang, T. Huang, et al., Single-phase high-entropy intermetallic compounds (HEICs): bridging high-entropy alloys and ceramics, Sci. Bull. 64 (2019) 856–864.
[11] W. Obrowski, B2-Phasen von Aluminium mit T-Metallen der VII. und VIII. Gruppe des Periodischen Systems, Naturwissenschaften 47 (1960) 14.
[12] L. Fleischer, R.D. Field, C.L. Briant, Mechanical properties of high-temperature alloys of AlRu, Metall Trans A 22 (1990) 403–414.
[13] R.L. Fleischer, Substitutional solutes in AlRu-I. Effects of solute on moduli, lattice parameters and vacancy production, Acta Metall. Mater. 41 (1993) 863–869.
[14] R.L. Fleischer, Substitutional solutes in AlRu-II. Hardening and correlations with defect structure, Acta Metall. Mater. 41 (1993) 1197–1205.
[15] T. Gemming, M. Seifert, E. Brachmann, G.K. Rane, S.B. Menzel, S. Oswald, Pt-RuAl bilayers as a model system for Pt wire bonding of high-temperature RuAl electrodes, J. Alloy. Compd. 813 (2020) 152107.
[16] W.J. LaBarge, C. Anderson, J. Kupe, US Patent US8 20 (2011) 378. B2.
[17] B. Tryon, F. Cao, K.S. Murphy, et al., Ruthenium-containing bond coats for thermal barrier coating systems, JOM (J. Occup. Med.) 58 (2006) 53–59.
[18] F. Mücklich, N. Ilić, RuAl and its alloys. Part I. Structure, physical properties, microstructure and processing, Intermetallics 13 (2005) 5–21.
[19] L.E. Edshammar, The crystal structure of $RuAl_6$, Acta Chem. Scand. 22 (1968) 2374–2400.
[20] L.E. Edshammar, The crystal structure of Ru_4Al_{13}, Acta Chem. Scand. 19 (1965) 2124–2130.
[21] S. Mi, S. Balanetskyy, B. Grushko, A study of the Al-rich part of the Al-Ru alloy system, Intermetallics 11 (2003) 643–649.
[22] W. Obrowski, Über Legierungen des Rutheniums mit Bor, Beryllium und Aluminium, Met 17 (1963) 108–112.
[23] O. Schwomma, H. Nowtny, A. Wittmann, Die Verbindungen $RuAl_2$ und $OsSi_{1,5}$, Monatsh. Chem. 94 (1963) 924–926.
[24] L.E. Edshammar, An X-ray investigation of ruthenium-aluminium alloys, Acta Chem. Scand. 20 (1966) 427–431.
[25] F. Mücklich, N. Ilić, K. Woll, RuAl and its alloys, Part II: mechanical properties, environmental resistance and applications, Intermetallics 16 (2008) 593–608.
[26] I.M. Wolff, G. Sauthoff, High-temperature behavior of precious metal base composites, Metall Mater Trans A Phys Metall Mater Sci 27 (1996) 2642–2652.
[27] K.W. Liu, F. Mücklich, R. Birringer, Synthesis of nano-RuAl by mechanical alloying, Intermetallics 9 (2001) 81–88.
[28] A. Borah, P.S. Robi, A. Srinivasan, Synthesis of nano-crystalline RuAl by mechanical alloying, Met. Mater. Int. 13 (2007) 293–302.
[29] K.E. Mohamed, D. Stover, H.P. Buchkremer, Some reactive processing aspects of high-temperature aluminides Nb_3Al and RuAl, J. Mater. Eng. Perform. 6 (1997) 771–779.
[30] H.A. Gobran, N. Ilić, F. Mücklich, Effects of particle size and pressure on the reactive sintering of RuAl intermetallic compound, Intermetallics 12 (2004) 555–562.
[31] C. Pauly, K. Woll, B. Bax, F. Mücklich, The role of transitional phase formation during ignition of reactive multilayers, Appl. Phys. Lett. 107 (2015) 113104.
[32] K. Woll, A. Bergamaschi, K. Avchachov, et al., Ru/Al multilayers integrate maximum energy density and ductility for reactive materials, Sci. Rep. 6 (2016) 19535.
[33] Bruker AXS. Karlsruhe, Topas 5.1. General Profile and Structure Analysis Software for Powder Diffraction Data, 2014.
[34] R.W. Cheary, A.A. Coelho, J.P. Cline, Fundamental parameters line profile fitting in laboratory diffractometers, J Res Natl Inst Stand Technol 109 (2004) 1–25.
[35] A. Merkys, A. Vaitkus, J. Butkus, et al., COD::CIF::Parser: an error-correcting CIF parser for the Perl language, J. Appl. Crystallogr. 49 (2016) 292–301.
[36] C.A. Schneider, W.S. Rasband, K.W. Eliceiri, ImageJ, Fundam Digit Imaging Med 9 (2010) 185–188.
[37] N.G. Garcia-Pena, R. Redon, A. Herrera-Gomez, et al., Solventless synthesis of ruthenium nanoparticles, Appl. Surf. Sci. 340 (2015) 25–34.
[38] T. Klein, G. Kickelbick, Synthesis of submicron aluminum particles via thermal decomposition of alkyl aluminum precursors in the presence of metal seeds and their application in the formation of ruthenium aluminides, Nanotechnology 31 (2020) 265605–265619.
[39] Klein T., Pauly C., Mücklich F., Kickelbick G., Preparation of Ni aluminides from submicron Al particles and Ni nanoparticles. Intermetallics, accepted.
[40] D. Hong, M. Muramaki, Y. Yamada, S. Fukuzumi, Efficient water oxidation by cerium ammonium nitrate with [IrIII(Cp*)(4,4'-bishydroxy-2,2'-bipyridine)$(H_2O)]^{2+}$ as a precatalyst, Energy Environ. Sci. 5 (2012) 5708–5716.
[41] S. Fukuzumi, Y. Yamada, Catalytic activity of metal-based nanoparticles for photocatalytic water oxidation and reduction, J. Mater. Chem. 22 (2012) 24284–24296.
[42] J.R. Rumble, D.R. Lide, T.J. Bruno. Handbook of Chemistry and Physics, 98th ed., CRC Press, Boca Raton, 2017.
[43] H.X. Zhu, R. Abbaschian, Reactive processing of nickel-aluminide intermetallic compounds, J. Mater. Sci. 38 (2003) 3861–3870.
[44] C. Nishimura, C.T. Liu, Reactive sintering of Ni_3Al under compression, Acta Metall. Mater. 41 (1993) 113–120.
[45] B. Wen, J. Zhao, F. Bai, T. Li, First-principle studies of Al-Ru intermetallic compounds, Intermetallics 16 (2008) 333–339.
[46] V.V. Barzykin, Initiation of shs processes, Pure Appl. Chem. 64 (1992) 909–918.
[47] C. Rossi, K. Zhang, D. Estève, et al., Nanoenergetic materials for MEMS: a review, J Microelectromechanical Syst 16 (2007) 919–931.
[48] G. Jian, S. Chowdhury, K. Sullivan, M.R. Zachariah, Nanothermite reactions: is gas phase oxygen generation from the oxygen carrier an essential prerequisite to ignition? Combust. Flame 160 (2013) 432–437.
[49] A.S. Mukasyan, A.S. Rogachev, S.T. Aruna, Combustion synthesis in nanostructured reactive systems, Adv. Powder Technol. 26 (2015) 954–976.
[50] E.L. Dreizin, M. Schoenitz, Correlating ignition mechanisms of aluminum-based reactive materials with thermoanalytical measurements, Prog. Energy Combust. Sci. 50 (2015) 81–105.
[51] E.L. Dreizin, Metal-based reactive nanomaterials, Prog. Energy Combust. Sci. 35 (2009) 141–167.
[52] X. Wang, M.R. Zachariah, What atomic properties of metal oxide control the reaction threshold of solid elemental fuels? Phys. Chem. Chem. Phys. 20 (2018) 26885–26891.
[53] S. Brotman, M.D. Rouhani, C. Rossi, A. Estève, A condensed phase model of the initial Al/CuO reaction stage to interpret experimental findings, J. Appl. Phys. 125 (2019), 035102.

As can be learned from these studies, the preparation of Ru aluminides is possible applying wet chemically prepared Ru nanoparticles and submicron Al particles. However, typically multiphase products were obtained, and a homogenization step would be necessary to achieve a complete conversion. The increased reactivity of the applied nanoparticles was particularly observed upon reacting the Ru-Al mixtures in an atmosphere of ambient air. The onset of the reaction was determined to be about 300 °C lower than in an atmosphere of Ar, which was attributed to a partial oxidation of the Ru nanoparticles and of organics. In contrast, samples prepared from micrometer sized particles could not be ignited in an atmosphere of ambient air up to a temperature of 600 °C. In order to test if the ignition temperature of the pellets prepared from micrometer sized particles could be lowered by the addition of a certain amount of wet chemically prepared Ru nanoparticles, samples containing up to 50 % Ru nanoparticles instead of micrometer sized Ru particles were prepared. However, no lowering of the ignition temperature was observed in these samples and they did not ignite up to a temperature of 600 °C.

Since good results for the preparation of Ni and Ru aluminides were observed applying the two-step synthesis protocol developed within this work, the applicability of this approach for preparation of additional aluminides was briefly tested. The results of these preliminary studies will be summarized in the following chapter and shall be an outlook to possible future work.

3.2.5 Synthesis of additional aluminides and aluminothermic reactions

The two-step synthesis protocol developed in Chapters 3.2.3.2 and 3.2.4.3 for the preparation of Ni and Ru aluminides was adapted for the preparation of additional aluminides. For both aluminides, the first step consisted of preparing the submicron Al particles via a thermal decomposition of triisobutylaluminum in diphenylether before in a second step, the additional metal was synthesized via a thermal decomposition of a suitable precursor. The resulting powder mixtures were then compacted in a hydraulic press and reacted to the respective aluminides via a thermal treatment. To adapt this method for the preparation of other aluminides, suitable metal precursors need to be selected. Particularly metal carbonyls are promising precursors, since only the metal as well as gaseous carbon monoxide are formed upon decomposition, resulting in the formation of high purity products. Accordingly the applicability of $Co_2(CO)_8$, $Fe(CO)_5$, $W(CO)_6$, and $Re_2(CO)_{10}$ was tested. However, carbonyls are not available for every element. Thus, the applicability of other precursors such Ag(acac), $Cu(acac)_2$, and Karstedt's catalyst for the preparation of the respective aluminides was also studied.

The following sections are summarizing the first few results regarding the preparation of CoAl, FeAl, ReAl, WAl_4, Ag_2Al, CuAl as well as $PtAl_2$ applying metal-aluminum mixtures prepared via a two-step synthesis protocol. Although promising results were observed in some examples, they have to be

understood as preliminary experiments and further studies are necessary to fully characterize the formed products as well as the respective reactions. They might however point out that the synthesis of many more aluminides is possible applying the approach developed within this work.

Cobalt aluminide

Dicobaltoctacarbonyl decomposes to metallic Co and CO at temperatures > 50 °C and was thus chosen as a precursor for the preparation of Al-Co powder mixtures. For their synthesis, a similar approach as for the preparation of the Ni-Al mixtures was applied: Submicron Al particles were prepared in a first step by the decomposition of triisobutylaluminum and in a second reaction step, metallic Co was prepared via a thermal decomposition of dicobaltoctacarbonyl (Scheme 13).

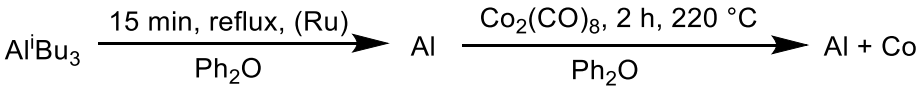

***Scheme 13**: Synthesis of Al-Co particle mixtures.*

The diffraction pattern of the as prepared powders clearly shows the presence of metallic Al (Figure 53a) with a crystallite size of 170 ± 36 nm as determined from Rietveld refinements. Although Co was present in the sample after heating to temperatures > 600 °C (Figure 53b and c), no reflections of Co were observed in the as prepared powder mixtures, indicating its amorphous state. The TEM image of the as prepared Al and Co particle mixture clearly shows the submicron Al particles as well as the Co nanoparticles, deposited on the Al surfaces. The diameter of the Co particles determined from the TEM images was 13 ± 2 nm (Figure 53d and e).

Starting from these Al-Co powder mixtures, the synthesis of CoAl was easily possible by heating compacted samples to a temperature of 800 °C in an atmosphere of Ar as well as in an atmosphere of ambient air at 600 °C on a hot plate. The onset temperature determined on a hot-plate in an atmosphere of ambient air was 564 °C, while an onset temperature of 578 °C – 593 °C was observed in an Ar atmosphere. Similar to the Ni-Al mixtures, CoAl was the only crystalline phase being observed in both cases in the respective XRD measurements (Figure 53b and c).

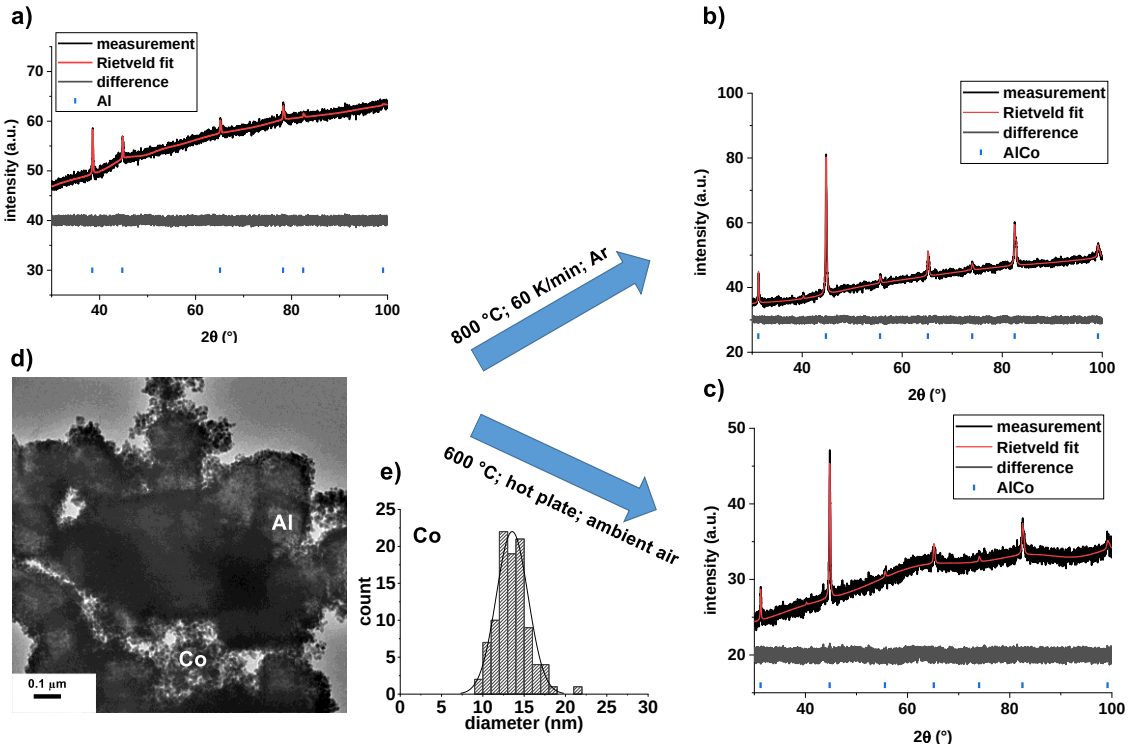

***Figure 53**: XRD measurements and Rietveld refinements of Al-Co pellets prepared from wet chemically synthesized submicron Al particles and Co nanoparticles. The particles were synthesized in a one-pot, two-step protocol via thermal decomposition of triisobutylaluminum and dicobaltoctacarbonyl **a)** as prepared, **b)** reacted under Ar (800 °C; Ar; 60 K/min) **c)** reacted unter ambient air on a hot plate (600 °C) **d)** TEM image of the Al-Co mixtures and **e)** particle size distribution of the Co particles determined from the TEM image shown in d).*

Upon heating in an Ar atmosphere, the applied heating rate was found to play only a minor role regarding the final product composition and in all samples CoAl was observed as the only crystalline phase (Figure 54a and b). This can again likely be attributed to the good intermixing as well as the good interfacial contact between Al and Co, similar as reported for the Ni-Al system described in Chapter 3.2.3.2. The onset temperature of the reaction was found to shift from 593 °C to 573 °C upon decreasing the heating rate from 60 K/min to 5 K/min and the activation energy determined by a Kissinger analysis (Figure 54c**)** was 275 ± 34 kJ/mol. This value is in good agreement with a value of 247 ± 19 kJ/mol reported in the literature for a Co/Al multilayer with a bilayer thickness of 50 nm[326]. In addition, AlCo was also observed to form as the only intermetallic phase upon heating the loose powders to a temperature of 800 °C in an atmosphere of Ar with an onset temperature of 593 °C. Accordingly, no endothermic melting was observed in the STA traces of the loose powders, indicating an initiation of the reaction via a solid-state reaction. Similar as it was discussed for the Ni-Al mixtures, this further confirms the proposed good interelemental contact.

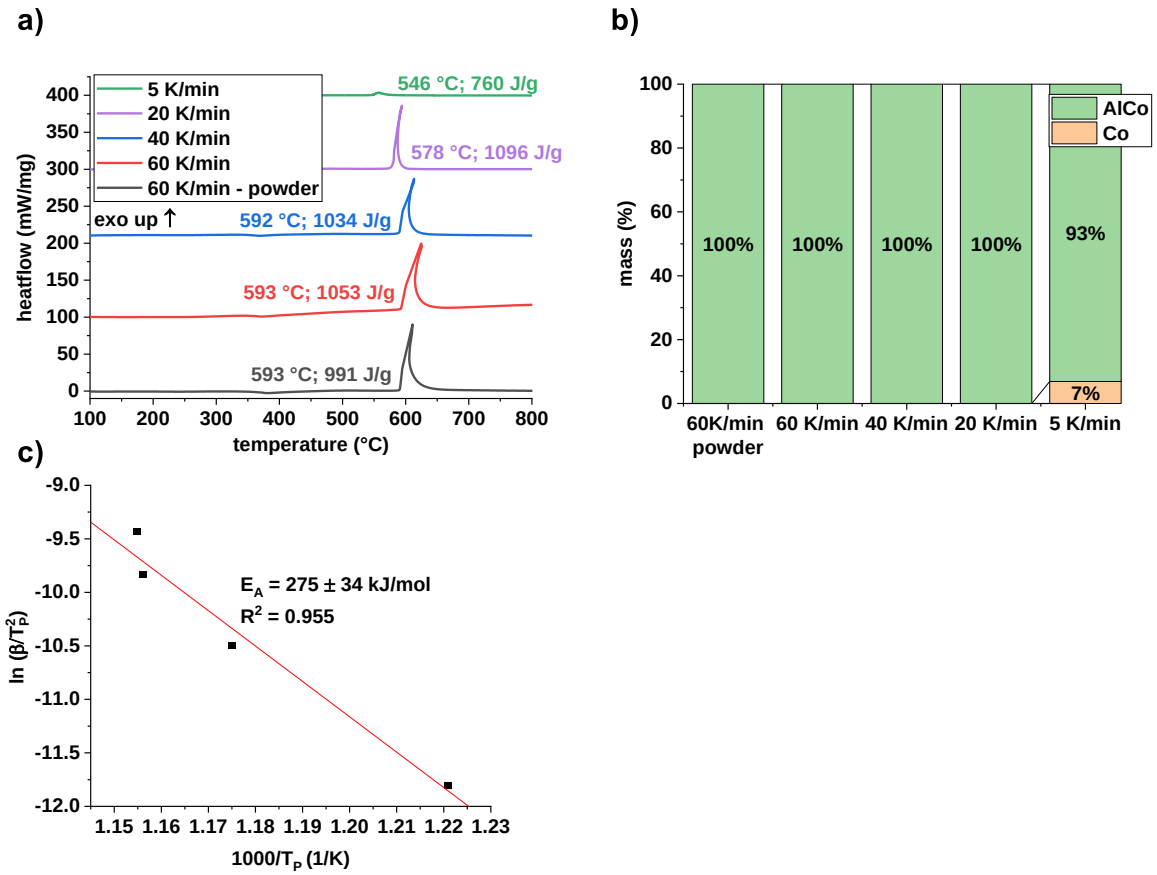

Figure 54: a) *STA traces of Co-Al pellets and loose powder prepared from wet chemically synthesized submicron Al particles and Co nanoparticles upon applying various heating rates. The particles were synthesized in a one-pot, two-step protocol via thermal decomposition of triisobutylaluminum and dicobaltoctacarbonyl;* ***b****) sample compositions of the samples after the STA measurements shown in a) determined from Rietveld refinements;* ***c)*** *Kissinger plot obtained from the data shown in a).*

In contrast, in mixtures of micrometer sized Al (14 ± 7 µm) and Co (0.9 ± 0.2 µm) particles, a poorer intermixing as well as longer diffusion pathways can be expected to occur. Characterizations of these powders can be found in Chapter 7. Accordingly, upon heating a loose powder mixture of micrometer sized Al and Co particles, the onset of the reaction occurred after the formation of a liquid phase via solid-liquid reactions as is indicated by the low intensity endothermic event prior to the exothermic reaction at a temperature of 658 °C (Figure 55a). Moreover, due to the larger diffusion pathways, incomplete reactions were observed within these loose powder mixtures (Figure 55b). Upon heating compacted pellets of these micrometer sized Al and Co particle mixtures in an atmosphere of Ar to a temperature of 800 °C, increased onset temperatures of 640 – 645 °C were observed. This lower reactivity might be attributed to the lower reactivity of such micrometer sized particles in general as well as to a poorer intermixing and interelemental contact. In contrast, in the wet-chemical preparation method described above, the Co was deposited on the submicron Al particles prior to air contact, thus resulting in an improved Al-Co interfacial contact. Moreover, the larger diffusion pathways were particularly problematic upon applying low heating rates of 5 K/min, where incomplete

reactions were observed resulting in the formation of products containing AlCo, Al rich Al_5Co_2 as well as residual Co. In contrast to the wet chemically prepared Al-Co mixtures, no ignition was observed on a hot plate in an atmosphere of ambient air up to a maximum temperature of 650 °C, further indicating their lower reactivity described above.

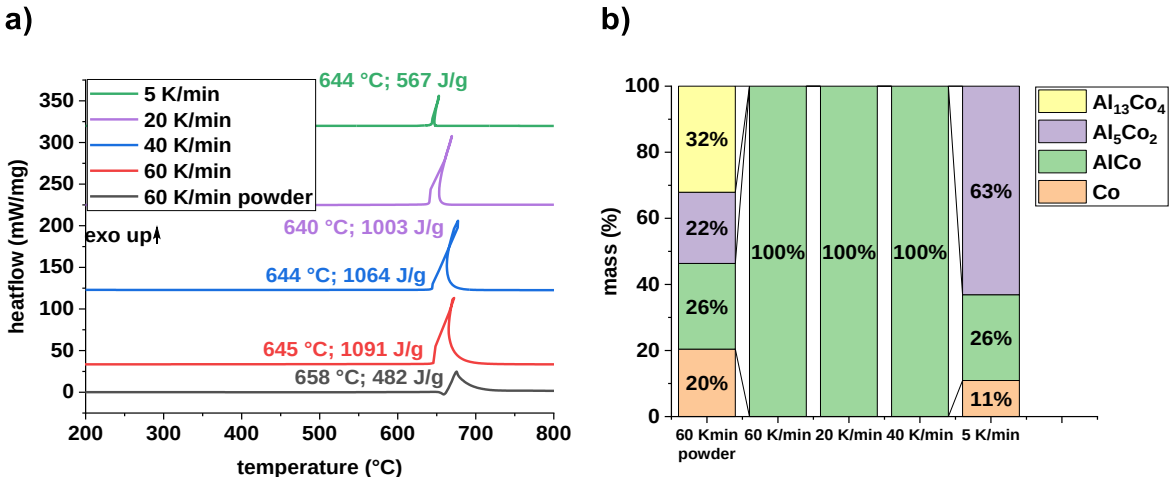

***Figure 55**: **a)** STA traces of Co-Al pellets and loose powder prepared from commercial Al and Co powders upon applying various heating rates; **b)** sample compositions of the samples after the STA measurements shown in a) determined from Rietveld refinements.*

Iron aluminide

Typical synthesis methods for the preparation of Fe nanoparticles are based on the application of $NaBH_4$ as a reducing agent[327] or on a thermal decomposition of $Fe(CO)_5$[48]. Similar as reported above for the Ni nanoparticles, impurities such as Fe borides or carbides were easily introduced into the final product via the resulting Fe particles (Figure 56a and b). While the formation of Fe borides could not be avoided upon applying $NaBH_4$ as a reducing agent, the formation of carbides upon applying $Fe(CO)_5$ could be largely avoided by varying the reaction conditions.

Thus, the applicability of $Fe(CO)_5$ for the preparation of Fe-Al powder mixtures via a two-step synthesis protocol as described above was studied in more detail. Within this approach, Al particles were prepared via thermal decomposition of triisobutylaluminum in refluxing diphenylether and, in a second reaction step, Fe powder was prepared via thermal decomposition of $Fe(CO)_5$ in diphenylether at various reaction temperatures (Scheme 14) with or without the presence of oleylamine. The as prepared powders were compacted to pellets and were then heated to a temperature of 800 °C in an atmosphere of Ar applying a heating rate of 60 K/min. The sample compositions of the reacted pellets were determined from Rietveld refinements and are given in Figure 57a.

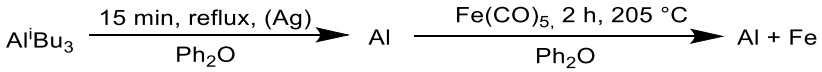

***Scheme 14**: Synthesis of Al-Fe particle mixtures.*

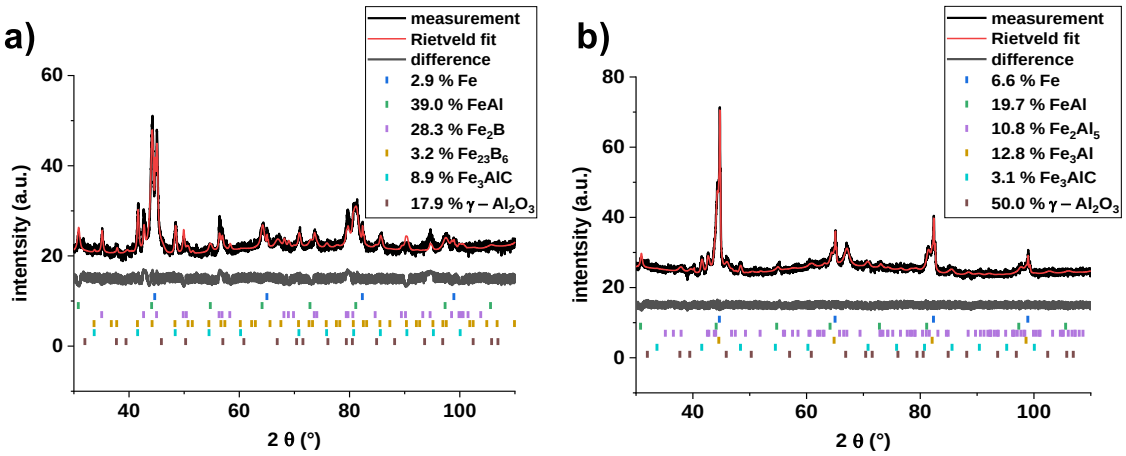

***Figure 56**: Reaction products obtained from mixtures of Al nanoparticles and **a)** Fe particles prepared applying $NaBH_4$ as a reducing agent, and **b)** Fe particles prepared by decomposing $Fe(CO)_5$. The reactions were carried out by heating the compacted mixtures to a temperature of 800 °C in an Ar atmosphere applying a heating rate of 60 K/min.*

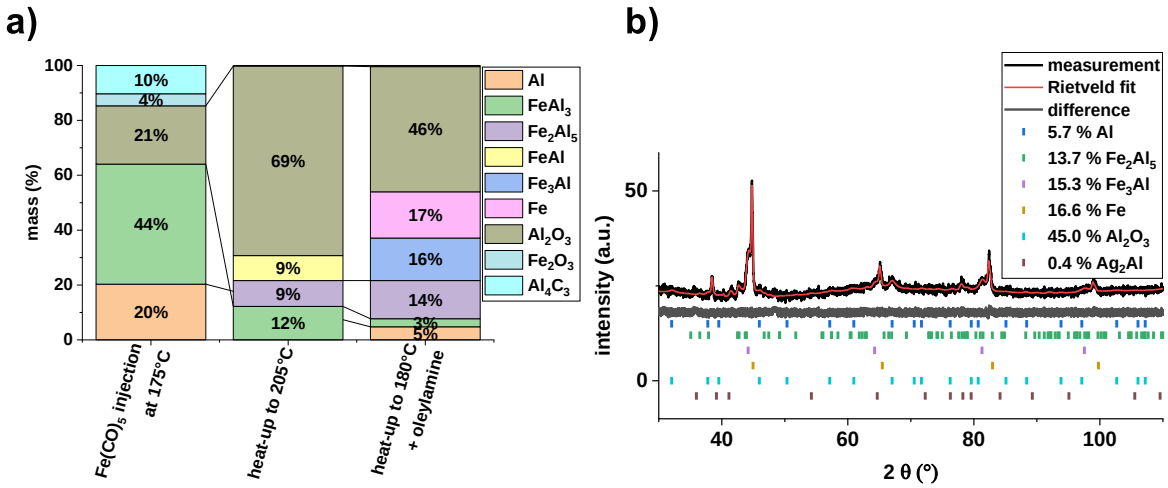

***Figure 57**: **a)** Sample compositions of reacted Al-Fe pellets prepared from particle mixtures synthesized via thermal decomposition of triisobutylaluminum and ironpentacarbonyl (800 °C; Ar; 60 K/min) determined from Rietveld refinements; **b)** XRD measurement and Rietveld refinement of the sample prepared from the powder mixture synthesized by heating up to 180 °C in the presence of oleylamine shown in a).*

The preparation of FeAl via such a two-step synthesis approach was not as trivial as for Ni or Co (Figure 57a). When the $Fe(CO)_5$ was injected into the preheated reaction mixture containing the submicron Al particles, the formation of Al carbides occurred. Accordingly, a further optimization of the reaction conditions would be required, which was however not carried out due to time reasons.

Alternatively, the carbide formation was prevented by adding the $Fe(CO)_5$ at room temperature and applying a slow heat-up procedure (Figure 57a). However, the oxidation sensitivity of the Fe remained problematic. The Fe oxide can be expected to react in an aluminothermic reaction with Al^0 yielding Al_2O_3 and Fe, ultimately resulting in the formation of the large amounts Al_2O_3 detected within these samples. Moreover, due to this undesired reaction, the total composition of the formed intermetallic phases is difficult to control. As a result, the formed intermetallic phases had an Al rich total composition (mainly Fe_2Al_5 or $FeAl_3$ and unreacted Al), although a 1:1 Fe:Al ratio was aimed to be prepared.

To cap and protect the formed Fe particles from oxidation, the reaction was carried out in the presence of additional oleylamine. However, the application of oleylamine was not capable of preventing the Fe oxidation and large Al_2O_3 contents were still observed within the reacted pellets (Figure 57). Although the total oxide mass content was lower compared to the sample prepared without oleylamine, this does not necessarily point towards a lower degree of Fe oxidation, since the samples are exhibiting different total Fe contents. Moreover, the reactions were still incomplete, resulting in the formation of multiphase products containing Fe_3Al and unreacted Fe as well as Fe_2Al_5 and unreacted residual Al. As shown in Chapter 3.2.2 these incomplete reactions might be due to the increased organic content of oleylamine and the increased oxide contents.

Accordingly, this method is only partially suitable for the preparation of Fe aluminides and further studies including a handling of the prepared samples in an inert atmosphere or a capping of the Fe particles would be clearly necessary in a possible future work.

Tungsten and rhenium aluminides

For the preparation of tungsten aluminides, $W(CO)_6$ was chosen as a precursor and a similar two - step reaction approach as reported above was applied (Scheme 15).

$$Al^iBu_3 \xrightarrow[Ph_2O]{\text{15 min, reflux, (Ru)}} Al \xrightarrow[Ph_2O]{W(CO)_6,\ 2\ h,\ 230\ °C} Al + W$$

***Scheme 15**: Synthesis of Al-W particle mixtures.*

Again, the Al reflections were clearly visible in the as prepared powders, while no reflections belonging to W were observed, indicating its amorphous nature (Figure 58a). The crystallite size of the Al was 80 ± 7 nm as determined from Rietveld refinements. However, during the decomposition, the sublimation of $W(CO)_6$ was very problematic regarding the control of the Al:W ratio in the prepared powders, as the $W(CO)_6$ sublimed in the reflux condenser and was effectively removed from the

reaction mixture. As a result, upon applying 1 eq of $W(CO)_6$, the obtained aluminide was highly understoichiometric in W (Figure 58b) and only the formation of Al_5W was observed. Accordingly, although the preparation of tungsten aluminides seems theoretically possible applying this method, more studies to prevent the sublimation of $W(CO)_6$ or an empirical determination of the amount of $W(CO)_6$ necessary to achieve a 1:1 stoichiometry in the prepared aluminide are needed. The onset of the reaction was found to occur at a temperature of 737 °C (Figure 58c).

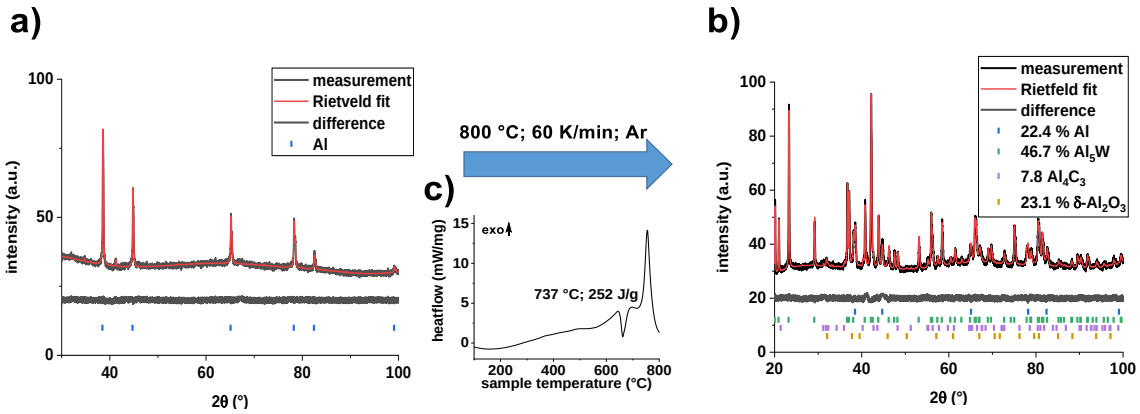

***Figure 58**: XRD measurements and Rietveld refinements of Al-W pellets prepared from a Al-W particle mixture synthesized via thermal decomposition of triisobutylaluminum and tungstenhexacarbonyl **a)** as prepared, **b)** reacted (800 °C; Ar; 60 K/min); **c)** STA trace of the reaction of the compacted Al-W pellet leading to the formation of the product shown in b) (800 °C; Ar; 60 K/min).*

The preparation of rhenium aluminum powder mixtures was attempted by adding $Re_2(CO)_{10}$ to a mixture of Al particles in diphenylether and heating the reaction mixture to 250 °C for 3 h with or without the addition of 20 ml of oleylamine. However, in both samples, XRD measurements of the as prepared powders only revealed the presence of Al^0 and no additional crystalline phase was visible. Similarly, upon heating to 800 °C in an atmosphere of Ar applying a heating rate of 60 K/min, no formation of any intermetallic Al-Re compound was observed via XRD measurements. In the reacted samples, unreacted Al was identified together with at least one additional crystalline phase, which did not match any known Al-Re intermetallic compound, Al-Re oxide, or Al-Re carbide and which could not be further identified.

Although metal carbonyls are ideal metal precursors within this synthesis approach, they are known only for a limited number of elements. However, for many elements, other precursors are available that allow their preparation by thermal decomposition reactions. Typical examples are including acetylacetonates, which are also known to decompose often yielding the respective metal and volatile decomposition products[328]. Thus, the applicability of metal acetylacetonates within the developed approach was studied and as a first example, the preparation of Al-Cu and Al-Ag powder mixtures was examined by thermally decomposing $Cu(acac)_2$ and Ag(acac) as metal precursors (Scheme 16 and Scheme 17).

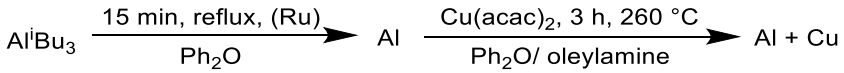

***Scheme 16**: Synthesis of Al-Cu particle mixtures.*

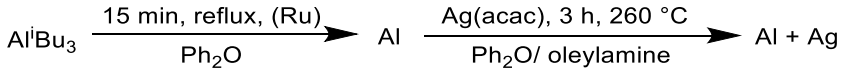

***Scheme 17**: Synthesis of Al-Ag particle mixtures.*

The as prepared mixtures were consisting of elemental Al and Cu or Al and Ag respectively, indicating a successful decomposition of both precursors (Figure 59a and Figure 60a). The decomposition was complete, as was proven by low total CHN contents determined from CHN analyses (Ag: 1.35 % C; 0.23 % H and Cu: 3.63 % C; 0.96 % H). Upon heating in an Ar atmosphere to 800 °C applying a heating rate of 60 K/min the formation of CuAl as well as Ag_2Al were observed, confirming the suitability of acetylacetonates as possible metal precursors in this reaction system (Figure 59b and Figure 60b). Particularly in the Al-Cu system, AlCu was the only crystalline intermetallic phase being present, although the as prepared mixture had a total composition of $Al_{70}Cu_{30}$. This can likely be ascribed to the presence of Cu_2O within the sample, which reacts with excess Al to yield Al_2O_3 and Cu. The presence of this Cu_2O is also indicated by the presence of a very broad reflection at around 30 – 40 °C in the as prepared sample, which can be ascribed to the Cu_2O (111) reflection, but which was not considered within the Rietveld refinement. In the STA trace two exothermic events at temperatures of 313 °C and 515 °C were observed (Figure 59c). The exact nature of these signals needs to be further evaluated, which was however not carried out within this work. The observed heat of reaction of 306 J/g is considerably lower than the theoretical value of 452 J/g[161], which can likely be attributed to the dilution by oxides.

Similarly, Ag_2Al was prepared in a good yield of 88 %. The onset of the reaction was 604 °C (Figure 60c), which is significantly higher than the values reported for Al/Ag multilayers, which are capable to react

at temperatures < 300 °C[329]. These increased reaction temperatures can likely be attributed to the presence of oxidic passivation layers on the Al surfaces. It also has to be noted, that the reaction flask was opened to the atmosphere prior to the decomposition of the Ag(acac) in order to allow an air passivation of the submicron Al particles to prevent a premature formation of any Ag-Al intermetallic phases during the synthesis, which was reported to occur at temperatures as low as 70 °C in multilayer systems[330]. The endothermic signals at 627 °C and 754 °C can be attributed to the melting of intermetallic Al-Ag compounds formed during the reaction.

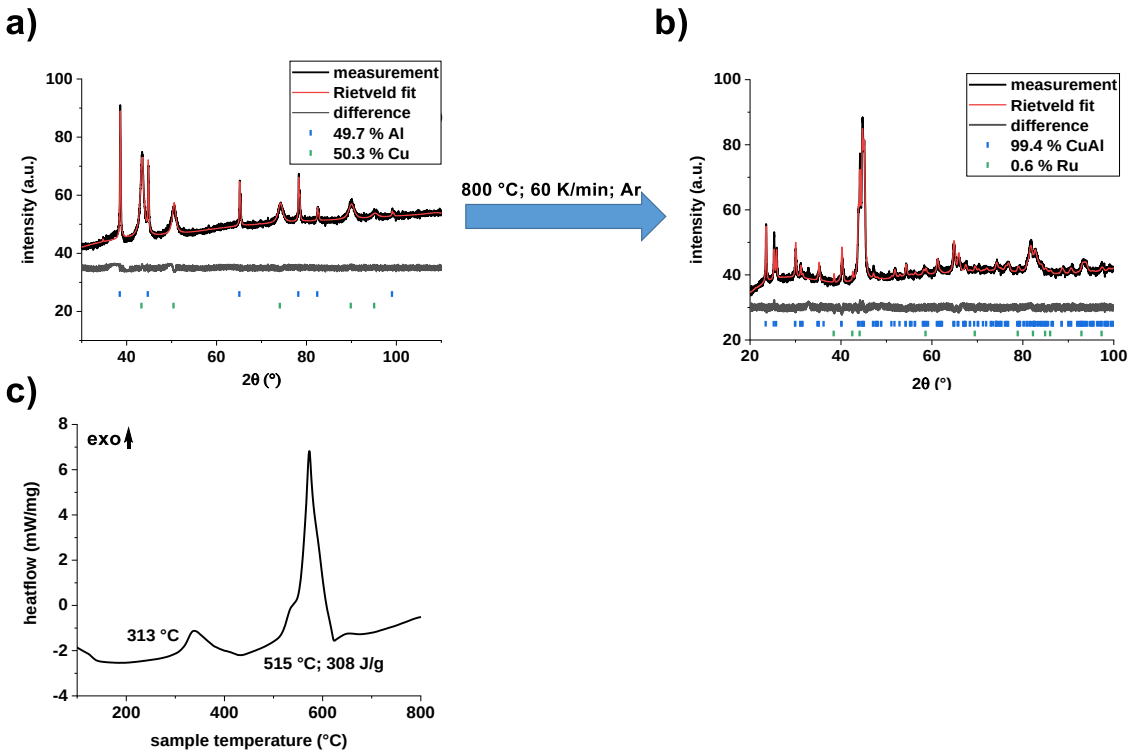

***Figure 59**: XRD measurements and Rietveld refinements of Al-Cu pellets prepared from a Al-Cu particle mixture synthesized via thermal decomposition of triisobutylaluminum and $Cu(acac)_2$ **a)** as prepared, **b)** reacted (800 °C; Ar; 60 K/min), and **c)** STA trace of the Al-Cu pellet (800 °C; Ar; 60 K/min).*

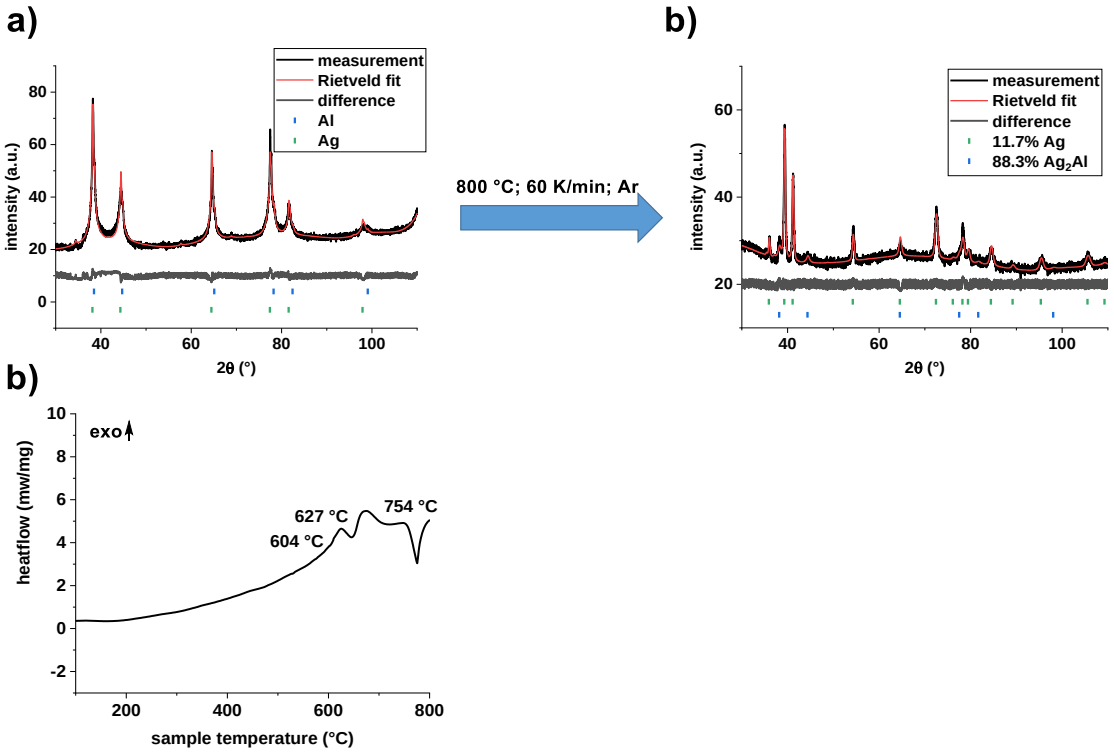

***Figure 60**: XRD measurements and Rietveld refinements of Al-Ag pellets prepared from a Al-Ag particle mixture synthesized via thermal decomposition of triisobutylaluminum and Ag(acac) **a)** as prepared, **b)** reacted (800 °C; Ar; 60 K/min), and **c)** STA trace of the Al-Ag pellet (800 °C; Ar; 60 K/min).*

Platinum aluminides

For the synthesis of platinum aluminides, Karstedt's catalyst was chosen as an Pt precursor, since it is known to decompose yielding Pt^0 upon heating (Scheme 18).

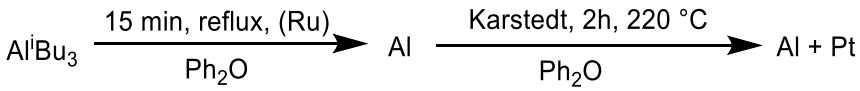

***Scheme 18**: Synthesis of Al-Pt particle mixtures.*

Again, the XRD measurement of the as prepared powder only confirmed the presence of Al^0 with a crystallite size of 71 ± 2 nm, indicating the amorphous nature of the formed Pt (Figure 61a). Although the formation of Al_2Pt was evident upon heating the compacted samples to 800 °C in an atmosphere of Ar, the presence of numerous side products such as Al_4C_3, Al_2OC, Al_2O_3 and SiO_2 was observed (Figure 61b). The formation of these products can likely be ascribed to the presence of residual ligands from the Karstedt catalyst during the heat-up, making the use of the Karstedt catalyst as a Pt^0 precursor problematic. The presence of the ligands was confirmed by CHN analysis, in which a total CHN content of 13.27 % (10.23 % C; 3.04 % H) was determined. Thus, although the formation of Pt aluminides applying this approach seems possible in general, alternative clean-up procedures or Pt precursors

need to be studied in order to reduce the amount of impurity phases. The onset of the reaction was 754 °C (Figure 61c).

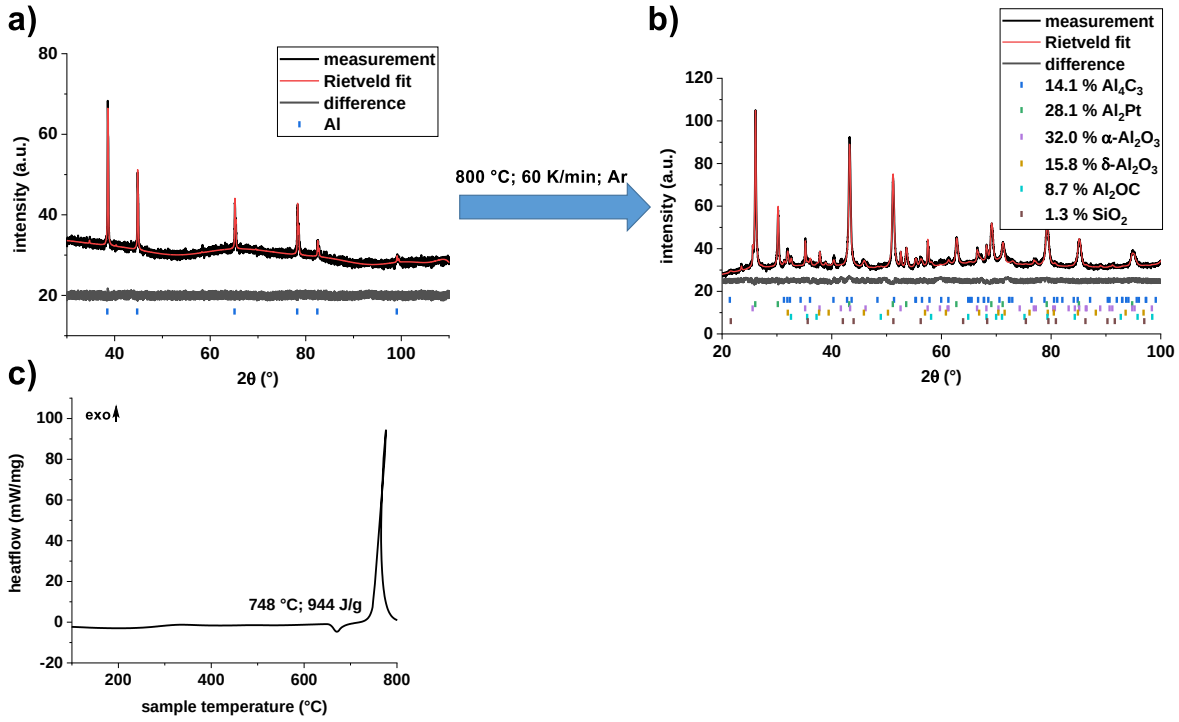

***Figure 61**: XRD measurements and Rietveld refinements of Al-Pt pellets prepared from a Al-Pt particle mixture synthesized via thermal decomposition of triisobutylaluminum and karstedt's catalyst **a)** as prepared, **b)** reacted (800 °C; Ar; 60 K/min) **c)** STA trace of the Al-W pellet (800 °C; Ar; 60 K/min).*

In conclusion, these results indicate that that two-step synthesis protocol can be applied for the preparation of various aluminides. However, in many cases, an optimization of the reaction conditions still needs to be carried out to minimize the formation of side products or to achieve a complete decomposition of the applied precursors. Accordingly, no general protocol applicable to any metal precursor could be determined yet.

Aluminothermic reactions

Besides the synthesis of intermetallic Al compounds, which was studied within this work, Al particles are commonly applied within aluminothermic reactions. In these, typically highly exothermic reactions, the Al particles are reacted with metal oxides yielding alumina and the respective metal. Thus, a first few studies were conducted to examine the suitability of the submicron Al particles prepared via the thermal decomposition approach developed within this work for these reactions. For this purpose, the submicron Al particles were reacted with wet chemically prepared Fe_2O_3, Cu_2O as well as V_2O_5 powders. The Fe_2O_3 particles were prepared by decomposing $Fe(acac)_3$ in oleylamine/ benzyl ether

solutions and exhibited a size of 7 ± 1 nm[331,332]. The Cu_2O and V_2O_5 particles were synthesized by reacting $Cu(acac)_2$ and $VO(O^iPr)_3$ in diethyleneglycol at a temperature of 180 °C according to the procedures published by C. Feldmann[333,334] and exhibited crystallite sizes of 273(13) nm and 36(2) nm respectively. The XRD measurements of these powders are given in Chapter 7. The metal oxide particles were thoroughly mixed with the Al particles in an agate mortar and the mixture was then compacted to a pellet in a hydraulic press (350 MPa, 1 t, 10 min, Ø 6 mm) and reacted by heating in a TGA/DSC thermal analyzer up to a temperature of 800 °C in an Ar atmosphere applying a heating rate of 60 K/min. After cooling to room temperature, the pellets were homogenized, and their composition was determined from Rietveld refinements.

An aluminothermic reaction was possible upon applying the wet chemically synthesized Al and metal oxide particles (Figure 62). Upon reacting Cu_2O and Al, the product was found to consist of a mixture of 69 % Cu and 31 % Cu_2O, while a mixture of 83 % Fe and 17 % Fe_3Al was observed upon reacting Fe_2O_3 and Al. The presence of Cu_2O and Fe_3Al are a result of the reacting mixtures being slightly off stoichiometric due to the presence of organics and oxidic phases. However, due to time reason no further attempts were made to prepare additional samples with a 1:1 stoichiometry.

Figure 62a and b shows the STA traces of the Al metal oxide particle mixtures measured in an Ar atmosphere applying a heating rate of 60 K/min. For the Al - V_2O_5 mixtures a highly exothermic reaction with an onset temperature of 655 °C was observed. Although this exothermic signal strongly suggests the occurrence of an aluminothermic reaction, this could not be confirmed via an XRD measurement since the sample spilled out of the crucible during the reaction. The mixtures of Al with Cu_2O and Fe_2O_3 exhibited onset temperatures of 576 °C and 491 °C respectively. However, only weak exothermic signals, with the determined heats of reaction being well below the literature values of 2405 J/g[161] and 3956 J/g[161] were observed in both cases. These low values might be explained by i) dilution by residual organics, ii) dilution by the oxide layer on the Al surfaces, or iii) incomplete reactions, and iv) diffusion processes. For the Al - V_2O_5 mixtures the sample spilled out of the crucible during the measurement, explaining the low heat of reaction of 1511 J/g compared to the literature value of 4568 J/g[161].

Moreover, these reactions could also be carried out in an atmosphere of ambient air on a hot plate and the ignition temperatures determined within this method generally agreed well with the values observed in the STA measurements. The Al-Fe_2O_3 mixtures ignited at a temperature of 495 °C, the Al-Cu_2O mixtures at 600 °C and the Al-V_2O_5 mixtures at 557 °C.

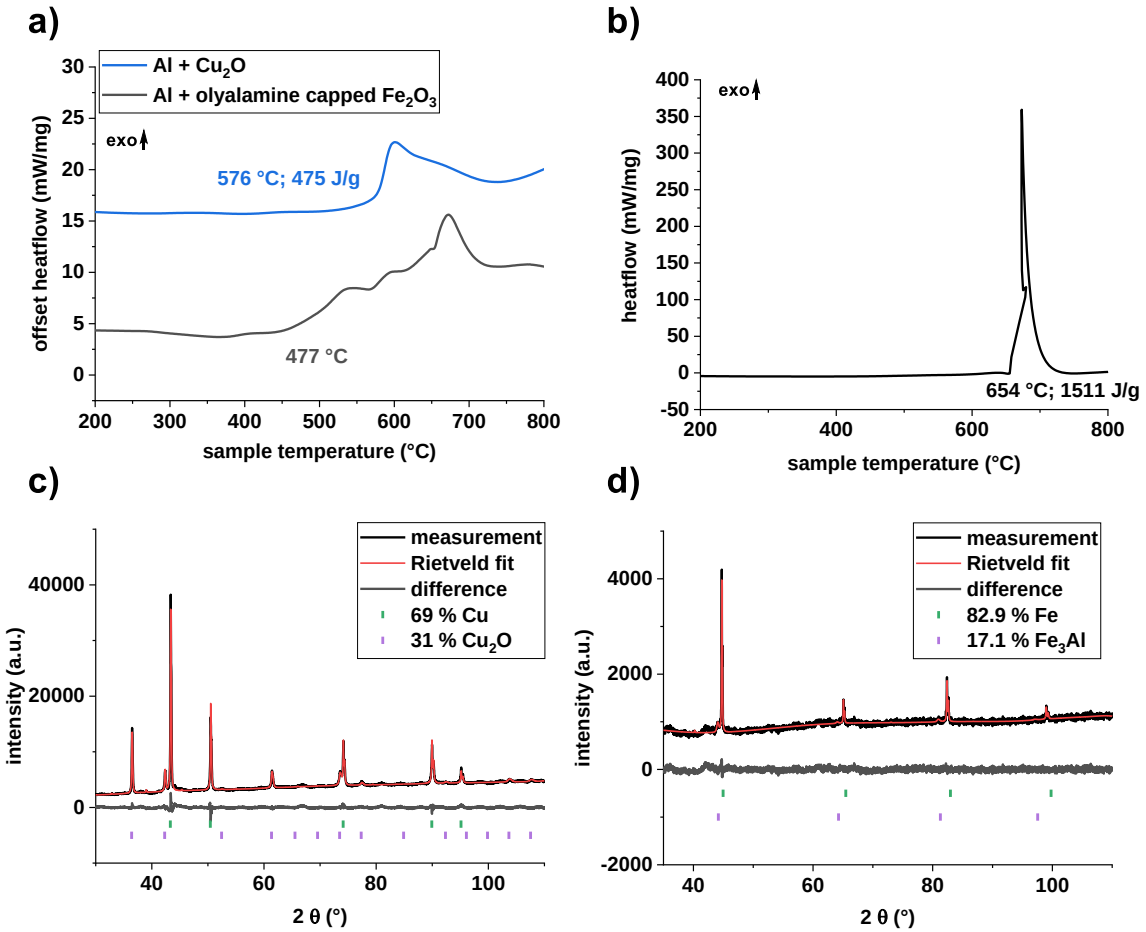

***Figure 62**: STA traces of Al-metal oxide pellets prepared from wet chemically synthesized Al and metal oxide particles **a)** Al - Cu_2O and Al - Fe_2O_3 (800 °C; Ar; 60 K/min), **b)** Al - V_2O_5 (800 °C; Ar; 60 K/min); **c)** and **d)** XRD measurement and Rietveld refinements of the reaction products obtained from the reactions shown in a) and b).*

4. Experimental

The majority of the experimental procedures can be found within the published articles contained in Chapters 3.1.3, 3.1.4, 3.2.3.2 as well as 3.2.4.3[308,309,324,325]**.** Within this chapter only the materials, methods, and syntheses relevant for the results not already described in these chapters will be given.

4.1 Materials

The purity and supplier of the applied reagents is summarized in Table 15. All listed chemicals were used as received without any further purification. Unless stated otherwise all solvents were received from the ZChL and used as received. Dry hexane, THF, diethylether, and toluene were obtained from a MBraun solvent purification system. Oleylamine, tetraglyme, diphenylether, and oleic acid were dried and degassed by heating to 100 °C in vacuo for 2 h and stored over molecular sieves (3 Å). Diphenylether was filtered through 0.45 µm PTFE syringe filters prior to use. PPh_3, PPh_3O and TOPO were dried by heating to 80 °C in vacuo. Fe_2O_3/ Fe_3O_4 nanoparticles with a size of 7 nm were available from a previous work[332].

Table 15*: Purity and supplier of the applied chemicals within this work.*

Chemical	Purity [%]	Supplier
Ag(acac)	98	Sigma-Aldrich (St. Louis, USA)
$AlCl_3$	98.5	Acros Organics (Geel, Belgium)
Al_2O_3-NP (< 50 nm)	n/a	Sigma-Aldrich (St. Louis, USA)
benzyl ether	98	Sigma-Aldrich (St. Louis, USA)
Co	> 99	Sigma-Aldrich (St. Louis, USA)
$Co_2(CO)_8$, stab. with hexanes	95	Acros Organics (Geel, Belgium)
$Cu(acac)_2$	97	Sigma-Aldrich (St. Louis, USA)
diethylene glycol	99.5	TCI (Eschborn, Germany)
diphenylether	99	Alfa-Aesar (Kandel, Germany)
$Fe(acac)_3$	> 99	Acros Organics (Geel, Belgium)
$Fe(CO)_5$	> 95	Acros Organics (Geel, Belgium)
Li	> 98	Sigma-Aldrich (St. Louis, USA)
$LiAlH_4$	95	Sigma-Aldrich (St. Louis, USA)
Ni	> 99	Fluka (Buchs, Switzerland)
$N(Oct)_3$	> 92.5	Merck (Darmstadt, Germany)
oleic acid	90	Alfa-Aesar (Kandel, Germany)

Table 15 *(Continued): Purity and supplier of the applied chemicals within this work.*

Chemical	Purity [%]	Supplier
oleylamine	70	Sigma-Aldrich (St. Louis, USA)
$P(^nBu)_3$	93	abcr (Karlsruhe, Germany)
PPh_3	99 %	Sigma-Aldrich (St. Louis, USA)
PPh_3O	99 %	Alfa-Aesar (Kandel, Germany)
$Re_2(CO)_{10}$	98 %	abcr (Karlsruhe, Germany)
tetraglyme	98 %	abcr (Karlsruhe, Germany)
TOP	97 %	abcr (Karlsruhe, Germany)
TOPO	99 %	Sigma-Aldrich (St. Louis, USA)
triisobutylaluminum (1M in hexane)	---	Sigma-Aldrich (St. Louis, USA)
$VO(O^iPr)_3$	96 %	Alfa-Aesar (Kandel, Germany)
$W(CO)_6$	97 %	Schuchardt (München, Germany)

4.2 Methods

The characterizations were carried out as described in the published articles[308,309,324,325]. The methods relevant for the results not already described in the published papers will be briefly summarized below.

Elemental analyses (CHN analyses) were carried out on an Elementar Vario Micro Cube.

Powder X-ray diffractograms were recorded on a Bruker D8-A25-Advance diffractometer in a Bragg-Brentano geometry using Cu K_α-radiation (λ = 1.5406 Å). A 2θ range from 7 to 120 °, a step size of 0,013 ° as well as a total measurement time of 1 h were applied. The specimens were prepared by drop coating the dispersed samples on glass sample holders. Alternatively, standard steel sample holders were applied for larger sample amounts. Rietveld refinements using TOPAS 5.1[335] were carried out to determine the sample compositions. The background was fitted using a Chebychev polynom (15th degree) and a fundamental parameter approach[336] was chosen to take into account the instrumental line broadening. Literature known crystal structures from the crystallographic open database (COD)[337], the inorganic crystal structure database (ICSD) or the materials project[338] were applied to conduct the Rietveld refinements. Entries with the following ID's were applied: Al 2300250 (*Fm*$\bar{3}$*m*; COD), Ni 2100640 (*Fm*$\bar{3}$*m;* COD), NiAl 9008802 (*Pm*$\bar{3}$*m;* COD), Ni_3Al 20000627 (*Pm*$\bar{3}$*m;* COD), $NiAl_3$ 58040 (*Pnma;* ICSD), Ni_2Al_3 mp-1057 (*P*$\bar{3}$*m*1*;* materials project), Ni_3P 9011823 (*I*$\bar{4}$*;* COD), Ag_2Al 1509011 (*P*6$_3$/*mmc;* COD), γ-Al_2O_3 2107301 (*Fd*$\bar{3}$*m;* COD), Ru 1539052 (*P*6$_3$/*mmc;* COD), RuAl 1527371 (*Pm*$\bar{3}$*m;* COD), $RuAl_2$ 58156 (*Fddd*; ICSD), Ru_4Al_{13} 58158 (*P*$\bar{3}$*m*1; ICSD), Ru_2Al_3 609226 (*I*4/*mmm*; ICSD), AlCo 57596 (*Pm*$\bar{3}$*m;* ICSD), Co 1534891 (*Fm*$\bar{3}$*m;* COD), Al_5Co_2 109470 (*P*6$_3$/*mmc;* ICSD), $Al_{13}Co_4$ 104638 (*Pmn*2$_1$; ICSD), Fe

230020 (*Im*$\bar{3}$*m;* COD), FeAl 1541193 (*Pm*$\bar{3}$*m;* COD), Fe_2Al_5 57796 (*Cmcm*; ICSD), $AlFe_3$ 607483 (*Fm*$\bar{3}$*m;* ICSD), $FeAl_3$ 57795 (*C*12/*m*1; ICSD), Fe_2O_3 101240 (*R*$\bar{3}$*c:R;* COD), Fe_3AlC 43853 (ICSD), Al_4C_3 2310414 (COD), Al_5W 58206 (ICSD), CuAl 40332 (ICSD), Ag_2Al 1509011 (*Pm*$\bar{3}$*m;* COD), Ag 1100136 (*Fm*$\bar{3}$*m;* COD), Al_2Pt 58132 (*Fm*$\bar{3}$*m;* ICSD), Al_2CO 1537347 (*P*6$_3$*mc;* COD), SiO_2 1010944 (*Fd*$\bar{3}$*m;* COD), Cu 4105040 (*Fm*$\bar{3}$*m;* COD), Cu_2O 1010941 (*Pn*$\bar{3}$*m* COD), AlCu (C12/m1; ICSD).

TEM images were taken on a JEOL JEM-2010 electron microscope and an accelerating voltage of 200 kV was applied. The samples were prepared from the dispersed nanoparticles in hexane or methanol by drop coating onto carbon coated copper grids followed by air drying. A JEOL JSM-7000F scanning electron microscope was applied to record the SEM images of the dried samples without any pretreatment. The particle size distributions were determined from the TEM or SEM images by measuring at least 100 particles using the software ImageJ[339].

A FEI Helios NanoLab600 was applied to carry out the focused ion beam (FIB) measurements using a gallium ion beam at an observation angle of 52 °. Prior to the measurements, the samples were contacted with conductive carbon.

Thermogravimetric analyses (TGA) were conducted on a TG F1 Iris from Netzsch. The measurements were carried out in a constant flow of N_2/O_2 32:8 (40 ml/min) or N_2 (40 ml/min) using a heating rate of 10 K/min in open alumina crucibles. Buoyancy effects occurring during the measurements were corrected by subtracting a measurement of an empty crucible measured with the same temperature program. A temperature calibration was carried out employing In, Sn, Zn, Bi, Al and Ag melt standards. From the TGA traces Al^0 contents were calculated as described in Chapter 1.5.1.

Simultaneous thermal analyses (STA) were carried out on a Mettler-Toledo STAre system. The measurements were carried out in open alumina crucibles in a constant flow of Ar (40 ml/min). Heating rates ranging from 5 K/min to 60 K/min were used and the maximum temperature in the measurements was 800 °C. For all samples, a second scan was used as a background after the absence of any signals (particularly Al melting) was confirmed. The tau lag, the sample temperature and the heatflow was calibrated applying Al, Au, In and Zn melt standards.

An ALV Compact Goniometer was applied to carry out the dynamic light scattering (DLS) measurements. They were conducted at room temperature at a scattering angle of 90 °. Prior to the measurements, the particles were dispersed in methanol or hexane, ultrasonicated for 10 min, filtered through 0.45 µm PTFE filters and equilibrated for 5 min at room temperature.

ATR-FTIR spectra were recorded on A Bruker Vertex 70 spectrometer in an atmosphere of ambient air or flowing Ar. The spectra were obtained as an average of 16 scans for both, the background, and the

sample. The measurements were carried out in a wavelength range of 4000 – 400 cm^{-1} applying a resolution of 4 cm^{-1} in a DIAMOND ATR-QL measurement cell from Bruker.

An AV400WB spectrometer from Bruker was used to carry out the solid-state ^{27}Al SPE-MAS and ^{31}P CPMAS NMR spectra. The measurements were conducted in ZrO_2 rotors applying a rotation of 13 kHz. ^{31}P spectra were recorded at 162 MHz and ^{27}Al spectra at 104 MHz. 85 % H_3PO_4 was used as an external standard for the ^{31}P NMR spectra, while an $AlCl_3$ solution (1 M in H_2O) was used as a standard for the ^{27}Al spectra.

Ignition temperatures of the compacted pellets in an atmosphere of ambient air were determined by dropping small pellet pieces (1 – 2 mg) onto a hot plate preheated to a set temperature. The experimental setup is described in Chapter 1.5.3. An ignition and thus a reaction of the powder mixture could be recognized with the naked eye by the formation of sparks. If no reaction was observed, the temperature of the plate was raised, and the procedure was repeated. The ignition temperature was then determined as the median of the lowest temperature at which an ignition was observed and the highest temperature at which no ignition was observed. At around the observed onset temperature, the temperature of the hot plate was generally increased in increments < 5 °C to allow a precise determination of the individual ignition temperature. In these measurements a constant temperature distribution in the reaction spot (Ø 2 cm) was assumed and the set temperature of the PID controller was assumed to be the surface temperature. The reaction onset temperatures in an atmosphere of Ar were determined from the STA traces as the onset of the corresponding exothermic signals.

4.3 Syntheses

Al particles via metal reduction

550 mg (4 mmol) of $AlCl_3$ were dissolved in 20 ml of THF. 100 mg of Li (14 mmol) were added in small pieces and the mixture was heated to reflux for 3 h. The formed black solid was separated via centrifugation (8000 rpm; 10 min) and washed three times with 15 ml of isopropanol (8000 rpm; 10 min). The solid was dried at room temperature in vacuo.

For the preparation of oleic acid capped Al powder, a similar procedure was applied. After heating to reflux for 3 h, 2 ml of oleic acid were added, and the mixture was stirred at room temperature overnight. The isolation of the formed Al particles was carried out as described above.

Yield: 59 mg black solid (10 % based on Al^0).

Al particles via hydride reduction

The particles were synthesized following a modified literature procedure[340]. Briefly, 0.54 g (14 mmol) of $LiAlH_4$, 0.46 g (3 mmol) $AlCl_3$, and the desired amount of phosphine stabilizer were dissolved in 120 ml of mesitylene. The reaction mixture was heated to 165 °C for 1 h and the formed solid was collected by centrifugation (12000 rpm; 10 min). The obtained grey solid was washed twice with methanol (20 ml), twice with THF (20 ml) and dried in vacuo at room temperature.

Yield: 363 mg grey solid (61 % based on Al^0) (for PPh_3 stabilized Al particles).

Al particles via catalytic decomposition

The synthesis is described in Chapter 3.1.3[308].

Al particles via thermal decomposition

The synthesis is described in Chapter 3.1.4[309].

Ni nanoparticles

The synthesis is described in Chapter 3.2.3.2 and was carried out following known literature procedures[310].

The syntheses applying PPh_3 were carried out analogously applying PPh_3 instead of TOP.

Mechanochemical synthesis of Ru (Ru nanopowder)

The synthesis is described in Chapter 3.1.4 and was carried out following known literature procedures[319].

Ag nanoparticles

The synthesis is described in Chapter 3.1.4 and was carried out following known literature procedures[341].

Synthesis of Ru nanoparticles via reduction of $RuCl_3$

The synthesis was carried out according to known literature methods[313]. 800 mg (3 mmol) $RuCl_3 \cdot H_2O$ were added to 80 ml oleylamine and degassed for 30 min at a temperature of 30 °C. The mixture was heated to 350 °C for 1 h. After cooling to room temperature, the Ru nanoparticles were precipitated by adding 80 ml ethanol and isolated by centrifugation (8000 rpm; 10 min). The particles were washed three times with methanol (8000 rpm; 10 min) and dried in vacuo at 80 °C.

Yield: 656 mg brown gel (52 % based on Ru^0).

Synthesis of Ru nanoparticles via decomposition of $Ru(acac)_3$

The synthesis was carried out according to known literature methods[314]. 1.22 g (3 mmol) $Ru(acac)_3$ were added to 80 ml oleylamine and degassed in vacuo at 70 °C for 30 min. The mixture was heated for 1 h to 120 °C before the temperature was increased to 300 °C for 1 h. After cooling to room temperature, the Ru nanoparticles were precipitated by adding 80 ml ethanol and isolated by centrifugation (8000 rpm; 10 min). The resulting black solid was washed by three cycles of redispersing in 5 ml of hexane, precipitating with 40 ml of acetone, and centrifugation (8000 rpm; 10 min). The particles were dried in vacuo at 80 °C.

Yield: 2.4 g brown gel (70 % based on Ru^0)

Synthesis of Ru nanoparticles via decomposition of $Ru_3(CO)_{12}$

The synthesis is described in Chapter 3.2.4.3[325].

Synthesis of Fe nanoparticles via $NaBH_4$ reduction

The particles were synthesized following a modified literature procedure[327]. 1.1 g (4 mmol) $FeSO_4 \cdot 7H_2O$ and 0.23 g (0.8 mmol) sodium dodecyl sulfate were dissolved in 100 ml H_2O/ EtOH (3:1 v/v). 0.57 g (15 mmol) of $NaBH_4$ was dissolved in 20 ml of cold water and added dropwise to the above mixture under stirring. The formed black solid was magnetically separated, washed three times with 40 ml ethanol and dried in vacuo.

Yield: 195 mg black solid (87 %)

Synthesis of Fe nanoparticles via decomposition of $Fe(CO)_5$

The synthesis was carried out according to known literature methods[48]. 20 ml 1-octadecene and 0.3 ml (1 mmol) oleylamine were degassed at 120 °C for 30 min and then heated to a temperature of 180 °C. At this temperature 0.7 ml (5 mmol) $Fe(CO)_5$ were injected and the mixture was stirred at 180 °C for an additional 20 min. The formed black solid was magnetically separated, washed 3 times with 20 ml of hexane and dried in vacuo at 80 °C.

Yield: 167 mg black solid (60 %)

Nanocrystalline Cu_2O

The synthesis was carried out according to published literature methods[333]. Briefly, 600 mg (2.3 mmol) of $Cu(acac)_2$ were dispersed in 50 ml of diethylene glycol. 2 ml H_2O were added, and the mixture was heated to 180 °C for 5 h. After cooling to room temperature, the mixture was centrifuged (13000 rpm; 10 min) and washed 3 times with 20 ml of ethanol (13000 rpm; 10 min). The resulting solid was dried in vacuo at room temperature.

Yield: 57 mg red/ brown solid (35 %)

Nanocrystalline V_2O_5

V_2O_5 was synthesized according to published literature procedures[334]. Briefly, 3.9 g (16 mmol) $VO(^iOiPr)_3$ were dissolved in 50 ml of diethylene glycol. 2 ml of H_2O were added, and the reaction mixture was heated to 180 °C for 6 h. After cooling to room temperature, the mixture was centrifuged (13000 rpm; 10 min) and the resulting solid was washed 3 times with 20 ml of ethanol (13000 rpm; 10 min). The resulting solid was dried in vacuo at room temperature and sintered for 30 min at 450 °C in an atmosphere of ambient air.

Yield: 1.04 g yellow solid (71 %)

Pellet preparation

For the preparation of pellets starting from separately synthesized Al and metal particles, both reactants were dispersed in hexane, thoroughly mixed in an agate mortar or an ultrasonication bath (10 min) and allowed to air dry. Prior to the mixing the Al^0 content of the Al particles was determined from TG measurements to allow the preparation of pellets with exact stoichiometries.

The pellets were then prepared from the resulting mixtures or directly from the particle mixtures prepared via the two-step synthesis protocol developed within this work applying a hydraulic press. Unless stated otherwise, at about 15 mg of powder were compacted by a piston with a diameter of 6 mm for 10 min applying a pressure of 350 MPa.

Aluminide preparation

The aluminides were typically prepared starting from the pellets prepared as described above. For the preparation in an atmosphere of flowing Ar (40 ml/min), a 3 – 15 mg portion of the pellet was placed in an open alumina crucible which was heated in a TGA/DSC thermal analyzer. Typically, the sample was heated up to a temperature of 800 °C applying heating rates ranging from 5 to 60 K/min. The cooling was carried out with a heating rate of 20 K/min and a second heating cycle was carried out for background correction in all samples. The preparation in an atmosphere of ambient air was carried out on a hot plate as described above.

Al-polystyrene mixtures

In a first step, Al particles were prepared via the thermal decomposition approach as described in Chapter 3.1.4. The resulting Al particles were separated from the diphenylether solvent by centrifugation (8000 rpm; 10 min) and washed three times with 20 ml of toluene. The desired amount of polystyrene was dissolved in 20 ml of toluene and added to the prepared Al particles. The mixture was homogenized for 30 min in an ultrasonication bath and the toluene was removed in vacuo. The formed Al-polystyrene mixtures were dried in vacuo at room temperature.

Oxidation of Al particles with HNO_3

The oxidation was carried out according to reports in the literature[323]. In a first step, Al particles were prepared via the thermal decomposition approach as described in Chapter 3.1.4, including the separation and drying steps. 35 mg of the resulting particles were stirred for 10 and 20 min in

concentrated HNO_3 (69 wt%). The particles were separated by centrifugation (8000 rpm; 10 min), washed two times with H_2O (8000 rpm; 10 min) and dried in vacuo at 80 °C.

Al-Ni particle mixtures

The synthesis is described in Chapter 3.2.3.2[324].

Al-Ru particle mixtures

The synthesis is described in Chapter 3.2.4.3[325].

Al-Co particle mixtures

The synthesis was carried by adapting the method applied for the preparation of the Ni-Al mixtures[324]. 60 ml of diphenylether were degassed at 100 °C for 30 min. After cooling to 40 °C, 2 ml of triisobutylaluminium (1 M in hexane) (2 mmol) and 3 mg (0.03 mmol) of Ru nanopowder were added. The hexane was removed in vacuo and the mixture was homogenized using an ultrasonication bath for 15 min. The mixture was refluxed for 15 min resulting in the formation of submicron Al particles. After cooling to room temperature 0.26 g (1.5 mmol) $Co_2(CO)_8$ were added and the mixture was heated to 220 °C for 2 h. The formed solid was centrifuged (8000 rpm; 10 min), washed three times with 15 ml of toluene (8000 rpm; 10 min) and dried in vacuo at room temperature.

Yield: 151 mg black solid.

Al-Fe particle mixtures

The synthesis was carried by adapting the method applied for the preparation of the Ni-Al mixtures[324]. 60 ml of diphenylether were degassed at 100 °C for 30 min. After cooling to 40 °C 2 ml, of triisobutylaluminium (1 M in hexane) (2 mmol) and 3 mg (0.03 mmol) of Ru nanopowder were added. The hexane was removed in vacuo and the mixture was homogenized using an ultrasonication bath for 15 min. The mixture was refluxed for 15 min resulting in the formation of submicron Al particles. After cooling to room temperature 0.3 ml (1.5 mmol) $Fe(CO)_5$ were added and the mixture was heated to 205 °C for 2 h. In alternative synthesis approaches, the $Fe(CO)_5$ was injected at a temperature of 175 °C or decomposed at 180 °C in the presence of an additional 20 ml of oleylamine. In all samples, the

formed solid was centrifuged (8000 rpm; 10 min), washed three times with 15 ml of toluene (8000 rpm; 10 min) and dried in vacuo at room temperature.

Yield: 120 mg black solid.

Al-W particle mixtures

The synthesis was carried by adapting the method applied for the preparation of the Ni-Al mixtures[324]. 60 ml of diphenylether were degassed at 100 °C for 30 min. After cooling to 40 °C 2 ml, of triisobutylaluminium (1 M in hexane) (2 mmol) and 3 mg (0.03 mmol) of Ag nanoparticles were added. The hexane was removed in vacuo and the mixture was homogenized using an ultrasonication bath for 15 min. The mixture was refluxed for 15 min resulting in the formation of submicron Al particles. After cooling to room temperature 0.5 g (1.5 mmol) $W(CO)_6$ were added and the mixture was heated to 230 °C for 2 h. The formed solid was centrifuged (8000 rpm; 10 min), washed three times with 15 ml of toluene (8000 rpm; 10 min) and dried in vacuo at room temperature.

Yield: 45 mg grey solid.

Al-Re particle mixtures

The synthesis was carried by adapting the method applied for the preparation of the Ni-Al mixtures[324]. 60 ml of diphenylether were degassed at 100 °C for 30 min. After cooling to 40 °C 2 ml, of triisobutylaluminium (1 M in hexane) (2 mmol) and 3 mg (0.03 mmol) of Ru nanoparticles were added. The hexane was removed in vacuo and the mixture was homogenized using an ultrasonication bath for 15 min. The mixture was refluxed for 15 min resulting in the formation of submicron Al particles. After cooling to room temperature 0.49 g (1.5 mmol) $Re_2(CO)_{10}$ were added and the mixture was heated to 250 °C for 3 h. The formed solid was centrifuged (8000 rpm; 10 min), washed three times with 15 ml of toluene (8000 rpm; 10 min) and dried in vacuo at room temperature.

Yield: 32 mg, grey solid.

Al-Ag particle mixtures

The synthesis was carried out by adapting the method applied for the preparation of the Ni-Al mixtures[324]. 60 ml of diphenylether were degassed at 100 °C for 30 min. After cooling to 40 °C, 2 ml of triisobutylaluminium (1 M in hexane) (2 mmol) and 3 mg (0.03 mmol) of Ru nanoparticles were added. The hexane was removed in vacuo and the mixture was homogenized using an ultrasonication bath for 15 min. The mixture was refluxed for 15 min resulting in the formation of submicron Al particles. After cooling to room temperature 0.64 g (1.5 mmol) Ag(acac) were added and the mixture was heated to 200 °C for 2 h. The formed solid was centrifuged (13000 rpm; 10 min), washed three times with 15 ml of toluene (13000 rpm; 10 min) and dried in vacuo at room temperature.

Yield: 350 mg grey solid.

Al-Cu particle mixtures

The synthesis was carried out by adapting the method applied for the preparation of the Ni-Al mixtures[324]. 60 ml of diphenylether were degassed at 100 °C for 30 min. After cooling to 40 °C, 2 ml of triisobutylaluminium (1 M in hexane) (2 mmol) and 3 mg (0.03 mmol) of Ru nanoparticles were added. The hexane was removed in vacuo and the mixture was homogenized using an ultrasonication bath for 15 min. The mixture was refluxed for 15 min resulting in the formation of submicron Al particles. After cooling to room temperature 0.36 g (1.5 mmol) $Cu(acac)_2$ were added and the mixture was heated to 260 °C for 3 h. The formed solid was centrifuged (13000 rpm; 10 min), washed three times with 15 ml of toluene (13000 rpm; 10 min) and dried in vacuo at room temperature.

Yield: 152 mg red-brown solid.

Al-Pt particle mixtures

The synthesis was carried out by adapting the method applied for the preparation of the Ni-Al mixtures[324]. 60 ml of diphenylether were degassed at 100 °C for 30 min. After cooling to 40 °C, 2 ml of triisobutylaluminium (1 M in hexane) (2 mmol) and 3 mg (0.03 mmol) of Ru nanoparticles were added. The hexane was removed in vacuo and the mixture was homogenized using an ultrasonication bath for 15 min. The mixture was refluxed for 15 min resulting in the formation of submicron Al particles. After cooling to room temperature 0.95 g (2 wt% Pt) Karstedt`s catalyst was added, and the mixture was heated to 250 °C for 3 h. The formed solid was centrifuged (13000 rpm; 10 min), washed three times with 15 ml of toluene (13000 rpm; 10 min) and dried in vacuo at room temperature.

Yield: 34 mg black solid.

5. Summary and Outlook

Summary

Ni and Ru aluminides were successfully prepared starting from wet chemically synthesized Al and Ni or Ru particles. The Al particles applied for this purpose were synthesized applying metal reduction, hydride reduction and catalytic decomposition approaches as well as a thermal decomposition approach developed within this work. Particularly the catalytic and thermal decomposition approaches were studied in more detail.

Al nanoparticles were prepared via the catalytic decomposition approach. The reaction conditions were systematically studied and optimized regarding homogenous reaction mixtures, short reaction times, small particle sizes of 30 – 50 nm as well as mild reaction temperatures. For this purpose, various reaction parameters including the Al precursor, the decomposition catalyst, the reaction temperature, the solvent, the stabilizer as well as the reactant concentrations were systematically varied. The application of Ti catalysts should be preferred over other Lewis acid catalysts for which increased reaction times were necessary. Bulky Ti catalysts like $Ti(O^tBu)_4$ were slightly less efficient and resulted in the formation of larger particles compared to smaller catalysts like $Ti(O^iPr)_4$. The application of increased temperatures >90 °C was necessary to achieve a fast decomposition (<15 min). Similarly, the shortest reaction times as well as the smallest particles were observed upon applying nonpolar solvents such as toluene or cyclohexane. In contrast, significantly decreased decomposition rates were observed upon applying polar solvents, resulting in incomplete reactions after a reaction time of 15 min. The application of bulky alane precursors resulted in the formation of products with a complex, network-like morphology, while small, non-agglomerated particles were obtained from small alane precursors such as H_3AlNEt_3 or $H_3Al(THF)$. Within the reaction system studied in this work, PPh_3 as well as $N(Oct)_3$ were identified as suitable stabilizers, which were largely removed during the clean-up procedures and resulted in a content of organics <10 %. Moreover, a decrease of the particle size as well as a narrowing of the particle size distribution was observed upon decreasing the precursor concentration or upon increasing the concentration of the decomposition catalyst. Considering the requirements and results summarized above, the most promising results were obtained by applying an increased reaction temperature of 90 °C in toluene solutions, a concentration of 35 ppm of a $Ti(O^iPr)_4$ catalyst, and a concentration of 35 mM of a H_3AlNEt_3 or a $H_3Al(THF)$ precursor in the presence of 5 eq PPh_3 acting as a stabilizer. These conditions resulted in the formation of nanoparticles with a size of 35 nm within a short reaction time of < 15 min.

A thermal decomposition approach for the preparation of Al particles was developed. Within this approach, triisobutylalumium was thermally decomposed in refluxing diphenylether in the presence

of nanoparticulate seeds of Ni, Ru and Ag within 15 min. No additional stabilizers were necessary during this synthesis and the resulting submicron Al particles exhibited sizes of about 100 – 250 nm, Al^0 contents of about 80 wt% as well as very low organic contents < 5 %. However, a capping with oleic acid was also possible in a second, optional synthesis step. The size of the resulting particles was decreased to about 70 nm by the addition of PPh_3 during the decomposition. The content of the seed metal within in the final product could be reduced by applying the resulting particles themselves as seeds. A decrease of the particle size as well as narrower particle size distributions were observed when the triisobutylalumium was injected into the reaction mixture at an increased temperature of 270 °C.

The performance of the Al particles prepared from the different synthesis approaches for the preparation of Ni and Ru aluminides was studied. The most promising results regarding complete reactions, high yields and low oxidic contents were observed upon applying the submicron Al particles prepared via the thermal decomposition approach. This was attributed to the low organic and oxidic contents of these particles, since high contents of organics and oxides were found to have a negative influence on the aluminide formation, ultimately resulting in incomplete reactions.

For the preparation of Ni aluminides starting from separately prepared Ni and Al particles, the formation of multiphase products was observed upon applying small sample amounts. This was ascribed to heat loss effects ultimately resulting in incomplete reactions. Thus, a one-pot, two-step synthesis protocol was developed, which resulted in the deposition of small Ni crystallites with a size of about 2 nm on the surface of Al particles with a size of about 150 nm. In a first step, submicron Al particles were prepared via thermal decomposition of triisobutylaluminum in refluxing diphenylether in the presence of nanoparticulate Ni seeds before in a second step, Ni was deposited via a thermal decomposition of $Ni(COD)_2$. Upon heating the resulting mixtures to 800 °C in an Ar atmosphere or to 600 °C on a hot plate, the formation of products containing NiAl as the only crystalline phase was observed, which can likely be attributed to the excellent interelemental contact as well as mixing. Besides, due the application of oxide passivated Al particles, at about 20 % of amorphous Al_2O_3 was detected within these samples.

For the formation of Ru aluminides, an analogous one-pot, two-step synthesis protocol was developed. Again, in a first step, submicron Al particles with a size of about 150 nm were prepared via thermal decomposition of triisobutylaluminum in refluxing diphenylether, before in a second step, Ru was prepared by adding and decomposing $Ru_3(CO)_{12}$ in oleylamine solutions at a temperature of 220 °C. The resulting Ru nanoparticles exhibited sizes of 6.4 ± 0.8 nm and upon heating the resulting particle mixtures in an atmosphere of Ar to a temperature of 800 °C, the formation of Ru aluminides was observed starting at a temperature of about 600 °C. In contrast, on a hot plate in an atmosphere of

ambient air, the onset of the reaction was found to occur at temperatures as low as 300 °C, which was attributed to additional heat released during the decomposition of residual organics as well as to an oxidation of the Ru nanoparticles.

The general applicability of the developed two-step synthesis protocol for the preparation of various other aluminides was moreover shown by a successful preparation of Co, Ag, Cu and Fe aluminides.

Outlook

One aspect on which future work might be focused is the reduction of the oxide content within the prepared aluminides, which can possibly be achieved via various synthetic approaches. The first and most obvious approach is the simple repetition of the work presented throughout this work under strictly air-free conditions, particularly including the pellet preparation steps. Alternatively, the synthesis of core-shell particles, ideally with the shell consisting of the less air sensitive compound, or the application of Al rich aluminides as Al sources would be plausible approaches (Figure 63). Besides the lower oxide contents, the intermixing as well as the interelemental contact can also be expected to significantly improve compared to the particle mixtures applied throughout this work upon applying such core-shell morphologies. Ultimately, these different approaches might be compared regarding the resulting products as well as the influence of the oxide shell during the combustion reaction. Moreover, particularly the performance of the core-shell systems, which can be considered as a particulate equivalent to the commonly applied multilayer systems, should be evaluated in comparison to these systems.

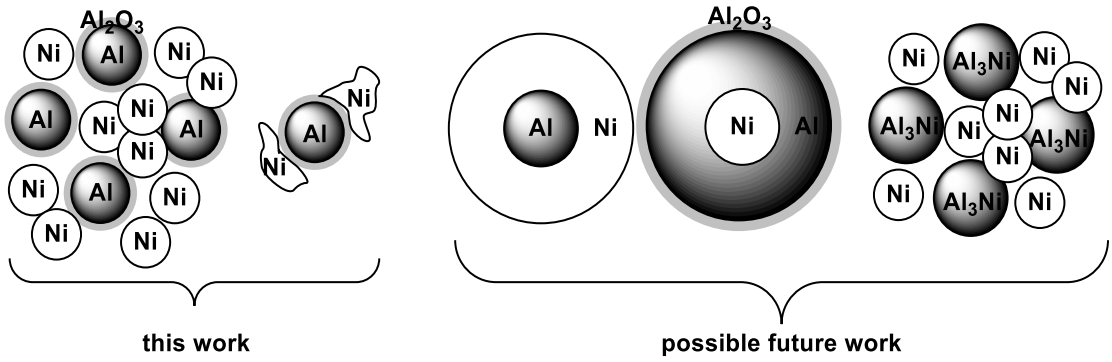

***Figure 63**: Plausible precursors for the preparation of oxide free aluminides.*

Since wet chemical synthesis methods allow a facile functionalization of the prepared nanoparticles, a method for the preparation of well dispersed particle mixtures in various solvents such as hexane or ethanol should be developed. As aluminides are typically applied as coating materials for many materials, the suitability of such particle dispersions for the preparation of aluminide coatings might

be examined. The preparation of aluminide coatings via facile processes such as dip, spray or spin coating would represent a convenient and fast method even for coating components with large or very complex geometries. Simultaneously, a scale-up of the methods developed within the present work might be carried out in order to increase the sample amounts obtainable via the wet chemical methods and ideally, a synthesis would be possible applying a continuous wet chemical synthesis approach.

In addition, Al is known to form intermetallic compounds with many more elements. As was shown within this work, the preparation of these compounds starting from wet chemically synthesized powders is not straightforward and tailored approaches might be necessary for many of these compounds. As was shown, their synthesis is generally possible, however further studies would be necessary to develop synthesis approaches suitable for the preparation of additional aluminides in high yields.

Another field of application for which Al particles are commonly applied, but which was not studied in detail within this work, is the field of aluminothermic reactions. Accordingly, in a future work, the suitability of the Al particles prepared via the different synthesis methods for the preparation of various metals by aluminothermic reactions might be evaluated and the influence of various parameters, such as for example particle sizes, organic and oxide contents as well as the applied temperature programs might be studied. Ultimately, similar as described above, Al core- metal oxide shell particles might be synthesized and their applicability within these reactions may be evaluated.

6. References

(1) ISO/TS 80004-2:2015 Nanotechnologies - Vocabulary - Part 2: Nano-Objects.

(2) Hsu, C. Y.; Chan, Y. P. Identification and Localization of Proteins Associated with Biomineralization in the Iron Deposition Vesicles of Honeybees (Apis Mellifera). *PLoS One* **2011**, *6*, e19088.

(3) Tepe, N.; Bau, M. Importance of Nanoparticles and Colloids from Volcanic Ash for Riverine Transport of Trace Elements to the Ocean: Evidence from Glacial-Fed Rivers after the 2010 Eruption of Eyjafjallajökull Volcano, Iceland. *Sci. Total Environ.* **2014**, *488–489*, 243–251.

(4) Krukemeyer, M.; Krenn, V.; Huebner, F.; Wagner, W.; R, R. History and Possible Uses of Nanomedicine Based on Nanoparticles and Nanotechnological Progress. *J. Nanomed. Nanotechnol.* **2015**, *06*, 1000336.

(5) Bayda, S.; Adeel, M.; Tuccinardi, T.; Cordani, M.; Rizzolio, F. The History of Nanoscience and Nanotechnology: From Chemical-Physical Applications to Nanomedicine. *Molecules* **2020**, *25*, 1–15.

(6) Hulla, J. E.; Sahu, S. C.; Hayes, A. W. Nanotechnology: History and Future. *Hum. Exp. Toxicol.* **2015**, *34*, 1318–1321.

(7) Nanotechnology Timeline https://www.nano.gov/timeline (accessed Jun 4, 2020).

(8) Freestone, I.; Meeks, N.; Sax, M.; Higgitt, C. The Lycurgus Cup - A Roman Nanotechnology. *Gold Bull.* **2007**, *40*, 270–277.

(9) Leonhardt, U. Invisibility Cup. *Nat. Photonics* **2007**, *1*, 207–208.

(10) Pérez-Arantegui, J.; Molera, J.; Larrea, A.; Pradell, T.; Vendrell-Saz, M.; Borgia, I.; Brunetti, B. G.; Cariati, F.; Fermo, P.; Mellini, M.; et al. Luster Pottery from the Thirteenth Century to the Sixteenth Century: A Nanostructured Thin Metallic Film. *J. Am. Ceram. Soc.* **2001**, *84*, 442–446.

(11) Horikoshi, S.; Serpone, N. Introduction to Nanoparticles. In *Microwaves in Nanoparticle Synthesis: Fundamentals and Applications*; Wiley VCH: Weinheim, 2013; pp 1–24.

(12) https://commons.wikimedia.org/wiki/File:British_Museum_The_Lycurgus_Cup_03_15022019_4320.jpg (accessed Dec 13, 2019).

(13) https://commons.wikimedia.org/wiki/File:Lusterware_Tile_MET_DP140850.jpg (accessed Dec 13, 2019).

(14) https://commons.wikimedia.org/wiki/File:Paryż_notre-dame_witraż.JPG (accessed Dec 13, 2019).

(15) Faraday, M. The Bakerian Lecture : Experimental Relations of Gold (and Other Metals) to Light. *Philos. Trans. R. Soc. London* **1857**, *147*, 145–181.

(16) Siedentopf, H.; Zsigmondy, R. Über Sichtbarmachung Und Größenbestimmung Ultramikroskopischer Teilchen, Mit Besonderer Anwendung Auf Godrubingläser. *Ann. Phys.* **1902**, *315*, 1–39.

(17) https://www.nobelprize.org/prizes/chemistry/1925/summary/ (accessed Nov 15, 2019).

(18) Feynman, R. P. There's Plenty of Room at the Bottom. *J. Eng. Sci.* **1960**, *4*, 22–36.

(19) Roduner, E. Size Matters: Why Nanomaterials Are Different. *Chem. Soc. Rev.* **2006**, *35*, 583–592.

(20) Rumble, J. R.; Lide, D. R.; Bruno, T. J. *Handbook of Chemistry and Physics*, 98th ed.; CRC Press: Boca Raton, 2017.

(21) Sun, J.; Simon, S. L. The Melting Behavior of Aluminum Nanoparticles. *Thermochim. Acta* **2007**, *463*, 32–40.

(22) Puri, P.; Yang, V. Effect of Particle Size on Melting of Aluminum at Nano Scales. *J. Phys. Chem. C* **2007**, *111*, 11776–11783.

(23) Hunt, E. M.; Plantier, K. B.; Pantoya, M. L. Nano-Scale Reactants in the Self-Propagating High-Temperature Synthesis of Nickel Aluminide. *Acta Mater.* **2004**, *52*, 3183–3191.

(24) Gangopadhyay, S.; Gangopadhyay, K.; Thiruvengadathan, R.; Bezmelnitsyn, A. Nanothermite Thrusters with a Nanothermite Propellant. US Patent US20110167795 A1, 2011.

(25) Glavier, L.; Nicollet, A.; Jouot, F.; Martin, B.; Barberon, J.; Renaud, L.; Rossi, C. Nanothermite/RDX-Based Miniature Device for Impact Ignition of High Explosives. *Propellants, Explos. Pyrotech.* **2017**, *42*, 308–317.

(26) Ekinci, Y.; Solak, H. H.; Löffler, J. F. Plasmon Resonances of Aluminum Nanoparticles and Nanorods. *J. Appl. Phys.* **2008**, *104*, 083107.

(27) Sharma, V.; Chotia, C.; Tarachand; Ganesan, V.; Okram, G. S. Influence of Particle Size and Dielectric Environment on the Dispersion Behaviour and Surface Plasmon in Nickel Nanoparticles. *Phys. Chem. Chem. Phys.* **2017**, *19*, 14096–14106.

(28) Liu, P.; Wang, H.; Li, X.; Rui, M.; Zeng, H. Localized Surface Plasmon Resonance of Cu Nanoparticles by Laser Ablation in Liquid Media. *RSC Adv.* **2015**, *5*, 79738–79745.

(29) Zhang, J.; Lan, C. Q. Nickel and Cobalt Nanoparticles Produced by Laser Ablation of Solids in Organic Solution. *Mater. Lett.* **2008**, *62*, 1521–1524.

(30) Noguez, C. Surface Plasmons on Metal Nanoparticles: The Influence of Shape and Physical Environment. *J. Phys. Chem. C* **2007**, *111*, 3806–3819.

(31) Sun, Y.; Xia, Y. Shape-Controlled Synthesis of Gold and Silver Nanoparticles. *Science* **2002**, *298*, 2176–2179.

(32) Xia, Y.; Xiong, Y.; Lim, B.; Skrabalak, S. E. Shape-Controlled Synthesis of Metal Nanocrystals: Simple Chemistry Meets Complex Physics? *Angew. Chemie - Int. Ed.* **2009**, *48*, 60–103.

(33) Zeng, W.; Buckner, S. W.; Jelliss, P. A. Poly(Methyl Methacrylate) as an Environmentally Responsive Capping Material for Aluminum Nanoparticles. *ACS Omega* **2017**, *2*, 2034–2040.

(34) Schöttle, C.; Bockstaller, P.; Popescu, R.; Gerthsen, D.; Feldmann, C. Sodium-Naphthalenide-Driven Synthesis of Base-Metal Nanoparticles and Follow-up Reactions. *Angew. Chemie Int. Ed.* **2015**, *54*, 9866–9870.

(35) Schöttle, C.; Doronkin, D. E.; Popescu, R.; Gerthsen, D.; Grunwaldt, J. D.; Feldmann, C. Ti^0 Nanoparticles via Lithium-Naphthalenide-Driven Reduction. *Chem Commun* **2016**, *52*, 6316–6319.

(36) Song, M.-R.; Chen, M.; Zhang, Z. J. Preparation and Characterization of Mg Nanoparticles. *Mater. Charact.* **2008**, *59*, 514–518.

(37) Norberg, N. S.; Arthur, T. S.; Fredrick, S. J.; Prieto, A. L. Size-Dependent Hydrogen Storage Properties of Mg Nanocrystals Prepared from Solution. *J. Am. Chem. Soc.* **2011**, *133*, 10679–10681.

(38) Pickering, A. L.; Mitterbauer, C.; Browning, N. D.; Kauzlarich, S. M.; Power, P. P. Room Temperature Synthesis of Surface-Functionalised Boron Nanoparticles. *Chem. Commun.* **2007**, *43*, 580–582.

(39) Baldwin, R. K.; Pettigrew, K. A.; Ratai, E.; Augustine, M. P.; Kauzlarich, S. M. Solution Reduction Synthesis of Surface Stabilized Silicon Nanoparticles. *Chem. Commun.* **2002**, *38*, 1822–1823.

(40) Rieke, R. D.; Hudnall, P. M.; Kenan, W. R. Activated Metals. I. Preparation of Highly Reactive Magnesium Metal. *J. Am. Chem. Soc.* **1972**, *94*, 7178–7179.

(41) Rieke, R. D.; Sell, M. S.; Klein, W. R.; Chen, T. A.; Brown, J. D.; Hanson, M. V. Rieke Metals: Highly Reactive Metal Powders Prepared by Alkali Metal Reduction of Metal Salts. In *Active Metals: Preparation, Characterization, Applications*; Wiley VCH: Weinheim, 2007; pp 1–59.

(42) Halalay, I. C.; Balogh, M. P. Sonochemical Method for Producing Titanium Metal Powder. *Ultrason. Sonochem.* **2008**, *15*, 684–688.

(43) Nador, F.; Moglie, Y.; Vitale, C.; Yus, M.; Alonso, F.; Radivoy, G. Reduction of Polycyclic Aromatic Hydrocarbons Promoted by Cobalt or Manganese Nanoparticles. *Tetrahedron* **2010**, *66*, 4318–4325.

(44) Liu, W.; Aguey-Zinsou, K.-F. Size Effects and Hydrogen Storage Properties of Mg Nanoparticles Synthesised by an Electroless Reduction Method. *J. Mater. Chem. A* **2014**, *2*, 9718–9726.

(45) Schöttle, C.; Bockstaller, P.; Gerthsen, D.; Feldmann, C. Tungsten Nanoparticles from Liquid-Ammonia-Based Synthesis. *Chem. Commun.* **2014**, *50*, 4547–4550.

(46) Bondi, J. F.; Oyler, K. D.; Ke, X.; Schiffer, P.; Schaak, R. E.; Park, U. V; Pennsyl, V. Chemical Synthesis of Air-Stable Manganese Nanoparticles. *J. Am. Chem. Soc* **2009**, *131*, 9144–9145.

(47) Ghosh, D.; Pradhan, S.; Chen, W.; Chen, S. Titanium Nanoparticles Stabilized by Ti-C Covalent Bonds. *Chem. Mater.* **2008**, *20*, 1248–1250.

(48) Peng, S.; Wang, C.; Xie, J.; Sun, S. Synthesis and Stabilization of Monodisperse Fe Nanoparticles. *J. Am. Chem. Soc.* **2006**, *128*, 10676–10677.

(49) Yang, H.; Ito, F.; Hasegawa, D.; Ogawa, T.; Takahashi, M. Facile Large-Scale Synthesis of Monodisperse Fe Nanoparticles by Modest-Temperature Decomposition of Iron Carbonyl. *J. Appl. Phys.* **2007**, *101*, 09J112.

(50) Yamamuro, S.; Ando, T.; Sumiyama, K.; Uchida, T.; Kojima, I. Monodisperse Metallic Iron Nanoparticles Synthesized from Noncarbonyl Complex. *Jpn. J. Appl. Phys.* **2004**, *43*, 4458–4459.

(51) He, X.; Zhong, W.; Au, C.-T.; Du, Y. Size Dependence of the Magnetic Properties of Ni Nanoparticles Prepared by Thermal Decomposition Method. *Nanoscale Res. Lett.* **2013**, *8*, 446.

(52) Mourdikoudis, S.; Liz-Marzán, L. M. Oleylamine in Nanoparticle Synthesis. *Chem. Mater.* **2013**, *25*, 1465–1476.

(53) McClain, M. J.; Schlather, A. E.; Ringe, E.; King, N. S.; Liu, L.; Manjavacas, A.; Knight, M. W.; Kumar, I.; Whitmire, K. H.; Everitt, H. O.; et al. Aluminum Nanocrystals. *Nano Lett.* **2015**, *15*, 2751–2755.

(54) Cui, Y.; Huang, D.; Li, Y.; Huang, W.; Liang, Z.; Xu, Z.; Zhao, S. Aluminium Nanoparticles Synthesized by a Novel Wet Chemical Method and Used to Enhance the Performance of Polymer Solar Cells by the Plasmonic Effect. *J. Mater. Chem. C* **2015**, *3*, 4099–4103.

(55) Chung, S. W.; Guliants, E. A.; Bunker, C. E.; Hammerstroem, D. W.; Deng, Y.; Burgers, M. A.; Jelliss, P. A.; Buckner, S. W. Capping and Passivation of Aluminum Nanoparticles Using Alkyl-Substituted Epoxides. *Langmuir* **2009**, *25*, 8883–8887.

(56) Gottapu, S.; Padhi, S. K.; Krishna, M. G.; Muralidharan, K. Poly(Vinylpyrrolidone) Stabilized Aluminum Nanoparticles Obtained by the Reaction of $SiCl_4$ with $LiAlH_4$. *New J. Chem.* **2015**, *39*, 5203–5207.

(57) Johnson, C. E.; Higa, K. T. Preparation of Nanometer Sized Aluminum Powders. *MRS Proc.* **1996**, *457*, 131–135.

(58) Crouse, C. A.; Pierce, C. J.; Spowart, J. E. Influencing Solvent Miscibility and Aqueous Stability of Aluminum Nanoparticles through Surface Functionalization with Acrylic Monomers. *ACS Appl. Mater. Interfaces* **2010**, *2*, 2560–2569.

(59) Cheng, Z. peng; Yang, Y.; Li, F. sheng; Pan, Z. hua. Synthesis and Characterization of Aluminum Particles Coated with Uniform Silica Shell. *Trans. Nonferrous Met. Soc. China (English Ed.* **2008**, *18*, 378–382.

(60) Eliezer, S.; Eliaz, N.; Grossman, E.; Fisher, D.; Gouzman, I.; Henis, Z.; Pecker, S.; Horovitz, Y.; Fraenkel, M.; Maman, S.; et al. Synthesis of Nanoparticles with Femtosecond Laser Pulses. *Phys. Rev. B* **2004**, *69*, 144119.

(61) Stratakis, E.; Barberoglou, M.; Fotakis, C.; Viau, G.; Garcia, C.; Shafeev, G. A. Generation of Al Nanoparticles via Ablation of Bulk Al in Liquids with Short Laser Pulses. *Opt. Express* **2009**, *17*, 12650–12659.

(62) Zhang, K.; Ivanov, D. S.; Ganeev, R. A.; Boltaev, G. S.; Krishnendu, P. S.; Singh, S. C.; Garcia, M. E.; Zavestovskaya, I. N.; Guo, C. Pulse Duration and Wavelength Effects of Laser Ablation on the Oxidation, Hydrolysis, and Aging of Aluminum Nanoparticles in Water. *Nanomaterials* **2019**, *9*, 767.

(63) Dudoitis, V.; Ulevičius, V.; Račiukaitis, G.; Špirkauskaitė, N.; Plauškaitė, K. Generation of Metal Nanoparticles by Laser Ablation. *Lith. J. Phys.* **2011**, *51*, 248–259.

(64) Sindhu, T. K.; Sarathi, R.; Chakravarthy, S. R. Generation and Characterization of Nano Aluminium Powder Obtained through Wire Explosion Process. *Bull. Mater. Sci.* **2007**, *30*, 187–195.

(65) Lerner, M. I.; Glazkova, E. A.; Lozhkomoev, A. S.; Svarovskaya, N. V.; Bakina, O. V.; Pervikov, A. V.; Psakhie, S. G. Synthesis of Al Nanoparticles and Al/AlN Composite Nanoparticles by Electrical Explosion of Aluminum Wires in Argon and Nitrogen. *Powder Technol.* **2016**, *295*, 307–314.

(66) Kwon, Y. S.; Gromov, A. A.; Strokova, J. I. Passivation of the Surface of Aluminum Nanopowders by Protective Coatings of the Different Chemical Origin. *Appl. Surf. Sci.* **2007**, *253*, 5558–5564.

(67) Gromov, A. A.; Förter-Barth, U.; Teipel, U. Aluminum Nanopowders Produced by Electrical Explosion of Wires and Passivated by Non-Inert Coatings: Characterisation and Reactivity with Air and Water. *Powder Technol.* **2006**, *164*, 111–115.

(68) Sen, P.; Ghosh, J.; Abdullah, A.; Kumar, P.; Vandana. Preparation of Cu, Ag, Fe and Al Nanoparticles by the Exploding Wire Technique. *J. Chem. Sci.* **2003**, *115*, 499–508.

(69) Kwon, Y. S.; Gromov, A. A.; Ilyin, A. P.; Rim, G. H. Passivation Process for Superfine Aluminum Powders Obtained by Electrical Explosion of Wires. *Appl. Surf. Sci.* **2003**, *211*, 57–67.

(70) Oshima, K.; Fujita, T.; Wada, N.; Yoshioka, H.; Uyeda, R. Superconductivity in Films of Aluminium Fine Particles Prepared by Evaporation in Helium Gas. *J. Phys. Soc. Japan* **1969**, *26*, 862.

(71) Wada, N.; Garbini, M.; Makimura, T.; Sakuramoto, T.; Murakami, K.; Injected, M. V. Preparation of Fine Metal Particles by Means of Evaporation in Xenon Gas. *Jpn. J. Appl. Phys.* **1968**, *7*, 1287–1293.

(72) Kimoto, K.; Kamiya, Y.; Nonoyama, M.; Uyeda, R. An Electron Microscope Study on Fine Metal Particles Prepared by Evaporation in Argon Gas at Low Pressure. *Jpn. J. Appl. Phys.* **1963**, *2*, 702–713.

(73) Yatsuya, S.; Kasukabe, S.; Uyeda, R. Formation of Ultrafine Metal Particles by Gas Evaporation Technique. I. Aluminium in Helium. *Jpn. J. Appl. Phys.* **1973**, *12*, 1675–1684.

(74) Kimoto, K.; Nishida, I. The Crystal Habits of Small Particles of Aluminium and Silver Prepared by Evaporation in Clean Atmosphere of Argon. *Jpn. J. Appl. Phys.* **1977**, *16*, 941–948.

(75) Sun, X. K.; Xu, J.; Chen, W. X.; Wei, W. D. Preparation of Al Nanoparticles in a Controlled Environment. *Nanostructured Mater.* **1994**, *4*, 337–344.

(76) Mhadhbi, M.; Khitouni, M.; Azabou, M.; Kolsi, A. Characterization of Al and Fe Nanosized Powders Synthesized by High Energy Mechanical Milling. *Mater. Charact.* **2008**, *59*, 944–950.

(77) Yu, J.; McMahon, B. W.; Boatz, J. A.; Anderson, S. L. Aluminum Nanoparticle Production by Acetonitrile-Assisted Milling: Effects of Liquid- vs Vapor-Phase Milling and of Milling Method on Particle Size and Surface Chemistry. *J. Phys. Chem. C* **2016**, *120*, 19613–19629.

(78) Jiang, A.; Wang, F.; Xia, D.; Li, M.; Qiang, L.; Zhu, Z.; Wang, P.; Fan, R.; Lin, K.; Yang, Y. Aluminum Nanoparticles Manufactured Using a Ball-Milling Method with Ammonium Chloride as a Grinding Aid: Achieving Energy Release at Low Temperature. *New J. Chem.* **2019**, *43*, 1851–1856.

(79) https://www.ssnano.com/inc/sdetail/aluminum_nanoparticles__nanopowder__al__99_7__40_60_nm_/276 (accessed May 19, 2020).

(80) http://www.nanosized-powders.com/en/prices/ (accessed Nov 15, 2019).

(81) http://www.sk-steel-powder.de/price-en.html (accessed May 19, 2020).

(82) https://nanografi.com/nanoparticles/element-alloys-nanoparticles/aluminum-nanoparticles/ (accessed May 19, 2020).

(83) Clark, B. D.; Jacobson, C. R.; Lou, M.; Yang, J.; Zhou, L.; Gottheim, S.; DeSantis, C. J.; Nordlander, P.; Halas, N. J. Aluminum Nanorods. *Nano Lett.* **2018**, *18*, 1234–1240.

(84) Zhang, L. *On the Chemical Synthesis of Manganese-Based High Magnetocrystalline Anisotropy Energy Density Magnetic Nanoparticles*; University of Alabama Libraries: Tuscaloosa, 2013.

(85) Rieke, R. D.; Chao, L. C. Activated Metals IV. The Preparation of Highly Reactive Aluminum Metal and the Direct Synthesis of Phenylaluminum Halides. *Synth. React. Inorg. Met. Org. Chem.* **1974**, *4*, 101–105.

(86) Tzu-jung, P. *Preparations and Reactions of Rieke Metals Activated Aluminum and Zinc*; University of Nebraska: Lincoln, 1981.

(87) Pyo, S. H.; Byung, H. H. Reduction of Nitroarenes by Activated Metals. *Bull. Korean Chem. Soc.* **1995**, *16*, 181–183.

(88) Zhu, H.; Sadoway, D. R. Synthesis of Nanoscale Particles of Ta and Nb_3Al by Homogeneous Reduction in Liquid Ammonia. *J. Mater. Res.* **2001**, *16*, 2544–2549.

(89) Haber, J. A.; Buhro, W. E. Kinetic Instability of Nanocrystalline Aluminum Prepared by Chemical Synthesis; Facile Room-Temperature Grain Growth. *J. Am. Chem. Soc.* **1998**, *120*, 10847–10855.

(90) Cui, Y.; Zhao, S.; Tao, D.; Liang, Z.; Huang, D.; Xu, Z. Synthesis of Size-Controlled and Discrete Core-Shell Aluminum Nanoparticles with a Wet Chemical Process. *Mater. Lett.* **2014**, *121*, 54–57.

(91) Ghanta, S. R.; Muralidharan, K. Solution Phase Chemical Synthesis of Nano Aluminium Particles Stabilized in Poly(Vinylpyrrolidone) and Poly(Methylmethacrylate) Matrices. *Nanoscale* **2010**, *2*, 976–980.

(92) Lee, H. M.; Yun, J.-Y. Preparation of Aluminum-Oleic Acid Nano-Composite for Application to Electrode for Si Solar Cells. *Mater. Trans.* **2011**, *52*, 1222–1227.

(93) Mahendiran, C.; Ganesan, R.; Gedanken, A. Sonoelectrochemical Synthesis of Metallic Aluminum Nanoparticles. *Eur. J. Inorg. Chem.* **2009**, *2009*, 2050–2053.

(94) Ghanta, S. R.; Muralidharan, K. Chemical Synthesis of Aluminum Nanoparticles. *J. Nanoparticle Res.* **2013**, *15*, 1715.

(95) Shabana, S.; Sonawane, S. H.; Ranganathan, V.; Pujjalwar, P. H.; Pinjari, D. V.; Bhanvase, B. A.; Gogate, P. R.; Ashokkumar, M. Improved Synthesis of Aluminium Nanoparticles Using Ultrasound Assisted Approach and Subsequent Dispersion Studies in Di-Octyl Adipate. *Ultrason. Sonochem.* **2017**, *36*, 59–69.

(96) Chandra, S.; Kumar, A.; Tomar, P. K. Synthesis of Al Nanoparticles: Transmission Electron Microscopy, Thermal and Spectral Studies. *Spectrochim. Acta A* **2012**, *92*, 392–397.

(97) Bunker, C. E.; Smith, M. J.; Shiral Fernando, K. A.; Harruff, B. A.; Lewis, W. K.; Gord, J. R.; Guliants, E. A.; Phelps, D. K. Spontaneous Hydrogen Generation from Organic-Capped Al Nanoparticles and Water. *ACS Appl. Mater. Interfaces* **2010**, *2*, 11–14.

(98) Lewis, W. K.; Rosenberger, A. T.; Gord, J. R.; Crouse, C. A.; Harruff, B. A.; Fernando, K. A. S.; Smith, M. J.; Phelps, D. K.; Spowart, J. E.; Guliants, E. A.; et al. Multispectroscopic (FTIR, XPS, and TOFMS-TPD) Investigation of the Core-Shell Bonding in Sonochemically Prepared Aluminum Nanoparticles Capped with Oleic Acid. *J. Phys. Chem. C* **2010**, *114*, 6377–6380.

(99) Fernando, K. A. S.; Smith, M. J.; Harruff, B. A.; Lewis, W. K.; Guliants, E. A.; Bunker, C. E. Sonochemically Assisted Thermal Decomposition of Alane N,N- Dimethylethylamine with Titanium (IV) Isopropoxide in the Presence of Oleic Acid to Yield Air-Stable and Size-Selective Aluminum Core - Shell Nanoparticles. *J. Phys. Chem. C* **2009**, *113*, 500–503.

(100) Jouet, R. J.; Warren, A. D.; Rosenberg, D. M.; Bellitto, V. J.; Park, K.; Zachariah, M. R. Surface Passivation of Bare Aluminum Nanoparticles Using Perfluoroalkyl Carboxylic Acids. *Chem. Mater.* **2005**, *17*, 2987–2996.

(101) Jouet, R. J.; Granholm, R. H.; Sandusky, H. W.; Warren, A. D. Preparation and Shock Reactivity Analysis of Novel Perfluoroalkyl-Coated Aluminum Nanocomposites. *Mater. Sci. Technol.* **2006**, *22*, 422–429.

(102) Meziani, M. J.; Bunker, C. E.; Lu, F.; Li, H.; Wang, W.; Guliants, E. A.; Quinn, R. A.; Sun, Y. P.

Formation and Properties of Stabilized Aluminum Nanoparticles. *ACS Appl. Mater. Interfaces* **2009**, *1*, 703–709.

(103) Hammerstroem, D. W.; Burgers, M. A.; Chung, S. W.; Guliants, E. A.; Bunker, C. E.; Wentz, K. M.; Hayes, S. E.; Buckner, S. W.; Jelliss, P. A. Aluminum Nanoparticles Capped by Polymerization of Alkyl-Substituted Epoxides: Ratio-Dependent Stability and Particle Size. *Inorg. Chem.* **2011**, *50*, 5054–5059.

(104) Jelliss, P. A.; Buckner, S. W.; Chung, S. W.; Patel, A.; Guliants, E. A.; Bunker, C. E. The Use of 1,2-Epoxyhexane as a Passivating Agent for Core-Shell Aluminum Nanoparticles with Very High Active Aluminum Content. *Solid State Sci.* **2013**, *23*, 8–12.

(105) Thomas, B. J.; Bunker, C. E.; Guliants, E. A.; Hayes, S. E.; Kheyfets, A.; Wentz, K. M.; Buckner, S. W.; Jelliss, P. A. Synthesis of Aluminum Nanoparticles Capped with Copolymerizable Epoxides. *J. Nanoparticle Res.* **2013**, *15*, 1729.

(106) Higa, K. T.; Johnson, C. E.; Hollins, R. A. Preparation of Fine Aluminum Powders by Solution Methods. United States Patent 5885321, 1999.

(107) Foley, T. J.; Johnson, C. E.; Higa, K. T. Inhibition of Oxide Formation on Aluminum Nanoparticles by Transition Metal Coating. *Chem. Mater.* **2005**, *17*, 4086–4091.

(108) Atmane, Y. A.; Sicard, L.; Lamouri, A.; Pinson, J.; Sicard, M.; Masson, C.; Nowak, S.; Decorse, P.; Piquemal, J. Y.; Galtayries, A.; et al. Functionalization of Aluminum Nanoparticles Using a Combination of Aryl Diazonium Salt Chemistry and Iniferter Method. *J. Phys. Chem. C* **2013**, *117*, 26000–26006.

(109) Clark, B. D.; DeSantis, C. J.; Wu, G.; Renard, D.; McClain, M. J.; Bursi, L.; Tsai, A.-L.; Nordlander, P.; Halas, N. J. Ligand-Dependent Colloidal Stability Controls the Growth of Aluminum Nanocrystals. *J. Am. Chem. Soc.* **2019**, *141*, 1716–1724.

(110) Renard, D.; Tian, S.; Ahmadivand, A.; Desantis, C. J.; Clark, B. D.; Nordlander, P.; Halas, N. J. Polydopamine-Stabilized Aluminum Nanocrystals: Aqueous Stability and Benzo[a]Pyrene Detection. *ACS Nano* **2019**, *13*, 3117–3124.

(111) Smith, M. J. *Aluminum Core-Shell Nanoparticles: Synthesis, Properties, and Applications*; University of Dayton: Dayton, 2010.

(112) Lu, S.; Yu, H.; Gottheim, S.; Gao, H.; Desantis, C. J.; Clark, B. D.; Yang, J.; Jacobson, C. R.; Lu, Z.; Nordlander, P.; et al. Polymer-Directed Growth of Plasmonic Aluminum Nanocrystals. *J. Am. Chem. Soc.* **2018**, *140*, 15412–15418.

(113) Clark, B. D.; Jacobson, C. R.; Lou, M.; Renard, D.; Wu, G.; Bursi, L.; Ali, A. S.; Swearer, D. F.; Tsai, A.-L.; Nordlander, P.; et al. Aluminum Nanocubes Have Sharp Corners. *ACS Nano* **2019**, *13*, 9682–9691.

(114) Bogdanović, B.; Schwickardi, M. Ti-Doped Alkali Metal Aluminium Hydrides as Potential Novel Reversible Hydrogen Storage Materials. *J. Alloys Compd.* **1997**, *253–254*, 1–9.

(115) Frankcombe, T. J. Proposed Mechanisms for the Catalytic Activity of Ti in $NaAlH_4$. *Chem. Rev.* **2012**, *112*, 2164–2178.

(116) Wiberg, E.; Bauer, R.; Schmidt, M.; Uson, R. Zur Kenntnis Des Lithium-Aluminium-Wasserstoffs. *Z. Naturforsch. B* **1951**, *6*, 393–394.

(117) Gavrilenko, V. V.; Chekulaeva, L. A.; Zakharkin, L. I. Decomposition of Solvates of Aluminum Hydride and Its Derivatives in Ethereal Solutions under the Influence of Titanium Compounds. *Russ. Chem. Bull.* **1977**, *26*, 1131–1134.

(118) Zhang, S.; Taniguchi, A.; Xu, Q.; Takeichi, N.; Takeshita, H. T.; Kuriyama, N.; Kiyobayashi, T. Understanding the Effect of Titanium Species on the Decomposition of Alanates in Homogeneous Solution. *J. Alloys Compd.* **2006**, *413*, 218–221.

(119) Tiwari, D.; Dunn, S. Photochemical Reduction of Al^{3+} to Al^0 over a Ferroelectric Photocatalyst — $LiNbO_3$. *Mater. Lett.* **2012**, *79*, 18–20.

(120) Cokoja, M. *Nanometallurgy in Organic Solution: Organometallic Synthesis of Intermetallic Transition Metal Aluminide and -Zincide Nanoparticles*; Ruhr-Universität Bochum: Bochum, 2007.

(121) Shevchenko, E. V.; Talapin, D. V.; Schnablegger, H.; Kornowski, A.; Festin, Ö.; Svedlindh, P.; Haase, M.; Weller, H. Study of Nucleation and Growth in the Organometallic Synthesis of Magnetic Alloy Nanocrystals: The Role of Nucleation Rate in Size Control of $CoPt_3$ Nanocrystals. *J. Am. Chem. Soc.* **2003**, *125*, 9090–9101.

(122) Watzky, M. A.; Finke, R. G. Nanocluster Size-Control and "Magic Number" Investigations. Experimental Tests of the "Living-Metal Polymer" Concept and of Mechanism-Based Size-Control Predictions Leading to the Syntheses of Iridium (0) Nanoclusters Centering about Four Sequential Magic. *Chem. Mater.* **1997**, *9*, 3083–3095.

(123) Mozaffari, S.; Li, W.; Thompson, C.; Ivanov, S.; Seifert, S.; Lee, B.; Kovarik, L.; Karim, A. M. Colloidal Nanoparticle Size Control: Experimental and Kinetic Modeling Investigation of the Ligand-Metal Binding Role in Controlling the Nucleation and Growth Kinetics. *Nanoscale* **2017**, *9*, 13772–13785.

(124) Bakshi, M. S. How Surfactants Control Crystal Growth of Nanomaterials. *Cryst. Growth Des.* **2016**, *16*, 1104–1133.

(125) Swearer, D. F.; Leary, R. K.; Newell, R.; Yazdi, S.; Robatjazi, H.; Zhang, Y.; Renard, D.; Nordlander, P.; Midgley, P. A.; Halas, N. J.; et al. Transition-Metal Decorated Aluminum Nanocrystals. *ACS Nano* **2017**, *11*, 10281–10288.

(126) Zhou, L.; Zhang, C.; McClain, M. J.; Manjavacas, A.; Krauter, C. M.; Tian, S.; Berg, F.; Everitt, H. O.; Carter, E. A.; Nordlander, P.; et al. Aluminum Nanocrystals as a Plasmonic Photocatalyst for Hydrogen Dissociation. *Nano Lett.* **2016**, *16*, 1478–1484.

(127) Sánchez-López, J. C.; Fernández, A.; Conde, C. F.; Conde, A.; Morant, C.; Sanz, J. M. The Melting Behavior of Passivated Nanocrystalline Aluminum. *Nanostruct. Mater.* **1996**, *7*, 813–822.

(128) Eckert, J.; Holzer, J. C.; Ahn, C. C.; Fu, Z.; Johnson, W. L. Melting Behavior of Nanocrystalline Aluminum Powders. *Nanostruct. Mater.* **1993**, *2*, 407–413.

(129) Trunov, M. A.; Umbrajkar, S. M.; Schoenitz, M.; Mang, J. T.; Dreizin, E. L. Oxidation and Melting of Aluminum Nanopowders. *J. Phys. Chem. B* **2006**, *110*, 13094–13099.

(130) Trunov, M. A.; Schoenitz, M.; Dreizin, E. L. Effect of Polymorphic Phase Transformations in Alumina Layer on Ignition of Aluminium Particles. *Combust. Theor. Model.* **2006**, *10*, 603–623.

(131) Trunov, M. A.; Schoenitz, M.; Zhu, X.; Dreizin, E. L. Effect of Polymorphic Phase Transformations in Al_2O_3 Film on Oxidation Kinetics of Aluminum Powders. *Combust. Flame* **2005**, *140*, 310–318.

(132) Jeurgens, L. P. H.; Sloof, W. G.; Tichelaar, F. D.; Mittemeijer, E. J. Growth Kinetics and Mechanisms of Aluminum-Oxide Films Formed by Thermal Oxidation of Aluminum. *J. Appl. Phys.* **2002**, *92*, 1649–1656.

(133) Jeurgens, L. P. H.; Sloof, W. G.; Tichelaar, F. D.; Mittemeijer, E. J. Thermodynamic Stability of Amorphous Oxide Films on Metals: Application to Aluminum Oxide Films on Aluminum Substrates. *Phys. Rev. B* **2000**, *62*, 4707–4719.

(134) Gorham, C. S.; Gaskins, J. T.; Parsons, G. N.; Losego, M. D.; Hopkins, P. E. Density Dependence of the Room Temperature Thermal Conductivity of Atomic Layer Deposition-Grown Amorphous Alumina (Al_2O_3). *Appl. Phys. Lett.* **2014**, *104*, 253107.

(135) Kniep, R.; Lamparter, P.; Steep, S. Structure of Anodic Oxide Coating on Aluminum. *Adv. Mater.* **1989**, *7*, 229–231.

(136) Wefers, K.; Misra, C. *Oxides and Hydroxides of Aluminum*; Alcoa Research Laboratories: New Kensington, 1987.

(137) Laboureur, D.; Glabeke, G.; Gouriet, J. B. Aluminum Nanoparticles Oxidation by TGA/DSC. *J. Therm. Anal. Calorim.* **2019**, *137*, 1199–1210.

(138) Chen, L.; Song, W. L.; Lv, J.; Wang, L.; Xie, C. S. Effect of Heating Rates on TG-DTA Results of Aluminum Nanopowders Prepared by Laser Heating Evaporation. *J. Therm. Anal. Calorim.* **2009**, *96*, 141–145.

(139) Knight, M. W.; King, N. S.; Liu, L.; Everitt, H. O.; Nordlander, P.; Halas, N. J. Aluminum for Plasmonics. *ACS Nano* **2014**, *8*, 834–840.

(140) Chen, X.; Jia, B.; Zhang, Y.; Gu, M. Exceeding the Limit of Plasmonic Light Trapping in Textured Screen-Printed Solar Cells Using Al Nanoparticles and Wrinkle-like Graphene Sheets. *Light Sci. Appl.* **2013**, *2*, e92.

(141) Villesen, T. F.; Uhrenfeldt, C.; Johansen, B.; Nylandsted Larsen, A. Self-Assembled Al Nanoparticles on Si and Fused Silica, and Their Application for Si Solar Cells. *Nanotechnology* **2013**, *24*, 275606.

(142) Akimov, Y. A.; Koh, W. S. Resonant and Nonresonant Plasmonic Nanoparticle Enhancement for Thin-Film Silicon Solar Cells. *Nanotechnology* **2010**, *21*, 235201.

(143) Olson, J.; Manjavacas, A.; Liu, L.; Chang, W. S.; Foerster, B.; King, N. S.; Knight, M. W.; Nordlander, P.; Halas, N. J.; Link, S. Vivid, Full-Color Aluminum Plasmonic Pixels. *Proc. Natl. Acad. Sci. U. S. A.* **2014**, *111*, 14348–14353.

(144) Olson, J.; Manjavacas, A.; Basu, T.; Huang, D.; Schlather, A. E.; Zheng, B.; Halas, N. J.; Nordlander, P.; Link, S. High Chromaticity Aluminum Plasmonic Pixels for Active Liquid Crystal Displays. *ACS Nano* **2016**, *10*, 1108–1117.

(145) Chowdhury, M. H.; Ray, K.; Gray, S. K.; Pond, J.; Lakowicz, J. R. Aluminum Nanoparticles as Substrates for Metal-Enhanced Fluorescence in the Ultraviolet for the Label-Free Detection of Biomolecules. *Anal. Chem.* **2009**, *81*, 1397–1403.

(146) Bunker, C. E.; Fernando, K. A. S.; Guliants, E. A.; Smith, M. J.; Harruff, B. A. Method of Generating Hydrogen from the Reaction of Stabilized Aluminum Nanoparticles with Water and Method of Forming Stabilized Aluminum Nanoparticles. US Patent US10384937B2, 2019.

(147) Risha, G. A.; Connell, T. L.; Yetter, R. A.; Yang, V.; Wood, T. D.; Pfeil, M. A.; Pourpoint, T. L.; Son, S. F.; Engineering, N.; Lafayette, W.; et al. Aluminum-Ice (ALICE) Propellants for Hydrogen Generation and Propulsion. *45 th AIAA/ASME/SAE/ASEE Jt. Propuls. Conf. Exhib.* **2009**.

(148) Risha, G. A.; Connell Jr., T. L.; Yetter, R. A.; Sundaram, D. S.; Yang, V. Combustion of Frozen Nanoaluminum and Water Mixtures. *J. Propul. Power* **2014**, *30*, 133–142.

(149) Zhu, Y. L.; Huang, H.; Ren, H.; Jiao, Q. J. Effects of Aluminum Nanoparticles on Thermal

Decomposition of Ammonium Perchlorate. *J. Korean Chem. Soc.* **2013**, *57*, 109–114.

(150) Armstrong, R. W.; Baschung, B.; Booth, D. W.; Samirant, M. Enhanced Propellant Combustion with Nanoparticles. *Nano Lett.* **2003**, *3*, 253–255.

(151) Young, G.; Wang, H.; Zachariah, M. R. Application of Nano-Aluminum/Nitrocellulose Mesoparticles in Composite Solid Rocket Propellants. *Propellants, Explos. Pyrotech.* **2015**, *40*, 413–418.

(152) Tyagi, H.; Phelan, P. E.; Prasher, R.; Peck, R.; Lee, T.; Pacheco, J. R.; Arentzen, P. Increased Hot-Plate Ignition Probability for Nanoparticle-Laden Diesel Fuel. *Nano Lett.* **2008**, *8*, 1410–1416.

(153) Hou, C.; Geng, X.; An, C.; Wang, J.; Xu, W.; Li, X. Preparation of Al Nanoparticles and Their Influence on the Thermal Decomposition of RDX. *Cent. Eur. J. Energ. Mater.* **2013**, *10*, 123–133.

(154) Zhu, Y. L.; Huang, H.; Ren, H.; Jiao, Q. J. Influence of Aluminum Particle Size on Thermal Decomposition of RDX. *J. Energ. Mater.* **2013**, *31*, 178–191.

(155) Zhou, Z.; Chen, J.; Yuan, H.; Nie, J. Effects of Aluminum Particle Size on the Detonation Pressure of TNT/Al. *Propellants, Explos. Pyrotech.* **2017**, *42*, 1401–1409.

(156) Gottfried, J. L.; Smith, D. K.; Wu, C. C.; Pantoya, M. L. Improving the Explosive Performance of Aluminum Nanoparticles with Aluminum Iodate Hexahydrate (AIH). *Sci. Rep.* **2018**, *8*, 8036.

(157) Ji, X.; Qin, W.; Li, X.; Zheng, S.; Zhou, J.; Xin, Z.; Li, Y.; Wang, L. Initiation of CL-20 Doped with Aluminum Nanoparticles by Using a Laser Pulse through an Optical Fiber. *Propellants, Explos. Pyrotech.* **2018**, *43*, 1210–1214.

(158) Yang, Y.; Wang, S.; Sun, Z.; Dlott, D. D. Propagation of Shock-Induced Chemistry in Nanoenergetic Materials: The First Micrometer. *J. Appl. Phys.* **2004**, *95*, 3667–3676.

(159) Morlock, M. J. Method and System for Welding Railroad Rails. US Patent US5877468A, 1999.

(160) Wang, L. L.; Munir, Z. A.; Maximov, Y. M. Thermite Reactions: Their Utilization in the Synthesis and Processing of Materials. *J. Mater. Sci.* **1993**, *28*, 3693–3708.

(161) Fischer, S.; Grubelich, M. *Theoretical Energy Release of Thermites, Intermetallics, and Combustible Metals*; Sandia National Laboratories: Albuquerque, 1998.

(162) Piercey, D. G.; Klapötke, T. M. Nanoscale Aluminum -Metal Oxide (Thermite) Reactions for Application in Energetic Materials. *Cent. Eur. J. Energ. Mater.* **2010**, *7*, 115–129.

(163) Weir, C.; Pantoya, M. L.; Daniels, M. A. The Role of Aluminum Particle Size in Electrostatic Ignition Sensitivity of Composite Energetic Materials. *Combust. Flame* **2013**, *160*, 2279–2281.

(164) Sun, J.; Pantoya, M. L.; Simon, S. L. Dependence of Size and Size Distribution on Reactivity of Aluminum Nanoparticles in Reactions with Oxygen and MoO_3. *Thermochim. Acta* **2006**, *444*, 117–127.

(165) Bale, C. W.; Bélisle, E.; Chartrand, P.; Decterov, S. A.; Eriksson, G.; Gheribi, A. E.; Hack, K.; Jung, I. H.; Kang, Y. B.; Melançon, J.; et al. FactSage Thermochemical Software and Databases, 2010-2016. *Calphad* **2016**, *54*, 35–53.

(166) Woll, K.; Bergamaschi, A.; Avchachov, K.; Djurabekova, F.; Gier, S.; Pauly, C.; Leibenguth, P.; Wagner, C.; Nordlund, K.; Mücklich, F. Ru/Al Multilayers Integrate Maximum Energy Density and Ductility for Reactive Materials. *Sci. Rep.* **2016**, *6*, 19535.

(167) Wen, B.; Zhao, J.; Bai, F.; Li, T. First-Principle Studies of Al-Ru Intermetallic Compounds.

Intermetallics **2008**, *16*, 333–339.

(168) Lim, S. S.; Rossiter, P. L.; Tibballs, J. E. Assessment of the Al-Ag Binary Phase Diagram. *Calphad* **1995**, *19*, 131–141.

(169) Inoue, M.; Watanabe, H.; Niihara, K.; Suganuma, K. Synthetic Processes of Uniform Nickel Aluminides by Reactive Infiltration and Post Hot-Pressing of Infiltrated Precursors. *Mater. Lett.* **1998**, *34*, 55–59.

(170) Wolff, I. M. Synthesis of RuAl by Reactive Powder Processing. *Metall. Mater. Trans. A* **1996**, *27A*, 3688–3699.

(171) Mukasyan, A. S.; White, J. D. E.; Kovalev, D. Y.; Kochetov, N. A.; Ponomarev, V. I.; Son, S. F. Dynamics of Phase Transformation during Thermal Explosion in the Al-Ni System: Influence of Mechanical Activation. *Phys. B* **2010**, *405*, 778–784.

(172) Dunand, D. C. Reactive Synthesis of Aluminide Intermetallies. *Mater. Manuf. Process.* **1995**, *10*, 373–403.

(173) Rogachev, A. S.; Makasyan, A. S. *Combustion for Material Synthesis*, 1st Editio.; CRC Press: Boca Raton, 2014.

(174) Picard, Y. N.; Adams, D. P.; Palmer, J. A.; Yalisove, S. M. Pulsed Laser Ignition of Reactive Multilayer Films. *Appl. Phys. Lett.* **2006**, *88*, 144102.

(175) Peng, J. H.; Binner, J.; Bradshaw, S. Microwave Initiated Self-Propagating High Temperature Synthesis of SiC. *J. Mater. Synth. Process.* **2001**, *9*, 363–368.

(176) Wada, T.; Kinoshita, H. Rapid Exothermic Synthesis of Chalcopyrite-Type $CuInSe_2$. *J. Phys. Chem. Solids* **2005**, *66*, 1987–1989.

(177) Kim, D. W.; Kim, K. T.; Kwon, G. H.; Song, K.; Son, I. Self-Propagating Heat Synthetic Reactivity of Fine Aluminum Particles via Spontaneously Coated Nickel Layer. *Sci. Rep.* **2019**, *9*, 1033.

(178) White, J. D. E.; Reeves, R. V.; Son, S. F.; Mukasyan, A. S. Thermal Explosion in Ni-Al System: Influence of Mechanical Activation. *J. Phys. Chem. A* **2009**, *113*, 13541–13547.

(179) Liu, K. W.; Mücklich, F.; Birringer, R. Synthesis of Nano-RuAl by Mechanical Alloying. *Intermetallics* **2001**, *9*, 81–88.

(180) Haber, J. A.; Gunda, N. V.; Balbach, J. J.; Conradi, M. S.; Buhro, W. E. Chemical Syntheses of Nanocrystalline Nickel Aluminides. *Chem. Mater.* **2000**, *12*, 973–982.

(181) Bönnemann, H.; Brijoux, W.; Hofstadt, H. W.; Ould-Ely, T.; Schmidt, W.; Waßmuth, B.; Weidenthaler, C. Wet Chemistry Synthesis of β-Nickel Aluminide NiAl. *Angew. Chemie - Int. Ed.* **2002**, *41*, 599–603.

(182) Mücklich, F.; Ilić, N. RuAl and Its Alloys. Part I. Structure, Physical Properties, Microstructure and Processing. *Intermetallics* **2005**, *13*, 5–21.

(183) Obrowski, W. B2-Phasen von Aluminium Mit T-Metallen Der VII. Und VIII. Gruppe Des Periodischen Systems. *Naturwissenschaften* **1960**, *47*, 14.

(184) Boniface, T. D.; Cornish, L. A. Investigation of the High Aluminium End of the Aluminium-Ruthenium Phase Diagram. *J. Alloys Compd.* **1996**, *233*, 241–245.

(185) Boniface, T. D.; Cornish, L. A. Investigation of the Aluminium-Ruthenium Phase Diagram above 25 at.% Ruthenium. *J. Alloys Compd.* **1996**, *234*, 275–279.

(186) Mi, S.; Balanetskyy, S.; Grushko, B. A Study of the Al-Rich Part of the Al-Ru Alloy System.

Intermetallics **2003**, *11*, 643–649.

(187) Okamoto, H. Al-Ru (Aluminum-Ruthenium). *J. Phase Equilibria* **1997**, *18*, 105.

(188) Gobran, H. A.; Heger, D.; Mücklich, F. Determination of RuAl Phase Boundaries in Binary Ru-Al Phase Diagram at Room Temperature and 1200°C. *Zeitschrift für Met.* **2005**, *96*, 794–800.

(189) Xu, Y.; Makhlouf, S. A.; Ivanov, E.; Wakoh, K.; Sumiyama, K.; Suzuki, K. Nanocrystalline B2 Type $Ru_{40}Al_{60}$ and Ru Powders Produced by Mechanical Alloying and Leaching. *Nanostructured Mater.* **1994**, *4*, 437–444.

(190) Cooper, A. S. Precise Lattice Constants of Germanium, Aluminum, Gallium Arsenide, Uranium, Sulphur, Quartz and Sapphire. *Acta Crystallogr.* **1962**, *15*, 578–582.

(191) Edshammar, L. E. The Crystal Structure of $RuAl_6$. *Acta Chem. Scand.* **1968**, *22*, 2374–2400.

(192) Edshammar, L. E. The Crystal Structure of Ru_4Al_{13}. *Acta Chem. Scand.* **1965**, *19*, 2124–2130.

(193) Edshammar, L. E. An X-Ray Investigation of Ruthenium-Aluminium Alloys. *Acta Chem. Scand.* **1966**, *20*, 427–431.

(194) Ross, R. G.; Hume-Rothery, W. High Temperature X-Ray Metallography I. A New Debye-Scherrer Camera for Use at Very High Temperatures II. A New Parafocusing Camera III. Applications to the Study of Chromium, Hafnium, Molybdenum, Rhodium, Ruthenium and Tungsten. *J. Less-Common Met.* **1963**, *5*, 258–270.

(195) Mücklich, F.; Ilić, N.; Woll, K. RuAl and Its Alloys, Part II: Mechanical Properties, Environmental Resistance and Applications. *Intermetallics* **2008**, *16*, 593–608.

(196) Soldera, F.; Ilić, N.; Brännström, S.; Barrientos, I.; Gobran, H.; Mücklich, F. Formation of Al_2O_3 Scales on Single-Phase RuAl Produced by Reactive Sintering. *Oxid. Met.* **2003**, *59*, 529–542.

(197) Soldera, F.; Ilić, N.; Conesa, N. M.; Barrientos, I.; Mücklich, F. Influence of the Microstructure on the Formation of Alumina Scales on near Stoichiometric RuAl Produced by Arc Melting. *Intermetallics* **2005**, *13*, 101–107.

(198) Wolff, I. M. Toward a Better Understanding of Ruthenium Aluminide. *J. Miner. Met. Mater. Soc.* **1997**, *49*, 34–39.

(199) Fleischer, L.; Field, R. D.; Briant, C. L. Mechanical Properties of High-Temperature Alloys of AlRu. *Metall. Trans. A* **1991**, *22*, 403–414.

(200) Ilić, N.; Rein, R.; Göken, M.; Kempf, M.; Soldera, F.; Mücklich, F. Properties of Eutectic Ru-Al Alloy Produced by Ingot Metallurgy. *Mater. Sci. Eng. A* **2002**, *329–331*, 38–44.

(201) Fleischer, R. L.; Briant, C. L.; Field, R. D.; Engines, E. A. Tough, Ductile High-Temperature Intermetallic Compounds: Results of a Four-Year Survey. *MRS Proc.* **1991**, *213*, 463–474.

(202) Fleischer, R. L. Substitutional Solutes in AlRu-I. Effects of Solute on Moduli, Lattice Parameters and Vacancy Production. *Acta Metall. Mater.* **1993**, *41*, 863–869.

(203) Fleischer, R. L. Substitutional Solutes in AlRu-II. Hardening and Correlations with Defect Structure. *Acta Metall. Mater.* **1993**, *41*, 1197–1205.

(204) Reynolds, T. D.; Johnson, D. R. Microstructure and Mechanical Properties of Ru-Al-Mo Alloys. *Intermetallics* **2004**, *12*, 157–164.

(205) Fleischer, R. L. Ruthenium Aluminum Intermetallic Compounds. US patent 5011554, 1991.

(206) Fleischer, R. L. Ruthenium Aluminum Intermetallic Compounds with Scandium and Boron. US

Patent 5152853, 1992.

(207) King, W. W. Intermetallic Aluminide Polycrystalline Diamond Compact (PDC) Cutting Elements. US Patent US20100038148 A1, 2010.

(208) LaBarge, W. J.; Anderson, C.; Kupe, J. Exhaust Manifold Comprising Aluminide. US Patent US8020378B2, 2011.

(209) Tryon, B.; Cao, F.; Murphy, K. S.; Levi, C. G.; Pollock, T. M. Ruthenium-Containing Bond Coats for Thermal Barrier Coating Systems. *JOM* **2006**, *58*, 53–59.

(210) Alperine, S. A.; Fournes, J.; Moulineaux, I.; Leger, L.; Ville, C.; Malie, H. L.; Manesse, G. Thermal Barrier Coating with Improved Sub-Layer and Parts Coated with Said Thermal Barrier. US Patent 5843585, 1998.

(211) Seifert, M.; Brachmann, E.; Rane, G. K.; Menzel, S. B.; Oswald, S.; Gemming, T. Pt-RuAl Bilayers as a Model System for Pt Wire Bonding of High-Temperature RuAl Electrodes. *J. Alloys Compd.* **2020**, *813*, 152107.

(212) Borah, A.; Robi, P. S.; Srinivasan, A. Synthesis of Nano-Crystalline RuAl by Mechanical Alloying. *Met. Mater. Int.* **2007**, *13*, 293–302.

(213) Pauly, C.; Woll, K.; Bax, B.; Mücklich, F. The Role of Transitional Phase Formation during Ignition of Reactive Multilayers. *Appl. Phys. Lett.* **2015**, *107*, 113104.

(214) Zotov, N.; Woll, K.; Mücklich, F. Phase Formation of B2-RuAl during Annealing of Ru/Al Multilayers. *Intermetallics* **2010**, *18*, 1507–1516.

(215) Woll, K.; Chinnam, R. K. S.; Mücklich, F. Thin-Film Synthesis and Cyclic Oxidation Behavior of B2-RuAl. *MRS Proc.* **2008**, *1128*, 1128-U06-10.

(216) Mohamed, K. E.; Stover, D.; Buchkremer, H. P. Some Reactive Processing Aspects of High-Temperature Aluminides Nb_3Al and RuAl. *J. Mater. Eng. Perform.* **1997**, *6*, 771–779.

(217) Gobran, H. A.; Ilić, N.; Mücklich, F. Effects of Particle Size and Pressure on the Reactive Sintering of RuAl Intermetallic Compound. *Intermetallics* **2004**, *12*, 555–562.

(218) Okamoto, H. Al-Ni (Aluminum-Nickel). *J. Phase Equilibria Diffus.* **2004**, *25*, 394.

(219) Wöhler, F.; Michel, F. Ueber Krystallisirte Verbindungen von Aluminium Mit Metallen. *Justus Liebigs Ann. Chem.* **1860**, *115*, 102–105.

(220) Brunck, O. Über Einige Krystallisirte, Metallische Verbindungen Des Aluminium. *Berichte der Dtsch. Chem. Gesellschaft* **1901**, *34*, 2733–2735.

(221) Gwyer, A. G. C. Über Die Legierungen Des Aluminium Mit Kupfer, Eisen, Nickel, Kobalt, Blei Und Cadmium. *Z. anorg. Chem* **1908**, *57*, 113–153.

(222) Alexander, W. O.; Vaughan, N. B. The Constitution of the Nickel-Aluminium System. *J. Inst. Met.* **1937**, *61*, 247–260.

(223) Bradley, A. J.; Taylor, A. An X-Ray Analysis of the Nickel-Aluminium System. *Proc. R. Soc. A* **1937**, *159*, 56–72.

(224) Enami, K.; Nenno, S. A New Orderd Phase in Tempered 63.8Ni-1Co-Al Martensite. *Trans. Jpn. Inst. Met.* **1978**, *19*, 571–580.

(225) Bremer, F. J.; Beyss, M.; Karthaus, E.; Hellwig, A.; Schober, T.; Welter, J. M.; Wenzl, H. Experimental Analysis of the Ni-Al Phase Diagram. *J. Cryst. Growth* **1988**, *87*, 185–192.

(226) Okamoto, H. Al-Ni (Aluminum-Nickel). *J. Phase Equilibria* **1993**, *14*, 257–259.

(227) Bitterlich, H.; Löser, W.; Schultz, L. Reassessment of Ni-Al and Ni-Fe-Al Solidus Temperatures. *J. Phase Equilibria* **2002**, *23*, 301–304.

(228) Taylor, A.; Doyle, N. J. Further Studies on the Nickel–Aluminium System. I. β-NiAl and δ-Ni_2Al_3 Phase Fields. *J. Appl. Crystallogr.* **1972**, *5*, 201–209.

(229) Iwasaki, Y.; Katayama, Y.; Komatsu, S. Y.; Amano, H. Equilibrium Solid Solubility of Nickel to Aluminum Re-Investigated by Resistometry. *J. Japan Inst. Light Met.* **2007**, *57*, 157–162.

(230) Bradley, A. J.; Taylor, A. The Crystal Structures of Ni2Al3 and NiAl3. *Philos. Mag.* **1937**, *23*, 1049–1067.

(231) Chrifi-Alaoui, F. Z.; Nassik, M.; Mahdouk, K.; Gachon, J. C. Enthalpies of Formation of the Al-Ni Intermetallic Compounds. *J. Alloys Compd.* **2004**, *364*, 121–126.

(232) Rzyman, K.; Moser, Z. Calorimetric Studies of the Enthalpies of Formation of Al_3Ni_2, AlNi and $AlNi_3$. *Prog. Mater. Sci.* **2004**, *49*, 581–606.

(233) Wyckoff, R. W. G. *Crystal Structures*, 2nd Editio.; Interscience Publishers: New York, 1963.

(234) Zhou, S. H.; Wang, Y.; Zhu, J. Z.; Wang, T.; Chen, L. Q.; MacKay, R. A.; Liu, Z. K. Computational Tools for Designing Ni-Base Superalloys. *Proc. Int. Symp. Superalloys* **2004**, 969–975.

(235) Mohan Rao, P. V.; Suryanarayana, S. V.; Satyanarayana Murthy, K.; Nagender Naidu, S. V. The High-Temperature Thermal Expansion of Ni_3Al Measured by X-Ray Diffraction and Dilation Methods. *J. Phys. Condens. Matter* **1989**, *1*, 5357–5361.

(236) Barrett, C. A. Effect of 0.1 at.% Zirconium on the Cyclic Oxidation Resistance of β-NiAl. *Oxid. Met.* **1988**, *30*, 361–390.

(237) Doychak, J.; Smialek, J. L.; Barrett, C. A. *The Oxidation of Ni-Rich Ni-Al Intermetallics*; NASA Lewis Research Center: Cleveland, 1988.

(238) Doychak, J.; Riihle, M. TEM Studies of Oxidized NiAl and Ni_3Al Cross Sections. *Oxid. Met.* **1989**, *31*, 431–452.

(239) Doychak, J.; Smialek, J. L.; Mitchell, T. E. Transient Oxidation of Single-Crystal β-NiAl. *Metall. Trans. A* **1989**, *20A*, 499–518.

(240) Albiter, A.; Espinosa-Medina, M. A.; Gonzalez-Rodriguez, J. G.; Perez, R. Effect of Mo, Ga and Fe on the Corrosion Resistance of Nanocrystalline NiAl Alloy in Acidic Media. *Int. J. Hydrogen Energy* **2005**, *30*, 1311–1315.

(241) George, E. P.; Liu, C. T. Brittle Fracture and Grain Boundary Chemistry of Microalloyed NiAl. *J. Mater. Res.* **1990**, *5*, 754–762.

(242) Noebe, R. D.; Bowman, R. R.; Nathal, M. V. Physical and Mechanical Properties of the B2 Compound NiAl. *Int. Mater. Rev.* **1993**, *38*, 193–232.

(243) Noebe, R. D.; Bowman, R. R.; Nathal, M. V. The Physical and Mechanical Metallurgy of NiAl. In *Physical Metallurgy and processing of Intermetallic Compounds*; Springer: Boston, US, 1996; pp 212–296.

(244) Miracle, D. B. The Physical and Mechanical Properties of NiAl. *Acta Metall. Mater.* **1993**, *41*, 649–684.

(245) Nagaraj, B. .; Schaeffler, J. C.; Rosenzweig, M. A. Thermal Barrier Coating System and Method Therefore. US Patent 5975852, 1999.

(246) Raj, S. V. Blanch Resistant and Thermal Barrier NiAl Coating Systems for Advanced Copper Alloys. US Patent 6838191 B1, 2005.

(247) Grylls, R. J.; Lau, Y.-C. Method for Modifying Stoichiometric NiAl Coatings Applied to Turbine Airfoils by Thermal Processes. US Patent 6403165 B1, 2002.

(248) Darolia, R. Bond Coat for a Thermal Barrier Coating System and Method Therefor. US Patent 6255001 B1, 2001.

(249) Chigasaki, M.; Otaka, K.; Okayama, A.; Onisawa, K.; Soeno, K. Method of Producing Nickel Base Alloy Structure with NiAl Coating. US Patent 4486245, 1984.

(250) Chen, C.-H.; Maddox, G. M.; Orth, J. E.; Turbeville, E. L. Nickel Aluminide Intermetallic Alloys for Tooling Applications. US Patent 6066291, 2000.

(251) Liu, C. T. Nickel Aluminides and Nickel-Iron Aluminides for Use in Oxidizing Environments. US Patent 4731221, 1988.

(252) Darolia, R. NiAI Alloys for High-Temperature Structural Applications. *JOM* **1991**, *43*, 44–49.

(253) Liu, C. T. Castable Nickel Aluminide Alloys for Structural Applications. US Patent 5108700, 1992.

(254) Liu, C. T. Nickel Aluminide Alloy Suitable for Structural Applications. US Patent 5725691, 1998.

(255) Liu, C. T.; Sikka, V. K. Nickel Aluminide Alloy for High Temperature Structural Use. US Patent 5006308, 1991.

(256) Bochenek, K.; Basista, M. Advances in Processing of NiAl Intermetallic Alloys and Composites for High Temperature Aerospace Applications. *Prog. Aerosp. Sci.* **2015**, *79*, 136–146.

(257) Deevi, S. C.; Sikka, V. K. Electronic Circuits Having NiAl and Ni_3Al Substrates. US Patent 5965274, 1999.

(258) Deevi, S. C.; Sikka, V. K. Method for Making Electronic Circuits Habing NiAl and Ni_3Al Substrates. US Patent US6179953 B1, 2001.

(259) Schwenk, E.; Papa, D.; Hankin, H.; Ginsberg, H. γ-n-Propylbutyrolactone and β-(Tetrahydrofuryl)Propionic Acid. *Org. Synth.* **1947**, *27*, 68–70.

(260) Page, G.A. Tarbell, D. S. β-(o-Carboxyphenyl)Propionic Acid. *Org. Synth.* **1954**, *34*, 8.

(261) Freel, J.; Pieters, W. J. M.; Anderson, R. B. The Structure of Raney Nickel. II. Electron Microprobe Studies. *J. Catal.* **1970**, *16*, 281–291.

(262) Murty, B. S.; Singh, K. H. S.; Pabi, S. K. Synthesis of Nanocrystalline NiAl over a Wide Composition Range by Mechanical Alloying. *Bull. Mater. Sci.* **1996**, *19*, 565–571.

(263) Akbari, G. H.; Attarzadeh, H.; Khajesarvi, A. Effect of Milling Time on the Formation of NiAl Nanostructure Intermetallic Produced by the Mechanical Alloying Process. *Adv. Mater. Res.* **2014**, *829*, 115–119.

(264) Portnoi, V. K.; Blinov, A. M.; Tomilin, I. A.; Kulik, T. Mechanochemical Synthesis of Mo-Doped Nickel Aluminides. *Inorg. Mater.* **2002**, *38*, 900–904.

(265) Fritz, G. M.; Spey, S. J.; Grapes, M. D.; Weihs, T. P. Thresholds for Igniting Exothermic Reactions in Al/Ni Multilayers Using Pulses of Electrical, Mechanical, and Thermal Energy. *J. Appl. Phys.* **2013**, *113*, 014901.

(266) Fritz, G. M.; Grzyb, J. A.; Knio, O. M.; Grapes, M. D.; Weihs, T. P. Characterizing Solid-State

Ignition of Runaway Chemical Reactions in Ni-Al Nanoscale Multilayers under Uniform Heating. *J. Appl. Phys.* **2015**, *118*, 135101.

(267) Rogachev, A. S.; Vadchenko, S. G.; Baras, F.; Politano, O.; Rouvimov, S.; Sachkova, N. V.; Mukasyan, A. S. Structure Evolution and Reaction Mechanism in the Ni/Al Reactive Multilayer Nanofoils. *Acta Mater.* **2014**, *66*, 86–96.

(268) Rogachev, A. S.; Vadchenko, S. G.; Baras, F.; Politano, O.; Rouvimov, S.; Sachkova, N. V.; Grapes, M. D.; Weihs, T. P.; Mukasyan, A. S. Combustion in Reactive Multilayer Ni/Al Nanofoils: Experiments and Molecular Dynamic Simulation. *Combust. Flame* **2016**, *166*, 158–169.

(269) Trenkle, J. C.; Koerner, L. J.; Tate, M. W.; Walker, N.; Gruner, S. M.; Weihs, T. P.; Hufnagel, T. C. Time-Resolved x-Ray Microdiffraction Studies of Phase Transformations during Rapidly Propagating Reactions in Al/Ni and Zr/Ni Multilayer Foils. *J. Appl. Phys.* **2010**, *107*, 113511.

(270) Zhu, P.; Li, J. C. M.; Liu, C. T. Reaction Mechanism of Combustion Synthesis of NiAl. *Mater. Sci. Eng. A* **2002**, *329–331*, 57–68.

(271) Ma, E.; Thompson, C. V.; Clevenger, L. A. Nucleation and Growth during Reactions in Multilayer Al/Ni Films: The Early Stage of Al_3Ni Formation. *J. Appl. Phys.* **1991**, *69*, 2211–2218.

(272) Blobaum, K. J.; Van Heerden, D.; Gavens, A. J.; Weihs, T. P. Al/Ni Formation Reactions: Characterization of the Metastable Al_9Ni_2 Phase and Analysis of Its Formation. *Acta Mater.* **2003**, *51*, 3871–3884.

(273) https://www.indium.com/nanofoil/ (aufgerufen am 13.11.2019).

(274) Wong, J.; Larson, E. M.; Holt, J. B.; Waide, P. A.; Rupp, B.; Frahm, R. Time-Resolved X-Ray Diffraction Study of Solid Combustion Reactions. *Science (80-.).* **1990**, *249*, 1406–1409.

(275) Tingaud, D.; Stuppfler, L.; Paris, S.; Vrel, D.; Bernard, F.; Penot, C.; Nardou, F. Time-Resolved X-Ray Diffraction Study of SHS-Produced NiAl and NiAl-ZrO_2 Composites. *Int. J. Self-Propagating High-Temperature Synth.* **2007**, *16*, 12–17.

(276) Biswas, A.; Roy, S. K. Comparison between the Microstructural Evolutions of Two Modes of SHS of NiAl: Key to a Common Reaction Mechanism. *Acta Mater.* **2004**, *52*, 257–270.

(277) Curfs, C.; Turrillas, X.; Vaughan, G. B. M.; Terry, A. E.; Kvick, Å.; Rodríguez, M. A. Al-Ni Intermetallics Obtained by SHS; A Time-Resolved X-Ray Diffraction Study. *Intermetallics* **2007**, *15*, 1163–1171.

(278) Fan, Q.; Chai, H.; Jin, Z. Dissolution-Precipitation Mechanism of Self-Propagating High-Temperature Synthesis of Mononickel Aluminide. *Intermetallics* **2001**, *9*, 609–619.

(279) Gasparyan, A. G.; Shteinberg, A. S. Macrokinetics of Reaction and Thermal Explosion in Ni and Al Powder Mixtures. *Combust. Explos. Shock Waves* **1988**, *24*, 324–330.

(280) Sina, H.; Iyengar, S.; Melin, S. Ignition Temperatures for Cu-Al and Ni-Al Reactions in Elemental Powder Mixtures Using Differential Scanning Calorimetry. *Int. Conf. Powder Metall. Part. Mater.* **2012**, 09-40-09–51.

(281) Thiers, L.; Mukasyan, A. S.; Varma, A. Thermal Explosion in Ni-Al System: Influence of Reaction Medium Microstructure. *Combust. Flame* **2002**, *131*, 198–209.

(282) Plazanet, L.; Nardou, F. Reaction Process during Relative Sintering of NiAl. *J. Mater. Sci.* **1998**, *3*, 2129–2136.

(283) Miura, S.; Ohashi, T.; Mishima, Y. Amount of Liquid Phase during Reaction Synthesis of Nickel

Aluminides. *Intermetallics* **1997**, *5*, 45–59.

(284) Dong, H. X.; Jiang, Y.; He, Y. H.; Song, M.; Zou, J.; Xu, N. P.; Huang, B. Y.; Liu, C. T.; Liaw, P. K. Formation of Porous Ni-Al Intermetallics through Pressureless Reaction Synthesis. *J. Alloys Compd.* **2009**, *484*, 907–913.

(285) Farber, L.; Klinger, L.; Gotman, I. Modeling of Reactive Synthesis in Consolidated Blends of Fine Ni and Al Powders. *Mater. Sci. Eng. A* **1998**, *254*, 155–165.

(286) Nishimura, C.; Liu, C. T. Reactive Sintering of Ni_3Al under Compression. *Acta Metall. Mater.* **1993**, *41*, 113–120.

(287) Zhu, H. X.; Abbaschian, R. Reactive Processing of Nickel-Aluminide Intermetallic Compounds. *J. Mater. Sci.* **2003**, *38*, 3861–3870.

(288) Bhaumik, S. K.; Divakar, C.; Rangaraj, L.; Singh, A. K. Reaction Sintering of NiAl and TiB2-NiAl Composites under Pressure. *Mater. Sci. Eng. A* **1998**, *257*, 341–348.

(289) Chang, S. Y.; Lin, S. J. Processing Stainless Steel Fibre Reinforced NiAl Matrix Composites by Reactive Hot Pressing. *J. Mater. Sci.* **1997**, *32*, 5127–5135.

(290) Munir, Z. A. Reaction Synthesis Processes: Mechanisms and Characteristics. *Metall. Trans. A* **1992**, *23A*, 7–13.

(291) Maslov, V. A.; Borovinskaya, I. P.; Merzhanov, A. G. Problem of the Mechanism of Gasless Combustion. *Combust. Explos. Shock Waves* **1976**, *12*, 631–636.

(292) Naibodorenko, Y. S.; Itin, V. I. Gasless Combustion of Metal Powder Mixtures 1. Mechanism and Details. *Combust. Explos. Shock Waves* **1975**, *11*, 293–300.

(293) Zhu, X.; Zhang, T.; Morris, V.; Marchant, D. Combustion Synthesis of $NiAl/Al_2O_3$ Composites by Induction Heating. *Intermetallics* **2010**, *18*, 1197–1204.

(294) Lebrat, J. P.; Varma, A.; McGinn, P. J. Mechanistic Studies in Combustion Synthesis of Ni_3Al and Ni_3Al-Matrix Composites. *J. Mater. Res.* **1994**, *9*, 1184–1192.

(295) Li, H. P.; Sekhar, J. A. The Influence of the Reactant Size on the Micropyretic Synthesis of NiAl Intermetallic Compounds. *J. Mater. Res.* **1995**, *10*, 2471–2480.

(296) Morsi, K. Review: Reaction Synthesis Processing of Ni-Al Intermetallic Materials. *Mater. Sci. Eng. A* **2001**, *299*, 1–15.

(297) Misiolek, W.; German, R. M. Reactive Sintering and Reactive Hot Isostatic Compaction of Aluminide Matrix Composites. *Mater. Sci. Eng. A* **1991**, *144*, 1–10.

(298) Biswas, A.; Roy, S. K.; Gurumurthy, K. R.; Prabhu, N.; Banerjee, S. A Study of Self-Propagating High-Temperature Synthesis of NiAl in Thermal Explosion Mode. *Acta Mater.* **2002**, *50*, 757–773.

(299) Dumez, M. C.; Marin-Ayral, R. M.; Tédenac, J. C. The Role of Experimental Parameters in Combustion Synthesis of NiAl under High Gas Pressure. *J. Alloys Compd.* **1998**, *268*, 141–151.

(300) Dong, S.; Hou, P.; Yang, H.; Zou, G. Synthesis of Intermetallic NiAl by SHS Reaction Using Coarse-Grained Nickel and Ultrafine-Grained Aluminum Produced by Wire Electrical Explosion. *Intermetallics* **2002**, *10*, 217–223.

(301) Granier, J. J.; Plantier, K. B.; Pantoya, M. L. The Role of the Al_2O_3 Passivation Shell Surrounding Nano-Al Particles in the Combustion Synthesis of NiAl. *J. Mater. Sci.* **2004**, *39*, 6421–6431.

(302) Hunt, E. M.; Pantoya, M. L. Ignition Dynamics and Activation Energies of Metallic Thermites:

From Nano- to Micron-Scale Particulate Composites. *J. Appl. Phys.* **2005**, *98*, 034909.

(303) Bucher, P.; Yetter, R. A.; Dryer, F. L.; Vicenzi, E. P.; Parr, T. P.; Hanson-Parr, D. M. Condensed-Phase Species Distributions about Al Particles Reacting in Various Oxidizers. *Combust. Flame* **1999**, *117*, 351–361.

(304) Vorozhtsov, A. B.; Lerner, M.; Rodkevich, N.; Nie, H.; Abraham, A.; Schoenitz, M.; Dreizin, E. L. Oxidation of Nano-Sized Aluminum Powders. *Thermochim. Acta* **2016**, *636*, 48–56.

(305) Kissinger, H. E. Reaction Kinetics in Differential Thermal Analysis. *Anal. Chem.* **1957**, *29*, 1702–1706.

(306) Sharma, R.; Holland, G. P.; Solomon, V. C.; Zimmermann, H.; Schiffenhaus, S.; Amin, S. A.; Buttry, D. A.; Yarger, J. L. NMR Characterization of Ligand Binding and Exchange Dynamics in Triphenylphosphine-Capped Gold Nanoparticles. *J. Phys. Chem. C* **2009**, *113*, 16387–16393.

(307) Son, S. U.; Jang, Y.; Yoon, K. Y.; Kang, E.; Hyeon, T. Facile Synthesis of Various Phosphine-Stabilized Monodisperse Palladium Nanoparticles through the Understanding of Coordination Chemistry of the Nanoparticles. *Nano Lett.* **2004**, *4*, 1147–1151.

(308) Klein, T.; Kickelbick, G. Aluminum Nanoparticle Preparation via Catalytic Decomposition of Alane Adducts – Influence of Reaction Parameters on Nanoparticle Size, Morphology and Reactivity. *Dalt. Trans.* **2020**, *49*, 9820–9834.

(309) Klein, T.; Kickelbick, G. Synthesis of Submicron Aluminum Particles via Thermal Decomposition of Alkyl Aluminum Precursors in the Presence of Metal Seeds and Their Application in the Formation of Ruthenium Aluminides. *Nanotechnology* **2020**, *31*, 265605.

(310) Carenco, S.; Boissière, C.; Nicole, L.; Sanchez, C.; Le Floch, P.; Mézailles, N. Controlled Design of Size-Tunable Monodisperse Nickel Nanoparticles. *Chem. Mater.* **2010**, *22*, 1340–1349.

(311) Henkes, A. E.; Vasquez, Y.; Schaak, R. E. Converting Metals into Phosphides: A General Strategy for the Synthesis of Metal Phosphide Nanocrystals. *J. Am. Chem. Soc.* **2007**, *129*, 1896–1897.

(312) Carroll, K. J.; Reveles, J. U.; Shultz, M. D.; Khanna, S. N.; Carpenter, E. E. Preparation of Elemental Cu and Ni Nanoparticles by the Polyol Method: An Experimental and Theoretical Approach. *J. Phys. Chem. C* **2011**, *115*, 2656–2664.

(313) Yang, J.; Ye, F.; Liu, H.; Yang, J.; Cao, H. Morphology and Structure Controlled Synthesis of Ruthenium Nanoparticles in Oleylamine. *Dalt. Trans.* **2013**, *42*, 12309–12316.

(314) Can, H.; Metin, Ö. A Facile Synthesis of Nearly Monodisperse Ruthenium Nanoparticles and Their Catalysis in the Hydrolytic Dehydrogenation of Ammonia Borane for Chemical Hydrogen Storage. *Appl. Catal. B Environ.* **2012**, *125*, 304–310.

(315) Yu, M.; Diao, X.; Huang, T.; Liu, H.; Li, J. Shape-Controlled Synthesis of Ruthenium Nanoparticles. *Funct. Mater. Lett.* **2011**, *4*, 337–340.

(316) Lee, J. Y.; Yang, J.; Deivaraj, T. C.; Too, H. P. A Novel Synthesis Route for Ethylenediamine-Protected Ruthenium Nanoparticles. *J. Colloid Interface Sci.* **2003**, *268*, 77–80.

(317) Quek, X. Y.; Pestman, R.; Van Santen, R. A.; Hensen, E. J. M. Structure Sensitivity in the Ruthenium Nanoparticle Catalyzed Aqueous-Phase Fischer-Tropsch Reaction. *Catal. Sci. Technol.* **2014**, *4*, 3510–3523.

(318) Yang, Y.; Yang, X.; Zhao, Y.; Song, Q.; Luo, Y. Tunable Preparation of Ruthenium Nanoparticles with Superior Size-Dependent Catalytic Hydrogenation Properties. *J. Hazard. Mater.* **2017**, *332*, 124–131.

(319) Garcia-Pena, N. G.; Redon, R.; Herrera-Gomez, A.; Fernandez-Osorio, A. L.; Bravo-Sanchez, M.; Gomez-Sosa, G. Solventless Synthesis of Ruthenium Nanoparticles. *Appl. Surf. Sci.* **2015**, *340*, 25–34.

(320) Fedotova, T. D.; Glotov, O. G.; Zarko, V. E. Chemical Analysis of Aluminum as a Propellant Ingredient and Determination of Aluminum and Aluminum Nitride in Condensed Combustion Products. *Propellants, Explos. Pyrotech.* **2000**, *25*, 325–332.

(321) Yang, S.-P.; Tsai, R.-Y. Complexometric Titration of Aluminum and Magnesium Ions in Commercial Antacids. An Experiment for General and Analytical Chemistry Laboratories. *J. Chem. Educ.* **2006**, *83*, 906–909.

(322) Peterson, J. D.; Vyazovkin, S.; Wight, C. A. Kinetics of the Thermal and Thermo-Oxidative Degradation of Polystyrene, Polyethylene and Poly(Propylene). *Macromol. Chem. Phys.* **2001**, *202*, 775–784.

(323) Iwata, T.; Matsumoto, T.; Terakawa, S.; Kobayashi, H. Fabrication of Al_2O_3/Al Structure by Nitric Acid Oxidation at Room Temperature. *Cent. Eur. J. Phys.* **2010**, *8*, 1015–1020.

(324) Klein, T.; Pauly, C.; Mücklich, F.; Kickelbick, G. Al and Ni Nanoparticles as Precursors for Ni Aluminides. *Intermetallics* **2020**, *124*, 106839.

(325) Klein, T.; Pauly, C.; Mücklich, F.; Kickelbick, G. Al and Ru Nanoparticles as Precursors for Al-Ru Intermetallics. *Intermetallics* **2020**, *124*, 106851.

(326) Rodriguez, M. A.; Adams, D. P.; Tissot, R. G. Determination of Activation Energy of Intermixing in Textured Metal-Metal Multilayer Films via Two-Dimensional X-Ray Diffraction. *Powder Diffr.* **2009**, *24*, 82–84.

(327) Mikhailov, I.; Levina, V.; Leybo, D.; Masov, V.; Tagirov, M.; Kuznetsov, D. Synthesis, Characterization and Reactivity of Nanostructured Zero-Valent Iron Particles for Degradation of Azo Dyes. *Int. J. Nanosci.* **2017**, *16*, 3–9.

(328) Von Hoene, J.; Charles, R. G.; Hickam, W. M. Thermal Decomposition of Metal Acetylacetonates Mass Spectrometer Studies. *J. Phys. Chem.* **1958**, *62*, 1098–1101.

(329) Roy, R.; Sen, S. K. Calorimetric and Other Studies of Intermetallic Phase Formation in Ag/Al Bilayer Thin Films. *J. Mater. Sci.* **1992**, *27*, 6098–6104.

(330) Aboulfadl, H.; Gallino, I.; Busch, R.; Mücklich, F. Atomic Scale Analysis of Phase Formation and Diffusion Kinetics in Ag/Al Multilayer Thin Films. *J. Appl. Phys.* **2016**, *120*, 195306.

(331) Shouheng Sun, Hao Zeng, David B. Robinson, Simone Raoux, Philip M. Rice, Shan X. Wang, and G. L. Controlled Synthesis of MFe_2O_4 (M = Mn, Fe, Co, Ni and Zn) Nanoparticles. *J.Am.Chem.Soc.* **2004**, *126*, 273–279.

(332) Schäfer, S.; Kickelbick, G. Diels-Alder Reactions on Surface-Modified Magnetite/Maghemite Nanoparticles: Application in Self-Healing Nanocomposites. *ACS Appl. Nano Mater.* **2018**, *1*, 2640–2652.

(333) Feldmann, C.; Jungk, H. O. Polyol-Mediated Preparation of Nanoscale Oxide Particles. *Angew. Chemie - Int. Ed.* **2001**, *40*, 359–362.

(334) Feldmann, C. Darstellung Und Charakterisierung Der Nanoskaligen Vb-Metalloxide M_2O_5 (M = V, Nb, Ta). *Zeitschrift fur Anorg. und Allg. Chemie* **2004**, *630*, 2473–2477.

(335) Bruker AXS Karlsruhe. Topas 5.1. General Profile and Structure Analysis Software for Powder Diffraction Data. Karlsruhe 2014.

(336) Cheary, R. W.; Coelho, A. A.; Cline, J. P. Fundamental Parameters Line Profile Fitting in Laboratory Diffractometers. *J. Res. Natl. Inst. Stand. Technol.* **2004**, *109*, 1–25.

(337) Merkys, A.; Vaitkus, A.; Butkus, J.; Okulič-Kazarinas, M.; Kairys, V.; Gražulis, S. COD::CIF::Parser: An Error-Correcting CIF Parser for the Perl Language. *J. Appl. Crystallogr.* **2016**, *49*, 292–301.

(338) Jain, A.; Ong, S. P.; Hautier, G.; Chen, W.; Richards, W. D.; Dacek, S.; Cholia, S.; Gunter, D.; Skinner, D.; Ceder, G.; et al. Commentary: The Materials Project: A Materials Genome Approach to Accelerating Materials Innovation. *APL Mater.* **2013**, *1*, 011002.

(339) Schneider, C. A.; Rasband, W. S.; Eliceiri, K. W. NIH Image to ImageJ: 25 Years of Image Analysis. *Nat. Methods* **2012**, *9*, 671–675.

(340) Cui, Y.; Huang, D.; Li, Y.; Huang, W.; Liang, Z.; Xu, Z.; Zhao, S. Aluminium Nanoparticles Synthesized by a Novel Wet Chemical Method and Used to Enhance the Performance of Polymer Solar Cells by the Plasmonic Effect. *J. Mater. Chem. C* **2015**, *3*, 4099–4103.

(341) Park, J.; Kwon, S. G.; Jun, S. W.; Kim, B. H.; Hyeon, T. Large-Scale Synthesis of Ultra-Small-Sized Silver Nanoparticles. *ChemPhysChem* **2012**, *13*, 2540–2543.

7. Appendix

7.1 Characterization of the commercial Ni powder

The Ni powder obtained from Fluka (Buchs, Switzerland) consisted of quasi spherical particles with irregular surfaces. The mean diameter of the particles determined from the SEM images was 7 ± 2 µm. The crystallite size determined from Rietveld refinement was 258(8) nm (Figure 64).

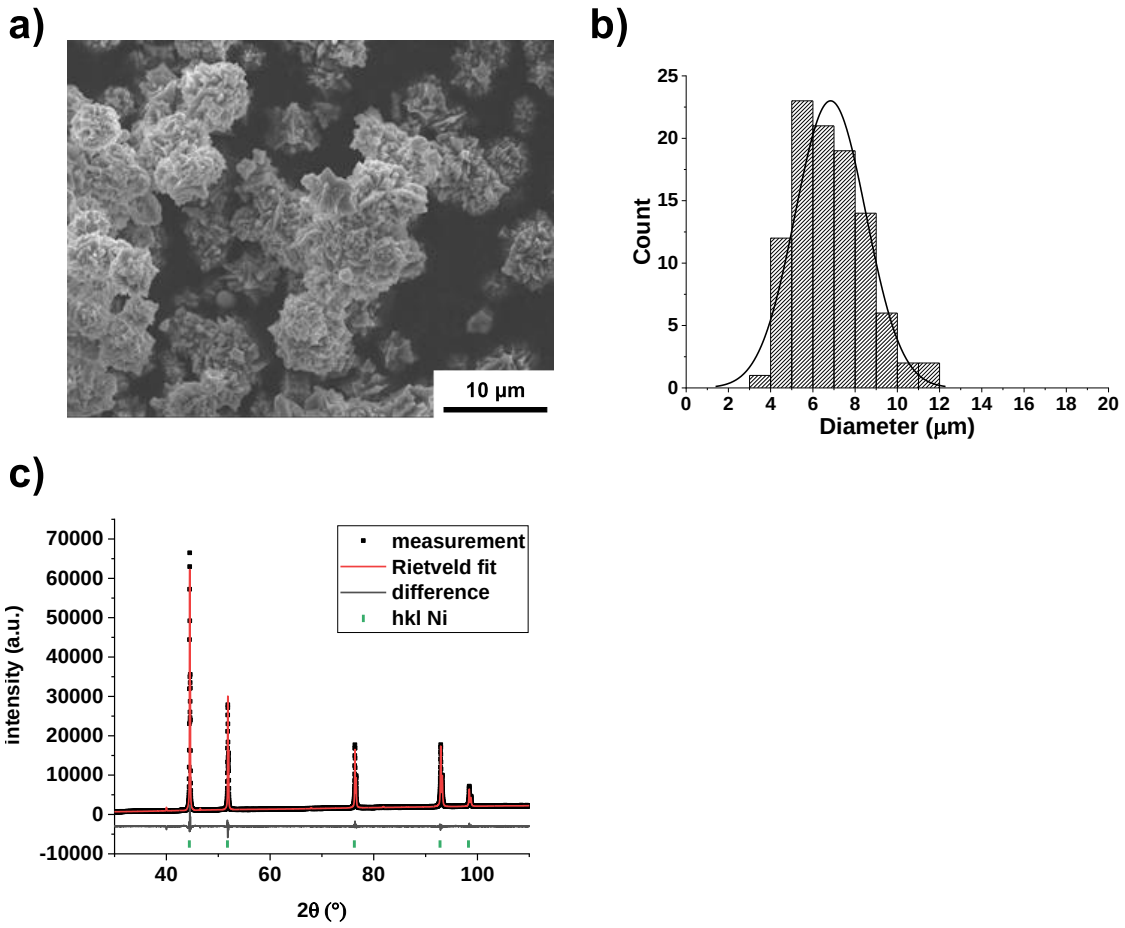

***Figure 64**: **a)** SEM images of commercial Ni powder used for the synthesis of aluminides; **b)** particle size distribution obtained from the SEM images by measuring 100 particles; **c)** XRD measurement and Rietveld refinement of the commercial Ni powder.*

7.2 Characterization of the commercial Co powder

The Co powder obtained from Aldrich (St. Louis, USA) consisted of severely agglomerated and sintered spherical particles with a mean diameter determined from the SEM images of 0.9 ± 0.2 µm (Figure 65).

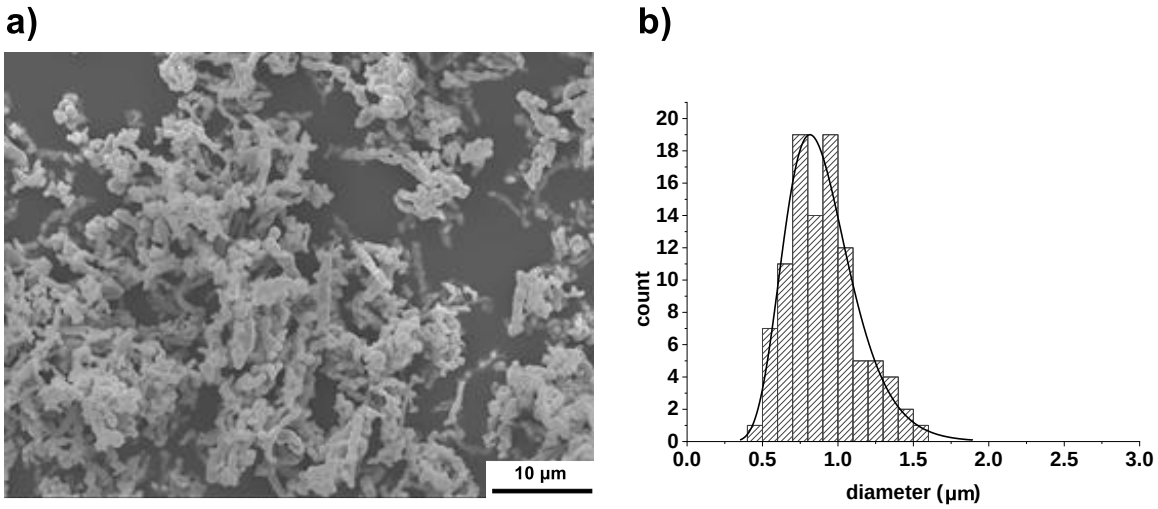

***Figure 65**: **a)** SEM images of commercial Co powder used for the synthesis of aluminides; **b)** particle size distribution obtained from the SEM images by measuring 100 particles.*

7.3 Diffractograms of the nanocrystalline Cu_2O and V_2O_5

XRD measurements revealed the presence of Cu_2O with a crystallite size of 273(13) nm (Figure 66).

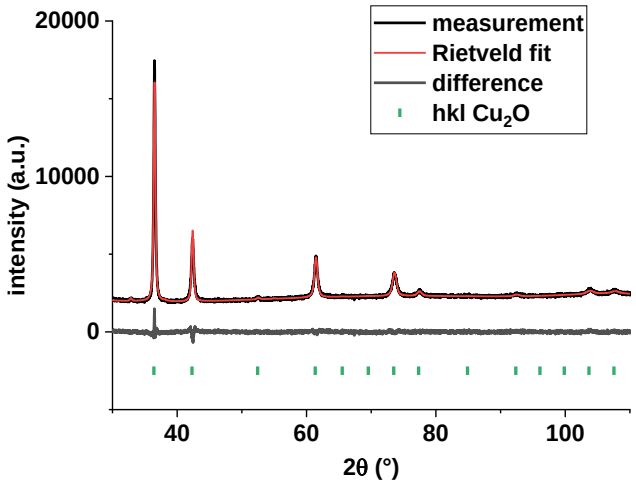

***Figure 66**: XRD measurement and Rietveld refinement of nanocrystalline Cu_2O prepared from $Cu(acac)_2$ in diethylene glycol.*

XRD measurements revealed the presence of V_2O_5 with a crystallite size of 36(2) nm. Moreover, the sample was found to contain 5 wt% of Vanadium(IV)oxide as an impurity phase (Figure 67).

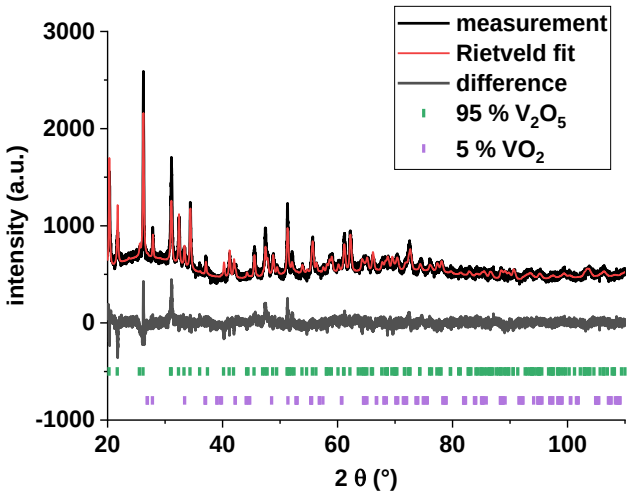

***Figure 67**: XRD measurement and Rietveld refinement of nanocrystalline V_2O_5 prepared from $VO(O^iPr)_3$ in diethylene glycol.*

7.4 Supporting information for Chapter 3.1.3.2

Supporting information

Aluminum nanoparticle preparation via catalytic decomposition of alane adducts – Influence of reaction parameters on nanoparticle size, morphology and reactivity

Thomas Klein, Guido Kickelbick

Saarland University, Inorganic Solid State Chemistry, Campus $C4_1$, 66123 Saarbrücken, Germany

E-mail: guido.kickelbick@uni-saarland.de

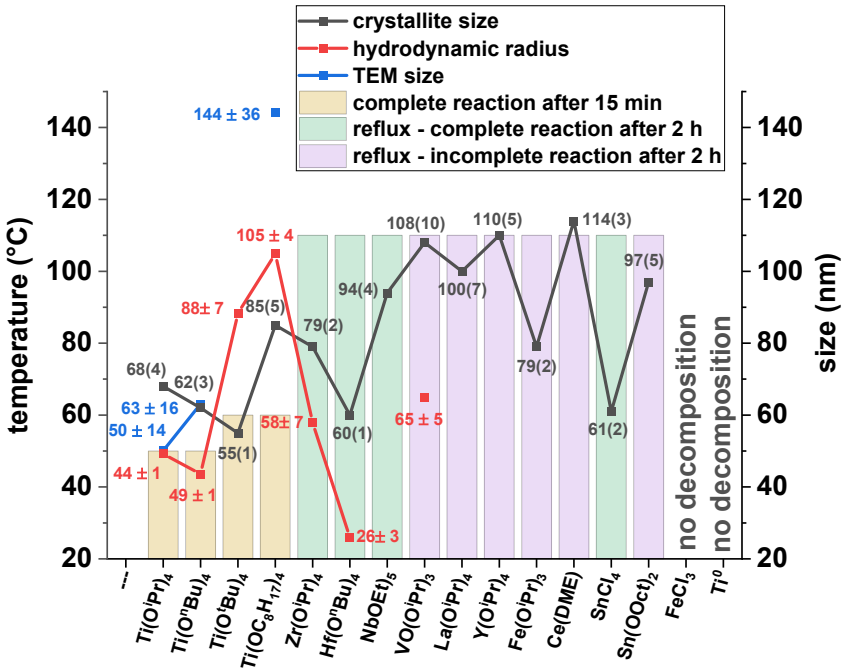

Figure S1: The concentrations used were as follows: 35 mM H_3AlNEt_3, Al: PPh_3 5:1 and cat.:Al 2 ppm. The crystallite sizes were determined from Rietveld refinements of the dried powders.

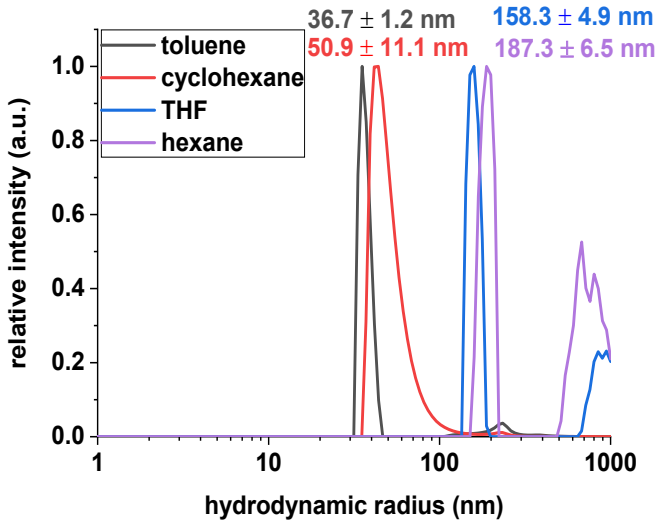

Figure S2: DLS measurements of Al nanoparticles synthesized from H_3AlNEt_3 in different solvents in methanol. The concentrations used were as follows: 35 mM H_3AlNEt_3, Al: epoxyhexane 4:1 and cat.:Al 2 ppm.

a)

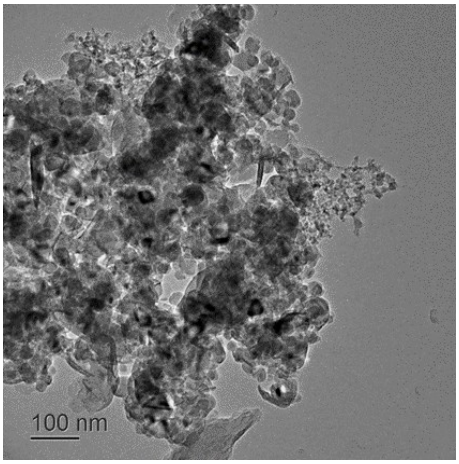
100 nm

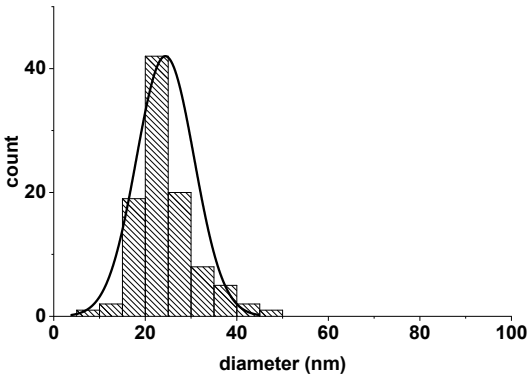
count
diameter (nm)
0
20
40
0
20
40
60
80
100

b)

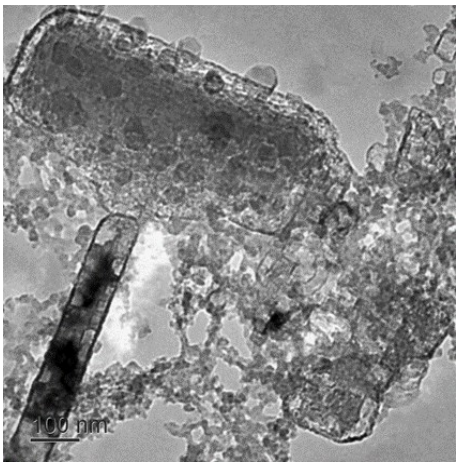
100 nm

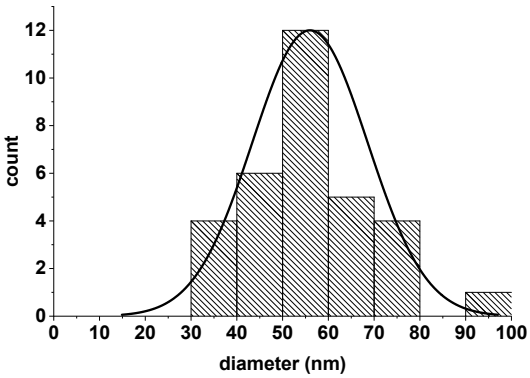
count
diameter (nm)
0
2
4
6
8
10
12
0
10
20
30
40
50
60
70
80
90
100

c)

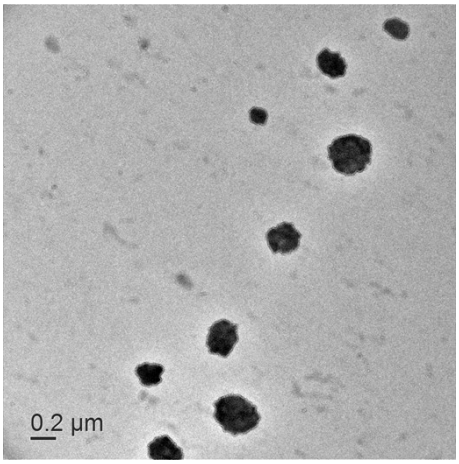
0.2 µm

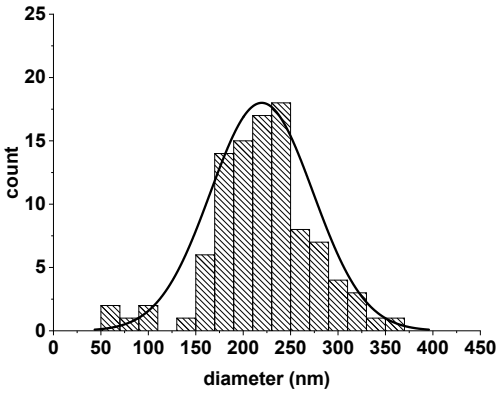
count
diameter (nm)
0
5
10
15
20
25
0
50
100
150
200
250
300
350
400
450

d)

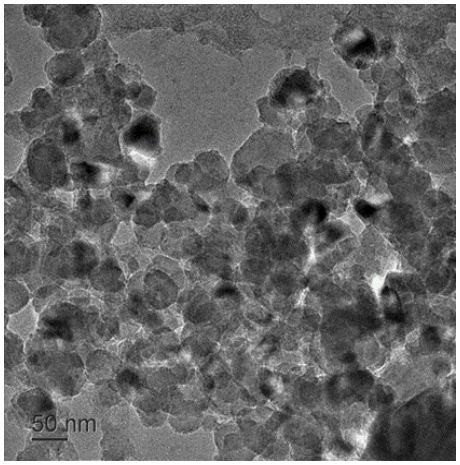
50 nm

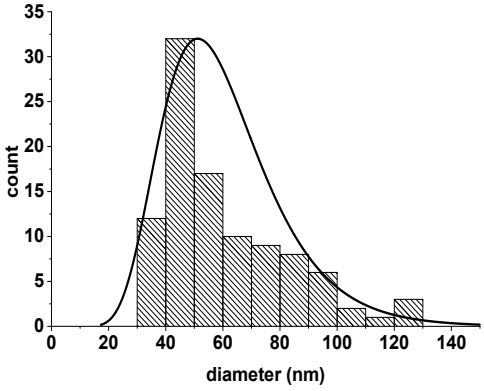
count
diameter (nm)
0
5
10
15
20
25
30
35
0
20
40
60
80
100
120
140

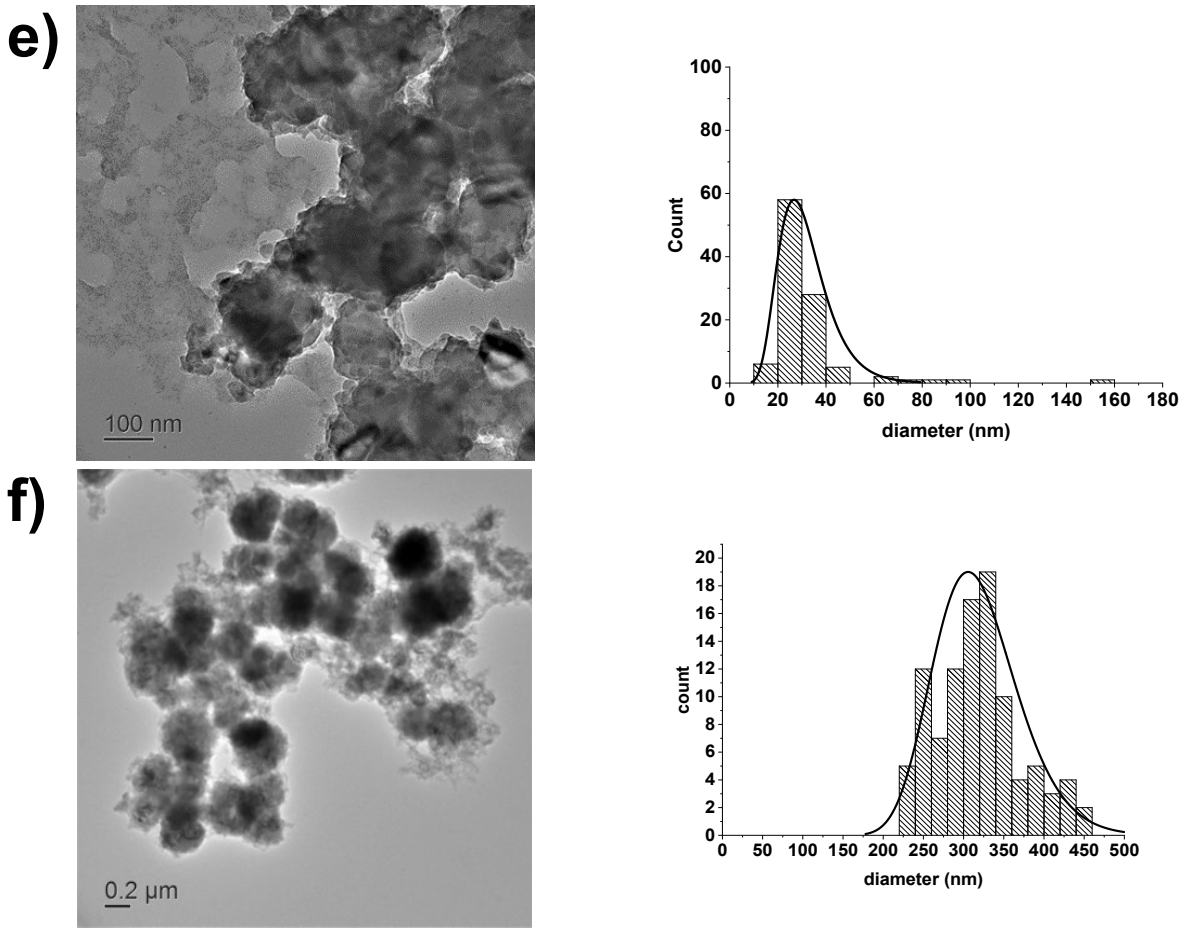

Figure S3: a) TEM image of Al particles synthesized from H_3AlNMe_2Et, **b)** H_3AlNBu_3, **c)** $H_3AlNOct_3$, **d)** $H_3Al{\cdot}THF$, **e)** $H_3Al{\cdot}IMes$, **f)** $H_3Al{\cdot}PCy_3$ and the respective particle size distributions

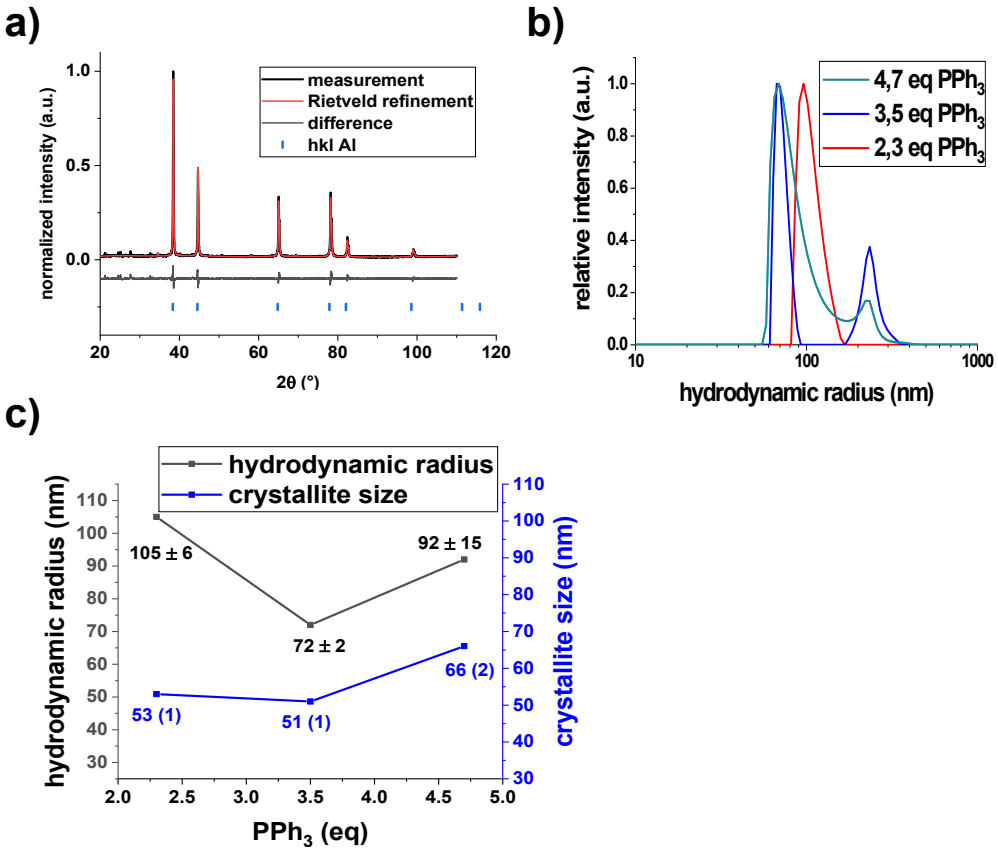

Figure S4: **a)** PXRD measurement and Rietveld refinement, **b)** DLS measurements in methanol, and **c)** a comparison of hydrodynamic radii as well as crystallite sizes of Al nanoparticles synthesized via a chemical reduction approach.

Table S1: CHN analyses of Al nanoparticles synthesized using different stabilizers in toluene. The concentrations used were as follows: 35 mM H_3AlNEt_3 (unless stated otherwise), and cat.:Al 2 ppm

stabilizer	C [%]	H[%]	N[%]	Σ (CHN) [%]
---	3.16	1.29	0.45	4.90
--- - $H_3AlNOct_3$ as precursor				
5.0 eq PPh_3	8.36	1.89	---	7.5
5.0 eq TOP	4.72	1.82	0.97	7.51
0.25 eq TOP				
5.0 eq $N(Oct)_3$		no decomposition		
0.25 eq $N(Oct)_3$	5.27	1.68	0.53	7.48
0.12 TOEDA	4.73	1.44	0.48	6.65
0.25 eq $N(Bu)_3$	2.82	0.95	0.33	4.10
0.25 eq NPh_3	3.01	1.01	0.50	4.52

0.25 eq $N(^iBu)_3$	4.74	1.63	0.53	6.90
0.25 eq TOPO	2.34	0.99	3.19	6.52
5.0 eq PCy_3				
5.0 eq NPh_3				

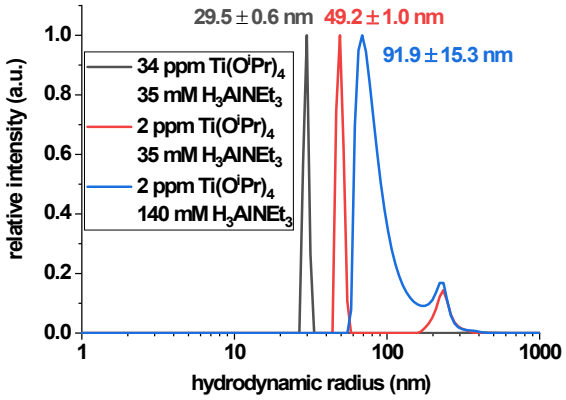

Figure S5: DLS measurements of Al nanoparticles synthesized in the presence of 5 eq. PPh_3 applying different concentrations of the precursor and decomposition catalyst.

Synthesis and characterization of the alane precursors

Methods

^1H, ^{13}C, ^{31}P and ^{27}Al NMR spectra were recorded on a Bruker Avance III HD 400 MHz spectrometer. ^1H spectra were recorded at 400 MHz, ^{13}C at 101 MHz, ^{31}P at 162 MHz and ^{27}Al at 104 MHz. All spectra were recorded at room temperature in benzene-d_6 (C_6D_6) or chloroform-d ($CDCl_3$).

A Bruker Vertex 70 ATR-FTIR spectrometer was used for recording the IR spectra. The spectra were recorded as an average of 16 scans for background and sample in a range from 4000 – 400 cm^{-1} in a resolution of 4 cm^{-1} applying a DIAMOND ATR-QL measurement cell from Bruker in an atmosphere of flowing Ar.

A titriometric determination of the hydride content of the alane precursors was carried out according to methods described in the literature for $LiAlH_4$ [1,2]: The alane (~ 0.5 mmol) to be determined was dissolved in 10 ml of THF. To this solution 9-fluorenone was added dropwise (1 M in THF) under stirring until a yellow coloration remained visible.

Materials

Tributylamine (NBu_3, >98 %) was purchased from TCI Japan (Tokyo, Japan) and trioctylamine ($N(Oct)_3$ < 92.5 %) was obtained from Merck (Darmstadt, Germany). Bis(2-dimethylaminoethyl)-methylamine (PMDTA, 99 %) and $LiAlH_4$ (95 %) were purchased from Sigma-Aldrich (Munich, Germany). Triethylamine (> 99 %) was purchased from applichem (Darmstadt, Germany). 1,4-Diazabicyclo[2.2.2]octane (DABCO, 98 %) was obtained from Alfa Aesar (Ward Hill, USA). $AlCl_3$ (98.5 %) was from Acros Organics (Geel, Belgium). Tricyclohexylphosphine (>97 %) was delivered from Carbosynth (Berkshire, United Kingdom). Toluene, THF, hexane, and diethylether were purified in a MBraun solvent purification system. All chemicals were used as received unless stated otherwise. The reactions were carried out under an Ar atmosphere using either a glove box or Schlenk line techniques.

Synthesis of H_3AlNR_3

Triethylamine alane, tributylamine alane and trioctylamine alane were synthesized following known literature methods[3]. A typical synthesis was carried out as follows: 1.81 g $LiAlH_4$ (48 mmol) and 1.89 g $AlCl_3$ (14 mmol) were slurried in 50 ml of dry toluene. To this suspension 14.2 ml (60 mmol) tributylamine was added dropwise under stirring. The mixture was stirred over night at room temperature and filtered through a glass frit. The volume of the filtrate reduced to half of its volume and the resulting solution was stored at - 25 °C overnight. The resulting white solid was recrystallized from toluene and stored under Ar at - 25 °C. When Trioctylamine was used, no crystallization could be observed over a period of 3 months. Thus, the remaining solvent was removed in vacuo resulting in the formation of a colorless liquid, which was stored at -25 °C under Ar.

Yields: H_3AlNMe_2Et: colorless liquid, 5.4 g (85 % based on Al)

H_3AlNEt_3: colorless liquid, 24.7 g (76 % based on Al)

H_3AlNBu_3: white solid, 10.7 g (80 % based on Al)

$H_3AlNOct_3$: colorless liquid, yield could not be determined

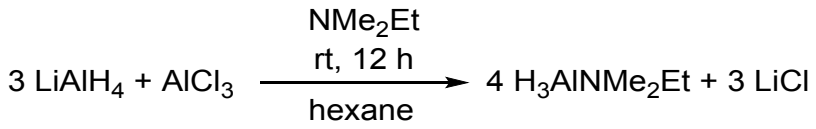

Scheme S1*: Synthesis procedure for H_3AlNMe_2Et.*

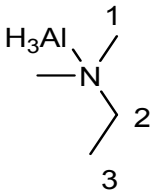

^{1}H NMR (C_6D_6; 400 MHz): 0.78 (tr; 3H; H3; J = 4 Hz), 1.94 (s; 6H; H1). 2.29 (q; 2H; H2; J = 8 Hz), 3.98 (br s; AlH) ppm. ^{13}C NMR (C_6D_6; 101 MHz): 9.18 (C3), 44.23 (C1), 53.93 (C2) ppm. ^{27}Al NMR (C_6D_6; 104 MHz): 140.84 ppm.

H_3AlNEt_3

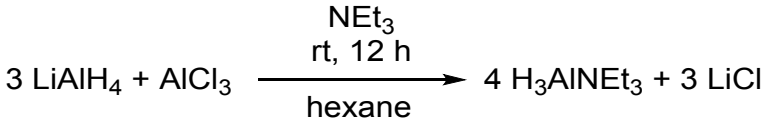

Scheme S2*: Synthesis procedure for H_3AlNEt_3.*

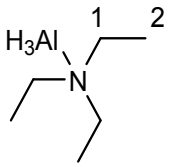

^{1}H NMR (C_6D_6; 400 MHz): 0.86 (tr; 9H; H2; J = 8 Hz), 2.39 (q; 6H; H1; J = 8 Hz), 4.00 (br s; AlH) ppm. ^{13}C NMR (C_6D_6; 101 MHz): 9.05 (C2), 48.17 (C1) ppm. ^{27}Al NMR (C_6D_6; 104 MHz): 140.84 ppm. δ

IR: Al-H: 1762 cm^{-1}.

H_3AlNBu_3

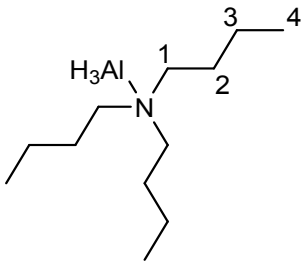

^{1}H NMR (C_6D_6; 400 MHz): 0.78 (tr; 9H; H4; J = 8 Hz), 1.06 (sxt; 6H; H3; J = 8 Hz), 1.48-1.56 (m; 6H; H2), 2.46-2.51 (m; 6H; H1), 4.28 (br s; AlH) ppm. ^{13}C NMR (C_6D_6; 101 MHz): 13.90 (C4), 20.97 (C3), 26.42 (C2), 55.23 (C1) ppm. ^{27}Al NMR (C_6D_6; 104 MHz): 163.78 ppm.

IR: Al-H: 1753 cm^{-1}.

$H_3AlN(Oct)_3$

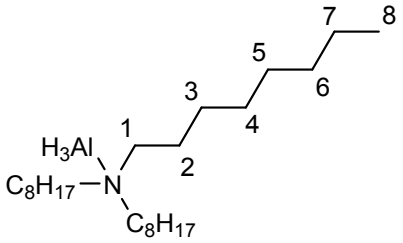

^{1}H NMR (C_6D_6; 400 MHz): 0.91 (tr; 9H; H8; J = 8 Hz), 1.14-1.31 (m; 30H; H7+H6+H5+H4+H3), 1.55-1.61 (m; 6H; H2), 2.53-2.57 (m; 6H; H1), 4.25 (br s; AlH) ppm. Aromatic signals + 2.12 ppm: residual toluene.

^{13}C NMR (C_6D_6; 101 MHz):14.40 (C8), 23.11, 27.94, 29.74, 29.75, 32.24, 55.36 ppm.

IR: Al-H: 1769 cm^{-1}.

Synthesis of H_3AlNMe_3

The synthesis was carried out according the methods reported in the literature[4]: 0.5 g (13 mmol) of $LiAlH_4$ and 1.02 g (11 mmol) of $NMe_3 \cdot HCl$ were placed in a 100 ml Schlenk flask and cooled to -50 °C. 50 ml of diethylether were added and the reaction mixture was stirred for 4 h while slowly warming up to room temperature. The solvent was removed in vacuo and 30 ml of hexane were added to the resulting white residue. The reaction mixture was filtered and the filtrate was concentrated in vacuo. After storage at – 25 °C the resulting white solid was collected by filtration and dried in vacuo at 0 °C.

Yield: white solid, 847 mg (72 % based on Al)

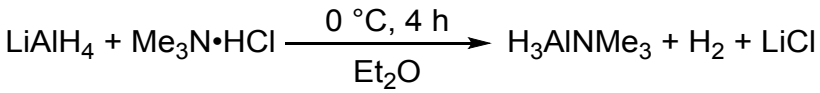

Scheme S3: Synthesis procedure for H_3AlNMe_3.

^1H NMR (C_6D_6; 400 MHz): 1.87 (s; 9H), 4.08 (br s; Al-H) ppm.

^{13}C NMR (C_6D_6; 101 MHz): 47.46 ppm. ^{27}Al NMR (C_6D_6; 104 MHz): 140.46 ppm.

IR: Al-H: 1779 cm^{-1}.

Synthesis of $H_3Al \cdot THF$

The preparation was carried out following literature procedures[5]: 1.09 g $LiAlH_4$ (29 mmol) were dissolved in 50 ml THF and the resulting mixture was cooled to 0 °C. 1.26 g $AlCl_3$ (9 mmol) were added in portions and after the complete addition the mixture was stirred for 3 h at 0 °C. The reaction mixture was filtered and the filtrate was concentrated to dryness. 50 ml of hexane were added and the mixture was stirred for 30 min. A white solid was removed by filtration and the filtrate was concentrated in vacuo at room temperature yielding a white solid which was stored under Ar at -10 °C.

Yield: white solid, 3.62 g (92 % based on Al)

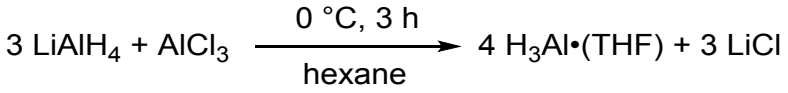

Scheme S4: Synthesis procedure for $H_3Al{\cdot}THF$.

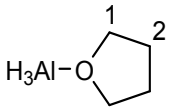

^{1}H NMR (C_6D_6; 400 MHz): 1.12-1.16 (m; 4H; H2), 3.59-3.63 (m; 4H; H1), 4.21 (br s; AlH) ppm. ^{13}C NMR (C_6D_6; 101 MHz): 25.33 (C2), 69.74 (C1) ppm. ^{27}Al NMR (C_6D_6; 104 MHz): 119.74 ppm.

IR: Al-H: 1807 cm^{-1}.

Synthesis of $[H_2Al(PMDTA)]^+[AlH]^-$

The synthesis was carried out applying known literature methods[6]: Briefly, 1.12 g H_3AlNEt_3 (9 mmol) were dissolved in 25 ml of diethylether. To this solution 1.8 ml (5 mmol) of PMDTA in 15 ml diethylether were added dropwise at 0 °C. The resulting white reaction mixture was stirred for 2 more hours at room temperature before the solvent was evaporated in vacuo. The remaining white solid was recrystallized from THF and stored under Ar at -10 °C.

Yield: white solid, 877 mg (84 % based on Al)

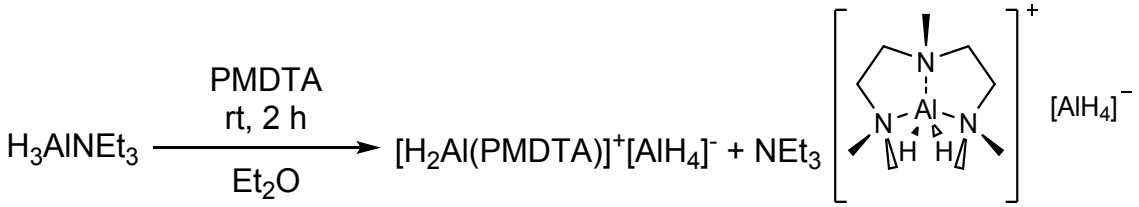

Scheme S5: Synthesis procedure for $[H_2Al(PMDTA)]^+[AlH]^-$.

IR: Al-H: 1662 cm^{-1} + 1826 cm^{-1}

Synthesis of H_3Al·DABCO

The synthesis was carried out applying known literature methods[7]. 1.02 g DABCO (9 mmol) were dissolved in 30 ml of toluene. To this solution 2.33 g of H_3AlNEt_3 (17 mmol) were added in portions under stirring. The resulting mixture was stirred for 2 h at room temperature. The solvent was evaporated in vacuo and the resulting white solid was washed with diethylether and stored under Ar at –10 °C.

Yield: white solid, 2.49 g (97%). The product was obtained as a mixture of H_3AlNEt_3 and H_3Al·DABCO

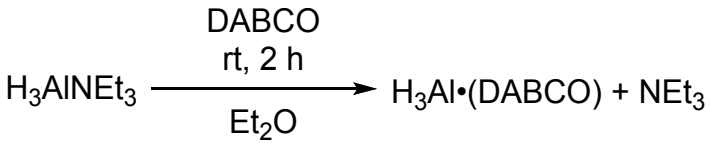

Scheme S6: Synthesis procedure for H_3Al·DABCO.

IR: Al-H: 1691 cm^{-1} + 1762 cm^{-1}

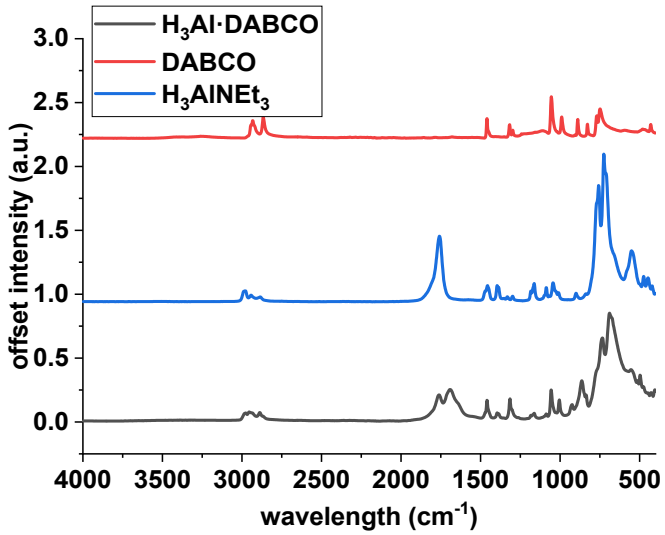

Figure S29: ATR-FTIR spectra of H_3Al·DABCO, H_3AlNEt_3 and DABCO.

Synthesis of $H_3Al{\cdot}PCy_3$

Protocols reported in the literature were applied[8]: Briefly, a solution of 1.5 g of PCy_3 (5 mmol) in 10 ml of diethylether was bubbled with HCl under stirring for 30 min. A white solid was formed and the solvent was removed in vacuo.

Yield: 1.63 g (97 %)

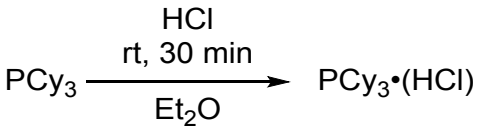

Scheme S7: Synthesis procedure for $PCy_3{\cdot}HCl$.

^1H NMR ($CDCl_3$; 400 MHz): 1.29-2.57 (m; 33H; Cy), 7.81 (d; 1H; P-H; J = 492 Hz). ^{31}P NMR ($CDCl_3$; 162 MHz): 31.35 (d; J = 491 Hz) ppm.

To a mixture of 302 mg $LiAlH_4$ (8 mmol) and 1.6 g $PCy_3{\cdot}HCl$ (5 mmol) was added 70 ml of diethylether at -78 °C. The mixture was stirred over night while warming up to room temperature. The formed solid was filtered off and the filtrate was concentrated to dryness. The resulting white solid was recrystallized from diethylether and stored under Ar at -10 °C.

Yield: white solid, 490 mg (32 % based on Al)

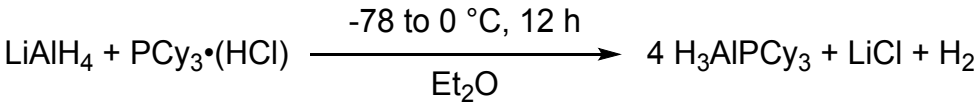

Scheme S8: Synthesis procedure for $H_3Al{\cdot}PCy_3$.

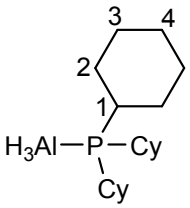

^{1}H NMR (C_6D_6; 400 MHz): 0.98-1.08 (m; 9H; Cy), 1.42-1.59 (m; 15H; Cy), 1.81-1.87 (m; 9H; Cy), 4.26 (br s; AlH) ppm. ^{31}P NMR (C_6D_6; 162 MHz): 3.57 ppm. ^{27}Al NMR (C_6D_6; 104 MHz): 118.67 ppm. IR: Al-H: 1750 cm^{-1}

Synthesis of H_3Al·IMes

The synthesis was carried out applying known literature methods[9,10]. Under an atmosphere of air, 58 ml (0.5 mol) glyoxal (40 % w/w in H_2O) were added to 54 g (0.4 mol) of 2,4,6-trimethylaniline in 200 ml of methanol. 0.5 ml of formic acid were added dropwise and the reaction mixture was stirred over night at room temperature. The formed yellow solid was collected, washed with 50 ml of methanol and dried in vacuo.

Yield: yellow solid, 54 g (92 %)

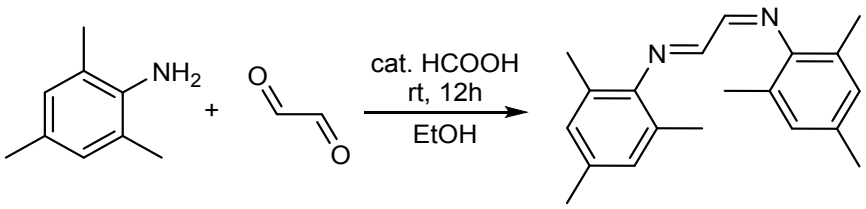

Scheme S9: Synthesis procedure for N^1,N^2-dimesitylethane-1,2-diimine.

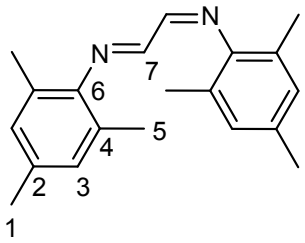

^{1}H NMR ($CDCl_3$; 400 MHz): 2.16 (s; 12H; H5), 2.30 (s; 6H; H1), 6.91 (s; 4H; H3), 8.11 (s; 2H; H7) ppm. ^{13}C NMR ($CDCl_3$; 101MHz): 18.34 (C5), 20.91 (C1), 126.70 (C4), 129.13 (C3), 134.40 (C2), 147.60 (C6), 163.63 (C7) ppm.

Under an atmosphere of air, 5 g of (17 mmol) N^1,N^2-dimesitylethane-1,2-diimine were dissolved in 120 ml of ethylacetate and 0.55 g (18 mmol) paraformaldehyde were added. 2.5 ml (20 mmol) TMSCl dissolved in 15 ml of ethylacetate were added dropwise and the reaction mixture was heated to 70 °C for 2 h. The formed solid was collected by filtration, washed with ethylacetate and dried at 100 °C.

Yield: very slight yellow solid, 2.6 g (45 %)

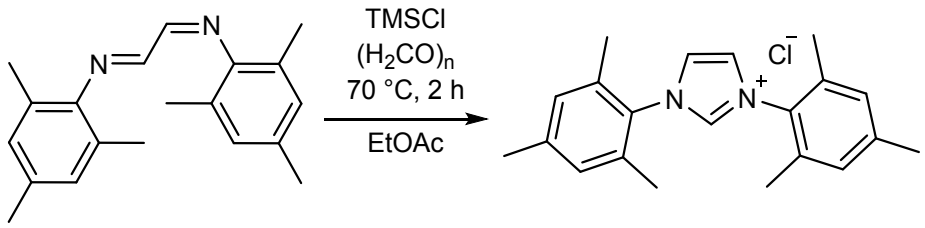

Scheme S10: Synthesis procedure for 1,3-bis-(2,4,6-trimethylphenyl)imidazolium chloride.

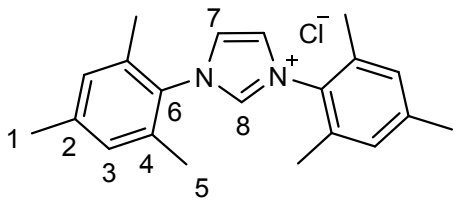

^{1}H NMR ($CDCl_3$; 400 MHz): 2.19 (s; 12H; H5), 2.34 (s; 6H; H1), 7.03 (s; 4H; H3), 6.91 (s; 4H; H3), 7.58 (s; 2H; H7), 11.03 (s; 1H; H8) ppm. ^{13}C NMR ($CDCl_3$; 101MHz): 17.82 (C5), 21.28 (C1), 124.37 (C6), 130.09 (C3), 130.77 (C2), 134.22 (C4), 141.49 (C7) ppm.

1 g (3 mmol) of 1,3-bis-(2,4,6-trimethylphenyl)imidazolium chloride were dispersed in 40 ml of THF. 150 mg (6 mmol) NaH and a grain of KO^{t}Bu were added and the resulting mixture was stirred over night at room temperature. The remaining solid was filtered off and the filtrate was concentrated in vacuo. The product was precipitated by adding 40 ml of Hexane, collected by filtration and dried in vacuo.

Yield: white solid, 687 mg (75 %)

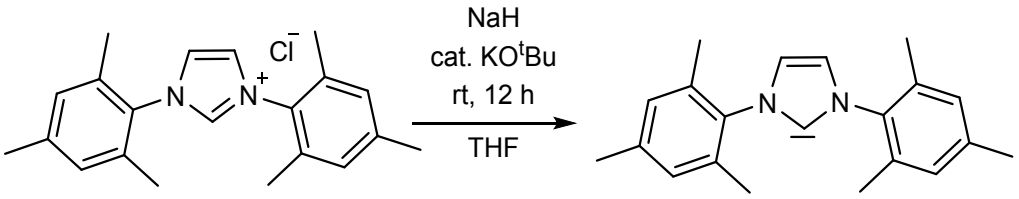

Scheme 11: Synthesis procedure for 1,3-bis-(2,4,6-trimethylphenyl)imidazolylidene (IMes).

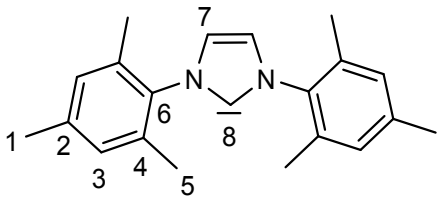

^{1}H NMR (C_6D_6; 400 MHz): 2.16 (s; 18H; H1+H5), 6.49 (s; 2H; H7), 6.81 (s; 4H; H3) ppm.
^{13}C NMR (C_6D_6; 101MHz): 18.07 (C5), 21.04 (C1), 120.56 (C7), 135.46 (C6), 137.28 (C4), 139.28 (C3), 219.18 (C8) ppm.

To a solution of 201 mg (0.7 mmol) of 1,3-bis-(2,4,6-trimethylphenyl)imidazolylidene in 20 ml of toluene were added 1.3 ml (0.7 mmol) of a 0.5 M solution of H_3AlNMe_2Et in toluene. The mixture was stirred for 2 h at room temperature and then dried in vacuo yielding a white to light yellow solid.

Yield: white solid, 154 mg (66%)

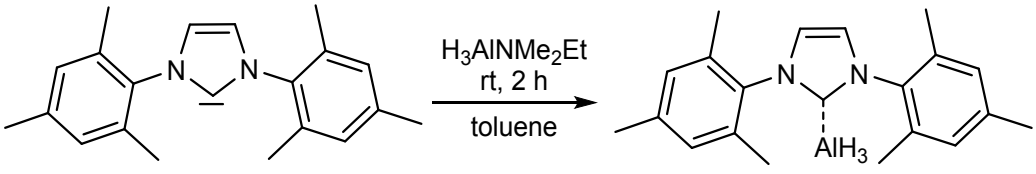

Scheme S12: Synthesis procedure for H_3Al·IMes.

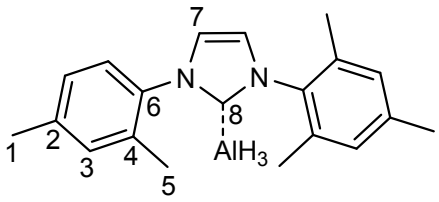

^{1}H NMR (C_6D_6; 400 MHz): 2.04 (s; 12H; H5), 2.07 (s; 6H; H1), 6.49 (s; 2H; H7), 3.79 (br s; AlH), 6.04 (s; 2H; H7), 6.74 (s; 4H; H3) ppm. ^{13}C NMR (C_6D_6; 101MHz): 17.63 (C5), 21.09 (C1), 122.50 (C7), 129.48 (C4), 130.02 (C2), 135.04 (C3), 139.55 (C6) ppm. ^{27}Al NMR (C_6D_6; 104 MHz): 117.54 ppm. IR: Al-H: 1741 cm^{-1}.

Synthesis of N,N,N′,N′-tetraoctylethylendiamine (TOEDA)

The synthesis was carried out applying known literature methods[11]. In an atmosphere of air, 1,45 ml (22 mmol) of ethylendiamine were dissolved in 5 ml of methanole/ hexane (50/50 v/v) and 15 ml of triethylamine were added. 15 ml (87 mmol) of 1-bromoctane were added dropwise and the reaction mixture was heated to reflux for 4 days. The formed solid was filtered off and the filtrate was concentrated to dryness. The viscous residue was dissolved in toluene, and the pH was adjusted to 7 using HCl/ NaOH. The organic phase was washed three times with 50 ml of H_2O, dried with $MgSO_4$ and the solvent was removed in vacuo.

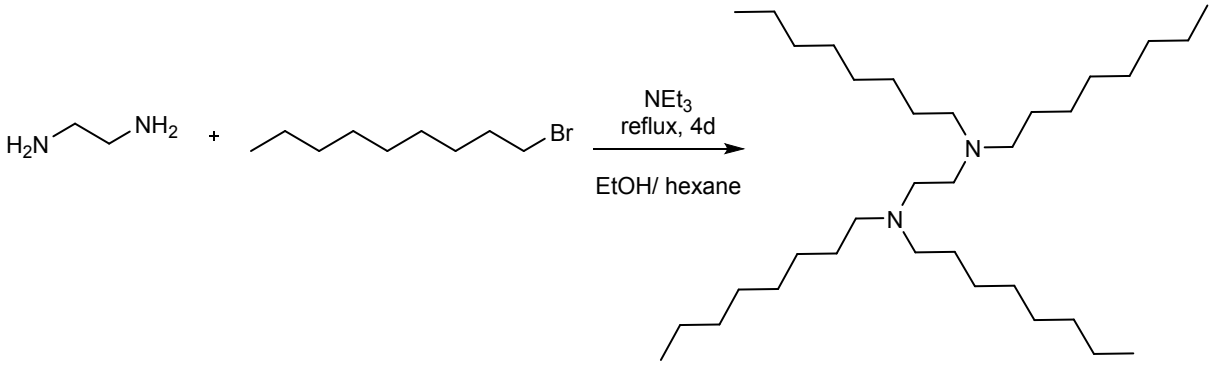

Scheme S13: Synthesis procedure for N,N,N′,N′-tetraoctylethylendiamine (TOEDA).

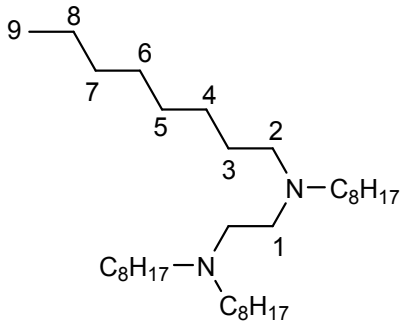

^{1}H NMR ($CDCl_3$; 400 MHz): 0.86 (tr; 12H; H9; J = 8 Hz), 1.25-1.40(m; 48H; H2+H3+H4+H5+H6+H7), 2.38 (tr; 8H; H2), 2.48 (s; 4H; H1) ppm. ^{13}C NMR ($CDCl_3$; 101MHz): 14.14 (C9), 22.74, 27.27, 27.69, 29.41, 29.69, 31.96, 52.41(C1), 54.95 (C2) ppm.

From the selected precursors the hydrogen content was determined by NMR spectroscopy and from a titriometric method (**Table S2**)[1] [2], in order the determine the excatct amount of Al introduced into the reaction mixtures. The titriometric method was used in addition to the NMR integration for the determination of the hydride content, since the hydridic protons are typically resulting in broad ^{1}H NMR signals making their integration difficult. However, in our studies a good agreement between the two methods could be achieved. The observed hydride content typically is slightly below the expected value of three, most likely based on the formation of a few 2:1 complexes.

Table S2: Overview of the Al precursors applied for the synthesis of Al nanoparticles.

Donor atom	**Precursor**	**M_w [g/mol]**	**H/Al[1]**	**H/Al[2]**
N	H_3AlNMe_3	89.12	2.54	2.66
	H_3AlNEt_3	131,19	2,64	2,73
	$H_3AlNEtMe_2$	101,14	2,76	---
	$H_3AlN^nBu_3$	215,35	2,39	2,35
	$H_3AlN^nOct_3$	383,67	2,60	2,18
polymeric	H_3Al·DABCO	142,17	2,27	---
ionic	H_3Al·PMDTA	233,30	2,23	---
O	H_3Al·THF	110,11	1,72	2,28
P	H_3Al·PCy_3	310,43	2,87	2,60
C	H_3Al·IMes	334,43	2,44	2,35

[1]titriometric method, [2]NMR integration

References

(1) Fedotova, T. D.; Glotov, O. G.; Zarko, V. E. Chemical Analysis of Aluminum as a Propellant Ingredient and Determination of Aluminum and Aluminum Nitride in Condensed Combustion Products. *Propellants, Explos. Pyrotech.* **2000**, *25*, 325–332.

(2) Yang, S.-P.; Tsai, R.-Y. Complexometric Titration of Aluminum and Magnesium Ions in Commercial Antacids. An Experiment for General and Analytical Chemistry Laboratories. *J. Chem. Educ.* **2006**, *83*, 906.

(3) Reuvers, P. J.; Smit, C. J. Preparation and Properties of Alane Dimethylethylamine, a Liquid Precursor for MOCVD. *Chem. Mater.* **1994**, *6*, 190–195.

(4) Ruff, J. K.; Hawthorne, M. F. The Amine Complexes of Aluminum Hydride. I. *J. Am. Chem. Soc.* **1960**, *82*, 2141–2144.

(5) Finholt, A. E.; Bond, A. C.; Schlesinger, H. I. Lithium Aluminum Hydride, Aluminum Hydride and Lithium Gallium Hydride, and Some of Their Applications in Organic and Inorganic Chemistry 1. *J. Am. Chem. Soc.* **1947**, *69*, 1199–1203.

(6) Atwood, J. L.; Robinson, K. D.; Jonesb, C.; Raston, C. L. Cationic Aluminium Hydrides: $[H_2AlL]+[AlH_4]-$, L = N,N,N',N",N"-Pentamethyldiethylenetriamine and 1,4,8,11-Tetramethyl-1,4,8,11-Tetraazacyclotetradecane. *J. Chem. Soc., Chem. Commun.* **1991**, *3*, 1697–1699.

(7) Brown, H. C.; Singaram, B. Molecular Addition Compounds. 7. Synthesis of Addition Compounds of Boron Trifluoride, Borane, and Alane with N, N, N, 'N'-Tetramethylethylenediamine and Triethylenediamine by Precipitation from Ether Solvents. *Inorg. Chem.* **1980**, *19*, 455–457.

(8) Bennett, F. R.; Elms, F. M.; Gardiner, M. G.; Koutsantonis, G. A.; Raston, C. L.; Roberts, N. K. Stable Tertiary Phosphine Adducts of Alane. *Organometallics* **1992**, *11*, 1457–1459.

(9) Bantreil, X.; Nolan, S. P. Synthesis of N-Heterocyclic Carbene Ligands and Derived Ruthenium Olefin Metathesis Catalysts. *Nat. Protoc.* **2011**, *6*, 69–77.

(10) Hintermann, L. Expedient Syntheses of the N-Heterocyclic Carbene Precursor Imidazolium Salts IPr·HCl, IMes·HCl and IXy·HCl. *Beilstein J. Org. Chem.* **2007**, *3*, 2–6.

(11) Preez, J. G. H. du; Shillington, D. P.; Brecht, B. J. A. M. van. Polynitrogen Reagents in Metal Separation. Part 1. Ditertiary and Diquaternary Ammonium Extractants for Cobalt (II) and Copper (II) in HCL Medium. *Solvent Extr. Ion Exch.* **2007**, *2*, 839–858.

7.5 Supporting information for Chapter 3.1.4

Supporting information

Synthesis of submicron aluminum particles via thermal decomposition of alkyl aluminum precursors in the presence of metal seeds and their application in the formation of ruthenium aluminides.

Thomas Klein, Guido Kickelbick[1]

Inorganic Solid State Chemistry, Saarland University, Campus C4.1, 66123 Saarbrücken

E-mail: guido.kickelbick@uni-saarland.de
Homepage: www.uni-saarland.de/lehrstuhl/kickelbick.html

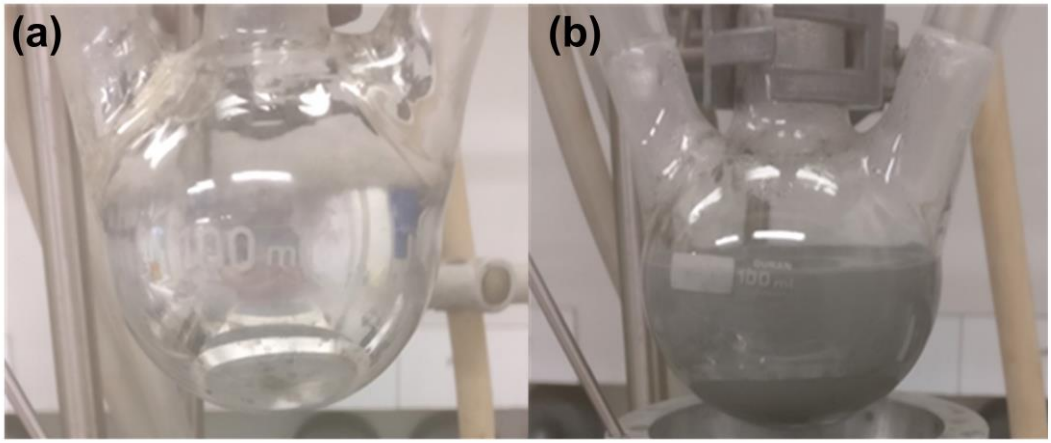

Figure S1. Images of the reaction flask after the synthesis **a)** without and **b)** with the presence of metal nanoparticle seeds.

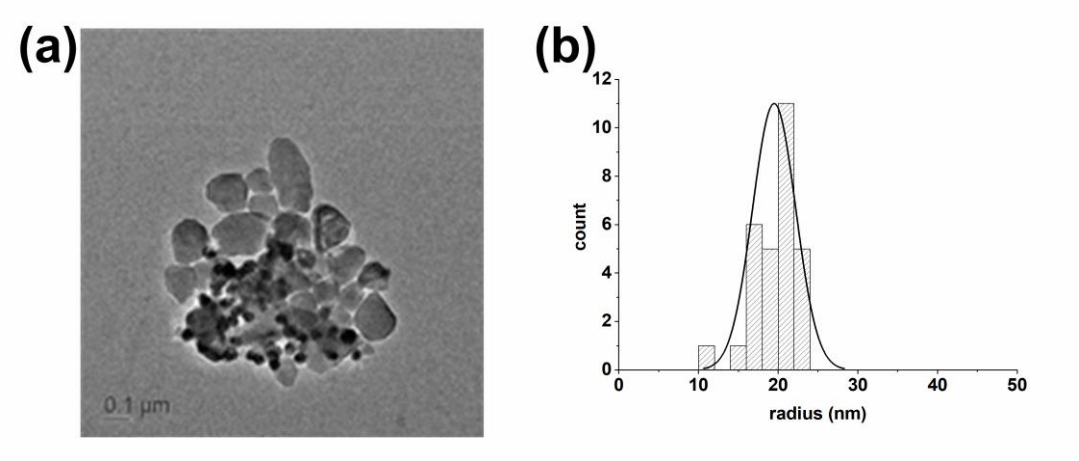

Figure S2. (a) TEM image of Al(Ni) particles, showing the synthesized Al particles as well as the Ni seed particles; **(b)** particle size distribution obtained by measuring 100 particles.

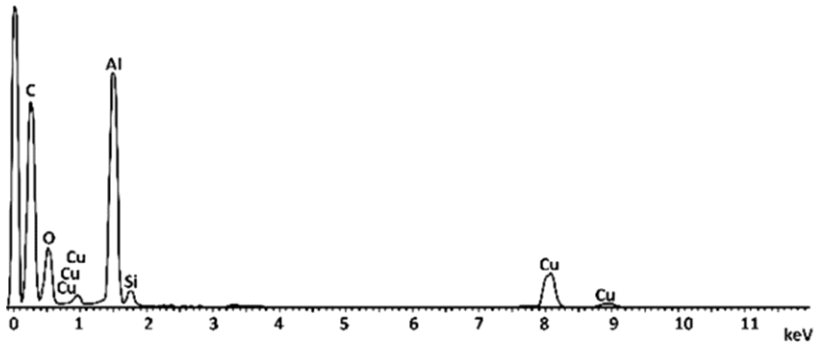

Figure S3. EDX measurements of Al submicron particles from Ag seeds synthesized via thermal decomposition of TIBAl in Ph_2O.

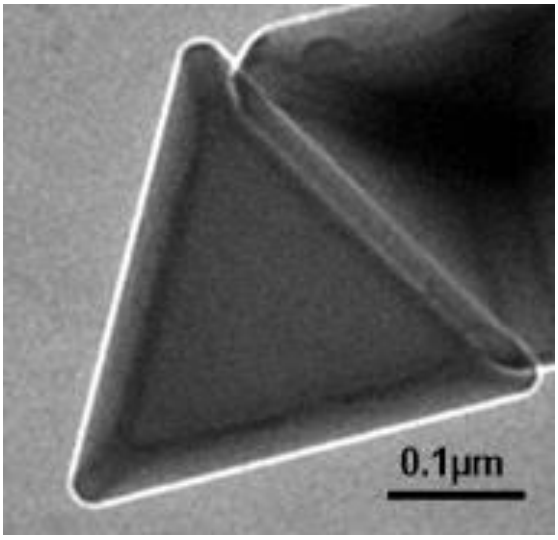

Figure S4. TEM image of a triangular Al platelet synthesized from Ag seeds.

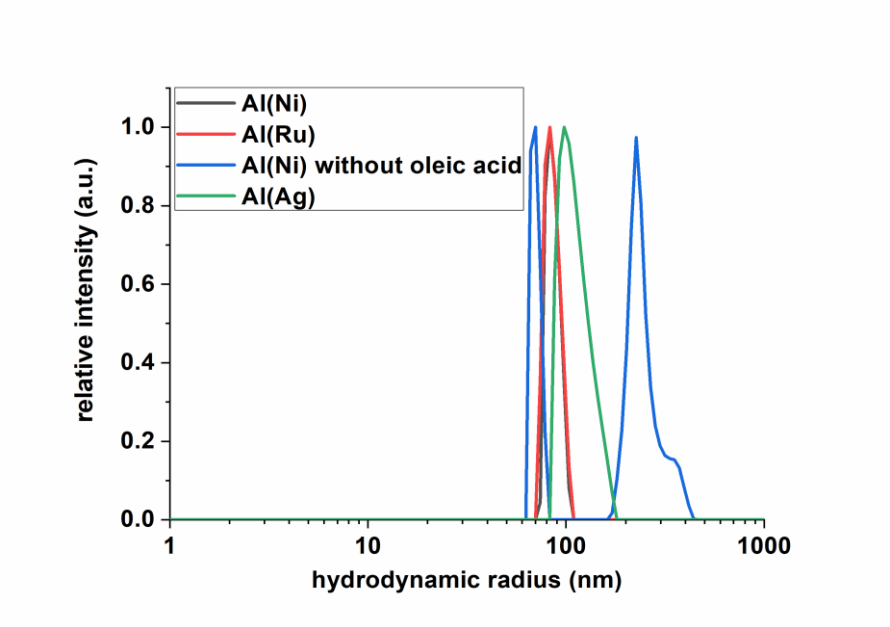

Figure S5. DLS measurements of Al particles synthesized via thermal decomposition of TIBAL in Ph_2O using different metal nanoparticles as seeds in hexane. The particles were capped by oleic acid unless stated otherwise.

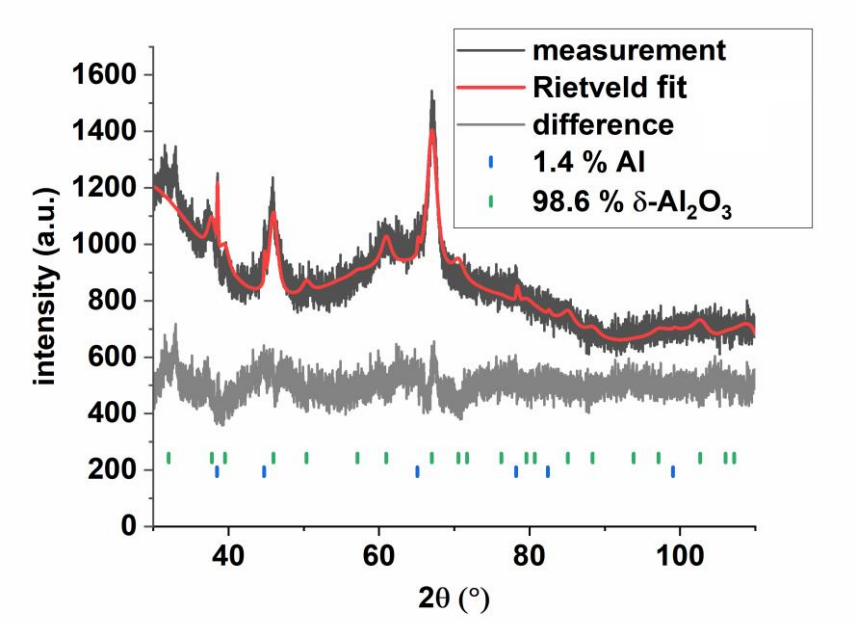

Figure S6. XRD measurement and Rietveld fit of the oxidized submicron Al particles measured after a TG measurement under an atmosphere of synthetic air.

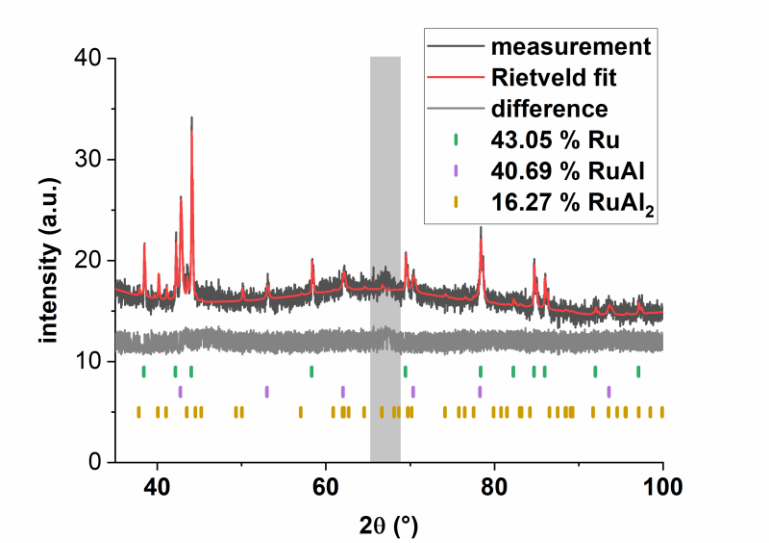

Figure S7. PXRD measurements and Rietveld refinement of the reaction product obtained from Ru-powder and oleic acid capped Al particles after heating up to 800 °C under an atmosphere of flowing argon. The formation of Al_2O_3 is clearly visible (highlighted in grey), likely to be caused by the presence of the additional oxygen contained within the oleic acid.

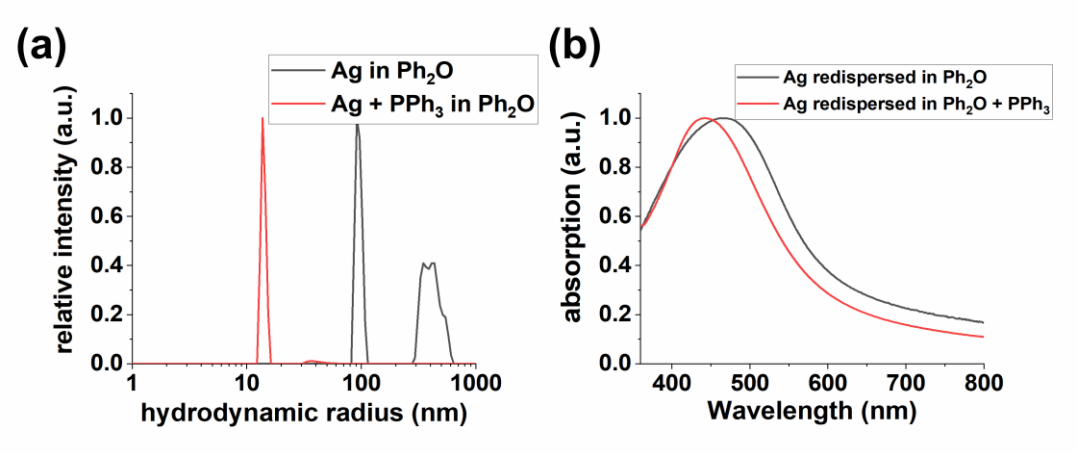

Figure S8. a) DLS measurements of Ag seeds in diphenylether: shown are the number weighted results **b)** normalized UV/VIS spectra of Ag seeds in diphenylether.

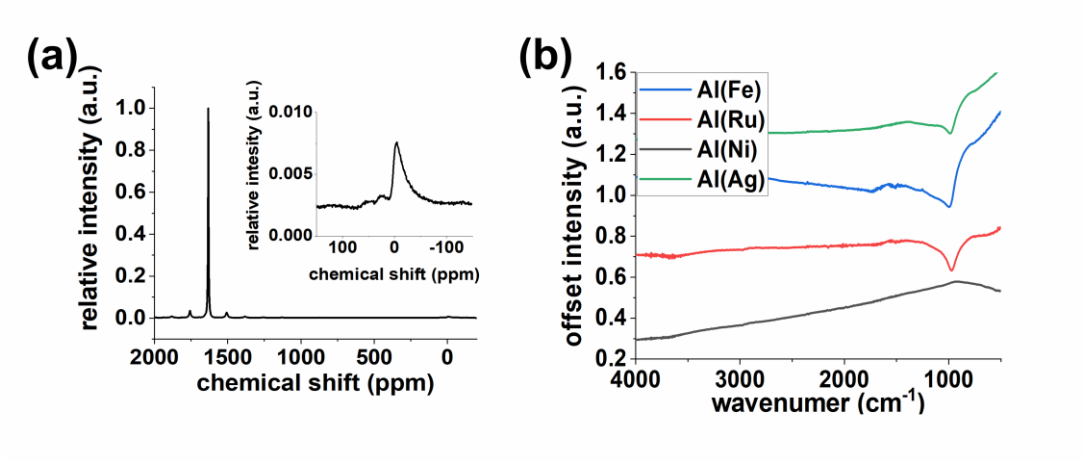

Figure S9. a) ATR-FTIR spectra and **b)** SPE-MAS-NMR of uncapped submicron Al particles synthesized via thermal decomposition of TIBAL in Ph_2O using different metal nanoparticles as seeds. The inset shows the enlarged spectra around 0 ppm. Syntheses were carried out using a metal:Al ratio of 1:80.

Ag Nanoparticles

Figure S10 shows the TEM images, XRD and TG measurements of the Ag nanoparticles used as seeds for the synthesis of the Al nanoparticles. The particles have a spherical shape, a size of 6±1 nm and a narrow particle size distribution. The Ag silver content determined from TG measurements of the particles is about 75 %.

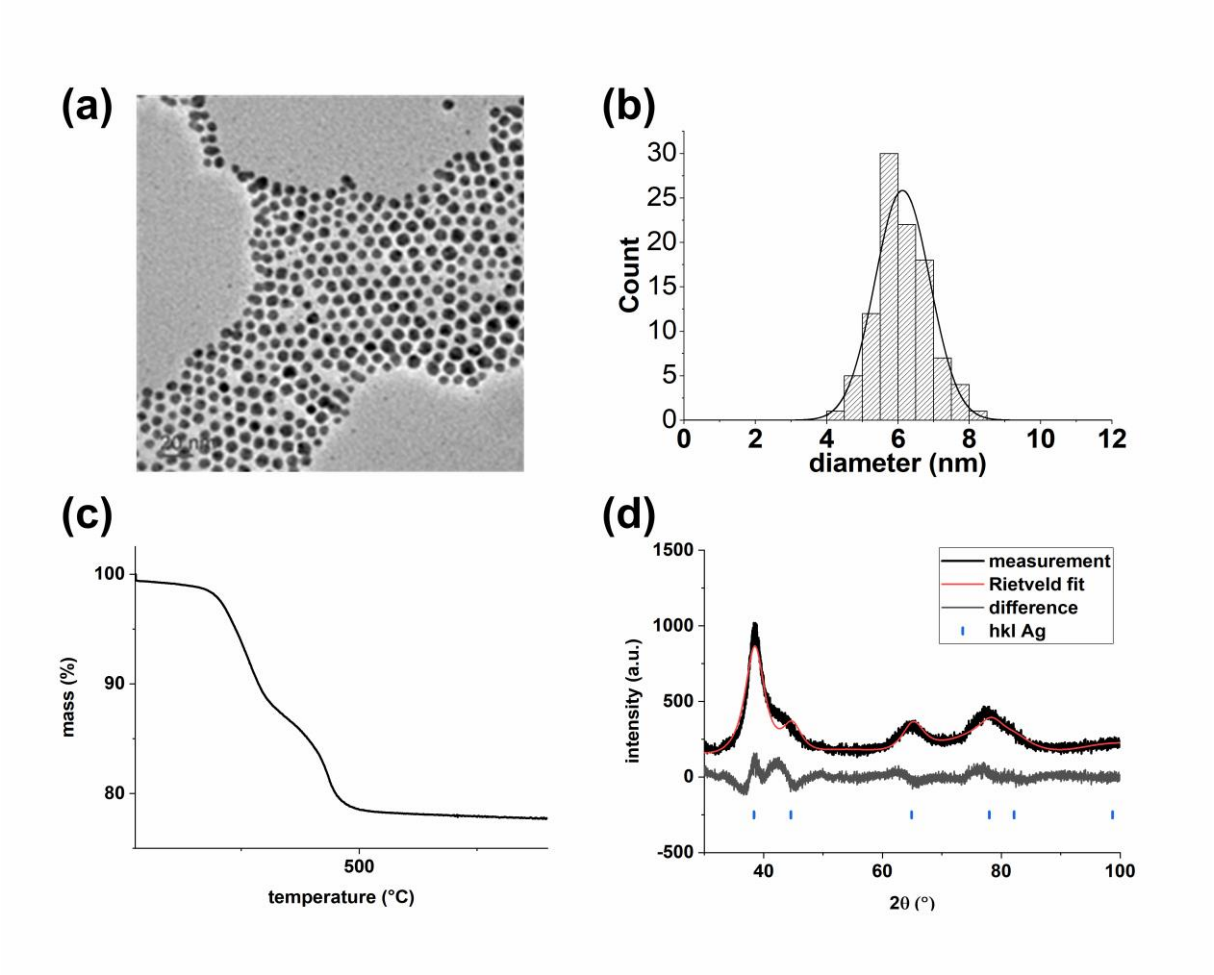

Figure S10. a) TEM image of oleic acid capped Ag nanoparticles used as seeds for synthesis of Al nanoparticles **b)** particle size distribution obtained from TEM images by measuring 100 particles **c)** TGA measurements of oleic acid capped Ag nanoparticles using a heating rate of 20 K/min under an atmosphere of N_2:O_2 32:8 **d)** PXRD measurement and Rietveld refinement of the oleic acid capped Ag nanoparticles.

Ni Nanoparticles

The Ni nanoparticles show a mean radius of 8±1 nm and a narrow particle size distribution (Figure S11a and S11b). The crystallite size determined via Rietveld refinement was 10(1) nm (cf. Figure S11c). The organic content determined via CHN-analysis was as low as 4.3 %. This low value was confirmed by TG measurements were a mass loss of 0.8 % was observed up to a temperature of 200 °C (Figure S11d).

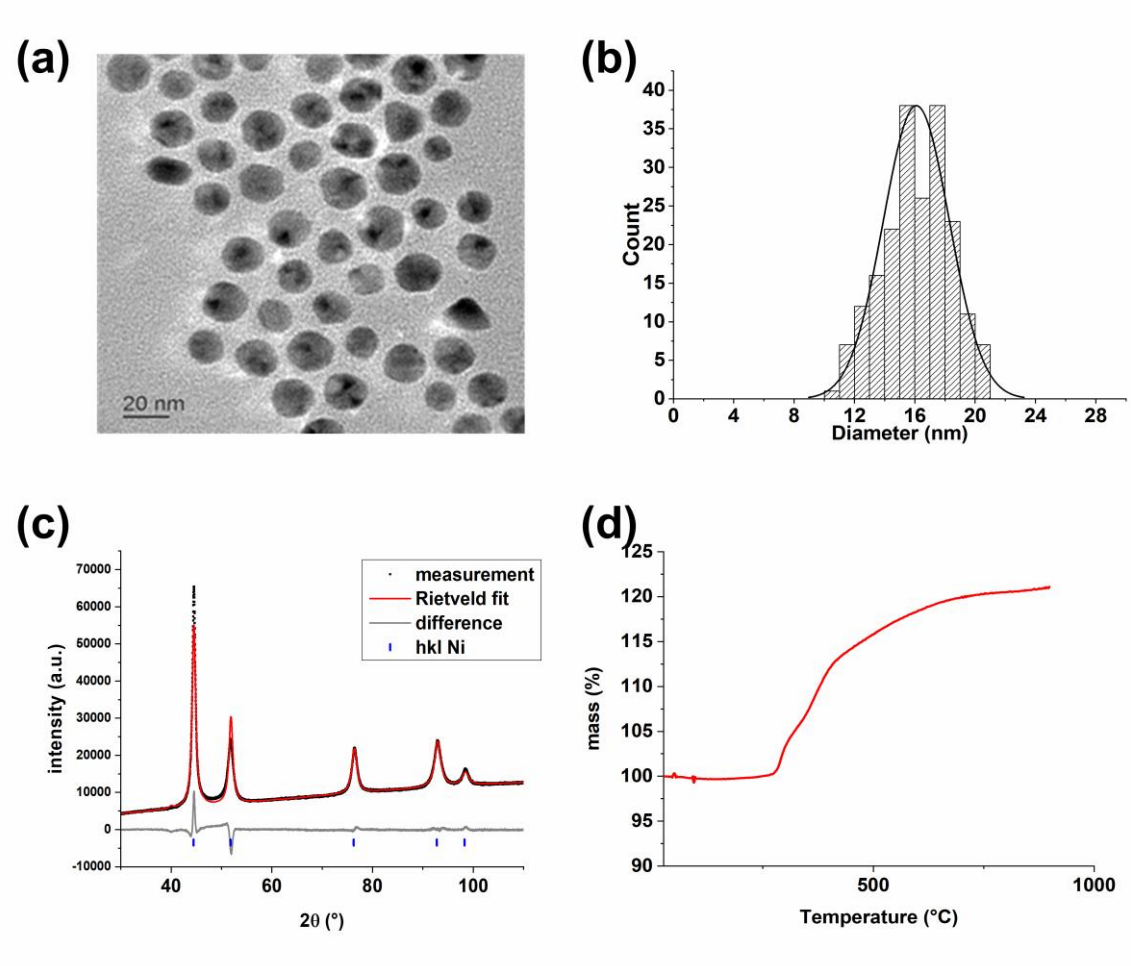

Figure S11. a) TEM image of TOP capped Ni nanoparticles used as seeds in the synthesis of Al nanoparticles **b)** particle size distribution obtained from TEM images by measuring 202 particles **c)** PXRD measurements and Rietveld refinement of TOP capped Ni nanoparticles used as seeds in the synthesis of Al nanoparticles **d)** TGA measurement of TOP capped Ni nanoparticles used as seeds in the synthesis of Al nanoparticles (20 °C/min) in an atmosphere of synthetic air (N_2:O_2 32:8).

Ru Nanoparticles

Figure S12 shows the TEM images and XRD measurements of the Ru nanoparticles used as seeds in the synthesis of submicron Al particles and for the formation of Ru aluminides. The particles are consisting of small crystallites with sizes of about 2-3 nm (Figure S12a). However, strong agglomeration to clusters with sizes > 100 nm is clearly visible. This formation of agglomerates is due to their synthesis via a mechanochemical approach without any stabilizer present. The crystallite size determined via Rietveld refinement (Figure S12b) is 2(1) nm.

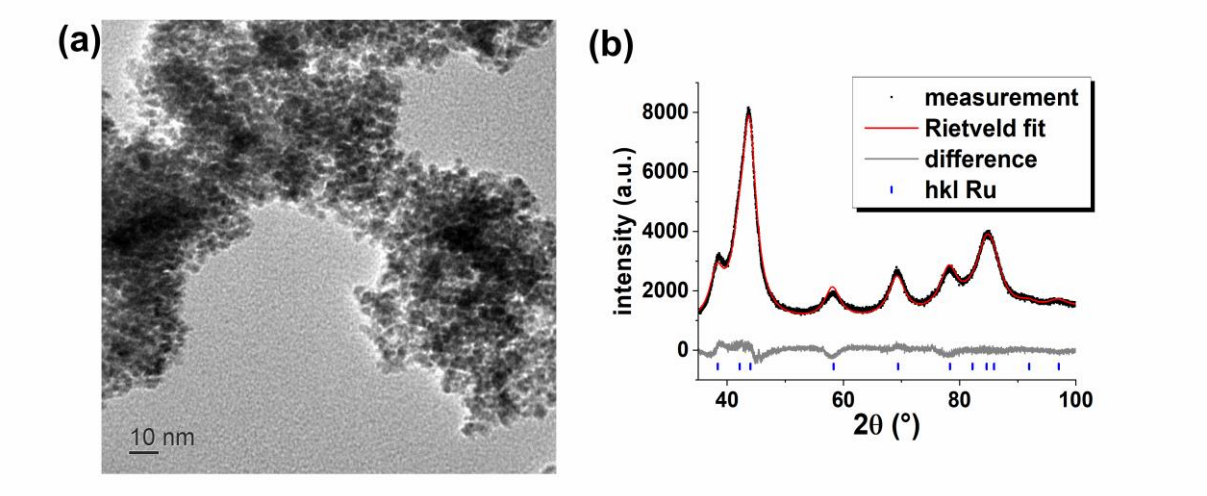

Figure S12. a) TEM image of Ru nanoparticles used as seeds in the synthesis of submicron Al particles and for the formation of Ru aluminides **b)** PXRD measurements and Rietveld refinement of the Ru nanoparticles used as seeds in the synthesis of submicron Al particles and for the formation of Ru aluminides.

Commercial Ru powder

The Ru powder (Figure S13) obtained from abcr (Karlsruhe, Germany; nominal size 60 µm) consisted of particles of irregular shapes with irregular surfaces. The mean diameter determined from light microscopic images was 57±12 µm. The crystallite size determined from Rietveld refinement was found to be 172(6) nm.

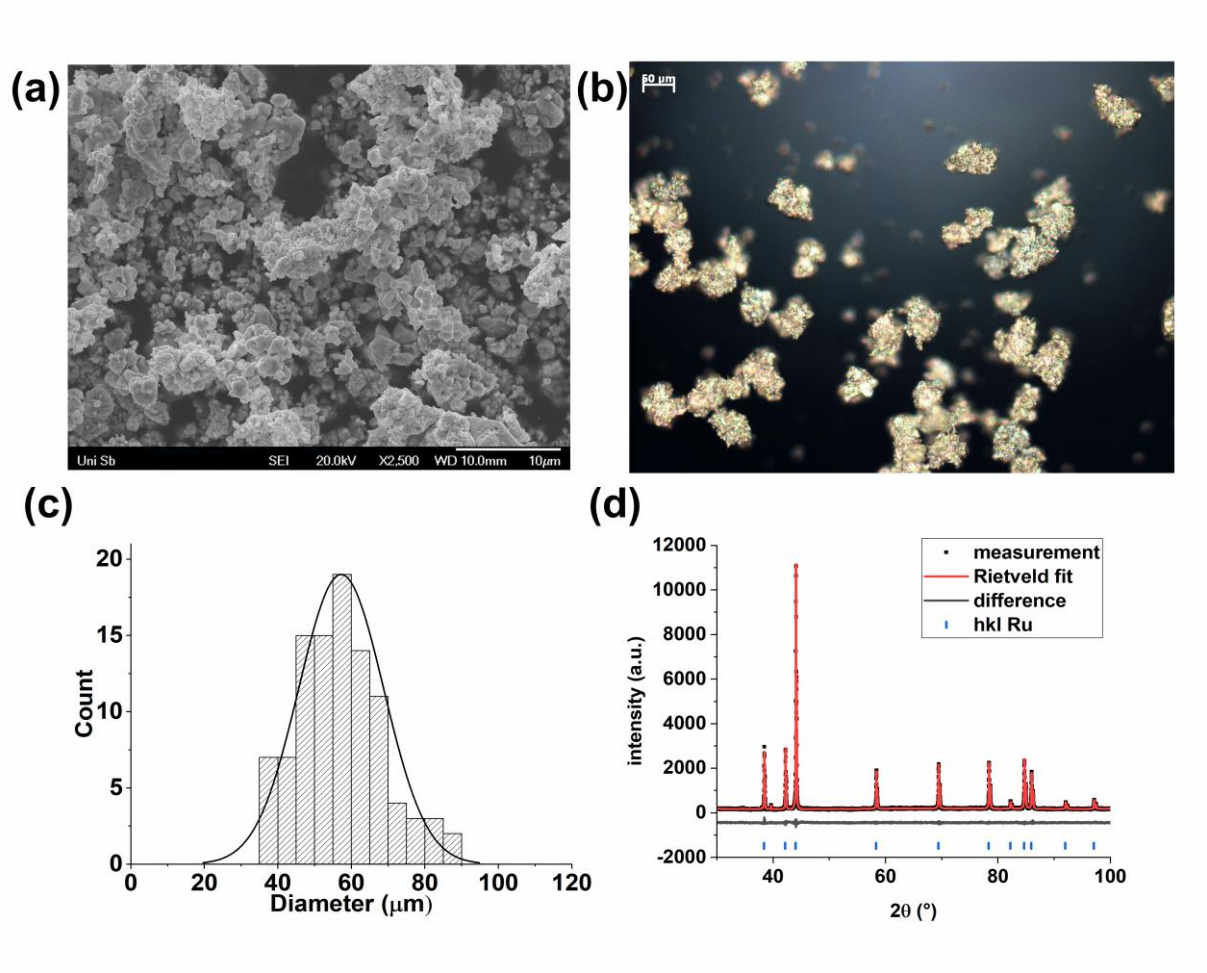

Figure S13. a) SEM images and **b)** light microscopic images of commercial Ru powder used for the synthesis of aluminides **c)** particle size distribution obtained from the light microscopic images by measuring 100 particles **d)** PXRD measurement and Rietveld refinement of the commercial Ru powder.

Commercial Al powder

The Al powder (Figure S14) obtained from abcr (Karlsruhe, Germany; nominal size <325 mesh) consisted of particles with irregular shapes, where some of the particles had quasi-spherical shapes, while others were elongated in one direction. They had smooth surfaces and the mean diameter was 14±7 µm as determined from the SEM images. The crystallite size determined from Rietveld refinement was found to be 318(16) nm.

The Al^0 content of the commercial Al powder determined via the back titration method was calculated to be around 99 %. The higher Al^0 content compared the synthesized Al particles is also clearly seen in the TG measurements showing only a mass gain of around 1 % in the first mass gain step at 600 °C.

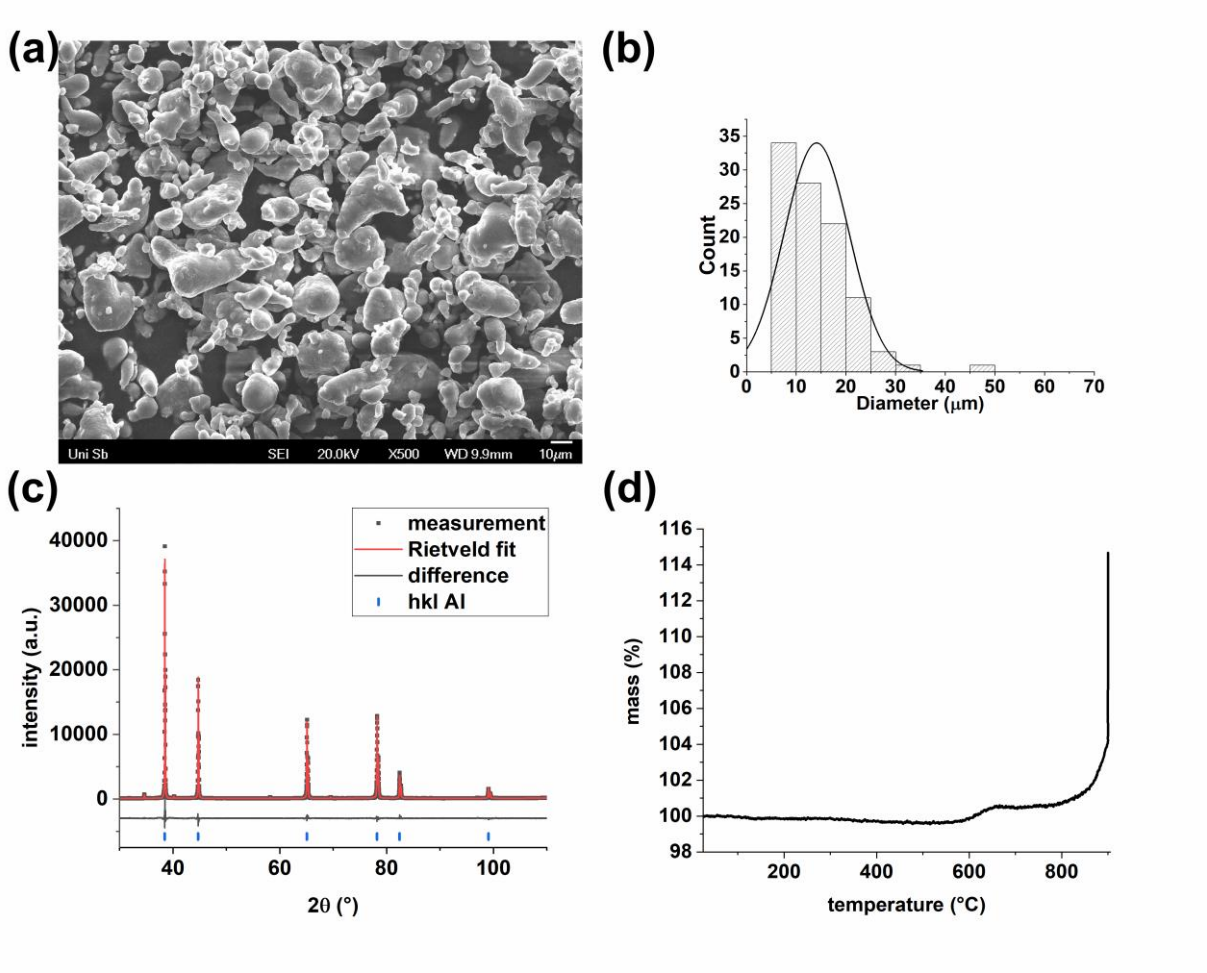

Figure S14. a) SEM images of commercial Al powder used for the synthesis of aluminides **b)** particle size distribution obtained from the SEM images by measuring 100 particles **c)** PXRD measurement and Rietveld refinement of the commercial Al powder **d)** TGA measurement of commercial Al powder (10 K/ min; N_2O_2 32:8).